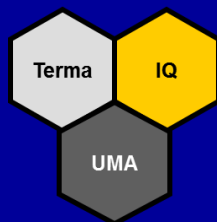


Programa de Doctorado:  
Química y Tecnologías Químicas. Materiales y Nanotecnología.



Grupo Terma  
(Tecnología de Residuos y Medioambiente)

Departamento de Ingeniería Química  
Universidad de Málaga

TESIS  
DOCTORAL

Estudio cinético de la reacción de ODH de propano sobre catalizadores de vanadio  
electrohilado con tamaño submicrométrico

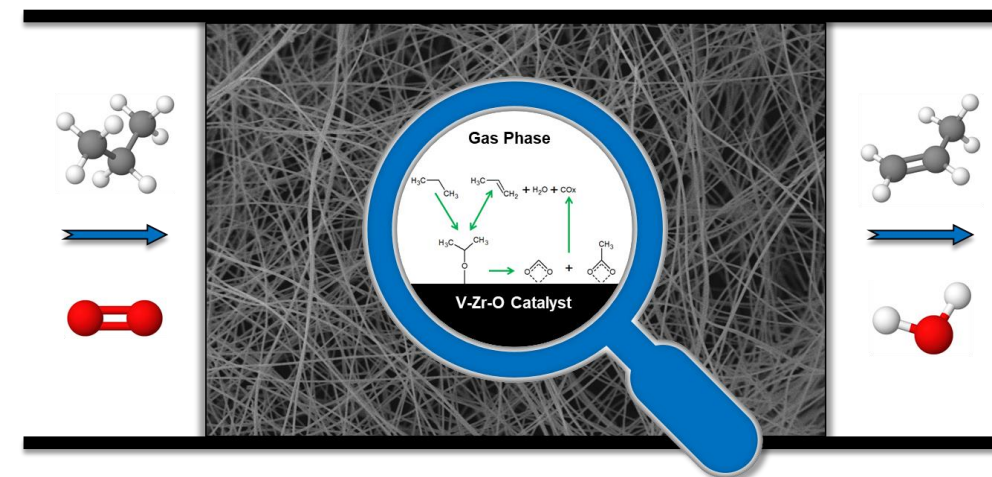
Juan José  
Ternero  
Hidalgo

2020

UNIVERSIDAD DE MÁLAGA  
Facultad de Ciencias  
Departamento de Ingeniería Química

TESIS DOCTORAL

ESTUDIO CINÉTICO DE LA REACCIÓN DE ODH DE  
PROPANO SOBRE CATALIZADORES DE VANADIO  
ELECTROHILADO CON TAMAÑO SUBMICROMÉTRICO



Programa de Doctorado:  
Química y Tecnologías Químicas. Materiales y Nanotecnología.

Directores:  
Dr. D. José Rodríguez Mirasol  
Dra. Dña. María Olga Guerrero Pérez

Juan José Ternero Hidalgo

Málaga, 2020



UNIVERSIDAD  
DE MÁLAGA



UNIVERSIDAD DE MÁLAGA

Facultad de Ciencias

*Departamento de Ingeniería Química*

## TESIS DOCTORAL

Para optar al Título de:

Doctor en Ingeniería Química con Mención Internacional

Estudio cinético de la reacción de ODH de  
propano sobre catalizadores de vanadio  
electrohilado con tamaño submicrométrico

Autor: Juan José Ternero Hidalgo

Directores: Dr. D. José Rodríguez Mirasol

Dra. Dña. María Olga Guerrero Pérez


Programa de doctorado: Química y Tecnologías Químicas.  
Materiales y Nanotecnología

Málaga, 2020



UNIVERSIDAD  
DE MÁLAGA

AUTOR: Juan José Ternero Hidalgo

 <http://orcid.org/0000-0001-5280-739X>

EDITA: Publicaciones y Divulgación Científica. Universidad de Málaga



Esta obra está bajo una licencia de Creative Commons Reconocimiento-NoComercial-SinObraDerivada 4.0 Internacional:

<http://creativecommons.org/licenses/by-nc-nd/4.0/legalcode>

Cualquier parte de esta obra se puede reproducir sin autorización pero con el reconocimiento y atribución de los autores.

No se puede hacer uso comercial de la obra y no se puede alterar, transformar o hacer obras derivadas.

Esta Tesis Doctoral está depositada en el Repositorio Institucional de la Universidad de Málaga (RIUMA): [riuma.uma.es](http://riuma.uma.es)

D. JOSÉ RODRÍGUEZ MIRASOL, Catedrático de Ingeniería Química de la Universidad de Málaga,

Dña. MARÍA OLGA GUERRERO PÉREZ, Profesora Titular de Ingeniería Química de la Universidad de Málaga,

CERTIFICAN: Que el trabajo de investigación recogido en la presente Memoria ha sido realizado bajo su dirección en el Departamento de Ingeniería Química de la Universidad de Málaga por el Ingeniero D. JUAN JOSÉ TERNERO HIDALGO, y reúne, a su juicio, contenido científico suficiente y las condiciones necesarias para ser presentado y defendido ante el Tribunal correspondiente para optar al Grado de Doctor con Mención Internacional.

Málaga, octubre de 2019

Fdo.: José Rodríguez Mirasol

Fdo.: María Olga Guerrero Pérez





*A mi familia*



## OVERVIEW AND OBJECTIVES

Propylene is the second most-demanded building block in the petrochemical industry to produce many interest products. The propylene demand was about 67 and 89-109 million tons in 2005 and 2014, respectively, and it is estimated to increase up to around 165 Million tons by 2030. Traditionally, this demand has been covered by the propylene obtained as byproduct in the oil refining during the production of ethylene and gasoline from steam cracking and from fluid catalytic cracking, respectively. Since last decade, these technologies are only covering the 85-90% of the global demand, then “on-purpose propylene technologies” are necessary to fill such gap. This situation has encouraged the production of propylene from propane, which is an abundant and low-cost feedstock due to the current proliferation of the shale gas.

Nowadays, Oleflex and Catofin technologies are commercially implemented for the non-oxidative dehydrogenation of propane to produce propylene using catalysts of Pt-Sn or Cr<sub>2</sub>O<sub>3</sub> supported on alumina, respectively. They are energy-intensive processes, where the conversion and selectivity are thermodynamically restricted and catalyst deactivation is occurred by coke deposition. In this way, propane ODH has the potential to overcome these above disadvantages and has been extensively studied over supported vanadium-based catalysts for the last decades. In terms of energy saving, it is estimated that propane ODH could potentially consume 45% less energy than the non-oxidative counterpart. However, propane ODH has not been industrially implemented yet, despite its higher energetic efficiency, due to its too low values of yield and productivity towards propylene, as a result of the undesired overoxidation reactions to CO<sub>x</sub>, which are difficult to control. Until now, the highest productivity found in the literature is 9 g<sub>C<sub>3</sub>H<sub>6</sub></sub>·g<sub>cat</sub><sup>-1</sup>·h<sup>-1</sup>, and most of the yields obtained are below 30% with propylene selectivity below 70%, while the yield in the pure propane dehydrogenation is usually around 40% with a propylene selectivity above 90%. Therefore, this reaction is still in the research state, since it would be



definitely necessary to improve the existing catalysts or to find new ones, to optimize the reaction conditions and/or to find the optimal reactor obtaining higher yield and/or productivity in order to become profitable as an industrial process.

This PhD thesis is divided into four sections: the introduction, where the state of art is shown; the experimental methodology, where the general aspects about the preparation and characterization of the catalysts and the reactors used for the propane ODH are described; the results and discussions, which consists of five subsections; and the general conclusions. Regarding the results and discussions section, each of the subsections contain its own abstract, introduction, experimental methodology, results and discussions, and conclusions. Overall, this section gathers three main objectives:

1. The preparation and characterization of submicrometric fibrous catalysts based on Zr, Zr-V, Zr-Mo, Zr-Nb, Zr-V-Mo and Zr-V-Nb mixed oxides by using the electrospinning technique, in order to be studied in the propane ODH reaction. In this way, a new versatile, simple and straightforward procedure is proposed for the preparation of such catalysts, which involves the electrospun of a polymer solution containing all the required metallic precursors, followed by only one calcination step. Compared to the traditional powdered catalysts, the submicrometric fibrillar structure would confer to these materials several advantages such as small internal diffusion resistance, less temperature gradients and lower pressure drop when they are packed in a fixed bed reactor.
2. The study of the propane ODH reaction mechanism to gain deeper insight about the structure-activity relationships of the catalysts during reaction. For such goal, a new homemade *operando* IRRaman reactor has been used. This reactor allows to obtain in a single experiment, with space and time consistency, information about the structure of the

catalyst (mainly from Raman), the adsorbed species (mainly from FTIR) and the reactivity (online gases measurements) during reaction.

3. The kinetic study of the propane ODH reaction over the submicron diameter fiber catalysts already prepared by electrospinning and thoroughly characterized, establishing the kinetic equations in a rigorous way using the reaction mechanism previously proposed according to the FTIR-Raman *operando* results obtained in the IRRaman reactor. Thereby, it will be attempted to find out kinetic information from the different active species present on the catalysts such as polyvanadate, monovanadate, crystalline  $ZrV_2O_7$  and V-Mo-O species. The kinetic model will be used to simulate values of yield and productivity to study their dependence and to try to find the theoretical optimum conditions to get their maximum values, what could be very useful to determine if a catalyst can be suitable to be used on an industrial scale.





# CONTENTS

<b>OVERVIEW AND OBJECTIVES.....</b>	<b>V</b>
<b>1. INTRODUCTION.....</b>	<b>3</b>
<b>1.1. Propylene.....</b>	<b>3</b>
1.1.1. Propylene gap.....	3
1.1.2. Current technologies to obtain propylene.....	5
1.1.2.1. Steam cracking.....	5
1.1.2.2. Fluid catalytic cracking.....	8
1.1.2.3. Catalytic dehydrogenation.....	12
<b>1.2. Oxidative dehydrogenation (ODH) of propane.....</b>	<b>21</b>
1.2.1 Propane ODH as alternative.....	21
1.2.2. Catalysts for propane ODH reaction.....	24
1.2.2.1. Alkali and Alkaline earth-based catalysts.....	27
1.2.2.2. Reducible transition metal oxides-based catalysts.....	27
1.2.2.3. Boron based catalysts.....	29
1.2.3. Vanadium oxide based catalysts.....	32
1.2.3.1. Vanadia species and active sites.....	34
1.2.3.2. Effect of support.....	36
1.2.3.3. Red-ox properties.....	38
1.2.3.4. Acid-basic properties.....	39
1.2.3.5. Effect of additives.....	39
1.2.4 Aspects of the propane ODH reaction mechanism over vanadium oxide based catalysts.....	41
1.2.5. Kinetic models.....	48
1.2.5.1. Eley-Rideal.....	50
1.2.5.2. Langmuir-Hinshelwood.....	51
1.2.5.3. Power Law.....	52
1.2.5.4. Rake.....	52
1.2.5.5. Mars van Krevelen (redox).....	54
1.2.6. Reactor configurations.....	55
<b>1.3. References.....</b>	<b>59</b>
<b>2. EXPERIMENTAL METHODOLOGY.....</b>	<b>115</b>
<b>2.1. Catalysts preparation.....</b>	<b>115</b>
2.1.1. Reagents.....	115



2.1.2. Polymer solutions .....	115
2.1.3. Electrospinning .....	116
2.1.4. Incipient wetness method .....	118
2.1.5. Samples nomenclature .....	119
<b>2.2. Catalysts characterization .....</b>	<b>120</b>
2.2.1. Porous texture .....	120
2.2.2. Morphology .....	120
2.2.3. Surface chemistry and crystal structure .....	121
<b>2.3. Propane ODH experiments .....</b>	<b>121</b>
2.3.1. Fixed bed reactor .....	121
2.3.2. IRRaman <i>operando</i> reactor .....	123
<b>2.4. References .....</b>	<b>124</b>
<b>3. RESULTS AND DISCUSSION .....</b>	<b>129</b>
<b>3.1. Electrospun vanadium oxide based submicron diameter fiber catalysts. Part I: Preparation procedure and propane ODH application .....</b>	<b>129</b>
3.1.1. Introduction .....	130
3.1.2. Materials and methods .....	133
3.1.2.1. Catalysts preparation .....	133
3.1.2.2. Characterization .....	136
3.1.2.3. Propane oxidative dehydrogenation .....	137
3.1.3. Results .....	139
3.1.4. Discussion .....	154
3.1.5. Conclusions .....	157
3.1.6. Supplementary information .....	157
3.1.7. References .....	160
<b>3.2. Electrospun vanadium oxide based submicron diameter fiber catalysts. Part II: Effect of chemical formulation and dopants .....</b>	<b>168</b>
3.2.1. Introduction .....	169
3.2.2. Materials and methods .....	170
3.2.2.1. Catalysts preparation .....	170
3.2.2.2. Characterization .....	173
3.2.2.3. Propane oxidative dehydrogenation .....	173
3.2.3. Results and discussion .....	175
3.2.4. Conclusions .....	186
3.2.5. Supplementary information .....	187
3.2.6. References .....	187

<b>3.3. A simultaneous <i>operando</i> FTIR &amp; Raman study of propane ODH mechanism over V-Zr-O catalysts .....</b>	<b>190</b>
3.3.1. Introduction.....	191
3.3.2. Experimental .....	194
3.3.2.1. Catalysts preparation .....	194
3.3.2.2. ODH reaction conditions .....	194
3.3.3. Results and discussion.....	198
3.3.3.1. Fresh Catalysts characterization .....	198
3.3.3.2. Catalysts during reaction.....	200
3.3.3.2.1. ODH conditions .....	200
3.3.3.2.2. DH conditions .....	210
3.3.3.3. Proposed mechanism.....	215
3.3.4. Conclusions .....	220
3.3.5. Supplementary information .....	221
3.3.6. References .....	223
<b>3.4. Kinetic study of propane ODH on electrospun vanadium oxide-based submicron diameter fiber catalyst. Part I .....</b>	<b>234</b>
3.4.1. Introduction.....	236
3.4.2. Materials and methods.....	239
3.4.2.1. Catalyst preparation and characterization.....	239
3.4.2.2. Propane ODH experiments .....	242
3.4.3. Results.....	243
3.4.3.1. Propane ODH mechanism .....	243
3.4.3.2. Rate equations .....	245
3.4.3.3. Kinetic study .....	255
3.4.3.4. Influence of space-time .....	260
3.4.3.5. Influence of inlet partial pressure of propane and oxygen .....	266
3.4.4. Conclusions .....	269
3.4.5. References .....	271
<b>3.5. Kinetic study of propane ODH on electrospun vanadium oxide-based submicron diameter fiber catalysts. Part II .....</b>	<b>278</b>
3.5.1. Introduction.....	280
3.5.2. Materials and methods.....	283
3.5.2.1. Catalysts preparation and characterization.....	283
3.5.2.2. Propane ODH experiments .....	285
3.5.3. Results and discussion.....	286
3.5.3.1. Kinetic model .....	286
3.5.3.2. Kinetic study .....	290
3.5.3.3. Influence of space-time and oxygen inlet partial pressure .....	298
3.5.3.4. Simulation of yield and productivity to propylene .....	304
3.5.4. Conclusions .....	317
3.5.5. Supplementary information .....	320
3.5.6. References .....	324

<b>4. GENERAL CONCLUSIONS .....</b>	<b>337</b>
<b>SUMMARY IN ENGLISH .....</b>	<b>343</b>
<b>RESUMEN EN ESPAÑOL .....</b>	<b>365</b>
<b>ACKNOWLEDGEMENTS .....</b>	<b>387</b>
<b>CURRICULUM .....</b>	<b>391</b>



# **INTRODUCTION**





# 1. INTRODUCTION

## 1.1. Propylene

### 1.1.1. Propylene gap

Propylene is a gas at standard temperature and pressure (STP) conditions with a high vapor pressure and flammable. It is a compound intended for industrial applications and not for the direct consumer use. Over recent decades, the propylene demand has been increasing and currently is the second most-used building block, after ethylene, to produce many chemical and plastic products in the petrochemical industry (polypropylene, acrylonitrile, oxo-alcohols, propylene oxide, cumene, acrylic acid, etc) [1–3]. The propylene demand was about 67 and 89-109 million tons in 2005 and 2014, respectively, and it is estimated to increase up to around 165 Million tons by 2030 [2,4,5]. Traditionally, this demand has been covered by the propylene obtained as byproduct in the oil refining during the production of ethylene and gasoline from steam cracking (SC) and from fluid catalytic cracking (FCC), respectively [2,4,6] (Figure 1.1), which means that the propylene production has been always strongly influenced by the ethylene and gasoline demand. However, the propylene supply by these technologies only represents around the 85-90% of the global demand since last decade. This is not only due to the increase of the propylene demand, but also to the improvement of the ethylene and gasoline (target products) yields obtained by SC and FCC, respectively, in detriment of propylene [4,6,7]. Therefore, “on-purpose propylene technologies” are necessary to fill the propylene gap created between the demand and the supply by SC and FCC (Figure 1.1).

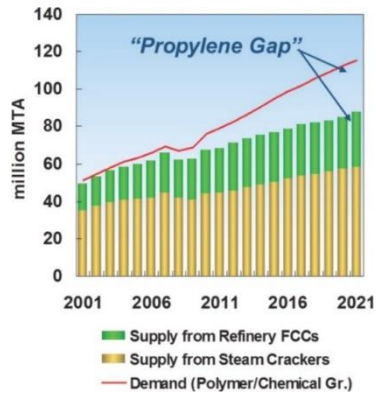


Figure 1.1. Predicted propylene demand and supply from FCC and SC (adapted from [6]).

In this way, the propylene production using propane as a feedstock appears as the main alternative, since propane has become abundant and very cheap due to the exploitation of shale gas and stranded gas by hydraulic fracturing or “fracking” technologies [3,4,7,8], which has been significantly improved to date by increasing the volume of production and reducing operating costs. As shown in Table 1.1, shale gas usually contains methane as main component and considerable amounts of light alkanes or so-called gas liquids (NGL), such as ethane, propane and lower amounts of larger hydrocarbon as butane, which can be easily separated. The main economic motivation to consider propane as a raw material to obtain propylene is the increasing price differential between the alkane feed and the olefin product [9]. In fact, the increasing availability and low-cost shale gas and stranded gas have led to a profound impact on the light olefin market. On one hand, it has made more profitable the production of light olefins from gas-based dehydrogenation routes [10], even though the separation of the alkane/alkene mixture sometimes requires a lot of energy due to the small volatility difference, as in the case of propylene/propane separation that is normally achieved in cryogenic or high-pressure distillation columns [11,12]. On the other hand, the feed for SC has been progressively changed from naphtha to the abundant and cheap ethane, resulting in a great improvement of the ethylene yield at the expense of propylene in such process (Figure 1.2) increasing the propylene gap [4,7].

**Table 1.1.** Average gas composition of six different shale gas deposits in the United States<sup>a</sup> (adapted from [3]).

Shale deposit	Methane (%)	Ethane (%)	Propane (%)	Carbon oxides (%)	Nitrogen (%)
Barnett	86.8	6.7	2.0	1.7	2.9
Marcellus	85.2	11.3	2.9	0.4	0.3
Fayetteville	97.3	1.0	0	1.0	0.7
New Albany <sup>b</sup>	89.9	1.1	1.1	7.9	-
Antrim	62.0	4.2	1.1	3.8	29.0
Haynesville	95.0	0.1	0	4.8	0.1

<sup>a</sup>Larger hydrocarbons, hydrogen, and oxygen are present in trace amounts and are not given.

<sup>b</sup>Nitrogen not reported.

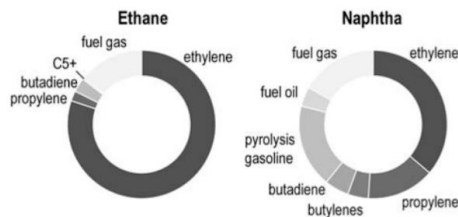


**Figure 1.2.** Steam cracker product yield by weight for ethane and naphtha feedstocks (adapted from [13]).

## 1.1.2. Current technologies to obtain propylene

### 1.1.2.1. Steam cracking

Steam cracking (SC) of gaseous or liquid saturated hydrocarbon (ethane, LPG or naphtha) is a petrochemical process where complex organic molecules are broken down into simpler ones such as olefins, paraffins and hydrogen [14]. The oxycracking reactions can also produce hydrocarbons that are heavier than the feed. For instance, ethane could be converted to propylene or butadiene (Figure 1.2 [13]). SC represents the main route for producing light olefins, especially ethylene (principal product) and propylene (byproduct), as well as small amounts of higher olefins (byproducts) (Figure 1.2). A significant amount of coke is also formed during the process that results in certain operating constraints and frequent plant shut-downs [10,15,16]. SC is a gas phase homogenous and highly endothermic reaction that involves the breaking of C-C and C-H bonds in the precursor, which requires a high amount of energy (around 70% of the total production cost).

In this process, the hydrocarbon feedstock is diluted with steam (steam/ethane ratio of 0.5-0.8) without the presence of oxygen and heated at around 850°C in a tubular furnace at a slightly higher pressure than 1

atm for a brief period of time (Figure 1.3) [17,18]. The residence time can be as short as in the order of milliseconds (gas velocities around the speed of sound) in modern cracking furnaces, in order to avoid secondary reactions and to improve the yield to desired products. In fact, the products leaving the tubular reactor are quickly quenched to stop the reaction. The feed is diluted with steam to decrease the partial pressure of the hydrocarbon feedstock and to diminish the coke formation, as well as the steam can react with the carbon deposits formed on the walls of the reactor. These deposits reduce the heat transfer through the alloy tubes of the reactor and halt the reaction [10,15,16].

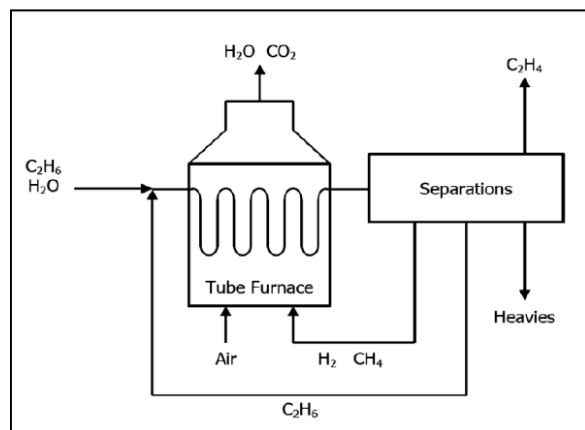


Figure 1.3. Schematic of a steam-cracking furnace [19].

The distribution of the products can be controlled adjusting the temperature, residence time in the tubular furnace and the hydrocarbon to steam ratio [20]. The production of ethane and benzene is favored at high temperature, whereas higher amounts of propylene, C4-hydrocarbons, and liquid products are produced in relatively higher proportions at low temperatures. Moreover, the composition of the feed has a strong influence in the selectivity of the process [14]. Light hydrocarbon feeds (ethane, LPG or light naphthas) tend to form light olefins (ethylene, propylene and butadiene), and heavy hydrocarbon feeds (heavy naphthas and other refinery products) tend to produce aromatics hydrocarbons and other

compounds that can be used for inclusion in gasoline or fuel oil. Propylene yields can be higher using thermal cracking of propane and liquid hydrocarbon feedstocks (around 14-16%), and the ethylene yields reach the highest values when ethane is used as raw material. Typically, the steam cracking of ethane at high temperatures (800-1000°C) result in a per-pass ethylene molar yield of ~50% (and close to 80% molar yield upon recycling of the unconverted ethane (Figure 1.2 and 1.3)), with ~60% conversion of ethane and ~85% of ethylene selectivity [10,21].

The addition of oxygen (oxycracking) in a molar feed ratio oxygen/ethane of 0.2 can improve the conversion and make the overall reaction become thermoneutral, due to the heat generated by the combustion of a fraction of the hydrocarbon feed that can compensate the high endothermic cracking reactions [21,22]. In this case, reforming and water-gas shift reactions can also take place as secondary reactions. Sometimes, the addition of reactive 'fuel' components (Co-fed H<sub>2</sub>, CO, methanol and acetone) has also been used for the combustion. Moreover, the use of a catalyst allows operating at lower temperatures, contact times and/or reactor volumes reaching the same yields than when the process is performed without catalyst, resulting in a more energy-efficient process. The role of the catalyst is to promote the exothermic combustion reaction towards CO<sub>2</sub> and H<sub>2</sub>O to release some energy, while avoiding the reforming and water-gas shift reactions, and without directly affecting the gas phase homogenous cracking reactions significantly [22].

It can be found in the literature papers addressing the oxidative dehydrogenation or oxydehydrogenation (ODH) and the oxycracking as equivalent processes. However, they are quite different, since the oxycracking takes place via ignition and subsequent non-catalytic homogenous cracking reactions at high temperature (>700°C) that can result in alkenes with different carbon number, and the ODH reactions are performed with redox catalysts at much lower temperatures (300-600°C)

without the breaking of C-C bonds and leading to the corresponding alkene of the inlet alkane and  $\text{CO}_x$  [22].

#### 1.1.2.2. Fluid catalytic cracking

Fluid catalytic cracking (FCC) is probably the most important process in modern petroleum refineries. Essentially, catalytic cracking consists of the rupture of C-C bonds to convert heavy hydrocarbon fractions of petroleum (vacuum gas oil, residues, and deasphalted oil) into more valuable and lower molecular weight hydrocarbons (diesel, gasoline, olefinic gases, and other products) [23–25]. Originally, cracking of petroleum was only performed by thermal cracking, but FCC using zeolite catalysts [26] has become more important nowadays since provides an alternative route with lower activation energy for the breaking of C-C bonds, which results in a temperature decrease of 150-250°C and more production of gasoline with a higher octane rating with respect to SC [6].

FCC usually operates at moderate pressure around 550°C and it requires a significant amount of energy due to the endothermic nature of the reactions. As in the case of SC, coke is also formed during the process, which is deposited on the catalyst producing its deactivation. This problem can be overcome by continuous catalyst regeneration and frequent fresh catalyst addition, what makes possible the FCC unit can be run for a few years without shut-downs [27]. The operational conditions are usually constrained by environmental permits that limits the amount of coke burned in the regenerator and emissions rate of particulates, CO,  $\text{SO}_2$ ,  $\text{SO}_3$ , NO,  $\text{N}_2\text{O}$ , etc [28].

FCC units can adopt two different configurations: the “stacked” type where a single vessel contains both the reactor and the catalyst regenerator, and the “side-by-side” type where there are two independent vessels, one for the reactor and other one for the catalyst regenerator. The schematic flow diagram of Figure 1.4 represents a conventional FCC unit with the “side-by-side” configuration, which consists of a feed injection system, a riser

reactor, a stripper, a regenerator and a fractionator. The feedstock is preheated and mixed with the recycle slurry oil from the bottom of the fractionator and injected to the riser reactor, where the hydrocarbons interact with the hot powdered catalyst coming from the regenerator. The catalyst breaks the C-C bonds of the large molecules cracking into shorter ones that are collected as a vapor. The cracking reaction occurs within the period of 2-4 seconds while coke is deposited on the catalyst decreasing the catalytic activity, although the catalyst always presents a significant residual activity [29]. At the end of the riser reactor, the catalyst is separated from the gas products by a stripper and sent to the regenerator to burn the coke under airflow at about 715°C and reactivate the catalyst. The heat released by the coke combustion is partially absorbed by the regenerated catalyst, and then, this energy will be enough to evaporate the feedstock for the endothermic cracking reactions again [25,30,31]. Therefore, the catalyst is the one that transports the heat or the potential heat from the regenerator to the reactor (catalyst at high temperature) and vice versa (coke deposits that can be burned in the regenerator). The heat available for conversion in the reactor will be determined by the amount of coke burned in the regenerator, and in turn, it will be influenced by the operation conditions.

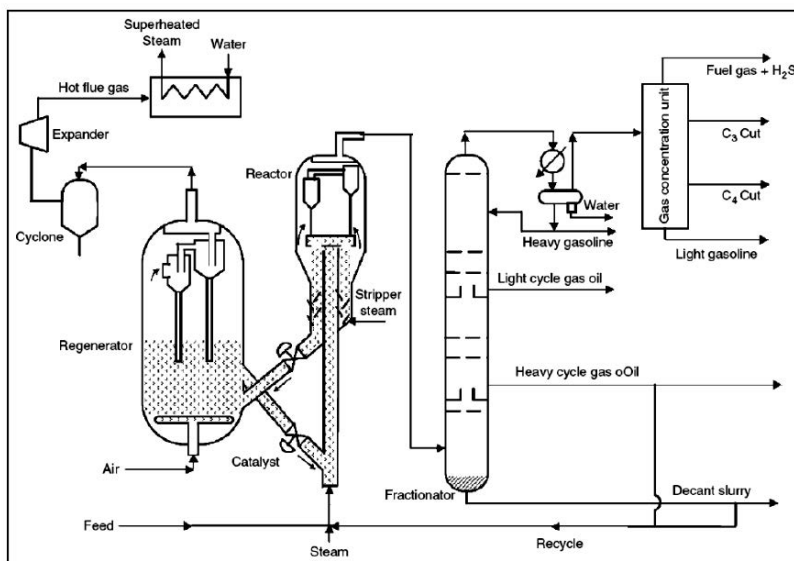


Figure 1.4. Schematic of FCC unit [27].



In FCC, propylene is a byproduct of gasoline, being the latter the most desired and the main product. Moreover, about 40% of the propylene obtained is usually used to produce high-octane gasoline blends [27]. However, the increasing propylene demand has promoted an extensive research effort in developing new FCC processes with higher propylene yields [32,33]. The conventional FCC presents a propylene yield around 5%, whereas the emerging high-olefins FCC technologies presents yields around 14-22% (Table 1.2). FCC is a very flexible unit of the refinery and allows modifications in the feed, the catalyst and operating conditions, which can result in different yield values to propylene and gasoline as shown in Figure 1.5 [6]. It can be observed that higher propylene yield is in detrimental of the gasoline yield and vice versa. However, maximizing the gasoline yield is the target in traditional refineries.

**Table 1.2.** Product yields of conventional and emerging FCC processes [33,34].

Parameter	FCC	DCC	PetroFCC	HS-FCC
Reaction Temperature (°C)	500	530	590	600
Product yield (wt. %)				
<i>Ethylene</i>	1.5	5.4	6.0	2.3
<i>Propylene</i>	4.8	14.3	22.0	15.9
<i>Mixed butanes</i>	6.9	14.7	14.0	17.4
<i>Gasoline</i>	51.5	39.0	28.0	37.8
<i>Heavy and light oils</i>	21.0	15.6	14.5	9.9
<i>Coke</i>	4.5	4.3	5.5	6.5

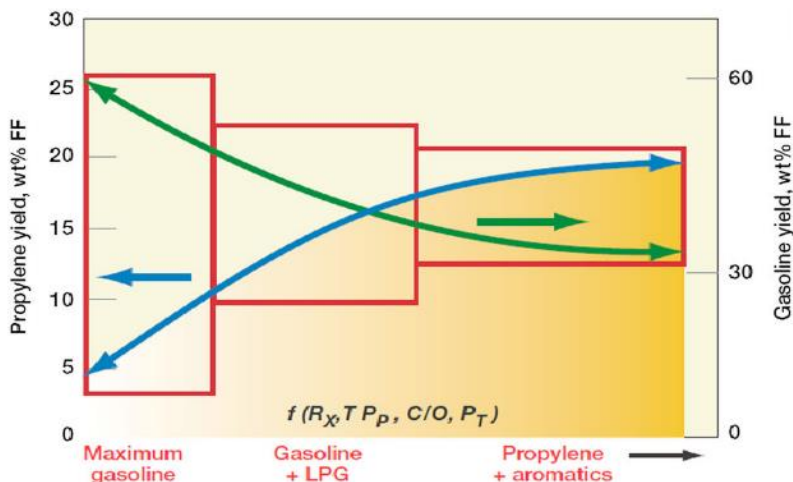
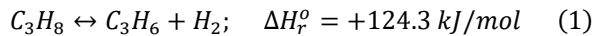


**Figure 1.5.** FCC design and operating modes [6].

The greatest revolution in the FCC process took place in 1962 when amorphous silica-alumina was replaced by faujasite zeolites as the main component of the catalysts [35]. An extensive research has been done to modify the Y zeolite for improving the activity, gasoline selectivity and its octane number, coke selectivity and stability. Gas oil cracking reactions require the presence of strong Brønsted acid sites and the conversion/selectivity will depend on the framework composition. Dealuminated Y zeolites with low framework Al content are more selective to diesel at the expense of gasoline, more selective to olefins and more stable under severe conditions. Furthermore, the activity and selectivity will be also determined by the accessibility to the acid sites. Since the molecules of the gas oil feedstocks can hardly access the acid sites located in the micropores, then, mesoporosity play an important role in the catalytic cracking. It is also well-known that the addition of ZSM-5 zeolite to the FCC improves gasoline octane and increases the yield to light olefins (propylene and butenes) in detriment of gasoline [36]. A strong research has been done to improve the hydrothermal stability of ZSM-5 zeolite under the regenerator conditions and about the potential use of MCM-22 zeolite as a cracking additive for FCC processes [37]. On the other hand, vanadium (among other metals) is the most important deactivation compound for the catalysts used in the FCC processes. Since there are high amounts of metals in some crude oils (e.g. Brazilian oils), it has been necessary to develop novel catalysts with higher resistance to metal contamination [38]. The low melting point of  $V_2O_5$  (690°C) facilitates the migration of the vanadium into the zeolite framework that is the responsible for the permanent deactivation effect due to the completely destruction of the zeolite structure [39–42]. The addition of rare earth elements (e.g. cerium) in the catalyst formulation has been used as metal traps to avoid such metal contamination [38]. However, it seems that there is still a room for improvement, since it is not so clear the interaction between rare earth, vanadium and the catalysts due to the complexity in the metal environment changes occurred over the 10000-50000 reaction-regeneration (i.e. reduction-oxidation) cycles during the life time of the catalyst.

### 1.1.2.3. Catalytic dehydrogenation

The alkane dehydrogenation reaction is an on-purpose technology where the corresponding olefin and hydrogen are obtained as products. The cheap price of light alkanes from shale gas makes this process worth considering [8]. In addition, this process allows to obtain very high selectivity to a single and desired olefin, instead of a mixture of products as in SC or FCC processes [7]. However, it encounters the same problems than in SC and FCC, since it also consumes a large amount of energy and occurs the catalyst deactivation due to coke formation. The reaction Eq. (1) describes the dehydrogenation of propane:



where  $\Delta H_r^\circ$  is the standard enthalpy of reaction at 25°C and 1 atm. This reaction is highly endothermic and equilibrium-limited; hence, according to Le Chatelier's principle, high temperatures and low pressures are necessary to obtain adequate conversions [3,43]. Indeed, withdrawing the hydrogen produced during reaction and/or diluting the alkane partial pressure are the two more common strategies to increase the conversion (i.e. shifting the equilibrium toward higher olefin yields) [3].

On one hand, the hydrogen formed during dehydrogenation can be removed by selective hydrogen combustion using an oxidant that is introduced to the reaction feed. Generally, mild oxidants such as CO<sub>2</sub> are preferred instead of strong oxidants like O<sub>2</sub>, in order to prevent the combustion of hydrocarbon reactants and products [3]. In this case, CO<sub>2</sub> can remove the hydrogen via the reverse water gas shift reaction, as well as can decrease the coke deposition on the catalyst surface by elimination of acid sites that catalyze its formation and by the Boudouart reaction [44–49]. Sometimes has been added solid oxygen carrier such as ceria to oxidize the hydrogen formed. Subsequently, the reduced solid need to be reoxidized in a regeneration step [50]. Another method to separate the hydrogen from the system is the use of semipermeable membranes. Different membranes have been investigated, such as Pd-coated

mesoporous alumina, Pt-Ag composites and molecular sieves based on molybdenum or carbon [51–57]. However, this approach has the limitation of the temperature, since the thermal stability of these membranes is limited and it could be only used for dehydrogenation at relatively low temperatures (e.g. dehydrogenation of isobutene) [58–60]. On the other hand, steam dehydrogenation is a technique to decrease the alkane partial pressure. The steam introduced in the feed can also be used as heat carrier and as coke remover to elongate the catalyst activity [61,62]. In the case that selective hydrogen oxidation is incorporated to the process, the steam generated during such combustion could be introduced in the dehydrogenation reactors. It should be noted that steam in excess can be detrimental, since it could compete with propane to adsorb on active sites hindering the dehydrogenation reaction [61].

The temperature and pressure dependence on the equilibrium conversion is represented in Figure 1.6, showing that temperatures higher than 600°C is necessary to obtain higher conversion than 50% at 1 atm. Moreover, it can be also seen that higher conversions can be obtained at lower pressures for a given temperature. Unfortunately, these operation conditions promote side reactions as coke formation, cracking (reaction Eq. (2)) and hydrogenolysis (reaction Eq. (3)) that can occur in an appreciable extent at elevated temperatures avoiding the total selectivity to the desired olefin production, and being these reactions difficult to control [18,43].



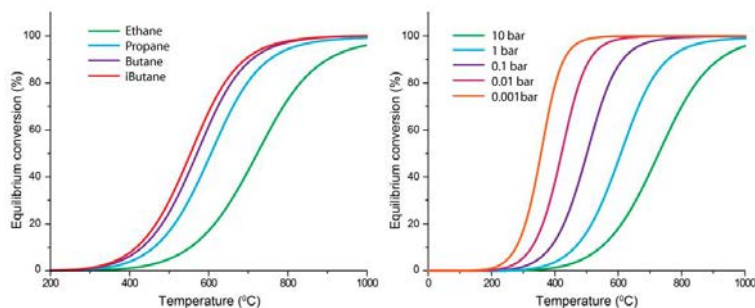


**Figure 1.6.** Equilibrium of C2-C4 paraffins to olefins as a function of temperature at 1 bar (left) and pressure dependence of the dehydrogenation of propane as a function of temperature (right) [3].

In this way, the use of catalysts in the dehydrogenation process is not only to improve the reaction rate and consequently the productivity, but also to increase the selectivity to the desired olefin by avoiding side reactions. This means that it is desirable that the catalyst also favors the C-H over C-C bond cleavage promoting the dehydrogenation reaction and improving the yield towards the olefin. Generally, nonoxidative dehydrogenation reactions of light olefins are performed using two types of catalyst formulations: metal oxide-based and noble metal-based catalysts. Both chromium oxide or platinum based catalysts supported on alumina, which presents excellent thermal stability and mechanical strength, are the most commonly used in the industry, although vanadium oxide, molybdenum oxide, gallium oxide, indium oxide, supported iron oxide, silica supported metal sulfides (ZnS, FeS, CuS, CoS, MnS, NiS, and MoS) or carbon based catalysts have also been reported [3,7,63–66].

Chromium oxide and platinum based catalysts have been investigated for dehydrogenation processes since the 1930s and 1960s, respectively [18,67]. In these catalysts, Cr-O and Pt are the active sites, respectively, where the adsorption of the alkane molecules takes place for the subsequent dehydrogenation. In the former, the oxidation state of chromium atoms in the dispersed  $\text{CrO}_x$  presents a strong influence on the dehydrogenation activity. Indeed, coordinatively unsaturated  $\text{Cr}^{3+}$  or  $\text{Cr}^{2+}$  sites and/or a mixture of both have been proposed as the active sites, whereas  $\text{Cr}^{6+}$  or  $\text{Cr}^{5+}$  sites have not been observed to be active [68–73]. Unlike supported Pt-based catalysts, metal loading in supported chromium

oxide-based catalysts has an influence on the type of surface species formed and their catalytic activity, and in turn, on the yield to olefin, as can be observed in Figure 1.7. Highly dispersed and active phase of chromium oxide is formed at low chromium loadings, and the activity is linearly increased as the loading increases until reaching a point where crystalline  $\text{Cr}_2\text{O}_3$  starts to be formed, which is not active due to the high stability of these fully coordinated species [74–76]. With respect to the platinum-based catalysts, highly dispersion of the Pt atoms on the catalyst surface is also important to make easier the accessibility of the reactant to the active sites and improve the catalytic activity, although the nature of the species formed may not be influenced by the platinum loading [3].

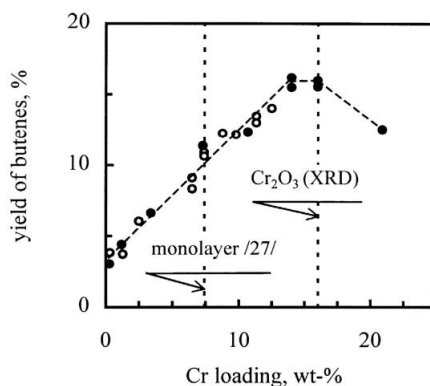
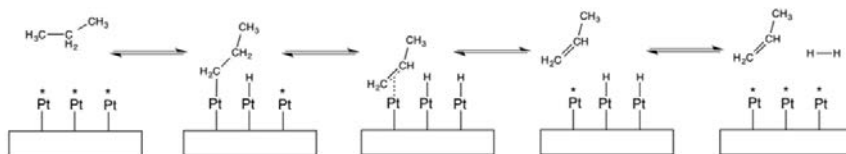


Figure 1.7. Yield of butenes at 540°C over a chromia-alumina catalyst as a function of Cr loading [3].

The so-called Horiuti–Polanyi mechanism proposed in 1934 is the most used to describe catalytic dehydrogenation reactions [77]. This mechanism follows a Langmuir–Hinshelwood kinetic and consists of four general steps (Scheme 1.1): dissociative adsorption of the alkane, a second C–H bond cleavage, formation of a hydrogen molecule and subsequent desorption of both the hydrogen and the olefin. Generally, both the C–H cleavage steps and the dissociative adsorption of the alkane have been considered in the literature as the rate limiting step (RDS) of the overall dehydrogenation reaction [68,78–84].



**Scheme 1.1.** Horiuti-Polanyi mechanism in the catalytic dehydrogenation reaction in Pt based catalysts.

All dehydrogenation catalysts are progressively deactivated with time-on-stream by different processes. These deactivation processes are similar for all the catalysts, being coke deposition the main cause of deactivation [3,85–88]. The term coke involves a large family of highly graphitized hydrocarbon molecules, and it is produced in many processes of the petroleum industry. These compounds tend to deposit on the catalyst surface during reaction, hindering the reactants diffusion by blocking both pores and active sites of the catalyst. As a result, the catalytic activity decreases, being the extension of this effect dependent on the nature, structure, morphology and location of the coke deposits [89]. The mechanism of coke formation is very complex and not completely understood yet, despite it has been studied for many decades to develop strategies to prevent the formation of such carbonaceous deposits. It is well known that Brønsted acid and others active sites are responsible for the formation of coke deposits. Firstly, carbocation intermediates are formed on the acid sites, and then paraffins and more easily olefins present in the stream react with these carbocations forming large graphitic structures. Typical intermediates in this mechanism are acetylene, ethylidyne, propylidyne and similar molecules, which can follow several pathways to form the first aromatic ring structures by cracking, deep dehydrogenation and polymerization reactions [84,90,91]. Then, coke species may continue growing via Diels-Alder addition, propylene addition to a radical or fusion of graphitic sheets into larger ones by a radical mechanism [92–94].

It should be noted that the presence of carbonaceous deposits on the catalyst surface is not always negative for the dehydrogenation reaction and it is not completely undesirable. It has been observed that low amount of coke deposition can increase the catalytic activity by promoting the

alkane adsorption next to the active site [89]. Moreover, it can first deactivate the most active sites, which normally tend to be responsible for side reactions, giving rise to higher selectivity towards the desired olefin. However, if the graphitic sheets continue growing and progressively cover all the active sites, a drop in the catalyst activity is occurred showing the detrimental effect of coke deposition [95,96]. On the other hand, the presence of coke deposits on deactivated catalysts is important in the industrial processes, since the combustion of these carbonaceous compounds during the catalyst regeneration is the main source of heat for the dehydrogenation reaction. The amount of coke formation can be decreased adding a promoter element to the catalyst (e.g. Sn to Pt-based catalysts) or introducing steam, hydrogen or CO<sub>2</sub> in the feed, whereas higher partial pressures of paraffins and olefins promote the coke deposition. The nature of the coke will also depend on the operation conditions and alkane reactant used [91].

In addition to the catalyst deactivation by coke deposition, which is relatively reversible, there is other deactivation processes that are not entirely reversible, and then, a loss of activity is observed after each reaction-regeneration cycle. These processes are normally related to the high temperatures of both the regeneration and dehydrogenation reactions. This results in the agglomeration or sintering of the active species and/or the support with the concomitant loss of active sites and surface area giving rise to catalyst deactivation. In the case of Pt-based catalysts, Pt can be almost fully redispersed on the catalyst at 500°C with the addition of low amounts of oxygen and chlorine in the feed [97–102]. The PtO<sub>x</sub> and PtO<sub>x</sub>Cl<sub>y</sub> species formed present such interaction with the support that improves their mobility on the surface and promotes their redispersion. With respect to CrO<sub>x</sub>-based catalysts, the redispersion is achieved by the oxidation of Cr<sup>+3</sup> to Cr<sup>+6</sup> species during the regeneration [3]. It should be noted that the oxidized species, formed during the regeneration of the above catalysts to favor the redispersion, are reduced again with the alkane feed in the dehydrogenation reactor obtaining the active species again. However, the



redispersion is not fully achieved for both catalysts, due to the loss of support surface area during each reaction-regeneration cycle, which results in a lower dispersion capacity each time. In the case of  $\text{CrO}_x$ -based catalysts, it is even possible the incorporation of Cr atoms inside the bulk of the support forming inactive species for the dehydrogenation reaction [103,104].

In the case of  $\gamma$ -alumina, which is the most commonly used support for these types of catalysts, the loss of surface area during the reaction-regeneration cycles is due to the transformation of  $\gamma$ -alumina to more thermodynamically stable structures as  $\theta$ - or  $\alpha$ -alumina. This transformation can be restrained by doping the support with silica, zirconia, magnesia, or lanthane [105,106]. The use of alumina as support has other drawbacks. It is an acid support that can catalyze cracking and coking reactions, which results in a drop in both activity and selectivity. Doping of the alumina support with alkali ions (Li, Na, K, Rb and Cs) to poison these undesirable acid sites has been extensively investigated [69,107–112]. These alkali cations also present the ability to stabilize the support structure and to increase the active phase dispersion [69,112]. Zn and Mg have also been used to dope the alumina support decreasing the acidity and increasing the thermal stability, as well as avoiding the sintering of the dispersed platinum in the case of  $\text{Pt}/\text{Al}_2\text{O}_3$ -based catalysts [113–116]. The use of other supports such as zirconia has been also investigated, since for  $\text{CrO}_x$ -based catalysts, chromia presents higher sintering resistance and prevents the formation of chromia-alumina spinels. However, the deactivation process is faster when zirconia is used as support with respect to alumina, since the formation of the inactive chromium carbides is favored with the former support [117].

Sn is the promoter most studied and is included in all the platinum-based catalysts industrially used. This post-transition metal modifies both the active phase and the support, avoiding side reactions such as cracking, coking, hydrogenolysis and isomerization, as well as minimizing the metal sintering and neutralizing the acidity of the support. Most of these



advantages are due to the higher dispersion and smaller size of the Pt nanoparticles obtained when Sn is added to the catalyst as promoter [79,118–121]. Moreover, the adsorptive and catalytic properties of the active sites are also altered, weakening the adsorption of the alkane and favoring the desorption of the olefin, while the formation of coke precursors (acetylene, ethylidyne, propylidyne, etc) is partially suppressed [122–127]. This results in higher selectivity to the desired olefin and in lower conversion when Sn is present in the catalyst formulation. This means that there is an optimum ratio of Pt and Sn, which is Pt<sub>3</sub>Sn according to DFT calculations [125–127]. Other promoters such as Zn, Ga, In and Ge have been also investigated [91,128–137].

Although Pt-based and CrO<sub>x</sub>-based catalysts are the catalytic materials commercially used for alkane dehydrogenation to obtain olefins in the industry, some problems such as catalyst poisoning, high cost of Pt and environmental concerns associated with the use of Cr have encouraged the search for improvements or alternatives. In this way, other dispersed metal oxides such as GaO<sub>x</sub>, VO<sub>x</sub> and MoO<sub>x</sub> based catalysts, usually supported on alumina, have been also widely studied over the last decades [80,138–145]. As in the case of CrO<sub>x</sub>-based catalysts, all these alternative catalysts have in common that the metal atoms need to be coordinatively unsaturated to form active species. The species formed will depend on the dispersion capacity of the support and the surface density of such dispersed metal oxides. Normally, higher surface density will result in more polymerized species, until reaching a point where the dispersion capacity of the support is exceeded, and crystalline phases (normally undesired) of the corresponding metal oxide is formed. Then, a broad range of species with different catalytic activity can be expected in this kind of catalysts, unlike in the case of Pt-based catalysts, where any Pt<sup>0</sup> located at the surface catalyze the reaction, and the only issue is to avoid the formation of big clusters of platinum that can promote undesired side reactions decreasing the selectivity to the desired olefin [79,118–121]. Pt-based catalysts typically have much lower loadings of metal than the other metal oxide

(CrO<sub>x</sub>, GaO<sub>x</sub>, VO<sub>x</sub> and MoO<sub>x</sub>) based catalysts, while giving comparable yields to the desired olefin. In fact, the specific activity calculated for Pt is around 4 magnitude orders higher than for metal oxide species. Moreover, Pt-based catalysts present lower deactivation rates than metal oxide-based catalysts. Then, the catalysts with the best dehydrogenation and deactivation rate ratios are Pt-based catalysts followed by CrO<sub>x</sub>-based catalysts, and so far, better alternatives have not been developed yet, even though after several decades of investigation. The main drawback of the alternative formulations is the rapid deactivation of the catalysts [3].

Nowadays, there are four industrial dehydrogenation processes for propylene production: CATOFIN from ABB Lummus, OLEFLEX from UOP, Fluidized Bed Dehydrogenation (FBD) from Snamprogetti, and Steam Active Reforming (STAR) from Phillips Petroleum. These technologies differ in the catalyst type, the reactor design, and operating conditions. Table 1.3 summarizes the main characteristics of these processes, including typical operating conditions and product yields. Currently, Oleflex and the Catofin technologies are the most commercially available dehydrogenation units used for propylene production. All these processes include both a dehydrogenation section and a catalyst regeneration section.

**Table 1.3.** Typical properties of commercial propane dehydrogenation [18,146–150].

	<b>CATOFIN</b>	<b>OLEFLEX</b>	<b>FBD<sup>a</sup></b>	<b>STAR<sup>b</sup></b>	<b>PDH</b>
<b>Licensors</b>	SudChemie/ ABB Lummus	UOP Inc.	Snamprogetti	Uhde/Phillips Petroleum	Linde- BASF-Statoil
<b>Reactor</b>	Adiabatic fixed-bed	Adiabatic moving-bed	Fluidized-bed	Adiabatic fixed-bed	Isothermal fixed-bed
<b>Operation</b>	Cyclic	Continuous	Continuous	Cyclic	Cyclic
<b>Feedstock</b>	C <sub>3</sub> or C <sub>4</sub>	C <sub>3</sub> or C <sub>4</sub>	C <sub>3</sub> or C <sub>4</sub>	C <sub>3</sub>	C <sub>3</sub>
<b>Catalyst</b>	Cr <sub>2</sub> O <sub>3</sub> /Al <sub>2</sub> O <sub>3</sub> with alkaline promoter	Pt/Sn/Al <sub>2</sub> O <sub>3</sub> with alkaline promoter	CrO <sub>x</sub> /Al <sub>2</sub> O <sub>3</sub> with alkaline promoter	Pt/Sn on ZnAl <sub>2</sub> O <sub>4</sub> /Ca Al <sub>2</sub> O <sub>4</sub>	CrO <sub>x</sub> /Al <sub>2</sub> O <sub>3</sub>
<b>T (°C)</b>	590-650	550-620	550-600	550-590	590
<b>P (bar)</b>	0.3-0.5	2-5	1.1-1.5	5-6	>1
<b>Conversion (%)</b>	C <sub>3</sub> :48-65 C <sub>4</sub> :60-65	C <sub>3</sub> :25 C <sub>4</sub> :35	C <sub>3</sub> :40 C <sub>4</sub> :50	C <sub>3</sub> :40	C <sub>3</sub> :30
<b>Olefins Selectivity (%)</b>	C <sub>3</sub> :82-87 C <sub>4</sub> :93	C <sub>3</sub> :89-91 C <sub>4</sub> :91-93	C <sub>3</sub> :89 C <sub>4</sub> :91	C <sub>3</sub> :89	C <sub>3</sub> :90

<sup>a</sup>Fluidized Bed Dehydrogenation (FBD)

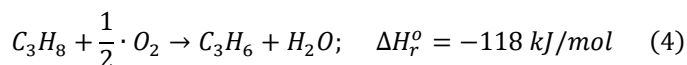
<sup>b</sup>Steam Active Reforming (STAR)

## 1.2. Oxidative dehydrogenation (ODH) of propane

### 1.2.1 Propane ODH as alternative

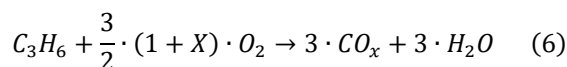
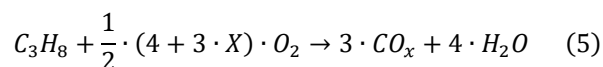
Selective oxidation technologies have been extensively studied in the literature and play an important role in the petrochemical industry to produce numerous value-added chemicals mainly used in organic synthesis [151–155]. Overall, these reactions usually involve a Mars-van Krevelen type mechanism with a parallel and consecutive reaction network through olefins and oxygenates as intermediates in the formation of CO<sub>2</sub> and water, which are the thermodynamically stable products. This results in a challenging process, since overoxidation pathways are usually difficult to avoid with the subsequent decrease of the selective towards the desired product [152,156,157]. Selective oxidation of hydrocarbons usually goes through C-H bond activation [151,156], while the structure of C-C bonds is normally unchanged (unlike in SC and FCC processes) unless that the undesired total oxidation occurs. Alkane molecules are more easily oxidized as contain higher number of carbon atoms due to C-H bonds become weaker [158].

Among the different processes included in selective oxidation, the oxidative dehydrogenation (ODH) of propane to obtain propylene has been extensively studied over the past decades [21,159,160]. Unlike non-oxidative dehydrogenation, ODH is an irreversible and exothermic reaction that takes place in the presence of an oxidizing agent as molecular oxygen (or other oxidizing agents as N<sub>2</sub>O [161,162]) as described in Eq. (4):



Propane ODH is a very promising technology to replace the non-oxidative propane dehydrogenation [147,157], which it is a technology used today in the industry despite the thermodynamic limitations on the propane conversion, the presence of side reactions (e.g. thermal cracking), the required very high energy consumption due to the strong endothermic

reactions that need to be performed at high temperatures (550-650°C) and the coke formation on the catalyst that needs regeneration during the process [147,160]. ODH has the potential to overcome these above disadvantages of thermodynamic limitations, being an exothermic reaction that can be performed at low temperatures (300-500°C) and practically avoiding the catalyst deactivation by coke deposition [147,157]. It is estimated that around 45% of the energy consumption can be potentially saved by using propane ODH with respect the non-oxidative counterpart [157,163]. It should be noted that the propane dehydrogenation presents a valuable side product, hydrogen, but it does not compensate the extra energy that is necessary to supply with respect to the propane ODH reaction, even though the potential energy that can be obtained burning hydrogen (producing water as in the case of ODH) is taken into account. On the other hand, the energetic efficiency in the propane dehydrogenation can be improved by coupling with other processes to obtain other valuable products. However, propane ODH would be easier integrated than propane dehydrogenation into the typical propylene selective oxidation processes (such as the acrylic acid production) for the process intensification [164,165]. The direct linking of the exit streams from the propylene obtained in an ODH process into the following propylene selective oxidation processes would be possible and safer without needing the prior separation of hydrogen as in the case of the propane dehydrogenation [164,165], since the presence of hydrogen in the feed of an oxidation reactor could be dangerous. However, despite its higher energetic efficiency, propane ODH has not been industrially implemented yet, even after decades of research, due to its too low propylene yields and productivity as a result of the undesired overoxidation reactions to CO<sub>x</sub>, which are difficult to control and are described in Eqs. (5) and (6):



Until now, the highest productivity found in the literature is  $9 \text{ g}_{\text{C}_3\text{H}_6} \cdot \text{g}_{\text{cat}}^{-1} \cdot \text{h}^{-1}$  for transition metals [163], and most of the yields obtained are below 30% with propylene selectivity below 70% [21], while the yield in the pure propane dehydrogenation is usually around 40% with a propylene selectivity above 90% [4,61]. Moreover, ODH reaction presents other problems such as the removal of heat, flammability of the reaction mixture, and the possibility of reaction runaway [147,148]. Some of the last drawbacks have been already minimized to some extent using fixed bed and fluidized bed membrane reactors [147,167–169], which allow to homogeneously distribute the oxygen feed along the reactor. Nevertheless, this reaction is still in the research state and would require further optimization of the catalysts and/or reaction conditions in order to improve the yield and/or productivity to become profitable as an industrial process [21].

A wide variety of catalysts have been developed for propane ODH [21,160], being vanadium based catalysts the most studied and one of the most active and selective. These catalytic systems can be also used for the ODH of ethane and butane [21,147], although the optimum catalyst for each alkane is different in each case. Most of the authors have focused on the preparation and the characterization of the catalysts, followed by catalytic tests to compare conversion-selectivity profiles, propane consumption TOF rates, yields and/or productivity values under a given reaction conditions. However, there are several concepts under discussion related to the mechanism and the structure-activity relationships of the catalysts during ODH reaction. For example, although is generally accepted that lattice oxygens in the bridging form (V-O-V/V-O-Support) are the most active sites [156,159,170–196], there are still authors reporting that terminal oxygen bonds (V=O) are the active sites from 1968 to today [197–206]. Furthermore, there is no complete unanimity about the nature of the path leading to propylene formation and, despite the vast propane ODH literature, not many details are usually given about the nature and number of steps of the mechanism involving the formation of  $\text{CO}_x$  [160]. It would be

convenient to understand these concepts in order to know how the activity and selectivity is related to the reaction mechanism and operation conditions. In this way, it could be possible to prepare better catalysts and to optimize the operation conditions increasing the activity and avoiding the overoxidation steps as much as possible, and consequently improving the yield and/or productivity, what it would allow to definitely show if propane ODH could be really industrially implemented.

### 1.2.2. Catalysts for propane ODH reaction

Three main groups of different catalysts have been studied for ODH in the literature [10,21,159,160]:

- Alkali and Alkaline earth-based catalysts
- Reducible transition metal oxides-based catalysts
- Boron based catalysts

The activity of a catalyst, in addition to being determined by its intrinsic nature, will depend on the reaction conditions. Thus, the selection of the best catalytic system will be determined by the reaction conditions used [160]. Table 4 shows an overview of some ODH catalysts used by different authors at the temperature range of 300-500°C. It is noteworthy the wide variety of catalysts and reaction conditions that has been used in the literature. It can be observed that scarcely propane conversions of 30% are obtained, whose respective propylene selectivity are around 40-60%. This leads to propylene yields that are usually below 15%. Propylene productivity covers a broad range of values, being 11.9 and 9  $\text{g}_{\text{C}_3\text{H}_6} \cdot \text{g}_{\text{cat}}^{-1} \cdot \text{h}^{-1}$  the highest values obtained using elemental boron and V/Ti/SBA-15 catalysts, respectively.

**Table 4.** Literature overview of ODH catalysts used by different authors. Catalyst composition, reaction conditions, catalytic activity and selectivity values and references are shown.

Catalyst	Temperature (°C)	Space-time (g·s·mL <sup>-1</sup> <sub>C<sub>3</sub>H<sub>8</sub></sub> )	Propane Conversion (%)	Propylene Selectivity (%)	Propylene Yield (%)	Propylene Productivity (g <sub>C<sub>3</sub>H<sub>6</sub></sub> /g <sub>cat</sub> ·h)	Reference
Ni/Ti/O	300	0.25	0.29	0.41	0.12	0.55	[207]
Ce/Ni/O	300	0.67	0.19	0.59	0.11	0.04	[208]
V <sub>2</sub> O <sub>5</sub> /Zn-Al <sub>2</sub> O <sub>3</sub>	350	0.34	0.11	0.29	0.03	0.01	[209]
CeNbNiO <sub>x</sub>	350	0.35	0.23	0.49	0.11	1.91	[210]
B <sub>x</sub> CN	350	11.39	0.08	0.81	0.06	0.04	[211]
V <sub>2</sub> O <sub>5</sub> -CeO <sub>2</sub>	370	0.24	0.12	0.32	0.04	0.05	[212]
Cs <sub>0.9</sub> H <sub>2.1</sub> PW <sub>12</sub> O <sub>40</sub>	380	68.36	0.19	0.38	0.07	0.01	[213]
V/Nb/O-TiO <sub>2</sub>	400	0.48	0.20	0.30	0.06	0.02	[214]
Ni/V/O	400	0.60	0.20	0.50	0.10	0.11	[215]
Nb <sub>2</sub> O <sub>5</sub> -TiO <sub>2</sub>	400	0.74	0.20	0.36	0.07	0.01	[214]
V <sub>2</sub> O <sub>5</sub> /K-TiO <sub>2</sub>	400	1.00	0.17	0.21	0.04	0.01	[216,217]
Nb <sub>2</sub> O <sub>5</sub> /CeO <sub>2</sub>	400	1.95	0.19	0.26	0.05	0.17	[218]
Ni/Co/Mo/O	420	0.38	0.22	0.41	0.09	0.21	[219]
Cr/Mo/Cs/O-Al <sub>2</sub> O <sub>3</sub>	420	0.80	0.15	0.65	0.10	0.20	[220]
V/Nb/O	425	0.48	0.11	0.43	0.05	0.21	[221]
Ni/V/O	425	0.60	0.18	0.50	0.09	0.20	[222]
V/Zr/O-PILC	445	1.00	0.13	0.30	0.04	0.03	[223]
V <sub>2</sub> O <sub>5</sub> -Ga <sub>2</sub> O <sub>3</sub>	450	0.06	0.29	0.20	0.06	0.24	[224]
Ni/Mo/O+Sb/O+prom N <sub>2</sub> O	450	0.50	0.14	0.30	0.04	0.05	[225]
V/Sm/O	450	0.60	0.22	0.38	0.08	0.03	[226,227]
Cr <sub>2</sub> O <sub>3</sub> -Al <sub>2</sub> O <sub>3</sub>	450	0.80	0.17	0.55	0.09	0.19	[228]
Co/Sr/O-hydr. apatite	450	1.00	0.23	0.50	0.12	0.10	[229,230]
Cr <sub>2</sub> O <sub>3</sub> /Al <sub>2</sub> O <sub>3</sub>	450	2.85	0.17	0.54	0.09	0.19	[231]
Ni/Al/O	450	3.00	-	-	-	0.01	[232]
MoO <sub>3</sub> /K-Si-TiO <sub>2</sub>	450	4.27	0.22	0.63	0.14	0.33	[233]
CMK-3	450	5.70	0.21	0.55	0.11	0.13	[234]
NiO-POM	450	13.67	0.23	0.65	0.15	0.07	[235]
V <sub>2</sub> O <sub>5</sub> -ZrO <sub>2</sub>	455	0.10	0.22	0.35	0.08	0.58	[236]
MoO <sub>3</sub> -Al <sub>2</sub> O <sub>3</sub>	470	0.13	0.10	0.50	0.05	0.12	[237]
V <sub>2</sub> O <sub>5</sub> /K-Al <sub>2</sub> O <sub>3</sub>	475	1.33	0.22	0.52	0.11	0.05	[238]
Meso-NiMoO <sub>4</sub>	475	19.53	0.18	0.64	0.12	0.35	[239]



Table 4. (Continued).

Catalyst	Temperature (°C)	Space-time (g·s·mL <sup>-1</sup> <sub>C<sub>3</sub>H<sub>8</sub></sub> )	Propane Conversion (%)	Propylene Selectivity (%)	Propylene Yield (%)	Propylene Productivity (g <sub>C<sub>3</sub>H<sub>6</sub></sub> /g <sub>cat</sub> ·h)	Reference
V/Mg/Al/O	480	0.60	0.28	0.30	0.08	0.16	[240]
V/Ti/SBA-15	500	0.03	-	-	-	9.00	[166]
V/Mg/Al/O	500	0.07	0.13	0.52	0.07	0.23	[241]
Elemental Boron	500	0.07	0.10	0.83	0.08	11.90	[242]
Ga-USY	500	0.17	0.13	0.28	0.04	0.16	[243]
V-MCM-41	500	0.24	0.14	0.60	0.08	0.26	[244]
V <sub>2</sub> O <sub>5</sub> -ZrO <sub>2</sub>	500	0.30	0.19	0.32	0.06	0.06	[156]
MoO <sub>3</sub> -Al <sub>2</sub> O <sub>3</sub>	500	0.36	0.19	0.38	0.07	0.06	[245]
V <sub>2</sub> O <sub>5</sub> -TiO <sub>2</sub>	500	0.36	0.21	0.31	0.07	0.05	[245]
MoO <sub>3</sub> -Al <sub>2</sub> O <sub>3</sub>	500	0.42	0.29	0.28	0.08	0.05	[246]
V/silic. Beta	500	0.50	0.26	0.27	0.07	0.06	[247]
V-Mg-O	500	0.58	0.24	0.58	0.14	1.45	[248]
V-HMS	500	0.60	0.17	0.66	0.11	0.20	[249]
V/Mg/O	500	0.60	0.24	0.58	0.14	1.45	[248]
V <sub>2</sub> O <sub>5</sub> -SmVO <sub>4</sub>	500	0.60	0.31	0.28	0.09	0.03	[250]
V-HMS	500	0.60	0.34	0.35	0.12	0.21	[251]
V/Sb/O	500	0.60	0.34	0.39	0.13	0.14	[252]
MoO <sub>3</sub> /K-ZrO <sub>2</sub>	500	0.80	0.16	0.45	0.07	0.06	[253]
Co/Mo/O-MCM-41	500	0.80	0.26	0.25	0.07	0.14	[254]
SrVMoO <sub>x</sub> /Al <sub>2</sub> O <sub>3</sub>	500	1.29	0.22	0.68	0.15	0.75	[255]
Na-V <sub>2</sub> O <sub>5</sub> /Al <sub>2</sub> O <sub>3</sub>	500	1.37	0.20	0.51	0.10	0.45	[256]
Ag/Mo/P/O	500	1.5	0.11	0.69	0.08	0.12	[257]
P <sub>2</sub> O <sub>5</sub> -Nanodiamond	500	1.95	0.23	0.45	0.10	0.12	[258]
Mesoporous NiO	500	9.63	0.22	0.47	0.10	0.71	[259]

### 1.2.2.1. Alkali and Alkaline earth-based catalysts

These catalysts contain non-reducible alkali and alkaline earth ions and oxides, which do not follow the conventional Mars-van Krevelen type mechanism. The reaction mechanism usually involves the formation of radical species on the catalyst surface, which evolve to the gas phase with the subsequently homogeneous reactions to obtain the different reaction products such as propylene [21]. They present a good ethylene selectivity in the ethane ODH reaction, but a high temperature (above 600°C) [160]. The best performance for this reaction has been achieved using a Li-promoted MgO catalyst [260,261]. Other catalysts doped with Na, B, lanthanide oxides and SnO<sub>2</sub> [261,262], as well as other catalytic systems such as LiCl/NiO, LiTiO, LiMnTiO [263,264] and LaF<sub>3</sub> associated with a rare oxide (CeO<sub>2</sub> and SmO<sub>2</sub>) and doped with BaF<sub>2</sub> have been also reported in the literature [265,266]. Moreover, the highest selectivities have been obtained when the catalysts have been doped with halides or adding chlorine containing compounds to the feed mixture [267]. The presence of chlorine ions promotes the generation of ethyl radical species that are necessary for the ethylene formation.

On the other hand, propane ODH has been less studied over this kind of catalysts [268,269], being the ones containing MgO mixed and promoted by alkali metal (Li) oxides, halogens (mainly Cl) and dysprosium (Dy) [270–275]. In these catalysts, the acidity due to the halides resulted in a positive effect on the reaction. The Li/Cl/MgO/Dy<sub>2</sub>O<sub>3</sub> catalytic system has reported one of the best performances in the propane ODH at 500-650°C.

### 1.2.2.2. Reducible transition metal oxides-based catalysts

Among the available catalysts for ODH reaction, non-noble transition metal oxides are of special interest, since they can work at relatively low temperatures (300-600°C) [153,160]. They are normally used as supported catalysts and/or mixed with other metal oxides [21], while hardly are used as bulk catalysts since are not so effective for the reaction. These transition

metals contain lattice oxygen that is removable and can accept hydrogen atoms from alkanes during the oxidation reactions, both in the selective formation of propylene and in the undesired total oxidation to  $\text{CO}_x$  [160]. Subsequently, the reoxidation of the reduced catalysts is carried out by molecular oxygen [147,158] or other oxidizing agents such as  $\text{N}_2\text{O}$  [161,162]. This kind of catalysts mainly includes:

- V-based catalysts.
- Mo-based catalysts.
- Mixed oxides catalysts such as V-Mg-O, V-Nb-O, Mo-V-Nb-O, Mo-V-Sb-O or Mo-V-Te-Nb-O.
- Other catalysts based on Ni, W, Cr or Mn oxides.

Considering the different transition metal oxides for the alkane ODH reaction, supported V-catalysts are more active than supported Mo- or W-catalysts [276] and more selective than  $\text{CrO}_x$ - or  $\text{MnO}_x$ -catalysts [277–279]. In fact, vanadium based catalysts have become the most studied systems over the last decades [21,159,280], and its development as supported catalyst has extensively contributed in the knowledge of the factors influencing on the alkane ODH reactions [280].

The most common catalytic systems used for propane ODH are vanadium or molybdenum based catalysts [21,160], which are usually supported or dispersed on different oxides such as  $\text{SiO}_2$ ,  $\text{Al}_2\text{O}_3$ ,  $\text{TiO}_2$ ,  $\text{ZrO}_2$ , CeO,  $\text{Nb}_2\text{O}_5$ , MgO or zeolite [21,159,281–284]. Both catalysts based on supported vanadium oxide or molybdenum oxide present many similarities, although vanadia based catalysts are more active regardless of the support used [21]. Among these catalysts, V-Mg-O mixed oxide systems are characterized by high values of selectivity and yield to propylene in the propane ODH [171,285–287]. In this way, V-Nb-O systems have been also reported to present a relatively good productivity to propylene [288]. The other mixed oxide catalysts such as Mo-V-Nb-O [289–295], Mo-V-Sb-O [296,297], Mo-V-Te-Nb-O [298–300] and Ni-O [301–307] have been mainly studied in the ethane ODH, but hardly investigated in the propane ODH.

On the other hand, the use of additives such as alkalis (e.g. Li, Na, K, and Rb) and transition metals (e.g. Ti, Cr, Mn, Fe, Co, Ni, Nb, Ce, V, and Mo) as promoters in the vanadia or molybdena based catalysts have been investigated to modulate the catalytic activity and selectivity [208,216,217,223,308-316]. Generally, the addition of redox elements or P leads to an increase of the activity and a decrease of the selectivity, while the doping with alkalis elements or Bi leads to a decrease of the activity and an increase of the selectivity. The doping of the support with ions (e.g.  $\text{Ca}^{+2}$ ,  $\text{Al}^{+3}$ ,  $\text{Fe}^{+3}$ ,  $\text{W}^{+6}$  and  $\text{K}^{+}$ ) to modify its physicochemical and catalytic properties in ODH has also been studied [216,308].

### 1.2.2.3. Boron based catalysts

Recently, it has been reported that catalysts based on boron nitride (BN) seem to present an extraordinary selectivity to propylene in the propane ODH [10,157,242,317,318]. These catalysts usually work at 500°C and lead to ethylene (a highly valuable olefin) as the main byproduct, rather than  $\text{CO}_x$  as in the typical catalysts based on transition metals [21,159,160]. As an example, at propane conversion of 14% using a boron nitride catalyst, the selectivity to propylene and ethylene could be 79 and 12%, respectively; while for supported vanadia catalysts, at propane conversion of 9%, typical selectivity to propylene and  $\text{CO}_x$  could be 67 and 33%, respectively, depending on the catalyst and the reaction conditions. It should be noted that the olefin selectivity obtained by the boron-containing catalyst, including propylene and ethylene, was relatively constant over a wide conversion range, what indicated that cracking reactions via C–C cleavage prevailed versus the consecutive combustion during the ODH reaction [10]. No propane conversion was observed in the absent of oxygen, unlike supported vanadia catalysts that can present some activity until the lattice oxygen is exhausted and the role of the gas phase oxygen is reoxidizing the catalyst to perpetuate the catalytic cycle. Therefore, it has been suggested that the role of the gas phase oxygen in boron catalysts must be different, although is not completely clear yet. Actually, boron catalysts are not usually redox active and do not follow a Mars van Krevelen type

mechanism [318]. In fact, it has been proposed that the acid/base properties of the surface could govern the catalyst reactivity. Furthermore, the catalyst activity does not correlate with the C–H bond strength of the alkane substrate used, as it occurs with the typical catalysts for ODH reaction. It has been proposed that the reaction mechanism in boron catalysts consists of the propyl radicals formation on the catalyst surface, and then, the reaction continues in the gas phase via alkyl hydroperoxides [318], where somehow the oxygen participation should be also required.

Later, Grant *et al.* described that other boron-containing catalysts such as boron carbide ( $B_4C$ ), titanium boride ( $TiB_2$ ), nickel boride ( $NiB$ ), cobalt boride ( $Co_2B/Co_3B$ ), hafnium boride ( $HfB_2$ ), tungsten boride ( $WB$ ) and elemental boron lead to the same behavior as boron nitride [242,318]. Although they differed in their propane consumption rates, all these catalysts showed similar propylene selectivity at isoconversion values, what suggested that similar active sites are present in all the catalysts, being boron a crucial element in such sites. In fact, elemental boron was the most active catalyst among the boron-containing catalytic systems, reaching propylene productivity values of about  $12 \text{ g}_{C_3H_6} \cdot \text{g}_{cat}^{-1} \cdot \text{h}^{-1}$  at 9.8% propane conversion, which has been the highest propylene productivity reported for the propane ODH in the literature to date ( $9 \text{ g}_{C_3H_6} \cdot \text{g}_{cat}^{-1} \cdot \text{h}^{-1}$  [166]), whereas the other tested borides resulted in productivity values below  $1 \text{ g}_{C_3H_6} \cdot \text{g}_{cat}^{-1} \cdot \text{h}^{-1}$ . These high productivity values obtained by these boron catalysts are promising results, and further investigations and improvement could mean in their industrial implementation.

The reactivity differences between elemental boron and the other borides, which did not follow a correlation with the different specific surface areas of each catalyst, may be due to the density of active sites and/or the electronic interactions between the subsurface bulk structure and the surface boron species [242,318]. Both of these possibilities are related to the bulk material over which the boron species layer is formed during reaction, what in turn will depend on the non-boron constituent element. The fact that the propylene selectivity at isoconversion values seemed to be always similar

for all boron-containing catalysts suggested that the non-boron constituent element is not directly involved or crucial in the active site. In fact, all the boron-containing catalysts presented similar surface elemental compositions upon exposure to propane ODH reaction [242], where the surface oxygen concentration increased in detriment of the concentrations of the non-boron elements, achieving a surface composition primarily comprised of B and O atoms. The coordination of boron with oxygen was confirmed by infrared and X-ray photoelectron spectroscopy results, where the B1s XPS feature shifted to higher binding energies due to the presence of boron in higher oxidation state. It should be noted that such oxyfunctionalization was only occurred when both alkane and oxygen were simultaneously present in the feed. These results suggested the formation of  $\text{BO}_x$  sites on the surface of all the boron-containing catalysts during the propane ODH reaction, which would be active and very selective for the formation of olefins. The formation of a  $\text{B}_2\text{O}_3$  layer on the catalyst surface was discarded, since the typical reaction temperature used with these catalysts (around  $500^\circ\text{C}$ ) exceeded the melting point of this oxide (around  $450^\circ\text{C}$ ). So, this would result in a  $\text{B}_2\text{O}_3$  gradually leaching off of the catalyst with the concomitant deactivation, as already observed for  $\text{Al}_2\text{O}_3$ -supported  $\text{B}_2\text{O}_3$  catalysts [319]. However, the boron catalysts have been found to be very stable during reaction.

It should be noted that different understandings of the catalysts nature of boron nitride can be found, although it seems to be universally acknowledged that oxygen-containing boron sites, gas-phase oxygen and propane molecules participate in the catalytic cycle [10]. In this way, it is necessary to get more insights about the active sites and the reaction mechanism, since there is still a large room to improve these catalysts. In addition to the relatively high olefin productivity already obtained, these materials are very stable and present an excellent thermal conductivity, what is important for the removal of the reaction heat in the highly exothermic alkane ODH reaction. Furthermore, boron catalysts may also be of interest for other reactions such as olefin hydrogenation [320],

acetylene hydrochlorination [321], dibenzothiophene oxidation [322], nitroaldol reaction [323] and oxidative desulfurization [324].

### 1.2.3. Vanadium oxide based catalysts

Vanadium oxide based catalysts are widely used for partial oxidation reactions in the chemical, petroleum and environmental industries [21,158,170,172,196,325–328] due to the favorable redox properties of the active vanadium sites [329] that can easily change its oxidation state accepting or giving their lattice oxygens [329–334]. Vanadium is used as catalyst in the most important commercial process of alkane activation on an industrial scale, which is the selective oxidation of n-butane to maleic anhydride using vanadium-phosphorus oxide (VPO) catalysts [335,336]. This has encouraged the study of vanadium catalysts in other selective oxidations such as the propane ODH reaction.

The catalytic properties of vanadia based catalysts can be significantly improved by supporting the vanadium oxide onto a support or by doping with other elements [21,147]. In contrast, big and pure  $V_2O_5$  crystals are not good catalysts for most of the reactions [147,170]. The incipient wetness impregnation method is the most used technique to prepare supported catalysts. This method requires the previous preparation of the catalytic support via calcination of the corresponding precursor/s, followed by its impregnation with the active phase precursor and a subsequent calcination [156,337–341]. The active phase deposition usually results in a decrease of the surface area of the catalytic support [159]. Although is less commonly reported in the literature, some authors have mixed both the support and the active phase precursors to be calcined in only one step giving rise to the simultaneously formation of the support and the dispersion of the active phase along the entire catalyst bulk [342].

A lot of papers have reported that the preparation method can affect the nature of the supported vanadium oxide phases. However, it has been demonstrated that the surface vanadia species are thermodynamically controlled and are not really influenced by the vanadium precursors or

preparation methods [173,196]. In fact, vanadia can be spontaneously dispersed after heating (above 500°C) a physical mixture of crystalline  $V_2O_5$  and oxide support powder (Figure 1.8).

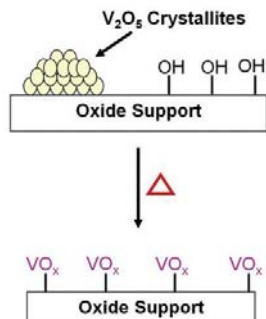


**Figure 1.8.** Schematic representation of the formation of a surface vanadia monolayer by heating a physical mixture of crystalline  $V_2O_5$  and oxide support powder (spontaneous dispersion) [196].

The anchoring bonds between the vanadium species and the support are formed via titration of the Support-OH bonds. This reaction presents reversible nature via dehydration/hydration of the supported vanadia phase. Generally, when the dispersion capacity of the support is exceeded,  $V_2O_5$  crystals start to be formed and remain stable on the solid surface (Figure 1.9). The capacity dispersion of a support will be influenced by its specific area and by the interaction forces between the vanadia species and the underlying oxide support [193].

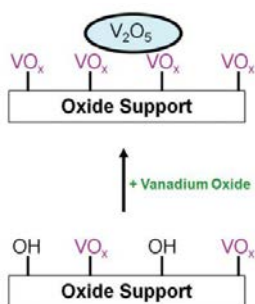


**Figure 1.9.** Schematic representation of  $V_2O_5$  nanoparticle formation on top of a surface vanadia monolayer with increasing vanadium oxide loading [196].

The catalytic behavior of supported vanadia catalysts is strongly influenced by several factors [158,172,174,281,325–327,343–346]:



- The coordination and aggregation of the vanadia species, which depend on the vanadium surface concentration of the catalyst.
- The redox properties of the vanadia active sites, which are determined by the reducibility of the catalyst (i.e. the ease of the oxygen removal from the lattice or the V-O bond energy).
- The acid-base character of the support, which strongly influences on the adsorption/desorption steps of the reactants and products determining the selectivity.
- All the above factors influence each other and are in turn determined by the nature of the metal oxide support and by the presence of additives as promoter.

#### 1.2.3.1. Vanadia species and active sites

The molecular structures of supported or dispersed vanadium oxide species have been extensively studied by different spectroscopic techniques such as IR, Raman, XANES/EXAFS, UV-vis diffuse reflectance spectroscopy (DRS), solid-state  $^{51}\text{V}$  NMR [175,347–363]. In dehydrated conditions, these  $\text{VO}_x$  species can be present forming four different structures [156,170,176,364] (Figure 1.10):

- Isolated surface  $\text{VO}_4$  species containing three bridging V-O-Support bonds and one terminal V=O bond.
- Polymeric surface  $\text{VO}_4$  species containing three bridging V-O-V/O-support bonds and one terminal V=O bond.
- Crystalline  $\text{V}_2\text{O}_5$  nanoparticles.
- Mixed oxide compounds containing vanadium and the metal oxide support may be also formed (e.g.,  $\text{ZrV}_2\text{O}_7$ ,  $\text{AlVO}_4$ ,  $\text{V}_x\text{Ti}_{1-x}\text{O}_2$ ,  $\text{NbVO}_5$ ,  $\text{Mg}_2\text{V}_2\text{O}_7$ ), usually at high temperatures.

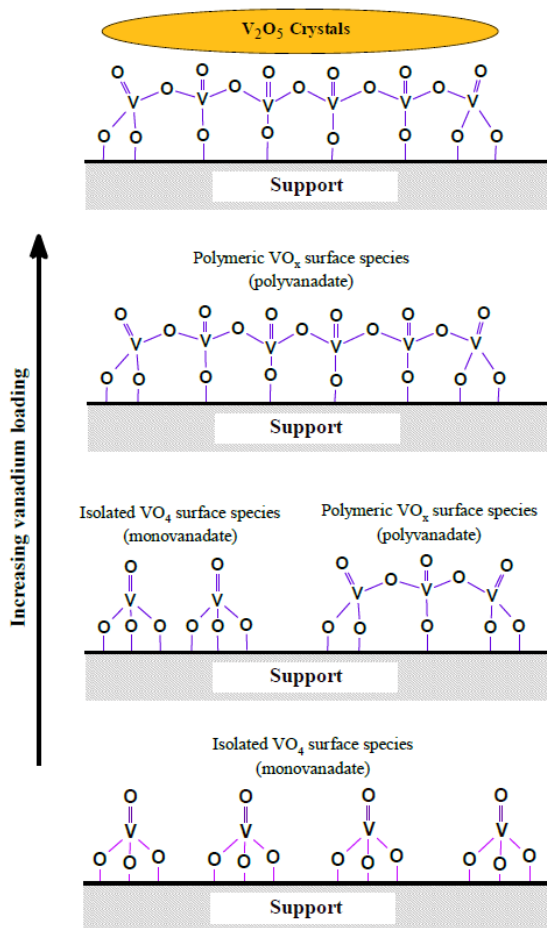


Figure 1.10. Vanadia species on the catalyst surface as the vanadium loading increases.

These species can coexist and their proportion in the catalyst will be determined by the surface density of vanadium, specific surface area and nature of the support [3]. Therefore, different combinations of V-O-Support, V-O-V, or V=O moieties can be obtained and may result in different catalytic activity. In fact, the reducibility of polyvanadates is higher than monovanadates because V-O-V and V=O bonds are more easily reduced than V-O-Support [3,280].

At vanadium loadings below monolayer coverage, isolated and polymeric surface  $VO_x$  species are the most abundant species on the oxide support, increasing the relative concentration of polyvanadates as the surface

density of vanadium is higher, as shown in Figure 1.10 [176,365]. At vanadium loadings greater than monolayer coverage, in addition to polyvanadate and monovanadate species,  $V_2O_5$  crystallites are expected to be present (Figure 1.10), although it has been found that they can also appear below monolayer coverage [159]. In these cases, the spontaneous dispersion of such crystalline phases onto the support as surface vanadia species is possible by heating at elevated temperatures (above 500°C) [363].

It is well known that monomeric and polymeric surface  $VO_4$  species are the most active species in supported vanadia catalysts, whereas crystalline phases are less active due to their more condensed structures that results in lower exposed active sites [176]. For this reason, in order to avoid the formation of  $V_2O_5$  crystallites, catalysts with coverage below monolayer are usually synthesized in the literature. However, it has been recently found that crystalline  $V_2O_5$  nanoparticles in the 1-3 nm range can exhibit high activity in the ODH reaction [159,337]. It should be noted that although it is well-known that the  $VO_x$  lattice oxygen are the active species [21,159], the individual catalytic contributions of monovanadate and polyvanadate species during reaction are still not completely resolved in the literature [156,159,337].

#### 1.2.3.2. Effect of support

$SiO_2$ ,  $Al_2O_3$ ,  $TiO_2$ ,  $ZrO_2$ ,  $CeO$ ,  $Nb_2O_5$ ,  $MgO$  or zeolite are the supports most reported in the literature to disperse vanadium oxide [21,159,281–284]. Depending on the support material, vanadium monolayer coverage is reached with a different vanadium surface density. It is generally agreed that, with the exception of supported  $V_2O_5/SiO_2$  catalysts, the theoretical monolayer coverage in most of the supports corresponds approximately to 8-9 vanadium atoms per  $nm^2$  [159,176,236]. Moreover, the polymerization degree of vanadia species is also influenced by the nature of the support and the number of available -OH surface groups on such support. For instance, at an intermediate surface vanadia density, the polyvanadate to

monovanadate ratio is higher in the order of  $\text{SiO}_2 \ll \text{ZrO}_2 \ll \text{Al}_2\text{O}_3$  supports [176], what could already result in different catalytic activity. Furthermore, the influence of the support on the reactivity of the vanadia active sites has been studied by several authors and it has been observed that the acidic and basic nature together with the redox properties of the support has a significant influence on the reducibility of the vanadia species, and in turn, in their catalytic activity [256]. In this way, higher reducibility of the active sites results in higher catalyst activity. It should be noted that some confusions about the real effect of certain supports have been found in the literature as a result of their different synthesis processes that can introduce additives, which can significantly change the catalyst properties [177].

It has been found that the TOF values can vary by more than one order of magnitude, for both the isolated and polymeric surface  $\text{VO}_x$  species, as the oxide support was varied:  $\text{SiO}_2 < \text{Al}_2\text{O}_3 < \text{Nb}_2\text{O}_5 < \text{TiO}_2 < \text{ZrO}_2 < \text{CeO}_2$  [174,176,177,193,196,366]. This trend inversely correlates with the Sanderson electronegativity of the oxide support cations [174]. The lower support cation electronegativity could result in a higher electron density on the vanadia sites enhancing the specific rate for the redox cycle. According to this effect, Wachs *et al.* have concluded that bridging V-O-Support bonds are the critical active sites in the rate determining step (RDS) of the reaction mechanism [178]. DFT calculations have suggested that the oxygen defect formation enthalpy of the vanadia sites can be significantly induced by the support affecting the redox properties of the active sites [367,368]. In this way, lower oxygen defect formation enthalpies of the vanadia sites would result in higher reaction rates for oxidation reactions.

On the other hand, the selectivity at isoconversion values on supported vanadia catalysts increase according to the order:  $\text{Al}_2\text{O}_3 < \text{TiO}_2 < \text{ZrO}_2 < \text{MgO}$  [256]. Corma *et al.* observed that the most selective vanadia species were those supported on basic metal oxide supports such as  $\text{MgO}$ ,  $\text{Bi}_2\text{O}_3$ ,  $\text{La}_2\text{O}_3$  and  $\text{Sm}_2\text{O}_3$ , whereas those supported in acidic metal oxide support such as  $\text{SiO}_2$ ,  $\text{TiO}_2$ , or  $\text{Al}_2\text{O}_3$  resulted in lower selectivity [281]. Moreover, it has been generally found that basic metal oxide supports, such as  $\text{MgO}$ ,

strongly interact with the dispersed vanadia and the mixed metal oxide may be formed [285,369], rather than the surface vanadia overlayer as in other supports such as alumina, titania or zirconia that allow good dispersion of surface vanadia species [256,330,370]. In the case of silica support, the dispersion of vanadia is more difficult due to the weak interaction between the vanadia species and the acidic support, then crystalline  $V_2O_5$  can be found even at low vanadium surface density [371]. It should be noted that it has also been reported that the free -OH groups on the support can act as unselective sites [175]. It can be concluded that the acid-base properties of the metal oxide support will determine the distribution of the surface vanadia species and the selectivity of such active sites.

#### 1.2.3.3. Red-ox properties

Vanadium-based catalysts are frequently used for the selective oxidation of alkanes due to their properties redox, since these materials easily change its oxidation state from  $V^{II}$  to  $V^V$  [329–334]. Indeed, catalytic reactions of selective oxidation usually occur by a redox mechanism, and then the reducibility of the active sites tends to proportional correlate with the catalytic activity [344,372,373]. Furthermore, the reducibility of a catalyst (i.e. the ease of the oxygen removal from the lattice or the V-O bond energy) can be modified by the incorporation of promoters enhancing the catalytic activity [147,158].

In a cycle of propane ODH, during the C-H activation step, the transfers of two electrons are involved from the propane molecule to the  $VO_x$  species, which are usually present in the  $V^V$  oxidation state, unless they are under reduction conditions [156,374]. Subsequently, these reduced metal centers are reoxidized using  $O_2$ , being this step much faster than the catalyst reduction rate [372,373]. In a cycle of the ODH reaction is generally accepted that is easier the reduction of two  $V^V$  species to two adjacent  $V^{IV}$  ones, than the reduction of a single  $V^V$  site to a single  $V^{III}$  one. This is because the  $V^{IV}$  species are less stable than the  $V^{III}$  ones, and then  $V^{IV}$  species are easily converted back to  $V^V$  ones during the catalytic cycle.

Moreover, the formation of the transition state is favored with the presence of two adjacent vanadium atoms. For these reasons, the catalytic activity in the propane ODH could be improved with the presence of polyvanadates with two or more adjacent vanadium atoms, instead of monovanadates with an isolated vanadium atom [201,344]. In fact, polymeric surface  $\text{VO}_4$  species are more easily reduced than isolated surface  $\text{VO}_4$  species [179].

#### *1.2.3.4. Acid-basic properties*

The acid-base character of the catalysts determines the distribution of the surface species (e.g. polymerization degree of the species), the mean distance between the vanadium active centers and the metal-oxygen bond strength (i.e. catalyst reducibility) [173,375,376]. These factors are crucial in the catalytic performance of these catalysts in selective oxidations such as propane ODH, especially in the product desorption/adsorption rates, as well as also have influence on the reactivity of the active sites [280].

It has been found that higher basic character of the catalysts usually results in higher propylene selectivity at isoconversion values, since basic sites seem to promote a fast desorption from the catalyst surface of the produced olefin during reaction [281]. In this way, the incorporation of other elements (e.g. potassium or magnesium oxide) on the catalyst surface can eliminate certain acid sites and/or provide the base properties of the vanadia sites to suppress the overoxidation with the subsequent increase of the propylene selectivity [147,158,326,377].

#### *1.2.3.5. Effect of additives*

The addition of additives such as alkalis or alkaline earth (e.g. Li, Na, K, Rb, Mg and Ca), transition metals (e.g. Ti, Cr, Mn, Fe, Co, Ni, Nb, Zn, W, Au, Ce and Mo) and P as promoters in the vanadia based catalysts have been reported to affect their redox and acid-basic properties, and hence their catalytic activity and selectivity [216,217,223,238,256,308,310–313,316,378–385]. The additives introduced in the catalyst can have an influence on the catalytic performance by forming point defects in both



cationic and anionic sublattices, including interstitial or substitutional cations, oxygen, and cationic vacancies. At low content (so called “doping”), the additives generally just affect the electronic properties of the catalyst, whereas at high content the additives can also geometrically block the strongest Brønsted acid sites or eliminate them by substitution (e.g. a proton in an acidic OH group by atoms of alkali metals) and/or modify the structure and hence affecting the structure related properties of the active sites. The formation of mixed oxide phases can also occur, resulting in the stabilization of certain oxidized or reduced vanadium sites during the redox cycle, which can have an influence on the catalytic performance of the catalyst. Besides, additives can also induce segregation effects and change the distribution of surface species, decreasing the amount of polymeric forms [310,386] and increasing the dispersion and spreading (wetting) of vanadia on the support oxide [217,312] and promoting the amorphization of such species [387]. Wachs distinguished two types of additives [388]: Non-interacting, which only coordinate to the support affecting the distribution of vanadia surface species; and interacting, which coordinate with vanadia species modifying the V-O bond energies or forming other surface compounds.

The addition of alkalis and alkaline earth metals is the most commonly reported and usually results in a selectivity improvement at isoconversion values [256,381]. On the one hand, they can exert the poisoning effect of the most unselective strong acid sites that favour the total oxidation to CO<sub>x</sub>, being this effect more evident as the ionic radius of the promoter increases: Li (0.68 Å) > K (1.33 Å) > Rb (1.48 Å) [217]. On the other hand, these metals also induce an increase of the basic character of the catalyst facilitating the quick desorption of the olefinic products before further oxidation to CO<sub>x</sub> [217,256,312,313,316]. Therefore, both effects contribute increasing the catalyst selectivity by preventing secondary reactions. Moreover, these additives may decrease the reducibility of the catalysts by increasing the V-O bond energy of the active sites, what may result in a decrease of the catalytic activity [256]. Kinetic studies of the propane ODH reaction have

concluded that the addition of alkali metals to the catalyst leads to an increase of the selectivity as a result of the relative higher rate of propane oxidation to obtain propylene versus the rate of propylene overoxidation to  $\text{CO}_x$  [217,389]. This is due to the relatively favoured propylene desorption (i.e. the decrease of the heat of propene adsorption [313]) and the relatively increase of the activation energy related to the propylene oxidation after the addition of such additives, which inhibit the secondary propylene combustion. In contrast, there is also a concomitant decrease of the propane oxidation rate denoting the influence of the presence of such metals lowering the catalytic activity.

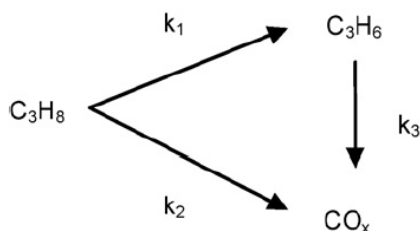
The addition of redox elements (normally a transition metal such as Ni, Cr, Nb and Mo) or P tends to increase the reducibility of the catalysts, which in turn result in an increase of the catalytic activity [311,379,380]. However, it has been found that these additives also affected the acid-base properties of the catalysts by increasing the number of acidic sites, resulting in a decrease of the propylene selectivity in the propane ODH reaction. In fact it has been reported that addition of phosphorus to  $\text{VO}_x/\text{TiO}_2$  catalysts leads to a decrease in the selectivity towards the basic olefinic products as butadiene in butene oxidation [390], whereas it increases the selectivity values towards the acidic products such as maleic anhydride in butadiene oxidation [390], benzoic acid in toluene oxidation [391,392], and phthalic anhydride in o-xylene oxidation at high conversions [393]. These results support the assumption that the adsorption of basic products and their overoxidation to  $\text{CO}_x$  is promoted in acidic surfaces and vice versa, which suggests that basic catalyst surfaces will trend to increase the selectivity towards basic products and acidic catalyst surfaces will lead to better selectivity values to acidic products.

#### **1.2.4 Aspects of the propane ODH reaction mechanism over vanadium oxide based catalysts**

It has been established that reaction proceeds via Mars-van Krevelen type mechanism [159–161,338,394–398], which means that the lattice oxygens



of the catalyst are the active sites. In this way, the mechanism involves the simultaneous reduction and oxidation of the catalyst surface by the reaction with propane and oxygen (or other oxidizing agents as  $N_2O$  [161,162]), respectively. The general reaction network most accepted in the literature is a parallel-consecutive pathway as shown in Scheme 1.2, where propane is oxidized to propylene, and both can be totally oxidized to  $CO_x$  [160]. Moreover, it is commonly reported that it is difficult to control such undesired combustion in order to obtain high propylene yields [276], since the same active sites are responsible for both the selective ODH reaction and the total oxidation. Moreover, it is also generally accepted that most of the  $CO_x$  produced during reaction usually comes from the consecutive combustion of propylene due to the lower energy requirement to activate propylene with respect to propane [159,160,399].



**Scheme 1.2.** Simplified reaction network of propane ODH [326,338].

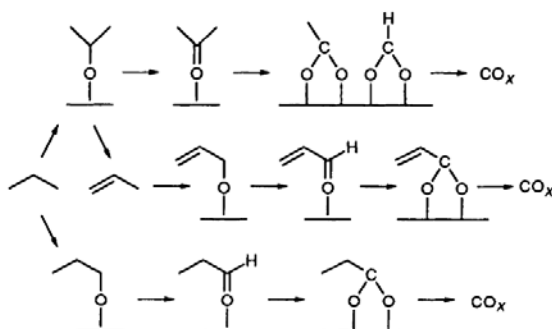
On the one hand, it appears to be a consensus that the activation of the secondary C-H bond of propane is the rate determining step (RDS) occurring via formation of propyl or (iso)propoxy species as first reaction intermediates, which leads to propylene in the gas phase or adsorbed oxygenate species on the catalyst that are usually further oxidized giving rise to  $CO_x$  [276,400,160]. On the other hand, the oxidation of the propylene formed during reaction seems to occur via activation of allylic C-H bonds with the subsequent formation of allyl-alkoxide surface species, followed by several oxidation steps required to complete the combustion [276]. Iglesia *et al.* carried out isotopic tracer studies to investigate the propane ODH reaction mechanism over  $VO_x/ZrO_2$  catalysts [276,401]. The results suggested that the C-H bond activation step of propane and the dissociative oxygen chemisorption step to reoxidize the catalyst are both irreversible,

while the OH groups formed on the catalyst during the different reactions are reversibly recombined forming water, oxygen active sites and vacancy centers.

However, there is no consensus about the nature of the path leading to propylene formation and, despite the vast propane ODH literature, not many details are usually given about the nature and number of steps of the mechanism involving the formation of CO<sub>x</sub> [160]. Probably, because this is a very challenging reaction to study, since the first proton abstraction of propane is the rate-determining step, hence the steady-state coverages of subsequent intermediates are likely too small to be accessible by traditional methods. The nature of the activation step of the C-H bond is still unclear and depend on the nature of the active sites [151,160]. In redox catalysts, as it is the case for those based on vanadium oxide, the activation seems to occur via heterolytic dissociation of the C-H bond by abstraction of a proton on a nucleophilic site [158,402], which leads to the formation of an organic fragment of the anion type. The decisive factor in the nucleophilic attack can be the nucleophilicity of the oxygen or the electrophilicity of the metal. However, the heterolytic cleavage of the C-H bond could also occur via abstraction of a hydride ion leading to a fragment of the cation type. Furthermore, homolytic dissociation of the C-H bond is also possible via abstraction of a hydrogen atom leading to a radical fragment [158,326,402]. Many DFT studies have focused on the C-H bond activation during the propane ODH [201–203,311,403–406], but hardly any works study in detail the deep oxidation reactions network, what would be important to understand the properties of the catalysts that determine the propylene selectivity.

In this way, it seems that the most detailed investigations are provided by Busca *et al.*, who performed IR studies of the total oxidation of propane and its ODH to propene over catalysts of Mn<sub>3</sub>O<sub>4</sub>, Co<sub>3</sub>O<sub>4</sub> and MgCr<sub>2</sub>O<sub>4</sub> [396,400,407–410]. From these results and their comparison with the data available in literature by then, they proposed different possible reaction pathways for the propane activation and oxidation depending on the

catalyst nature (Scheme 1.3 [408]), which could be extrapolated over other transition metal oxide based catalytic systems [400,409].



**Scheme 1.3.** Scheme for propane oxidation pathways over transition metal oxide based catalysts (adapted from [408]).

According to Busca *et al.*, they suggested that all the oxidation steps involved in the hydrocarbon oxidation mechanism over such catalysts occur at the expense of nucleophilic lattice oxygen species [409]. They also proposed that propane is most probably attacked at C(2), the weakest C-H bond, forming isopropoxide species, whose evolution can give rise to propylene or chemisorbed acetone that is overoxidized to  $\text{CO}_x$  through acetate and formate species as intermediates with the formation of carbonates. Oxidation of propane hardly occurred via attack at C(1), since it was observed in a very low extent and only using the catalyst of  $\text{Co}_3\text{O}_4$  [408], forming n-propoxide species, which are evolved as propylene or are totally oxidized through formation of chemisorbed propanal, followed by propanoate species and finally  $\text{CO}_x$ . Simultaneously, the formed propylene during reaction can be adsorbed on the catalyst and oxidized through an OH surface group to form 2-propoxide and continue with the total oxidation via the acetone pathway. Moreover, according to their results obtained in [407,408,410], propylene can be also oxidized through allyl-alkoxides as first intermediate species, followed by formation of chemisorbed acrolein, then acrylate species, and finally carboxylates and carbonates species with the subsequent formation of  $\text{CO}_x$ . These propylene oxidation routes could be supported by the investigations performed by Wachs *et al.* about selective oxidation of propylene to acrolein over supported  $\text{V}_2\text{O}_5/\text{Nb}_2\text{O}_5$

catalysts [180,365], where surface allyl intermediate species were found as the most abundant surface intermediate species, and acrolein together with acetone were the major compound in the gas phase.

Furthermore, although it is generally accepted that bridging oxygens sites (V-O-V/V-O-Support) are the most active sites, there are still authors reporting that terminal oxygen sites (V=O) are the active sites. Terminal V=O bonds were firstly reported as the most active sites [197–206]. In 1968, vanadyl oxygen (V=O) was already proposed by Tarama *et al.* as active sites in the catalytic oxidation reactions according to adsorption experiments and using IR spectroscopy [197]. In 1985, Mori *et al.* found that V=O is the active site for the oxidation of butane [198]. In 1991, Oyama *et al.* suggested that the vanadyl oxygen is also the active site for the selective oxidation of ethane to ethylene and acetaldehyde [199]. In 1982, Andersson proposed that the V=O species are the active sites for hydrocarbons catalytic oxidation according to electronic structure calculations of V<sub>2</sub>O<sub>5</sub> [200]. In 2000, Gilardoni *et al.* found that V=O bonds are the active sites for the propane ODH in agreement with the results obtained by DFT, and it was justified by analysis of the Fukui function that revealed the higher nucleophilic character of vanadyl oxygens [201]. In 2006, Fu *et al.* found by doing DFT calculations that V=O sites are more active and V-O-V sites are more selective to ODH of ethane or propane [202]. In 2007, Cheng *et al.* reported that V=O sites play a key role in all the reaction steps of the catalytic cycle according to their results obtained by quantum mechanical methods [203]. In 2012, Alexopoulos *et al.* performed DFT calculations and they also reported that vanadyl oxygen (V=O) are more active, while bridging oxygens (V-O-V) are more selective in the propane ODH reaction [204]. Recently, in 2019, Deo *et al.* reported in a DFT investigation that the C-H activation of propane on titania or alumina support catalyst is favorable on the bridging oxygens, while on the silica support catalyst the activation is more favorable on the vanadyl oxygen [205]. In the same year, DFT calculations for propane dehydrogenation over aluminum supported

vanadium oxide performed by Xiong *et al.* have reported that V=O bonds present the dominant role during propane ODH [206].

Conversely, since the 1990s other authors have reported that the bridging oxygens are the catalytic active sites for the selective oxidation reactions assuming a minor participation of the vanadyl oxygen [156,159,170–196]. In this way, Wachs *et al.* [159,172,174–180,190–196] have made a large contribution showing experimental evidences by *in situ* or *operando* IR, Raman and UV-Vis DRS spectroscopy, as well as by  $^{18}\text{O}_2$ – $^{16}\text{O}_2$  isotopic labeling studies. They observed that changing the catalyst support had a great influence on the TOF values obtained, what suggested that V-O-Support bonds are the active sites having a key role in the kinetic of the rate determining step [178]. Nevertheless, the Raman and IR band positions of the vanadyl oxygens, which is directly related to the V=O bond strength, were similar for each support despite the TOF values variation observed, what could indicate that the vanadyl bonds are not critical in the catalytic oxidation and supporting, by elimination, the importance of bridging oxygens [190]. This was supported by *operando* and oxygen-18 labeling experiments, where no correlations of the TOF obtained during reaction were found with the reduction degree and perturbations observed in both the terminal V=O and bridging V-O-V bonds, as well as with the apparent isotopic exchange rate of such oxygens, which should be fully exchanged within the first catalytic cycle if they were kinetically critical active sites [172,174,192,193]. However, V=O bonds were not fully exchanged after ~10 or 20 catalytic cycles. On the other hand, the surface concentration of vanadium active sites, which affect the species proportion of polyvanadates with respect to monovanadates, did not seem to significantly alter the TOF values for the alkane ODH reactions or for the selective oxidation reactions of methane or methanol to formaldehyde. This suggested that both surface species present the same intrinsic catalytic activity, highlighting the moderate contribution of V-O-V bonds (present in polyvanadates and not in monovanadate) as critical active sites, and showing that only one active site is required to perform such reactions [177,193]. It should be noted that they

also reported that other partial oxidation reactions can require more than one active site and TOF values increase as the surface concentration of active sites is higher due to the geometric requirement of several sites in close vicinity for the reaction, as in the cases of the selective oxidations of butane or propylene to maleic anhydride or acrolein, respectively [172,194]. Later, quantum chemical calculations done by Witko *et al.* [186–189] modelling different  $V_2O_5$  crystallographic faces supported the above assumptions, showing the inactivity of the terminal vanadyl bonds and the higher activity of the bridging oxygens due to their higher nucleophilic character.

However, most of the previous insights reported by Wach *et al.* about the activity of each oxygen site were indirectly deduced from the experimental results. Since the Raman bands related to V-O-Support bonds, which were considered as active sites, were normally difficult to detect (depending on the support), due to their high ionic character and their very weak Raman scattering cross-sections [191,193], then only the relatively intense V=O and V-O-V bands were deeply studied, whose bonds were considered as non-crucial active sites. Furthermore, different opinions can be found in the literature regarding the activity of polyvanadates with respect to monovanadates [156,159,337], what have made difficult to find out the real contribution of V-O-V bonds in the catalytic oxidation reactions.

The variation of propane TOF values with respect to vanadium content of the catalysts have been widely used by many authors to discern if monovanadates are more, less or equally active than polyvanadates. It is well known that the polyvanadates to monovanadates ratio increases as the vanadium content in the catalyst is higher [176,365]. In an extensive review article by Carrero *et al.* [159] it was concluded that monovanadates present the same TOF than polivanadates. However, different tendencies can be found in the literature, it has been reported that TOF decreases [156,161], remains constant [159,175,411,412] or increases [214,337,344] as the vanadium content of the catalyst increases. The variation of TOF with vanadium content has been always explained with the different

catalytic performances between polyvanadates and monovanadates. The different catalytic activity between these species have been usually explained by the different reducibility and activity of the V-O-Support and V-O-V bonds [156,245,337], being the former present in higher proportion in monovanates and the latter only present in polyvanadates. The selectivity of these species is generally very similar, although it has been reported that V-O-S bonds are more selective than V-O-V bonds [162] and vice versa [343]. All these discrepancies can be due to the use of different preparation methods of the catalysts, supports and/or additives, which may result in different kind of vanadia surface species. Moreover, it cannot be discarded the possible existence of external and/or internal mass and/or heat transport limitations, contribution of homogenous phase reaction at high temperatures (above 500°C) and/or data with total oxygen conversion.

It can be concluded that there is still some controversy in the literature about the propane ODH regarding the active sites and intermediate species during reaction and their relationship with the conversion and selectivity. Not many articles describe a detailed reaction mechanism or kinetic study. The use of *operando* spectroscopy together with a kinetic study could be a good combination to get new insights about the reaction mechanism and determine the kinetic parameters in order to be able to understand the structure-activity relationship for the propane ODH. In this way, it could be possible to improve the catalyst and to operate under the optimal reactor and reactions conditions in order to increase the yield and productivity to propylene and try to make feasible its industrial implementation.

### 1.2.5. Kinetic models

In gas-solid heterogeneous catalysis, the reaction mainly proceeds the following stages [160]:

1. Diffusion of the reactants towards the surface of the catalyst.
2. Adsorption of the reactants on the surface.
3. Reaction on the surface.

4. Desorption of the products from the surface.
5. Diffusion of the reaction products from the catalyst surface.

The rate of each stage depends on different factors, as well as on the reactant concentrations and temperature. Stages 1 and 5 are mainly influenced by the fluid dynamics characteristics of the system (e.g. flow velocity, diffusional properties, etc). Stages 2 and 4 are determined by the adsorption/desorption constants of the gas phase reactants/products on/from the catalyst surface, respectively. Stage 3 depend on the reaction constants such as the activation energy required for the reaction on the catalyst surface. Only in the case that stages 2, 3 and 4 (related to adsorption/desorption and reaction steps) are significantly slower than the stage 1 and 5 (related to diffusion process), the intrinsic kinetic data can be obtained from traditional experiments. Otherwise, the experimental data obtained will totally or partly describe the diffusion process, and the apparent kinetic constants obtained will not be representative of the intrinsic catalytic reactivity of the catalyst or comparable with kinetic data obtained in other conditions or reactor.

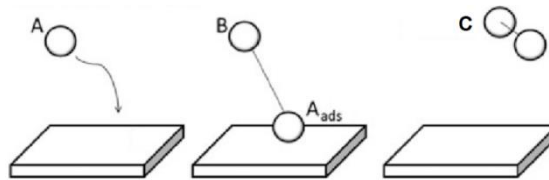
Different kinetics models have been used for the description of propane ODH: Eley-Rideal, Langmuir-Hinshelwood, Power Law, Rake, etc. [282,413–416], but the Mars-van Krevelen [394] is the most commonly used [159–161,338,395–398]. Generally, first-order dependence is considered for propane and propylene in the selective and non-selective reactions, respectively; while order of 0.5 is usually considered for gas phase oxygen indicating dissociative chemisorption of oxygen on the surface catalyst during the reoxidation step. However, many authors have simplified to zero-order dependence with respect to oxygen for the reoxidation reaction rate, assuming that the reoxidation reaction of the catalyst is much faster than the reduction reaction [166,337,343,399,414,415,417,418], and consequently, sometimes, even taking for granted that the catalyst is fully oxidized or nearly saturated with oxygen under reaction conditions [166,415]. These assumptions have become generalized and accepted in



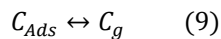
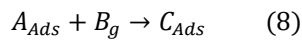
the literature for this kind of catalysts in ODH reactions, and probably it is correct for a broad range of catalysts and operation conditions. However, it is possible that sometimes these assumptions are not true even at low conversions, since it will depend on the catalyst nature and reaction conditions. The kinetic constant usually compared between different catalysts is the activation energy of the first hydrogen abstraction from propane, which is considered the RDS [159,160]. However, a wide range of values can be found in the literature, probably due to the wide variety of different kinetic models used, which are sometimes oversimplified and/or frequently inconsistent and incorrect without physical relevance.

#### 1.2.5.1. Eley-Rideal

In this model it is considered that species A are adsorbed in equilibrium and react with molecules B of the gas phase (Scheme 1.4):



**Scheme 1.4.** Schematic representation of the Eley-Rideal Mechanism.

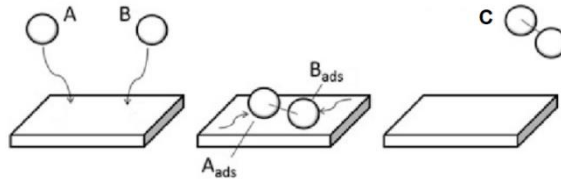


Assuming Langmuir adsorption of A, first-order dependence with respect to B and rapid desorption or low surface coverage of C, the reaction rate expression would be:

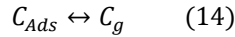
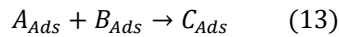
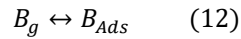
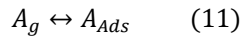
$$r = \frac{k \cdot K_{Ads A} \cdot P_A \cdot P_B}{1 + K \cdot P_A} \quad (10)$$

### 1.2.5.2. Langmuir-Hinshelwood

This model considers the Langmuir adsorption of both species, A and B, and the subsequent reaction of neighbor adsorbed species (Scheme 1.5):



**Scheme 1.5.** Schematic representation of the Langmuir-Hinshelwood Mechanism.



It is usually assumed that all the reaction steps are in thermodynamic equilibrium except the rate-determining step (RDS), which can be any of the step. The reaction rate expression will be determined by the RDS.

If the adsorption of A is the RDS:

$$r = k_{Ads A} \cdot P_A \cdot (1 - \theta_A - \theta_B - \theta_C) \quad (15)$$

while the equilibrium conditions of the other steps and components would be:

$$K_{Ads B} = \frac{\theta_B}{P_B \cdot (1 - \theta_A - \theta_B - \theta_C)} \quad (16)$$

$$K_{Ads C} = \frac{\theta_C}{P_C \cdot (1 - \theta_A - \theta_B - \theta_C)} \quad (17)$$

$$K_{Reaction} = \frac{\theta_C}{\theta_A \cdot \theta_B} \quad (18)$$

If the surface reaction is the RDS, then:

$$r = k \cdot \theta_A \cdot \theta_B \quad (19)$$

$$\theta_A = \frac{K_{Ads A} \cdot P_A}{(1 + K_A \cdot P_A + K_B \cdot P_B + K_C \cdot P_C)} \quad (20)$$

$$\theta_B = \frac{K_{Ads B} \cdot P_B}{(1 + K_A \cdot P_A + K_B \cdot P_B + K_C \cdot P_C)} \quad (21)$$

If the desorption of C is the RDS:

$$r = k_{Des C} \cdot \theta_C \quad (22)$$

$$K_{Reaction} = \frac{\theta_C}{\theta_A \cdot \theta_B} \quad (23)$$

$$K_{Ads A} = \frac{\theta_A}{P_C \cdot (1 - \theta_A - \theta_B - \theta_C)} \quad (24)$$

$$K_{Ads B} = \frac{\theta_B}{P_B \cdot (1 - \theta_A - \theta_B - \theta_C)} \quad (25)$$

#### 1.2.5.3. Power Law

This model is used when the mechanism of a reaction is very complex and/or there is not much knowledge about it. It is normally used as a first approximation in the kinetic studies of catalytic reactions. It correlates the reaction rate with the partial pressures as follow:

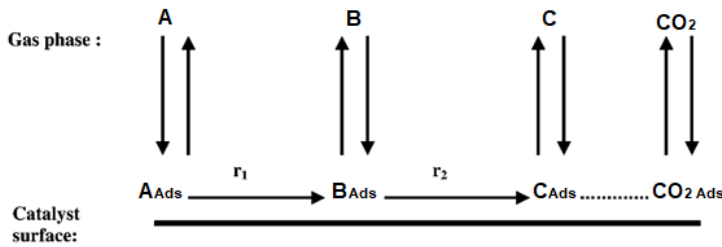
$$r = k \cdot P_A^m \cdot P_B^n \quad (26)$$

where “m” and “n” are the reaction orders experimentally obtained, which do not necessarily have to be equal to the stoichiometric coefficients of A and B in the reaction, respectively.

#### 1.2.5.4. Rake

This model is used for catalytic reactions of selective oxidations. The rake mechanism is a consecutive route of oxidation reactions by which a molecule is gradually oxidized giving rise to different species in the gas phase and CO<sub>2</sub> as shown in Scheme 1.6 [376]. Consequently, the desired

products (e.g. propylene in the propane ODH) are normally intermediate in the consecutive oxidation reactions, and their corresponding selectivity values will be determined by the ratio of the rate constants belonging to their formation and elimination/oxidation reactions. A good catalyst should have appropriate values of the adsorption and desorption parameters for the desired product. A high desorption rate of a certain product will require a low bonding heat of such product to the catalyst surface. In some oxidations the concerted reaction can be occurred and no desorption of intermediates to the gas phase is observed (e.g. in n-butane oxidation to maleic anhydride).



Scheme 1.6. Rake mechanism of oxidation reactions (adapted from [376]).

Making balance and assuming pseudo-steady state for each adsorbed species, the rate of change in their respective surface coverages would be approximately zero and the surface coverage of species A, B and C would be as follow:

$$\theta_A = \frac{k_{Ads A} \cdot P_A \cdot \theta_{\square}}{(k_{Des A} + k_1)} \quad (27)$$

$$\theta_B = \frac{(k_1 \cdot \theta_A + k_{Ads B} \cdot P_B \cdot \theta_{\square})}{(k_{Des B} + k_2)} \quad (28)$$

$$\theta_C = \frac{(k_2 \cdot \theta_B + k_{Ads C} \cdot P_C \cdot \theta_{\square})}{k_{Des C}} \quad (29)$$

where  $\theta_{\square}$  is the surface coverage of vacancy sites and a balance of sites would be:

$$1 = \theta_A + \theta_B + \theta_C + \theta_{\square} \quad (30)$$

It should be noted that first-order dependence with respect to the partial pressures of A, B and C is assumed. The balance of each species results in the following system of differential equations:

$$\frac{dP_A}{dt} = -k_{Ads A} \cdot P_A \cdot \theta_{\square} + k_{Des A} \cdot \theta_A \quad (31)$$

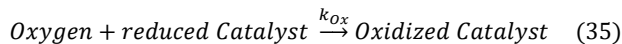
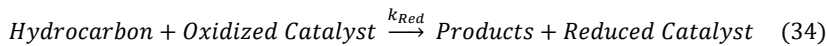
$$\frac{dP_B}{dt} = -k_{Ads B} \cdot P_B \cdot \theta_{\square} + k_{Des B} \cdot \theta_B \quad (32)$$

$$\frac{dP_C}{dt} = -k_{Ads C} \cdot P_C \cdot \theta_{\square} + k_{Des C} \cdot \theta_C \quad (33)$$

These system of differential equations (Eqs. (31)-(33)) together with the equations of the surface coverage of each adsorbed species (Eqs. (27)-(29)) and the balance of sites (Eq. (30)) is usually numerically solved and fitted to the experimental data to determine the kinetic constants of the catalyst for the corresponding selective oxidation reaction.

#### 1.2.5.5. Mars van Krevelen (redox)

According to this redox model, the oxygen consumed during the reaction comes from the lattice of the catalyst, which needs to be reoxidized by the gas phase oxygen to recover the catalytic activity and continue with the catalytic cycle. The general mechanism can be schematized in two general steps, reduction of the oxidized catalyst and oxidation of the reduced catalyst, Eqs. (34) and (35), respectively.



It should be noted that both the reduction and the reoxidation reactions can be quite complex involving several elemental steps. At the steady state, the reduction and reoxidation reactions rate are equal, being the oxidation state of the catalyst determined by the ratio of the rate constants of both reactions. The rate expression derived by Mars and Van Krevelen in their work [346] is:

$$r = \frac{k_{Red} \cdot k_{Ox} \cdot P_R \cdot P_{O_2}^n}{k_{Red} \cdot P_R + k_{Ox} \cdot P_{O_2}^n} \quad (36)$$

However, this equation (Eq. (36)) is inconsistent for several reasons, despite has been widely used by many authors to describe redox reactions [159–161,338,395–398], and it should be only considered as a mathematical fitting function without physical relevance [419]. The major inconsistency (among others) is found in the rate of oxygen adsorption. Since if it is assumed that lattice oxygen are the active sites, the oxygen adsorption must have dissociative character. However, the equation used is the corresponding to molecular oxygen adsorption in a single site. Other inconsistencies come from the consideration of non-elementary steps in the rate equations and the non-inclusion of intermediate species or final products in the site balance, considering only oxygen ions (even though the equation represents molecular oxygen adsorption).

### 1.2.6. Reactor configurations

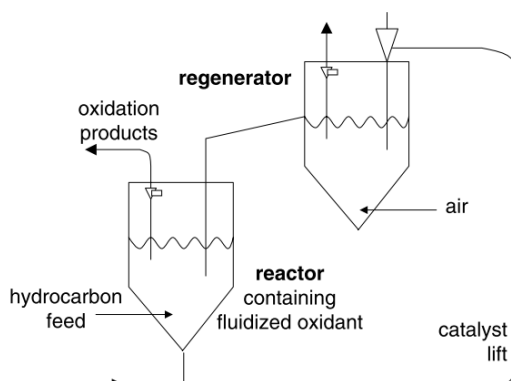
Fixed bed are the most used reactors on the laboratory scale, since they are probably the simplest and cheapest reactor configuration to perform gas-solid heterogeneous catalysis. However, propane ODH reaction is a very exothermic reaction that easily can form hot spots in fixed bed reactors (FBR) [152,168], especially at moderate or high propane partial pressures, what may damage the catalyst and/or produce runaway with the subsequent risk of explosion. Then, this reactor configuration could not be suitable for industrial-scale operation. The appearance of hot spots can be avoided by both improving the heat removal efficiency of the reactor or dosing the oxidant continuously along the reactor decreasing the overall oxygen concentration that interact with the catalyst [152,168].

In this way, the use of fluidized bed reactors (FLBR) can prevent the hot spot formation during reaction [169]. These reactors usually present a high thermal homogeneity along the reaction media, being safer in this respect compared to FBR. Multitubular reactors can be also used for a fast heat removal avoiding the formation of hot spots, although these reactors are

quite expensive to manufacture [152]. Microchannel reactors could be also considered to avoid explosions, even in the highly explosive regime, due to the high surface to volume ratio in these reactors that allow an efficient heat removal [152]. In fact, radical chain reactions can be quenched at the walls of these metal reactors. However, these reactors present some problems such as high pressure drop or clogging of the channels due to their small dimensions. The increasing of the channel diameter to overcome these problems gives rise to the catalytic wall reactor (CWR), which is characterized by its isothermal behavior unlike the FBR. The main problem of CWR is to find a reliable coating procedure that guarantee a good adhesion and distribution of the catalyst layers on the wall of the reactor [152].

A good example of air and hydrocarbon separation is the two-bed concept, which allows feed with high hydrocarbon concentration without risk of explosion. This concept is industrially used in the oxidation of butane to maleic anhydride [336]. It uses a solid as oxygen carrier to oxidize the hydrocarbon in the reactor as shown in the Scheme 1.7. Subsequently, the reduced solid is oxidized with air in the regenerator. The plant work at steady state and the conditions for the two semi-cycles can be independently optimized. With similar strategy, membrane reactors are the most studied alternative to FBR [11,152,153,167–169,420]. In a membrane reactor the chemical reaction and the separation take place in the same apparatus. There are two options: (i) one of the reaction products is separated through the membrane from the reaction mixture; (ii) one of the reactants is fed to the reaction zone through the membrane to control its concentration along the reactor. On the one hand, the first option is generally used to remove the target product from the reaction media to avoid its further oxidation, as well as shifting the equilibrium to the product side. In this way, higher selectivity and yield towards the desired product may be obtained. The use of H<sub>2</sub>-selective membranes in the case of non-oxidative dehydrogenation reaction is the most reported in the literature. However, the current membranes are not still good enough to perform such

separations under typical conditions of industrial oxidations. On the other hand, the second option is used for a distributed dosing of the oxygen into the reaction media lowering the average oxygen partial pressure along the reactor during the oxidative dehydrogenation process. This can result in an increase of the selectivity by suppression of the deep oxidation reactions hindering the formation of hot spots and the risk of explosions.

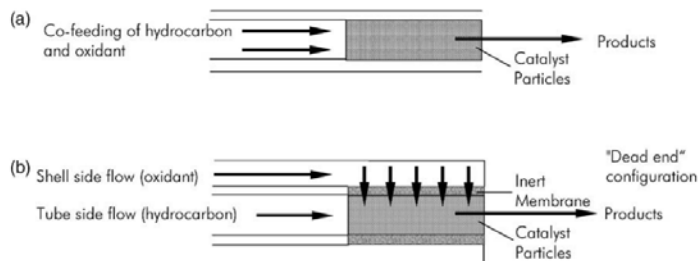


**Scheme 1.7.** Schematic representation of a two-bed partial oxidation [152].

In this way, selective oxidation reactions have been studied using fixed bed membrane reactors (FBMR), what can result in an increase of the selectivity and safety with respect to the use of the conventional FBR due to the uniform dosing of oxygen along the reactor [153,167]. Furthermore, these membrane reactors allow to operate under high hydrocarbon excess improving the olefin productivity without explosion, even at the explosive hydrocarbon to oxygen ratios. However, in case of membrane damage or other reactor leakages the risk of explosion is quite high. In most of the studies, the hydrocarbon is inserted in the inner side of the membrane, while the oxidant is fed in the shell side with a slightly higher pressure to allow the oxidant is fed across the membrane as shown in the Scheme 1.8. Thus, the oxidant is continuously added along the catalyst. Both ends of the membrane are normally vitrified only leaving as permeable the catalyst bed zone. Moreover, the shell side outlet is usually closed to force all the shell side flow pass through membrane allowing the uniform distribution of the oxidant along the catalyst. The membrane is inert and normally only has



separation purpose, as can be observed in the Scheme 1.8, unlike some membranes that can be found in other different processes, which also incorporate the catalyst functionality.



**Scheme 1.8.** Schematic representation of (a) feed configuration for fixed-bed reactor and (b) fixed-bed membrane reactor [153].

Some authors have investigated the use of fluidized bed membrane reactors (FLBMR) with distributed oxidant supply for alkanes ODH [168,169]. The combination of the excellent heat transfer of fluidized bed with advantageous principle of distributed oxidant dosing appears to be as a favorable strategy, especially for strongly exothermic reactions, which allow the operation in a broad conditions range with respect to the hydrocarbon to oxygen ratio. Moreover, these reactors are especially robust against oscillations and disturbances in the reactant feed, what confers a higher operation safety. It has been shown that the use of FLBMR can improve the selectivity and yield value towards olefin with respect to FBMR and FBR [168,169], the latter with the co-feed operation. However, it seems that the use of membrane reactors in the propane ODH has not brought remarkable improvements with respect to the conventional reactor configurations as the FBR.

### 1.3. References

- [1] J. Lazonby, Propene (Propylene), (n.d.). <http://www.essentialchemicalindustry.org/chemicals/propene.html> (accessed June 3, 2019).
- [2] The Propylene Gap: How Can It Be Filled?, Am. Chem. Soc. (n.d.). <https://www.acs.org/content/acs/en/pressroom/cutting-edge-chemistry/the-propylene-gap-how-can-it-be-filled.html> (accessed June 3, 2019).
- [3] J.J.H.B. Sattler, J. Ruiz-Martinez, E. Santillan-Jimenez, B.M. Weckhuysen, Catalytic Dehydrogenation of Light Alkanes on Metals and Metal Oxides, Chem. Rev. 114 (2014) 10613–10653. <https://doi.org/10.1021/cr5002436>.
- [4] A. Agarwal, D. Sengupta, M. El-Halwagi, Sustainable Process Design Approach for On-Purpose Propylene Production and Intensification, ACS Sustain. Chem. Eng. 6 (2018) 2407–2421. <https://doi.org/10.1021/acssuschemeng.7b03854>.
- [5] Ethylene, propylene demand will experience increased growth in 2005-10, (n.d.). <http://www.ogj.com/articles/print/volume-103/issue-45/special-report/ethylene-propylene-demand-will-experience-increased-growth-in-2005-10.html> (accessed September 20, 2016).
- [6] A. Akah, M. Al-Ghrami, Maximizing propylene production via FCC technology, Appl. Petrochem. Res. 5 (2015) 377–392. <https://doi.org/10.1007/s13203-015-0104-3>.
- [7] I. Amghizar, L.A. Vandewalle, G. Van, G.B. Marin, New Trends in Olefin Production, 3 (2017) 171–178. <https://doi.org/10.1016/J.ENG.2017.02.006>.
- [8] J.J.H.B. Sattler, I.D. Gonzalez-Jimenez, L. Luo, B.A. Stears, A. Malek, D.G. Barton, B.A. Kilos, M.P. Kaminsky, T.W.G.M. Verhoeven, E.J. Koers, M. Baldus, B.M. Weckhuysen, Platinum-Promoted Ga/Al<sub>2</sub>O<sub>3</sub> as Highly Active, Selective, and Stable Catalyst for the Dehydrogenation of Propane, Angew. Chem. Int. Ed. 53 (2014) 9251–9256. <https://doi.org/10.1002/anie.201404460>.

- [9] J.F. Brazdil, Strategies for the selective catalytic oxidation of alkanes, *Top. Catal.* 38 (2006) 289–294. <https://doi.org/10.1007/s11244-006-0027-4>.
- [10] L. Shi, Y. Wang, B. Yan, W. Song, D. Shao, A.-H. Lu, Progress in selective oxidative dehydrogenation of light alkanes to olefins promoted by boron nitride catalysts, *Chem. Commun.* 54 (2018) 10936–10946. <https://doi.org/10.1039/C8CC04604B>.
- [11] S.-W. Choi, D.S. Sholl, S. Nair, J.S. Moore, Y. Liu, R.S. Dixit, J.G. Pendergast, Modeling and process simulation of hollow fiber membrane reactor systems for propane dehydrogenation, *AIChE J.* 63 (2017) 4519–4531. <https://doi.org/10.1002/aic.15785>.
- [12] J.R. Alcántara-Avila, F.I. Gómez-Castro, J.G. Segovia-Hernández, K.-I. Sotowa, T. Horikawa, Optimal design of cryogenic distillation columns with side heat pumps for the propylene/propane separation, *Chem. Eng. Process. Process Intensif.* 82 (2014) 112–122. <https://doi.org/10.1016/j.cep.2014.06.006>.
- [13] M. Abraham, *Encyclopedia of Sustainable Technologies*, Elsevier, 2017.
- [14] *Applied Plastics Engineering Handbook*, Elsevier, 2011. <https://doi.org/10.1016/C2010-0-67336-6>.
- [15] E.P. Schulz, J.A. Bandoni, M.S. Diaz, Optimal Shutdown Policy for Maintenance of Cracking Furnaces in Ethylene Plants, *Ind. Eng. Chem. Res.* 45 (2006) 2748–2757. <https://doi.org/10.1021/ie050341r>.
- [16] M.M. Bhasin, Is True Ethane Oxydehydrogenation Feasible?, *Top. Catal.* 23 (2003) 145–149. <https://doi.org/10.1023/A:1024884623238>.
- [17] L. Albright, *Novel Production Methods for Ethylene, Light Hydrocarbons, and Aromatics*, CRC Press, 1991.
- [18] M.M. Bhasin, J.H. McCain, B.V. Vora, T. Imai, P.R. Pujadó, Dehydrogenation and oxydehydrogenation of paraffins to olefins, *Appl. Catal. Gen.* 221 (2001) 397–419. [https://doi.org/10.1016/S0926-860X\(01\)00816-X](https://doi.org/10.1016/S0926-860X(01)00816-X).

- [19] C.H. Bartholomew, R.J. Farrauto, *Fundamentals of Industrial Catalytic Processes*, John Wiley & Sons, 2011.
- [20] S.A.R. Mulla, O.V. Buyevskaya, M. Baerns, A comparative study on non-catalytic and catalytic oxidative dehydrogenation of ethane to ethylene, *Appl. Catal. Gen.* 226 (2002) 73–78.  
[https://doi.org/10.1016/S0926-860X\(01\)00884-5](https://doi.org/10.1016/S0926-860X(01)00884-5).
- [21] F. Cavani, N. Ballarini, A. Cericola, Oxidative dehydrogenation of ethane and propane: How far from commercial implementation?, *Catal. Today.* 127 (2007) 113–131.  
<https://doi.org/10.1016/j.cattod.2007.05.009>.
- [22] J.-P. Lange, R.J. Schoonebeek, P.D.L. Mercera, F.W. van Breukelen, Oxycracking of hydrocarbons: chemistry, technology and economic potential, *Appl. Catal. Gen.* 283 (2005) 243–253.  
<https://doi.org/10.1016/j.apcata.2005.01.011>.
- [23] J.H. Gary, G.E. Handwerk, M.J. Kaiser, *Petroleum Refining: Technology and Economics*, Fifth Edition, CRC Press, 2007.
- [24] J.G. Speight, *The Chemistry and Technology of Petroleum*, Fifth Edition, CRC Press, 2014.
- [25] R. Sadeghbeigi, *Fluid Catalytic Cracking Handbook: An Expert Guide to the Practical Operation, Design, and Optimization of FCC Units*, Gulf Professional Publishing, 2000.
- [26] T.F. Degnan, Applications of zeolites in petroleum refining, *Top. Catal.* 13 (2000) 349–356.  
<https://doi.org/10.1023/A:1009054905137>.
- [27] M.A. Fahim, T.A. Al-Sahhaf, A. Elkilani, *Fundamentals of Petroleum Refining*, Elsevier, 2009.  
<https://linkinghub.elsevier.com/retrieve/pii/C20090163481>.
- [28] J.F. Cuadros, D.N.C. Melo, N.M. Nascimento, R.M. Filho, M.R. Wolf Maciel, A hybrid GA-SQP multi-objective optimization methodology for carbon monoxide pollution minimization in Fluid Catalytic Cracking Process, in: A. Kraslawski, I. Turunen (Eds.), *Comput. Aided Chem. Eng.*, Elsevier, 2013: pp. 763–768.  
<https://doi.org/10.1016/B978-0-444-63234-0.50128-7>.

- [29] M.A. den Hollander, M. Makkee, J.A. Moulijn, Prediction of the Performance of Coked and Regenerated FCC Catalyst Mixtures, in: J.J. Spivey, G.W. Roberts, B.H. Davis (Eds.), *Stud. Surf. Sci. Catal.*, Elsevier, 2001: pp. 197–204. [https://doi.org/10.1016/S0167-2991\(01\)80198-1](https://doi.org/10.1016/S0167-2991(01)80198-1).
- [30] J.G. Speight, B. Ozum, *Petroleum Refining Processes*, CRC Press, 2001.
- [31] J.W. Wilson, *Fluid Catalytic Cracking Technology and Operations*, PennWell Books, 1997.
- [32] A. M Aitani, Propylene Production, in: *Encycl. Chem. Process.*, 2006: pp. 12–2461.
- [33] A.G. Maadhah, Y. Fujiyama, H. Redhwi, M. Abul-Hamayel, A. Aitani, M. Saeed, C. Dean, A new catalytic cracking process to maximize refinery propylene, *Arab. J. Sci. Eng.* 33 (2008) 17–28.
- [34] A. Aitani, T. Yoshikawa, T. Ino, Maximization of FCC light olefins by high severity operation and ZSM-5 addition, *Catal. Today*. 60 (2000) 111–117. [https://doi.org/10.1016/S0920-5861\(00\)00322-9](https://doi.org/10.1016/S0920-5861(00)00322-9).
- [35] A. Corma, A. Martínez, Zeolites in refining and petrochemistry, in: J. Čejka, H. van Bekkum (Eds.), *Stud. Surf. Sci. Catal.*, Elsevier, 2005: pp. 337–366. [https://doi.org/10.1016/S0167-2991\(05\)80018-7](https://doi.org/10.1016/S0167-2991(05)80018-7).
- [36] R.H. Harding, A.W. Peters, J.R.D. Nee, New developments in FCC catalyst technology, *Appl. Catal. Gen.* 221 (2001) 389–396. [https://doi.org/10.1016/S0926-860X\(01\)00814-6](https://doi.org/10.1016/S0926-860X(01)00814-6).
- [37] A. Corma, J. Martínez-Triguero, The Use of MCM-22 as a Cracking Zeolitic Additive for FCC, *J. Catal.* 165 (1997) 102–120. <https://doi.org/10.1006/jcat.1997.1474>.
- [38] C.R. Moreira, M. Schmal, M.M. Pereira, The effect of cerium introduction on vanadium-USY catalysts, in: E. Gaigneaux, D.E. De Vos, P. Grange, P.A. Jacobs, J.A. Martens, P. Ruiz, G. Poncelet (Eds.), *Stud. Surf. Sci. Catal.*, Elsevier, 2000: pp. 915–923. [https://doi.org/10.1016/S0167-2991\(00\)80736-3](https://doi.org/10.1016/S0167-2991(00)80736-3).
- [39] M. Torrealba, M.R. Goldwasser, G. Perot, M. Guisnet, Influence of vanadium on the physicochemical and catalytic properties of USHY

- zeolite and FCC catalyst, *Appl. Catal. Gen.* 90 (1992) 35–49. [https://doi.org/10.1016/0926-860X\(92\)80246-9](https://doi.org/10.1016/0926-860X(92)80246-9).
- [40] J. Biswas, I.E. Maxwell, Recent process- and catalyst-related developments in fluid catalytic cracking, *Appl. Catal.* 63 (1990) 197–258. [https://doi.org/10.1016/S0166-9834\(00\)81716-9](https://doi.org/10.1016/S0166-9834(00)81716-9).
- [41] C.A. Trujillo, U.N. Uribe, P.-P. Knops-Gerrits, L.A. Oviedo A, P.A. Jacobs, The Mechanism of Zeolite Y Destruction by Steam in the Presence of Vanadium, *J. Catal.* 168 (1997) 1–15. <https://doi.org/10.1006/jcat.1997.1550>.
- [42] G. Martino, Catalysis for oil refining and petrochemistry, recent developments and future trends, *Stud. Surf. Sci. Catal.* 130 A (2000) 83–103.
- [43] S. Sahebdehfar, M.T. Ravanchi, F. Tahiri Zangeneh, S. Mehrazma, S. Rajabi, Kinetic study of propane dehydrogenation and side reactions over Pt–Sn/Al<sub>2</sub>O<sub>3</sub> catalyst, *Chem. Eng. Res. Des.* 90 (2012) 1090–1097. <https://doi.org/10.1016/j.cherd.2011.11.004>.
- [44] K. Takehira, Y. Ohishi, T. Shishido, T. Kawabata, K. Takaki, Q. Zhang, Y. Wang, Behavior of active sites on Cr-MCM-41 catalysts during the dehydrogenation of propane with CO<sub>2</sub>, *J. Catal.* 224 (2004) 404–416. <https://doi.org/10.1016/j.jcat.2004.03.014>.
- [45] X. Shi, S. Ji, K. Wang, Oxidative Dehydrogenation of Ethane to Ethylene with Carbon dioxide over Cr–Ce/SBA-15 Catalysts, *Catal. Lett.* 125 (2008) 331–339. <https://doi.org/10.1007/s10562-008-9569-3>.
- [46] P. Michorczyk, J. Ogonowski, M. Niemczyk, Investigation of catalytic activity of CrSBA-1 materials obtained by direct method in the dehydrogenation of propane with CO<sub>2</sub>, *Appl. Catal. Gen.* 374 (2010) 142–149. <https://doi.org/10.1016/j.apcata.2009.11.040>.
- [47] J. Ogonowski, E. Skrzyńska, Dehydrogenation of isobutane in the presence of carbon dioxide over supported vanadium oxide catalysts, *React. Kinet. Catal. Lett.* 88 (2006) 293–300. <https://doi.org/10.1007/s11144-006-0064-9>.

- [48] J. Ogonowski, E. Skrzyńska, Activity of vanadium magnesium oxide supported catalysts in the dehydrogenation of isobutane, *Catal. Lett.* 111 (2006) 79–85. <https://doi.org/10.1007/s10562-006-0132-9>.
- [49] J. Ogonowski, E. Skrzyńska, Deactivation of VMgOx Catalysts by Coke in the Process of Isobutane Dehydrogenation with Carbon Dioxide, *Catal. Lett.* 121 (2008) 234–240. <https://doi.org/10.1007/s10562-007-9320-5>.
- [50] R.K. Grasselli, Advances and future trends in selective oxidation and ammoxidation catalysis, *Catal. Today.* 49 (1999) 141–153. [https://doi.org/10.1016/S0920-5861\(98\)00418-0](https://doi.org/10.1016/S0920-5861(98)00418-0).
- [51] T. Matsuda, I. Koike, N. Kubo, E. Kikuchi, Dehydrogenation of isobutane to isobutene in a palladium membrane reactor, *J. Membr. Sci.* 77 (1993) 283. [https://doi.org/10.1016/0376-7388\(93\)85076-9](https://doi.org/10.1016/0376-7388(93)85076-9).
- [52] J.P. Collins, R.W. Schwartz, R. Sehgal, T.L. Ward, C.J. Brinker, G.P. Hagen, C.A. Udovich, Catalytic Dehydrogenation of Propane in Hydrogen Permselective Membrane Reactors, *Ind. Eng. Chem. Res.* 35 (1996) 4398–4405. <https://doi.org/10.1021/ie960133m>.
- [53] L. Kiwi-Minsker, O. Wolfrath, A. Renken, Membrane reactor microstructured by filamentous catalyst, *Chem. Eng. Sci.* 57 (2002) 4947–4953. [https://doi.org/10.1016/S0009-2509\(02\)00294-4](https://doi.org/10.1016/S0009-2509(02)00294-4).
- [54] G. Szejner, M. Sheintuch, Application of a carbon membrane reactor for dehydrogenation reactions, *Chem. Eng. Sci.* 59 (2004) 2013–2021. <https://doi.org/10.1016/j.ces.2004.01.051>.
- [55] V.S. Bobrov, N.G. Dígurov, V.V. Skudin, Propane dehydrogenation using catalytic membrane, *J. Membr. Sci.* 253 (2005) 233–242. <https://doi.org/10.1016/j.memsci.2004.11.037>.
- [56] W. Liang, R. Hughes, The catalytic dehydrogenation of isobutane to isobutene in a palladium/silver composite membrane reactor, *Catal. Today.* 104 (2005) 238–243. <https://doi.org/10.1016/j.cattod.2005.03.045>.
- [57] J.A. Medrano, I. Julián, F.R. García-García, K. Li, J. Herguido, M. Menéndez, Two-Zone Fluidized Bed Reactor (TZFBR) with Palladium Membrane for Catalytic Propane Dehydrogenation:

- Experimental Performance Assessment, *Ind. Eng. Chem. Res.* 52 (2013) 3723–3731. <https://doi.org/10.1021/ie303185p>.
- [58] R. Dittmeyer, V. Höllein, K. Daub, Membrane reactors for hydrogenation and dehydrogenation processes based on supported palladium, *J. Mol. Catal. Chem.* 173 (2001) 135–184. [https://doi.org/10.1016/S1381-1169\(01\)00149-2](https://doi.org/10.1016/S1381-1169(01)00149-2).
- [59] M. Takht Ravanchi, T. Kaghazchi, A. Kargari, Application of membrane separation processes in petrochemical industry: a review, *Desalination*. 235 (2009) 199–244. <https://doi.org/10.1016/j.desal.2007.10.042>.
- [60] M.D. Falco, L. Marrelli, G. Iaquaniello, eds., *Membrane Reactors for Hydrogen Production Processes*, Springer-Verlag, London, 2011. <https://www.springer.com/gp/book/9780857291509> (accessed July 14, 2019).
- [61] Y. Shan, Z. Sui, Y. Zhu, D. Chen, X. Zhou, Effect of steam addition on the structure and activity of Pt–Sn catalysts in propane dehydrogenation, *Chem. Eng. J.* 278 (2015) 240–248. <https://doi.org/10.1016/j.cej.2014.09.107>.
- [62] D. Duprez, M. Hadj-Aissa, J. Barbier, Effect of steam on the coking of platinum catalysts: I. Inhibiting effect of steam at low partial pressure for the dehydrogenation of cyclopentane and the coking reaction, *Appl. Catal.* 49 (1989) 67–74. [https://doi.org/10.1016/S0166-9834\(00\)81422-0](https://doi.org/10.1016/S0166-9834(00)81422-0).
- [63] B.M. Weckhuysen, R.A. Schoonheydt, Alkane dehydrogenation over supported chromium oxide catalysts, *Catal. Today*. 51 (1999) 223–232. [https://doi.org/10.1016/S0920-5861\(99\)00047-4](https://doi.org/10.1016/S0920-5861(99)00047-4).
- [64] R.A. Meyers, R.A. Meyers, *Handbook of Petrochemicals Production Processes*, McGraw-Hill Prof Med/Tech, 2005.
- [65] P.R. Pujado, B.V. Vora, Make C3-C4 olefins selectively, *Hydrocarb. Process.* 69 (1990) 65–70.
- [66] I. Miracca, L. Piovesan, Light paraffins dehydrogenation in a fluidized bed reactor, *Catal. Today*. 52 (1999) 259–269. [https://doi.org/10.1016/S0920-5861\(99\)00080-2](https://doi.org/10.1016/S0920-5861(99)00080-2).



- [67] F.E. Frey, W.F. Huppke, Equilibrium Dehydrogenation of Ethane, Propane, and the Butanes, *Ind. Eng. Chem.* 25 (1933) 54–59. <https://doi.org/10.1021/ie50277a013>.
- [68] U. Olsbye, A. Virnovskaia, Ø. Prytz, S.J. Tinnemans, B.M. Weckhuysen, Mechanistic Insight in the Ethane Dehydrogenation Reaction over Cr/Al<sub>2</sub>O<sub>3</sub> Catalysts, *Catal. Lett.* 103 (2005) 143–148. <https://doi.org/10.1007/s10562-005-6521-7>.
- [69] Ch. Marcilly, B. Delmon, The activity of true Cr<sub>2</sub>O<sub>3</sub>/Al<sub>2</sub>O<sub>3</sub> solid solutions in dehydrogenation, *J. Catal.* 24 (1972) 336–347. [https://doi.org/10.1016/0021-9517\(72\)90078-4](https://doi.org/10.1016/0021-9517(72)90078-4).
- [70] F.M. Ashmawy, Surface composition and catalytic activity of chromia–alumina catalysts, *J. Chem. Soc. Faraday Trans. 1 Phys. Chem. Condens. Phases.* 76 (1980) 2096–2101. <https://doi.org/10.1039/F19807602096>.
- [71] H.J. Lugo, J.H. Lunsford, The dehydrogenation of ethane over chromium catalysts, *J. Catal.* 91 (1985) 155–166. [https://doi.org/10.1016/0021-9517\(85\)90297-0](https://doi.org/10.1016/0021-9517(85)90297-0).
- [72] W. Grünert, W. Saffert, R. Feldhaus, K. Anders, Reduction and aromatization activity of chromia-alumina catalysts: I. Reduction and break-in behavior of a potassium-promoted chromia-alumina catalyst, *J. Catal.* 99 (1986) 149–158. [https://doi.org/10.1016/0021-9517\(86\)90208-3](https://doi.org/10.1016/0021-9517(86)90208-3).
- [73] F.J. Pérez-Reina, E. Rodríguez-Castellón, A. Jiménez-López, Dehydrogenation of Propane over Chromia-Pillared Zirconium Phosphate Catalysts, *Langmuir.* 15 (1999) 8421–8428. <https://doi.org/10.1021/la990504e>.
- [74] A. Hakuli, A. Kytökivi, A.O.I. Krause, Dehydrogenation of i-butane on CrO<sub>x</sub>/Al<sub>2</sub>O<sub>3</sub> catalysts prepared by ALE and impregnation techniques, *Appl. Catal. Gen.* 190 (2000) 219–232. [https://doi.org/10.1016/S0926-860X\(99\)00310-5](https://doi.org/10.1016/S0926-860X(99)00310-5).
- [75] A. Kytökivi, J.-P. Jacobs, A. Hakuli, J. Meriläinen, H.H. Brongersma, Surface Characteristics and Activity of Chromia/Alumina Catalysts

- Prepared by Atomic Layer Epitaxy, *J. Catal.* 162 (1996) 190–197.  
<https://doi.org/10.1006/jcat.1996.0276>.
- [76] P. Michorczyk, P. Pietrzyk, J. Ogonowski, Preparation and characterization of SBA-1–supported chromium oxide catalysts for CO<sub>2</sub> assisted dehydrogenation of propane, *Microporous Mesoporous Mater.* 161 (2012) 56–66.  
<https://doi.org/10.1016/j.micromeso.2012.05.011>.
- [77] I. Horiuti, M. Polanyi, Exchange reactions of hydrogen on metallic catalysts, *Trans. Faraday Soc.* 30 (1934) 1164–1172.  
<https://doi.org/10.1039/TF9343001164>.
- [78] R.D. Cortright, P.E. Levin, J.A. Dumesic, Kinetic Studies of Isobutane Dehydrogenation and Isobutene Hydrogenation over Pt/Sn-Based Catalysts, *Ind. Eng. Chem. Res.* 37 (1998) 1717–1723.  
<https://doi.org/10.1021/ie970917f>.
- [79] R.D. Cortright, J.M. Hill, J.A. Dumesic, Selective dehydrogenation of isobutane over supported Pt/Sn catalysts, *Catal. Today.* 55 (2000) 213–223. [https://doi.org/10.1016/S0920-5861\(99\)00249-7](https://doi.org/10.1016/S0920-5861(99)00249-7).
- [80] B. Zheng, W. Hua, Y. Yue, Z. Gao, Dehydrogenation of propane to propene over different polymorphs of gallium oxide, *J. Catal.* 232 (2005) 143–151. <https://doi.org/10.1016/j.jcat.2005.03.001>.
- [81] Q. Li, Z. Sui, X. Zhou, D. Chen, Kinetics of propane dehydrogenation over Pt–Sn/Al<sub>2</sub>O<sub>3</sub> catalyst, *Appl. Catal. Gen.* 398 (2011) 18–26.  
<https://doi.org/10.1016/j.apcata.2011.01.039>.
- [82] S. Sokolov, M. Stoyanova, U. Rodemerck, D. Linke, E.V. Kondratenko, Comparative study of propane dehydrogenation over V-, Cr-, and Pt-based catalysts: Time on-stream behavior and origins of deactivation, *J. Catal.* 293 (2012) 67–75.  
<https://doi.org/10.1016/j.jcat.2012.06.005>.
- [83] A.W. Hauser, J. Gomes, M. Bajdich, M. Head-Gordon, A.T. Bell, Subnanometer-sized Pt/Sn alloy cluster catalysts for the dehydrogenation of linear alkanes, *Phys. Chem. Chem. Phys.* 15 (2013) 20727–20734. <https://doi.org/10.1039/C3CP53796J>.

- [84] V. Galvita, G. Siddiqi, P. Sun, A.T. Bell, Ethane dehydrogenation on Pt/Mg(Al)O and PtSn/Mg(Al)O catalysts, *J. Catal.* 271 (2010) 209–219. <https://doi.org/10.1016/j.jcat.2010.01.016>.
- [85] J.A. Moulijn, A.E. van Diepen, F. Kapteijn, Catalyst deactivation: is it predictable?: What to do?, *Appl. Catal. Gen.* 212 (2001) 3–16. [https://doi.org/10.1016/S0926-860X\(00\)00842-5](https://doi.org/10.1016/S0926-860X(00)00842-5).
- [86] H. Noda, S. Tone, T. Otake, Kinetics of Isopentane Dehydrogenation on Chromia-Alumina Catalyst with Catalyst Fouling, *J. Chem. Eng. Jpn.* 7 (1974) 110–116. <https://doi.org/10.1252/jcej.7.110>.
- [87] R. Toei, K. Nakanishi, K. Yamada, M. Okazaki, Catalyst Fouling in the Dehydrogenation of n-Butane over Chromia-Alumina Catalysts, *J. Chem. Eng. Jpn.* 8 (1975) 131–136. <https://doi.org/10.1252/jcej.8.131>.
- [88] H.E. Swift, H. Beuther, R.J. Rennard, Elimination of Excessive Carbon Formation during Catalytic Butene Dehydrogenation, *Prod. RD.* 15 (1976) 131–136. <https://doi.org/10.1021/i360058a006>.
- [89] P.G. Menon, Coke on catalysts-harmful, harmless, invisible and beneficial types, *J. Mol. Catal.* 59 (1990) 207–220. [https://doi.org/10.1016/0304-5102\(90\)85053-K](https://doi.org/10.1016/0304-5102(90)85053-K).
- [90] M.-L. Yang, Y.-A. Zhu, C. Fan, Z.-J. Sui, D. Chen, X.-G. Zhou, Density functional study of the chemisorption of C1, C2 and C3 intermediates in propane dissociation on Pt(111), *J. Mol. Catal. Chem.* 321 (2010) 42–49. <https://doi.org/10.1016/j.molcata.2010.01.017>.
- [91] G. Siddiqi, P. Sun, V. Galvita, A.T. Bell, Catalyst performance of novel Pt/Mg(Ga)(Al)O catalysts for alkane dehydrogenation, *J. Catal.* 274 (2010) 200–206. <https://doi.org/10.1016/j.jcat.2010.06.016>.
- [92] F. Zaera, D. Chrysostomou, Propylene on Pt(111), *Surf. Sci.* 457 (2000) 89–108. [https://doi.org/10.1016/S0039-6028\(00\)00337-X](https://doi.org/10.1016/S0039-6028(00)00337-X).

- [93] D. Chrysostomou, F. Zaera, Thermal Chemistry of C3 Allyl Groups on Pt(111), *J. Phys. Chem. B.* 105 (2001) 1003–1011. <https://doi.org/10.1021/jp0028608>.
- [94] Y. Chen, D.G. Vlachos, Hydrogenation of Ethylene and Dehydrogenation and Hydrogenolysis of Ethane on Pt(111) and Pt(211): A Density Functional Theory Study, *J. Phys. Chem. C.* 114 (2010) 4973–4982. <https://doi.org/10.1021/jp909163z>.
- [95] T.A. (Xander) Nijhuis, S.J. Tinnemans, T. Visser, B.M. Weckhuysen, Operando spectroscopic investigation of supported metal oxide catalysts by combined time-resolved UV-VIS/Raman/on-line mass spectrometry, *Phys. Chem. Chem. Phys.* 5 (2003) 4361–4365. <https://doi.org/10.1039/B305786K>.
- [96] S.J. Tinnemans, M.H.F. Kox, T.A. Nijhuis, T. Visser, B.M. Weckhuysen, Real time quantitative Raman spectroscopy of supported metal oxide catalysts without the need of an internal standard, *Phys. Chem. Chem. Phys.* 7 (2005) 211–216. <https://doi.org/10.1039/B414427A>.
- [97] R.M.J. Fiedorow, B.S. Chahar, S.E. Wanke, The sintering of supported metal catalysts: II. Comparison of sintering rates of supported Pt, Ir, and Rh catalysts in hydrogen and oxygen, *J. Catal.* 51 (1978) 193–202. [https://doi.org/10.1016/0021-9517\(78\)90293-2](https://doi.org/10.1016/0021-9517(78)90293-2).
- [98] S.F. Adler, J.J. Keavney, The Physical Nature of Supported Platinum, *J. Phys. Chem.* 64 (1960) 208–212. <https://doi.org/10.1021/j100831a005>.
- [99] H. Lieske, G. Lietz, H. Spindler, J. Völter, Reactions of platinum in oxygen- and hydrogen-treated Pt $\gamma$ -Al $_2$ O $_3$  catalysts: I. Temperature-programmed reduction, adsorption, and redispersion of platinum, *J. Catal.* 81 (1983) 8–16. [https://doi.org/10.1016/0021-9517\(83\)90142-2](https://doi.org/10.1016/0021-9517(83)90142-2).
- [100] T.J. Lee, Y.G. Kim, Redispersion of supported platinum catalysts, *J. Catal.* 90 (1984) 279–291. [https://doi.org/10.1016/0021-9517\(84\)90256-2](https://doi.org/10.1016/0021-9517(84)90256-2).

- [101] F. Le Normand, A. Borgna, T.F. Garetto, C.R. Apesteguia, B. Moraweck, Redispersion of Sintered Pt/Al<sub>2</sub>O<sub>3</sub> Naphtha Reforming Catalysts: An in Situ Study Monitored by X-ray Absorption Spectroscopy, *J. Phys. Chem.* 100 (1996) 9068–9076. <https://doi.org/10.1021/jp960080m>.
- [102] A. Monzón, T.F. Garetto, A. Borgna, Sintering and redispersion of Pt/ $\gamma$ -Al<sub>2</sub>O<sub>3</sub> catalysts: a kinetic model, *Appl. Catal. Gen.* 248 (2003) 279–289. [https://doi.org/10.1016/S0926-860X\(03\)00300-4](https://doi.org/10.1016/S0926-860X(03)00300-4).
- [103] B.M. Weckhuysen, L.M. De Ridder, R.A. Schoonheydt, A quantitative diffuse reflectance spectroscopy study of supported chromium catalysts, *J. Phys. Chem.* 97 (1993) 4756–4763. <https://doi.org/10.1021/j100120a030>.
- [104] B.M. Weckhuysen, L.M. De Ridder, P.J. Grobet, R.A. Schoonheydt, Redox Behavior and Dispersion of Supported Chromium Catalysts, *J. Phys. Chem.* 99 (1995) 320–326. <https://doi.org/10.1021/j100001a048>.
- [105] S. Rossignol, C. Kappenstein, Effect of doping elements on the thermal stability of transition alumina, *Int. J. Inorg. Mater.* 3 (2001) 51–58. [https://doi.org/10.1016/S1466-6049\(00\)00088-X](https://doi.org/10.1016/S1466-6049(00)00088-X).
- [106] L. Wachowski, P. Kirszenstejn, R. Łopatka, B. Czajka, Studies of physicochemical and surface properties of alumina modified with rare-earth oxides I. Preparation, structure and thermal stability, *Mater. Chem. Phys.* 37 (1994) 29–38. [https://doi.org/10.1016/0254-0584\(94\)90067-1](https://doi.org/10.1016/0254-0584(94)90067-1).
- [107] S.A. Bocanegra, A.A. Castro, A. Guerrero-Ruíz, O.A. Scelza, S.R. de Miguel, Characteristics of the metallic phase of Pt/Al<sub>2</sub>O<sub>3</sub> and Na-doped Pt/Al<sub>2</sub>O<sub>3</sub> catalysts for light paraffins dehydrogenation, *Chem. Eng. J.* 118 (2006) 161–166. <https://doi.org/10.1016/j.cej.2006.02.004>.
- [108] M.L. Casella, G.J. Siri, G.F. Santori, O.A. Ferretti, M.M. Ramírez-Corredores, Surface Characterization of Li-Modified Platinum/Tin Catalysts for Isobutane Dehydrogenation, *Langmuir.* 16 (2000) 5639–5643. <https://doi.org/10.1021/la991437r>.

- [109] G.J. Siri, G.R. Bertolini, M.L. Casella, O.A. Ferretti, PtSn/ $\gamma$ -Al<sub>2</sub>O<sub>3</sub> isobutane dehydrogenation catalysts: The effect of alkaline metals addition, *Mater. Lett.* 59 (2005) 2319–2324. <https://doi.org/10.1016/j.matlet.2005.03.013>.
- [110] S.R. de Miguel, S.A. Bocanegra, I.M.J. Vilella, A. Guerrero-Ruiz, O.A. Scelza, Characterization and Catalytic Performance of PtSn Catalysts Supported on Al<sub>2</sub>O<sub>3</sub> and Na-doped Al<sub>2</sub>O<sub>3</sub> in n-butane Dehydrogenation, *Catal. Lett.* 119 (2007) 5–15. <https://doi.org/10.1007/s10562-007-9215-5>.
- [111] M. Tasbihi, F. Feyzi, M.A. Amlashi, A.Z. Abdullah, A.R. Mohamed, Effect of the addition of potassium and lithium in Pt–Sn/Al<sub>2</sub>O<sub>3</sub> catalysts for the dehydrogenation of isobutane, *Fuel Process. Technol.* 88 (2007) 883–889. <https://doi.org/10.1016/j.fuproc.2007.04.007>.
- [112] H. Zhao, H. Song, L. Xu, L. Chou, Isobutane dehydrogenation over the mesoporous Cr<sub>2</sub>O<sub>3</sub>/Al<sub>2</sub>O<sub>3</sub> catalysts synthesized from a metal-organic framework MIL-101, *Appl. Catal. Gen.* 456 (2013) 188–196. <https://doi.org/10.1016/j.apcata.2013.02.018>.
- [113] R.J. Rennard, J. Freel, The role of sulfur in deactivation of PtMgAl<sub>2</sub>O<sub>4</sub> for propane dehydrogenation, *J. Catal.* 98 (1986) 235–244. [https://doi.org/10.1016/0021-9517\(86\)90312-X](https://doi.org/10.1016/0021-9517(86)90312-X).
- [114] G. Aguilar-Ríos, M.A. Valenzuela, H. Armendariz, P. Salas, J.M. Domínguez, D.R. Acosta, I. Schifter, Metal-support effects and catalytic properties of platinum supported on zinc aluminate, *Appl. Catal. Gen.* 90 (1992) 25–34. [https://doi.org/10.1016/0926-860X\(92\)80245-8](https://doi.org/10.1016/0926-860X(92)80245-8).
- [115] S.A. Bocanegra, A. Guerrero-Ruiz, S.R. de Miguel, O.A. Scelza, Performance of PtSn catalysts supported on MAI<sub>2</sub>O<sub>4</sub> (M: Mg or Zn) in n-butane dehydrogenation: characterization of the metallic phase, *Appl. Catal. Gen.* 277 (2004) 11–22. <https://doi.org/10.1016/j.apcata.2004.08.016>.
- [116] Y. Lai, S. He, X. Li, C. Sun, K. Seshan, Dehydrogenation of n-dodecane over PtSn/MgAlO catalysts: Investigating the catalyst

- performance while monitoring the products, *Appl. Catal. Gen.* 469 (2014) 74–80. <https://doi.org/10.1016/j.apcata.2013.09.042>.
- [117] X. Zhang, Y. Yue, Z. Gao, Chromium Oxide Supported on Mesoporous SBA-15 as Propane Dehydrogenation and Oxidative Dehydrogenation Catalysts, *Catal. Lett.* 83 (2002) 19–25. <https://doi.org/10.1023/A:1020693028720>.
- [118] J.M. Hill, R.D. Cortright, J.A. Dumesic, Silica- and L-zeolite-supported Pt, Pt/Sn and Pt/Sn/K catalysts for isobutane dehydrogenation, *Appl. Catal. Gen.* 168 (1998) 9–21. [https://doi.org/10.1016/S0926-860X\(97\)00338-4](https://doi.org/10.1016/S0926-860X(97)00338-4).
- [119] H. Lieske, A. Sárkány, J. Völter, Hydrocarbon adsorption and coke formation on Pt/Al<sub>2</sub>O<sub>3</sub> and Pt-Sn/Al<sub>2</sub>O<sub>3</sub> catalysts, *Appl. Catal.* 30 (1987) 69–80. [https://doi.org/10.1016/S0166-9834\(00\)81012-X](https://doi.org/10.1016/S0166-9834(00)81012-X).
- [120] J. Wu, Z. Peng, A.T. Bell, Effects of composition and metal particle size on ethane dehydrogenation over Pt<sub>x</sub>Sn<sub>100-x</sub>/Mg(Al)O (70 ≤ x ≤ 100), *J. Catal.* 311 (2014) 161–168. <https://doi.org/10.1016/j.jcat.2013.11.017>.
- [121] B.M. Nagaraja, C.-H. Shin, K.-D. Jung, Selective and stable bimetallic PtSn/θ-Al<sub>2</sub>O<sub>3</sub> catalyst for dehydrogenation of n-butane to n-butenes, *Appl. Catal. Gen.* 467 (2013) 211–223. <https://doi.org/10.1016/j.apcata.2013.07.022>.
- [122] R.D. Cortright, J.A. Dumesic, Effects of Potassium on Silica-Supported Pt and Pt/Sn Catalysts for Isobutane Dehydrogenation, *J. Catal.* 157 (1995) 576–583. <https://doi.org/10.1006/jcat.1995.1322>.
- [123] M.A. Natal-Santiago, S.G. Podkolzin, R.D. Cortright, J.A. Dumesic, Microcalorimetric studies of interactions of ethene, isobutene, and isobutane with silica-supported Pd, Pt, and PtSn, *Catal. Lett.* 45 (1997) 155–163.
- [124] J. Shen, J.M. Hill, R.M. Watwe, B.E. Spiewak, J.A. Dumesic, Microcalorimetric, Infrared Spectroscopic, and DFT Studies of Ethylene Adsorption on Pt/SiO<sub>2</sub> and Pt–Sn/SiO<sub>2</sub> Catalysts, *J. Phys.*

- Chem. B. 103 (1999) 3923–3934.  
<https://doi.org/10.1021/jp9902452>.
- [125] M.-L. Yang, Y.-A. Zhu, X.-G. Zhou, Z.-J. Sui, D. Chen, First-Principles Calculations of Propane Dehydrogenation over PtSn Catalysts, *ACS Catal.* 2 (2012) 1247–1258.  
<https://doi.org/10.1021/cs300031d>.
- [126] L. Nykänen, K. Honkala, Density Functional Theory Study on Propane and Propene Adsorption on Pt(111) and PtSn Alloy Surfaces, *J. Phys. Chem. C.* 115 (2011) 9578–9586.  
<https://doi.org/10.1021/jp1121799>.
- [127] J. Gao, H. Zhao, X. Yang, B.E. Koel, S.G. Podkolzin, Geometric Requirements for Hydrocarbon Catalytic Sites on Platinum Surfaces, *Angew. Chem. Int. Ed.* 53 (2014) 3641–3644.  
<https://doi.org/10.1002/anie.201309043>.
- [128] J. Silvestre-Albero, M.A. Sanchez-Castillo, R. He, A. Sepúlveda-Escribano, F. Rodríguez-Reinoso, J.A. Dumesic, Microcalorimetric, reaction kinetics and DFT studies of Pt–Zn/X-zeolite for isobutane dehydrogenation, *Catal. Lett.* 74 (2001) 17–25.  
<https://doi.org/10.1023/A:1016630622312>.
- [129] J. Silvestre-Albero, J.C. Serrano-Ruiz, A. Sepúlveda-Escribano, F. Rodríguez-Reinoso, Modification of the catalytic behaviour of platinum by zinc in crotonaldehyde hydrogenation and iso-butane dehydrogenation, *Appl. Catal. Gen.* 292 (2005) 244–251.  
<https://doi.org/10.1016/j.apcata.2005.06.005>.
- [130] P.L. De Cola, R. Gläser, J. Weitkamp, Non-oxidative propane dehydrogenation over Pt–Zn-containing zeolites, *Appl. Catal. Gen.* 306 (2006) 85–97. <https://doi.org/10.1016/j.apcata.2006.03.028>.
- [131] C. Yu, H. Xu, Q. Ge, W. Li, Properties of the metallic phase of zinc-doped platinum catalysts for propane dehydrogenation, *J. Mol. Catal. Chem.* 266 (2007) 80–87.  
<https://doi.org/10.1016/j.molcata.2006.10.025>.
- [132] J. Silvestre-Albero, J.C. Serrano-Ruiz, A. Sepúlveda-Escribano, F. Rodríguez-Reinoso, Zn-modified MCM-41 as support for Pt



- catalysts, *Appl. Catal. Gen.* 351 (2008) 16–23. <https://doi.org/10.1016/j.apcata.2008.08.021>.
- [133] B.K. Vu, M.B. Song, I.Y. Ahn, Y.-W. Suh, D.J. Suh, W.-I. Kim, H.-L. Koh, Y.G. Choi, E.W. Shin, Pt–Sn alloy phases and coke mobility over Pt–Sn/Al<sub>2</sub>O<sub>3</sub> and Pt–Sn/ZnAl<sub>2</sub>O<sub>4</sub> catalysts for propane dehydrogenation, *Appl. Catal. Gen.* 400 (2011) 25–33. <https://doi.org/10.1016/j.apcata.2011.03.057>.
- [134] E.L. Jablonski, A.A. Castro, O.A. Scelza, S.R. de Miguel, Effect of Ga addition to Pt/Al<sub>2</sub>O<sub>3</sub> on the activity, selectivity and deactivation in the propane dehydrogenation, *Appl. Catal. Gen.* 183 (1999) 189–198. [https://doi.org/10.1016/S0926-860X\(99\)00058-7](https://doi.org/10.1016/S0926-860X(99)00058-7).
- [135] P. Sun, G. Siddiqi, M. Chi, A.T. Bell, Synthesis and characterization of a new catalyst Pt/Mg(Ga)(Al)O for alkane dehydrogenation, *J. Catal.* 274 (2010) 192–199. <https://doi.org/10.1016/j.jcat.2010.06.017>.
- [136] P. Sun, G. Siddiqi, W.C. Vining, M. Chi, A.T. Bell, Novel Pt/Mg(In)(Al)O catalysts for ethane and propane dehydrogenation, *J. Catal.* 282 (2011) 165–174. <https://doi.org/10.1016/j.jcat.2011.06.008>.
- [137] A.D. Ballarini, S.R. de Miguel, A.A. Castro, O.A. Scelza, n-Decane dehydrogenation on Pt, PtSn and PtGe supported on spinels prepared by different methods of synthesis, *Appl. Catal. Gen.* 467 (2013) 235–245. <https://doi.org/10.1016/j.apcata.2013.07.030>.
- [138] K. Nakagawa, M. Okamura, N. Ikenaga, T. Suzuki, K. Nakagawa, M. Okamura, T. Suzuki, T. Kobayashi, T. Kobayashi, Dehydrogenation of ethane over gallium oxide in the presence of carbon dioxide, *Chem. Commun.* (1998) 1025–1026. <https://doi.org/10.1039/A800184G>.
- [139] K. Nakagawa, C. Kajita, K. Okumura, N. Ikenaga, M. Nishitani-Gamo, T. Ando, T. Kobayashi, T. Suzuki, Role of Carbon Dioxide in the Dehydrogenation of Ethane over Gallium-Loaded Catalysts, *J. Catal.* 203 (2001) 87–93. <https://doi.org/10.1006/jcat.2001.3306>.

- [140] A.S. Russell, J.J. Stokes, Role of Surface Area in Dehydrocyclization Catalysis, *Ind. Eng. Chem.* 38 (1946) 1071–1074. <https://doi.org/10.1021/ie50442a027>.
- [141] M.E. Harlin, L.B. Backman, A.O.I. Krause, O.J.T. Jylhä, Activity of Molybdenum Oxide Catalyst in the Dehydrogenation of n-Butane, *J. Catal.* 183 (1999) 300–313. <https://doi.org/10.1006/jcat.1999.2413>.
- [142] R. López Cordero, F.J. Gil Llambias, A. López Agudo, Temperature-programmed reduction and zeta potential studies of the structure of Mo/O<sub>3</sub>Al<sub>2</sub>O<sub>3</sub> and Mo/O<sub>3</sub>SiO<sub>2</sub> catalysts effect of the impregnation pH and molybdenum loading, *Appl. Catal.* 74 (1991) 125–136. [https://doi.org/10.1016/0166-9834\(91\)90013-X](https://doi.org/10.1016/0166-9834(91)90013-X).
- [143] Z. Wu, P.C. Stair, UV Raman spectroscopic studies of V/ $\theta$ -Al<sub>2</sub>O<sub>3</sub> catalysts in butane dehydrogenation, *J. Catal.* 237 (2006) 220–229. <https://doi.org/10.1016/j.jcat.2005.11.005>.
- [144] S.D. Jackson, S. Rugmini, Dehydrogenation of n-butane over vanadia catalysts supported on  $\theta$ -alumina, *J. Catal.* 251 (2007) 59–68. <https://doi.org/10.1016/j.jcat.2007.07.015>.
- [145] J. McGregor, Z. Huang, G. Shiko, L.F. Gladden, R.S. Stein, M.J. Duer, Z. Wu, P.C. Stair, S. Rugmini, S.D. Jackson, The role of surface vanadia species in butane dehydrogenation over VO<sub>x</sub>/Al<sub>2</sub>O<sub>3</sub>, *Catal. Today.* 142 (2009) 143–151. <https://doi.org/10.1016/j.cattod.2008.07.022>.
- [146] Report: New propylene production technologies hold great promise, *Oil Gas J.* 102 (2004) 50–52.
- [147] F. Cavani, F. Trifirò, The oxidative dehydrogenation of ethane and propane as an alternative way for the production of light olefins, *Catal. Today.* 24 (1995) 307–313. [https://doi.org/10.1016/0920-5861\(95\)00051-G](https://doi.org/10.1016/0920-5861(95)00051-G).
- [148] G. Centi, F. Cavani, F. Trifirò, *Selective Oxidation by Heterogeneous Catalysis*, Springer US, 2001. <https://www.springer.com/gp/book/9780306462658> (accessed August 16, 2019).

- [149] D. Sanfilippo, I. Miracca, Dehydrogenation of paraffins: synergies between catalyst design and reactor engineering, *Catal. Today*. 111 (2006) 133–139. <https://doi.org/10.1016/j.cattod.2005.10.012>.
- [150] D. Sanfilippo, Dehydrogenation of Paraffins; Key Technology for Petrochemicals and Fuels, *CATTECH*. 4 (2000) 56–73. <https://doi.org/10.1023/A:1011947328263>.
- [151] V.D. Sokolovskii, Principles of Oxidative Catalysis on Solid Oxides, *Catal. Rev.* 32 (1990) 1–49. <https://doi.org/10.1080/01614949009349939>.
- [152] G. Emig, M.A. Liauw, New Reaction Engineering Concepts for Selective Oxidation Reactions, *Top. Catal.* 21 (2002) 11–24. <https://doi.org/10.1023/A:1020543729259>.
- [153] F. Klose, T. Wolff, S. Thomas, A. Seidel-Morgenstern, Operation modes of packed-bed membrane reactors in the catalytic oxidation of hydrocarbons, *Appl. Catal. Gen.* 257 (2004) 193–199. <https://doi.org/10.1016/j.apcata.2003.07.009>.
- [154] R.H. Crabtree, Alkane C–H activation and functionalization with homogeneous transition metal catalysts: a century of progress—a new millennium in prospect, *J. Chem. Soc. Dalton Trans.* (2001) 2437–2450. <https://doi.org/10.1039/B103147N>.
- [155] F. Cavani, J.H. Teles, Sustainability in Catalytic Oxidation: An Alternative Approach or a Structural Evolution?, *ChemSusChem*. (2009). <https://doi.org/10.1002/cssc.200900020>.
- [156] A. Christodoulakis, M. Machli, A.A. Lemonidou, S. Boghosian, Molecular structure and reactivity of vanadia-based catalysts for propane oxidative dehydrogenation studied by in situ Raman spectroscopy and catalytic activity measurements, *J. Catal.* 222 (2004) 293–306. <https://doi.org/10.1016/j.jcat.2003.10.007>.
- [157] J.T. Grant, C.A. Carrero, F. Goeltl, J. Venegas, P. Mueller, S.P. Burt, S.E. Specht, W.P. McDermott, A. Chiericato, I. Hermans, Selective oxidative dehydrogenation of propane to propene using boron nitride catalysts, *Science*. 354 (2016) 1570–1573. <https://doi.org/10.1126/science.aaf7885>.

- [158] E.A. Mamedov, V. Cortés Corberán, Oxidative dehydrogenation of lower alkanes on vanadium oxide-based catalysts. The present state of the art and outlooks, *Appl. Catal. Gen.* 127 (1995) 1–40. [https://doi.org/10.1016/0926-860X\(95\)00056-9](https://doi.org/10.1016/0926-860X(95)00056-9).
- [159] C.A. Carrero, R. Schloegl, I.E. Wachs, R. Schomaecker, Critical Literature Review of the Kinetics for the Oxidative Dehydrogenation of Propane over Well-Defined Supported Vanadium Oxide Catalysts, *ACS Catal.* 4 (2014) 3357–3380. <https://doi.org/10.1021/cs5003417>.
- [160] R. Grabowski, Kinetics of oxidative dehydrogenation of C2-C3 alkanes on oxide catalysts, *Catal. Rev. - Sci. Eng.* 48 (2006) 199–268. <https://doi.org/10.1080/01614940600631413>.
- [161] E.V. Kondratenko, M. Cherian, M. Baerns, D. Su, R. Schlögl, X. Wang, I.E. Wachs, Oxidative dehydrogenation of propane over V/MCM-41 catalysts: comparison of O<sub>2</sub> and N<sub>2</sub>O as oxidants, *J. Catal.* 234 (2005) 131–142. <https://doi.org/10.1016/j.jcat.2005.05.025>.
- [162] E.V. Kondratenko, M. Baerns, Catalytic oxidative dehydrogenation of propane in the presence of O<sub>2</sub> and N<sub>2</sub>O—the role of vanadia distribution and oxidant activation, *Appl. Catal. Gen.* 222 (2001) 133–143. [https://doi.org/10.1016/S0926-860X\(01\)00836-5](https://doi.org/10.1016/S0926-860X(01)00836-5).
- [163] T. Ren, M. Patel, K. Blok, Olefins from conventional and heavy feedstocks: Energy use in steam cracking and alternative processes, *Energy.* 31 (2006) 425–451. <https://doi.org/10.1016/j.energy.2005.04.001>.
- [164] E.G. Rightor, C.L. Tway, Global energy & emissions reduction potential of chemical process improvements, *Catal. Today.* 258 (2015) 226–229. <https://doi.org/10.1016/j.cattod.2015.02.023>.
- [165] F. Cavani, Catalytic selective oxidation faces the sustainability challenge: turning points, objectives reached, old approaches revisited and solutions still requiring further investigation, *J. Chem. Technol. Biotechnol.* 85 (2010) 1175–1183. <https://doi.org/10.1002/jctb.2389>.

- [166] C. Carrero, M. Kauer, A. Dinse, T. Wolfram, N. Hamilton, A. Trunschke, R. Schlögl, R. Schomäcker, High performance (VOx)<sub>n</sub>–(TiOx)<sub>m</sub>/SBA-15 catalysts for the oxidative dehydrogenation of propane, *Catal. Sci. Technol.* 4 (2014) 786–794. <https://doi.org/10.1039/C3CY00625E>.
- [167] F. Klose, T. Wolff, S. Thomas, A. Seidel-Morgenstern, Concentration and residence time effects in packed bed membrane reactors, *Catal. Today.* 82 (2003) 25–40. [https://doi.org/10.1016/S0920-5861\(03\)00199-8](https://doi.org/10.1016/S0920-5861(03)00199-8).
- [168] P. Marín, C. Hamel, S. Ordóñez, F.V. Díez, E. Tsotsas, A. Seidel-Morgenstern, Analysis of a fluidized bed membrane reactor for butane partial oxidation to maleic anhydride: 2D modelling, *Chem. Eng. Sci.* 65 (2010) 3538–3548. <https://doi.org/10.1016/j.ces.2010.02.041>.
- [169] D. Ahchieva, M. Peglow, S. Heinrich, L. Mörl, T. Wolff, F. Klose, Oxidative dehydrogenation of ethane in a fluidized bed membrane reactor, *Appl. Catal. Gen.* 296 (2005) 176–185. <https://doi.org/10.1016/j.apcata.2005.07.040>.
- [170] M.O. Guerrero-Pérez, Supported, bulk and bulk-supported vanadium oxide catalysts: A short review with an historical perspective, *Catal. Today.* 285 (2017) 226–233. <https://doi.org/10.1016/j.cattod.2017.01.037>.
- [171] P.M. Michalakos, M.C. Kung, I. Jahan, H. Kung, Selectivity Patterns in Alkane Oxidation over Mg<sub>3</sub>(VO<sub>4</sub>)<sub>2</sub>·MgO, Mg<sub>2</sub>V<sub>2</sub>O<sub>7</sub>, and (VO)<sub>2</sub>P<sub>2</sub>O<sub>7</sub>, *J. Catal.* 140 (1993) 226–242. <https://doi.org/10.1006/jcat.1993.1080>.
- [172] I.E. Wachs, J.-M. Jehng, G. Deo, B.M. Weckhuysen, V.V. Gulians, J.B. Benziger, S. Sundaresan, Fundamental Studies of Butane Oxidation over Model-Supported Vanadium Oxide Catalysts: Molecular Structure-Reactivity Relationships, *J. Catal.* 170 (1997) 75–88. <https://doi.org/10.1006/jcat.1997.1742>.

- [173] J.G. Eon, R. Olier, J.C. Volta, Oxidative Dehydrogenation of Propane on  $\gamma$ -Al<sub>2</sub>O<sub>3</sub> Supported Vanadium Oxides, *J. Catal.* 145 (1994) 318–326. <https://doi.org/10.1006/jcat.1994.1040>.
- [174] I.E. Wachs, B.M. Weckhuysen, Structure and reactivity of surface vanadium oxide species on oxide supports, *Appl. Catal. Gen.* 157 (1997) 67–90. [https://doi.org/10.1016/S0926-860X\(97\)00021-5](https://doi.org/10.1016/S0926-860X(97)00021-5).
- [175] X. Gao, J.-M. Jehng, I.E. Wachs, In Situ UV–vis–NIR Diffuse Reflectance and Raman Spectroscopic Studies of Propane Oxidation over ZrO<sub>2</sub>-Supported Vanadium Oxide Catalysts, *J. Catal.* 209 (2002) 43–50. <https://doi.org/10.1006/jcat.2002.3635>.
- [176] H. Tian, E.I. Ross, I.E. Wachs, Quantitative Determination of the Speciation of Surface Vanadium Oxides and Their Catalytic Activity, *J. Phys. Chem. B.* 110 (2006) 9593–9600. <https://doi.org/10.1021/jp055767y>.
- [177] I.E. Wachs, Recent conceptual advances in the catalysis science of mixed metal oxide catalytic materials, *Catal. Today.* 100 (2005) 79–94. <https://doi.org/10.1016/j.cattod.2004.12.019>.
- [178] G. Deo, I.E. Wachs, Surface oxide-support interaction (SOSI) for surface redox sites, *J. Catal.* 129 (1991) 307–312. [https://doi.org/10.1016/0021-9517\(91\)90036-4](https://doi.org/10.1016/0021-9517(91)90036-4).
- [179] I.E. Wachs, C.J. Keturakis, 7.06 - Monolayer Systems, in: J. Reedijk, K. Poeppelmeier (Eds.), *Compr. Inorg. Chem. II Second Ed.*, Elsevier, Amsterdam, 2013: pp. 131–151. <https://doi.org/10.1016/B978-0-08-097774-4.00717-8>.
- [180] C. Zhao, I.E. Wachs, An Operando Raman, IR, and TPSR Spectroscopic Investigation of the Selective Oxidation of Propylene to Acrolein over a Model Supported Vanadium Oxide Monolayer Catalyst, *J. Phys. Chem. C.* 112 (2008) 11363–11372. <https://doi.org/10.1021/jp801562g>.
- [181] A.D. Costa, C. Mathieu, Y. Barbaux, H. Poelman, G. Dalmai-Vennik, L. Fiermans, Observation of the V<sub>2</sub>O<sub>5</sub>(001) surface using ambient atomic force microscopy, *Surf. Sci.* 370 (1997) 339–344. [https://doi.org/10.1016/S0039-6028\(96\)00956-9](https://doi.org/10.1016/S0039-6028(96)00956-9).

- [182] J. Sambeth, A. Juan, L. Gambaro, H. Thomas, Catalytic oxidation of CH<sub>3</sub>OH to HCOOCH<sub>3</sub> on V<sub>2</sub>O<sub>5</sub>: A theoretical study, *J. Mol. Catal. Chem.* 118 (1997) 283–291. [https://doi.org/10.1016/S1381-1169\(96\)00900-4](https://doi.org/10.1016/S1381-1169(96)00900-4).
- [183] A. Kämper, A. Auroux, M. Baerns, A molecular mechanics study of the adsorption of ethane and propane on a V<sub>2</sub>O<sub>5</sub>(001) surface, *Phys. Chem. Chem. Phys.* 2 (2000) 1069–1075. <https://doi.org/10.1039/A908988H>.
- [184] A. Kämper, I. Hahndorf, M. Baerns, A molecular mechanics study of the adsorption of ethane and propane on V<sub>2</sub>O<sub>5</sub>(001) surfaces with oxygen vacancies, *Top. Catal.* 11 (2000) 77–84. <https://doi.org/10.1023/A:1027239612464>.
- [185] M.V. Martínez-Huerta, G. Deo, J.L.G. Fierro, M.A. Bañares, Operando Raman-GC Study on the Structure–Activity Relationships in V<sup>5+</sup>/CeO<sub>2</sub> Catalyst for Ethane Oxidative Dehydrogenation: The Formation of CeVO<sub>4</sub>, *J. Phys. Chem. C* 112 (2008) 11441–11447. <https://doi.org/10.1021/jp802827t>.
- [186] M. Witko, Quantum-chemical description of the active sites for the selective oxidation of hydrocarbons, *Catal. Today* 32 (1996) 89–95. [https://doi.org/10.1016/S0920-5861\(96\)00187-3](https://doi.org/10.1016/S0920-5861(96)00187-3).
- [187] M. Witko, R. Tokarz, J. Haber, Vanadium pentoxide. II. Quantum chemical modeling, *Appl. Catal. Gen.* 157 (1997) 23–44. [https://doi.org/10.1016/S0926-860X\(97\)00019-7](https://doi.org/10.1016/S0926-860X(97)00019-7).
- [188] A. Michalak, M. Witko, K. Hermann, Density functional cluster studies on the (010) surface of vanadium pentoxide, *Surf. Sci.* 375 (1997) 385–394. [https://doi.org/10.1016/S0039-6028\(96\)01286-1](https://doi.org/10.1016/S0039-6028(96)01286-1).
- [189] M. Witko, K. Hermann, R. Tokarz, Adsorption and reactions at the (010) V<sub>2</sub>O<sub>5</sub> surface: cluster model studies, *Catal. Today* 50 (1999) 553–565. [https://doi.org/10.1016/S0920-5861\(98\)00490-8](https://doi.org/10.1016/S0920-5861(98)00490-8).
- [190] G. Deo, I.E. Wachs, Reactivity of Supported Vanadium Oxide Catalysts: The Partial Oxidation of Methanol, *J. Catal.* 146 (1994) 323–334. <https://doi.org/10.1006/jcat.1994.1071>.

- [191] L.J. Burcham, G. Deo, X. Gao, I.E. Wachs, In situ IR, Raman, and UV-Vis DRS spectroscopy of supported vanadium oxide catalysts during methanol oxidation, *Top. Catal.* 11 (2000) 85–100. <https://doi.org/10.1023/A:1027275225668>.
- [192] M.A. Bañares, M. Martínez-Huerta, X. Gao, I.E. Wachs, J.L.G. Fierro, Identification and roles of the different active sites in supported vanadia catalysts by in situ techniques, in: A. Corma, F.V. Melo, S. Mendioroz, J.L.G. Fierro (Eds.), *Stud. Surf. Sci. Catal.*, Elsevier, 2000: pp. 3125–3130. [https://doi.org/10.1016/S0167-2991\(00\)80502-9](https://doi.org/10.1016/S0167-2991(00)80502-9).
- [193] M.A. Bañares, I.E. Wachs, Molecular structures of supported metal oxide catalysts under different environments, *J. Raman Spectrosc.* 33 (2002) 359–380. <https://doi.org/10.1002/jrs.866>.
- [194] C. Zhao, I.E. Wachs, Selective oxidation of propylene over model supported V<sub>2</sub>O<sub>5</sub> catalysts: Influence of surface vanadia coverage and oxide support, *J. Catal.* 257 (2008) 181–189. <https://doi.org/10.1016/j.jcat.2008.04.022>.
- [195] I.E. Wachs, M. Bañares, In Situ and Operando Raman Spectroscopy of Oxidation Catalysts, in: *Handb. Adv. Methods Process. Oxid. Catal.*, IMPERIAL COLLEGE PRESS, 2011: pp. 420–446. [https://doi.org/10.1142/9781848167513\\_0017](https://doi.org/10.1142/9781848167513_0017).
- [196] I.E. Wachs, Catalysis science of supported vanadium oxide catalysts, *Dalton Trans.* 42 (2013) 11762–11769. <https://doi.org/10.1039/C3DT50692D>.
- [197] K. Tarama, S. Yoshida, S. Ishida, H. Kakioka, Spectroscopic Studies of Catalysis by Vanadium Pentoxide, *Bull. Chem. Soc. Jpn.* 41 (1968) 2840–2845. <https://doi.org/10.1246/bcsj.41.2840>.
- [198] K. Mori, A. Miyamoto, Y. Murakami, Catalytic reactions on well-characterized vanadium oxide catalysts. 4. Oxidation of butane, *J. Phys. Chem.* 89 (1985) 4265–4269. <https://doi.org/10.1021/j100266a024>.



- [199] S.T. Oyama, Adsorbate bonding and the selection of partial and total oxidation pathways, *J. Catal.* 128 (1991) 210–217. [https://doi.org/10.1016/0021-9517\(91\)90078-I](https://doi.org/10.1016/0021-9517(91)90078-I).
- [200] A. Andersson, An oxidized surface state model of vanadium oxides and its application to catalysis, *J. Solid State Chem.* 42 (1982) 263–275. [https://doi.org/10.1016/0022-4596\(82\)90005-6](https://doi.org/10.1016/0022-4596(82)90005-6).
- [201] F. Gilardoni, A.T. Bell, A. Chakraborty, P. Boulet, Density functional theory calculations of the oxidative dehydrogenation of propane on the (010) surface of  $\text{V}_2\text{O}_5$ , *J. Phys. Chem. B.* 104 (2000) 12250–12255.
- [202] H. Fu, Z.-P. Liu, Z.-H. Li, W.-N. Wang, K.-N. Fan, Periodic Density Functional Theory Study of Propane Oxidative Dehydrogenation over  $\text{V}_2\text{O}_5(001)$  Surface, *J. Am. Chem. Soc.* 128 (2006) 11114–11123. <https://doi.org/10.1021/ja0611745>.
- [203] M.-J. Cheng, K. Chenoweth, J. Oxgaard, A. van Duin, W.A. Goddard, Single-Site Vanadyl Activation, Functionalization, and Reoxidation Reaction Mechanism for Propane Oxidative Dehydrogenation on the Cubic  $\text{V}_4\text{O}_{10}$  Cluster, *J. Phys. Chem. C.* 111 (2007) 5115–5127. <https://doi.org/10.1021/jp0663917>.
- [204] K. Alexopoulos, M.-F. Reyniers, G.B. Marin, Reaction path analysis of propane selective oxidation over  $\text{V}_2\text{O}_5$  and  $\text{V}_2\text{O}_5/\text{TiO}_2$ , *J. Catal.* 289 (2012) 127–139. <https://doi.org/10.1016/j.jcat.2012.01.019>.
- [205] A.S. Sandupatla, S.C. Nayak, C. Sivananda, G. Deo, DFT investigation into the experimentally observed influence of oxide support in the ODH of propane over supported vanadia catalysts, *Catal. Today.* (2019). <https://doi.org/10.1016/j.cattod.2018.05.058>.
- [206] C. Xiong, S. Chen, P. Yang, S. Zha, Z.-J. Zhao, J. Gong, Structure-Performance Relationships for Propane Dehydrogenation over Aluminum Supported Vanadium Oxide, *ACS Catal.* 9 (2019) 5816–5827. <https://doi.org/10.1021/acscatal.8b04701>.
- [207] Y. Wu, Y. He, T. Chen, W. Weng, H. Wan, Low temperature catalytic performance of nanosized  $\text{TiNiO}$  for oxidative dehydrogenation of

- propane to propene, *Appl. Surf. Sci.* 252 (2006) 5220–5226. <https://doi.org/10.1016/j.apsusc.2005.08.002>.
- [208] P. Boizumault-Moriceau, A. Pennequin, B. Grzybowska, Y. Barbaux, Oxidative dehydrogenation of propane on Ni-Ce-O oxide: effect of the preparation method, effect of potassium addition and physical characterization, *Appl. Catal. Gen.* 245 (2003) 55–67. [https://doi.org/10.1016/S0926-860X\(02\)00611-7](https://doi.org/10.1016/S0926-860X(02)00611-7).
- [209] A.R.J.M. Mattos, R.A. da Silva San Gil, M.L.M. Rocco, J.-G. Eon, Zinc-modified, alumina-supported vanadium oxides as catalysts for propane oxidative dehydrogenation, *J. Mol. Catal. Chem.* 178 (2002) 229–237. [https://doi.org/10.1016/S1381-1169\(01\)00339-9](https://doi.org/10.1016/S1381-1169(01)00339-9).
- [210] J. Li, C. Wang, C. Huang, W. Weng, H. Wan, Low Temperature Catalytic Performance of Nanosized CeNbNiO Mixed Oxide for Oxidative Dehydrogenation of Propane to Propene, *Catal. Lett.* 137 (2010) 81–87. <https://doi.org/10.1007/s10562-010-0333-0>.
- [211] R. Goyal, B. Sarkar, A. Bag, F. Lefebvre, S. Sameer, C. Pendem, A. Bordoloi, Single-step synthesis of hierarchical BxCN: a metal-free catalyst for low-temperature oxidative dehydrogenation of propane, *J. Mater. Chem. A.* 4 (2016) 18559–18569. <https://doi.org/10.1039/C6TA06972J>.
- [212] W. Daniell, A. Ponchel, S. Kuba, F. Anderle, T. Weingand, D.H. Gregory, H. Knözinger, Characterization and Catalytic Behavior of VO<sub>x</sub>-CeO<sub>2</sub> Catalysts for the Oxidative Dehydrogenation of Propane, *Top. Catal.* 20 (2002) 65–74. <https://doi.org/10.1023/A:1016399315511>.
- [213] J. Zhang, M. Sun, C. Cao, Q. Zhang, Y. Wang, H. Wan, Effects of acidity and microstructure on the catalytic behavior of cesium salts of 12-tungstophosphoric acid for oxidative dehydrogenation of propane, *Appl. Catal. Gen.* 380 (2010) 87–94. <https://doi.org/10.1016/j.apcata.2010.03.033>.
- [214] P. Viparelli, P. Ciambelli, L. Lisi, G. Ruoppolo, G. Russo, J.C. Volta, Oxidative dehydrogenation of propane over vanadium and niobium

- oxides supported catalysts, *Appl. Catal. Gen.* 184 (1999) 291–301. [https://doi.org/10.1016/S0926-860X\(99\)00104-0](https://doi.org/10.1016/S0926-860X(99)00104-0).
- [215] B. Zhaorigetu, W. Li, R. Kieffer, H. Xu, Synergetic effect between NiO and Ni<sub>3</sub>V<sub>2</sub>O<sub>8</sub> in propane oxidative dehydrogenation, *React. Kinet. Catal. Lett.* 75 (2002) 275–287. <https://doi.org/10.1023/A:1015298912903>.
- [216] D. Courcot, A. Ponchel, B. Grzybowska, Y. Barbaux, M. Rigole, M. Guelton, J.P. Bonnelle, Effect of the sequence of potassium introduction to V<sub>2</sub>O<sub>5</sub>/TiO<sub>2</sub> catalysts on their physicochemical properties and catalytic performance in oxidative dehydrogenation of propane, *Catal. Today.* 33 (1997) 109–118. [https://doi.org/10.1016/S0920-5861\(96\)00098-3](https://doi.org/10.1016/S0920-5861(96)00098-3).
- [217] R. Grabowski, B. Grzybowska, K. Samson, J. Słoczyński, J. Stoch, K. Wcisło, Effect of alkaline promoters on catalytic activity of V<sub>2</sub>O<sub>5</sub>/TiO<sub>2</sub> and MoO<sub>3</sub>/TiO<sub>2</sub> catalysts in oxidative dehydrogenation of propane and in isopropanol decomposition, *Appl. Catal. Gen.* 125 (1995) 129–144. [https://doi.org/10.1016/0926-860X\(94\)00274-6](https://doi.org/10.1016/0926-860X(94)00274-6).
- [218] R. You, X. Zhang, L. Luo, Y. Pan, H. Pan, J. Yang, L. Wu, X. Zheng, Y. Jin, W. Huang, NbO<sub>x</sub>/CeO<sub>2</sub>-rods catalysts for oxidative dehydrogenation of propane: Nb–CeO<sub>2</sub> interaction and reaction mechanism, *J. Catal.* 348 (2017) 189–199. <https://doi.org/10.1016/j.jcat.2016.12.012>.
- [219] M.M. Barsan, F.C. Thyron, Kinetic study of oxidative dehydrogenation of propane over Ni-Co molybdate catalyst, *Catal. Today.* 81 (2003) 159–170. [https://doi.org/10.1016/S0920-5861\(03\)00109-3](https://doi.org/10.1016/S0920-5861(03)00109-3).
- [220] B.Y. Jibril, S.M. Al-Zahrani, A.E. Abasaeed, R. Hughes, Oxidative dehydrogenation of propane over supported chromium–molybdenum oxides catalysts, *Catal. Commun.* 4 (2003) 579–584. <https://doi.org/10.1016/j.catcom.2003.07.001>.
- [221] L. Yuan, S. Bhatt, G. Beaucage, V.V. Guliants, S. Mamedov, R.S. Soman, Novel Mesoporous Mixed Nb–M (M = V, Mo, and Sb)

- Oxides for Oxidative Dehydrogenation of Propane, *J. Phys. Chem. B.* 109 (2005) 23250–23254. <https://doi.org/10.1021/jp054218p>.
- [222] B. Zhaorigetu, W. Li, H. Xu, R. Kieffer, Correlation Between the Characteristics and Catalytic Performance of Ni–V–O Catalysts in Oxidative Dehydrogenation of Propane, *Catal. Lett.* 94 (2004) 125–129. <https://doi.org/10.1023/B:CATL.0000019342.03708.f3>.
- [223] K. Bahranowski, R. Grabowski, B. Grzybowska, A. Kielski, E.M. Serwicka, K. Wcisło, E. Wisła-Walsh, K. Wodnicka, Synthesis and physicochemical properties of vanadium-doped zirconia-pillared montmorillonites in relation to oxidative dehydrogenation of propane, *Top. Catal.* 11 (2000) 255. <https://doi.org/10.1023/A:1027247914281>.
- [224] A. Pérez Pujol, R.X. Valenzuela, A. Fuerte, E. Wloch, A. Kubacka, Z. Olejniczak, B. Sulikowski, V. Cortés Corberán, High performance of V–Ga–O catalysts for oxidehydrogenation of propane, *Catal. Today.* 78 (2003) 247–256. [https://doi.org/10.1016/S0920-5861\(02\)00348-6](https://doi.org/10.1016/S0920-5861(02)00348-6).
- [225] O. Demoulin, F. Dury, M. Navez, E.M. Gaigneaux, P. Ruiz, Modification of active catalytic sites with N<sub>2</sub>O and CO<sub>2</sub> as gas promoters during oxidation reactions, *Catal. Today.* 91–92 (2004) 27–31. <https://doi.org/10.1016/j.cattod.2004.03.005>.
- [226] B.P. Barbero, L.E. Cadus, Evaluation and characterization of Sm–V–O catalytic system for propane oxydehydrogenation: Sm<sub>2</sub>O<sub>3</sub>-impregnated V<sub>2</sub>O<sub>5</sub> catalysts, *Appl. Catal. Gen.* 234 (2002) 245–258. [https://doi.org/10.1016/S0926-860X\(02\)00228-4](https://doi.org/10.1016/S0926-860X(02)00228-4).
- [227] B.P. Barbero, L.E. Cadus, V<sub>2</sub>O<sub>5</sub>–SmVO<sub>4</sub> mechanical mixture: oxidative dehydrogenation of propane, *Appl. Catal. Gen.* 237 (2002) 263–273. [https://doi.org/10.1016/S0926-860X\(02\)00336-8](https://doi.org/10.1016/S0926-860X(02)00336-8).
- [228] S.M. Al-Zahrani, B.Y. Jibril, A.E. Abasaeed, Activities of  $\gamma$ -Al<sub>2</sub>O<sub>3</sub>-Supported Metal Oxide Catalysts in Propane Oxidative Dehydrogenation, *Catal. Lett.* 85 (2003) 57–67. <https://doi.org/10.1023/A:1022116723773>.

- [229] S. Sugiyama, H. Hayashi, Role of Hydroxide Groups in Hydroxyapatite Catalysts for the Oxidative Dehydrogenation of Alkanes, *Int. J. Mod. Phys. B.* 17 (2003) 1476–1481. <https://doi.org/10.1142/S0217979203019186>.
- [230] S. Sugiyama, T. Shono, D. Makino, T. Moriga, H. Hayashi, Enhancement of the catalytic activities in propane oxidation and H–D exchangeability of hydroxyl groups by the incorporation with cobalt into strontium hydroxyapatite, *J. Catal.* 214 (2003) 8–14. [https://doi.org/10.1016/S0021-9517\(02\)00101-X](https://doi.org/10.1016/S0021-9517(02)00101-X).
- [231] B.Y. Jibril, Propane oxidative dehydrogenation over chromium oxide-based catalysts, *Appl. Catal. Gen.* 264 (2004) 193–202. <https://doi.org/10.1016/j.apcata.2003.12.054>.
- [232] J. Słoczyński, J. Ziółkowski, B. Grzybowska, R. Grabowski, D. Jachewicz, K. Wcisło, L. Gengembre, Oxidative Dehydrogenation of Propane on  $\text{Ni}_x\text{Mg}_{1-x}\text{Al}_2\text{O}_4$  and  $\text{NiCr}_2\text{O}_4$  Spinel, *J. Catal.* 187 (1999) 410–418. <https://doi.org/10.1006/jcat.1999.2626>.
- [233] R.B. Watson, U.S. Ozkan, K/Mo Catalysts Supported over Sol–Gel Silica–Titania Mixed Oxides in the Oxidative Dehydrogenation of Propane, *J. Catal.* 191 (2000) 12–29. <https://doi.org/10.1006/jcat.1999.2781>.
- [234] P. Michorczyk, P. Kuśtrowski, P. Niebrzydowska, A. Wach, Catalytic performance of sucrose-derived CMK-3 in oxidative dehydrogenation of propane to propene, *Appl. Catal. Gen.* 445–446 (2012) 321–328. <https://doi.org/10.1016/j.apcata.2012.08.044>.
- [235] Q. Zhang, C. Cao, T. Xu, M. Sun, J. Zhang, Y. Wang, H. Wan, NiO–polyoxometalate nanocomposites as efficient catalysts for the oxidative dehydrogenation of propane and isobutane, *Chem. Commun.* (2009) 2376–2378. <https://doi.org/10.1039/B823369A>.
- [236] C.L. Pieck, M.A. Bañares, J.L.G. Fierro, Propane oxidative dehydrogenation on  $\text{VO}_x/\text{ZrO}_2$  catalysts, *J. Catal.* 224 (2004) 1–7. <https://doi.org/10.1016/j.jcat.2004.02.024>.
- [237] M.A. Bañares, S.J. Khatib, Structure–activity relationships in alumina-supported molybdena–vanadia catalysts for propane

- oxidative dehydrogenation, *Catal. Today*. 96 (2004) 251–257. <https://doi.org/10.1016/j.cattod.2004.06.152>.
- [238] G. Garcia Cortez, J.L.G. Fierro, M.A. Bañares, Role of potassium on the structure and activity of alumina-supported vanadium oxide catalysts for propane oxidative dehydrogenation, *Catal. Today*. 78 (2003) 219–228. [https://doi.org/10.1016/S0920-5861\(02\)00341-3](https://doi.org/10.1016/S0920-5861(02)00341-3).
- [239] B. Farin, P. Eloy, C. Poleunis, M. Devillers, E.M. Gaigneaux, Self-assembled hybrid precursors towards more efficient propane ODH NiMoO<sub>4</sub> catalysts, *Catal. Sci. Technol.* 6 (2016) 6046–6056. <https://doi.org/10.1039/C6CY00167J>.
- [240] R. Dula, K. Wcisło, J. Stoch, B. Grzybowska, E.M. Serwicka, F. Kooli, K. Bahranowski, A. Gawęł, Layered double hydroxide-derived vanadium catalysts for oxidative dehydrogenation of propane: Influence of interlayer-doping versus layer-doping, *Appl. Catal. Gen.* 230 (2002) 281–291. [https://doi.org/10.1016/S0926-860X\(02\)00041-8](https://doi.org/10.1016/S0926-860X(02)00041-8).
- [241] K. Bahranowski, G. Bueno, V. Cortés Corberán, F. Kooli, E.M. Serwicka, R.X. Valenzuela, K. Wcisło, Oxidative dehydrogenation of propane over calcined vanadate-exchanged Mg,Al-layered double hydroxides, *Appl. Catal. Gen.* 185 (1999) 65–73. [https://doi.org/10.1016/S0926-860X\(99\)00113-1](https://doi.org/10.1016/S0926-860X(99)00113-1).
- [242] J.T. Grant, W.P. McDermott, J.M. Venegas, S.P. Burt, J. Micka, S.P. Phivilay, C.A. Carrero, I. Hermans, Boron and Boron-Containing Catalysts for the Oxidative Dehydrogenation of Propane, *ChemCatChem*. 9 (2017) 3622–3622. <https://doi.org/10.1002/cctc.201701473>.
- [243] A. Kubacka, E. Włoch, B. Sulikowski, R.X. Valenzuela, V. Cortés Corberán, Oxidative dehydrogenation of propane on zeolite catalysts, *Catal. Today*. 61 (2000) 343–352. [https://doi.org/10.1016/S0920-5861\(00\)00394-1](https://doi.org/10.1016/S0920-5861(00)00394-1).
- [244] Y. Wang, Q. Zhang, Y. Ohishi, T. Shishido, K. Takehira, Synthesis of V-MCM-41 by template-ion exchange method and its catalytic

- properties in propane oxidative dehydrogenation, *Catal. Lett.* 72 (2001) 215–219. <https://doi.org/10.1023/A:1009001707280>.
- [245] E. Heracleous, M. Machli, A.A. Lemonidou, I.A. Vasalos, Oxidative dehydrogenation of ethane and propane over vanadia and molybdena supported catalysts, *J. Mol. Catal. Chem.* 232 (2005) 29–39. <https://doi.org/10.1016/j.molcata.2005.01.027>.
- [246] M.C. Abello, M.F. Gomez, O. Ferretti, Oxidative Conversion of Propane over Al<sub>2</sub>O<sub>3</sub>-Supported Molybdenum and Chromium Oxides, *Catal. Lett.* 87 (2003) 43–49. <https://doi.org/10.1023/A:1022801126269>.
- [247] S. Dźwigaj, I. Gressel, B. Grzybowska, K. Samson, Oxidative dehydrogenation of propane on VSi $\beta$  catalysts, *Catal. Today*. 114 (2006) 237–241. <https://doi.org/10.1016/j.cattod.2006.02.022>.
- [248] E.V. Kondratenko, O.V. Buyevskaya, M. Baerns, Characterisation of vanadium-oxide-based catalysts for the oxidative dehydrogenation of propane to propene, *Top. Catal.* 15 (2001) 175–180. <https://doi.org/10.1023/A:1016649731881>.
- [249] R. Zhou, Y. Cao, S. Yan, K. Fan, Rare earth (Y, La, Ce)-promoted V-HMS mesoporous catalysts for oxidative dehydrogenation of propane, *Appl. Catal. Gen.* 236 (2002) 103–111. [https://doi.org/10.1016/S0926-860X\(02\)00281-8](https://doi.org/10.1016/S0926-860X(02)00281-8).
- [250] B.P. Barbero, L.E. Cadus, Vanadium species: Sm-V-O catalytic system for oxidative dehydrogenation of propane, *Appl. Catal. Gen.* 244 (2003) 235–249. [https://doi.org/10.1016/S0926-860X\(02\)00568-9](https://doi.org/10.1016/S0926-860X(02)00568-9).
- [251] R. Zhou, Y. Cao, S. Yan, J. Deng, Y. Liao, B. Hong, Oxidative Dehydrogenation of Propane over Mesoporous HMS Silica Supported Vanadia, *Catal. Lett.* 75 (2001) 107–112. <https://doi.org/10.1023/A:1016684218041>.
- [252] P. Moggi, M. Devillers, P. Ruiz, G. Predieri, D. Cauzzi, S. Morselli, O. Ligabue, Oxidative dehydrogenation of propane on pure and silica-dispersed multimetallic oxides based on vanadium and niobium prepared via hydrolytic and non-hydrolytic sol–gel methods,

- Catal. Today. 81 (2003) 77–85. [https://doi.org/10.1016/S0920-5861\(03\)00114-7](https://doi.org/10.1016/S0920-5861(03)00114-7).
- [253] S.N. Koc, G. Gurdag, S. Geissler, M. Guraya, M. Orbay, M. Muhler, The oxidative dehydrogenation of propane over potassium-promoted molybdenum oxide/sol–gel zirconia catalysts, J. Mol. Catal. Chem. 225 (2005) 197–202. <https://doi.org/10.1016/j.molcata.2004.09.009>.
- [254] B.Y. Jibril, S. Ahmed, Oxidative dehydrogenation of propane over Co, Ni and Mo mixed oxides/MCM-41 catalysts: Effects of intra- and extra-framework locations of metals on product distributions, Catal. Commun. 7 (2006) 990–996. <https://doi.org/10.1016/j.catcom.2006.04.017>.
- [255] M.D. Putra, S.M. Al-Zahrani, A.E. Abasaeed, Oxidative dehydrogenation of propane to propylene over Al<sub>2</sub>O<sub>3</sub>-supported Sr–V–Mo catalysts, Catal. Commun. 14 (2011) 107–110. <https://doi.org/10.1016/j.catcom.2011.07.025>.
- [256] A.A. Lemonidou, L. Nalbandian, I.A. Vasalos, Oxidative dehydrogenation of propane over vanadium oxide based catalysts: Effect of support and alkali promoter, Catal. Today. 61 (2000) 333–341. [https://doi.org/10.1016/S0920-5861\(00\)00393-X](https://doi.org/10.1016/S0920-5861(00)00393-X).
- [257] X. Zhang, H. Wan, W. Weng, X. Yi, Effect of Ag promoter on redox properties and catalytic performance of Ag–Mo–P–O catalysts for oxidative dehydrogenation of propane, Appl. Surf. Sci. 220 (2003) 117–124. [https://doi.org/10.1016/S0169-4332\(03\)00837-7](https://doi.org/10.1016/S0169-4332(03)00837-7).
- [258] X. Sun, Y. Ding, B. Zhang, R. Huang, D. Chen, D.S. Su, Insight into the Enhanced Selectivity of Phosphate-Modified Annealed Nanodiamond for Oxidative Dehydrogenation Reactions, ACS Catal. 5 (2015) 2436–2444. <https://doi.org/10.1021/acscatal.5b00042>.
- [259] J.-H. Li, C.-C. Wang, C.-J. Huang, Y.-F. Sun, W.-Z. Weng, H.-L. Wan, Mesoporous nickel oxides as effective catalysts for oxidative dehydrogenation of propane to propene, Appl. Catal. Gen. 382 (2010) 99–105. <https://doi.org/10.1016/j.apcata.2010.04.034>.



- [260] S.J. Conway, J.H. Lunsford, The oxidative dehydrogenation of ethane over chlorine-promoted lithium-magnesium oxide catalysts, *J. Catal.* 131 (1991) 513–522. [https://doi.org/10.1016/0021-9517\(91\)90283-A](https://doi.org/10.1016/0021-9517(91)90283-A).
- [261] S.J. Conway, D.J. Wang, J.H. Lunsford, Selective oxidation of methane and ethane over Li<sup>+</sup>-MgO-Cl<sup>-</sup> catalysts promoted with metal oxides, *Appl. Catal. Gen.* 79 (1991) L1–L5. [https://doi.org/10.1016/0926-860X\(91\)85001-E](https://doi.org/10.1016/0926-860X(91)85001-E).
- [262] H.M. Swaan, A. Toebes, K. Seshan, J.G. van Ommen, J.R.H. Ross, The effect of addition of a third component on the behaviour of the lithium doped magnesium catalysts for the oxidative dehydrogenation of ethane, *Catal. Today.* 13 (1992) 629–634. [https://doi.org/10.1016/0920-5861\(92\)80100-2](https://doi.org/10.1016/0920-5861(92)80100-2).
- [263] K. Otsuka, M. Hatano, T. Komatsu, Synthesis of C<sub>2</sub>H<sub>4</sub> by Partial Oxidation of CH<sub>4</sub> Over Transition Metal Oxides With Alkali-Chlorides, in: D.M. Bibby, C.D. Chang, R.F. Howe, S. Yurchak (Eds.), *Stud. Surf. Sci. Catal.*, Elsevier, 1988: pp. 383–387. [https://doi.org/10.1016/S0167-2991\(09\)60529-2](https://doi.org/10.1016/S0167-2991(09)60529-2).
- [264] K. Otsuka, M. Hatano, T. Komatsu, Synthesis of C<sub>2</sub>H<sub>4</sub> by partial oxidation of CH<sub>4</sub> over LiCl/NiO, *Catal. Today.* 4 (1989) 409–419. [https://doi.org/10.1016/0920-5861\(89\)85037-0](https://doi.org/10.1016/0920-5861(89)85037-0).
- [265] J.Z. Luo, H.L. Wan, Oxidative dehydrogenation of ethane over LaF<sub>3</sub>CeO<sub>2</sub> catalysts, *Appl. Catal. Gen.* 158 (1997) 137–144. [https://doi.org/10.1016/S0926-860X\(97\)00039-2](https://doi.org/10.1016/S0926-860X(97)00039-2).
- [266] J.Z. Luo, X.P. Zhou, Z.S. Chao, H.L. Wan, Oxidative dehydrogenation of ethane over BaF<sub>2</sub> promoted SmO<sub>3</sub>LaF<sub>3</sub> catalysts, *Appl. Catal. Gen.* 159 (1997) 9–19. [https://doi.org/10.1016/S0926-860X\(97\)00046-X](https://doi.org/10.1016/S0926-860X(97)00046-X).
- [267] R. Burch, S. Chalker, S.J. Hibble, The role of chlorine in the partial oxidation of methane to ethene on MgO catalysts, *Appl. Catal. Gen.* 96 (1993) 289–303. [https://doi.org/10.1016/0926-860X\(90\)80017-9](https://doi.org/10.1016/0926-860X(90)80017-9).
- [268] R. Burch, E.M. Crabb, Homogeneous and heterogeneous contributions to the oxidative dehydrogenation of propane on oxide

- catalysts, *Appl. Catal. Gen.* 100 (1993) 111–130. [https://doi.org/10.1016/0926-860X\(93\)80120-F](https://doi.org/10.1016/0926-860X(93)80120-F).
- [269] H. Yamamoto, H.Y. Chu, M.T. Xu, C.L. Shi, J.H. Lunsford, Oxidative Coupling of Methane over a Li+/MgO Catalyst Using N<sub>2</sub>O as an Oxidant, *J. Catal.* 142 (1993) 325–336. <https://doi.org/10.1006/jcat.1993.1211>.
- [270] S. Fuchs, L. Leveles, K. Seshan, L. Lefferts, A. Lemonidou, J.A. Lercher, Oxidative dehydrogenation and cracking of ethane and propane over LiDyMg mixed oxides, *Top. Catal.* 15 (2001) 169–174. <https://doi.org/10.1023/A:1016662101839>.
- [271] C.P. Kumar, S. Gaab, T.E. Müller, J.A. Lercher, Oxidative Dehydrogenation of Light Alkanes on Supported Molten Alkali Metal Chloride Catalysts, *Top. Catal.* 50 (2008) 156–167. <https://doi.org/10.1007/s11244-008-9102-3>.
- [272] L. Leveles, K. Seshan, J.A. Lercher, L. Lefferts, Oxidative conversion of propane over lithium-promoted magnesia catalyst: I. Kinetics and mechanism, *J. Catal.* 218 (2003) 296–306. [https://doi.org/10.1016/S0021-9517\(03\)00112-X](https://doi.org/10.1016/S0021-9517(03)00112-X).
- [273] L. Leveles, K. Seshan, J.A. Lercher, L. Lefferts, Oxidative conversion of propane over lithium-promoted magnesia catalyst: II. Active site characterization and hydrocarbon activation, *J. Catal.* 218 (2003) 307–314. [https://doi.org/10.1016/S0021-9517\(03\)00113-1](https://doi.org/10.1016/S0021-9517(03)00113-1).
- [274] L. Leveles, S. Fuchs, K. Seshan, J.A. Lercher, L. Lefferts, Oxidative conversion of light alkanes to olefins over alkali promoted oxide catalysts, *Appl. Catal. Gen.* 227 (2002) 287–297. [https://doi.org/10.1016/S0926-860X\(01\)00944-9](https://doi.org/10.1016/S0926-860X(01)00944-9).
- [275] C. Trionfetti, I.V. Babich, K. Seshan, L. Lefferts, Formation of high surface area Li/MgO—Efficient catalyst for the oxidative dehydrogenation/cracking of propane, *Appl. Catal. Gen.* 310 (2006) 105–113. <https://doi.org/10.1016/j.apcata.2006.05.029>.
- [276] K. Chen, A.T. Bell, E. Iglesia, Kinetics and Mechanism of Oxidative Dehydrogenation of Propane on Vanadium, Molybdenum, and

- Tungsten Oxides, *J. Phys. Chem. B.* 104 (2000) 1292–1299. <https://doi.org/10.1021/jp9933875>.
- [277] M. Cherian, M.S. Rao, A.M. Hirt, I.E. Wachs, G. Deo, Oxidative Dehydrogenation of Propane over Supported Chromia Catalysts: Influence of Oxide Supports and Chromia Loading, *J. Catal.* 211 (2002) 482–495. <https://doi.org/10.1006/jcat.2002.3759>.
- [278] T.V. Malleswara Rao, G. Deo, J.-M. Jehng, I.E. Wachs, In Situ UV–Vis–NIR Diffuse Reflectance and Raman Spectroscopy and Catalytic Activity Studies of Propane Oxidative Dehydrogenation over Supported CrO<sub>3</sub>/ZrO<sub>2</sub> Catalysts, *Langmuir.* 20 (2004) 7159–7165. <https://doi.org/10.1021/la049590v>.
- [279] M. Baldi, V. Sanchez Escribano, J.M. Gallardo Amores, F. Milella, E. Finocchio, C. Pistarino, G. Busca, Propane catalytic oxidation and oxy-dehydrogenation over manganese-based metal oxides., in: A. Parmaliana, D. Sanfilippo, F. Frusteri, A. Vaccari, F. Arena (Eds.), *Stud. Surf. Sci. Catal.*, Elsevier, 1998: pp. 635–640. [https://doi.org/10.1016/S0167-2991\(98\)80503-X](https://doi.org/10.1016/S0167-2991(98)80503-X).
- [280] J.M.L. Nieto, The selective oxidative activation of light alkanes. From supported vanadia to multicomponent bulk V-containing catalysts, *Top. Catal.* 41 (2006) 3–15. <https://doi.org/10.1007/s11244-006-0088-4>.
- [281] A. Corma, J.M. López-Nieto, N. Paredes, M. Pérez, Y. Shen, H. Cao, S.L. Suib, Oxidative Dehydrogenation Of Propane Over Supported-Vanadium Oxide Catalysts, in: P. Ruiz, B. Delmon (Eds.), *Stud. Surf. Sci. Catal.*, Elsevier, 1992: pp. 213–220. [https://doi.org/10.1016/S0167-2991\(08\)61673-0](https://doi.org/10.1016/S0167-2991(08)61673-0).
- [282] B. Frank, A. Dinse, O. Ovsitser, E.V. Kondratenko, R. Schomäcker, Mass and heat transfer effects on the oxidative dehydrogenation of propane (ODP) over a low loaded VO<sub>x</sub>/Al<sub>2</sub>O<sub>3</sub> catalyst, *Appl. Catal. Gen.* 323 (2007) 66–76. <https://doi.org/10.1016/j.apcata.2007.02.006>.
- [283] Y.-M. Liu, Y. Cao, K.-K. Zhu, S.-R. Yan, W.-L. Dai, H.-Y. He, K.-N. Fan, Highly efficient VO<sub>x</sub>/SBA-15 mesoporous catalysts for

- oxidative dehydrogenation of propane, *Chem. Commun.* 0 (2002) 2832–2833. <https://doi.org/10.1039/B208177F>.
- [284] Y.-M. Liu, Y. Cao, N. Yi, W.-L. Feng, W.-L. Dai, S.-R. Yan, H.-Y. He, K.-N. Fan, Vanadium oxide supported on mesoporous SBA-15 as highly selective catalysts in the oxidative dehydrogenation of propane, *J. Catal.* 224 (2004) 417–428. <https://doi.org/10.1016/j.jcat.2004.03.010>.
- [285] D. Siew Hew Sam, V. Soenen, J.C. Volta, Oxidative dehydrogenation of propane over V-Mg-O catalysts, *J. Catal.* 123 (1990) 417–435. [https://doi.org/10.1016/0021-9517\(90\)90139-B](https://doi.org/10.1016/0021-9517(90)90139-B).
- [286] M.C. Kung, H.H. Kung, The effect of potassium in the preparation of magnesium orthovanadate and pyrovanadate on the oxidative dehydrogenation of propane and butane, *J. Catal.* 134 (1992) 668–677. [https://doi.org/10.1016/0021-9517\(92\)90351-H](https://doi.org/10.1016/0021-9517(92)90351-H).
- [287] X. Gao, P. Ruiz, Q. Xin, X. Guo, B. Delmon, Preparation and characterization of three pure magnesium vanadate phases as catalysts for selective oxidation of propane to propene, *Catal. Lett.* 23 (1994) 321–337. <https://doi.org/10.1007/BF00811367>.
- [288] R.H.H. Smits, K. Seshan, H. Leemreize, J.R.H. Ross, Influence of preparation method on the performance of vanadia-niobia catalysts for the oxidative dehydrogenation of propane, *Catal. Today.* 16 (1993) 513–523. [https://doi.org/10.1016/0920-5861\(93\)80092-F](https://doi.org/10.1016/0920-5861(93)80092-F).
- [289] E.M. Thorsteinson, T.P. Wilson, F.G. Young, P.H. Kasai, The oxidative dehydrogenation of ethane over catalysts containing mixed oxides of molybdenum and vanadium, *J. Catal.* 52 (1978) 116–132. [https://doi.org/10.1016/0021-9517\(78\)90128-8](https://doi.org/10.1016/0021-9517(78)90128-8).
- [290] P. Botella, J.M. López Nieto, A. Dejoz, M.I. Vázquez, A. Martínez-Arias, Mo–V–Nb mixed oxides as catalysts in the selective oxidation of ethane, *Catal. Today.* 78 (2003) 507–512. [https://doi.org/10.1016/S0920-5861\(02\)00338-3](https://doi.org/10.1016/S0920-5861(02)00338-3).
- [291] M. Merzouki, B. Taouk, L. Monceaux, E. Bordes, P. Courtine, Catalytic Properties Of Promoted Vanadium Oxide In The Oxidation Of Ethane In Acetic Acid, in: P. Ruiz, B. Delmon (Eds.), *Stud. Surf.*

- Sci. Catal., Elsevier, 1992: pp. 165–179.  
[https://doi.org/10.1016/S0167-2991\(08\)61669-9](https://doi.org/10.1016/S0167-2991(08)61669-9).
- [292] M. Merzouki, B. Taouk, L. Tessier, E. Bordes, P. Courtine, Correlation Between Catalytic and Structural Properties of Modified Molybdenum and Vanadium Oxides in the Oxidation of Ethane in Acetic Acid or Ethylene, in: L. Guzzi, F. Solymosi, P. Tétényi (Eds.), Stud. Surf. Sci. Catal., Elsevier, 1993: pp. 753–764.  
[https://doi.org/10.1016/S0167-2991\(08\)64054-9](https://doi.org/10.1016/S0167-2991(08)64054-9).
- [293] O. Desponds, R.L. Keiski, G.A. Somorjai, The oxidative dehydrogenation of ethane over molybdenum-vanadium-niobium oxide catalysts: the role of catalyst composition, Catal. Lett. 19 (1993) 17–32. <https://doi.org/10.1007/BF00765198>.
- [294] K. Ruth, R. Kieffer, R. Burch, Mo–V–Nb Oxide Catalysts for the Partial Oxidation of Ethane: I. Preparation and Structural Characterisation, J. Catal. 175 (1998) 16–26.  
<https://doi.org/10.1006/jcat.1998.1975>.
- [295] K. Ruth, R. Burch, R. Kieffer, Mo–V–Nb Oxide Catalysts for the Partial Oxidation of Ethane: II. Chemical and Catalytic Properties and Structure Function Relationships, J. Catal. 175 (1998) 27–39.  
<https://doi.org/10.1006/jcat.1998.1976>.
- [296] P. Botella, A. Dejoz, J.M. López Nieto, P. Concepción, M.I. Vázquez, Selective oxidative dehydrogenation of ethane over MoVSbO mixed oxide catalysts, Appl. Catal. Gen. 298 (2006) 16–23.  
<https://doi.org/10.1016/j.apcata.2005.09.018>.
- [297] W. Ueda, K. Oshihara, D. Vitry, T. Hisano, Y. Kayashima, Hydrothermal Synthesis of Mo-Based Oxide Catalysts and Selective Oxidation of Alkanes, Catal. Surv. Asia. 6 (2002) 33–44.  
<https://doi.org/10.1023/A:1020668816617>.
- [298] P. Botella, E. García-González, A. Dejoz, J.M. López Nieto, M.I. Vázquez, J. González-Calbet, Selective oxidative dehydrogenation of ethane on MoVTenbO mixed metal oxide catalysts, J. Catal. 225 (2004) 428–438. <https://doi.org/10.1016/j.jcat.2004.04.024>.

- [299] F. Ivars, P. Botella, A. Dejoz, J.M.L. Nieto, P. Concepción, M.I. Vázquez, Selective oxidation of short-chain alkanes over hydrothermally prepared MoVTeNbO catalysts, *Top. Catal.* 38 (2006) 59–67. <https://doi.org/10.1007/s11244-006-0071-0>.
- [300] J.M.L. Nieto, P. Botella, M.I. Vázquez, A. Dejoz, The selective oxidative dehydrogenation of ethane over hydrothermally synthesised MoVTeNb catalysts, *Chem. Commun.* (2002) 1906–1907. <https://doi.org/10.1039/B204037A>.
- [301] E. Heracleous, A.A. Lemonidou, Ni–Nb–O mixed oxides as highly active and selective catalysts for ethene production via ethane oxidative dehydrogenation. Part I: Characterization and catalytic performance, *J. Catal.* 237 (2006) 162–174. <https://doi.org/10.1016/j.jcat.2005.11.002>.
- [302] E. Heracleous, A.A. Lemonidou, Ni–Nb–O mixed oxides as highly active and selective catalysts for ethene production via ethane oxidative dehydrogenation. Part II: Mechanistic aspects and kinetic modeling, *J. Catal.* 237 (2006) 175–189. <https://doi.org/10.1016/j.jcat.2005.11.003>.
- [303] E. Heracleous, A.F. Lee, K. Wilson, A.A. Lemonidou, Investigation of Ni-based alumina-supported catalysts for the oxidative dehydrogenation of ethane to ethylene: structural characterization and reactivity studies, *J. Catal.* 231 (2005) 159–171. <https://doi.org/10.1016/j.jcat.2005.01.015>.
- [304] K.-I. Nakamura, T. Miyake, T. Konishi, T. Suzuki, Oxidative dehydrogenation of ethane to ethylene over NiO loaded on high surface area MgO, *J. Mol. Catal. Chem.* 260 (2006) 144–151. <https://doi.org/10.1016/j.molcata.2006.06.058>.
- [305] X. Zhang, J. Liu, Y. Jing, Y. Xie, Support effects on the catalytic behavior of NiO/Al<sub>2</sub>O<sub>3</sub> for oxidative dehydrogenation of ethane to ethylene, *Appl. Catal. Gen.* 240 (2003) 143–150. [https://doi.org/10.1016/S0926-860X\(02\)00426-X](https://doi.org/10.1016/S0926-860X(02)00426-X).

- [306] X. Zhang, Y. Gong, G. Yu, Y. Xie, Oxygen species on NiO/Al<sub>2</sub>O<sub>3</sub> and their reactivities, *J. Mol. Catal. Chem.* 180 (2002) 293–298. [https://doi.org/10.1016/S1381-1169\(01\)00452-6](https://doi.org/10.1016/S1381-1169(01)00452-6).
- [307] A. Kaddouri, R. Anouchinsky, C. Mazzocchia, L.M. Madeira, M.F. Portela, Oxidative dehydrogenation of ethane on the  $\alpha$  and  $\beta$  phases of NiMoO<sub>4</sub>, *Catal. Today.* 40 (1998) 201–206. [https://doi.org/10.1016/S0920-5861\(98\)00008-X](https://doi.org/10.1016/S0920-5861(98)00008-X).
- [308] B. Grzybowska, J. Słoczyński, R. Grabowski, K. Samson, I. Gressel, K. Wcisło, L. Gengembre, Y. Barboux, Effect of doping of TiO<sub>2</sub> support with altermultivalent ions on physicochemical and catalytic properties in oxidative dehydrogenation of propane of vanadia–titania catalysts, *Appl. Catal. Gen.* 230 (2002) 1–10. [https://doi.org/10.1016/S0926-860X\(01\)00951-6](https://doi.org/10.1016/S0926-860X(01)00951-6).
- [309] M. Ziolek, A. Lewandowska, B. Grzybowska, A. Klisińska, NbMCM-41 mesoporous molecular sieves in oxidative dehydrogenation of ethane and propane, *React. Kinet. Catal. Lett.* 80 (2003) 199–206. <https://doi.org/10.1023/B:REAC.0000006126.82581.83>.
- [310] D. Courcot, B. Grzybowska, Y. Barboux, M. Rigole, A. Ponchel, M. Guelton, Effect of potassium addition to the TiO<sub>2</sub> support on the structure of V<sub>2</sub>O<sub>5</sub>/TiO<sub>2</sub> and its catalytic properties in the oxidative dehydrogenation of propane, *J. Chem. Soc. Faraday Trans.* 92 (1996) 1609–1617. <https://doi.org/10.1039/FT9969201609>.
- [311] A. Klisińska, A. Haras, K. Samson, M. Witko, B. Grzybowska, Effect of additives on properties of vanadia-based catalysts for oxidative dehydrogenation of propane: Experimental and quantum chemical studies, *J. Mol. Catal. Chem.* 210 (2004) 87–92. <https://doi.org/10.1016/j.molcata.2003.08.026>.
- [312] B. Grzybowska, P. Mekšs, R. Grabowski, K. Wcisło, Y. Barboux, L. Gengembre, Effect of Potassium Addition to V<sub>2</sub>O<sub>5</sub>/TiO<sub>2</sub> and MoO<sub>3</sub>/TiO<sub>2</sub> Catalysts on Their Physicochemical and Catalytic Properties in Oxidative Dehydrogenation of Propane, in: V.C. Corberán, S.V. Bellón (Eds.), *Stud. Surf. Sci. Catal.*, Elsevier, 1994: pp. 151–158. [https://doi.org/10.1016/S0167-2991\(08\)63407-2](https://doi.org/10.1016/S0167-2991(08)63407-2).

- [313] R. Grabowski, B. Grzybowska, A. Kozłowska, J. Słoczyński, K. Wcisło, Y. Barbaux, Effect of alkali metals additives to V<sub>2</sub>O<sub>5</sub>/TiO<sub>2</sub> catalyst on physicochemical properties and catalytic performance in oxidative dehydrogenation of propane, *Top. Catal.* 3 (1996) 277–288. <https://doi.org/10.1007/BF02113854>.
- [314] D.L. Stern, R.K. Grasselli, Propane Oxydehydrogenation over Molybdate-Based Catalysts, *J. Catal.* 167 (1997) 550–559. <https://doi.org/10.1006/jcat.1997.1568>.
- [315] D.L. Stern, R.K. Grasselli, Reaction Network and Kinetics of Propane Oxydehydrogenation over Nickel Cobalt Molybdate, *J. Catal.* 167 (1997) 560–569. <https://doi.org/10.1006/jcat.1997.1569>.
- [316] C. Martín, V. Rives, A.R. González-Elipe, Effect of sodium on the reductibility of V(V) ions during propene adsorption on V<sub>2</sub>O<sub>5</sub>/TiO<sub>2</sub> catalysts, *J. Catal.* 114 (1988) 473–477. [https://doi.org/10.1016/0021-9517\(88\)90053-X](https://doi.org/10.1016/0021-9517(88)90053-X).
- [317] L. Shi, D. Wang, W. Song, D. Shao, W.-P. Zhang, A.-H. Lu, Edge-hydroxylated Boron Nitride for Oxidative Dehydrogenation of Propane to Propylene, *ChemCatChem.* 9 (2017) 1720–1720. <https://doi.org/10.1002/cctc.201700745>.
- [318] J.M. Venegas, W.P. McDermott, I. Hermans, Serendipity in Catalysis Research: Boron-Based Materials for Alkane Oxidative Dehydrogenation, *Acc. Chem. Res.* 51 (2018) 2556–2564. <https://doi.org/10.1021/acs.accounts.8b00330>.
- [319] O.V. Buyevskaya, D. Müller, I. Pitsch, M. Baerns, Selective Oxidative Conversion of Propane to Olefins and Oxygenates on Boria-Containing Catalysts, in: A. Parmaliana, D. Sanfilippo, F. Frusteri, A. Vaccari, F. Arena (Eds.), *Stud. Surf. Sci. Catal.*, Elsevier, 1998: pp. 671–676. [https://doi.org/10.1016/S0167-2991\(98\)80509-0](https://doi.org/10.1016/S0167-2991(98)80509-0).
- [320] D.J. Nash, D.T. Restrepo, N.S. Parra, K.E. Giesler, R.A. Penabade, M. Aminpour, D. Le, Z. Li, O.K. Farha, J.K. Harper, T.S. Rahman, R.G. Blair, Heterogeneous Metal-Free Hydrogenation over Defect-



- Laden Hexagonal Boron Nitride, ACS Omega. 1 (2016) 1343–1354. <https://doi.org/10.1021/acsomega.6b00315>.
- [321] P. Li, H. Li, X. Pan, K. Tie, T. Cui, M. Ding, X. Bao, Catalytically Active Boron Nitride in Acetylene Hydrochlorination, ACS Catal. 7 (2017) 8572–8577. <https://doi.org/10.1021/acscatal.7b01877>.
- [322] P. Wu, S. Yang, W. Zhu, H. Li, Y. Chao, H. Zhu, H. Li, S. Dai, Tailoring N-Terminated Defective Edges of Porous Boron Nitride for Enhanced Aerobic Catalysis, Small. 13 (2017) 1701857. <https://doi.org/10.1002/sml.201701857>.
- [323] S. Torii, K. Jimura, S. Hayashi, R. Kikuchi, A. Takagaki, Utilization of hexagonal boron nitride as a solid acid–base bifunctional catalyst, J. Catal. 355 (2017) 176–184. <https://doi.org/10.1016/j.jcat.2017.09.013>.
- [324] Y. Wu, P. Wu, Y. Chao, J. He, H. Li, L. Lu, W. Jiang, B. Zhang, H. Li, W. Zhu, Gas-exfoliated porous monolayer boron nitride for enhanced aerobic oxidative desulfurization performance, Nanotechnology. 29 (2017) 025604. <https://doi.org/10.1088/1361-6528/aa9bc7>.
- [325] M.A. Bañares, X. Gao, J.L.G. Fierro, I.E. Wachs, Partial oxidation of ethane over monolayers of vanadium oxide. effect of the support and surface coverage, in: R.K. Grasselli, S.T. Oyama, A.M. Gaffney, J.E. Lyons (Eds.), Stud. Surf. Sci. Catal., Elsevier, 1997: pp. 295–304. [https://doi.org/10.1016/S0167-2991\(97\)80990-1](https://doi.org/10.1016/S0167-2991(97)80990-1).
- [326] T. Blasco, J.M.L. Nieto, Oxidative dyhydrogenation of short chain alkanes on supported vanadium oxide catalysts, Appl. Catal. Gen. 157 (1997) 117–142. [https://doi.org/10.1016/S0926-860X\(97\)00029-X](https://doi.org/10.1016/S0926-860X(97)00029-X).
- [327] M.A. Bañares, Supported metal oxide and other catalysts for ethane conversion: a review, Catal. Today. 51 (1999) 319–348. [https://doi.org/10.1016/S0920-5861\(99\)00053-X](https://doi.org/10.1016/S0920-5861(99)00053-X).
- [328] B.M. Weckhuysen, R.A. Schoonheydt, Recent progress in diffuse reflectance spectroscopy of supported metal oxide catalysts, Catal.

- Today. 49 (1999) 441–451. [https://doi.org/10.1016/S0920-5861\(98\)00458-1](https://doi.org/10.1016/S0920-5861(98)00458-1).
- [329] J. Haber, Fifty years of my romance with vanadium oxide catalysts, *Catal. Today*. 142 (2009) 100–113. <https://doi.org/10.1016/j.cattod.2008.11.007>.
- [330] G.C. Bond, S.F. Tahir, Vanadium oxide monolayer catalysts Preparation, characterization and catalytic activity, *Appl. Catal.* 71 (1991) 1–31. [https://doi.org/10.1016/0166-9834\(91\)85002-D](https://doi.org/10.1016/0166-9834(91)85002-D).
- [331] M.O. Guerrero-Pérez, J.M. Rosas, R. López-Medina, M.A. Bañares, J. Rodríguez-Mirasol, T. Cordero, Lignocellulosic-derived catalysts for the selective oxidation of propane, *Catal. Commun.* 12 (2011) 989–992. <https://doi.org/10.1016/j.catcom.2011.03.010>.
- [332] M.O. Guerrero-Pérez, M.C. Herrera, I. Malpartida, M.A. Larrubia, L.J. Alemany, M.A. Bañares, Operando Raman study of propane oxidation over alumina-supported V-Mo-W-O catalysts, *Catal. Today*. 126 (2007) 177–183. <https://doi.org/10.1016/j.cattod.2006.10.004>.
- [333] G. Centi, F. Trifiro, J.R. Ebner, V.M. Franchetti, MECHANISTIC ASPECTS OF MALEIC ANHYDRIDE SYNTHESIS FROM C<sub>4</sub> HYDROCARBONS OVER PHOSPHORUS VANADIUM OXIDE., *Chem. Rev.* 88 (1988) 55–80.
- [334] M.J. Valero-Romero, A. Cabrera-Molina, M.O. Guerrero-Pérez, J. Rodríguez-Mirasol, T. Cordero, Carbon materials as template for the preparation of mixed oxides with controlled morphology and porous structure, *Catal. Today*. 227 (2014) 233–241. <https://doi.org/10.1016/j.cattod.2013.10.093>.
- [335] B.K. Hodnett, Vanadium-Phosphorus Oxide Catalysts for the Selective Oxidation of C<sub>4</sub> Hydrocarbons to Maleic Anhydride, *Catal. Rev. Sci. Eng.* (2006). <https://doi.org/10.1080/01614948508064740>.
- [336] R.M. Contractor, H.E. Bergna, H.S. Horowitz, C.M. Blackstone, B. Malone, C.C. Torardi, B. Griffiths, U. Chowdhry, A.W. Sleight, Butane oxidation to maleic anhydride over vanadium phosphate

- catalysts, *Catal. Today.* 1 (1987) 49–58.  
[https://doi.org/10.1016/0920-5861\(87\)80026-3](https://doi.org/10.1016/0920-5861(87)80026-3).
- [337] A. Khodakov, B. Olthof, A.T. Bell, E. Iglesia, Structure and catalytic properties of supported vanadium oxides: Support effects on oxidative dehydrogenation reactions, *J. Catal.* 181 (1999) 205–216.
- [338] A. Dinse, B. Frank, C. Hess, D. Habel, R. Schomäcker, Oxidative dehydrogenation of propane over low-loaded vanadia catalysts: Impact of the support material on kinetics and selectivity, *J. Mol. Catal. Chem.* 289 (2008) 28–37.  
<https://doi.org/10.1016/j.molcata.2008.04.007>.
- [339] J. Bedia, J.M. Rosas, J. Rodríguez-Mirasol, T. Cordero, Pd supported on mesoporous activated carbons with high oxidation resistance as catalysts for toluene oxidation, *Appl. Catal. B Environ.* 94 (2010) 8–18. <https://doi.org/10.1016/j.apcatb.2009.10.015>.
- [340] I. Hita, T. Cordero-Lanzac, A. Gallardo, J.M. Arandes, J. Rodríguez-Mirasol, J. Bilbao, T. Cordero, P. Castaño, Phosphorus-containing activated carbon as acid support in a bifunctional Pt–Pd catalyst for tire oil hydrocracking, *Catal. Commun.* 78 (2016) 48–51.  
<https://doi.org/10.1016/j.catcom.2016.01.035>.
- [341] M.O. Guerrero-Pérez, J.L.G. Fierro, M.A. Vicente, M.A. Banares, Support effect on the structure and reactivity of VSbO<sub>4</sub> catalysts for propane ammoxidation to acrylonitrile, *Chem. Mater.* 19 (2007) 6621–6628. <https://doi.org/10.1021/cm702022d>.
- [342] B.-Y. Zhao, X.-P. Xu, H.-R. Ma, D.-H. Sun, J.-M. Gao, Monolayer dispersion of oxides and salts on surface of ZrO<sub>2</sub> and its application in preparation of ZrO<sub>2</sub>-supported catalysts with high surface areas, *Catal. Lett.* 45 (1997) 237–244.
- [343] A. Khodakov, J. Yang, S. Su, E. Iglesia, A.T. Bell, Structure and properties of vanadium oxide-zirconia catalysts for propane oxidative dehydrogenation, *J. Catal.* 177 (1998) 343–351.  
<https://doi.org/10.1006/jcat.1998.2143>.
- [344] K. Chen, A.T. Bell, E. Iglesia, The Relationship between the Electronic and Redox Properties of Dispersed Metal Oxides and

- Their Turnover Rates in Oxidative Dehydrogenation Reactions, *J. Catal.* 209 (2002) 35–42. <https://doi.org/10.1006/jcat.2002.3620>.
- [345] B. Grzybowska-Świerkosz, Effect of Additives on the Physicochemical and Catalytic Properties of Oxide Catalysts in Selective Oxidation Reactions, *Top. Catal.* 21 (2002) 35–46. <https://doi.org/10.1023/A:1020547830167>.
- [346] J.C. Védrine, The Role of Redox, Acid-Base and Collective Properties and of Crystalline State of Heterogeneous Catalysts in the Selective Oxidation of Hydrocarbons, *Top. Catal.* 21 (2002) 97–106. <https://doi.org/10.1023/A:1020560200125>.
- [347] M.F. Hazenkamp, G. Blasse, A luminescence spectroscopy study on supported vanadium and chromium oxide catalysts, *J. Phys. Chem.* 96 (1992) 3442–3446. <https://doi.org/10.1021/j100187a049>.
- [348] N. Das, H. Eckert, H. Hu, I.E. Wachs, J.F. Walzer, F.J. Feher, Bonding states of surface vanadium(V) oxide phases on silica: structural characterization by vanadium-51 NMR and Raman spectroscopy, *J. Phys. Chem.* 97 (1993) 8240–8243. <https://doi.org/10.1021/j100133a020>.
- [349] H. Eckert, I.E. Wachs, Solid-state vanadium-51 NMR structural studies on supported vanadium(V) oxide catalysts: vanadium oxide surface layers on alumina and titania supports, *J. Phys. Chem.* 93 (1989) 6796–6805. <https://doi.org/10.1021/j100355a043>.
- [350] G.T. Went, S.Ted. Oyama, A.T. Bell, Laser Raman spectroscopy of supported vanadium oxide catalysts, *J. Phys. Chem.* 94 (1990) 4240–4246. <https://doi.org/10.1021/j100373a067>.
- [351] C. Resini, T. Montanari, G. Busca, J.-M. Jehng, I.E. Wachs, Comparison of alcohol and alkane oxidative dehydrogenation reactions over supported vanadium oxide catalysts: in situ infrared, Raman and UV–vis spectroscopic studies of surface alkoxide intermediates and of their surface chemistry, *Catal. Today.* 99 (2005) 105–114. <https://doi.org/10.1016/j.cattod.2004.09.029>.
- [352] N. Magg, B. Immaraporn, J.B. Giorgi, T. Schroeder, M. Bäumer, J. Döbler, Z. Wu, E. Kondratenko, M. Cherian, M. Baerns, P.C. Stair,

- J. Sauer, H.-J. Freund, Vibrational spectra of alumina- and silica-supported vanadia revisited: An experimental and theoretical model catalyst study, *J. Catal.* 226 (2004) 88–100. <https://doi.org/10.1016/j.jcat.2004.04.021>.
- [353] M.A. Vuurman, I.E. Wachs, In situ Raman spectroscopy of alumina-supported metal oxide catalysts, *J. Phys. Chem.* 96 (1992) 5008–5016. <https://doi.org/10.1021/j100191a051>.
- [354] S. Yoshida, T. Tanaka, T. Hanada, T. Hiraiwa, H. Kanai, T. Funabiki, Analysis of XANES for identification of highly dispersed transition metal oxides on supports, *Catal. Lett.* 12 (1992) 277–285. <https://doi.org/10.1007/BF00767210>.
- [355] X. Gao, S.R. Bare, B.M. Weckhuysen, I.E. Wachs, In Situ Spectroscopic Investigation of Molecular Structures of Highly Dispersed Vanadium Oxide on Silica under Various Conditions, *J. Phys. Chem. B.* 102 (1998) 10842–10852. <https://doi.org/10.1021/jp9826367>.
- [356] X. Gao, M.A. Bañares, I.E. Wachs, Ethane and n-Butane Oxidation over Supported Vanadium Oxide Catalysts: An in Situ UV–Visible Diffuse Reflectance Spectroscopic Investigation, *J. Catal.* 188 (1999) 325–331. <https://doi.org/10.1006/jcat.1999.2647>.
- [357] X. Gao, I.E. Wachs, Investigation of Surface Structures of Supported Vanadium Oxide Catalysts by UV–vis–NIR Diffuse Reflectance Spectroscopy, *J. Phys. Chem. B.* 104 (2000) 1261–1268. <https://doi.org/10.1021/jp992867t>.
- [358] M. Schraml-Marth, A. Wokaun, M. Pohl, H.-L. Krauss, Spectroscopic investigation of the structure of silica-supported vanadium oxide catalysts at submonolayer coverages, *J. Chem. Soc. Faraday Trans.* 87 (1991) 2635–2646. <https://doi.org/10.1039/FT9918702635>.
- [359] G. Catana, R.R. Rao, B.M. Weckhuysen, P. Van Der Voort, E. Vansant, R.A. Schoonheydt, Supported Vanadium Oxide Catalysts: Quantitative Spectroscopy, Preferential Adsorption of V<sup>4+</sup>/V<sup>5+</sup>, and

- Al<sub>2</sub>O<sub>3</sub> Coating of Zeolite Y, *J. Phys. Chem. B.* 102 (1998) 8005–8012. <https://doi.org/10.1021/jp981482s>.
- [360] M. Baltes, O. Collart, P. Van Der Voort, E.F. Vansant, Synthesis of Supported Transition Metal Oxide Catalysts by the Designed Deposition of Acetylacetonate Complexes, *Langmuir.* 15 (1999) 5841–5845. <https://doi.org/10.1021/la981362b>.
- [361] M. Baltes, P.V.D. Voort, B.M. Weckhuysen, R.R. Rao, G. Catana, R.A. Schoonheydt, E.F. Vansant, Synthesis and characterization of alumina-supported vanadium oxide catalysts prepared by the molecular designed dispersion of VO(acac)<sub>2</sub> complexes, *Phys. Chem. Chem. Phys.* 2 (2000) 2673–2680. <https://doi.org/10.1039/B002141P>.
- [362] M.D. Argyle, K. Chen, C. Resini, C. Krebs, A.T. Bell, E. Iglesia, Extent of Reduction of Vanadium Oxides during Catalytic Oxidation of Alkanes Measured by in-Situ UV–Visible Spectroscopy, *J. Phys. Chem. B.* 108 (2004) 2345–2353. <https://doi.org/10.1021/jp030989m>.
- [363] N. Steinfeldt, D. Müller, H. Berndt, VO<sub>x</sub> species on alumina at high vanadia loadings and calcination temperature and their role in the ODP reaction, *Appl. Catal. Gen.* 272 (2004) 201–213. <https://doi.org/10.1016/j.apcata.2004.05.050>.
- [364] I.E. Wachs, Molecular engineering of supported metal oxide catalysts, *Chem. Eng. Sci.* 45 (1990) 2561–2565. [https://doi.org/10.1016/0009-2509\(90\)80142-2](https://doi.org/10.1016/0009-2509(90)80142-2).
- [365] C. Zhao, I.E. Wachs, Selective oxidation of propylene to acrolein over supported V<sub>2</sub>O<sub>5</sub>/Nb<sub>2</sub>O<sub>5</sub> catalysts: An in situ Raman, IR, TPSR and kinetic study, *Catal. Today.* 118 (2006) 332–343. <https://doi.org/10.1016/j.cattod.2006.07.018>.
- [366] M.V. Martínez-Huerta, X. Gao, H. Tian, I.E. Wachs, J.L.G. Fierro, M.A. Bañares, Oxidative dehydrogenation of ethane to ethylene over alumina-supported vanadium oxide catalysts: Relationship between molecular structures and chemical reactivity, *Catal. Today.* 118 (2006) 279–287. <https://doi.org/10.1016/j.cattod.2006.07.034>.

- [367] B. Beck, M. Harth, N.G. Hamilton, C. Carrero, J.J. Uhlrich, A. Trunschke, S. Shaikhutdinov, H. Schubert, H.-J. Freund, R. Schlögl, J. Sauer, R. Schomäcker, Partial oxidation of ethanol on vanadia catalysts on supporting oxides with different redox properties compared to propane, *J. Catal.* 296 (2012) 120–131. <https://doi.org/10.1016/j.jcat.2012.09.008>.
- [368] H.Y. Kim, H.M. Lee, R.G.S. Pala, V. Shapovalov, H. Metiu, CO Oxidation by Rutile TiO<sub>2</sub>(110) Doped with V, W, Cr, Mo, and Mn, *J. Phys. Chem. C.* 112 (2008) 12398–12408. <https://doi.org/10.1021/jp802296g>.
- [369] H.H. Kung, M.C. Kung, Oxidative dehydrogenation of alkanes over vanadium-magnesium-oxides, *Appl. Catal. Gen.* 157 (1997) 105–116. [https://doi.org/10.1016/S0926-860X\(97\)00028-8](https://doi.org/10.1016/S0926-860X(97)00028-8).
- [370] F. Arena, F. Frusteri, A. Parmaliana, Structure and dispersion of supported-vanadia catalysts. Influence of the oxide carrier, *Appl. Catal. Gen.* 176 (1999) 189–199. [https://doi.org/10.1016/S0926-860X\(98\)00236-1](https://doi.org/10.1016/S0926-860X(98)00236-1).
- [371] J. Haber, A. Kozłowska, R. Kozłowski, The structure and redox properties of vanadium oxide surface compounds, *J. Catal.* 102 (1986) 52–63. [https://doi.org/10.1016/0021-9517\(86\)90140-5](https://doi.org/10.1016/0021-9517(86)90140-5).
- [372] J.M. López Nieto, J. Soler, P. Concepción, J. Herguido, M. Menéndez, J. Santamaría, Oxidative Dehydrogenation of Alkanes over V-based Catalysts: Influence of Redox Properties on Catalytic Performance, *J. Catal.* 185 (1999) 324–332. <https://doi.org/10.1006/jcat.1999.2467>.
- [373] M.D. Argyle, K. Chen, E. Iglesia, A.T. Bell, In situ UV–Visible Spectroscopic Measurements of Kinetic Parameters and Active Sites for Catalytic Oxidation of Alkanes on Vanadium Oxides, *J. Phys. Chem. B.* 109 (2005) 2414–2420. <https://doi.org/10.1021/jp040166c>.
- [374] M.A. Bañares, M.V. Martínez-Huerta, X. Gao, J.L.G. Fierro, I.E. Wachs, Dynamic behavior of supported vanadia catalysts in the selective oxidation of ethane: In situ Raman, UV–Vis DRS and

- reactivity studies, *Catal. Today*. 61 (2000) 295–301.  
[https://doi.org/10.1016/S0920-5861\(00\)00388-6](https://doi.org/10.1016/S0920-5861(00)00388-6).
- [375] T. Blasco, J.M.L. Nieto, A. Dejoz, M.I. Vazquez, Influence of the Acid-Base Character of Supported Vanadium Catalysts on Their Catalytic Properties for the Oxidative Dehydrogenation of n-Butane, *J. Catal.* 157 (1995) 271–282.  
<https://doi.org/10.1006/jcat.1995.1291>.
- [376] B. Grzybowska-Świerkosz, Thirty years in selective oxidation on oxides: what have we learned?, *Top. Catal.* 11 (2000) 23–42.  
<https://doi.org/10.1023/A:1027256116098>.
- [377] P. Concepción, P. Botella, J.M.L. Nieto, Catalytic and FT-IR study on the reaction pathway for oxidation of propane and propylene on V- or Mo–V-based catalysts, *Appl. Catal. Gen.* 278 (2004) 45–56.  
<https://doi.org/10.1016/j.apcata.2004.09.024>.
- [378] C. Pak, A.T. Bell, T.D. Tilley, Oxidative Dehydrogenation of Propane over Vanadia–Magnesia Catalysts Prepared by Thermolysis of  $\text{OV}(\text{OtBu})_3$  in the Presence of Nanocrystalline  $\text{MgO}$ , *J. Catal.* 206 (2002) 49–59. <https://doi.org/10.1006/jcat.2001.3473>.
- [379] A. Klisińska, K. Samson, I. Gressel, B. Grzybowska, Effect of additives on properties of  $\text{V}_2\text{O}_5/\text{SiO}_2$  and  $\text{V}_2\text{O}_5/\text{MgO}$  catalysts: I. Oxidative dehydrogenation of propane and ethane, *Appl. Catal. Gen.* 309 (2006) 10–16.  
<https://doi.org/10.1016/j.apcata.2006.04.028>.
- [380] A. Klisińska, S. Loridant, B. Grzybowska, J. Stoch, I. Gressel, Effect of additives on properties of  $\text{V}_2\text{O}_5/\text{SiO}_2$  and  $\text{V}_2\text{O}_5/\text{MgO}$  catalysts: II. Structure and physicochemical properties of the catalysts and their correlations with oxidative dehydrogenation of propane and ethane, *Appl. Catal. Gen.* 309 (2006) 17–27.  
<https://doi.org/10.1016/j.apcata.2006.04.040>.
- [381] M. Machli, E. Heracleous, A.A. Lemonidou, Effect of Mg addition on the catalytic performance of V-based catalysts in oxidative dehydrogenation of propane, *Appl. Catal. Gen.* 236 (2002) 23–34.  
[https://doi.org/10.1016/S0926-860X\(02\)00298-3](https://doi.org/10.1016/S0926-860X(02)00298-3).



- [382] O.R. Evans, A.T. Bell, T.D. Tilley, Oxidative dehydrogenation of propane over vanadia-based catalysts supported on high-surface-area mesoporous  $\text{MgAl}_2\text{O}_4$ , *J. Catal.* 226 (2004) 292–300. <https://doi.org/10.1016/j.jcat.2004.06.002>.
- [383] M. Ruszel, B. Grzybowska, M. Gąsior, K. Samson, I. Gressel, J. Stoch, Effect of Au in  $\text{V}_2\text{O}_5/\text{SiO}_2$  and  $\text{MoO}_3/\text{SiO}_2$  catalysts on physicochemical and catalytic properties in oxidation of  $\text{C}_3$  hydrocarbons and of CO, *Catal. Today.* 99 (2005) 151–159. <https://doi.org/10.1016/j.cattod.2004.09.035>.
- [384] S. Sugiyama, T. Osaka, T. Hashimoto, K.-I. Sotowa, Oxidative Dehydrogenation of Propane on Calcium Hydroxyapatites Partially Substituted with Vanadate, *Catal. Lett.* 103 (2005) 121–123. <https://doi.org/10.1007/s10562-005-6513-7>.
- [385] P. Rybarczyk, H. Berndt, J. Radnik, M.-M. Pohl, O. Buyevskaya, M. Baerns, A. Brückner, The Structure of Active Sites in  $\text{Me}-\text{V}-\text{O}$  Catalysts ( $\text{Me} = \text{Mg}, \text{Zn}, \text{Pb}$ ) and Its Influence on the Catalytic Performance in the Oxidative Dehydrogenation (ODH) of Propane, *J. Catal.* 202 (2001) 45–58. <https://doi.org/10.1006/jcat.2001.3251>.
- [386] P. Concepción, S. Kuba, H. Knözinger, B. Solsona, J.M. López Nieto, Effect of potassium on the structure and reactivity of vanadium species in  $\text{VO}_x/\text{Al}_2\text{O}_3$  catalysts, in: A. Corma, F.V. Melo, S. Mendioroz, J.L.G. Fierro (Eds.), *Stud. Surf. Sci. Catal.*, Elsevier, 2000: pp. 767–772. [https://doi.org/10.1016/S0167-2991\(00\)81051-4](https://doi.org/10.1016/S0167-2991(00)81051-4).
- [387] D.A. Bulushev, L. Kiwi-Minsker, V.I. Zaikovskii, O.B. Lapina, A.A. Ivanov, S.I. Reshetnikov, A. Renken, Effect of potassium doping on the structural and catalytic properties of V/Ti-oxide in selective toluene oxidation, *Appl. Catal. Gen.* 202 (2000) 243–250. [https://doi.org/10.1016/S0926-860X\(00\)00538-X](https://doi.org/10.1016/S0926-860X(00)00538-X).
- [388] G. Deo, I.E. Wachs, Effect of Additives on the Structure and Reactivity of the Surface Vanadium Oxide Phase in  $\text{V}_2\text{O}_5/\text{TiO}_2$  Catalysts, *J. Catal.* 146 (1994) 335–345. <https://doi.org/10.1006/jcat.1994.1072>.

- [389] R. Grabowski, Kinetics of the oxidative dehydrogenation of propane on vanadia/titania catalysts, pure and doped with rubidium, *Appl. Catal. Gen.* 270 (2004) 37–47. <https://doi.org/10.1016/j.apcata.2004.04.021>.
- [390] M. Ai, Oxidation Activity and Acid-base Properties of Mixed Oxide Catalysts Containing Titania. II. The TiO<sub>2</sub>–V<sub>2</sub>O<sub>5</sub>–P<sub>2</sub>O<sub>5</sub> System, *Bull. Chem. Soc. Jpn.* 50 (1977) 355–358. <https://doi.org/10.1246/bcsj.50.355>.
- [391] J. Zhu, B. Rebenstorf, S.L.T. Andersson, Influence of phosphorus on the catalytic properties of V<sub>2</sub>O<sub>5</sub>/TiO<sub>2</sub> catalysts for toluene oxidation, *J. Chem. Soc. Faraday Trans. 1 Phys. Chem. Condens. Phases.* 85 (1989) 3645–3662. <https://doi.org/10.1039/F19898503645>.
- [392] A.J. van Hengstum, J. Pranger, J.G. van Ommen, P.J. Gellings, Influence of phosphorus and potassium impurities on the properties of vanadium oxide supported on TiO<sub>2</sub>, *Appl. Catal.* 11 (1984) 317–330. [https://doi.org/10.1016/S0166-9834\(00\)81889-8](https://doi.org/10.1016/S0166-9834(00)81889-8).
- [393] M.G. Nobbenhuis, P. Hug, T. Mallat, A. Baiker, Promoted vanadia/titania catalysts for o-xylene oxidation: influence of acid-base and redox properties, *Appl. Catal. Gen.* 108 (1994) 241–260. [https://doi.org/10.1016/0926-860X\(94\)85073-9](https://doi.org/10.1016/0926-860X(94)85073-9).
- [394] P. Mars, D.W. van Krevelen, Oxidations carried out by means of vanadium oxide catalysts, *Chem. Eng. Sci.* 3 (1954) 41–59. [https://doi.org/10.1016/S0009-2509\(54\)80005-4](https://doi.org/10.1016/S0009-2509(54)80005-4).
- [395] B.Y. Jibril, S.M. Al-Zahrani, A.E. Abasaeed, R. Hughes, Propane oxidative dehydrogenation on Cs-doped Cr-Mo-Al-O catalyst: kinetics and mechanism, *Chem. Eng. J.* 103 (2004) 59–67. <https://doi.org/10.1016/j.cej.2004.03.006>.
- [396] M. Baldi, E. Finocchio, C. Pistarino, G. Busca, Evaluation of the mechanism of the oxy-dehydrogenation of propane over manganese oxide, *Appl. Catal. Gen.* 173 (1998) 61–74. [https://doi.org/10.1016/S0926-860X\(98\)00129-X](https://doi.org/10.1016/S0926-860X(98)00129-X).

- [397] K. Routray, K.R.S.K. Reddy, G. Deo, Oxidative dehydrogenation of propane on V<sub>2</sub>O<sub>5</sub>/Al<sub>2</sub>O<sub>3</sub> and V<sub>2</sub>O<sub>5</sub>/TiO<sub>2</sub> catalysts: understanding the effect of support by parameter estimation, *Appl. Catal. Gen.* 265 (2004) 103–113. <https://doi.org/10.1016/j.apcata.2004.01.006>.
- [398] S. Chakraborty, S.C. Nayak, G. Deo, TiO<sub>2</sub>/SiO<sub>2</sub> supported vanadia catalysts for the ODH of propane, *Catal. Today.* 254 (2015) 62–71. <https://doi.org/10.1016/j.cattod.2015.01.047>.
- [399] A. Dinse, S. Khennache, B. Frank, C. Hess, R. Herbert, S. Wrabetz, R. Schlögl, R. Schomäcker, Oxidative dehydrogenation of propane on silica (SBA-15) supported vanadia catalysts: A kinetic investigation, *J. Mol. Catal. Chem.* 307 (2009) 43–50. <https://doi.org/10.1016/j.molcata.2009.03.008>.
- [400] G. Busca, E. Finocchio, V. Lorenzelli, G. Ramis, M. Baldi, IR studies on the activation of C–H hydrocarbon bonds on oxidation catalysts, *Catal. Today.* 49 (1999) 453–465. [https://doi.org/10.1016/S0920-5861\(98\)00441-6](https://doi.org/10.1016/S0920-5861(98)00441-6).
- [401] K. Chen, A. Khodakov, J. Yang, A.T. Bell, E. Iglesia, Isotopic Tracer and Kinetic Studies of Oxidative Dehydrogenation Pathways on Vanadium Oxide Catalysts, *J. Catal.* 186 (1999) 325–333. <https://doi.org/10.1006/jcat.1999.2510>.
- [402] M.M. Bettahar, G. Costentin, L. Savary, J.C. Lavalley, On the partial oxidation of propane and propylene on mixed metal oxide catalysts, *Appl. Catal. Gen.* 145 (1996) 1–48. [https://doi.org/10.1016/0926-860X\(96\)00138-X](https://doi.org/10.1016/0926-860X(96)00138-X).
- [403] P.C. Redfern, P. Zapol, M. Sternberg, S.P. Adiga, S.A. Zygmunt, L.A. Curtiss, Quantum Chemical Study of Mechanisms for Oxidative Dehydrogenation of Propane on Vanadium Oxide, *J. Phys. Chem. B.* 110 (2006) 8363–8371. <https://doi.org/10.1021/jp056228w>.
- [404] X. Rozanska, R. Fortrie, J. Sauer, Oxidative Dehydrogenation of Propane by Monomeric Vanadium Oxide Sites on Silica Support, *J. Phys. Chem. C.* 111 (2007) 6041–6050. <https://doi.org/10.1021/jp071409e>.

- [405] X. Rozanska, J. Sauer, Oxidative conversion of C1–C3 alkanes by vanadium oxide catalysts. DFT results and their accuracy, *Int. J. Quantum Chem.* 108 (2008) 2223–2229. <https://doi.org/10.1002/qua.21737>.
- [406] X. Rozanska, E.V. Kondratenko, J. Sauer, Oxidative dehydrogenation of propane: Differences between N<sub>2</sub>O and O<sub>2</sub> in the reoxidation of reduced vanadia sites and consequences for selectivity, *J. Catal.* 256 (2008) 84–94. <https://doi.org/10.1016/j.jcat.2008.03.002>.
- [407] E. Finocchio, G. Busca, V. Lorenzelli, R.J. Willey, FTIR studies on the selective oxidation and combustion of light hydrocarbons at metal oxide surfaces. Propane and propene oxidation on MgCr<sub>2</sub>O<sub>4</sub>, *J. Chem. Soc. Faraday Trans.* 90 (1994) 3347–3356. <https://doi.org/10.1039/FT9949003347>.
- [408] E. Finocchio, G. Busca, V. Lorenzelli, V.S. Escribano, FTIR studies on the selective oxidation and combustion of light hydrocarbons at metal oxide surfaces. Part 2.—Propane and propene oxidation on Co<sub>3</sub>O<sub>4</sub>, *J. Chem. Soc. Faraday Trans.* 92 (1996) 1587–1593. <https://doi.org/10.1039/FT9969201587>.
- [409] E. Finocchio, R.J. Willey, G. Ramis, G. Busca, V. Lorenzelli, Hydrocarbon activation and oxidation on transition metal mixed oxides: Ft-IR and flow reactor studies, in: J.W. Hightower, W. Nicholas Delgass, E. Iglesia, A.T. Bell (Eds.), *Stud. Surf. Sci. Catal.*, Elsevier, 1996: pp. 483–492. [https://doi.org/10.1016/S0167-2991\(96\)80259-X](https://doi.org/10.1016/S0167-2991(96)80259-X).
- [410] E. Finocchio, R.J. Willey, G. Busca, V. Lorenzelli, FTIR studies on the selective oxidation and combustion of light hydrocarbons at metal oxide surfaces Part 3.—Comparison of the oxidation of C<sub>3</sub> organic compounds over Co<sub>3</sub>O<sub>4</sub>, MgCr<sub>2</sub>O<sub>4</sub> and CuO, *J. Chem. Soc. Faraday Trans.* 93 (1997) 175–180. <https://doi.org/10.1039/A605341F>.
- [411] D. Shee, T.V.M. Rao, G. Deo, Kinetic parameter estimation for supported vanadium oxide catalysts for propane ODH reaction:

- Effect of loading and support, *Catal. Today*. 118 (2006) 288–297.  
<https://doi.org/10.1016/j.cattod.2006.07.017>.
- [412] T.V.M. Rao, G. Deo, Kinetic parameter analysis for propane ODH: V<sub>2</sub>O<sub>5</sub>/Al<sub>2</sub>O<sub>3</sub> and MoO<sub>3</sub>/Al<sub>2</sub>O<sub>3</sub> catalysts, *AIChE J.* 53 (2007) 1538–1549. <https://doi.org/10.1002/aic.11176>.
- [413] A. Bottino, G. Capannelli, A. Comite, S. Storace, R. Di Felice, Kinetic investigations on the oxidehydrogenation of propane over vanadium supported on  $\gamma$ -Al<sub>2</sub>O<sub>3</sub>, *Chem. Eng. J.* 94 (2003) 11–18.  
[https://doi.org/10.1016/S1385-8947\(03\)00003-2](https://doi.org/10.1016/S1385-8947(03)00003-2).
- [414] M.D. Argyle, K. Chen, A.T. Bell, E. Iglesia, Effect of Catalyst Structure on Oxidative Dehydrogenation of Ethane and Propane on Alumina-Supported Vanadia, *J. Catal.* 208 (2002) 139–149.  
<https://doi.org/10.1006/jcat.2002.3570>.
- [415] D. Creaser, B. Andersson, Oxidative dehydrogenation of propane over V-Mg-O: kinetic investigation by nonlinear regression analysis, *Appl. Catal. Gen.* 141 (1996) 131–152.  
[https://doi.org/10.1016/0926-860X\(96\)00029-4](https://doi.org/10.1016/0926-860X(96)00029-4).
- [416] S.L.T. Andersson, Kinetic study of the oxidative dehydrogenation of propane over vanadia supported on amorphous AlPO<sub>4</sub>, *Appl. Catal. Gen.* 112 (1994) 209–218. [https://doi.org/10.1016/0926-860X\(94\)80220-3](https://doi.org/10.1016/0926-860X(94)80220-3).
- [417] S. Zhang, H. Liu, Oxidative dehydrogenation of propane over Mg-V-O oxides supported on MgO-coated silica: Structural evolution and catalytic consequence, *Appl. Catal. Gen.* 573 (2019) 41–48.  
<https://doi.org/10.1016/j.apcata.2019.01.012>.
- [418] J.N. Michaels, D.L. Stern, R.K. Grasselli, Oxydehydrogenation of propane over Mg-V-Sb-oxide catalysts. II. Reaction kinetics and mechanism, *Catal. Lett.* 42 (1996) 139–148.  
<https://doi.org/10.1007/BF00810679>.
- [419] M.A. Vannice, An analysis of the Mars–van Krevelen rate expression, *Catal. Today*. 123 (2007) 18–22.  
<https://doi.org/10.1016/j.cattod.2007.02.002>.

- [420] G. Saracco, H.W.J.P. Neomagus, G.F. Versteeg, W.P.M. van Swaaij, High-temperature membrane reactors: potential and problems, *Chem. Eng. Sci.* 54 (1999) 1997–2017. [https://doi.org/10.1016/S0009-2509\(99\)00009-3](https://doi.org/10.1016/S0009-2509(99)00009-3).





# **EXPERIMENTAL METHODOLOGY**





## 2. EXPERIMENTAL METHODOLOGY

### 2.1. Catalysts preparation

#### 2.1.1. Reagents

The reagents used in the preparation of the polymer solutions to be electrospun were zirconium(IV) propoxide solution (Sigma-Aldrich, CAS: 23519-77-9, 70 wt % in 1-propanol), zirconium acetate solution (Sigma-Aldrich, CAS 7585-20-8,  $Zr^{+x} \cdot xCH_3COOH$ , Zr ~16 wt % in acetic acid), polyvinylpyrrolidone (PVP) (Sigma-Aldrich, CAS: 9003-39-8, Mw ~1,300,000), acetylacetone (Sigma-Aldrich, CAS: 123-54-6, ≥99%), 1-propanol (Sigma-Aldrich, CAS: 71-23-8, ≥99.5%), vanadyl acetylacetonate (Sigma-Aldrich, CAS: 3153-26-2, ≥97.0%), ammonium niobate(V) oxalate hydrate (Sigma-Aldrich, 99.99%) and ammonium heptamolybdate tetrahydrate (Sigma-Aldrich, CAS: 12054-85-2, 99.98%).

#### 2.1.2. Polymer solutions

Both zirconium propoxide in n-propanol or zirconium acetate in acetic acid solutions were used as zirconia precursor [1,2], instead of zirconium oxychloride [3,4], because they are more environmentally friendly and do not produce corrosive chloride ions during the process. In the former case, the addition of acetylacetone (chelating agent) was required for the stabilization of the zirconium propoxide solution [5,6]. PVP was used to form the polymer and to increase the viscosity of the solution in order to be properly electrospun [1,7]. Vanadyl acetylacetonate, ammonium niobate oxalate and ammonium heptamolybdate were used as vanadium, niobium and molybdenum precursors, respectively, since they presented an adequate solubility in the corresponding polymer solutions.

For the preparation of the polymer solutions, all the corresponding reagents were mixed in the proper amounts in order to obtain the desired metallic content in vanadium, niobium and/or molybdenum of the final solid. Then,

these polymer solutions were vigorously stirred for 24 h at room temperature.

Part of some of the polymer solutions were dried overnight at 60 °C in a vacuum dryer and then calcined to obtain powdered catalysts. The calcinations were proceeded in a conventional tubular furnace (from Thermo Fisher Scientific, Carbolite CTF 12/100/900 model) at 500°C for 6 h under air flow (150 mL STP/min) in order to eliminate the remaining solvent, the PVP and the carbonaceous material of the precursors. The heating rate to reach the calcination temperature was always 10°C/min.

### 2.1.3. Electrospinning

Electrospinning is a simple and straightforward technique to obtain fibers in the submicron and nano scale [7,8]. This technique makes use of electrohydrodynamic forces to prepare polymeric fibers from solutions. The typical set up of electrospinning mainly consists of three components: a needle or spinneret, a grounded collecting plate or collector and a high voltage power supply used to apply an electric field between the needle and the collector (Figure 2.1).

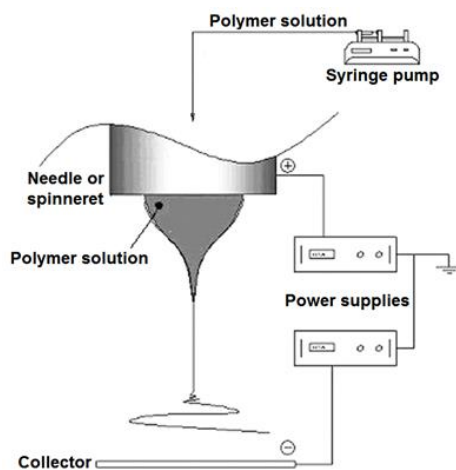


Figure 2.1. Schematic representation of a typical electrospinning equipment.

There are many parameters that have influence in the electrospinning process such as solution parameters (e.g. viscosity, density, concentration

of polymer solution, surface tension, etc.), process parameters (e.g. applied voltage, flow rate of the polymer solution, distance between the needle and the collector, etc.) and ambient parameters (e.g. humidity, temperature, etc). All these parameters have an influence one each other and determine the diameter and length of the fibers [5–8]. It should be noted that for a given solution and ambient parameters, the polymer solution is only spinnable in a range of values of the process parameters and vice versa, or even sometimes is not possible the electrospinning process. This range of values is determined by the polymer solution, which presents certain rheological and electrical properties.

In all the experiments the distance between the needle and the collector was 20 cm and the flow rate of the polymer solution was 0.5 mL/h. The electrical potential difference was adjusted/optimized depending on electrohydrodynamic properties of each polymer solution to find the stability of the jet during the electrospinning process. It should be noted that the applied voltage for the polymer solutions prepared using zirconium propoxide was always 12 kV, while for the ones prepared using zirconium acetate was required higher applied voltage (from 14 to 34 kV), probably due to the higher surface tension of the latter polymer solutions. Moreover, in some polymer solutions made of zirconium acetate were necessary to dilute them with acetic acid to avoid gel formation and to decrease the viscosity, which made difficult the electrospinning process.

Subsequently, the electrospun fibers were calcined in the tubular furnace at 500°C for 6 h under air flow (150 mL STP/min) in order to remove the remaining solvent, the PVP and the organic part of the metallic precursors, and to stabilize the zirconia fibers. The heating rate to get such calcination temperature was always 10°C/min. Finally, the multimetallic catalysts with fiber shape based on V-Zr-O, Mo-Zr-O, Nb-Zr-O, V-Mo-Zr-O and V-Nb-Zr-O systems were obtained.

#### 2.1.4. Incipient wetness method

Typically, synthesis of supported catalysts consists of a first step of support preparation, and a second step of active phase deposition onto the support [9–13]. In the case of incipient wetness impregnation method, it is normally required to determine the maximum volume of the precursor solution that can be adsorbed per gram of sample support. Then, the desired amount of active phase precursor is dissolved in such volume to impregnate the corresponding sample.

Therefore, this method is highly influenced by the solubility of the active phase precursor and the adsorption capacity of the sample support, which sometimes are not high enough and the amount of metal loading that can be used during the impregnation is limited. This is one of the biggest drawbacks of the incipient wetness impregnation method. Moreover, this method usually leads to a decrease of the surface area, due to pore blockage during the deposition of the active phase, what results in a little control over their dispersion [14]. Then, in the case of support impregnation with vanadium, non-uniform distribution of  $\text{VO}_x$  surface density may be achieved, and local spots with surface coverage above monolayer can appear with the subsequent formation of non-desired  $\text{V}_2\text{O}_5$  crystallites, even if the vanadium content of the solution for the impregnation is prepared to obtain a catalyst with submonolayer coverage.

In this work, zirconia samples in fiber and powder shape were impregnated by the classic incipient wetness impregnation method with aqueous solutions of vanadyl acetylacetonate. It should be noted that the adsorption capacity of each sample was determined by using distilled water. After the impregnation, the samples were dried overnight at 60 °C in a vacuum dryer and then calcined in the tubular furnace at 500°C (10°C/min of heating rate) for 6 h under air flow (150 mL STP/min) to obtain the final catalysts.



### 2.1.5. Samples nomenclature

All the catalysts prepared are summarized in Table 2.1. In the nomenclature, the first letter, “F” or “P”, indicates fibrillar or powdered shape of the catalysts, respectively. If this letter is followed by “I”, it means that the catalyst has been impregnated with the incipient wetness impregnation. With respect to the middle part of the name, “PZr” or “AZr” refers to the zirconium precursor used, zirconium propoxide or zirconium acetate, respectively. The final part of the name indicates the mass concentration of V, Nb and Mo. Thus, F-PZr is zirconia fiber free of V, Nb or Mo prepared using zirconium propoxide, PI-PZr-V5.0 is a powdered catalyst prepared using zirconium propoxide containing 5.0 wt % of vanadium and that has been impregnated by the incipient wetness impregnation method, and F-AZr-V0.8-Mo4.3 is zirconia fiber prepared using zirconium acetate with a mass content of V and Mo of 0.8 and 4.3%, respectively. Note that when the catalysts F-PZr-V2.5, F-PZr-V5.0 and F-PZr-V6.4 were grinded and pressed into self-supported wafers in order to perform *operando* experiments in the IRRaman reactor, their names became Zr-V2.5, Zr-V5.0 and Zr-V6.4, respectively.



**Table 2.1.** Summary of the samples prepared and their composition, shape and preparation method.

Name	Shape	Zirconia Precursor	V content (wt %)	Nb content (wt %)	Mo content (wt %)	Preparation method <sup>a</sup>
P-PZr	Powder	Propoxide	-	-	-	One-step
PI-PZr-V1.0	Powder	Propoxide	1.0	-	-	IWI
PI-PZr-V5.0	Powder	Propoxide	5.0	-	-	IWI
P-PZr-V5.0	Powder	Propoxide	5.0	-	-	One-step
F-PZr	Fiber	Propoxide	-	-	-	Electrospinning one-step
FI-PZr-V5.0	Fiber	Propoxide	5.0	-	-	Electrospinning and IWI
F-PZr-V1.3	Fiber	Propoxide	1.3	-	-	Electrospinning one-step
F-PZr-V2.5	Fiber	Propoxide	2.5	-	-	Electrospinning one-step
F-PZr-V3.7	Fiber	Propoxide	3.7	-	-	Electrospinning one-step
F-PZr-V5.0	Fiber	Propoxide	5.0	-	-	Electrospinning one-step
F-PZr-V6.4	Fiber	Propoxide	6.4	-	-	Electrospinning one-step
F-PZr-V13.3	Fiber	Propoxide	13.3	-	-	Electrospinning one-step
F-PZr-Nb5.0	Fiber	Propoxide	-	5.0	-	Electrospinning one-step
F-PZr-Mo5.0	Fiber	Propoxide	-	-	5.0	Electrospinning one-step
F-PZr-V3.1-Nb1.9	Fiber	Propoxide	3.1	1.9	-	Electrospinning one-step
F-PZr-V3.1-Mo1.9	Fiber	Propoxide	3.1	-	1.9	Electrospinning one-step
F-PZr-V0.8-Mo4.3	Fiber	Propoxide	0.8	-	4.3	Electrospinning one-step
F-AZr	Fiber	Acetate	-	-	-	Electrospinning one-step
F-AZr-V5.0	Fiber	Acetate	5.0	-	-	Electrospinning one-step
F-AZr-Nb5.0	Fiber	Acetate	5.0	5.0	-	Electrospinning one-step
F-AZr-Mo5.0	Fiber	Acetate	5.0	-	5.0	Electrospinning one-step
F-AZr-V3.1-Nb1.9	Fiber	Acetate	3.1	1.9	-	Electrospinning one-step
F-AZr-V3.1-Mo1.9	Fiber	Acetate	3.1	-	1.9	Electrospinning one-step
F-AZr-V0.8-Mo4.3	Fiber	Acetate	0.8	-	4.3	Electrospinning one-step
Zr-V2.5	Pellet	Propoxide	2.5	-	-	Pelletized F-PZr-V2.5
Zr-V5.0	Pellet	Propoxide	5.0	-	-	Pelletized F-PZr-V5.0
Zr-V6.4	Pellet	Propoxide	6.4	-	-	Pelletized F-PZr-V6.4

<sup>a</sup>IWI= Incipient wetness impregnation

## 2.2. Catalysts characterization

### 2.2.1. Porous texture

The porous texture of the samples was characterized by N<sub>2</sub> adsorption-desorption isotherms at -196°C using a micromeritics instrument (ASAP 2020 model). The samples were previously outgassed for at least 8 h at 150°C. The apparent surface area ( $A_{\text{BET}}$ ) was determined by applying the BET equation to the N<sub>2</sub> adsorption isotherm.

### 2.2.2. Morphology

The surface morphology of the samples was studied by transmission electron microscopy (TEM) at an accelerating voltage of 200 kV, in a FEI Talos F200X microscope equipped with energy-dispersive X-ray analyzer (EDXA).

### 2.2.3. Surface chemistry and crystal structure

Surface chemistry and crystal structure of the samples was analyzed by X-ray photoelectron spectroscopy (XPS), X-ray diffraction patterns (XRD) and *In situ* Raman.

XPS analyses of the samples were obtained by a 5700C model Physical Electronics apparatus with MgK $\alpha$  radiation (1253.6 eV). The maximum of the C1s peak was set at 284.5 eV and used as a reference to shift the other peaks.

XRD were recorded in the region of  $2\theta=5-80^\circ$  for 30 min on an EMPYREAN diffractometer of PANalytical using CuK $\alpha$ 1,2 (1.5406 Å) monochromatic radiation (operational value 45 kV and 40 mA), a detector PIXcel and Soller slits (incident and diffracted beam) of 0.04 rad.

*In situ* Raman spectra of the samples were acquired in the 200-3200 cm $^{-1}$  region, using an Invia Reflex Raman Confocal (RENISHAW) spectrometer equipped with a RemCam deep depletion CCD detector using the 514.5 nm Ar line, with a spectral resolution of ca. 1 cm $^{-1}$ . The samples were treated at 200°C in air 2 h for obtaining the spectra under dehydrated conditions.

## 2.3. Propane ODH experiments

### 2.3.1. Fixed bed reactor

A schematic representation of the set-up to perform the propane ODH reaction over the catalysts prepared is shown in Figure 2.2. The set-up consisted of a fixed bed microreactor with an internal diameter of 4 mm. This quartz tubular reactor (from Mervilab) was placed inside a vertical furnace (from Forns Hobersal, TR2-A model). The desired temperature for each experiment was achieved using a temperature controller (from Forns Hobersal, TR2-A model) connected to both the furnace and the thermocouple located inside the fixed bed in contact with the catalyst during reaction. The reactor was fed by a mixture of three gases (from Abello



Linde): propane (99.95%), oxygen (99.999%) and helium (99.999%), which were individually controlled by mass flow controllers (from BROOKS, serie GF040) to mix the gases in the desired composition. All the lines were heated above 120°C with a flexible heating cable (from Dicsa, KM-HC-G (3 M/450 W) model) connected to a power regulator (from Dicsa, KM-L116LLG 9642660 model) in order to pre-heat the reactant mixture before entering the reactor and to avoid the condensation of any product leaving the reactor. Reactants and products were analyzed by an on-line gas chromatograph (from Perkin-Elmer, Clarus 500 GC model), equipped with a Hayesep D 80/100 (length: 3 m; diameter: 1/8"; internal diameter: 2.1 mm) and an active carbon 80/100 (length: 2 m; diameter 1/8"; internal diameter: 2,1 mm) packed columns. Light gases ( $O_2$ , CO and  $CO_2$ ) were detected by a thermal conductivity detector (TCD); and  $CH_4$ ,  $C_2H_4$ ,  $C_2H_6$ ,  $C_3H_6$  and  $C_3H_8$  were detected using a flame ionization detector (FID). The duration of each GC analysis was always 15 min.

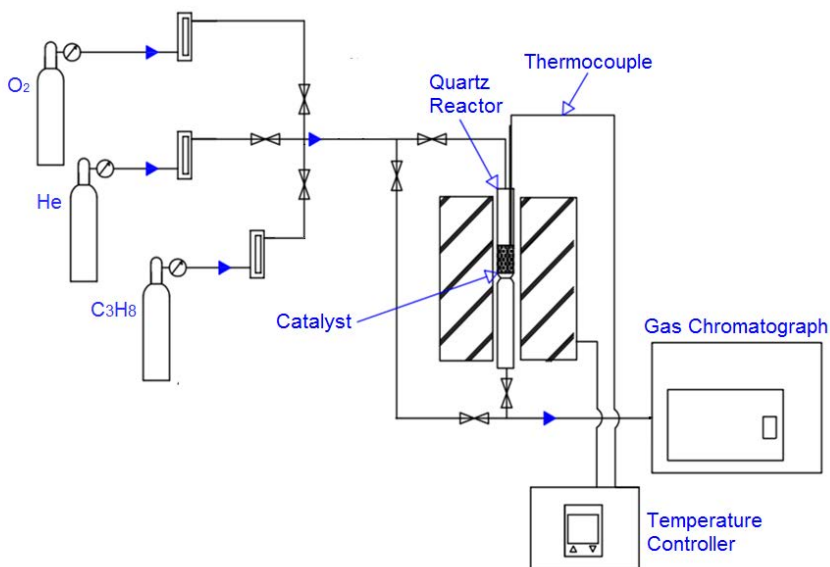


**Figure 2.2.** Schematic representation of the set-up for the fixed bed reactor.

### 2.3.2. IRRaman *operando* reactor

The IRRaman *operando* reactor was specifically designed at Laboratoire Catalyse et Spectrochimie (Caen, France) in a joint CSIC-UNICAEN collaboration, adapting a home-made *operando* IR reactor [15] to also host a Raman probe (Figure 2.3).

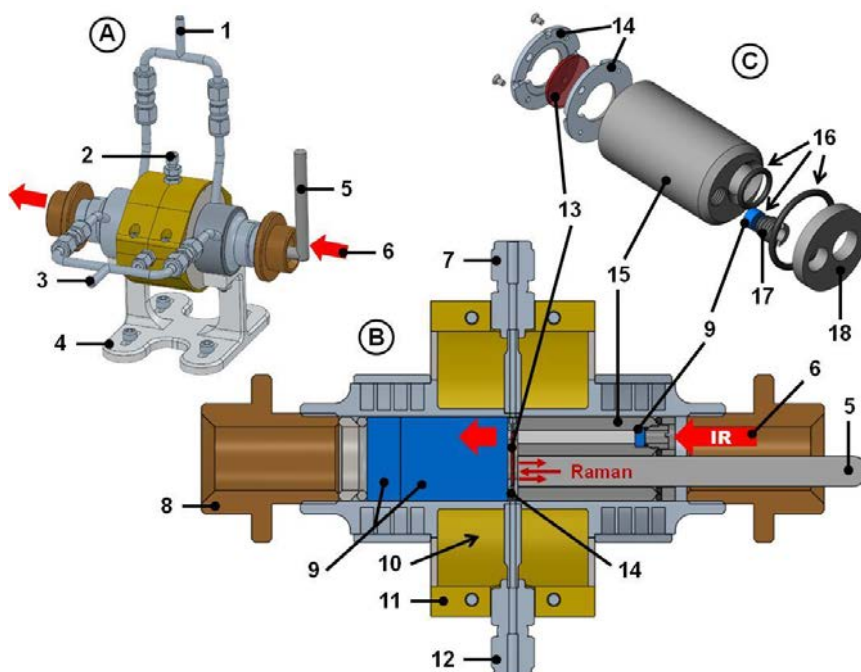


**Figure 2.3.** Description of the IRRaman device: (A) general view of the cell in perspective, (B) longitudinal view and (C) exploded view of the IRRaman accessory. (1) air cooling outlet, (2) thermocouple location, (3) air cooling inlet, (4) IRRaman cell support, (5) Raman probe, (6) IR beam, (7) gas outlet, (8) adjusting nut for airtightness, (9) KBr windows, (10) oven location, (11) external shell, (12) gas inlet, (13) sample (wafer), (14) wafer holder, (15) barrel of the IRRaman accessory, (16) Kalrez O-ring, (17) hollow clamping nut (for the passage of the IR beam), (18) cap of the IRRaman accessory.

The cell was placed in the IR spectrometer bench (Nicolet 6700 FT-IR spectrometer (64 scans/spectrum) equipped with a MCT/A detector) and allowed direct acquisition of the transmission IR spectra. For the Raman spectra, the laser excitation (532 nm) was brought in the cell via an optical fibre and focused on the sample with an *ad hoc* InPhotonics Raman probe specially designed to withstand high temperatures. The Raman signal was analysed by a Horiba Jobin Yvon Labram300 spectrometer. The dual IR-Raman *operando* reactor can be heated for catalyst activation or reaction,

and can be fed with controlled gas flow. The presence of an additional capillary thermocouple on the catalyst pellet (not shown in Figure 2.3) providing temperature monitoring and oven feedback guaranteed the temperature control during the experiments. Downstream the catalyst wafer, the exhaust gases were directed towards an IR gas cell, a GC and/or a mass spectrometer for simultaneous on line analysis. The lines were heated at 60°C with a flexible heating cable to pre-heat the reactant mixture before entering the reactor-cell and to avoid condensation of products leaving the reactor-cell.

## 2.4. References

- [1] R. Ruiz-Rosas, J. Bedia, J.M. Rosas, M. Lallave, I.G. Loscertales, J. Rodríguez-Mirasol, T. Cordero, Methanol decomposition on electrospun zirconia nanofibers, *Catal. Today*. 187 (2012) 77–87. <https://doi.org/10.1016/j.cattod.2011.10.031>.
- [2] S. Singh, V. Singh, M. Vijayakumar, V.V. Bhanu Prasad, ZrO<sub>2</sub> fibers obtained from the halide free synthesis of non-beaded PVA/Zr n-propoxide electrospun fibrous composites, *Ceram. Int.* 39 (2013) 1153–1161. <https://doi.org/10.1016/j.ceramint.2012.07.039>.
- [3] C. Shao, H. Guan, Y. Liu, J. Gong, N. Yu, X. Yang, A novel method for making ZrO<sub>2</sub> nanofibres via an electrospinning technique, *J. Cryst. Growth*. 267 (2004) 380–384. <https://doi.org/10.1016/j.jcrysgro.2004.03.065>.
- [4] J.Y. Li, Y. Sun, Y. Tan, F.M. Xu, X.L. Shi, N. Ren, Zirconium nitride (ZrN) fibers prepared by carbothermal reduction and nitridation of electrospun PVP/zirconium oxychloride composite fibers, *Chem. Eng. J.* 144 (2008) 149–152. <https://doi.org/10.1016/j.cej.2008.04.037>.
- [5] S. Singh, V. Singh, M. Vijayakumar, V.V. Bhanu Prasad, Dual fiber behavior of polyvinyl alcohol/zirconium n-propoxide composite fibrous mats prepared via electrospinning, *Ceram. Int.* 39 (2013) 5031–5037. <https://doi.org/10.1016/j.ceramint.2012.11.101>.

- [6] S. Singh, V. Singh, M. Vijayakumar, V.V. Bhanu Prasad, Electrospun ZrO<sub>2</sub> fibers obtained from polyvinyl alcohol/zirconium n-propoxide composite fibers processed through halide free sol–gel route using acetic acid as a stabilizer, *Mater. Lett.* 115 (2014) 64–67. <https://doi.org/10.1016/j.matlet.2013.10.026>.
- [7] N. Bhardwaj, S.C. Kundu, Electrospinning: A fascinating fiber fabrication technique, *Biotechnol. Adv.* 28 (2010) 325–347. <https://doi.org/10.1016/j.biotechadv.2010.01.004>.
- [8] Z.-M. Huang, Y.-Z. Zhang, M. Kotaki, S. Ramakrishna, A review on polymer nanofibers by electrospinning and their applications in nanocomposites, *Compos. Sci. Technol.* 63 (2003) 2223–2253. [https://doi.org/10.1016/S0266-3538\(03\)00178-7](https://doi.org/10.1016/S0266-3538(03)00178-7).
- [9] A. Khodakov, B. Olthof, A.T. Bell, E. Iglesia, Structure and catalytic properties of supported vanadium oxides: Support effects on oxidative dehydrogenation reactions, *J. Catal.* 181 (1999) 205–216.
- [10] J. Bedia, J.M. Rosas, J. Rodríguez-Mirasol, T. Cordero, Pd supported on mesoporous activated carbons with high oxidation resistance as catalysts for toluene oxidation, *Appl. Catal. B Environ.* 94 (2010) 8–18. <https://doi.org/10.1016/j.apcatb.2009.10.015>.
- [11] A. Christodoulakis, M. Machli, A.A. Lemonidou, S. Boghosian, Molecular structure and reactivity of vanadia-based catalysts for propane oxidative dehydrogenation studied by in situ Raman spectroscopy and catalytic activity measurements, *J. Catal.* 222 (2004) 293–306. <https://doi.org/10.1016/j.jcat.2003.10.007>.
- [12] I. Hita, T. Cordero-Lanzac, A. Gallardo, J.M. Arandes, J. Rodríguez-Mirasol, J. Bilbao, T. Cordero, P. Castaño, Phosphorus-containing activated carbon as acid support in a bifunctional Pt–Pd catalyst for tire oil hydrocracking, *Catal. Commun.* 78 (2016) 48–51. <https://doi.org/10.1016/j.catcom.2016.01.035>.
- [13] A. Dinse, B. Frank, C. Hess, D. Habel, R. Schomäcker, Oxidative dehydrogenation of propane over low-loaded vanadia catalysts: Impact of the support material on kinetics and selectivity, *J. Mol.*

- Catal. Chem. 289 (2008) 28–37.  
<https://doi.org/10.1016/j.molcata.2008.04.007>.
- [14] C.A. Carrero, R. Schloegl, I.E. Wachs, R. Schomaecker, Critical literature review of the kinetics for the oxidative dehydrogenation of propane over well-defined supported vanadium oxide catalysts, ACS Catal. 4 (2014) 3357–3380.  
<https://doi.org/10.1021/cs5003417>.
- [15] S. Wuttke, P. Bazin, A. Vimont, C. Serre, Y.-K. Seo, Y.K. Hwang, J.-S. Chang, G. Férey, M. Daturi, Discovering the Active Sites for C3 Separation in MIL-100(Fe) by Using Operando IR Spectroscopy, Chem. – Eur. J. 18 (2012) 11959–11967.  
<https://doi.org/10.1002/chem.201201006>.

## **RESULTS AND DISCUSSION**



### 3. RESULTS AND DISCUSSION

#### 3.1. Electrospun vanadium oxide based submicron diameter fiber catalysts. Part I: Preparation procedure and propane ODH application

J. J. Ternero-Hidalgo, J. Torres-Liñán, M.O. Guerrero-Pérez, J. Rodríguez-Mirasol, T. Cordero

Universidad de Málaga, Departamento de Ingeniería Química, Campus de Teatinos s/n, E29071 Málaga, Spain

**Keywords:** Propane ODH; Mixed-oxide catalysts; Submicron fibers; Electrospinning; Vanadium; Zirconia

#### **Abstract**

V-Zr-O submicron diameter fibers have been prepared by electrospinning of V and Zr containing solutions in only one calcination step. This is a simple and versatile synthesis method, easy to scale up, that produces porous solids, with fibrous morphology and with VO<sub>x</sub> catalytically active species, being these solids attractive for alkane partial oxidation reactions, since the catalysts with fibrous morphology present several advantages with respect powered ones. With the new proposed method, at low vanadium loadings (V% w/w<6.4), surface dispersed VO<sub>x</sub> were found in the zirconia fiber as shown by Raman spectroscopy analysis, whereas crystalline ZrV<sub>2</sub>O<sub>7</sub> was observed when the V content was increased (V% w/w>6.4). These fibers were very active for the propane oxidative dehydrogenation (ODH) catalytic reaction, showing very promising results since the fibrous morphology of submicrometric diameter makes these solids quite suitable for fixed-bed catalytic reactors.





### **3.1.1. Introduction**

Vanadium oxide based materials are well known active and selective catalysts for partial oxidation reactions [1,2]. The mechanical and catalytic properties of Vanadium oxides can be modulated and improved by the incorporation of other elements into their crystal structure and by the use of a catalytic support, such as zirconia. Several steps are required to obtain a VO<sub>x</sub> supported catalyst, including the preparation of a suitable catalytic support, which usually requires a first calcination process, followed by the impregnation of such support with the active phase precursor and the subsequent calcination step [3–8]. In general, these methods lead to a decrease of the surface area of the catalytic support, due to pore blockage during the process of deposition of the active phase [9].

On the other hand, the use of catalytic materials with fibrous structure of submicrometric size may present several advantages with respect to powdered ones. They show very small resistance to internal diffusion and high surface area to volume ratio because of their submicrometric diameter; as well as less significant temperature gradients and lower pressure drop in a fixed bed than those in powder form due to the high void fractions or bed porosity offered by these fibrous structures [10]. Furthermore, they are easy to handle and can be packed or constructed in the best form to fit the particular use or application due to their geometric flexibility. All these differences would still be more appreciable in the use of these catalysts on an industrial scale. Since the powder catalysts can easily overcome all these intrinsic disadvantages at laboratory scale adding a diluting inert material (glass, quartz,  $\alpha$ -alumina or silicon carbide [11,12]) and/or making pellets (not necessary for submicrometric fibers), which may not be so operative at industrial level. Moreover, pellet size should be small enough to avoid high resistance to internal diffusion and big enough to avoid high pressure drop in a fixed bed, which is not possible sometimes. Consequently, fibers have potentially higher fluidodynamics and transfer properties which may make them more feasible to scale up to industrial level. Electrospinning is a simple and straightforward technique to obtain

fibers in the submicron and nano scale [13,14]. This technique makes use of electrohydrodynamic forces to prepare polymeric fibers from solutions. The fibers obtained by this procedure find their use in a wide variety of applications such as in biomedicine (tissue engineering), sensor technology, energy storage (supercapacitors, electrocatalysts), adsorption, heterogeneous catalysis, etc. [13–18]. The typical set up of electrospinning mainly consists of three components: a needle or spinneret, a grounded collecting plate or collector and a high voltage power supply used to apply an electric field between the needle and the collector. In the electrospinning process, an electric field is subjected to the end of a needle that contains the polymer solution held by its surface tension. As the intensity of the electric field is increased, the fluid at the tip of the needle elongates to form a conical shape known as Taylor cone. When the applied electric field reaches a critical value, the repulsive electrical forces overcome the surface tension forces and a charged jet of the solution is ejected from the tip of the Taylor cone to the collector. During this process, the polymer solution jet undergoes an instability and elongation process, which allows the jet to become very long and thin. Meanwhile, the solvent evaporates, leaving behind a charged polymer fiber. There are several parameters that have influence in the process such as viscosity, flow, concentration of polymer solution, applied voltage, or distance between the needle and the collector, controlling the diameter and length of the fibers [13,14,19,20].

On the other hand, the interest of petrochemical industry towards the use of propylene is growing up because it is the raw material for a wide variety of interest products (i.e., polypropylene, acrylonitrile, oxo-alcohols, propylene oxide, cumene, acrylic acid, etc.) [21]. The global demand for propylene in 2005 and in 2014 were about 67 and 89 Mt, respectively [22,23], and this is expected to grow to about 165 Mt by 2030 [24]. In fact, propylene is the second most important starting product in the petrochemical industry after ethylene [23]. Currently, propylene is mainly obtained as byproduct from steam cracking of naphtha, fluid catalytic cracking in the oil refining and natural gas processing, which are performed

at high temperatures and present high energy consumption [21,24,25]. A wide range of demanded light hydrocarbons can be obtained by these processes; however, the selectivity to propylene is very low. Consequently, the propylene produced by this way is not enough to face the current demand and growth rate in the future [23,24]. Alternatively, the production of propylene from propane has been investigated since the early 1990s, because propane is more abundant and significantly cheaper as feedstock [26–28]. In this way, catalytic dehydrogenation of propane to propylene is possible, but this is a strongly endothermic process performed at temperature above 873 K, which presents thermodynamic constraints that limit the propane conversion. Moreover, a major problem in this process is coke formation, which causes rapid catalyst deactivation [9,25]. Oxidative dehydrogenation (ODH) of propane is a promising alternative to produce propylene from propane. This reaction is exothermic and can be performed at lower temperatures, it is thermodynamically unrestricted and the coke deposition is minimized [9,25]. However, the propene yields are still not sufficiently high to be profitable at industrial scale due to the undesirable combustion reactions to CO and CO<sub>2</sub> (CO<sub>x</sub>) [25].

According to the literature, isolated and oligomerized surface dispersed vanadium species (VO<sub>x</sub>) are the active phases during alkane partial oxidation reactions [9,25,29–32]. These surface VO<sub>x</sub> species have three different oxygen atoms: forming a terminal vanadyl group (V=O), bridging two vanadium atoms (V-O-V), and linking a vanadium atom and the support (V-O-S) [1,2]. The reactivity of these catalytic systems is controlled by their redox properties, which are influenced by both redox and acid-base properties of the support [1,33,34]. Several oxide supports have been used for preparing vanadium supported catalysts, such as SiO<sub>2</sub>, Al<sub>2</sub>O<sub>3</sub>, TiO<sub>2</sub>, and ZrO<sub>2</sub> [1,2]. Zirconia presents quite valuable characteristics as catalyst support, such as high thermal and chemical stability; and acidic, basic, reducing and oxidizing properties [35].

The main objective of the present paper is the preparation of zirconia submicron sized fibrous catalytic materials with dispersed VO<sub>x</sub> species

active for partial oxidation of propane by electrospinning technique. In this new procedure, the electrospinning process is performed with a polymer solution that includes both the vanadium and the zirconia precursors. These catalysts present all the advantages of fibrous conventional catalytic materials, but with a simpler preparation method that avoid a second process of depositing the catalytic active phase on the zirconia fibrous support, followed by the calcination step. In order to evaluate the effect of the synthesis method proposed on the nature of the vanadium species in the final catalytic material of the new methodology proposed (addition of Vanadium during the synthesis of the fiber in only one step), a series of catalysts were prepared by conventional impregnation (preparation of the support followed by impregnation of the Vanadium precursor, two steps) was also prepared and characterized.

### **3.1.2. Materials and methods**

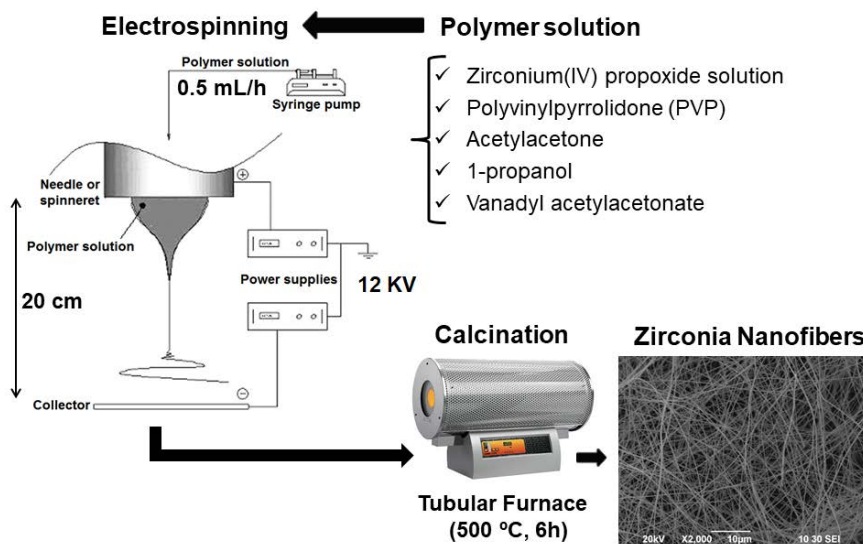
#### *3.1.2.1. Catalysts preparation*

Scheme 3.1.1 outlines the procedure followed for the preparation of zirconia fibers catalysts, which involves the preparation of the polymer solution containing both vanadium catalyst and zirconia precursors to be electrospun, followed by calcination to obtain the final submicron-fiber catalysts. The polymer solutions were prepared by using zirconium(IV) propoxide solution (Sigma-Aldrich, CAS: 23519-77-9, 70 wt % in 1-propanol), polyvinylpyrrolidone (PVP) (Sigma-Aldrich, CAS: 9003-39-8, Mw ~1,300,000), acetylacetone (Sigma-Aldrich, CAS: 123-54-6, ≥99%), 1-propanol (Sigma-Aldrich, CAS: 71-23-8, ≥99.5%), and Vanadyl acetylacetonate (Sigma-Aldrich, CAS: 3153-26-2, ≥97.0%).

Zirconium(IV) propoxide solution was used as zirconia precursor instead of zirconium oxychloride, as it has been previously published elsewhere [36,37], because it is more environmental friendly. The use of this precursor avoids the formation of corrosive chloride ions during the process. Vanadyl acetylacetonate is used as vanadium precursor since it presents an

adequate solubility in the polymer solution. PVP is used to form the polymer and to increase the viscosity of the solution in order to be properly electrospun [13,15]. Stabilization of zirconium(IV) propoxide is achieved by the addition of acetylacetonate (chelating agent) [19,20].

The Zr–PVP solutions have been prepared by mixing 2.1 g of zirconium(IV) propoxide solution, 0.317 g of PVP, 0.450 g of acetylacetonate and 2.984 g of 1-propanol. For preparing the V-containing zirconia fibers, vanadyl acetylacetonate was added to the above polymer solution, in the amounts of 0.038, 0.075, 0.110, 0.147, 0.190, and 0.521 g, to obtain final fibers with elemental vanadium mass concentrations of 1.3, 2.5, 3.7, 5.0, 6.4, and 13.3%, respectively. These amounts have been calculated in order to obtain V contents similar to those of active and selective conventional vanadium oxide supported catalysts that were prepared with the intention to obtain vanadium oxide contents close to a monolayer coverage [1,2]. Then, these polymer solutions were vigorously stirred for 24 h at room temperature before the electrospinning process.



**Scheme 3.1.1.** Schematic procedure followed for the preparation of vanadium-containing zirconia submicron-fibers.

Scheme 3.1.1 also shows the electrospinning set up used for the preparation of the fibers. This setup consists of a syringe pump, a needle

or spinneret, a collector and two high voltage power supplies (one positively polarized connected to the needle and the other negatively polarized attached to the collector). In every case, the electrospinning operation conditions were the same. The distance between the needle and the collector was 20 cm, the electrical potential difference was 12 kV (the tip at +6 kV and the collector was at -6 kV) and the flow rate of the polymer solution through the spinneret was 0.5 mL/h.

Then, the electrospun fibers were recovered in form of non-woven cloth and calcined in a conventional tubular furnace. In all the cases, the heating rate to reach the calcination temperature (500°C) was 10°C/min. The calcination temperature was kept for 6 h under air flow (150 mL STP/min) in order to eliminate the remaining solvent, the PVP and the organic part of the V and Zr precursors, and to stabilize the zirconia fibers. Finally, the fibers obtained were named F-PZr, F-PZr-V1.3, F-PZr-V2.5, F-PZr-V3.7, F-PZr-V5.0, F-PZr-V6.4, and F-PZr-V13.3. The letter F in the beginning of the names means that the sample presents a fibrillar shape whereas the letter P refers to the zirconia precursor (zirconium propoxide in this case). Thus, F-PZr is a zirconia fiber material without vanadium, and the others (F-PZr-VX.X) are zirconia fibers with a V mass content of X.X%. For comparative purposes, two samples in powder form (P-) were prepared via calcination of the polymer solutions before being electrospun without vanadium and with a 5.0% of V mass content, named P-PZr and P-PZr-V5.0, respectively. These polymer solutions for the preparation of the powdered samples were dried overnight at 60 °C in a vacuum dryer before the calcination. This drying process was performed to try to simulate the evaporation of the solvent that occurs during the electrospinning process for the sample with fiber shape. In this way, the calcination was proceeded with a dried material and in the same conditions for both cases, fibers and powder.

Catalysts with both powder and fiber forms were also prepared by classic incipient wetness impregnation method, for comparative purposes. In this case, the zirconia samples, P-PZr and F-PZr, were impregnated with aqueous solutions of vanadyl acetylacetonate obtaining the samples PI-

PZr-V5.0, PI-PZr-V1.0, and FI-PZr-V5.0. In the nomenclature, the letter I indicates that the samples were obtained via impregnation method of the zirconia support. Table 3.1.1 summarizes all the samples that have been prepared, their V contents, and their nomenclature.

**Table 3.1.1.** Summary of the samples prepared.

<b>Name</b>	<b>Shape</b>	<b>V content (wt %)</b>	<b>V incorporation method</b>
<b>F-PZr</b>	Fiber	0	Electrospinning one-step
<b>F-PZr-V1.3</b>	Fiber	1.3	Electrospinning one-step
<b>F-PZr-V2.5</b>	Fiber	2.5	Electrospinning one-step
<b>F-PZr-V3.7</b>	Fiber	3.7	Electrospinning one-step
<b>F-PZr-V5.0</b>	Fiber	5.0	Electrospinning one-step
<b>F-PZr-V6.4</b>	Fiber	6.4	Electrospinning one-step
<b>F-PZr-V13.3</b>	Fiber	13.3	Electrospinning one-step
<b>FI-PZr-V5.0</b>	Fiber	5.0	Electrospinning and Incipient wetness impregnation
<b>P-PZr</b>	Powder	0	One-step
<b>P-PZr-V5.0</b>	Powder	5.0	One-step
<b>PI-PZr-V1.0</b>	Powder	1.0	Incipient wetness impregnation
<b>PI-PZr-V5.0</b>	Powder	5.0	Incipient wetness impregnation

### 3.1.2.2. Characterization

The porous texture of the samples was characterized by N<sub>2</sub> adsorption-desorption at -196°C using a micromeritics instrument (ASAP 2020 model). The samples were previously outgassed for at least 8 h at 150°C. The apparent surface area ( $A_{\text{BET}}$ ) was determined by applying the BET equation to the N<sub>2</sub> adsorption isotherm.

The surface morphology of the samples was studied by transmission electron microscopy (TEM) at an accelerating voltage of 200 kV, in a FEI Talos F200X microscope equipped with energy-dispersive X-ray analyzer (EDXA).

Surface chemistry of the samples was analyzed by X-ray photoelectron spectroscopy (XPS). XPS analyses of the samples were obtained by a 5700C model Physical Electronics apparatus with MgK $\alpha$  radiation (1253.6 eV). The maximum of the C1s peak was set at 284.5 eV and used as a reference to shift the other peaks.

X-ray diffraction patterns (XRD) were recorded in the region of  $2\Theta=5-80^\circ$  for 30 min on an EMPYREAN diffractometer of PANalytical using  $\text{CuK}\alpha_{1,2}$  (1.5406 Å) monochromatic radiation (operational value 45 kV and 40 mA), a detector PIXcel and Soller slits (incident and diffracted beam) of 0.04 rad.

In situ Raman spectra of the samples were acquired in the 200-3200  $\text{cm}^{-1}$  region, using an Invia Reflex Raman Confocal (RENISHAW) spectrometer equipped with a RemCam deep depletion CCD detector using the 514.5 nm Ar line, with a spectral resolution of ca. 1  $\text{cm}^{-1}$ . The samples were treated at 200°C in air 2 h for obtaining the spectra under dehydrated conditions.

### 3.1.2.3. Propane oxidative dehydrogenation

The V-zirconia fibrous catalytic systems were tested for the propane oxidative dehydrogenation (ODH) in a fixed bed microreactor (i.d. 4 mm), with plug-flow behavior, placed inside a vertical furnace with temperature control. The temperature of reaction was varied from 300 to 400°C. The feed was prepared by a mixture of three gases: propane (99.95%), oxygen (99.999%) and helium (99.999%). The gases were always mixed in a composition of 20%  $\text{C}_3\text{H}_8$ , 10%  $\text{O}_2$  and 70% He by mass flow controllers, yielding a molar ratio of propane to oxygen of 2. The total volumetric gas flow ( $F_T$ ) and the mass of catalyst ( $W_{\text{cat}}$ ) were adjusted in order to vary the space-time ( $W_{\text{cat}}/F_{\text{C}_3\text{H}_8}$ ) in the range of 0.1-1.0  $\text{g}_{\text{cat}} \cdot \text{s} \cdot \text{mL}^{-1}_{\text{C}_3\text{H}_8}$  (Volume was always expressed in STP conditions). In the cases of the catalysts in powder form, the particle size was quite small, 25-75  $\mu\text{m}$ , and the samples were mixed with silicon carbide (100–300  $\mu\text{m}$  particle size) in a mass ratio of 1:1 in order to avoid both very high pressure drop and significant temperature gradients in the bed [11,12]. However, in the cases of the fibrous catalysts were not necessary to use silicon carbide. All the lines were heated above 120°C to pre-heat the reactant mixture before entering the reactor and to avoid the condensation of any product leaving the reactor.

Reactants and products were analyzed in steady state conditions by an on-line gas chromatograph (Perkin-Elmer, Clarus 500 GC), equipped with a



Hayesep D 80/100 (length: 3 m; diameter: 1/8"; internal diameter: 2.1 mm) and an active carbon 80/100 (length: 2 m; diameter 1/8"; internal diameter: 2,1 mm) packed columns. Light gases (O<sub>2</sub>, CO and CO<sub>2</sub>) were detected by a thermal conductivity detector (TCD); and CH<sub>4</sub>, C<sub>2</sub>H<sub>4</sub>, C<sub>2</sub>H<sub>6</sub>, C<sub>3</sub>H<sub>6</sub> and C<sub>3</sub>H<sub>8</sub> were detected using a flame ionization detector (FID). The duration of each GC analysis was 15 min. In all the cases carbon and oxygen molar balances were closed with errors lower than 5%. The propane conversion and the selectivity to *i* product are defined as *X* and *S<sub>i</sub>*, respectively:

$$X(\%) = \frac{\dot{F}_{C_{3,o}} - \dot{F}_{C_3}}{\dot{F}_{C_{3,o}}} \cdot 100 \quad (1)$$

$$S_i(\%) = \frac{n_i \cdot \dot{F}_i}{n_{C_3} \cdot \dot{F}_{C_{3,o}} \cdot X} \cdot 100 \quad (2)$$

Where  $\dot{F}_{C_{3,o}}$  and  $\dot{F}_{C_3}$  are the molar flows of propane in the inlet and in the outlet streams, respectively.  $\dot{F}_i$  is the molar flow of *i* product in the outlet stream, and  $n_{C_3}$  or  $n_i$  are the number of carbon atoms per molecule of propane ( $n_{C_3}=3$ ) or *i* product, respectively. Turn-over frequency was calculated from Eq. (3), it quantifies the specific activity of a catalytic surface active center under defined reaction conditions and so, describes the number of converted moles of propane per mol of vanadium and time:

$$TOF = \frac{\dot{F}_{C_{3,o}} \cdot X \cdot M_V}{W_{cat} \cdot W_V} \quad (3)$$

where  $M_V$  is denoted as the molar mass of vanadium and  $W_V$  mass of vanadium per gram catalyst determined by XPS. This method of quantification assumes that all the active sites are equal under reaction environment and that these sites are stable during the reaction. Propylene productivity values were calculated from Eq. (4). It indicates the propylene mass obtained per mass of catalyst and time:

$$Propylene\ productivity = \frac{\dot{F}_{C_{3,o}} \cdot X \cdot S_{C_3=} \cdot M_{C_3=}}{W_{cat}} \quad (4)$$

where  $M_{C_3=}$  is the molar mass of propylene.

As blank reactions, catalytic tests were also performed with the empty reactor (to check the contribution of homogeneous phase reaction), and with the V-free-fiber (to see the contribution of the zirconia). The propane conversion values were found negligible in both cases at lower temperatures than 500°C, where the homogeneous phase start to have a little contribution.

The internal mass transport limitation can be considered negligible due to the quite small diameter of the submicron-fibers and no pressure drop has been observed through the catalyst bed under the experimental conditions used, due to the fibrous morphology of the catalysts [10]. On the other hand, diagnostic experimental tests (see additional information Figure 3.1.1.S) for analyzing the presence of external mass transport limitations were performed under the most unfavorable experimental conditions as possible, checking the influence of the total gas flow rate at constant space-time in the observed conversions reaction [11]. It is noteworthy that no diffusion limitations were observed in the catalytic results shown using the catalysts with lower vanadium content than 13.3% prepared in this study. However, in the case of F-PZr-V13.3 at 400°C, it cannot be discarded some diffusional problems. Due to the high activity of this catalyst the oxygen is the limiting reactant, the selectivity to propylene is lower than those for the other catalysts and a high production of CO<sub>2</sub> is observed.

### **3.1.3. Results**

Figure 3.1.1 shows TEM images of F-PZr, F-PZr-V5.0, F-PZr-V13.3 and FI-PZr-V5.0 samples, which confirm the fibrous morphology of the samples. The TEM results for the rest of samples can be found in Figure 3.1.2.S at the additional information section. The samples show a quite high length to diameter ratio and they do not present fused zones or beads. V content affects the structure of these fibers, being mechanically resistant and with a smooth surface as V content is increased, up to a V content of 13.3% (see F-PZr-V13.3 sample in Figure 3.1.1e and 1f). At this high V content the fiber becomes quite fragile, probably because the maximum amount of

V that can be inserted into the zirconia fiber has been exceeded and some broken fibers are detected. F-PZr presents fiber diameters ranging from 420 to 830 nm, while for F-PZr-V5.0 diameters between 300 and 410 nm can be observed. These results indicate that the incorporation of V produces more uniform fibers with smaller diameters. This is probably due to the increase of the electrical conductivity of the electrospinning polymer solution when the vanadium precursor (vanadyl acetylacetonate) is added. It has been found that with the increase of electrical conductivity of the solution, coulombic forces further increase as result of higher amounts of charge carriers. Therefore, jet segment experiences more stretching, what results in smaller diameters and more uniform electrospun fibers [13]. However, at high vanadium content (F-PZr-V13.3) the fibers are less uniform and present a wider diameter distribution, with diameters ranging from 220 to 505 nm (Figure 3.1.1e). Figure 3.1.1g shows the TEM images for FI-PZr-V5.0 sample, similar to F-PZr-V5.0, but prepared by conventional incipient wetness V impregnation of a calcined electrospun zirconia fiber. This picture shows that some fibers have been broken during the impregnation method and that some crystalline particles, tentatively assigned to crystalline  $V_2O_5$ , have been formed around the fibers. These crystalline  $V_2O_5$  usually grows when the vanadium dispersion capacity on the surface has been exceeded. This can occur when vanadium content is higher to the corresponding of monolayer formation, or when vanadium species are not well distributed along the surface.

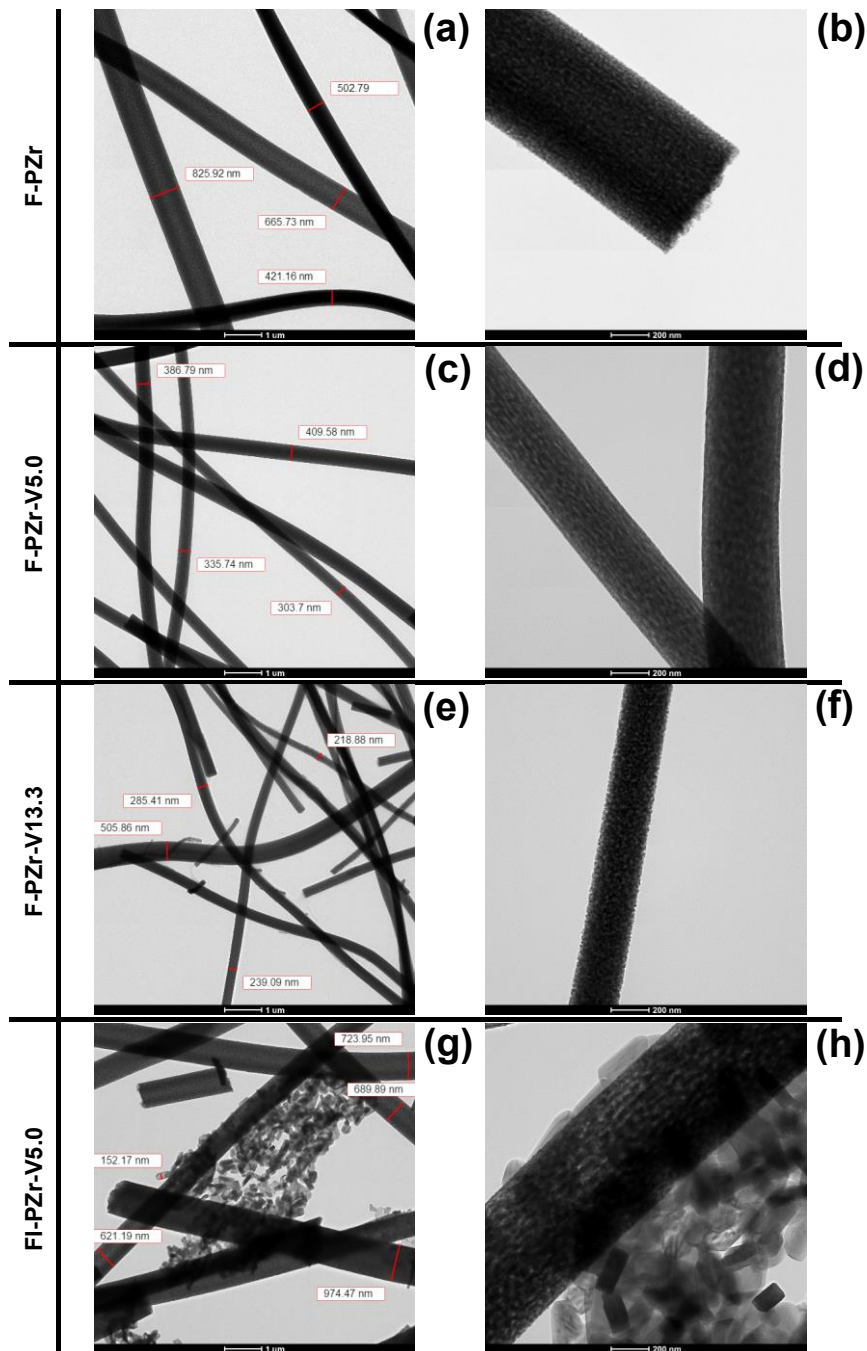
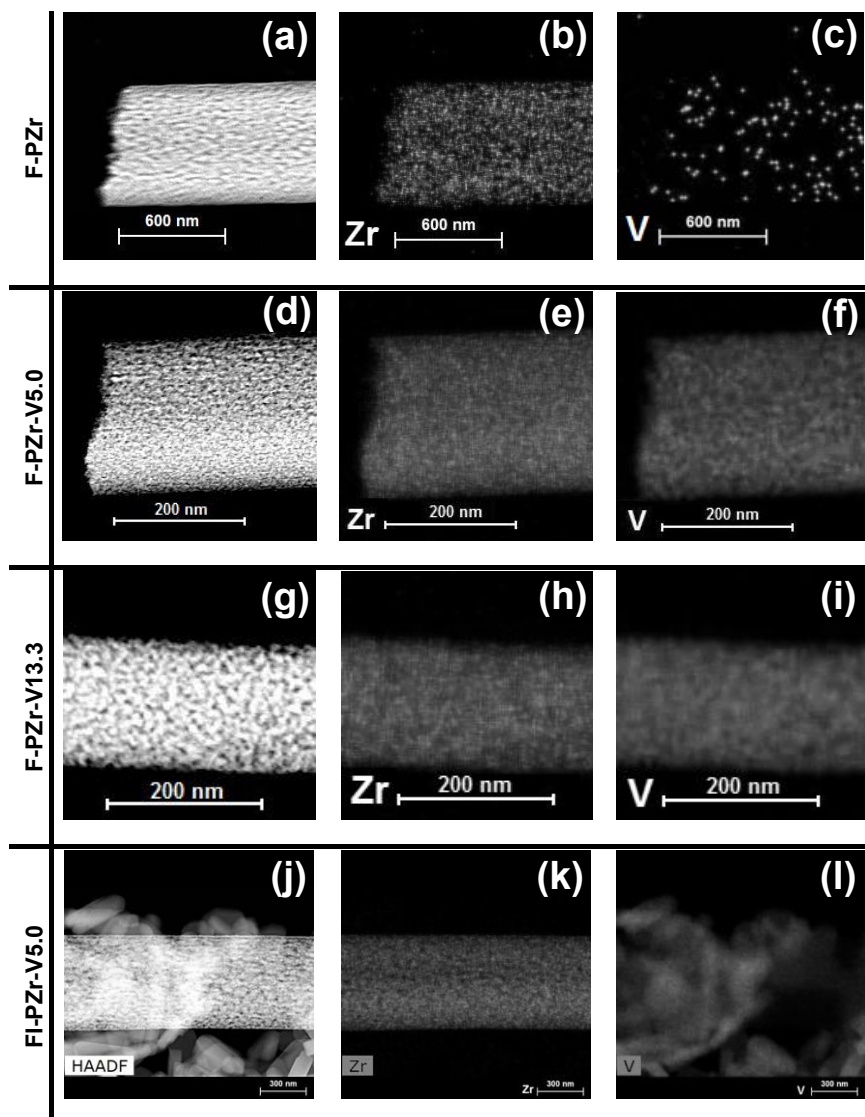


Figure 3.1.1. Transmission electron micrographs of F-PZr (a, b), F-PZr-V5.0 (c, d), F-PZr-V13.3 (e, f), and FI-PZr-V5.0 (g, h).

The Zr and V EDXA elemental mappings of F-PZr, F-PZr-V5.0, F-PZr-V13.3, and FI-PZr-V5.0 are presented in Figure 3.1.2. As expected, a high signal from Zirconium atoms is detected, and the results show that they are quite well dispersed. The images for V containing fibers, F-PZr-V5.0 and F-PZr-V13.3 (Figure 3.1.2f and 3.1.2i) indicate that vanadium oxide dispersion along the fiber material is good, whereas only some noise is detected, as expected, in the sample that do not contain V (Figure 3.1.2c). The images for the sample prepared by impregnation (Figure 3.1.2j, 3.1.2k and 3.1.2l) are quite different from those in which V was incorporated during the electrospinning step. In this case, most of the vanadium is in the particles instead of on the fiber surface. This support the idea exposed above about the formation of undesired  $V_2O_5$  in detrimental of dispersed vanadium species along the surface, what means that the dispersion has not been successfully achieved, in contrast with the samples prepared by the one-step method, whereby it is expected that the vanadium will be very well disperse, in all the fiber, due to the preparation by one step method.



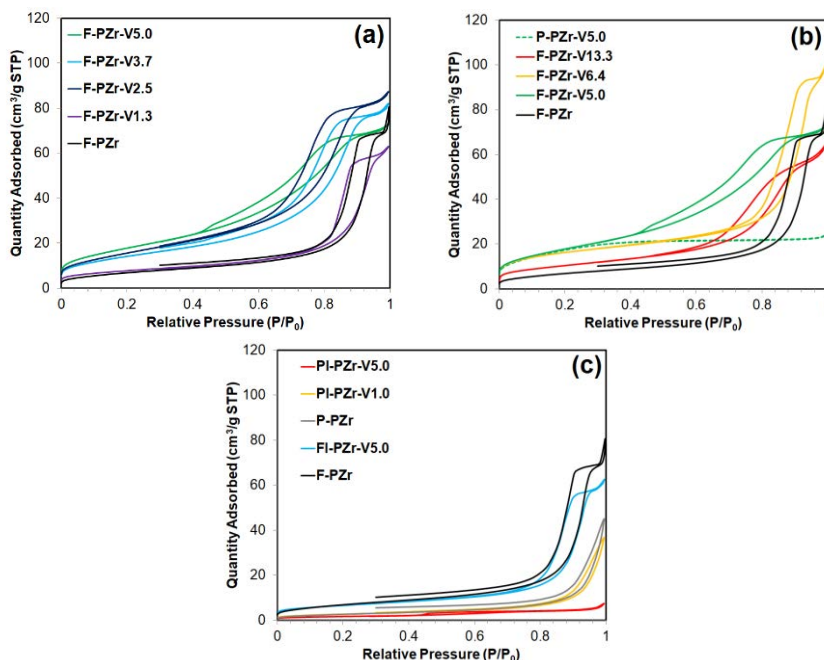
**Figure 3.1.2.** HAADF-STEM images and EDXA elemental mappings of Zr and V for the samples F-PZr (a, b, c), F-PZr-V5.0 (d, e, f), F-PZr-V13.3 (g, h, i), and FI-PZr-V5.0 (j, k, l). Note that the scale of each figure has been adapted to the size of the sample.

Figure 3.1.3 shows the N<sub>2</sub> isotherms of the samples, whereas Table 3.1.2 presents the BET surface areas obtained from them. Figures 3.1.3a and 3.1.3b show the data for the samples prepared with the one-step method. The samples with fibrous structure present a type IVa isotherm corresponding to mesoporous solid [38]. Most of the N<sub>2</sub> is adsorbed at high relative pressures showing a hysteresis loop in which the desorption occurs at lower relative pressures than the adsorption for equivalent volumes in each case. Type H1 hysteresis loops are observed in the fibers F-PZr, F-PZr-V1.3 and F-PZr-V6.4, associated to the presence of a narrow range of uniform mesopores [38]. However, type H5 hysteresis loops are observed in the fibers F-PZr-V2.5, F-PZr-V3.7, F-PZr-V5.0 and F-PZr-V13.3, often associated to pore textures containing both open and partially blocked mesopores [38]. The isotherm of the powder sample P-PZr-V5.0 presents a type Ib isotherm, indicative of mainly a microporous structure, including wider micropores and some narrow mesopores [38], as all the N<sub>2</sub> is adsorbed at low relative pressures. It should be noted that samples F-PZr-V5.0 and P-PZr-V5.0, both with the same vanadium content, show the same adsorption branch at low relative pressures in the N<sub>2</sub> adsorption-desorption isotherms (Figure 3.1.3b) and consequently a very similar BET surface area. However, the N<sub>2</sub> isotherms of both samples are very different at relative pressures higher than 0.3, where the adsorption of N<sub>2</sub> is almost negligible in P-PZr-V5.0, and is very appreciable in F-PZr-V5.0, indicating the presence of mesoporous in the latter sample, which could suggest that the mesoporous texture is developed during the electrospinning process and subsequent calcination.

N<sub>2</sub> isotherms of the submicron-fibers (Figure 3.1.3a and 3.1.3b) with (F-PZr-V1.3, F-PZr-V2.5, F-PZr-V3.7, F-PZr-V5.0, F-PZr-V6.4, and F-PZr-V13.3) and without (F-PZr) vanadium, indicate that the porous texture is influenced by the presence of the vanadium precursor (vanadyl acetylacetonate) during the electrospinning procedure. The isotherm profile found in the sample with the lowest vanadium content (F-PZr-V1.3) is very similar to that of the sample without vanadium (F-PZr), and only a decrease

in the  $N_2$  adsorption at high relative pressures is observed (Figure 3.1.3a). When V content is increased, also an increment of  $N_2$  adsorption is found to occur at low and medium relative pressures, achieving a maximum for F-PZr-V5.0 sample (Figure 3.1.3a). It is also detected a change in the hysteresis loop from type H1 to H5, whose closure is shifted to lower relative pressures (0.4 - 0.5), indicating the presence of narrower mesopores. These changes in the structure of V containing fibers results in a wider size distribution of mesoporous.

Figure 3.1.3c shows the isotherms of the samples prepared by the incipient wetness impregnation method. The samples with fibrous structure (F-PZr and FI-PZr-V5.0) present type IVa isotherms with a type H1 hysteresis loops. The powder samples (P-PZr, PI-PZr-V1.0, and PI-PZr-V5.0) show type II isotherms with hysteresis loops type H3 characteristic of nonporous or macroporous adsorbents [38]. These results show that the electrospinning process promote the development of the porous texture of the final catalyst during the one-step method used in this study.



**Figure 3.1.3.**  $N_2$  adsorption-desorption isotherms at  $-196\text{ }^\circ\text{C}$  of the (a, b) catalysts prepared with the one-step method, and (c) the ones prepared by the incipient wetness impregnation method.



Table 3.1.2. Physicochemical characteristics of the submicron-fibers.

	<sup>a</sup> A <sub>BET</sub> (m <sup>2</sup> /g)	V EDXA (wt %)	XPS (wt %)			
			V2p	Zr3d	O1s	C1s
<b>F-PZr</b>	26	0	0	67.7	28.0	4.3
<b>F-PZr-V1.3</b>	29	1.2	1.4	65.3	26.3	7.0
<b>F-PZr-V2.5</b>	59	2.4	2.7	66.1	24.2	7.0
<b>F-PZr-V3.7</b>	52	3.6	3.3	65.4	28.2	3.1
<b>F-PZr-V5.0</b>	66	4.7	4.9	64.3	27.9	2.9
<b>F-PZr-V6.4</b>	59	6.2	6.0	59.8	24.8	9.4
<b>F-PZr-V13.3</b>	38	11.4	12.9	48.0	31.4	7.7
<b>FI-PZr-V5.0</b>	24	-	2.2	66.5	28.1	3.2
<b>P-PZr</b>	10	-	0	69.5	26.3	4.2
<b>P-PZr-V5.0</b>	64	-	4.7	64.5	27.7	3.1
<b>PI-PZr-V1.0</b>	10	-	5.3	62.7	28.9	3.1
<b>PI-PZr-V5.0</b>	6	-	25.7	29.5	40.6	4.2

<sup>a</sup> from N<sub>2</sub> adsorption-desorption isotherms.

Table 3.1.2 summarizes some physicochemical characteristics of all the samples and the atomic compositions calculated from XPS spectra. Vanadium-containing samples prepared with the one-step method present the highest BET area values, achieving a maximum value around 66 m<sup>2</sup>/g for the samples with 5.0% of vanadium (P-PZr-V5.0 and F-PZr-V5.0), significantly higher than the samples without vanadium, 26 m<sup>2</sup>/g for F-PZr, and 10 m<sup>2</sup>/g for P-PZr. Regarding the samples prepared by the incipient wetness impregnation method, as expected, vanadium incorporation produces a slight decrease in the BET specific surface value, from 26 to 24 m<sup>2</sup>/g for the samples with fibrous structure (F-PZr and FI-PZr-V5.0, respectively), and from 10 to 6 m<sup>2</sup>/g for the powdered samples (P-PZr and PI-PZr-V5.0, respectively).

Figure 3.1.4 shows the X-ray diffractograms of the samples. The pattern of zirconia tetragonal phase is detected in all the samples, as expected, although the monoclinic phase is the thermodynamically stable one for pure zirconia up to 1170°C. This is because amorphous zirconia precursors tend to first crystallize forming the metastable tetragonal phase of zirconia and then, at temperature higher than 600°C, they start to be transformed into the monoclinic structure [15,39]. For fibrous shaped samples prepared by electrospinning, no crystalline V<sub>2</sub>O<sub>5</sub> pattern is detected, or at least they are not so big to be detected by this technique, indicative of a probable well

dispersion of this oxide in the fibrous material, in line with the EDXA mapping results (Figure 3.1.2). At high V loadings (F-PZr-V13.3 sample), it is detected the pattern of  $ZrV_2O_7$  (Figure 3.1.4a). The formation of this crystalline mixed oxide usually occurs at high temperatures ( $>600^\circ\text{C}$ ) [40] that should not have been reached in this case. However, the high V content could be responsible of this fact, given that in the presence of high concentration of V (as in F-PZr-V13.3),  $ZrV_2O_7$  could be form. Nevertheless, it is also possible that combustion of PVP and organic part of V and Zr precursor during calcination gives rise to hot spots in the fiber matrix, increasing the local temperatures of part of the fibers. On the other hand, PI-PZr-V5.0 and FI-PZr-V5.0, the reference materials prepared by impregnation, show  $V_2O_5$  pattern (Figure 3.1.4b).

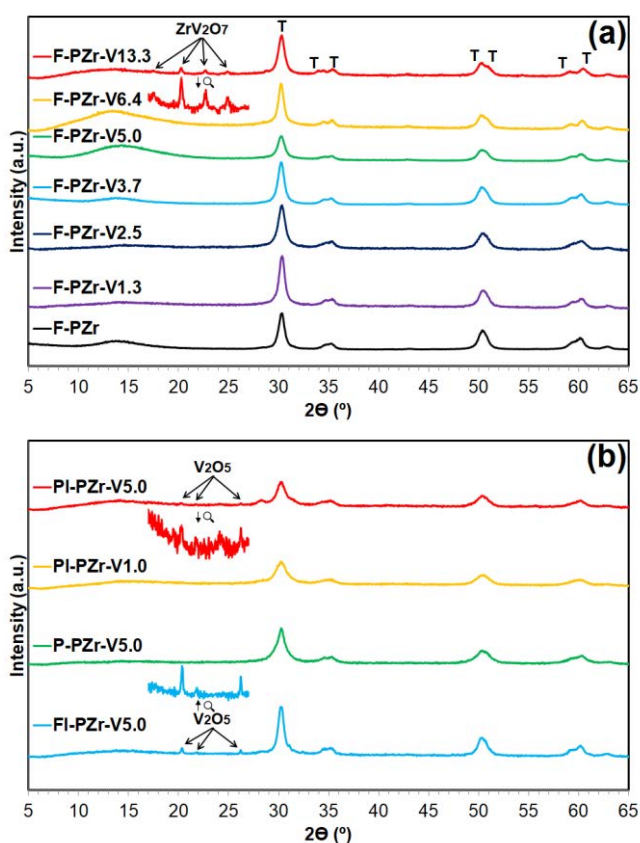


**Figure 3.1.4.** XRD patterns of (a) the zirconia fibers prepared by the one-step method, and (b) the samples FI-PZr-V5.0, P-PZr-V5.0, PI-PZr-V1.0, and PI-PZr-V5.0. Tetragonal  $ZrO_2$  (JCPDS 01-079-1769), cubic  $ZrV_2O_7$  (JCPDS 98-005-9396) and orthorhombic  $V_2O_5$  (JCPDS 01-085-0601) are found in the X-ray diffractograms.

Figure 3.1.5 shows the  $V2p_{3/2}$  XPS spectra of the samples and the typical binding energies of the powdered oxide standards of  $V_2O_5$  (517.2 eV),  $VO_2$  (516.2 eV) and  $V_2O_3$  (515.4 eV) as a reference, where vanadium is present in oxidation states of  $V^{+5}$ ,  $V^{+4}$  and  $V^{3+}$ , respectively [18,41–45]. The data indicate that as the vanadium content increases, the maximum value of the  $V2p_{3/2}$  spectrum shifts to higher binding energies corresponding to more oxidized species (Figure 3.1.5a). By this manner, the spectra of F-PZr-V1.3 and F-PZr-V2.5, are centered at 516 eV, close to the typical binding energy of  $V^{+4}$  present in the stoichiometric oxide  $VO_2$ ; and the spectrum of F-PZr-V13.3 is centered at 517.2 eV, corresponding to the typical binding energy of  $V^{+5}$  present in the stoichiometric oxide  $V_2O_5$ , but in this case vanadium is mainly forming  $ZrV_2O_7$  crystals as previously observed by the XRD results (Figure 3.1.4a). Figure 3.1.5b shows the  $V2p_{3/2}$  XPS spectra of the samples prepared by V-impregnation, FI-PZr-V5.0, PI-PZr-V1.0 and PI-PZr-V5.0, with a maximum value around 517.2 eV corresponding to  $V^{+5}$  forming  $V_2O_5$  crystals, as also mentioned in the XRD results (Figure 3.1.4b). The surface vanadium oxide species of the catalysts prepared in this study should practically be present as  $V^{+5}$  with a very moderate extent of reduction, unless they are under reaction/reduction conditions [5,46]. However, most of the prepared material present a  $V2p_{3/2}$  spectrum with binding energies between  $V^{+4}$  (in  $VO_2$ ) and  $V^{+5}$  (in  $V_2O_5$ ), typical in this kind of catalysts where vanadium is dispersed in zirconia [41], which indicates electron transfer from  $ZrO_2$  to V.

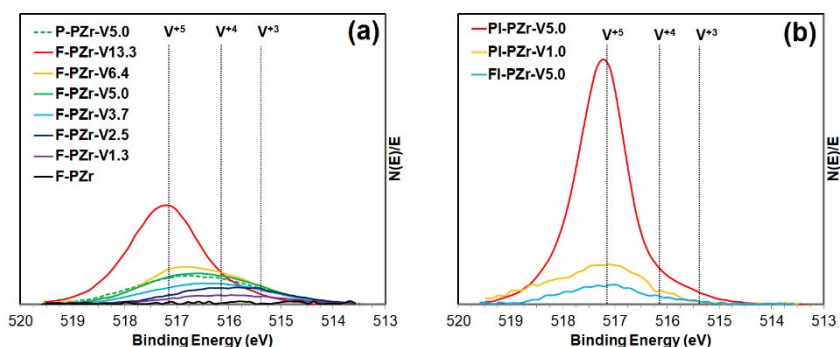


**Figure 3.1.5.**  $V2p_{3/2}$  XPS spectra of the (a) zirconia fibers prepared with the one-step method, and (b) the samples prepared by using the incipient wetness impregnation method.

Figure 3.1.6 shows the Raman spectra obtained under dehydrated conditions. Figure 3.1.6a shows the spectra for the catalysts in fiber form prepared by electrospinning in one step; it can be observed a different shape of the spectra for samples with higher V contents (F-PZr-V13.3 and F-PZr-6.4) with respect to samples with lower V concentrations. The catalysts with lower V contents (F-PZr-V1.3, F-PZr-V2.5, F-PZr-V3.7 and F-PZr-V5.0) present bands associated to tetragonal phase of zirconia (642, 604 (shoulder), 459, 314, 268 and 146  $\text{cm}^{-1}$  [47]) in agreement with the XRD results. For F-PZr-V3.7, it can be also observed some low intensity bands assigned to monoclinic phase (381, 189 and 177  $\text{cm}^{-1}$  [48]), which are not detected by XRD, due to the reduced size of these crystalline structures that are not able to give an XRD pattern. Moreover, these samples present a broad band between 700 and 950  $\text{cm}^{-1}$  associated to the presence of monovanadates and polyvanadates, due to V-O modes along V-O-V and/or V-O-Zr chains [5,49,50]. It can also be identified a broad band centered near 1020  $\text{cm}^{-1}$ , due to the V=O terminal stretching of isolated monovanadates (1019  $\text{cm}^{-1}$ ) and polyvanadates (1030  $\text{cm}^{-1}$ ) [5,51,52]. It can be also observed that the broad band at 700-950  $\text{cm}^{-1}$  grows in intensity by rising the vanadium content, at the same time that the V=O mode is blue-shifted close to 1030  $\text{cm}^{-1}$ . Therefore, it can be derived that increasing the vanadium content in the sample results in a higher proportion of polyvanadates, as reported in other studies in the literature [5,40,53]. As mentioned, the shape of spectra is different for samples with higher vanadium contents. F-PZr-V6.4 presents bands assigned to both monoclinic (637, 616, 559, 533, 502, 476, 381, 330, 305, 224, 190, 175 and 115  $\text{cm}^{-1}$  [48]) and tetragonal (146  $\text{cm}^{-1}$ ) phases (Figure 3.1.6a). Since only tetragonal phase was detected in the XRD pattern (Figure 3.1.4), this indicates that the monoclinic aggregates present a very small size. This could be also related to the hot spots (reaching temperatures >600 °C) occurring by combustion of PVP and organic part of the V and Zr precursors during calcination of the fibers. With respect to the bands associated to vanadium species, it can be detected the presence of two peaks, one at 747  $\text{cm}^{-1}$  and other one, smaller, at 925  $\text{cm}^{-1}$ , which can be related to a

mixture of monovanadates/polyvanadates species and crystalline  $ZrV_2O_7$  (988 and 777  $cm^{-1}$  [5,50,54]) indicating somehow that at this vanadium content the vanadium dispersion capacity in zirconia has been exceeded. In fact, as the vanadium content increases there is a turning point in the type of hysteresis loop observed in the  $N_2$  isotherms from H5 to H1 in this sample (F-PZr-V6.4), which could be related to the fact that vanadium species start to appear in a more condensed form as crystalline  $ZrV_2O_7$  having a repercussion in the final porous texture. In addition, a band at 1020  $cm^{-1}$  due to V=O mode is detected, indicating the presence of  $VO_x$ . With respect to the sample with highest vanadium content (F-PZr-V13.3), only bands associated to crystalline  $ZrV_2O_7$  are found. Therefore, it can be concluded that the V/Zr ratio in the initial polymer solution determine the vanadium species formed in the final sample after calcination, which in turn influences the porous texture.

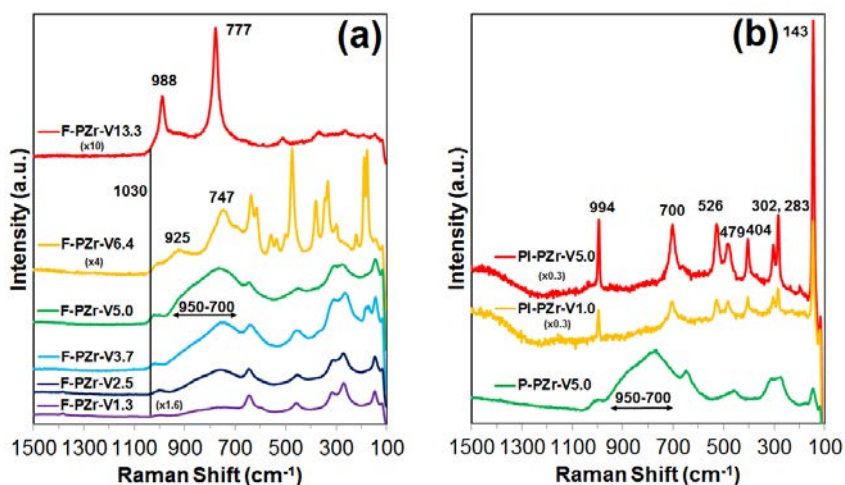


**Figure 3.1.6.** In situ Raman spectra of (a) the dehydrated vanadium-containing zirconia fibers prepared by the one-step method, and (b) the samples P-PZr-V5.0, PI-PZr-V1.0, and PI-PZr-V5.0.

Figure 3.1.6b shows the spectra for the reference samples in powder form, those prepared by incipient wetness impregnation method (PI-PZr-V1.0 and PI-PZr-V5.0) and the one prepared in one step (P-PZr-5.0). It can be observed that the Raman spectrum of the sample P-PZr-V5.0 is very similar to that of F-PZr-V5.0, indicative that the surface chemistry of the catalysts is not influenced by the electrospinning process, as suggested by the XRD

and XPS results. On the other hand, the samples PI-PZr-V1.0 and PI-PZr-V5.0 show Raman bands associated to  $V_2O_5$  crystals (994, 700, 526, 479, 404, 302, 283, and  $143\text{ cm}^{-1}$  [55]), whereas  $ZrV_2O_7$  is not detected. Thus, by impregnation of the fibers even with low amount of V, as in the case of PI-PZr-V1.0,  $V_2O_5$  crystals are detected, whereas the new proposed methods allow the incorporation of dispersed  $VO_x$  species on the surface of the zirconia fibers, as shown by the Raman spectra results (Figure 3.1.6a).

Table 3.1.3 shows steady state propane conversions and selectivity to propylene, CO and  $CO_2$ , as a function of reaction temperature at a space-time of  $0.1\text{ g}\cdot\text{s}\cdot\text{mL}^{-1}\text{C}_3\text{H}_8$ . At very low propane conversions the selectivity to propylene is 100%, as can be observed at  $300^\circ\text{C}$  for all the catalysts studied. At  $350^\circ\text{C}$ , when the propane conversions are higher, the selectivity to CO starts also to be appreciable for some catalysts, as well as that to propylene, but not to  $CO_2$ . Finally, at  $400^\circ\text{C}$  the presence of  $CO_2$  is also observed for most of the catalysts, together with propylene and CO. These results suggest that the reaction mechanism could occur in a consecutive pathway, where propylene is firstly formed, followed by CO and finally  $CO_2$ , although the direct combustion of propane cannot be discarded, especially at high temperatures.

**Table 3.1.3.** Propane conversions and selectivities to propylene, CO and  $CO_2$ , in the propane ODH reaction for the different vanadium-containing catalysts, as a function of temperature with a space-time of  $0.1\text{ g}\cdot\text{s}\cdot\text{mL}^{-1}\text{C}_3\text{H}_8$ .

Sample	300°C				350°C				400°C			
	X (%)	S <sub>C3=</sub> (%)	S <sub>CO</sub> (%)	S <sub>CO2</sub> (%)	X (%)	S <sub>C3=</sub> (%)	S <sub>CO</sub> (%)	S <sub>CO2</sub> (%)	X (%)	S <sub>C3=</sub> (%)	S <sub>CO</sub> (%)	S <sub>CO2</sub> (%)
F-PZr-V13.3	0.3	100	0	0	17.4	27.4	58.2	14.4	17.4	27.0	58.4	14.6
F-PZr-V6.4	0.3	100	0	0	1.0	71.6	28.4	0	4.2	30.5	56.6	12.9
F-PZr-V5.0	0.4	100	0	0	1.7	87.7	12.3	0	4.0	64.6	30.6	4.8
F-PZr-V3.7	-	-	-	-	0.5	100	0	0	2.7	66.7	27.3	6.0
F-PZr-V2.5	-	-	-	-	0.1	100	0	0	0.7	85.7	14.3	0
F-PZr-V1.3	-	-	-	-	-	-	-	-	0.2	100	0	0
P-PZr-V5.0	0.3	100	0	0	1.6	86.2	13.8	0	3.8	65.3	28.4	6.3
PI-PZr-V5.0	-	-	-	-	0.3	100	0	0	1.0	88.8	11.2	0
PI-PZr-V1.0	-	-	-	-	0.2	100	0	0	0.8	88.9	11.1	0

Figure 3.1.7 shows steady state propane conversions and selectivity to propylene as a function of reaction temperature and space time. The values for the samples prepared by the one-step method are shown in Figures

3.1.7a and 3.1.7b. The propylene selectivity profiles obtained for F-PZr-V6.4 and F-PZr-V13.3 catalysts are quite different, with lower values for the entire range of temperature studied, with respect to those for the other catalysts with lower V contents, which could indicate the presence of different active sites, in line with the characterization results that demonstrated the presence of the crystalline phase of  $ZrV_2O_7$  in F-PZr-V6.4 and F-PZr-V13.3 samples (Figures 3.1.4a and 3.1.6a). It is interesting to note that the oxygen profiles conversion is 100% during reaction of F-PZr-V13.3 at 350 and 400°C in the studied conditions. This is why the propane conversions are very similar at both different temperatures (Figure 3.1.7b and Table 3.1.3), since the reaction is truncated when all the oxygen is consumed.

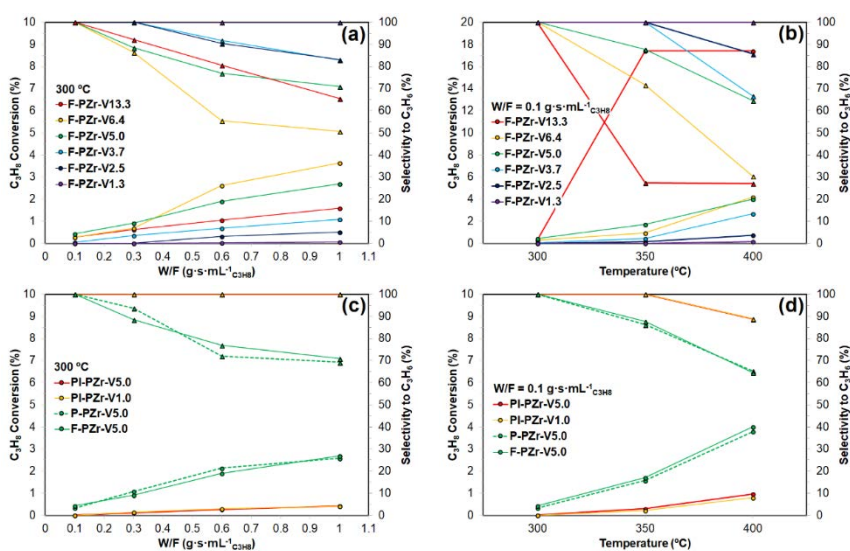


**Figure 3.1.7.** Reaction profiles in the propane ODH reaction of the different vanadium-containing catalysts. (●) Propane conversion and (▲) selectivity to propylene (a, c) as a function of space-time ( $W_{cat}/F_{C_3H_8}$ ) at 300 °C; and (b, d) as a function of temperature with a space-time of  $0.1 \text{ g} \cdot \text{s} \cdot \text{mL}^{-1} C_3H_8$ .

The conversion-selectivity profiles for the vanadium-containing catalysts F-PZr-V5.0, P-PZr-V5.0, PI-PZr-V1.0, and PI-PZr-V5.0 are shown in Figures 3.1.7c and 7d. These values are quite similar for the samples F-PZr-V5.0 and P-PZr-V5.0, in agreement with the results obtained by Raman spectroscopy (Figure 3.1.6), which suggests that both samples present a similar surface chemistry. Nevertheless, it has to be pointed out that F-PZr-

V5.0 catalyst works properly in its fibrous conformation under the operation conditions studied. However, P-PZr-V5.0 catalyst needs to be mixed with silicon carbide particles of 100-300 microns in size to avoid very high-pressure drop and temperature gradients through the catalytic bed or to prevent catalyst from severe reduction in surface area (and thus available active sites) that happen when agglomeration of catalyst particles takes place to increase the catalyst particle size, by addition of a binder. Figures 3.1.7c and 3.1.7d also show that PI-PZr-V1.0 and PI-PZr-V5.0 present relatively low conversion values, in agreement with its low BET area values (Table 3.1.2).

Propane conversions and selectivities to propylene as a function of time on stream for F-PZr-V1.3, F-PZr-V2.5, F-PZr-V3.7, F-PZr-V5.0, and F-PZr-V6.4 samples are shown in Figure 3.1.8. The results demonstrate that the fibrous catalysts are stable under time of stream up to 24 h at the operation conditions studied, without noticeable deactivation.

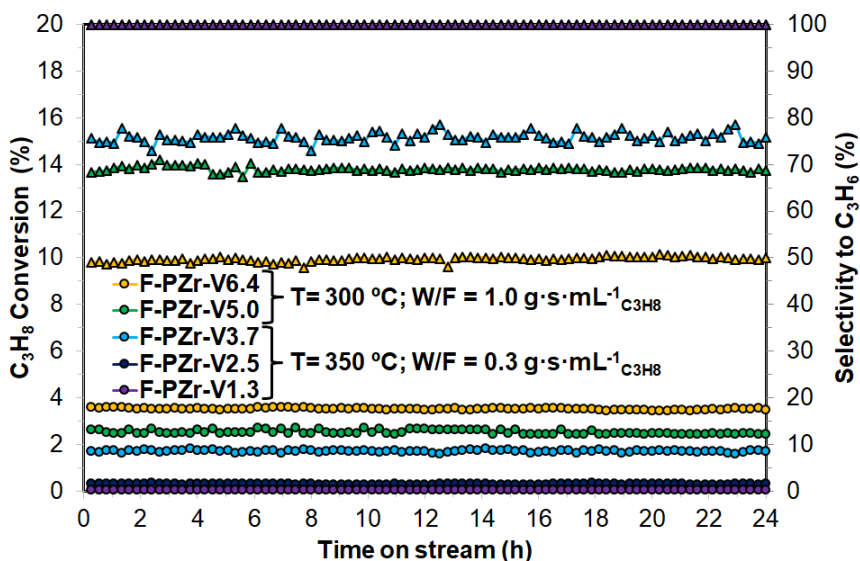


**Figure 3.1.8.** Time on Stream study of the activity in the propane ODH reaction of the vanadium-containing zirconia fibers (F-PZr-V1.3, F-PZr-V2.5, F-PZr-V3.7, F-PZr-V5.0, and F-PZr-V6.4) at different conditions. (●) Propane conversion and (▲) selectivity to propylene.



### 3.1.4. Discussion

The method described for the incorporation of V active sites throughout the synthesis of the fibrous catalysts, instead of by the synthesis of the catalyst support followed by the impregnation of the active phase, presents several advantages, generating fibers more uniform and mechanically resistant, as underlined the TEM results (Figure 3.1.1), and with a larger porosity and higher specific surface area values (Figure 3.1.3 and Table 3.1.2). In addition, by comparison with the samples prepared by impregnation, it has been showed how the one-step method allows the incorporation of a high amount of VO<sub>x</sub> species dispersed on the surface, which seems to be active and selective for the propane ODH reaction to propylene, avoiding the formation of non-selective V<sub>2</sub>O<sub>5</sub> crystals. Previous studies with powdered materials showed that carrying out the formation of the zirconia support and the dispersion of metal oxides in the same calcination step [56] presents also some advantages. According to Zhao *et al.* [56], the growth and sintering of crystallites takes place during the calcination process of the support, in addition to phase transformation via a mechanism of surface diffusion, which lead to a less developed porous texture. However, if in this process the active component is dispersed on the surface, it segregates the particles of the support from each other before the particles have grown into bigger ones. In this way, the surface diffusion is suppressed, and consequently the porous texture is improved.

The best catalytic activity results were obtained with the samples F-PZr-V5.0 and P-PZr-V5.0 (Figure 3.1.7 and Table 3.1.3), both with the same vanadium content, similar surface chemistry as showed in the XRD, XPS and Raman results (Figures 3.1.4, 3.1.5 and 3.1.6, respectively), and prepared using the one-step method with the only difference of using the electrospinning in F-PZr-V5.0. With respect to the porous texture, although the N<sub>2</sub> isotherms of F-PZr-V5.0 and P-PZr-V5.0 are different (Figure 3.1.3b), both samples present similar BET surface areas (Table 3.1.2), since they have the same adsorption branch at low relative pressures and this method only considers this range of low relative pressures to estimate

the surface area. In terms of catalytic activity, both samples are very similar (Figures 3.1.7c and 3.1.7d), although the sample F-PZr-V5.0 present a more developed mesoporous texture. Therefore, taking into account that the only differences among the two samples are the shape of the catalyst and the porous texture in the mesopore range, it can be concluded that the mesoporosity and the shape of the catalyst (fiber or powder) have not influence in the catalytic results of this reaction in the studied conditions. So, the type of isotherms at high relative pressures including the type of hysteresis loops are not relevant in the catalytic results, the only important points are the surface chemistry and the surface area of the catalyst, which it will be determined by the isotherm at low relative pressures corresponding to the micropores range. It is noteworthy that although the fiber shape does not have influence in the activity results, they present some important advantages with respect to the powder shape due to its superior fluidodynamics and transfer properties, which allow the use of this catalysts without adding a diluting inert material as silicon carbide, that it is necessary in the case of the powdered catalysts.

In order to compare the best propane ODH results of the catalysts prepared in this study with those reported in the literature, propylene productivity (Figure 3.1.9a) and propane TOF (Figure 3.1.9b) were used. The productivity and TOF results for other catalysts have been collected from two reviews articles published by Cavani *et al.* [25] and by Carrero *et al.* [9], respectively. Figure 3.1.9 shows that both parameters increase with temperature and with vanadium loading for the catalysts prepared in this work, in general. The results clearly indicate that the best values of propane TOF and propylene productivities obtained in this study correspond to F-PZr-V5.0, suggesting that VO<sub>x</sub> species are the most active and selective for propane ODH. Note that the results of propane TOF and propylene productivity obtained with P-PZr-V5.0 are not shown for the sake of brevity, but these results are very similar to those obtained with F-PZr-V5.0, since they present the same catalytic results as it was mentioned before (Figure 3.1.7 and Table 3.1.3).

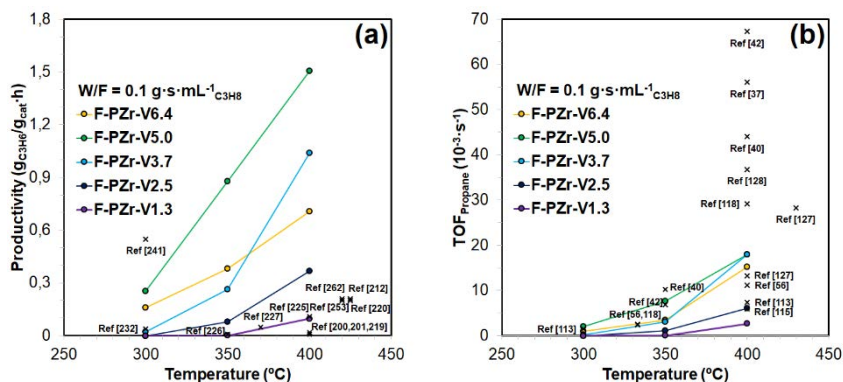


**Figure 3.1.9.** Comparison of the propane ODH results between the best catalysts prepared in this study and others reported in the literature. (a) Propylene productivity and (b) Propane consumption TOF rates as a function of the temperature at a space-time ( $W_{\text{cat}}/F_{\text{C}_3\text{H}_8}$ ) of  $0.1 \text{ g}\cdot\text{s}\cdot\text{mL}^{-1} \text{C}_3\text{H}_8$ . The literature results may have been obtained with different space-times and the numbers in (a) and in (b) indicate the cited reference in the reported reviews [25] and [9], respectively.

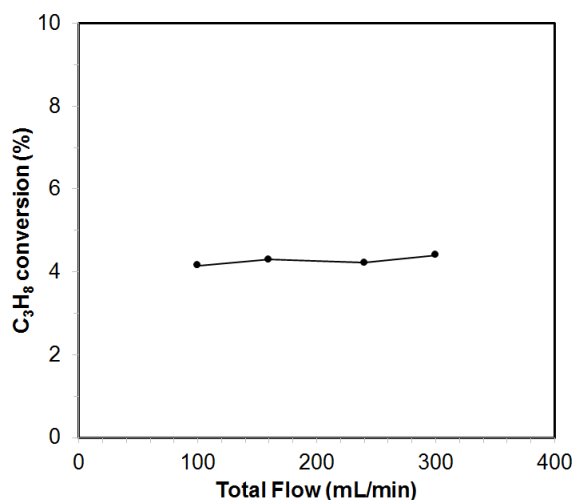
Table 3.1.3 results show that the highest propylene yields are obtained with the samples prepared with the one step method, which enhances the formation of  $\text{VO}_x$  dispersed species and avoids the formation of  $\text{V}_2\text{O}_5$  crystalline structures. If the surface V loading exceeds a certain value, corresponding probably to the monolayer, 5% in this case, the formation of  $\text{ZrV}_2\text{O}_7$  crystalline structures increases and that of  $\text{VO}_x$  decreases, reducing the TOF and propylene productivity, as in the case of F-PZr-V6.4 catalysts, shown in Figure 3.1.9.

On the other hand, it can be also observed in Figure 3.1.9 that the catalysts prepared in this study present similar results, in terms of TOF and productivity with respect to those reported in the literature. In fact, F-PZr-V5.0 presents higher or very similar TOF values in the temperature range of 300-350 $^\circ\text{C}$  than those of the catalysts reported in the literature and the highest propylene productivity values in the range of 350-400 $^\circ\text{C}$ . In this sense, it has to be pointed out that the propylene productivity values obtained for this catalyst between 300 and 400 $^\circ\text{C}$  correspond to typical values obtained at higher temperatures for the catalysts reported in the literature [25].

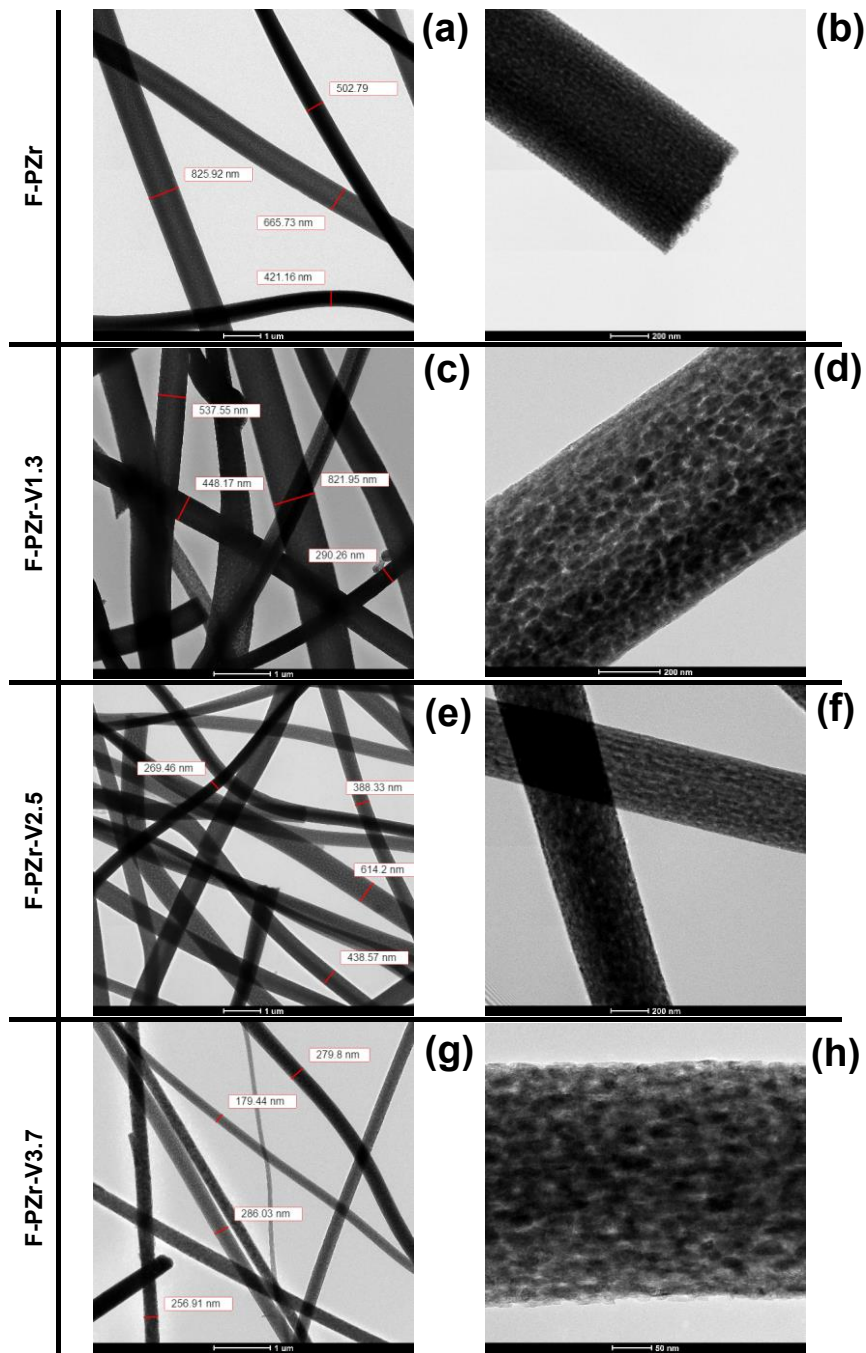
### 3.1.5. Conclusions

A new, versatile, simple and straightforward method to obtain highly dispersed vanadium oxide species on zirconia submicronfibers by electrospinning has been described in present work. This new method develops quite porous solids and enhances the formation of  $\text{VO}_x$  dispersed species on the surface of the  $\text{ZrO}_2$  fiber without an additional step for impregnation. Since these  $\text{VO}_x$  species are well-known as active species for alkane activation, the prepared solids are quite attractive as partial oxidation catalysts. The surface dispersion of vanadium oxide ( $\text{VO}_x$ ) during the zirconia oxide sub microfiber formation, delay the crystallization of amorphous  $\text{ZrO}_2$  and inhibit the conversion of metastable tetragonal to monoclinic phase in zirconia, while favoring the development of the porous texture and avoiding the formation of  $\text{V}_2\text{O}_5$  crystals. It has been also shown that these materials do not present deactivation processes under time on stream experiments. The propane ODH results in terms of conversion and selectivity are quite promising when they are compared with those already reported elsewhere.

### 3.1.6. Supplementary information



**Figure 3.1.1.S.** Diagnostic experimental test under the most unfavorable conditions as possible to discard the presence of external mass transport limitations. The experiment consisted of increasing the total flow ( $F_T$ ) at constant space-time ( $W/F_T = 0.1 \text{ g}\cdot\text{s}\cdot\text{mL}^{-1}$ ) to check if the observed conversion in the propane ODH reaction is constant for the catalyst F-PZr-V6.4 at  $400^\circ\text{C}$ .



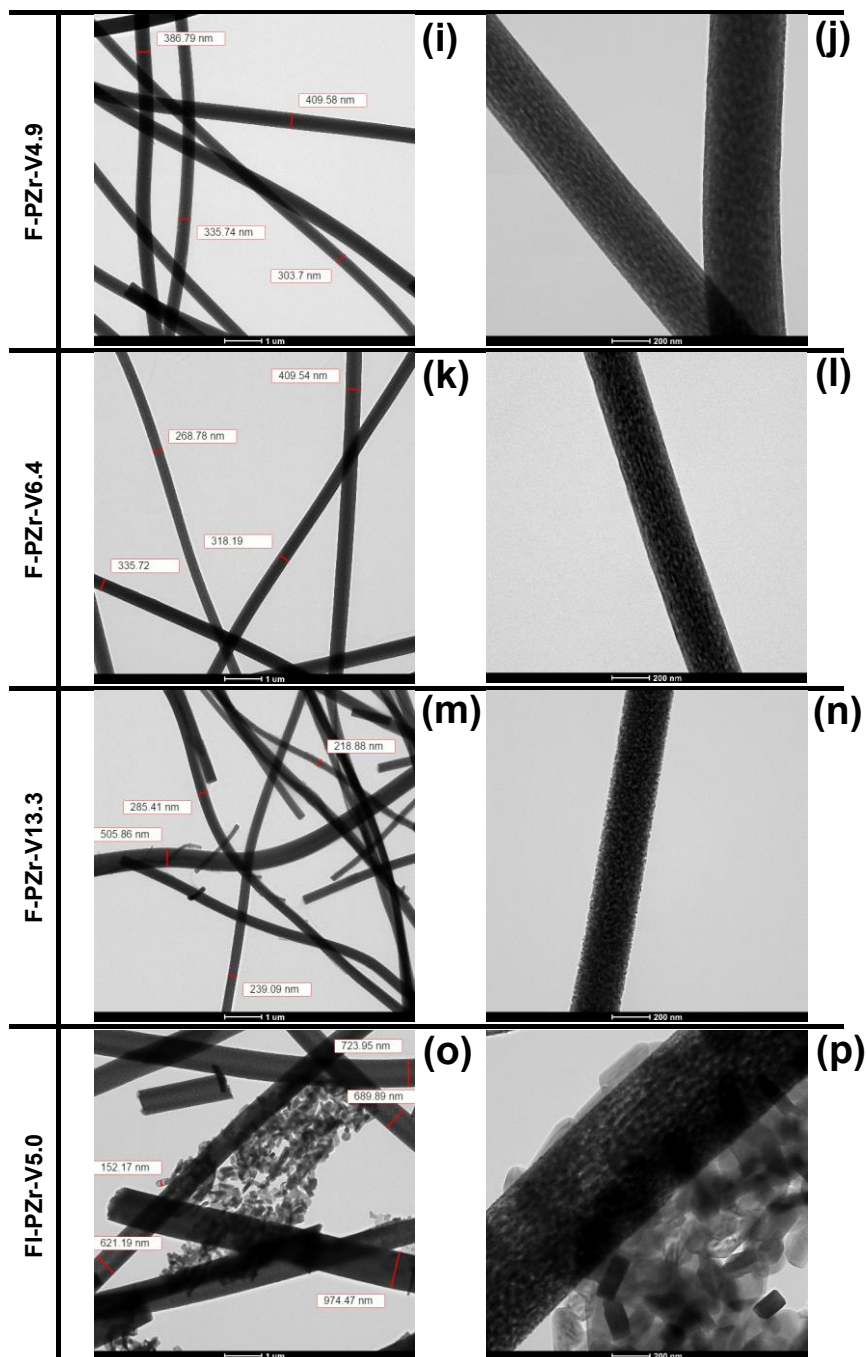


Figure 3.1.2.S. Transmission electron micrographs of F-PZr (a, b), F-PZr-V1.3 (c, d), F-PZr-V2.5 (e, f), F-PZr-V3.7 (g, h), F-PZr-V4.9 (i, j), F-PZr-V6.4 (k, l), F-PZr-V13.3 (m, n), and FI-PZr-V5.0 (o, p).

## Acknowledgements

This work was supported by the Spanish Ministry of Economy and Competitiveness and FEDER [CTQ-2012-36408 and CTQ-2015-68654-R]. J.J.T.H. and J.T.L. acknowledge the assistance of the Ministry of Economy and Competitiveness of Spain for the award of FPI Grants [BES-2013-064425 and BES-2016-079237, respectively].

### 3.1.7. References

- [1] I.E. Wachs, Molecular engineering of supported metal oxide catalysts, *Chem. Eng. Sci.* 45 (1990) 2561–2565. [https://doi.org/10.1016/0009-2509\(90\)80142-2](https://doi.org/10.1016/0009-2509(90)80142-2).
- [2] M.O. Guerrero-Pérez, Supported, bulk and bulk-supported vanadium oxide catalysts: A short review with an historical perspective, *Catal. Today.* 285 (2017) 226–233. <https://doi.org/10.1016/j.cattod.2017.01.037>.
- [3] A. Dinse, B. Frank, C. Hess, D. Habel, R. Schomäcker, Oxidative dehydrogenation of propane over low-loaded vanadia catalysts: Impact of the support material on kinetics and selectivity, *J. Mol. Catal. Chem.* 289 (2008) 28–37. <https://doi.org/10.1016/j.molcata.2008.04.007>.
- [4] A. Khodakov, B. Olthof, A.T. Bell, E. Iglesia, Structure and catalytic properties of supported vanadium oxides: Support effects on oxidative dehydrogenation reactions, *J. Catal.* 181 (1999) 205–216.
- [5] A. Christodoulakis, M. Machli, A.A. Lemonidou, S. Boghosian, Molecular structure and reactivity of vanadia-based catalysts for propane oxidative dehydrogenation studied by in situ Raman spectroscopy and catalytic activity measurements, *J. Catal.* 222 (2004) 293–306. <https://doi.org/10.1016/j.jcat.2003.10.007>.
- [6] J. Bedia, J.M. Rosas, J. Rodríguez-Mirasol, T. Cordero, Pd supported on mesoporous activated carbons with high oxidation resistance as catalysts for toluene oxidation, *Appl. Catal. B Environ.* 94 (2010) 8–18. <https://doi.org/10.1016/j.apcatb.2009.10.015>.

- [7] I. Hita, T. Cordero-Lanzac, A. Gallardo, J.M. Arandes, J. Rodríguez-Mirasol, J. Bilbao, T. Cordero, P. Castaño, Phosphorus-containing activated carbon as acid support in a bifunctional Pt–Pd catalyst for tire oil hydrocracking, *Catal. Commun.* 78 (2016) 48–51. <https://doi.org/10.1016/j.catcom.2016.01.035>.
- [8] M.O. Guerrero-Pérez, J.L.G. Fierro, M.A. Vicente, M.A. Bañares, Support effect on the structure and reactivity of VSbO<sub>4</sub> catalysts for propane ammoxidation to acrylonitrile, *Chem. Mater.* 19 (2007) 6621–6628. <https://doi.org/10.1021/cm702022d>.
- [9] C.A. Carrero, R. Schloegl, I.E. Wachs, R. Schomaecker, Critical literature review of the kinetics for the oxidative dehydrogenation of propane over well-defined supported vanadium oxide catalysts, *ACS Catal.* 4 (2014) 3357–3380. <https://doi.org/10.1021/cs5003417>.
- [10] E. Reichelt, M.P. Heddrich, M. Jahn, A. Michaelis, Fiber based structured materials for catalytic applications, *Appl. Catal. Gen.* 476 (2014) 78–90. <https://doi.org/10.1016/j.apcata.2014.02.021>.
- [11] J. Pérez-Ramírez, R.J. Berger, G. Mul, F. Kapteijn, J.A. Moulijn, The six-flow reactor technology a review on fast catalyst screening and kinetic studies, *Catal. Today.* 60 (2000) 93–109. [https://doi.org/10.1016/S0920-5861\(00\)00321-7](https://doi.org/10.1016/S0920-5861(00)00321-7).
- [12] R.J. Berger, J. Pérez-Ramírez, F. Kapteijn, J.A. Moulijn, Catalyst performance testing: The influence of catalyst bed dilution on the conversion observed, *Chem. Eng. J.* 90 (2002) 173–183. [https://doi.org/10.1016/S1385-8947\(02\)00078-5](https://doi.org/10.1016/S1385-8947(02)00078-5).
- [13] N. Bhardwaj, S.C. Kundu, Electrospinning: A fascinating fiber fabrication technique, *Biotechnol. Adv.* 28 (2010) 325–347. <https://doi.org/10.1016/j.biotechadv.2010.01.004>.
- [14] Z.-M. Huang, Y.-Z. Zhang, M. Kotaki, S. Ramakrishna, A review on polymer nanofibers by electrospinning and their applications in nanocomposites, *Compos. Sci. Technol.* 63 (2003) 2223–2253. [https://doi.org/10.1016/S0266-3538\(03\)00178-7](https://doi.org/10.1016/S0266-3538(03)00178-7).



- [15] R. Ruiz-Rosas, J. Bedia, J.M. Rosas, M. Lallave, I.G. Loscertales, J. Rodríguez-Mirasol, T. Cordero, Methanol decomposition on electrospun zirconia nanofibers, *Catal. Today*. 187 (2012) 77–87. <https://doi.org/10.1016/j.cattod.2011.10.031>.
- [16] R. Berenguer, F.J. García-Mateos, R. Ruiz-Rosas, D. Cazorla-Amorós, E. Morallón, J. Rodríguez-Mirasol, T. Cordero, Biomass-derived binderless fibrous carbon electrodes for ultrafast energy storage, *Green Chem.* 18 (2016) 1506–1515. <https://doi.org/10.1039/c5gc02409a>.
- [17] M. Lallave, J. Bedia, R. Ruiz-Rosas, J. Rodríguez-Mirasol, T. Cordero, J.C. Otero, M. Marquez, A. Barrero, I.G. Loscertales, Filled and Hollow Carbon Nanofibers by Coaxial Electrospinning of Alcell Lignin without Binder Polymers, *Adv. Mater.* 19 (2007) 4292–4296. <https://doi.org/10.1002/adma.200700963>.
- [18] R. Berenguer, J. Fornells, F.J. García-Mateos, M.O. Guerrero-Pérez, J. Rodríguez-Mirasol, T. Cordero, Novel Synthesis Method of porous VPO catalysts with fibrous structure by Electrospinning, *Catal. Today*. 277, Part 2 (2016) 266–273. <https://doi.org/10.1016/j.cattod.2016.03.002>.
- [19] S. Singh, V. Singh, M. Vijayakumar, V.V. Bhanu Prasad, Dual fiber behavior of polyvinyl alcohol/zirconium n-propoxide composite fibrous mats prepared via electrospinning, *Ceram. Int.* 39 (2013) 5031–5037. <https://doi.org/10.1016/j.ceramint.2012.11.101>.
- [20] S. Singh, V. Singh, M. Vijayakumar, V.V. Bhanu Prasad, Electrospun ZrO<sub>2</sub> fibers obtained from polyvinyl alcohol/zirconium n-propoxide composite fibers processed through halide free sol–gel route using acetic acid as a stabilizer, *Mater. Lett.* 115 (2014) 64–67. <https://doi.org/10.1016/j.matlet.2013.10.026>.
- [21] Propene (Propylene), (n.d.). <http://www.essentialchemicalindustry.org/chemicals/propene.html> (accessed March, 2018).
- [22] Ethylene, propylene demand will experience increased growth in 2005-10, (n.d.). <http://www.ogj.com/articles/print/volume-103/issue->

- [45/special-report/ethylene-propylene-demand-will-experience-increased-growth-in-2005-10.html](#) (accessed March 20, 2018).
- [23] The Propylene Gap: How Can It Be Filled?, Am. Chem. Soc. (n.d.). <https://www.acs.org/content/acs/en/pressroom/cutting-edge-chemistry/the-propylene-gap-how-can-it-be-filled.html> (accessed April, 2018).
- [24] A. Agarwal, D. Sengupta, M. El-Halwagi, Sustainable Process Design Approach for On-Purpose Propylene Production and Intensification, ACS Sustain. Chem. Eng. 6 (2018) 2407–2421. <https://doi.org/10.1021/acssuschemeng.7b03854>.
- [25] F. Cavani, N. Ballarini, A. Cericola, Oxidative dehydrogenation of ethane and propane: How far from commercial implementation?, Catal. Today. 127 (2007) 113–131. <https://doi.org/10.1016/j.cattod.2007.05.009>.
- [26] J.F. Brazdil, Strategies for the selective catalytic oxidation of alkanes, Top. Catal. 38 (2006) 289–294. <https://doi.org/10.1007/s11244-006-0027-4>.
- [27] R.K. Grasselli, Advances and future trends in selective oxidation and ammoxidation catalysis, Catal. Today. 49 (1999) 141–153.
- [28] I. Amghizar, L.A. Vandewalle, G. Van, G.B. Marin, New Trends in Olefin Production, 3 (2017) 171–178. <https://doi.org/10.1016/J.ENG.2017.02.006>.
- [29] A. Corma, J.M. López-Nieto, N. Paredes, M. Pérez, Y. Shen, H. Cao, S.L. Suib, Oxidative Dehydrogenation Of Propane Over Supported-Vanadium Oxide Catalysts, Stud. Surf. Sci. Catal. 72 (1992) 213–220. [https://doi.org/10.1016/S0167-2991\(08\)61673-0](https://doi.org/10.1016/S0167-2991(08)61673-0).
- [30] B. Frank, A. Dinse, O. Ovsitser, E.V. Kondratenko, R. Schomäcker, Mass and heat transfer effects on the oxidative dehydrogenation of propane (ODP) over a low loaded VO<sub>x</sub>/Al<sub>2</sub>O<sub>3</sub> catalyst, Appl. Catal. Gen. 323 (2007) 66–76. <https://doi.org/10.1016/j.apcata.2007.02.006>.
- [31] Y.-M. Liu, Y. Cao, K.-K. Zhu, S.-R. Yan, W.-L. Dai, H.-Y. He, K.-N. Fan, Highly efficient VO<sub>x</sub>/SBA-15 mesoporous catalysts for

- oxidative dehydrogenation of propane, *Chem. Commun.* (2002) 2832–2833.
- [32] Y.-M. Liu, Y. Cao, N. Yi, W.-L. Feng, W.-L. Dai, S.-R. Yan, H.-Y. He, K.-N. Fan, Vanadium oxide supported on mesoporous SBA-15 as highly selective catalysts in the oxidative dehydrogenation of propane, *J. Catal.* 224 (2004) 417–428. <https://doi.org/10.1016/j.jcat.2004.03.010>.
- [33] T. Blasco, J.M.L. Nieto, Oxidative dehydrogenation of short chain alkanes on supported vanadium oxide catalysts, *Appl. Catal. Gen.* 157 (1997) 117–142. [https://doi.org/10.1016/S0926-860X\(97\)00029-X](https://doi.org/10.1016/S0926-860X(97)00029-X).
- [34] J. Haber, Fifty years of my romance with vanadium oxide catalysts, *Catal. Today.* 142 (2009) 100–113. <https://doi.org/10.1016/j.cattod.2008.11.007>.
- [35] K.V.R. Chary, C.P. Kumar, T. Rajiah, C.S. Srikanth, Dispersion and reactivity of monolayer vanadium oxide catalysts supported on zirconia: The influence of molybdena addition, *J. Mol. Catal. Chem.* 258 (2006) 313–319. <https://doi.org/10.1016/j.molcata.2006.05.049>.
- [36] C. Shao, H. Guan, Y. Liu, J. Gong, N. Yu, X. Yang, A novel method for making ZrO<sub>2</sub> nanofibres via an electrospinning technique, *J. Cryst. Growth.* 267 (2004) 380–384. <https://doi.org/10.1016/j.jcrysgro.2004.03.065>.
- [37] J.Y. Li, Y. Sun, Y. Tan, F.M. Xu, X.L. Shi, N. Ren, Zirconium nitride (ZrN) fibers prepared by carbothermal reduction and nitridation of electrospun PVP/zirconium oxychloride composite fibers, *Chem. Eng. J.* 144 (2008) 149–152. <https://doi.org/10.1016/j.cej.2008.04.037>.
- [38] M. Thommes, K. Kaneko, A.V. Neimark, J.P. Olivier, F. Rodriguez-Reinoso, J. Rouquerol, K.S.W. Sing, Physisorption of gases, with special reference to the evaluation of surface area and pore size distribution (IUPAC Technical Report), *Pure Appl. Chem.* 87 (2015) 1051–1069. <https://doi.org/10.1515/pac-2014-1117>.

- [39] G.-Y. Guo, Y.-L. Chen, Unusual structural phase transition in nanocrystalline zirconia, *Appl. Phys. Mater. Sci. Process.* 84 (2006) 431–437. <https://doi.org/10.1007/s00339-006-3631-z>.
- [40] A. Khodakov, J. Yang, S. Su, E. Iglesia, A.T. Bell, Structure and properties of vanadium oxide-zirconia catalysts for propane oxidative dehydrogenation, *J. Catal.* 177 (1998) 343–351.
- [41] C.L. Pieck, M.A. Bañares, J.L.G. Fierro, Propane oxidative dehydrogenation on VOx/ZrO2 catalysts, *J. Catal.* 224 (2004) 1–7. <https://doi.org/10.1016/j.jcat.2004.02.024>.
- [42] B. Horvath, J. Strutz, J. Geyer-Lippmann, E.G. Horvath, Preparation, Properties, and ESCA Characterization of Vanadium Surface Compounds on Silicagel. I, *ZAAC - J. Inorg. Gen. Chem.* 483 (1981) 181–192. <https://doi.org/10.1002/zaac.19814831223>.
- [43] M.J. Valero-Romero, A. Cabrera-Molina, M.O. Guerrero-Pérez, J. Rodríguez-Mirasol, T. Cordero, Carbon materials as template for the preparation of mixed oxides with controlled morphology and porous structure, *Catal. Today.* 227 (2014) 233–241. <https://doi.org/10.1016/j.cattod.2013.10.093>.
- [44] R. López-Medina, J.L.G. Fierro, M.O. Guerrero-Pérez, M.A. Bañares, Nanoscaled rutile active phase in Mo-V-Nb-O supported catalysts for the oxidation of propane to acrylic acid, *Appl. Catal. Gen.* 375 (2010) 55–62. <https://doi.org/10.1016/j.apcata.2009.12.017>.
- [45] E. Hryha, E. Rutqvist, L. Nyborg, Stoichiometric vanadium oxides studied by XPS, *Surf. Interface Anal.* 44 (2012) 1022–1025. <https://doi.org/10.1002/sia.3844>.
- [46] M.A. Bañares, M.V. Martínez-Huerta, X. Gao, J.L.G. Fierro, I.E. Wachs, Dynamic behavior of supported vanadia catalysts in the selective oxidation of ethane: In situ Raman, UV–Vis DRS and reactivity studies, *Catal. Today.* 61 (2000) 295–301. [https://doi.org/10.1016/S0920-5861\(00\)00388-6](https://doi.org/10.1016/S0920-5861(00)00388-6).
- [47] L. Fernandez, E. Sanchez, M. Panizza, M.M. Carnasciali, G. Busca, Vibrational and electronic spectroscopic properties of zirconia

- powders, J. Mater. Chem. 11 (2001) 1891–1897. <https://doi.org/10.1039/b100909p>.
- [48] X. Zhao, D. Vanderbilt, Phonons and lattice dielectric properties of zirconia, Phys. Rev. B - Condens. Matter Mater. Phys. 65 (2002) 0751051–07510510.
- [49] S.C. Su, A.T. Bell, A study of the structure of vanadium oxide dispersed on zirconia, J. Phys. Chem. B. 102 (1998) 7000–7007.
- [50] D. Gazzoli, R. De, G. Ferraris, M. Valigi, L. Ferrari, S. Selci, Morphological and textural characterization of vanadium oxide supported on zirconia by ionic exchange, Appl. Surf. Sci. 255 (2008) 2012–2019. <https://doi.org/10.1016/j.apsusc.2008.06.139>.
- [51] I.E. Wachs, Raman and IR studies of surface metal oxide species on oxide supports: Supported metal oxide catalysts, Catal. Today. 27 (1996) 437–455. [https://doi.org/10.1016/0920-5861\(95\)00203-0](https://doi.org/10.1016/0920-5861(95)00203-0).
- [52] M.A. Bañares, I.E. Wachs, Molecular structures of supported metal oxide catalysts under different environments, J. Raman Spectrosc. 33 (2002) 359–380. <https://doi.org/10.1002/jrs.866>.
- [53] E. Heracleous, M. Machli, A.A. Lemonidou, I.A. Vasalos, Oxidative dehydrogenation of ethane and propane over vanadia and molybdena supported catalysts, J. Mol. Catal. Chem. 232 (2005) 29–39. <https://doi.org/10.1016/j.molcata.2005.01.027>.
- [54] J.R. Sohn, J.S. Han, J.S. Lim, Spectroscopic study of V<sub>2</sub>O<sub>5</sub> supported on zirconia and modified with MoO<sub>3</sub>, Mater. Chem. Phys. 91 (2005) 558–566. <https://doi.org/10.1016/j.matchemphys.2004.12.024>.
- [55] M.O. Guerrero-Pérez, J.L.G. Fierro, M.A. Vicente, M.A. Bañares, Effect of Sb/V ratio and of Sb + V coverage on the molecular structure and activity of alumina-supported Sb-V-O catalysts for the ammoxidation of propane to acrylonitrile, J. Catal. 206 (2002) 339–348. <https://doi.org/10.1006/jcat.2001.3494>.

- [56] B.-Y. Zhao, X.-P. Xu, H.-R. Ma, D.-H. Sun, J.-M. Gao, Monolayer dispersion of oxides and salts on surface of ZrO<sub>2</sub> and its application in preparation of ZrO<sub>2</sub>-supported catalysts with high surface areas, *Catal. Lett.* 45 (1997) 237–244.



### **3.2. Electrospun vanadium oxide based submicron diameter fiber catalysts. Part II: Effect of chemical formulation and dopants**

J. J. Ternero-Hidalgo, M.O. Guerrero-Pérez, J. Rodríguez-Mirasol, T. Cordero

Departamento de Ingeniería Química, Universidad de Málaga, Campus de Teatinos, E29071 Málaga, Spain

**Keywords:** Propane ODH; Mixed-oxide catalysts; Submicron fibers; Electrospinning; Vanadium; Zirconia

#### **Abstract**

The first part of present paper described the synthesis procedure for the preparation of  $\text{VO}_x/\text{ZrO}_2$  catalysts with fibrous morphology. In the present contribution, the same procedure is applied for the preparation of multimetallic catalysts, such as V-Mo-O/ $\text{ZrO}_2$  and V-Nb-O/ $\text{ZrO}_2$ . In all the cases, and in only one step, the multimetallic porous fibers were obtained. The characterization data has shown that the segregation of metal atoms is adequate, avoiding the formation of oxides such as  $\text{V}_2\text{O}_5$ ,  $\text{Nb}_2\text{O}_5$  and/or  $\text{Mo}_2\text{O}_3$ , and the activity under the propane ODH reaction of  $\text{VO}_x$  based catalysts is improved by the addition of Mo.

### **3.2.1. Introduction**

Vanadium is a key component for selective and environmental catalysts; and supported vanadium oxide catalysts find many industrial applications for selective oxidation, ammoxidation and reduction reactions. In this sense, mixed oxide catalysts containing Vanadium are one of the most studied heterogeneous catalytic systems for selective oxidation processes [1,2]. Moreover, the properties of these materials can be modulated and improved by the incorporation of other metals (Mo, Nb, Te, Sb, etc.) into their crystal structure, since the activity and selectivity of these catalysts can be modified by the addition of such atoms. In this way, there are several selective oxidation reactions in which Nb and/or Mo are used as promoting agent in vanadium-based catalysts [3-5]. The promoting effect of these atoms during partial oxidation process [5,6] are based on different facts: i) Nb and/or Mo partially substitutes V atoms, modulating the activity and decreasing the selectivity to total oxidation undesired products such as CO and CO<sub>2</sub>, ii) Mo and/or Nb can provide site isolation of the active centers from each other, resulting in a high selectivity to desired partial oxidation products, iii) Nb and/or Mo stabilize the crystal structure of vanadium oxide under catalytic reaction conditions with different V oxidation states, being possible a redox cycle for V species during reaction, and iv) Nb and/or Mo modify the number of acid sites on the surface of catalysts.

On the other hand, the use of a catalyst with fibrous structure of very low diameters in a fixed bed reactor has several advantages, such as low resistance to internal diffusion and pressure drop [7]. In the first part of this work ([8] or *Section 3.1*), it was described a new, versatile and simple synthesis method for preparing VO<sub>x</sub>/ZrO<sub>2</sub> fibers in only one-step by electrospinning. This new method proposed is able to develop quite porous fibers enhancing the formation of VO<sub>x</sub> catalytically active species on the surface of ZrO<sub>2</sub> oxide. It was also demonstrated how these porous fibers were catalysts active and selective for the propane oxidehydrogenation (ODH) reaction. This reaction is a promising alternative to the production of propylene by thermal cracking, which is a very energy demanding process



with quite low selectivity. Due to the promising results reported ([8] or *Section 3.1*) with the VOx/ZrO<sub>2</sub> fibers shape catalysts, the objective of present paper is to describe the synthesis, characterization and activity of fibers with compositions V-O-Nb/ZrO<sub>2</sub> and V-O-Mo/ZrO<sub>2</sub>. The effect of the composition (V/Mo or V/Nb), and the role of the synthesis method will be evaluated. Both zirconium propoxide or zirconium acetate solutions will be used as zirconia precursor during the preparation of the electrospinning polymer solutions in order to evaluate the effect of the precursor, since both have been described for this purpose [9-10].

### **3.2.2. Materials and methods**

#### *3.2.2.1. Catalysts preparation*

The synthesis of the different fibrous catalytic materials prepared in this study has been performed following the same procedure described before ([8] or *Section 3.1*), which involves the electrospun of a polymer solution containing the metallic precursors of Zirconium, Vanadium, Niobium and/or Molybdenum, followed by calcination to obtain the final submicron-fiber catalysts. The different reagents used for the preparation of the polymer solutions in this study were zirconium(IV) propoxide solution (Sigma-Aldrich, CAS: 23519-77-9, 70 wt % in 1-propanol), zirconium acetate solution (Sigma-Aldrich, CAS 7585-20-8, Zr<sup>x+</sup>·xCH<sub>3</sub>COOH, Zr ~16 wt % in acetic acid), polyvinylpyrrolidone (PVP) (Sigma-Aldrich, CAS: 9003-39-8, Mw ~1,300,000), acetylacetone (Sigma-Aldrich, CAS: 123-54-6, ≥99%), 1-propanol (Sigma-Aldrich, CAS: 71-23-8, ≥99.5%), vanadyl acetylacetonate (Sigma-Aldrich, CAS: 3153-26-2, ≥97.0%), ammonium niobate(V) oxalate hydrate (Sigma-Aldrich, 99.99%) and ammonium heptamolybdate tetrahydrate (Sigma-Aldrich, CAS: 12054-85-2, 99.98%).

Both zirconium propoxide in n-propanol or zirconium acetate in acetic acid solutions were used as zirconia precursor, as previously reported in others works [9-11], in order to compare the results and find the best precursor for every kind of catalyst. In the former case, the addition of acetylacetone

(chelating agent) [10] was required for the stabilization of the zirconium propoxide solution. PVP was used to form the polymer and to increase the viscosity of the solution in order to be properly electrospun [11]. Vanadyl acetylacetonate, ammonium niobate oxalate and ammonium heptamolybdate were used as vanadium, niobium and molybdenum precursors, respectively, since they presented an adequate solubility in the corresponding polymer solutions. Table 3.2.1 shows the amounts added of each reagent for the preparation of the polymer solutions to obtain the final fibers with the desired metallic content in vanadium, niobium and/or molybdenum. Then, these polymer solutions were vigorously stirred for 24 h at room temperature before the electrospinning process.

The electrospinning set up used for the preparation of the fibers has been described in the previous work ([8] or *Section 3.1*). In all the experiments the distance between the needle and the collector was 20 cm and the flow rate of the polymer solution was 0.5 mL/h. The electrical potential difference was adjusted/optimized depending on electrohydrodynamics properties of each polymer solution to find the stability during the electrospinning process. It should be noted that the applied voltage for the polymer solutions prepared using zirconium propoxide was always 12 kV (Table 3.2.1), while for the ones prepared using zirconium acetate was required higher applied voltage (from 14 to 34 kV), probably due to the higher surface tension of the latter polymer solutions. Moreover, in some polymer solutions made of zirconium acetate were necessary to dilute them with acetic acid to avoid gel formation and to decrease the viscosity, which made difficult the electrospinning process.

Finally, the electrospun fibers were calcined in a tubular furnace at 500°C for 6 h under air flow (150 mL STP/min) in order to remove the remaining solvent, the PVP and the organic part of the metallic precursors, and to stabilize the zirconia fibers. The heating rate to get the calcination temperature (500°C) was 10°C/min in all the cases. The name of all the fibers prepared in this study appears in Table 3.2.1, where the letter F in the beginning refers to the fibrillar shape of the samples. Then, PZr or AZr

are referring to the zirconium precursor used, zirconium propoxide or zirconium acetate, respectively. The rest of the name indicates the mass concentration of V, Nb and Mo. Thus, F-PZr is a zirconia fiber free of V, Nb or Mo prepared using zirconium propoxide, and F-AZr-VX.X-MoY.Y is zirconia fiber prepared using zirconium acetate with a mass content of V and Mo of X.X and Y.Y%, respectively.

**Table 3.2.1.** Summary of the samples prepared and their composition. Polymer solution and electrospinning conditions used for each sample.

Name	Metallic content (wt %)			Composition of the polymer solution	*Applied Voltage (kV)	
	V	Nb	Mo			
F-PZr	-	-	-	2.1000 g Zr Propoxide 0.3170 g PVP 0.4500 g Acetylacetone 2.9840 g n-Propanol	-	12
F-PZr-V5.0	5.0	-	-		0.1471 g C <sub>10</sub> H <sub>14</sub> O <sub>5</sub> V	12
F-PZr-Nb5.0	-	5.0	-		0.0971 g C <sub>4</sub> H <sub>4</sub> NNbO <sub>9</sub>	12
F-PZr-Mo5.0	-	-	5.0		0.0550 g (NH <sub>4</sub> ) <sub>6</sub> Mo <sub>7</sub> O <sub>24</sub> ·4H <sub>2</sub> O	12
F-PZr-V3.1-Nb1.9	3.1	1.9	-		0.1006 g C <sub>10</sub> H <sub>14</sub> O <sub>5</sub> V 0.0372 g C <sub>4</sub> H <sub>4</sub> NNbO <sub>9</sub>	12
F-PZr-V3.1-Mo1.9	3.1	-	1.9		0.1007 g C <sub>10</sub> H <sub>14</sub> O <sub>5</sub> V 0.0210 g (NH <sub>4</sub> ) <sub>6</sub> Mo <sub>7</sub> O <sub>24</sub> ·4H <sub>2</sub> O	12
F-PZr-V0.8-Mo4.3	0.8	-	4.3		0.0241 g C <sub>10</sub> H <sub>14</sub> O <sub>5</sub> V 0.0469 g (NH <sub>4</sub> ) <sub>6</sub> Mo <sub>7</sub> O <sub>24</sub> ·4H <sub>2</sub> O	12
F-AZr	-	-	-		5.0000 g Zr Acetate 0.3000 g PVP	-
F-AZr-V5.0	5.0	-	-	0.2943 g C <sub>10</sub> H <sub>14</sub> O <sub>5</sub> V		14
F-AZr-Nb5.0	-	5.0	-	0.1898 g C <sub>4</sub> H <sub>4</sub> NNbO <sub>9</sub> 5.0 mL Acetic Acid		34
F-AZr-Mo5.0	-	-	5.0	0.1075 g (NH <sub>4</sub> ) <sub>6</sub> Mo <sub>7</sub> O <sub>24</sub> ·4H <sub>2</sub> O 1.9 mL Acetic Acid		20
F-AZr-V3.1-Nb1.9	3.1	1.9	-	0.1966 g C <sub>10</sub> H <sub>14</sub> O <sub>5</sub> V 0.0726 g C <sub>4</sub> H <sub>4</sub> NNbO <sub>9</sub> 1.9 mL Acetic Acid		20
F-AZr-V3.1-Mo1.9	3.1	-	1.9	0.1968 g C <sub>10</sub> H <sub>14</sub> O <sub>5</sub> V 0.0410 g (NH <sub>4</sub> ) <sub>6</sub> Mo <sub>7</sub> O <sub>24</sub> ·4H <sub>2</sub> O 1.9 mL Acetic Acid		30
F-AZr-V0.8-Mo4.3	0.8	-	4.3	0.0471 g C <sub>10</sub> H <sub>14</sub> O <sub>5</sub> V 0.0916 g (NH <sub>4</sub> ) <sub>6</sub> Mo <sub>7</sub> O <sub>24</sub> ·4H <sub>2</sub> O 1.9 mL Acetic Acid		30

\*In all the experiments the distance between the needle and the collector was 20 cm and the flow rate of polymer solution was 0.5 mL/h.

### 3.2.2.2. Characterization

The porous texture of the samples was characterized by N<sub>2</sub> adsorption-desorption at -196°C using a micromeritics instrument (ASAP 2020 model). The samples were previously outgassed for at least 8 h at 150°C. The apparent surface area ( $A_{\text{BET}}$ ) was determined by applying the BET equation to the N<sub>2</sub> adsorption isotherm.

The surface morphology of the samples was studied by transmission electron microscopy (TEM) at an accelerating voltage of 200 kV, in a FEI Talos F200X microscope equipped with energy-dispersive X-ray analyzer (EDXA).

Surface chemistry of the samples was analyzed by X-ray photoelectron spectroscopy (XPS). XPS analyses of the samples were obtained by a 5700C model Physical Electronics apparatus with MgK $\alpha$  radiation (1253.6 eV). The maximum of the C1s peak was set at 284.5 eV and used as a reference to shift the other peaks.

X-ray diffraction patterns (XRD) were recorded in the region of  $2\theta=5-80^\circ$  for 30 min on an EMPYREAN diffractometer of PANalytical using CuK $\alpha$ <sub>1,2</sub> (1.5406 Å) monochromatic radiation (operational value 45 kV and 40 mA), a detector PIXcel and Soller slits (incident and diffracted beam) of 0.04 rad.

In situ Raman spectra of the samples were acquired in the 200-3200 cm<sup>-1</sup> region, using an Invia Reflex Raman Confocal (RENISHAW) spectrometer equipped with a RemCam deep depletion CCD detector using the 514.5 nm Ar line, with a spectral resolution of ca. 1 cm<sup>-1</sup>. The samples were treated at 200°C in air 2 h for obtaining the spectra under dehydrated conditions.

### 3.2.2.3. Propane oxidative dehydrogenation

The V-zirconia fibrous catalytic systems were tested for the propane oxidative dehydrogenation (ODH) in a fixed bed microreactor (i.d. 4 mm), with plug-flow behavior, placed inside a vertical furnace with temperature control. The temperature of reaction was varied from 300 to 480°C. The

feed was prepared by a mixture of three gases: propane (99.95%), oxygen (99.999%) and helium (99.999%). The gases were always mixed in a composition of 20% C<sub>3</sub>H<sub>8</sub>, 10% O<sub>2</sub> and 70% He by mass flow controllers, yielding a molar ratio of propane to oxygen of 2. The total volumetric gas flow ( $F_T$ ) and the mass of catalyst ( $W_{cat}$ ) were adjusted in order to vary the space-time ( $W_{cat}/F_{C3,o}$ ) in the range of 0.1-1.0 g<sub>cat</sub>·s·mL<sup>-1</sup>C<sub>3</sub>H<sub>8</sub> (Volume was always expressed in STP conditions). All the lines were heated above 120°C to pre-heat the reactant mixture before entering the reactor and to avoid the condensation of any product leaving the reactor.

Reactants and products were analyzed in steady state conditions by an on-line gas chromatograph (Perkin-Elmer, Clarus 500 GC), equipped with a Hayesep D 80/100 (length: 3 m; diameter: 1/8"; internal diameter: 2.1 mm) and an active carbon 80/100 (length: 2 m; diameter 1/8"; internal diameter: 2,1 mm) packed columns. Light gases (O<sub>2</sub>, CO and CO<sub>2</sub>) were detected by a thermal conductivity detector (TCD); and CH<sub>4</sub>, C<sub>2</sub>H<sub>4</sub>, C<sub>2</sub>H<sub>6</sub>, C<sub>3</sub>H<sub>6</sub> and C<sub>3</sub>H<sub>8</sub> were detected using a flame ionization detector (FID). The duration of each GC analysis was 15 min. In all the cases carbon and oxygen molar balances were closed with errors lower than 5%. The propane conversion and the selectivity to  $i$  product are defined as  $X$  and  $S_i$ , respectively:

$$X(\%) = \frac{\dot{F}_{C3,o} - \dot{F}_{C3}}{\dot{F}_{C3,o}} \cdot 100 \quad (1)$$

$$S_i(\%) = \frac{n_i \cdot \dot{F}_i}{n_{C3} \cdot \dot{F}_{C3,o} \cdot X} \cdot 100 \quad (2)$$

where  $\dot{F}_{C3,o}$  and  $\dot{F}_{C3}$  are the molar flows of propane in the inlet and in the outlet streams, respectively.  $\dot{F}_i$  is the molar flow of  $i$  product in the outlet stream, and  $n_{C3}$  or  $n_i$  are the number of carbon atoms per molecule of propane ( $n_{C3}=3$ ) or  $i$  product, respectively.

As blank reactions, catalytic tests were also performed with the empty reactor (to check the contribution of homogeneous phase reaction), and with the V/Nb/Mo-free-fiber (to see the contribution of the zirconia). The

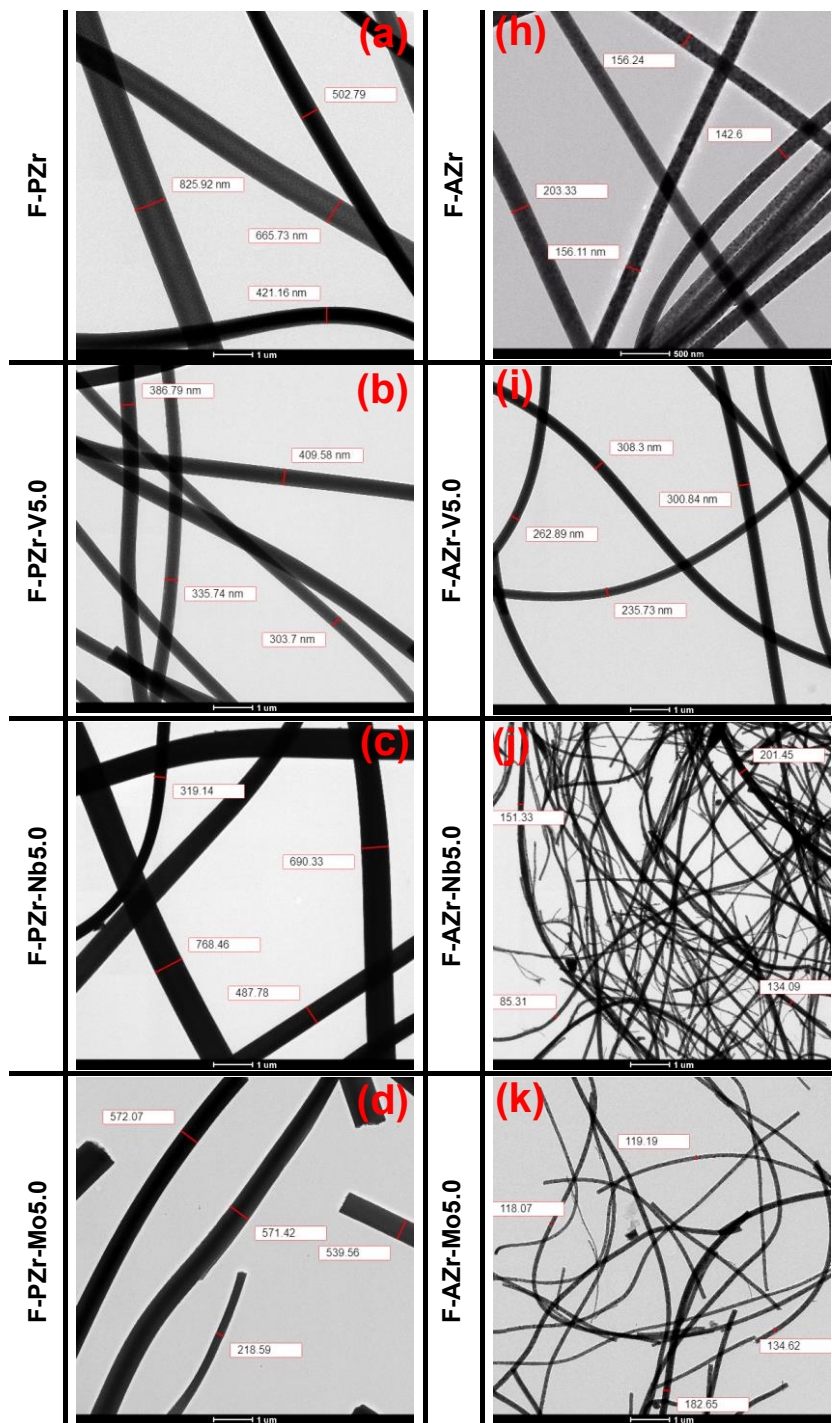
propane conversion values were found negligible in both cases when temperature was lower than 500°C.

The internal mass transport limitation can be considered negligible due to the quite small diameter of the submicron-fibers and no pressure drop has been observed through the catalyst bed under the experimental conditions used, due to the fibrous morphology of the catalysts. Under these conditions, it was concluded ([8] or *Section 3.1*) that the results were not affected by diffusional contribution, at least for all the reactions performed at 400°C or lower temperatures.

### **3.2.3. Results and discussion**

TEM images of all samples are shown in Figure 3.2.1, which confirms the fibrous morphology for all the samples, for all the compositions. The samples show a quite high length to diameter ratio and they do not present fused zones or beads. The first column shows the results for the samples prepared with propoxide, whereas the second one shows the micrographs obtained with the fibers obtained with acetate precursor. In all the cases, the diameters are thicker for the samples prepared with propoxide, probably due to the lower applied voltage during the electrospinning process in these samples compared to the ones prepared with acetate (Table 3.2.1), although the influence of other solution parameters as viscosity or electrical conductivity cannot be discarded. It has been reported that fiber diameter decreases with the increase of the applied voltage and/or electrical conductivity and with the decrease of the viscosity [11]. With respect the effect of composition in the diameter, it is observed that the incorporation of vanadium decreases the diameter in the case of the propoxide materials (F-PZr possess thicker diameters than F-PZr-V5.0), probably due to the increase of the electrical conductivity of the polymer solution when V precursor is incorporated. The same occurs, but to a much lesser extent, when the Nb or Mo precursor is added. However, different trends seem to occur when V, Mo or Nb are incorporated in the case of acetate materials (F-AZr, F-AZr-V5.0, F-AZr-Nb5.0, F-AZr-Mo5.0). Maybe because other

solution parameters, different of electrical conductivity, as surface tension and viscosity apparently also changed to a greater extent when V, Nb or Mo precursors were added in the acetate solutions. In fact, in this case the applied voltage was necessary to readjust in each acetate polymer solution, and sometimes was also necessary to dilute the solution with acetic acid to avoid gel formation and to decrease the viscosity. It also noteworthy that the fibers containing Mo prepared with propoxide were apparently more fragile than the ones prepared with acetate, which seems evident after comparing F-PZr-V3.1-Mo1.9 and F-PZr-V0.8-Mo4.3 with F-AZr-V3.1-Mo1.9 and F-AZr-V0.8-Mo4.3, since many broken fibers are observed in the first materials. It is the reason why the samples F-PZr-V3.1-Mo1.9 and F-PZr-V0.8-Mo4.3 were not tested in reaction and their characterization results will be not shown hereinafter.





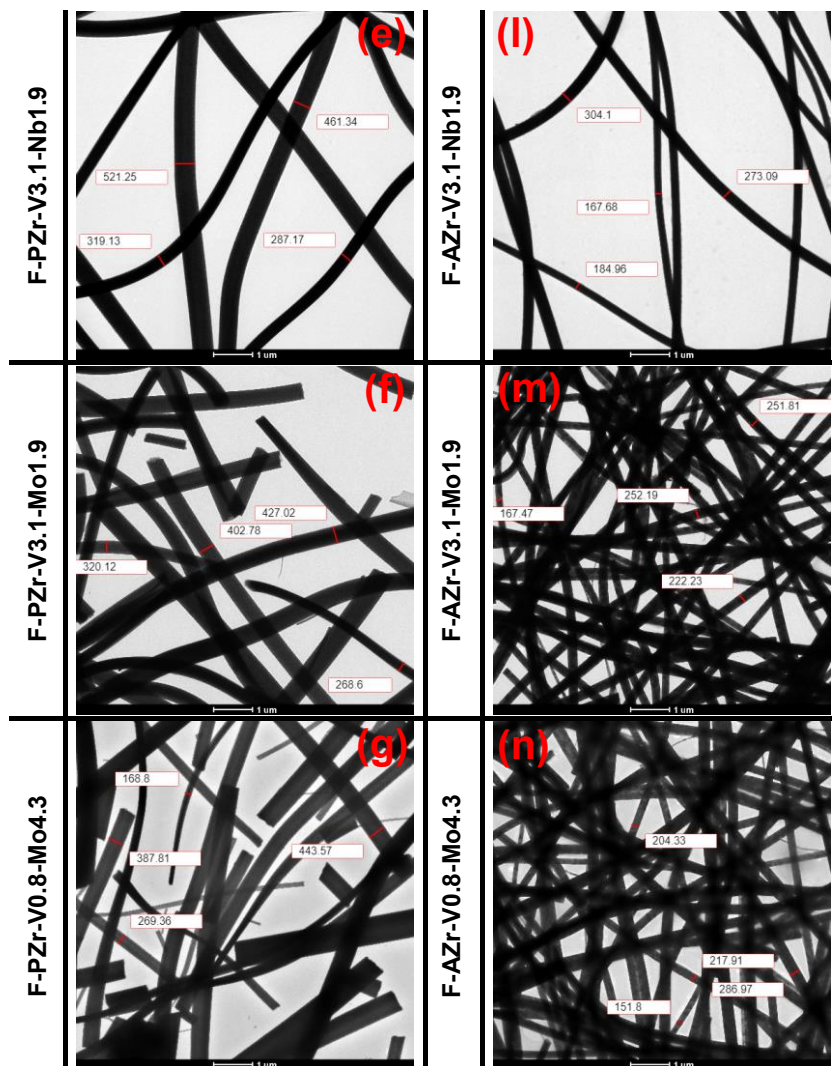


Figure 3.2.1. Transmission electron micrographs of the fibers prepared, on the left side using Zr propoxide (a-g) and on the right side using Zr acetate (h-n).

Figure 3.2.2 shows the N<sub>2</sub> adsorption-desorption isotherms, whereas Table 3.2.2 shows the BET surface area values of the fibers and the compositions obtained by both EDX and XPS (including the binding energies of the V2p, Nb3d and Mo3d XPS spectra). The samples prepared with propoxide (Figure 3.2.2a) present a typical mesoporous solid type IVa isotherm, and showing a hysteresis loop. Type H1 hysteresis loop is observed in the pure zirconia fiber (F-PZr), associated to the presence of a narrow range of uniform mesopores [12]. However, type H5 hysteresis loops are observed

in the zirconia fibers containing other metallic element such as V, Nb and/or Mo (F-PZr-V5.0, F-PZr-Nb5.0, F-PZr-Mo5.0 and F-PZr-V3.1-Nb1.9) often associated to pore textures containing both open and partially blocked mesopores [12]. On the contrary, type II isotherms with hysteresis loops type H3 are observed in the samples prepared with acetate (Figure 3.2.2b) characteristic of solids with a quite low developed porous structure [12]. Comparing the results obtained using both zirconium precursors, it is shown how the materials prepared using propoxide present a more developed porous texture and higher BET surface area values in all the cases. Moreover, the BET surface area values indicate that in both cases, these values increase when V is incorporated to the  $ZrO_2$  fiber (F-PZr presents a value of 26  $m^2/g$  whereas F-PZr-V5.0 of 66  $m^2/g$ ; and F-AZr a value of 7  $m^2/g$  versus 42  $m^2/g$  that presents F-AZr-V5.0 sample). This increase of the BET surface area value also occurs, but in a lower extent, when Nb or Mo is added to the fiber.

On the other hand, the binding energies of XPS spectra for the bands of V2p, Nb3d and Mo3d of the different samples prepared in this study (Table 3.2.2) present typical values of  $VO_x$ ,  $NbO_x$  and  $MoO_x$  species in  $ZrO_2$  [13-15], suggesting the presence of V-O-Zr, Nb-O-Zr and Mo-O-Zr bonds in the prepared materials. In all cases, the binding energies of these bands are lower than those in the crystalline phase of every metal (517.2 eV for  $V_2O_5$  [16], 207.3 eV for  $Nb_2O_5$  [14] and 233.2 eV for  $MoO_3$  [15]), probably due to electron transfer from  $ZrO_2$  to V, Nb or Mo. However, it cannot be discarded in any case the mixed oxides formation of Nb and V, or of Mo and V.

Table 3.2.2. Physicochemical characteristics of the fibers.

	<sup>a</sup> A <sub>BET</sub> (m <sup>2</sup> /g)	EDX (w/w %)			XPS (w/w %)			XPS BE (eV)		
		V	Nb	Mo	V2p	Nb3d	Mo3d	V2p	Nb3d	Mo3d
F-PZr	26	-	-	-	-	-	-	-	-	-
F-PZr-V5.0	66	4.7	-	-	4.9	-	-	516.6	-	-
F-PZr-Nb5.0	34	-	3.4	-	-	5.4	-	-	206.5	-
F-PZr-Mo5.0	44	-	-	5.3	-	-	8.5	-	-	232.8
F-PZr-V3.1-Nb1.9	54	3.5	0.9	-	2.6	3.4	-	516.6	207.0	-
F-AZr	7	-	-	-	-	-	-	-	-	-
F-AZr-V5.0	42	4.2	-	-	5.2	-	-	516.7	-	-
F-AZr-Nb5.0	12	-	0.8	-	-	3.5	-	-	207.0	-
F-AZr-Mo5.0	21	-	-	4.0	-	-	4.4	-	-	232.0
F-AZr-V3.1-Nb1.9	22	3.8	0.7	-	1.7	3.8	-	516.6	207.0	-
F-AZr-V3.1-Mo1.9	22	3.0	-	1.6	3.2	-	1.0	516.9	-	232.2
F-AZr-V0.8-Mo4.3	6	1.0	-	5.5	1.3	0	3.5	516.3	-	232.1

<sup>a</sup> from N<sub>2</sub> adsorption-desorption isotherms.

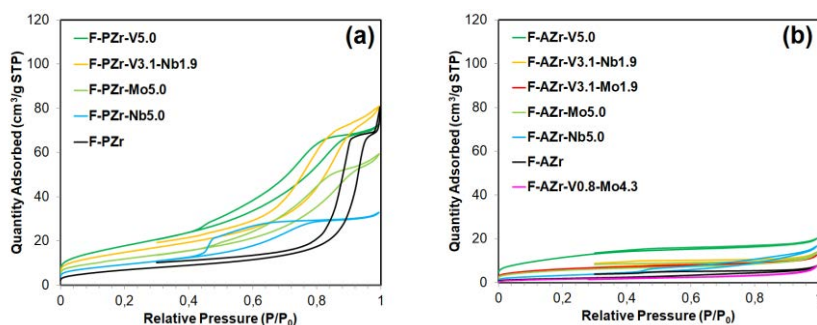
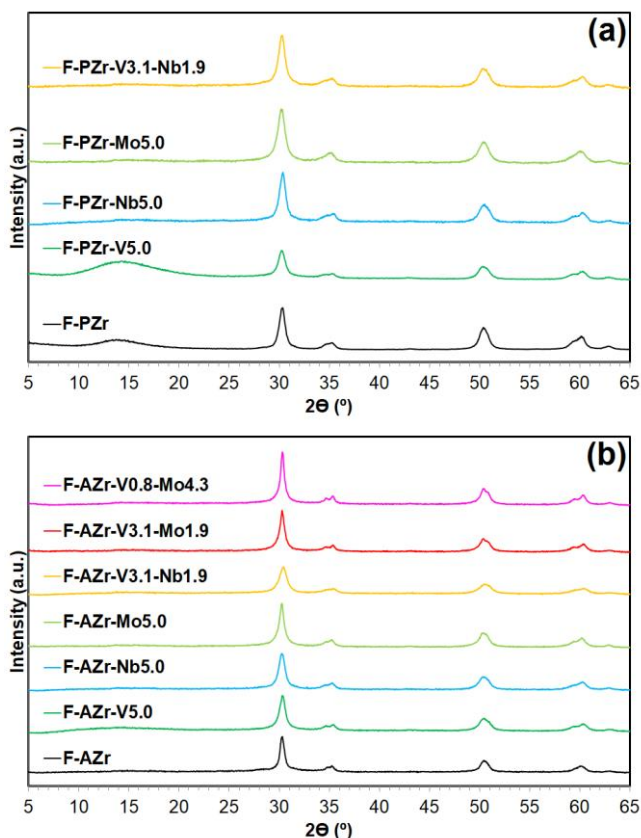


Figure 3.2.2. N<sub>2</sub> adsorption-desorption isotherms at -196 °C of the (a) samples prepared with Zr propoxide, and (b) the ones prepared with Zr acetate.

Bulk structure was analyzed by XRD (Figure 3.2.3), being these patterns quite similar for all the samples, and, as expected, showing the characteristic pattern of zirconia tetragonal phase [9]. Crystalline phases such as V<sub>2</sub>O<sub>5</sub>, Nb<sub>2</sub>O<sub>5</sub> or MoO<sub>3</sub>, including mixed oxides, are not observed, indicative that probably all the oxide phases are dispersed and not forming crystalline forms, or at least they are not so big to be detected by this technique. Figure 3.2.4 shows the Raman spectra of the dehydrated samples (although some of them could not be obtained due to fluorescence phenomena). All samples present the characteristic bands associated to tetragonal phase of zirconia, in agreement with the XRD results. In addition, they present a band around 950-1040 cm<sup>-1</sup>, sensitive under hydrating conditions, associated to V=O/Mo=O terminal bonds that corresponds to isolated mono and/or poly VO<sub>x</sub> and/or MoO<sub>x</sub> structures [17]. The samples

containing V present a broad band between 700 and 950  $\text{cm}^{-1}$ , centered around 765  $\text{cm}^{-1}$ , associated to the presence of monovanadates and polyvanadates, due to V-O modes along V-O-V and/or V-O-Zr chains [17,18]. Moreover, in the sample F-AZr-V5.0 can be detected the presence of two peaks, at 777  $\text{cm}^{-1}$  and 988  $\text{cm}^{-1}$ , which can be assigned to crystalline  $\text{ZrV}_2\text{O}_7$  [18,19], which is not observed in F-PZr-V5.0 despite having the same vanadium content. It seems that vanadium species trends to be in a more condensed form when zirconium acetate is used as zirconium precursor, which means that the vanadium is better dispersed when zirconium propoxide is used instead. On the other hand, the samples containing Mo (F-AZr-Mo5.0 and F-AZr-V0.8-Mo4.3) present a broad Raman band around 830  $\text{cm}^{-1}$  tentatively assigned to Mo-O-Zr and/or Mo-O-Mo bonds [17,20].



**Figure 3.2.3.** XRD patterns of the fibers prepared using Zr propoxide, and (b) the ones prepared using Zr acetate. Tetragonal  $\text{ZrO}_2$  (JCPDS 01-079-1769) are found in the X-ray diffractograms.

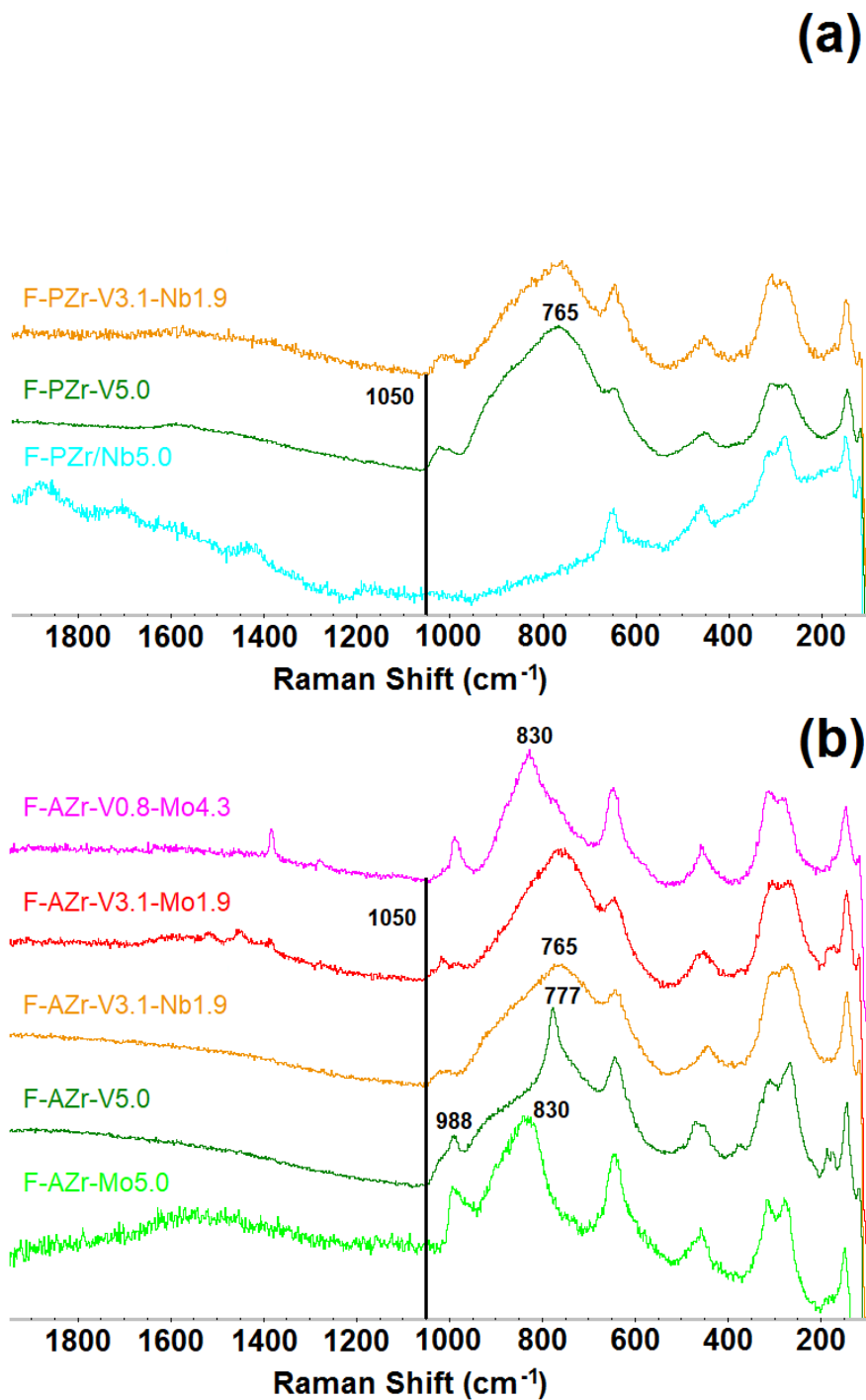


Figure 3.2.4. In situ Raman spectra of (a) the fibers prepared using Zr propoxide, and (b) the ones prepared using Zr acetate.

Activity results during ODH propane reaction are shown in Figure 3.2.5. If the activity results of the catalysts only containing vanadium are compared (F-AZr-V5.0 and F-PZr-V5.0), it can be observed that the propane conversion is always higher in the catalyst prepared using propoxide for the studied conditions (Figure 3.2.5a and b). Figure 3.2.5a shows that F-PZr-V5.0 presents similar propylene selectivities at low space-time ( $0.1 \text{ g}\cdot\text{s}\cdot\text{mL}^{-1}\text{C}_3\text{H}_8$ ) with respect temperature, despite the conversion values are always a bit higher than in F-AZr-V5.0. Figure 3.2.5b shows as the propane conversions for F-PZr-V5.0 are much higher than for F-AZr-V5.0 at  $300^\circ\text{C}$  when the space-time is increased from 0.1 to  $1.0 \text{ g}\cdot\text{s}\cdot\text{mL}^{-1}\text{C}_3\text{H}_8$ . In this case, F-PZr-V5.0 presents higher yields to propylene than F-AZr-V5.0, although the propylene selectivities is lower in each experiment. The higher activity of F-PZr-V5.0 than F-AZr-V5.0 could be explained by the higher BET surface area of the sample prepared using zirconium propoxide (66 versus  $42 \text{ m}^2/\text{g}$ ) (Table 3.2.2), together by the higher vanadium dispersion, which was already mentioned in the Raman results, where even some crystalline phase started to be detected in F-AZr-V5.0. Moreover, the reaction rate values per  $\text{m}^2$  of BET surface area of F-PZr-V5.0 and F-AZr-V5.0 for the conditions showed in the Figures 3.2.2a and 2b have been calculated (see additional information Figure 3.2.1.S). At low space-time ( $0.1 \text{ g}_{\text{cat}}\cdot\text{s}\cdot\text{mL}^{-1}\text{C}_3\text{H}_8$ ) the results are similar among the two catalysts. However, when the space-time is longer, the reaction rate value per  $\text{m}^2$  of F-PZr-V5.0 is the double with respect to F-AZr-V5.0. As these reaction rate values are different and these catalysts present the same amount of vanadium, these results suggest that not only the surface area is responsible of the higher activity of F-PZr-V5.0, but also the vanadium species are slightly different in both catalysts, as it was explained before in the Raman results. It is possible that in both catalysts adsorption of the reaction products and adsorption of the reagents is occurred on the same active sites in a competitive way, being the adsorption of the reactions products in F-AZr-V5.0 stronger than in F-PZr-V5.0, which could explain the differences found in the reaction rate values per  $\text{m}^2$  at high space-times. Since at higher

space-times, the products partial pressure is becoming higher and this effect would become more prominent.

Table 3.2.3 shows the activity results of the fibers containing only Nb or Mo (F-PZr-Nb5.0 and F-PZr-Mo5.0) as a function of temperature at space-times of 0.1 and 1.0 g·s·mL<sup>-1</sup><sub>C<sub>3</sub>H<sub>8</sub></sub>. No appreciable activity was detected until 480°C for both samples, where the sample containing Nb showed lower propane conversion and lower propylene selectivity than the one containing Mo. With respect to the fibers containing V and Nb (F-PZr-V3.1-Nb1.9 and F-AZr-V3.1-Nb1.9), the activity results are very similar and no great differences were observed between the samples prepared with different zirconium precursors (Figure 3.2.5a and c), although the BET surface area of F-PZr-V3.1-Nb1.9 is higher than of F-AZr-V3.1-Nb1.9, 54 and 22 m<sup>2</sup>/g, respectively (Table 3.2.2). Figure 3.2.5c also shows the results obtained with a fiber containing only V (F-PZr-V2.5) that presents quite similar propane conversions and propylene selectivities in the same reaction conditions, even though the V content of this catalyst is lower than the above ones (2.5 versus 3.1% wt). Therefore, in this case the mixture of Nb with V has not resulted in any improvement of the behaviour of the catalyst that only contains V.

**Table 3.2.3.** Propane conversions and selectivities to propylene in the propane ODH reaction for the catalysts F-PZr-Nb5.0 and F-PZr-Mo5.0 as a function of temperature with a space-time of 0.1 and 1.0 g·s·mL<sup>-1</sup><sub>C<sub>3</sub>H<sub>8</sub></sub>.

Sample	Space-time (g·s·mL <sup>-1</sup> <sub>C<sub>3</sub>H<sub>8</sub></sub> )	350°C		400°C		480°C	
		X (%)	S <sub>C<sub>3</sub>=</sub> (%)	X (%)	S <sub>C<sub>3</sub>=</sub> (%)	X (%)	S <sub>C<sub>3</sub>=</sub> (%)
F-PZr-Nb5.0	0.1	-	-	-	-	0.4	31.8
	1.0	-	-	-	-	1.6	29.9
F-PZr-Mo5.0	0.1	-	-	-	-	0.4	100
	1.0	-	-	0.1	100	3.9	41.9

The fibrous catalysts containing V and Mo prepared with acetate precursor, F-AZr-V3.1-Mo1.9 and F-AZr-V0.8-Mo4.3, has also been studied. Figure 3.2.5a shows that F-AZr-V3.1-Mo1.9 always presents higher propane conversions in the whole range of temperature than the samples prepared with the same content of V, but also adding Nb (F-PZr-V3.1-Nb1.9 and F-AZr-V3.1-Nb1.9). Moreover, at 400°C F-AZr-V3.1-Mo1.9 presents higher propane conversion and higher selectivity to propylene than F-PZr-V5.0

despite of having lower V content (3.1 versus 5.0 % wt) and lower BET surface area (22 versus 66 m<sup>2</sup>/g). On the other hand, the fiber F-AZr-V0.8-Mo4.3, which is the catalyst that showed the lowest activity in the whole conditions studied, did not show appreciable activity until 400°C. However, at higher temperatures (480°C) this catalyst presented high conversions together with relatively high propylene selectivities (Figure 3.2.5d). Figure 3.2.5d also shows the performance of a catalyst that only contains V (F-PZr-V1.3) and presents very similar propane conversion results with respect to F-AZr-V0.8-Mo4.3. It can be observed that the propylene selectivity obtained with F-AZr-V0.8-Mo4.3 is always 15-20% higher than the one obtained for the same conversions with the catalyst only containing V, F-PZr-V1.3. As above mentioned, the activity results of the catalyst prepared containing only Mo were negligible until 480°C. Moreover, at this high temperature the propylene selectivity was quite low. This means that when V and Mo are together somehow there should be a synergic interaction that improves the activity for the propane ODH with respect to the catalysts only containing V or Mo. Both Nb and Mo are well known as dopants for vanadium oxide based catalysts, whereas the radii and acid properties of both are quite different, for instance, Nb atoms present a bigger size than Mo ones. Mo and V oxide catalysts, even when they are in similar Mo/V molar ratio [4], thus, this is in line with the results obtained in present paper. Nb has a bigger size and a quite strong acid character, and it has been reported [6] that it is able to enhance the catalytic properties of several bulk oxide catalytic systems but only when it is in a quite low amount, by this way it is able to create vacancies and to modify the adsorption properties. But under certain synthesis conditions or when Nb is added in a high amount, it typically creates V-Nb-O stable structures that decrease the amount of V catalytically active species.



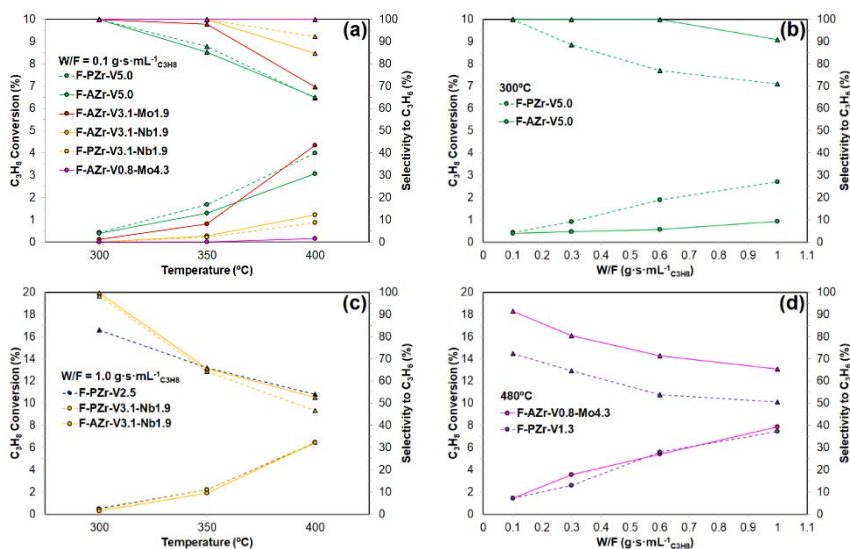


**Figure 3.2.5.** Reaction profiles in the propane ODH reaction of the different catalysts prepared. (●) Propane conversion and (▲) selectivity to propylene (a, c) as a function of temperature with a space-time of 0.1 and 1.0 g·s·mL<sup>-1</sup>C<sub>3</sub>H<sub>8</sub>, respectively; and (b, d) as a function of space-time ( $W/F_{cat}/F_{C_3H_8}$ ) at 300 and 480°C, respectively.

### 3.2.4. Conclusions

The first part of present work has proposed a new synthesis procedure for the preparation of porous ZrO<sub>2</sub> fiber with VOx catalytically active species on its surface in only one step, versatile, simple and straightforward procedure based on the electrospinning method. The second part demonstrated that this procedure is reproducible, and that can be used for the preparation of catalytic materials with different compositions, by the incorporation of other dopants in addition to vanadium. By this manner, it is possible to improve the catalytic activity during propane ODH reaction of V-containing catalysts by the addition of Mo.

### 3.2.5. Supplementary information

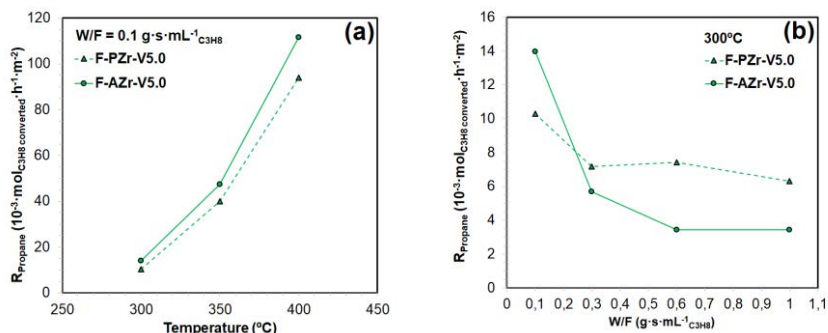


**Figure 3.2.1.S.** Propane reaction rates per  $\text{m}^2$  ( $R_{\text{Propane}}$ ) of the catalysts F-PZr-V5.0 and F-AZr-V5.0 (a) as a function of the temperature at a space-time ( $W_{\text{cat}}/F_{\text{C}_3\text{H}_8}$ ) of  $0.1 \text{ g} \cdot \text{s} \cdot \text{mL}^{-1} \cdot \text{C}_3\text{H}_8$  and (b) as a function of the space-time at  $300^{\circ}\text{C}$ . Note that the BET surface area values of each catalyst were used for the calculation of the  $R_{\text{Propane}}$  values.

### Acknowledgements

This work was supported by the Spanish Ministry of Economy and Competitiveness and FEDER [CTQ-2012-36408 and CTQ-2015-68654-R]. J.J.T.H. acknowledges the assistance of the Ministry of Economy and Competitiveness of Spain for the award of a FPI Grant [BES-2013-064425].

### 3.2.6. References

- [1] I.E. Wachs, Molecular engineering of supported metal oxide catalysts, *Chem. Eng. Sci.* 45 (1990) 2561–2565. [https://doi.org/10.1016/0009-2509\(90\)80142-2](https://doi.org/10.1016/0009-2509(90)80142-2).
- [2] M.O. Guerrero-Pérez, Supported, bulk and bulk-supported vanadium oxide catalysts: A short review with an historical perspective, *Catal. Today*. 285 (2017) 226–233. <https://doi.org/10.1016/j.cattod.2017.01.037>.
- [3] M.O. Guerrero-Pérez, M.A. Bañares, *Catalysis Today* 142, 245-251 (2009) “Niobium as Promoting Agent for Selective Oxidation Reactions” <https://doi.org/10.1016/j.cattod.2008.10.041> 36.
- [4] R. López-Medina, J.L.G. Fierro, M.O. Guerrero-Pérez, M.A. Bañares, “Nanoscaled Rutile Active Phase in Mo-V-Nb-O Supported Catalysts for the Oxidation of Propane to Acrylic Acid”, *Applied*

- Catalysis A: General 375(1), 55-62 (2010)  
<https://doi.org/10.1016/j.apcata.2009.12.017>
- [5] E. Rojas, M.O. Guerrero-Pérez, M.A. Bañares, "Niobia-Supported Nanoscaled Bulk-NiO Catalysts for the Ammoxidation of Ethane into Acetonitrile", *Catalysis Letters* 143 (2013) 31-42.  
<https://doi.org/10.1007/s10562-012-0937-7>.
- [6] R. López-Medina, I. Sobczak, H. Golinska-Mazwa, M. Ziolk, M.A. Bañares, M.O. Guerrero-Pérez, Spectroscopic Surface Characterization of MoVNbTe Nanostructured Catalysts for the Partial Oxidation of Propane", *Catal. Today* 187 (2012) 195-200.  
<https://doi.org/10.1016/j.cattod.2011.12.035>.
- [7] E. Reichelt, M.P. Heddrich, M. Jahn, A. Michaelis, Fiber based structured materials for catalytic applications, *Appl. Catal. Gen.* 476 (2014) 78–90. <https://doi.org/10.1016/j.apcata.2014.02.021>.
- [8] J.J. Ternero-Hidalgo, J. Torres-Liñán, M.O. Guerrero-Pérez, J. Rodríguez-Mirasol, T. Cordero, Electrospun vanadium oxide based submicron diameter fiber catalysts. Part I: Preparation procedure and propane ODH application, *Catal. Today.* (2018).  
<https://doi.org/10.1016/j.cattod.2018.10.073>.
- [9] Ruiz-Rosas, R., Bedia, J., Rosas, J. M. M., Lallave, M., Loscertales, I. G. G., Rodríguez-Mirasol, J., & Cordero, T. (2012). Methanol decomposition on electrospun zirconia nanofibers. *Catalysis Today*, 187(1), 77–87. <https://doi.org/10.1016/j.cattod.2011.10.031>.
- [10] Singh, S., Singh, V., Vijayakumar, M., & Bhanu Prasad, V. V. (2013). ZrO<sub>2</sub> fibers obtained from the halide free synthesis of non-beaded PVA/Zr n-propoxide electrospun fibrous composites. *Ceramics International*, 39(2), 1153–1161.  
<https://doi.org/10.1016/j.ceramint.2012.07.039>.
- [11] N. Bhardwaj, S.C. Kundu, Electrospinning: A fascinating fiber fabrication technique, *Biotechnol. Adv.* 28 (2010) 325–347.  
<https://doi.org/10.1016/j.biotechadv.2010.01.004>.
- [12] M. Thommes, K. Kaneko, A.V. Neimark, J.P. Olivier, F. Rodriguez-Reinoso, J. Rouquerol, K.S.W. Sing, Physisorption of gases, with

- special reference to the evaluation of surface area and pore size distribution (IUPAC Technical Report), *Pure Appl. Chem.* 87 (2015) 1051–1069. <https://doi.org/10.1515/pac-2014-1117>.
- [13] Pieck, C. L. L., Bañares, M. A. A., & Fierro, J. L. G. L. G. (2004). Propane oxidative dehydrogenation on VOx/ZrO2 catalysts. *Journal of Catalysis*, 224(1), 1–7. <https://doi.org/10.1016/j.jcat.2004.02.024>.
- [14] J. Goscianska, M. Ziolek, E. Gibson, M. Daturi, Meso-macroporous zirconia modified with niobia as support for platinum - Acidic and basic properties. *Catalysis Today*, 152(1–4), (2010) 33–41. <https://doi.org/10.1016/j.cattod.2009.10.016>.
- [15] N. K. Nag, A comparative study on the dispersion and carrier-catalyst interaction of molybdenum oxides supported on various oxides by electron spectroscopy for chemical analysis. *J. Phys. Chem.* 91(9), (1987) 2324–2327. <https://doi.org/10.1021/j100293a023>.
- [16] E. Hryha, E. Rutqvist, L. Nyborg, Stoichiometric vanadium oxides studied by XPS. *Surface and Interface Analysis*, 44(8), (2012) 1022–1025. <https://doi.org/10.1002/sia.3844>.
- [17] M.A. Bañares, I.E. Wachs, Molecular structures of supported metal oxide catalysts under different environments, *J. Raman Spectrosc.* 33 (2002) 359–380. <https://doi.org/10.1002/jrs.866>.
- [18] A. Christodoulakis, M. Machli, A.A. Lemonidou, S. Boghosian, Molecular structure and reactivity of vanadia-based catalysts for propane oxidative dehydrogenation studied by in situ Raman spectroscopy and catalytic activity measurements, *J. Catal.* 222 (2004) 293–306. <https://doi.org/10.1016/j.jcat.2003.10.007>.
- [19] J.R. Sohn, J.S. Han, J.S. Lim, Spectroscopic study of V2O5 supported on zirconia and modified with MoO3, *Mater. Chem. Phys.* 91 (2005) 558–566. <https://doi.org/10.1016/j.matchemphys.2004.12.024>.
- [20] Liu, Z., & Chen, Y. (1998). Spectroscopic Studies on Tetragonal ZrO2-Supported. *Journal of Catalysis*, 177, 314–324. <https://doi.org/10.1006/jcat.1998.2123>.

### **3.3. A simultaneous *operando* FTIR & Raman study of propane ODH mechanism over V-Zr-O catalysts**

J. J. Ternero-Hidalgo<sup>1</sup>, M. Daturi<sup>2</sup>, G. Clet<sup>2</sup>, P. Bazin<sup>2</sup>, M. A. Bañares<sup>3</sup>, R. Portela<sup>3</sup>, M.O. Guerrero-Pérez<sup>1</sup>, J. Rodríguez-Mirasol<sup>1</sup>, T. Cordero<sup>1</sup>

<sup>1</sup> *Universidad de Málaga, Departamento de Ingeniería Química, E29071 Málaga, Spain*

<sup>2</sup> *Normandie Univ, ENSICAEN, UNICAEN, CNRS, LCS, 14000 Caen, France*

<sup>3</sup> *Instituto de Catálisis y Petroleoquímica, CSIC, E28049 Madrid, Spain*

**Keywords:** Propane ODH; Reaction mechanism; Active sites; Structure-activity relationships; *Operando* IR-Raman

#### **Abstract**

Simultaneous *operando* Raman and transmission FTIR spectroscopic measurements have been combined for the study of the structure-activity relationships of V-Zr-O catalysts during propane OxyDeHydrogenation (ODH). The combination of both spectroscopies during reaction can allow the identification of reaction intermediates and yield structural information of the catalyst. The experimental results obtained are compared with the available data in the literature to propose a reaction mechanism for propane ODH, at least over V-Zr-O catalytic systems, and to identify the role of different oxygen species bound to vanadium sites. The results illustrate a Mars-van Krevelen type mechanism. Besides, they also directly and unambiguously show the higher activity of bridging oxygen sites (V-O-V, V-O-Zr) than terminal V=O bonds. In addition, the results reveal that polyvanadate are more active than monovanadate surface species.



### 3.3.1. Introduction

Nowadays, catalytic selective oxidation of hydrocarbons [1,2] is very important to obtain very demanded and useful value-added chemicals. Among these processes, the oxidative dehydrogenation (ODH) of propane to obtain propylene has been extensively studied over the past decades [3–5], since propylene has become the second most-demanded building block (after ethylene) in the petrochemical industry [6,7]. However, the low propylene yields obtained by propane ODH until now have hindered its industrial implementation [3]. Then, the non-oxidative dehydrogenation reaction is currently practiced in the industry instead [8], although it is an energy-intensive process with some other intrinsic drawbacks that could be solved by the ODH reaction [4,5].

Catalysts based on dispersed vanadia species over different supports ( $\text{ZrO}_2$ ,  $\text{TiO}_2$ ,  $\text{Al}_2\text{O}_3$ ,  $\text{SiO}_2$ , etc.) are the most reported in the literature for the propane ODH [3,4,9–12]. It has been established that reaction proceeds via Mars-van Krevelen type mechanism [4,5,13–19], which means that the lattice oxygens of the catalyst are the active sites for oxidation. In this way, the mechanism involves the consecutive reduction and oxidation of the catalyst surface by the reaction with propane and oxygen (or other oxidizing agents as  $\text{N}_2\text{O}$  [14,20]), respectively. The general reaction network most accepted in the literature is a parallel-consecutive pathway, where propane is oxidized to propylene, and both can be totally oxidized to  $\text{CO}_x$  [5]. Moreover, it is commonly reported that it is difficult to control such undesired combustion which lowers propylene yields [21], since the same active sites are responsible for both the selective ODH reaction and the total oxidation. Also, most of the  $\text{CO}_x$  produced during reaction usually comes from the consecutive combustion of propylene, due to the lower energy requirement to activate propylene with respect to propane [4,5,22,23]. Iglesia *et al.* carried out isotopic tracer studies to investigate the propane ODH reaction mechanism over  $\text{VO}_x/\text{ZrO}_2$  catalysts [21,24]. The results suggested that the C-H bond activation step of propane and the dissociative oxygen chemisorption step to reoxidize the catalyst are both irreversible, while the

OH groups formed on the catalyst during the different reactions are reversibly recombined forming water, oxygen active sites and vacancy centers.

However, there is no consensus about the nature of the path leading to propylene formation and, despite the vast propane ODH literature, not many details are usually given about the nature and number of steps of the mechanism involving the formation of  $\text{CO}_x$  [5]. Probably, because this is a very challenging reaction to study, since the first proton abstraction from propane is the rate-determining step, hence the steady-state coverages of subsequent intermediates are likely too small to be accessible by traditional methods. In this way, it seems that the most detailed investigations are provided by Busca *et al.*, who performed IR studies of the total oxidation of propane and its ODH to propylene over catalysts as  $\text{Mn}_3\text{O}_4$ ,  $\text{Co}_3\text{O}_4$  and  $\text{MgCr}_2\text{O}_4$  [17,25–29]. From these results and their comparison with the data available in literature by then, they proposed different possible reaction mechanisms for the propane activation and oxidation depending on the catalyst nature, which could be extrapolated over other transition metal oxide based catalytic systems [25,28]. According to them, it is suggested that all the oxidation steps involved in the hydrocarbon oxidation mechanism over such catalysts occur at the expense of nucleophilic lattice oxygen species [28]. They also propose that propane is most probably attacked at C(2), the weakest C-H bond, forming isopropoxide species, whose evolution can give rise to propylene or chemisorbed acetone that is overoxidized to  $\text{CO}_x$  through acetate and formate species as intermediates, with the consequent formation of carbonates. Oxidation of propane hardly occurs via attack at C(1), since it was observed in a very low extent and only using the catalyst  $\text{Co}_3\text{O}_4$  [27], forming n-propoxide species, which evolve as propylene or are totally oxidized through formation of chemisorbed propanal, followed by propanoate species and finally  $\text{CO}_x$ . Simultaneously, the formed propylene during reaction can be adsorbed on the catalyst and oxidized through an OH surface group to form 2-propoxide and continue towards the total oxidation via the acetone pathway.

Moreover, according to their results [26,27,29], propylene can be also oxidized through allyl-alkoxides as first intermediate species, followed by formation of chemisorbed acrolein, then acrylate species, and finally carboxylates and carbonates species, with the subsequent formation of CO<sub>x</sub>. These propylene oxidation routes could be supported by the investigations performed by Wachs *et al.* about selective oxidation of propylene to acrolein over supported V<sub>2</sub>O<sub>5</sub>/Nb<sub>2</sub>O<sub>5</sub> catalysts [30,31], where surface allyl intermediate species were found as the most abundant surface intermediate species, and acrolein together with acetone were the major compounds in the gas phase.

Furthermore, although is generally accepted that bridging oxygens sites (V-O-V/V-O-Support) are the most active sites, there are still authors reporting that terminal oxygen sites (V=O) are the active sites. Since 1968, terminal V=O bonds have been reported as the most active sites by many authors [32–41]. In fact, some DFT studies support that V=O bonds are the active sites for the propane ODH due to the higher nucleophilic character of vanadyl oxygens [37]. Conversely, since the 1990s other authors have evidenced that the bridging oxygens are the catalytic active sites for the selective oxidation reactions assuming a minor participation of the vanadyl oxygen [4,31,42–68]. In this way, quantum chemical calculations done by Witko *et al.* [51–54], modelling different V<sub>2</sub>O<sub>5</sub> crystallographic faces, supported the inactivity of the terminal vanadyl and the higher activity of the bridging oxygens, due to their higher nucleophilic character. Moreover, Wachs *et al.* [4,31,55–68] have provided a large support to this theory with experimental evidences by *in situ* or *operando* IR, Raman and UV-Vis DRS spectroscopy, as well as by <sup>18</sup>O<sub>2</sub>–<sup>16</sup>O<sub>2</sub> isotopic labeling studies. These results suggest the non-activity of the terminal vanadyl oxygens and the key role of the bridging V-O-support bonds in the kinetic rate determining step, as well as a minor participation of the bridging V-O-V bonds during the catalytic hydrocarbon oxidation reactions.

Thus, the aim of the present paper is to gain deeper insight about the role of the different oxygen sites and the propane ODH mechanism over V-Zr-



O catalysts. In this way, a new homemade *operando* IR-Raman cell, which was designed in a joint CSIC-UNICAEN collaboration, is used in order to obtain in a single experiment, with space and time consistency, information about the structure of the catalyst (mainly from Raman), the adsorbed species (mainly from FTIR) and the reactivity (online gases measurements) during reaction. Which offers a higher possibility to directly observe more relevant details about the structure-activity relationships of the catalysts during reaction. This will be used here to clarify some of the discrepancies found in the literature and/or confirm some speculative findings.

### **3.3.2. Experimental**

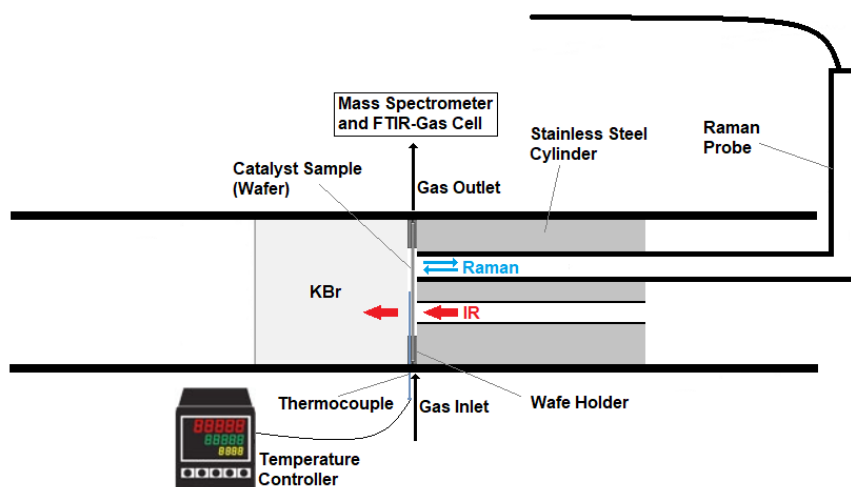
#### *3.3.2.1. Catalysts preparation*

The preparation of the catalysts has been published before ([69] or *Section 3.1*). The different reagents used were Zirconium (IV) propoxide, polyvinylpyrrolidone (PVP), acetylacetonate, 1-propanol and vanadyl acetylacetonate. The polymer solutions for the electrospinning process were prepared by mixing the zirconium precursor, the PVP, the acetylacetonate and the vanadyl acetylacetonate in 1-propanol in the adequate amounts to obtain final fibers with nominal mass concentrations of vanadium of 2.5% (Zr-V2.5), 5.0% (Zr-V5.0) and 6.4% (Zr-V6.4). These polymer solutions were vigorously stirred at room temperature for 24 h before the electrospinning process as described in previous articles ([69,70] or *Sections 3.1 and 3.2*). The electrospun fibers were calcined at 500°C (10°C·min<sup>-1</sup> of heating rate) for 6 h in air flow (150 mL·min<sup>-1</sup> STP). XPS analysis of the final catalysts Zr-V2.5, Zr-V5.0 and Zr-V6.4 resulted in vanadium mass concentrations of 2.7, 4.9 and 6.0%, respectively, as published in a previous work ([69] or *Section 3.1*).

#### *3.3.2.2. ODH reaction conditions*

Scheme 3.3.1 represents the IR-Raman *operando* reactor where the propane oxidative dehydrogenation (ODH) was performed for each catalyst. The cell is placed in the IR spectrometer bench (Nicolet 6700 FT-

IR spectrometer (64 scans/spectrum) equipped with a MCT/A detector) and allows direct acquisition of the transmission IR spectra. For the Raman spectra, the laser excitation (532 nm) is brought in the cell via an optical fibre and focused on the sample (using low power to prevent local heating, 5 mW in this case) with an *ad hoc* InPhotonics Raman probe specially designed to withstand high temperatures. The Raman signal was analysed by a Horiba Jobin Yvon Labram300 spectrometer. The dual IR-Raman *operando* reactor can be heated and fed with a controlled gas flow. Downstream the catalyst wafer, the exhaust gases are simultaneously measured using an IR gas cell, a GC and/or a mass spectrometer. The lines were heated at 60°C to pre-heat the reactant mixture before entering the reactor-cell and to avoid condensation of products leaving the reactor-cell. Additional technical details on the dual probe and coupled device will be provided in a dedicated technical paper.



**Scheme 3.3.1.** Schematic representation of the IRRaman device designed in a joint CSIC-UNICAEN collaboration.

The structured fiber catalysts were grinded and pressed into self-supported wafers to perform the catalytic experiments. The weight of catalyst wafer ( $W_{cat}$ ) and the total volumetric gas flow ( $F_T$ ) were always around 31.5 mg and 18.1 mL·min<sup>-1</sup>, respectively. The temperature of reaction was varied from 200 to 340°C. The “activation” flow contained 10% of oxygen in argon, while the “reaction” flow contained 20% of propane and 10% of oxygen in

argon (noted as ODH conditions in this case). Activation and reaction flow without oxygen were also used in the experiments (noted as DH conditions in this case).

Firstly, the samples were dehydrated heating from room temperature to 340°C (5°C·min<sup>-1</sup> of heating rate) under activation flow. After this step, the experiments were carried out at 200, 250, 300 and 340°C alternating the different flows, at each temperature, in the following order: activation, reaction, activation, reaction without oxygen, and activation flow. The conditions were never changed before achieving the steady or quasi-steady state in each experiment. In some cases, the temperature was increased until 340°C under activation flow to ascertain the complete removal of remaining surface species carrying on the following experiment.

FTIR and Raman *operando* spectra of the catalysts were acquired every 2 and 4 min, respectively, with an acquisition time of 39 s for the former and typically 180 s (sometimes changed to 60, 120 or 240 s) for the latter. Reactants and products of the gas phase were analyzed by both an online FTIR gas cell (one spectrum every 2 min), and online mass spectrometry (one measurement every ~3 seconds). In all the experiments performed under reaction flow the carbon molar balances were attained with a maximum error of 5%. Conversion of *i* reactant (propane or oxygen) and the selectivity to *i* product (propylene, carbon monoxide or carbon dioxide) are denoted as  $X_i$  and  $S_i$ , respectively, being:

$$X_i(\%) = \frac{\dot{F}_{i,o} - \dot{F}_i}{\dot{F}_{i,o}} \cdot 100 \quad (1)$$

$$S_i(\%) = \frac{n_i \cdot \dot{F}_i}{n_{C3} \cdot \dot{F}_{C3,o} \cdot X_{C3}} \cdot 100 \quad (2)$$

where  $\dot{F}_{i,o}$  and  $\dot{F}_i$  are the molar flows of *i* compound in the inlet and in the outlet streams, respectively, and  $n_i$  is the number of carbon atoms per molecule of *i* compound ( $n_{C3}=3$ ). Turn-over frequency (TOF) was calculated from Eq. (3); it quantifies the specific activity under defined reaction

conditions per vanadium atom describing the number of converted moles of propane per mol of vanadium and time:

$$TOF = \frac{\dot{F}_{C_3,o} \cdot X_{C_3} \cdot M_V}{W_{cat} \cdot W_V} \quad (3)$$

where  $M_V$  denotes the molar mass of vanadium and  $W_V$  the mass of vanadium per gram of catalyst based on nominal loading or determined by XPS in a previous work ([69] or *Section 3.1*). This parameter assumes that all the active sites have the same catalytic activity and that they are stable during the reaction. Therefore, it cannot be discarded that underestimated TOF values are obtained with Eq. (3), due to the possible presence of inaccessible active sites or vanadium atoms in the bulk.

In order to discard a possible contribution of the homogeneous phase reaction and/or of the zirconia support in the catalytic results of propane ODH at the temperatures studied, blank experiments were performed under reaction flow without catalyst and with a vanadium-free zirconia sample. In both cases propane conversion values were negligible. Moreover, the possible influence of the Raman laser on the catalytic activity was checked by performing FTIR *operando* experiments with and without the Raman probe to compare both results. The Raman laser effect was negligible, since no significant differences were found in the results obtained for each catalyst. The samples were also examined after the reaction experiments and no dark spots were observed due to the laser incidence. This apparently suggests that hotter zones, where coke could preferentially form, did not occur during reaction. The presence of a capillary thermocouple on the sample (providing temperature monitoring and oven feedback) guaranteed the thermal steady conditions over all the experimental process.

An experiment feeding a reaction flow with 20% of propylene instead of propane was also carried out. After activation at 340°C, the reaction flow of propylene was introduced in the reactor-cell at room temperature and heated to 100°C. During the experiment, the heating rate was kept at

5°C·min<sup>-1</sup>. At 48 minutes of the experiment the feed was changed to the activation flow and further heated to 150°C until steady state was achieved.

### 3.3.3. Results and discussion

#### 3.3.3.1. Fresh Catalysts characterization

Figure 3.3.1 shows the simultaneous infrared (Figure 3.3.1 A) and Raman spectra (Figure 3.3.1 B) of the dehydrated catalysts at 340°C. All the catalysts presented very similar Raman and infrared features. It can be observed the characteristic Raman bands (642, 459, 314 and 268 cm<sup>-1</sup>) of tetragonal phase of zirconia ([69,71] or *Section 3.1*), in concordance with the XRD results (Figure 3.3.1.S in Supplementary information). The broad Raman signal in the 700-950 cm<sup>-1</sup> range corresponds to V-O-V (around 880 cm<sup>-1</sup>) and V-O-Zr (around 770 cm<sup>-1</sup>) modes [42,61,69,72]. The typical Raman and infrared V=O modes of molecularly dispersed vanadium oxide species near 1020 cm<sup>-1</sup> [73–75] is detected at the same values of Raman shift and wavenumbers, respectively. It can be observed a relative intensity increase of the vanadium bands and a blue-shift of the V=O bands as the vanadium content increases. This shift is due to a higher relative population of polyvanadates with respect to monovanadates in the catalysts with higher vanadium contents [75]. The presence of crystalline V<sub>2</sub>O<sub>5</sub> can be excluded in all the catalysts, since its characteristic Raman bands near 143 and 994 cm<sup>-1</sup> are absent [72]. Moreover, some weak infrared bands around 3700 cm<sup>-1</sup> are apparent due to the hydroxyl groups. The infrared bands in the range of 1300-1600 cm<sup>-1</sup> can be attributed to carbonaceous deposits [76,77] and carbonate species [78]. The sharp band near 2339 cm<sup>-1</sup> is associated with occluded CO<sub>2</sub> [79,80], which could have been formed during the calcination step of the carbonaceous precursors for the preparation of the catalysts.

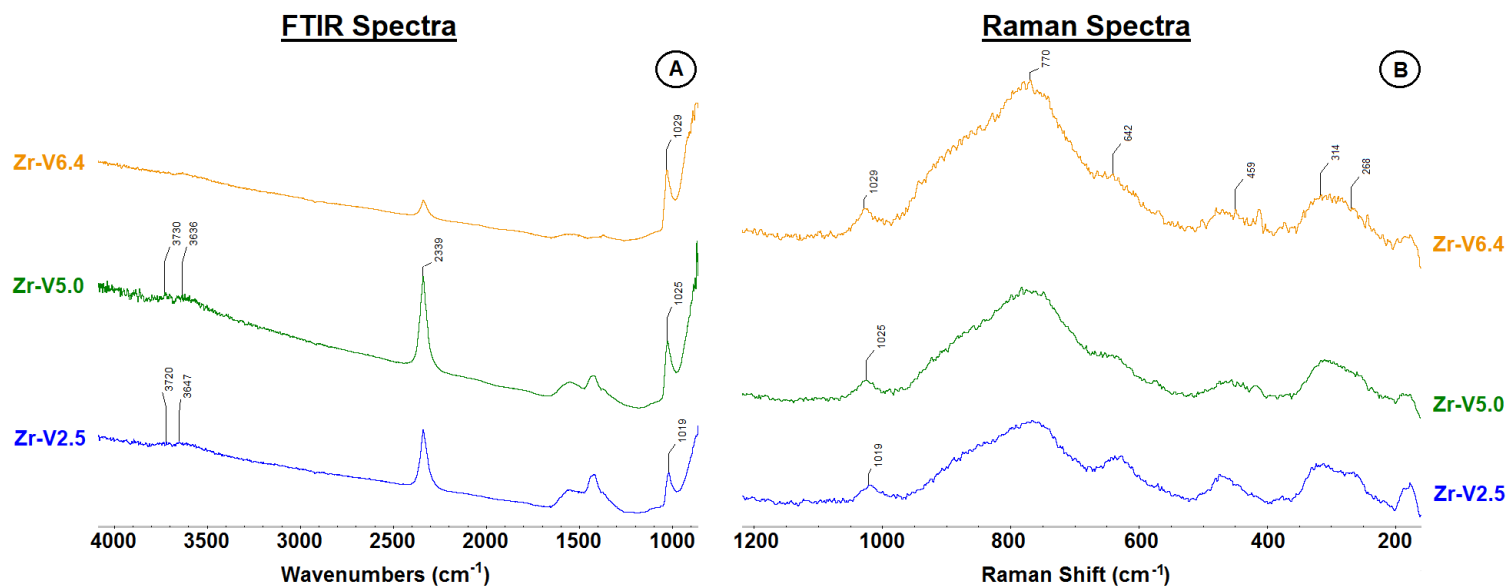


**Figure 3.3.1.** FTIR (A) and Raman (B) spectra obtained for the dehydrated catalysts Zr-V6.4, Zr-V5.0 and Zr-V2.5 in the IRRaman *operando* reactor under activation flow (10% O<sub>2</sub> in Ar) at 340°C.

### 3.3.3.2. Catalysts during reaction

#### 3.3.3.2.1. ODH conditions

The activity results obtained during propane ODH experiments in the IRRaman reactor are shown in Table 3.3.1. Conversion starts to be significant at 250°C for Zr-V6.4 and Zr-V5.0, and at 300°C for Zr-V2.5. In general terms, as reaction temperature increases, propane conversion increases and selectivity to propylene decreases due to the production of CO<sub>x</sub>, as a result of the undesirable combustion of both propane or propylene previously formed during reaction, in line with the known reaction pathway reported elsewhere [15,81]. The conversion, yield to propylene and TOF values obtained for the studied conditions indicates that the activity of the catalysts increases with vanadium content. Actually, the catalyst with the lowest vanadium concentration is not active at 250°C and always presents the lowest values of yield to propylene and TOF in each studied temperature. This means that Zr-V2.5 not only presents less amount of vanadium active sites, but also that these sites are less active than those present on the other catalysts with higher vanadia concentrations. This could suggest that the higher polyvanadates to monovanadates ratio present in Zr-V5.0 and Zr-V6.4 than in Zr-V2.5 could be responsible for the higher activity of the former, what may indicate that the oxygens sites on V-O-V structures are more active than those around V-O-Zr entities. It is noteworthy that TOF values based on both the vanadium concentration determined by XPS or the nominal vanadium concentration are very similar, suggesting that vanadium should be uniformly distributed along the catalysts studied in this work.

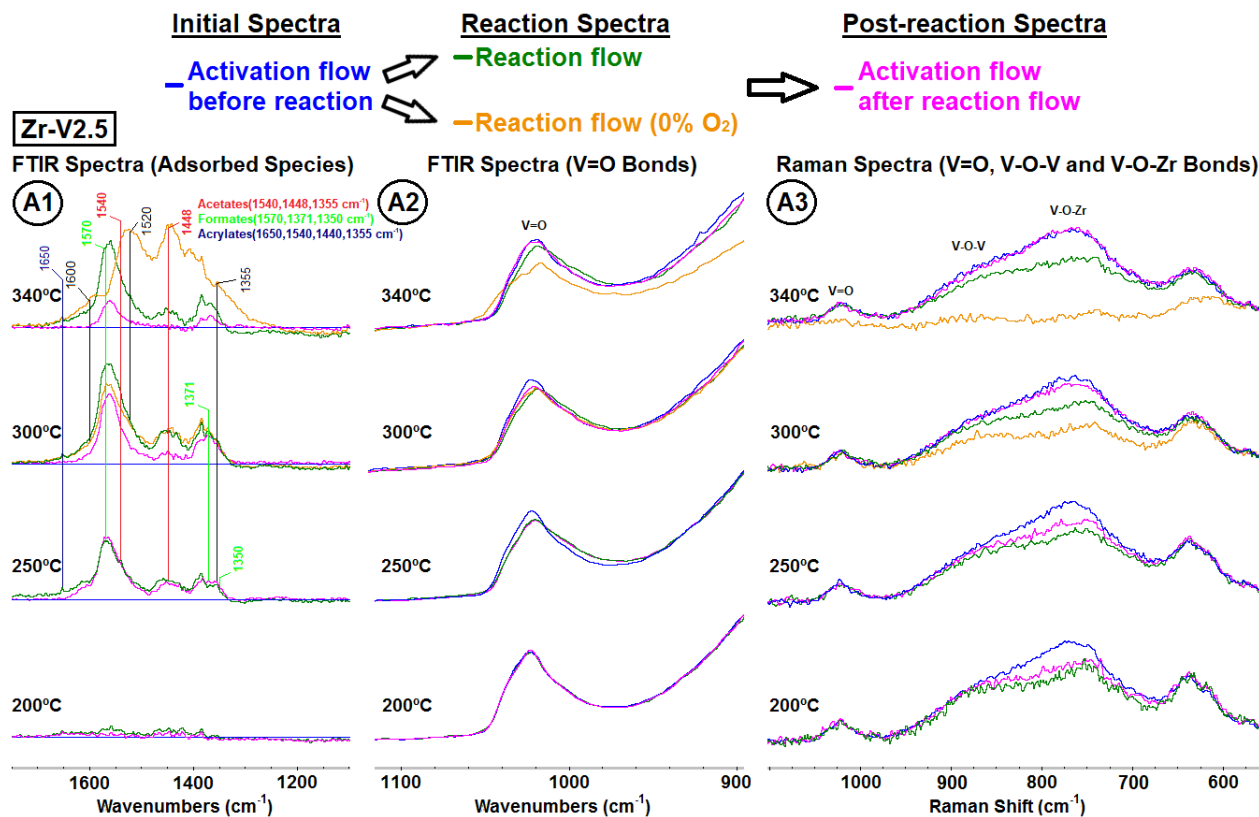
**Table 3.3.1.** Activity results obtained during the operando experiments in the IRRaman reactor (catalyst weight: ~31.5 mg, total flow: ~18.1 mL/min).

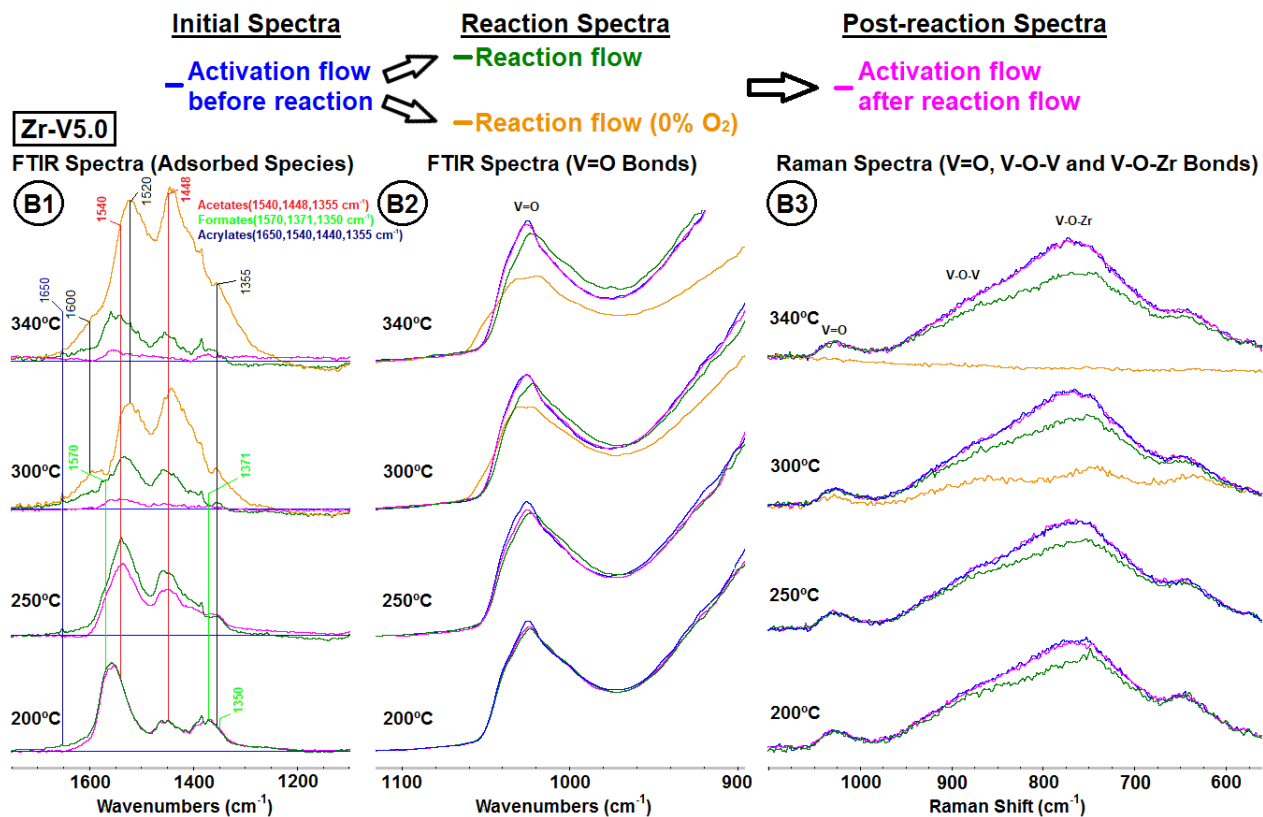
Temperature (°C)	Catalyst	X <sub>C3</sub> (%)	X <sub>O2</sub> (%)	S <sub>C3=</sub> (%)	Y <sub>C3=</sub> (%)	TOF <sup>a</sup> ·10 <sup>3</sup> (s <sup>-1</sup> )	TOF <sup>b</sup> ·10 <sup>3</sup> (s <sup>-1</sup> )
200	Zr-V2.5	-	-	-	-	-	-
	Zr-V5.0	-	-	-	-	-	-
	Zr-V6.4	-	-	-	-	-	-
250	Zr-V2.5	-	-	-	-	-	-
	Zr-V5.0	0.6	0.7	78.8	0.47	0.51	0.50
	Zr-V6.4	0.9	1.3	82.0	0.74	0.63	0.59
300	Zr-V2.5	0.7	1.3	82.8	0.58	1.09	1.18
	Zr-V5.0	1.6	3.5	74.5	1.19	1.37	1.34
	Zr-V6.4	2.1	5.9	68.3	1.43	1.47	1.38
340	Zr-V2.5	1.3	6.6	71.4	0.93	2.02	2.18
	Zr-V5.0	3.2	10.9	75.8	2.42	2.74	2.69
	Zr-V6.4	5.3	24.3	58.5	3.10	3.71	3.48

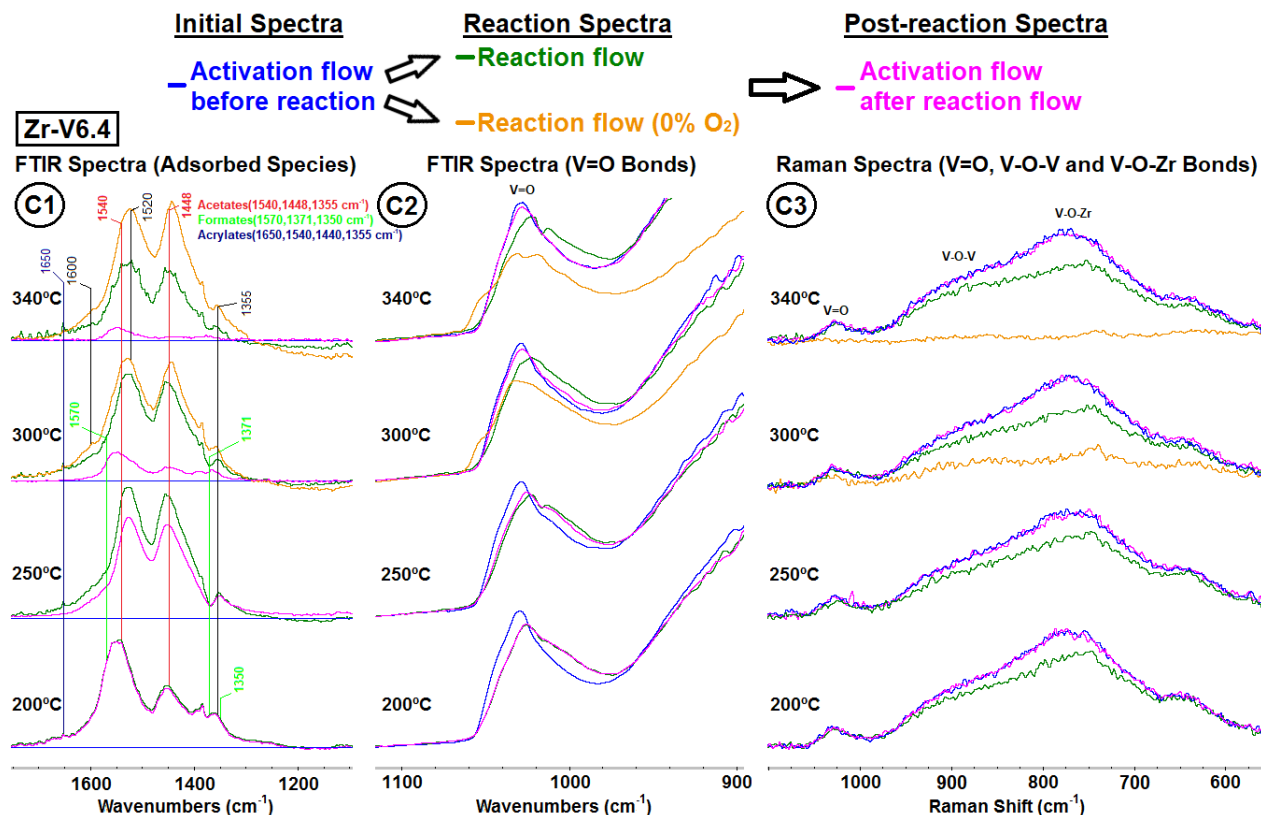
<sup>a</sup> TOF based on XPS analyses. <sup>b</sup> TOF based on nominal loading.

Figure 3.3.2 presents the FTIR and Raman operando spectra obtained during propane dehydrogenation in the presence and absence of oxygen (green and yellow traces, respectively), and activation flow before and after reaction (blue and pink lines, respectively), at different temperatures for the catalysts Zr-V2.5, Zr-V5.0 and Zr-V6.4 (Figures 3.3.2 A, B and C, respectively). Two regions of the FTIR spectra are shown, the 1750-1100 cm<sup>-1</sup> range (that provides information about the adsorbed oxygenated species - Figure 3.3.2 A1, B1 and C1), and the 1100-900 cm<sup>-1</sup> range, in which FTIR bands related to V=O bonds are detected (Figure 3.3.2 A2, B2 and C2). The Raman results are presented in the region 1100-525 cm<sup>-1</sup> (Figure 3.3.2 A3, B3 and C3). Adsorbed species were removed by heat treatment in presence of O<sub>2</sub> before starting each experiment, this is why the FTIR initial spectra under activation flow (blue lines) present no bands in the 1750-1100 cm<sup>-1</sup> region.









**Figure 3.3.2.** Operando FTIR (1 and 2) and Raman spectra (3) for Zr-V2.5 (A), Zr-V5.0 (B) and Zr-V6.4 (C). IR spectra shown at 1700-1100  $\text{cm}^{-1}$  (1) were all subtracted with the reference spectrum of the sample under activation flow at the same temperature. Green and yellow traces represent experiments using ODH and DH feeds, respectively. Blue and pink traces represent experiments using activation flow before and after reaction, respectively.

The catalytic activity of the samples in the conditions studied is almost negligible at 200°C (Table 3.3.1); however, Zr-V5.0 and Zr-V6.4 already exhibit some infrared bands in the 1600-1300 cm<sup>-1</sup> region (Figure 3.3.2 B1 and C1, respectively). These bands is attributed to a mixture of bidentate acetates (1540, 1448, and 1355 cm<sup>-1</sup>), acrylates (~1640, 1540, 1440, and 1355 cm<sup>-1</sup>) and bidentate formates (1570, 1371, and 1350 cm<sup>-1</sup>) [17,82–86], which appear stable during reaction (green lines) and remain on the surface upon subsequent oxidation (pink lines). For the Zr-V5.0 and Zr-V6.4 catalysts, a slight shift of the infrared V=O modes (Figure 3.3.2 B2 and C2, respectively) can be observed during reaction (green lines) with respect to the initial spectra (blue lines). This is not restored upon oxidation after reaction, since the post-reaction spectra (pink lines) at 200°C overlap with those during reaction (green lines). Raman spectra of all the catalysts (Figure 3.3.2 A3, B3 and C3) show an intensity decrease of the bands attributed to bridging V-O-V and V-O-Zr bonds in ODH conditions (green lines). These bands are quickly and totally recovered under oxidizing conditions, even though V=O bands are not restored and adsorbed species remain on the surface, since blue and pink lines overlap in all cases with the exception of Zr-V2.5 at 200°C. At this temperature, Zr-V2.5 is probably more difficult to reoxidize to the initial state, even though hardly any species are adsorbed in these conditions (Figure 3.3.2 A1) and the V=O bands keep unchanged (Figure 3.3.2 A2 and A3). This could be one further reason for the lower activity of Zr-V2.5 with respect to Zr-V5.0 and Zr-V6.4, as it was above mentioned when TOF values were compared (Table 3.3.1). Moreover, it can be also observed that in Zr-V2.5 the bridging oxygens can start to be slightly reduced in the presence of propane at 200°C, while the terminal bonds remain unperturbed (Figure 3.3.2 A2 and A3), what could suggest the higher activity of the former oxygen sites. It should be also noted that, although the propane conversion values measured at 200 °C are null for all the catalysts, it cannot be discarded the presence (at least for some moments) of some activity, very low or almost negligible and, below the detection limit of the measuring instruments used, since the apparition of oxygenate adsorbed species and the partial reduction of the

vanadia species observed in the FTIR and Raman spectra only could be explained by the propane oxidation with the concomitant catalyst reduction reactions. These reactions must be very slow at this low temperature (200°C), since it took long time (around 40 min) to reach the steady state in the spectra of the catalyst surface.

At 250°C, Zr-V2.5 is still apparently inactive but its features resemble those described above for Zr-V5.0 and Zr-V6.4 at 200°C with the development of a mixture of bidentate acetates, acrylates and bidentate formate species (Figure 3.3.2 A). Conversely, at 250°C, the catalytic activity starts to be appreciable for the samples Zr-V5.0 and Zr-V6.4 (Table 3.3.1), and some differences are found in the obtained spectra compared to those recorded at 200°C (Figure 3.3.2 B and C). The FTIR spectra in the region of adsorbed species show that the acetates to formates ratio increases with temperature for both catalysts (Figure 3.3.2 B1 and C1), since the bands attributed to acetates become more evident, and especially in Zr-V6.4, the most active catalyst. The relative decrease of formates may be explained as reported [27] by their transformation to CO without reducing the catalyst (lattice oxygen is not required during their decomposition) and by the fact that they are less thermally stable than the other species. This could explain why most of the formate species formed evolve at this temperature, while the most of acetate/acrylate species remains adsorbed. In fact, only a slight removal of acetate species is achieved with activation flow after reaction at 250°C. A decrease in the intensity of the Raman bands associated to V-O-V and V-O-Zr bonds is apparent during reaction (green lines), which are completely restored to the initial spectra (blue lines) upon reoxidation (pink lines) in the catalysts Zr-V5.0 and Zr-V6.4 (Figure 3.3.2 B3 and C3), unlike in Zr-V2.5 (Figure 3.3.2 A3).

At higher temperatures (300 and 340°C), the reaction rate becomes significantly faster, especially for the catalysts Zr-V5.0 and Zr-V6.4, as denoted by the higher conversion values measured (Table 3.3.1) and by the fact that steady state is quickly achieved (less than 15 min) for both the propane conversions and the catalyst surface spectra. Moreover, the

amounts of oxygenates that remain adsorbed (green lines) for catalysts Zr-V5.0 and Zr-V6.4 (Figure 3.3.2 B1 and C1) during reaction decrease significantly. These adsorbed species are almost completely removed upon reoxidation with activation flow (pink lines) while CO<sub>x</sub> and water are detected in the gas phase, evidencing that these oxygenate adsorbed species are active intermediates in the mechanism, and not just spectators, being precursors of CO<sub>x</sub> during the propane ODH reaction. Propylene is not detected in the gas phase during the evolution of these adsorbed species, as expected since the latter species present a higher oxidation state, what means that propylene is formed in earlier steps of the reaction and that the formation of carboxylate species is a consecutive and/or parallel reaction step with respect to the propylene formation. Regarding the FTIR spectra in the V=O region (Figure 3.3.2 B2 and C2), the small perturbation observed during reaction (green lines) disappears upon reoxidation (pink lines) along with the concomitant removal of oxygenate species (Figure 3.3.2 B1 and C1). Raman spectra changes become apparently increasing with temperature, although it does not seem to be proportional to any increase of the corresponding activity. Since the conversion will be determined by the catalyst reduction rate (i.e. propane oxidation rate), while the oxidation state of the catalyst under reaction conditions will depend on the steady state achieved when the reduction and oxidation reactions of the catalyst match with the same rate, this steady state will be determined by the ratio of the kinetic constants from the oxidation and reduction reactions at a given temperature, as well as by the operation conditions. On the other hand, the spectra (Figure 3.3.2) and the activity (Table 3.3.1) obtained for Zr-V2.5 at 300 and at 340°C, are similar to those afforded by Zr-V5.0 and Zr-V6.4 at lower temperatures, 250 and 300°C. However, it can be noted that the shape of FTIR spectra Zr-V2.5 in the region of adsorbed species under reaction (green lines) are not changed with increasing temperature (and activity) as happened with the other catalysts, which means that the proportion of acetate, acrylate and formate adsorbed species on surface is apparently constant. It seems that in the sample with the lowest catalytic activity, Zr-V2.5, the thermal stability of acetate, acrylate and formate

species is similar in the range of temperatures studied. This suggests that acetate and acrylate species could preferentially adsorb on sites that are more present on the catalysts with higher vanadium content, i.e. more polymerized species, where they are probably formed.

Overall, the *operando* results obtained in this work during propane ODH show that the catalyst is partly reduced during reaction, while part of the propane is oxidized giving rise to propylene (desired product), as well as oxygenated adsorbed species, behaving as active intermediates in the mechanism for the total oxidation to CO<sub>x</sub> (undesired products). It seems that acetate and formate species are the most abundant reaction intermediates (MARI), unlike acrylate species, for most of the reaction conditions studied. As observed in other researches [17,25,26], it cannot be discarded that the formation of carbonate surface species occurs during the evolution of such carboxylate species as CO<sub>x</sub>. Moreover, it is expected that other previous intermediate species than carboxylates could be formed during reaction (e.g. the precursor for the propylene formation), since surface oxidation reactions usually involve irreversible redox sequences where the adsorbed species are progressively oxidized into other ones [40]. However, these species are not detected in the studied conditions, probably due to their low or negligible surface concentrations, as a result of the relative low stability of such species with respect to those ones related to the rate determining step. The steady state is reached when the formation and oxidation/elimination rates of such species match with the same value, and then their steady state coverages will be determined by the operation conditions and the relative values between the kinetic constants of their corresponding oxidation steps and those constants belonging to the rate determining step at a given temperature. In the case of propane ODH, the assumption of the first proton abstraction of propane as rate determining step is commonly accepted in the literature [15,81,87]. As propane is significantly more stable towards oxidation than propylene and the formed intermediate species during reaction, the surface concentrations of most of these intermediates are very low and difficult to detect.

Moreover, the fact that the oxygenated species can be stable and accumulated on the surface below the reaction temperature suggests that the activation energy values for the oxidation steps of such species should be higher than the one for the rate determining step (propane activation). This is also consistent with the decrease of the amount of adsorbed species as the temperature increases, with the subsequent increase of the conversion to appreciable values. Furthermore, formates started to decompose as CO at lower temperatures than acetates, which suggests that the activation energy of the oxidation step for acetates is higher than for formates. This is consistent with the higher stability of acetates with respect to formates reported in the literature [27]. On the other hand, the slight decrease of bridging V-O-V/V-O-Zr bonds with the increase of the reaction temperature indicates a lower activation energy value for the catalyst reoxidation reaction of these bonds with respect to the activation energy value for the rate determining step, which will determine the rate of the different catalyst reduction reactions. In the case of the slight perturbations observed in the V=O band could somehow be associated with the interaction of these bonds with the adsorbed species, since these shifts are only observed when these species are present, and they disappear just when the oxygenates are removed, regardless of whether the catalyst has been reoxidized or not. It has already been reported that the coordination of surface vanadia species with hydrocarbon species or water results in small shifts in the V=O band [42,59], that are not detected in the bridging oxygens (V-O-V/V-O-Support) as a consequence of the broadness of this band.

In general, V=O and V-O-V/V-O-Zr bands show changes during reaction, which are quickly reversible under subsequent oxidation, but the biggest changes are observed in the bridging V-O-V and V-O-Zr bonds, as well as these bonds seem to start interacting with propane at lower temperature than the terminal oxygens, suggesting that bridging oxygens are most probably the active sites during propane ODH. These results, although are not definitive, are in agreement with previous works [45,55,88], where it has



been reported that bridging oxygens (V-O-V and V-O-Support) are more active than terminal oxygens (V=O). On the other hand, the increase of vanadium concentration in the catalysts, which leads to higher polyvanadates to monovanadates ratio on the catalyst surface, seems to increase the TOF values obtained during reaction, suggesting that polyvanadates are more active than monovanadates.

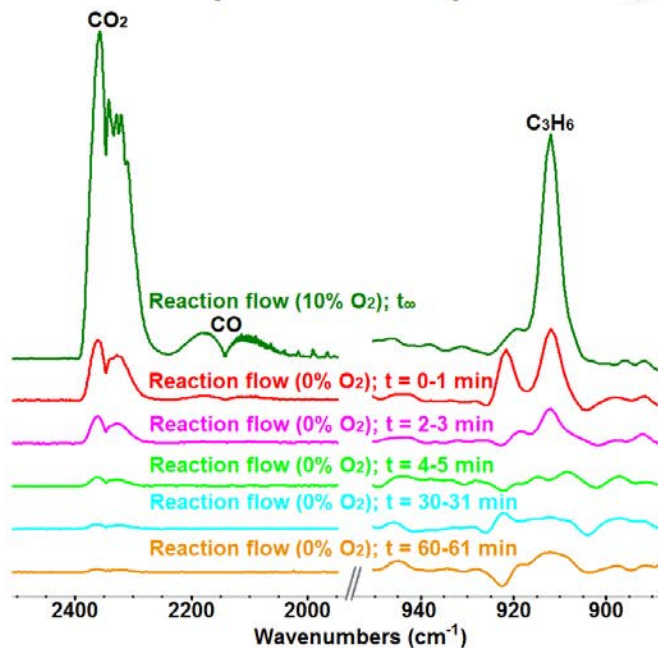
#### 3.3.3.2.2. DH conditions

Reaction without feeding oxygen (DH conditions) was also performed (yellow lines in Figure 3.3.2). Figure 3.3.2 shows only experiments at 300 and 340°C, since these at 200 and 250°C show no appreciable difference with those in the presence of oxygen, which was also the case for Zr-V2.5 at 300°C. At these temperatures, the spectra in DH conditions show a higher surface concentration of adsorbed oxygenates (mainly acetates) than in ODH conditions (Figure 3.3.2 A1, B1 and C1). As mentioned before, lattice oxygen is not required in the formates decomposition into CO. In contrast, the consumption of lattice oxygen is required for the evolution of acetate and acrylate species, what implies catalyst reduction. Therefore, during DH experiments, acetates dominate together with minor amounts of acrylates, because only the formates are removed while the acetates (and the acrylates to a lesser extent) are accumulated, since the oxygen necessary to their oxidation is lacking. However, during ODH experiments, both acetate and formate species are being simultaneously formed and removed giving rise to a steady state with a characteristic linear combination of both IR spectra. These differences are less obvious between the DH and ODH spectra for Zr-V5.0 and Zr-V6.4, since they already present a high acetates to formates ratio under ODH conditions. The results also show the formation of carbonaceous deposits form during DH experiments, as evidenced by a shoulder around 1600  $\text{cm}^{-1}$  in the FTIR spectra and Raman bands of carbon compounds around 1430 and 1600  $\text{cm}^{-1}$  (Figure 3.3.2.S in Supplementary information), while there is a significant decrease of V=O, V-O-V and V-O-Zr modes intensity (Figure 3.3.2 A2-A3, B2-B3 and C2-C3) (yellow lines). Argon flow was fed after

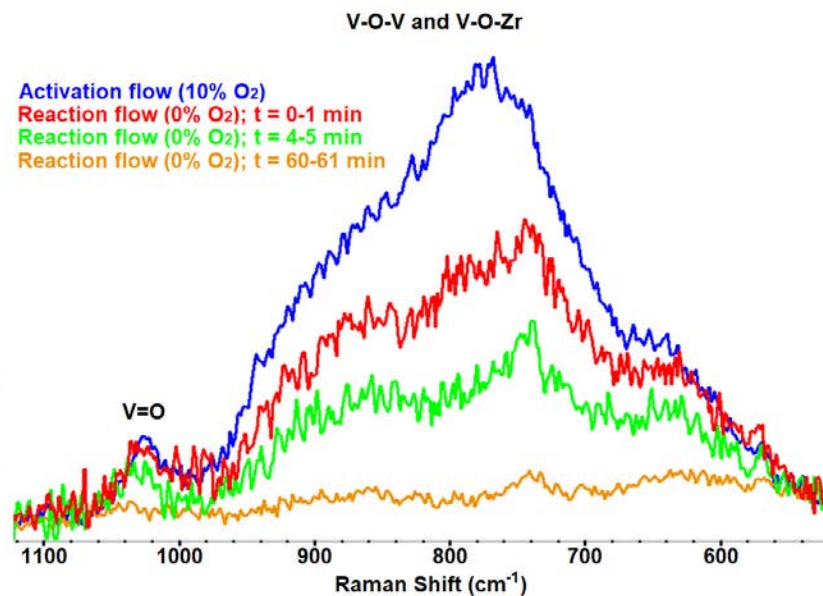
reaction to corroborate that the recovery of the vanadia bands to the initial state and the removal of the adsorbed species (mainly acetates and carbonaceous deposits) are only possible in the presence of gas phase oxygen.

The evolution of reaction products and of catalyst surface versus time during DH has been monitored and the results for Zr-V6.4 at 340°C are shown in Figure 3.3.3. It should be noted that the system was previously purged with argon to remove the oxygen in the gas phase. In addition, the acquisition time of the Raman spectra was reduced from 180 to 60 s in attempt to obtain more information about the first moments of the reaction, while the acquisition time of the FTIR spectra was kept in 39 s. The shorter data collection time in Raman resulted in worse quality Raman signals, but it was still acceptable. The ODH spectra obtained at 340°C from the gas phase under reaction flow in steady state and the spectra from the catalyst surface under activation flow are represented as reference showing both the steady state activity when oxygen is added to the feed and the catalyst surface in its highest oxidation state, respectively. Propylene, CO and CO<sub>2</sub> appear as initial products, whose concentrations decrease with time (Figure 3.3.3 A), as the lattice oxygen of the catalysts is being exhausted (Figure 3.3.3 B and D), while adsorbed species (mainly acetates) are formed (Figure 3.3.3 C). The fact that these products are being detected during some minutes, even though oxygen is not present in the gas phase, confirms the participation of lattice oxygen, as in a Mars-Van Krevelen type mechanism [13].

### Gas phase FTIR Spectra (A)



### Surface Raman Spectra (B)



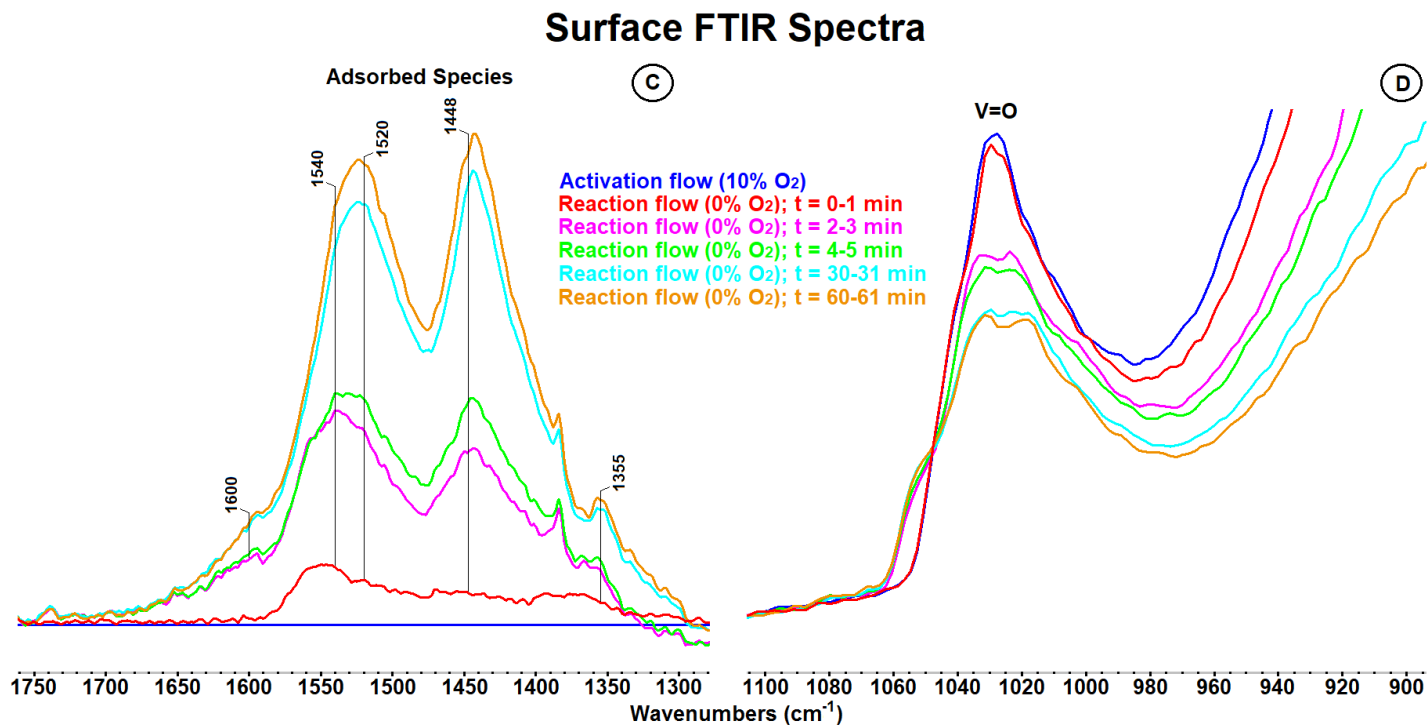


**Figure 3.3.3.** Evolution of the gas phase FTIR spectra (A), surface Raman spectra (B) and surface FTIR spectra (C and D) with time of Zr-V6.4 catalyst during DH reaction (20% C<sub>3</sub>H<sub>8</sub> in Ar) at 340°C.

With respect to the results obtained during the first minute in DH conditions, it can be derived from the gas phase spectra that the activity is already much lower than the reference (dark green line) obtained at steady state under ODH conditions (Figure 3.3.3 A). According to the Raman spectra (Figure 3.3.3 B), a significant intensity decrease of the Raman bands associated to V-O-V/V-O-Zr bonds is observed during the first minute of reaction (red line) compared to those previously obtained as reference under activation flow (dark blue line), showing the fast reduction rate of the catalyst in the studied conditions. However, Raman and FTIR bands belonging to V=O bonds practically keep unchanged (Figure 3.3.3 B and D, respectively), while FTIR bands associated to a mixture of bidentate acetate and formate species start to be apparent in Figure 3.3.3 C (red lines). Afterwards, the activity continues slowly decreasing with time on stream, being almost negligible after 3 minutes of reaction, while the lattice oxygen from V-O-V/V-O-Zr sites is further consumed and the reduction of V=O sites starts to be apparent, suggesting that V=O sites are much less active than V-O-V/V-O-Zr sites. From this point, the lattice oxygen of the catalyst is almost exhausted and acetate and acrylate species are progressively accumulated on the surface, without significant evolution to the gas phase. However, formate species are not noticeable, despite they should be also forming, since they can evolve to the gas phase even though the catalyst is totally reduced as above mentioned. The formation of coke is also observed when the catalyst is in a high reduced state, evidenced by the growing of a FTIR band by  $1600\text{ cm}^{-1}$ , absent during the first minute. Finally, quasi-steady state is achieved after 60 minutes in DH conditions, where it can be observed the total depletion of V=O bonds in the Raman spectrum, while these bands are still present in the FTIR spectrum, suggesting that there are vanadium sites not accessible in the catalyst pellets bulk. Since Raman is analyzing in backscattering and FTIR in transmission, then, most of the information collected by the Raman and FTIR spectra is from the surface ( $\sim 1\mu\text{m}$  of depth) and from the whole catalyst wafer, respectively.

These results show that the V-O-V/V-O-Zr sites (lattice bridging oxygens) are able to complete the whole catalytic cycle of the propane ODH reaction without the participation of oxygen from the gas phase or V=O sites (terminal vanadyl oxygens), since all the gas phase products and adsorbed species of such reaction have been fully formed during the first minute with the only use of the bridging oxygens in DH conditions. This is consistent with the assumptions made in the previous section, where V-O-V/V-O-Zr bonds are proposed as the most active sites instead of the V=O bonds, whose only slight changes observed during ODH can be mainly associated to the interaction of these bonds with the adsorbed species. It has also been revealed that terminal oxygen bonds (V=O) present some activity, but much lower than the bridging oxygens (V-O-V/V-O-Zr). These results definitely confirm the predictions made by other authors in the past, about the higher activity of bridging oxygens with respect to terminal oxygens [45,55,88]. It should be also noted that the simultaneous analysis by FTIR and Raman of the gas phase, of the catalyst structure and of the adsorbed species is crucial to fully and directly observe these findings in an unambiguous way. Furthermore, space and time consistency offered by the IRRaman reactor, due to its very small dead volume, was also crucial to successfully perform the transient experiment showed in Figure 3.3.3.

#### 3.3.3.3. Proposed mechanism

In Section 3.3.3.2, only acetate, acrylate and formate surface intermediate species were observed under reaction conditions, most of the intermediate species being undetected, as expected, since their surface concentrations must be very low by the fact that the very first C-H activation is the slowest step and the successive steps are much faster. In these cases, in order to determine the reaction mechanism, it is usually necessary to work at low reaction temperature or in the absence of one of the reactants to stop running the overall catalytic reaction, as well as to use an intermediate reactant in the gas phase that can form the successive surface intermediates at lower temperature, slowing down their evolution and allowing their detection [25]. Then, an experiment feeding propylene and

oxygen (ODH conditions) have been also performed, since propylene is much more reactive than propane and allows running experiments at lower temperatures than when propane was feed, which may enable the detection of less stable intermediates. Moreover, as the main source of CO<sub>x</sub> during propane ODH is the consecutive oxidation of the propylene formed [4,5,22], this experiment could give more information about the oxidations steps that take place during the total oxidation. Such results are shown in Figure 3.3.4 for Zr-V5.0. During propylene ODH, some bands, due to physisorbed propylene, appear at room temperature (1638, 1454, 1440, 1420 and 1372 cm<sup>-1</sup>) [26]. At 100°C, bands characteristic of adsorbed isopropoxide (1468, 1455, 1385, 1370, 1330, 1168, 1137 and 1115 cm<sup>-1</sup>) and chemisorbed acetone (1682, 1421, 1368, 1245 and 1090 cm<sup>-1</sup>) [82] can be detected; these species are also visible under oxidizing conditions (activation flow), and they are progressively oxidized, since the band of isopropoxide decreased and the band of acetone increased (dark blue line), reaching its maximum concentration after 86 minutes at 150°C. Then, acetone decreased and new bands characteristic of bidentate acetates and bidentate formates develop, similarly to the experiments where propane only was fed (Figure 3.3.2 A1, B1 and C1).

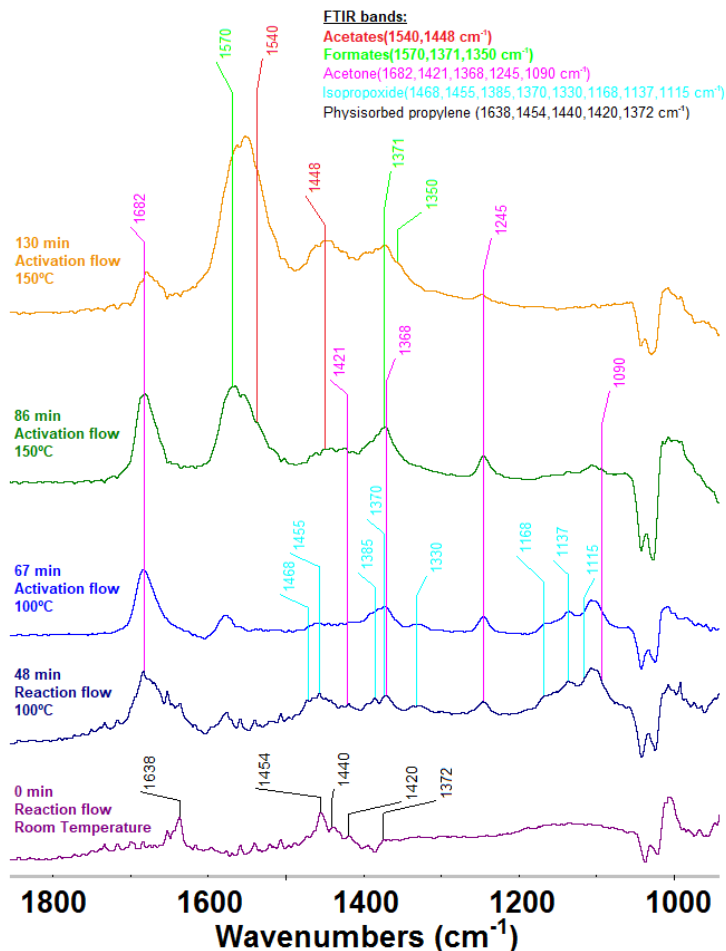
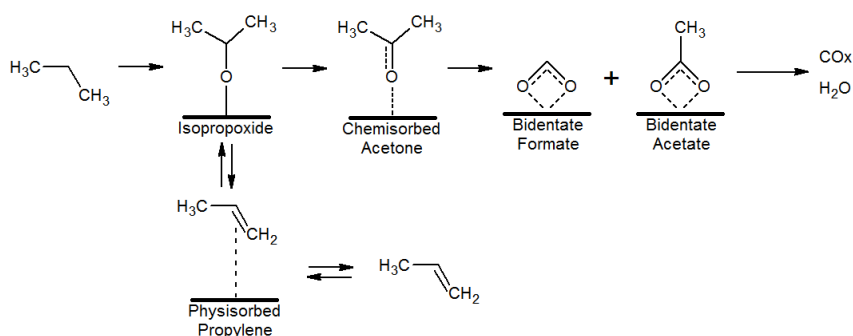


**Figure 3.3.4.** Operando FTIR spectra for Zr-V5.0 with a reaction flow of propylene (20%  $\text{C}_3\text{H}_6$  and 10%  $\text{O}_2$  in Ar), and with a subsequent activation flow (10%  $\text{O}_2$  in Ar).

The results obtained support the assumption that the consecutive total oxidation of propylene is responsible of most of the formed  $\text{CO}_x$ , in detriment of the parallel total oxidation of propane. Since practically the same final adsorbed species, which are precursors of  $\text{CO}_x$ , are obtained using propane or propylene under ODH conditions. It has also been observed that propylene activation mainly proceeds via isopropoxide species formation giving rise to chemisorbed acetone and carboxylates as observed in some previous studies [17,25–29], in contrast to other studies that have reported the activation through allyl-alkoxides giving rise to chemisorbed acrolein and acrylates surface species [21,26,27,29–31]. It is



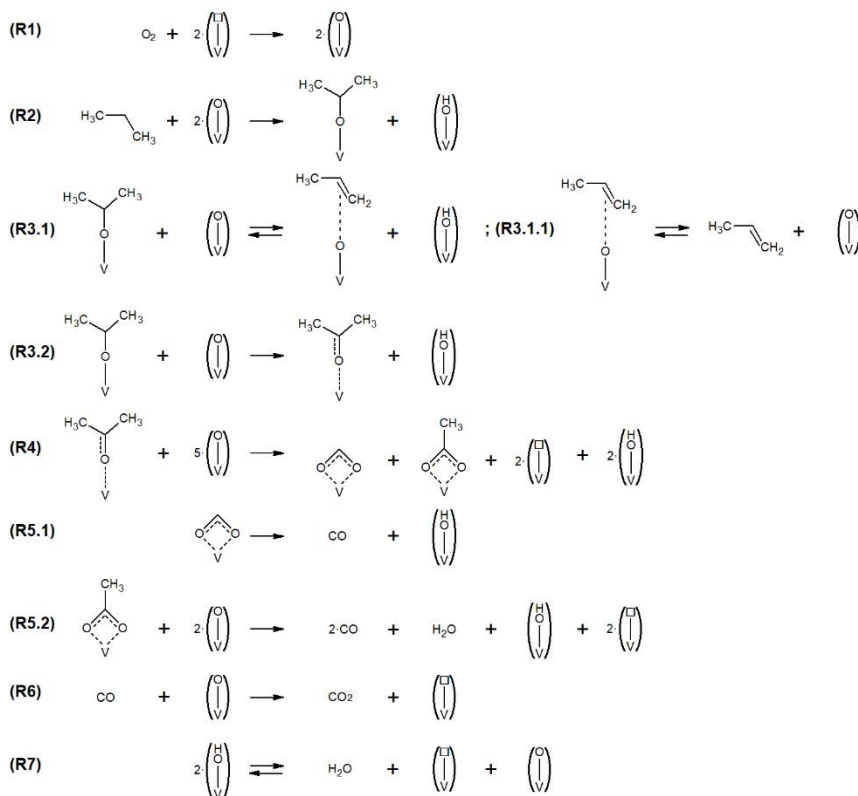
possible that both propylene oxidation routes simultaneously happen [26,28], and the catalyst nature will determine the most favorable pathway or the contribution of each one for the total oxidation steps. On the other hand, it has been assumed that propane is also activated via isopropoxide species formation as reported elsewhere [21,25,5], which would mean that a common surface intermediate is responsible of both parallel reactions [25,87], the propylene formation step and the total oxidation steps of propane or propylene. Scheme 3.3.2 illustrates the mechanism derived from these experiments and assumptions for the catalysts studied.



**Scheme 3.3.2.** Proposed mechanism derived from *operando* FTIR spectra obtained during propane/propylene partial oxidation reaction (ODH) and literature results.

Scheme 3.3.3 represents a proposed general mechanism that fits with the results obtained in this work, as have been described in present paper, and also with others already described in the literature [5,17,24–26,28]. It is assumed that only the lattice oxygen reacts with the adsorbed species, since it is the case of a Mars-van Krevelen type mechanism, and oxygen in the gas phase is necessary for the reoxidation of the catalyst, which perpetuates the catalytic cycle. To simplify the scheme, the lattice oxygens in the form of V-O-V or V-O-Zr bonds are represented as (V-O), where it has been assumed that both of them are the active sites having the same role in the mechanism. Moreover, the participation of V=O terminal groups in the reaction mechanism has not been represented in the scheme, since according to the here reported results, they are much less active than the bridging oxygens. (V-OH) and (V-□) represent a protonated lattice oxygen and a vacancy site, respectively. On the other hand, it is proposed that

propane oxidation occurs via the irreversible isopropoxide formation (R2), which can give rise to propylene in the gas phase (R3.1) or can be further oxidized to chemisorbed acetone (R3.2). The propylene formed can be adsorbed on the surface and be oxidized to isopropoxide species through a neighbour V-OH as Bronsted acidic site (R3.1.1 and R3.1, respectively) and continue with the subsequent oxidation steps (R3.2). Then, from chemisorbed acetone bidentate formates and acetates are formed by oxidative cleavage of the C(1)-C(2) bond (R4). Then, these oxygenate species evolve leading CO in the gas phase (R5.1 and R5.2). It has been assumed that these species evolve only as CO, and not as CO<sub>2</sub>, in line with a previous work with the same catalysts, where only CO was detected at low temperatures and at low space-time ([69] or *Section 3.1*). Finally, CO can be further oxidized to give rise to CO<sub>2</sub> in the gas phase (R6). Although it has not been represented in the scheme, the total oxidation through acrylates intermediate may be possible to some extent and it cannot be discarded the formation of carbonate surface species during the evolution of the carboxylates species as CO<sub>x</sub>, as reported in other works [17,25,26]. The equations R1 and R7 represent the reoxidation reactions of the catalyst, where the irreversible dissociative adsorption of O<sub>2</sub> from the gas phase is required, as well as the reversible OH recombination forming water, a V-O site and a vacancy center.



**Scheme 3.3.3.** Proposed detailed general mechanism based on the results obtained in this work and others found in the literature about propane ODH [5,17,24–26,28]. (V-O), (V-OH) and (V-□) represent lattice oxygens (V-O-V or V-O-Zr bonds), protonated lattice oxygens, and reduced vanadium sites, respectively.

As described, it has been possible to experimentally observe that the reaction occurs via a Mars-van Krevelen type mechanism showing clear evidences that the V-O-V/V-O-Zr sites are more active than terminal V=O bonds. In addition, also the required steps to total oxidation to CO<sub>x</sub> have been described, which could be useful to know how to proceed to avoid in some extent the total oxidation of propane, so increasing the selectivity towards propylene.

### 3.3.4. Conclusions

The new “IRRaman” reactor was used to study the structure-activity relationships of V-Zr-O based catalysts under propane ODH conditions. This multimodal *operando* cell allows activity measurement with the simultaneous obtention of Raman and FTIR spectra from the catalyst. The

results indicate that the reaction occurs via a Mars-van Krevelen type mechanism. It has been proposed that propane activation, considered the rate determining step, occurs through the formation of isopropoxide species, which can be desorbed giving rise to propylene or, parallelly, can be deeper oxidized to chemisorbed acetone, which can be converted into acetate and formate species by oxidative cleavage of the C(1)-C(2), being these carboxylates species precursors of CO<sub>x</sub>. It has been observed that the oxidation of the propylene formed during reaction mainly presents the same above pathway of oxidation, via reaction with an OH surface group as Bronsted acidic site to form isopropoxide species. Moreover, it has been directly and unambiguously observed that the V-O-V/V-O-Zr sites are significantly more active than terminal V=O bonds, so shedding additional light on the reaction mechanism, since some contradictory hypotheses regarding the real active bonds were proposed in the literature. The results also show that polyvanadates present a higher activity than monovanadates. In addition, valuable information was obtained to provide the required bases to perform a kinetic study in a future work. The simultaneous *operando* FTIR and Raman, together with the space and time consistency offered by the IRRaman reactor, have been very important to be able to observe the above insights about the propane ODH mechanism.

### 3.3.5. Supplementary information

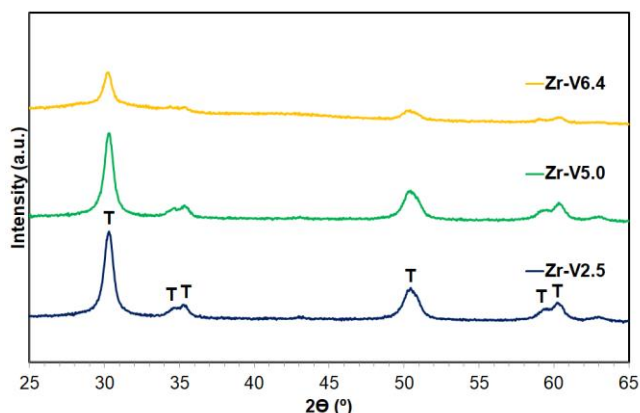


**Figure 3.3.1.S.** XRD patterns of the catalysts studied in this work (Zr-V2.5, Zr-V5.0 and Zr-V6.4). Tetragonal (T) ZrO<sub>2</sub> (JCPDS 01-079-1769) is found in all the X-ray diffractograms.

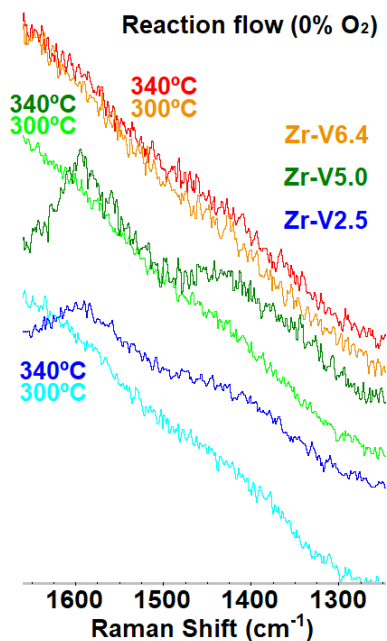


**Figure 3.3.2.S.** Operando Raman spectra for Zr-V2.5, Zr-V5.0 and Zr-V6.4 in the 1300-1600 cm<sup>-1</sup> region during DH conditions (20% propane in He) at 300 and 340°C.

### Acknowledgements

Authors acknowledge the FEDER-Region Basse-Normandie (France)-CNRS for a Chaire d'Excellence, which resulted in the implementation of the "IRRaman" rig and a research stay allowing to perform these investigations. This work was also supported by the Spanish Ministry of Economy and Competitiveness and FEDER (CTQ2012-36408, CTQ2015-68654-R and CTM2017-82335-R). J.J.T.H. acknowledges the assistance of the Ministry of Economy and Competitiveness of Spain for the award of a FPI Grant (BES-2013-064425) and the award for performing his stay at ENSICAEN (EEBB-I-16-10749).

### 3.3.6. References

- [1] R.H. Crabtree, Alkane C–H activation and functionalization with homogeneous transition metal catalysts: a century of progress—a new millennium in prospect, *J. Chem. Soc. Dalton Trans.* (2001) 2437–2450. <https://doi.org/10.1039/B103147N>.
- [2] F. Cavani, J.H. Teles, Sustainability in Catalytic Oxidation: An Alternative Approach or a Structural Evolution?, *ChemSusChem*. 2 (2009) 508–534. <https://doi.org/10.1002/cssc.200900020>.
- [3] F. Cavani, N. Ballarini, A. Cericola, Oxidative dehydrogenation of ethane and propane: How far from commercial implementation?, *Catal. Today*. 127 (2007) 113–131. <https://doi.org/10.1016/j.cattod.2007.05.009>.
- [4] C.A. Carrero, R. Schloegl, I.E. Wachs, R. Schomaecker, Critical Literature Review of the Kinetics for the Oxidative Dehydrogenation of Propane over Well-Defined Supported Vanadium Oxide Catalysts, *ACS Catal.* 4 (2014) 3357–3380. <https://doi.org/10.1021/cs5003417>.
- [5] R. Grabowski, Kinetics of oxidative dehydrogenation of C2-C3 alkanes on oxide catalysts, *Catal. Rev. - Sci. Eng.* 48 (2006) 199–268. <https://doi.org/10.1080/01614940600631413>.
- [6] J. Lazonby, Propene (Propylene), (n.d.). <http://www.essentialchemicalindustry.org/chemicals/propene.html> (accessed June 3, 2019).
- [7] The Propylene Gap: How Can It Be Filled?, *Am. Chem. Soc.* (n.d.). <https://www.acs.org/content/acs/en/pressroom/cutting-edge-chemistry/the-propylene-gap-how-can-it-be-filled.html> (accessed June 3, 2019).
- [8] I. Amghizar, L.A. Vandewalle, G. Van, G.B. Marin, New Trends in Olefin Production, 3 (2017) 171–178. <https://doi.org/10.1016/J.ENG.2017.02.006>.
- [9] A. Corma, J.M. López-Nieto, N. Paredes, M. Pérez, Y. Shen, H. Cao, S.L. Suib, Oxidative Dehydrogenation Of Propane Over Supported-

- Vanadium Oxide Catalysts, in: P. Ruiz, B. Delmon (Eds.), *Stud. Surf. Sci. Catal.*, Elsevier, 1992: pp. 213–220. [https://doi.org/10.1016/S0167-2991\(08\)61673-0](https://doi.org/10.1016/S0167-2991(08)61673-0).
- [10] B. Frank, A. Dinse, O. Ovsitser, E.V. Kondratenko, R. Schomäcker, Mass and heat transfer effects on the oxidative dehydrogenation of propane (ODP) over a low loaded VOx/Al<sub>2</sub>O<sub>3</sub> catalyst, *Appl. Catal. Gen.* 323 (2007) 66–76. <https://doi.org/10.1016/j.apcata.2007.02.006>.
- [11] Y.-M. Liu, Y. Cao, K.-K. Zhu, S.-R. Yan, W.-L. Dai, H.-Y. He, K.-N. Fan, Highly efficient VOx/SBA-15 mesoporous catalysts for oxidative dehydrogenation of propane, *Chem. Commun.* 0 (2002) 2832–2833. <https://doi.org/10.1039/B208177F>.
- [12] Y.-M. Liu, Y. Cao, N. Yi, W.-L. Feng, W.-L. Dai, S.-R. Yan, H.-Y. He, K.-N. Fan, Vanadium oxide supported on mesoporous SBA-15 as highly selective catalysts in the oxidative dehydrogenation of propane, *J. Catal.* 224 (2004) 417–428. <https://doi.org/10.1016/j.jcat.2004.03.010>.
- [13] P. Mars, D.W. van Krevelen, Oxidations carried out by means of vanadium oxide catalysts, *Chem. Eng. Sci.* 3 (1954) 41–59. [https://doi.org/10.1016/S0009-2509\(54\)80005-4](https://doi.org/10.1016/S0009-2509(54)80005-4).
- [14] E.V. Kondratenko, M. Cherian, M. Baerns, D. Su, R. Schlögl, X. Wang, I.E. Wachs, Oxidative dehydrogenation of propane over V/MCM-41 catalysts: comparison of O<sub>2</sub> and N<sub>2</sub>O as oxidants, *J. Catal.* 234 (2005) 131–142. <https://doi.org/10.1016/j.jcat.2005.05.025>.
- [15] A. Dinse, B. Frank, C. Hess, D. Habel, R. Schomäcker, Oxidative dehydrogenation of propane over low-loaded vanadia catalysts: Impact of the support material on kinetics and selectivity, *J. Mol. Catal. Chem.* 289 (2008) 28–37. <https://doi.org/10.1016/j.molcata.2008.04.007>.
- [16] B.Y. Jibril, S.M. Al-Zahrani, A.E. Abasaeed, R. Hughes, Propane oxidative dehydrogenation on Cs-doped Cr-Mo-Al-O catalyst:

- kinetics and mechanism, *Chem. Eng. J.* 103 (2004) 59–67.  
<https://doi.org/10.1016/j.cej.2004.03.006>.
- [17] M. Baldi, E. Finocchio, C. Pistarino, G. Busca, Evaluation of the mechanism of the oxy-dehydrogenation of propane over manganese oxide, *Appl. Catal. Gen.* 173 (1998) 61–74.  
[https://doi.org/10.1016/S0926-860X\(98\)00129-X](https://doi.org/10.1016/S0926-860X(98)00129-X).
- [18] K. Routray, K.R.S.K. Reddy, G. Deo, Oxidative dehydrogenation of propane on V<sub>2</sub>O<sub>5</sub>/Al<sub>2</sub>O<sub>3</sub> and V<sub>2</sub>O<sub>5</sub>/TiO<sub>2</sub> catalysts: understanding the effect of support by parameter estimation, *Appl. Catal. Gen.* 265 (2004) 103–113. <https://doi.org/10.1016/j.apcata.2004.01.006>.
- [19] S. Chakraborty, S.C. Nayak, G. Deo, TiO<sub>2</sub>/SiO<sub>2</sub> supported vanadia catalysts for the ODH of propane, *Catal. Today.* 254 (2015) 62–71.  
<https://doi.org/10.1016/j.cattod.2015.01.047>.
- [20] E.V. Kondratenko, M. Baerns, Catalytic oxidative dehydrogenation of propane in the presence of O<sub>2</sub> and N<sub>2</sub>O—the role of vanadia distribution and oxidant activation, *Appl. Catal. Gen.* 222 (2001) 133–143. [https://doi.org/10.1016/S0926-860X\(01\)00836-5](https://doi.org/10.1016/S0926-860X(01)00836-5).
- [21] K. Chen, A.T. Bell, E. Iglesia, Kinetics and Mechanism of Oxidative Dehydrogenation of Propane on Vanadium, Molybdenum, and Tungsten Oxides, *J. Phys. Chem. B.* 104 (2000) 1292–1299.  
<https://doi.org/10.1021/jp9933875>.
- [22] A. Dinse, S. Khennache, B. Frank, C. Hess, R. Herbert, S. Wrabetz, R. Schlögl, R. Schomäcker, Oxidative dehydrogenation of propane on silica (SBA-15) supported vanadia catalysts: A kinetic investigation, *J. Mol. Catal. Chem.* 307 (2009) 43–50.  
<https://doi.org/10.1016/j.molcata.2009.03.008>.
- [23] H.H. Kung, Oxidative Dehydrogenation of Light (C<sub>2</sub> to C<sub>4</sub>) Alkanes, in: D.D. Eley, H. Pines, W.O. Haag (Eds.), *Adv. Catal.*, Academic Press, 1994: pp. 1–38. [https://doi.org/10.1016/S0360-0564\(08\)60655-0](https://doi.org/10.1016/S0360-0564(08)60655-0).
- [24] K. Chen, A. Khodakov, J. Yang, A.T. Bell, E. Iglesia, Isotopic Tracer and Kinetic Studies of Oxidative Dehydrogenation Pathways on



- Vanadium Oxide Catalysts, *J. Catal.* 186 (1999) 325–333.  
<https://doi.org/10.1006/jcat.1999.2510>.
- [25] G. Busca, E. Finocchio, V. Lorenzelli, G. Ramis, M. Baldi, IR studies on the activation of C–H hydrocarbon bonds on oxidation catalysts, *Catal. Today*. 49 (1999) 453–465. [https://doi.org/10.1016/S0920-5861\(98\)00441-6](https://doi.org/10.1016/S0920-5861(98)00441-6).
- [26] E. Finocchio, G. Busca, V. Lorenzelli, R.J. Willey, FTIR studies on the selective oxidation and combustion of light hydrocarbons at metal oxide surfaces. Propane and propene oxidation on MgCr<sub>2</sub>O<sub>4</sub>, *J. Chem. Soc. Faraday Trans.* 90 (1994) 3347–3356.  
<https://doi.org/10.1039/FT9949003347>.
- [27] E. Finocchio, G. Busca, V. Lorenzelli, V.S. Escribano, FTIR studies on the selective oxidation and combustion of light hydrocarbons at metal oxide surfaces. Part 2.—Propane and propene oxidation on Co<sub>3</sub>O<sub>4</sub>, *J. Chem. Soc. Faraday Trans.* 92 (1996) 1587–1593.  
<https://doi.org/10.1039/FT9969201587>.
- [28] E. Finocchio, R.J. Willey, G. Ramis, G. Busca, V. Lorenzelli, Hydrocarbon activation and oxidation on transition metal mixed oxides: Ft-IR and flow reactor studies, in: J.W. Hightower, W. Nicholas Delgass, E. Iglesia, A.T. Bell (Eds.), *Stud. Surf. Sci. Catal.*, Elsevier, 1996: pp. 483–492. [https://doi.org/10.1016/S0167-2991\(96\)80259-X](https://doi.org/10.1016/S0167-2991(96)80259-X).
- [29] E. Finocchio, R.J. Willey, G. Busca, V. Lorenzelli, FTIR studies on the selective oxidation and combustion of light hydrocarbons at metal oxide surfaces Part 3.—Comparison of the oxidation of C<sub>3</sub> organic compounds over Co<sub>3</sub>O<sub>4</sub>, MgCr<sub>2</sub>O<sub>4</sub> and CuO, *J. Chem. Soc. Faraday Trans.* 93 (1997) 175–180.  
<https://doi.org/10.1039/A605341F>.
- [30] C. Zhao, I.E. Wachs, Selective oxidation of propylene to acrolein over supported V<sub>2</sub>O<sub>5</sub>/Nb<sub>2</sub>O<sub>5</sub> catalysts: An in situ Raman, IR, TPSR and kinetic study, *Catal. Today*. 118 (2006) 332–343.  
<https://doi.org/10.1016/j.cattod.2006.07.018>.

- [31] C. Zhao, I.E. Wachs, An Operando Raman, IR, and TPSR Spectroscopic Investigation of the Selective Oxidation of Propylene to Acrolein over a Model Supported Vanadium Oxide Monolayer Catalyst, *J. Phys. Chem. C.* 112 (2008) 11363–11372. <https://doi.org/10.1021/jp801562g>.
- [32] A.S. Sandupatla, S.C. Nayak, C. Sivananda, G. Deo, DFT investigation into the experimentally observed influence of oxide support in the ODH of propane over supported vanadia catalysts, *Catal. Today.* (2019). <https://doi.org/10.1016/j.cattod.2018.05.058>.
- [33] K. Tarama, S. Yoshida, S. Ishida, H. Kakioka, Spectroscopic Studies of Catalysis by Vanadium Pentoxide, *Bull. Chem. Soc. Jpn.* 41 (1968) 2840–2845. <https://doi.org/10.1246/bcsj.41.2840>.
- [34] K. Mori, A. Miyamoto, Y. Murakami, Catalytic reactions on well-characterized vanadium oxide catalysts. 4. Oxidation of butane, *J. Phys. Chem.* 89 (1985) 4265–4269. <https://doi.org/10.1021/j100266a024>.
- [35] S.T. Oyama, Adsorbate bonding and the selection of partial and total oxidation pathways, *J. Catal.* 128 (1991) 210–217. [https://doi.org/10.1016/0021-9517\(91\)90078-I](https://doi.org/10.1016/0021-9517(91)90078-I).
- [36] A. Andersson, An oxidized surface state model of vanadium oxides and its application to catalysis, *J. Solid State Chem.* 42 (1982) 263–275. [https://doi.org/10.1016/0022-4596\(82\)90005-6](https://doi.org/10.1016/0022-4596(82)90005-6).
- [37] F. Gilardoni, A.T. Bell, A. Chakraborty, P. Boulet, Density functional theory calculations of the oxidative dehydrogenation of propane on the (010) surface of C2O5, *J. Phys. Chem. B.* 104 (2000) 12250–12255. <https://doi.org/10.1021/jp001746m>.
- [38] H. Fu, Z.-P. Liu, Z.-H. Li, W.-N. Wang, K.-N. Fan, Periodic Density Functional Theory Study of Propane Oxidative Dehydrogenation over V2O5(001) Surface, *J. Am. Chem. Soc.* 128 (2006) 11114–11123. <https://doi.org/10.1021/ja0611745>.
- [39] M.-J. Cheng, K. Chenoweth, J. Oxgaard, A. van Duin, W.A. Goddard, Single-Site Vanadyl Activation, Functionalization, and Reoxidation Reaction Mechanism for Propane Oxidative

- Dehydrogenation on the Cubic V<sub>4</sub>O<sub>10</sub> Cluster, *J. Phys. Chem. C.* 111 (2007) 5115–5127. <https://doi.org/10.1021/jp0663917>.
- [40] K. Alexopoulos, M.-F. Reyniers, G.B. Marin, Reaction path analysis of propane selective oxidation over V<sub>2</sub>O<sub>5</sub> and V<sub>2</sub>O<sub>5</sub>/TiO<sub>2</sub>, *J. Catal.* 289 (2012) 127–139. <https://doi.org/10.1016/j.jcat.2012.01.019>.
- [41] C. Xiong, S. Chen, P. Yang, S. Zha, Z.-J. Zhao, J. Gong, Structure-Performance Relationships for Propane Dehydrogenation over Aluminum Supported Vanadium Oxide, *ACS Catal.* 9 (2019) 5816–5827. <https://doi.org/10.1021/acscatal.8b04701>.
- [42] A. Christodoulakis, M. Machli, A.A. Lemonidou, S. Boghosian, Molecular structure and reactivity of vanadia-based catalysts for propane oxidative dehydrogenation studied by in situ Raman spectroscopy and catalytic activity measurements, *J. Catal.* 222 (2004) 293–306. <https://doi.org/10.1016/j.jcat.2003.10.007>.
- [43] M.O. Guerrero-Pérez, Supported, bulk and bulk-supported vanadium oxide catalysts: A short review with an historical perspective, *Catal. Today.* 285 (2017) 226–233. <https://doi.org/10.1016/j.cattod.2017.01.037>.
- [44] P.M. Michalakos, M.C. Kung, I. Jahan, H. Kung, Selectivity Patterns in Alkane Oxidation over Mg<sub>3</sub>(VO<sub>4</sub>)<sub>2</sub>-MgO, Mg<sub>2</sub>V<sub>2</sub>O<sub>7</sub>, and (VO)<sub>2</sub>P<sub>2</sub>O<sub>7</sub>, *J. Catal.* 140 (1993) 226–242. <https://doi.org/10.1006/jcat.1993.1080>.
- [45] J.G. Eon, R. Olier, J.C. Volta, Oxidative Dehydrogenation of Propane on  $\gamma$ -Al<sub>2</sub>O<sub>3</sub> Supported Vanadium Oxides, *J. Catal.* 145 (1994) 318–326. <https://doi.org/10.1006/jcat.1994.1040>.
- [46] A.D. Costa, C. Mathieu, Y. Barbaux, H. Poelman, G. Dalmai-Vennik, L. Fiermans, Observation of the V<sub>2</sub>O<sub>5</sub>(001) surface using ambient atomic force microscopy, *Surf. Sci.* 370 (1997) 339–344. [https://doi.org/10.1016/S0039-6028\(96\)00956-9](https://doi.org/10.1016/S0039-6028(96)00956-9).
- [47] J. Sambeth, A. Juan, L. Gambaro, H. Thomas, Catalytic oxidation of CH<sub>3</sub>OH to HCOOCH<sub>3</sub> on V<sub>2</sub>O<sub>5</sub>: A theoretical study, *J. Mol. Catal. Chem.* 118 (1997) 283–291. [https://doi.org/10.1016/S1381-1169\(96\)00900-4](https://doi.org/10.1016/S1381-1169(96)00900-4).

- [48] A. Kämper, A. Auroux, M. Baerns, A molecular mechanics study of the adsorption of ethane and propane on a V<sub>2</sub>O<sub>5</sub>(001) surface, *Phys. Chem. Chem. Phys.* 2 (2000) 1069–1075. <https://doi.org/10.1039/A908988H>.
- [49] A. Kämper, I. Hahndorf, M. Baerns, A molecular mechanics study of the adsorption of ethane and propane on V<sub>2</sub>O<sub>5</sub>(001) surfaces with oxygen vacancies, *Top. Catal.* 11 (2000) 77–84. <https://doi.org/10.1023/A:1027239612464>.
- [50] M.V. Martínez-Huerta, G. Deo, J.L.G. Fierro, M.A. Bañares, Operando Raman-GC Study on the Structure–Activity Relationships in V<sup>5+</sup>/CeO<sub>2</sub> Catalyst for Ethane Oxidative Dehydrogenation: The Formation of CeVO<sub>4</sub>, *J. Phys. Chem. C.* 112 (2008) 11441–11447. <https://doi.org/10.1021/jp802827t>.
- [51] M. Witko, Quantum-chemical description of the active sites for the selective oxidation of hydrocarbons, *Catal. Today.* 32 (1996) 89–95. [https://doi.org/10.1016/S0920-5861\(96\)00187-3](https://doi.org/10.1016/S0920-5861(96)00187-3).
- [52] M. Witko, R. Tokarz, J. Haber, Vanadium pentoxide. II. Quantum chemical modeling, *Appl. Catal. Gen.* 157 (1997) 23–44. [https://doi.org/10.1016/S0926-860X\(97\)00019-7](https://doi.org/10.1016/S0926-860X(97)00019-7).
- [53] A. Michalak, M. Witko, K. Hermann, Density functional cluster studies on the (010) surface of vanadium pentoxide, *Surf. Sci.* 375 (1997) 385–394. [https://doi.org/10.1016/S0039-6028\(96\)01286-1](https://doi.org/10.1016/S0039-6028(96)01286-1).
- [54] M. Witko, K. Hermann, R. Tokarz, Adsorption and reactions at the (010) V<sub>2</sub>O<sub>5</sub> surface: cluster model studies, *Catal. Today.* 50 (1999) 553–565. [https://doi.org/10.1016/S0920-5861\(98\)00490-8](https://doi.org/10.1016/S0920-5861(98)00490-8).
- [55] G. Deo, I.E. Wachs, Surface oxide-support interaction (SOSI) for surface redox sites, *J. Catal.* 129 (1991) 307–312. [https://doi.org/10.1016/0021-9517\(91\)90036-4](https://doi.org/10.1016/0021-9517(91)90036-4).
- [56] G. Deo, I.E. Wachs, Reactivity of Supported Vanadium Oxide Catalysts: The Partial Oxidation of Methanol, *J. Catal.* 146 (1994) 323–334. <https://doi.org/10.1006/jcat.1994.1071>.
- [57] I.E. Wachs, J.-M. Jehng, G. Deo, B.M. Weckhuysen, V.V. Guliants, J.B. Benziger, S. Sundaresan, Fundamental Studies of Butane

- Oxidation over Model-Supported Vanadium Oxide Catalysts: Molecular Structure-Reactivity Relationships, *J. Catal.* 170 (1997) 75–88. <https://doi.org/10.1006/jcat.1997.1742>.
- [58] I.E. Wachs, B.M. Weckhuysen, Structure and reactivity of surface vanadium oxide species on oxide supports, *Appl. Catal. Gen.* 157 (1997) 67–90. [https://doi.org/10.1016/S0926-860X\(97\)00021-5](https://doi.org/10.1016/S0926-860X(97)00021-5).
- [59] L.J. Burcham, G. Deo, X. Gao, I.E. Wachs, In situ IR, Raman, and UV-Vis DRS spectroscopy of supported vanadium oxide catalysts during methanol oxidation, *Top. Catal.* 11 (2000) 85–100. <https://doi.org/10.1023/A:1027275225668>.
- [60] M.A. Bañares, M. Martínez-Huerta, X. Gao, I.E. Wachs, J.L.G. Fierro, Identification and roles of the different active sites in supported vanadia catalysts by in situ techniques, in: A. Corma, F.V. Melo, S. Mendioroz, J.L.G. Fierro (Eds.), *Stud. Surf. Sci. Catal.*, Elsevier, 2000: pp. 3125–3130. [https://doi.org/10.1016/S0167-2991\(00\)80502-9](https://doi.org/10.1016/S0167-2991(00)80502-9).
- [61] M.A. Bañares, I.E. Wachs, Molecular structures of supported metal oxide catalysts under different environments, *J. Raman Spectrosc.* 33 (2002) 359–380. <https://doi.org/10.1002/jrs.866>.
- [62] X. Gao, J.-M. Jehng, I.E. Wachs, In Situ UV–vis–NIR Diffuse Reflectance and Raman Spectroscopic Studies of Propane Oxidation over ZrO<sub>2</sub>-Supported Vanadium Oxide Catalysts, *J. Catal.* 209 (2002) 43–50. <https://doi.org/10.1006/jcat.2002.3635>.
- [63] I.E. Wachs, Recent conceptual advances in the catalysis science of mixed metal oxide catalytic materials, *Catal. Today.* 100 (2005) 79–94. <https://doi.org/10.1016/j.cattod.2004.12.019>.
- [64] H. Tian, E.I. Ross, I.E. Wachs, Quantitative Determination of the Speciation of Surface Vanadium Oxides and Their Catalytic Activity, *J. Phys. Chem. B.* 110 (2006) 9593–9600. <https://doi.org/10.1021/jp055767y>.
- [65] C. Zhao, I.E. Wachs, Selective oxidation of propylene over model supported V<sub>2</sub>O<sub>5</sub> catalysts: Influence of surface vanadia coverage

- and oxide support, *J. Catal.* 257 (2008) 181–189.  
<https://doi.org/10.1016/j.jcat.2008.04.022>.
- [66] I.E. Wachs, M. Bañares, *In Situ and Operando Raman Spectroscopy of Oxidation Catalysts*, in: *Handb. Adv. Methods Process. Oxid. Catal.*, IMPERIAL COLLEGE PRESS, 2011: pp. 420–446. [https://doi.org/10.1142/9781848167513\\_0017](https://doi.org/10.1142/9781848167513_0017).
- [67] I.E. Wachs, *Catalysis science of supported vanadium oxide catalysts*, *Dalton Trans.* 42 (2013) 11762–11769.  
<https://doi.org/10.1039/C3DT50692D>.
- [68] I.E. Wachs, C.J. Keturakis, 7.06 - Monolayer Systems, in: J. Reedijk, K. Poeppelemeier (Eds.), *Compr. Inorg. Chem. II Second Ed.*, Elsevier, Amsterdam, 2013: pp. 131–151.  
<https://doi.org/10.1016/B978-0-08-097774-4.00717-8>.
- [69] J.J. Ternero-Hidalgo, J. Torres-Liñán, M.O. Guerrero-Pérez, J. Rodríguez-Mirasol, T. Cordero, *Electrospun vanadium oxide based submicron diameter fiber catalysts. Part I: Preparation procedure and propane ODH application*, *Catal. Today.* (2018).  
<https://doi.org/10.1016/j.cattod.2018.10.073>.
- [70] J.J. Ternero-Hidalgo, M.O. Guerrero-Pérez, J. Rodríguez-Mirasol, T. Cordero, *Electrospun vanadium oxide based submicron diameter fiber catalysts. Part II: Effect of chemical formulation and dopants*, *Catal. Today.* (2018). <https://doi.org/10.1016/j.cattod.2018.10.072>.
- [71] L. Fernandez, E. Sanchez, M. Panizza, M.M. Carnasciali, G. Busca, *Vibrational and electronic spectroscopic properties of zirconia powders*, *J. Mater. Chem.* 11 (2001) 1891–1897.  
<https://doi.org/10.1039/b100909p>.
- [72] M.O. Guerrero-Pérez, J.L.G. Fierro, M.A. Vicente, M.A. Bañares, *Effect of Sb/V ratio and of Sb + V coverage on the molecular structure and activity of alumina-supported Sb-V-O catalysts for the ammoxidation of propane to acrylonitrile*, *J. Catal.* 206 (2002) 339–348. <https://doi.org/10.1006/jcat.2001.3494>.
- [73] L. Lietti, P. Forzatti, G. Ramis, G. Busca, F. Bregani, *Potassium doping of vanadia/titania de-NO<sub>x</sub>ing catalysts: Surface*

- characterisation and reactivity study, *Appl. Catal. B Environ.* 3 (1993) 13–35. [https://doi.org/10.1016/0926-3373\(93\)80065-L](https://doi.org/10.1016/0926-3373(93)80065-L).
- [74] N. Magg, B. Immaraporn, J.B. Giorgi, T. Schroeder, M. Bäumer, J. Döbler, Z. Wu, E. Kondratenko, M. Cherian, M. Baerns, P.C. Stair, J. Sauer, H.-J. Freund, Vibrational spectra of alumina- and silica-supported vanadia revisited: An experimental and theoretical model catalyst study, *J. Catal.* 226 (2004) 88–100. <https://doi.org/10.1016/j.jcat.2004.04.021>.
- [75] I.E. Wachs, Raman and IR studies of surface metal oxide species on oxide supports: Supported metal oxide catalysts, *Catal. Today.* 27 (1996) 437–455. [https://doi.org/10.1016/0920-5861\(95\)00203-0](https://doi.org/10.1016/0920-5861(95)00203-0).
- [76] D. Eisenbach, E. Gallei, Infrared spectroscopic investigations relating to coke formation on zeolites: I. Adsorption of hexene-1 and n-hexane on zeolites of type Y, *J. Catal.* 56 (1979) 377–389. [https://doi.org/10.1016/0021-9517\(79\)90130-1](https://doi.org/10.1016/0021-9517(79)90130-1).
- [77] J. Datka, Z. Sarbak, R.P. Eischens, Infrared Study of Coke on Alumina and Zeolite, *J. Catal.* 145 (1994) 544–550. <https://doi.org/10.1006/jcat.1994.1065>.
- [78] M. Daturi, C. Binet, J.C. Lavalley, G. Blanchard, Surface FTIR investigations on CexZr1-xO2 system, *Surf. Interface Anal.* 30 (2000) 273–277. [https://doi.org/10.1002/1096-9918\(200008\)30:1<273::AID-SIA715>3.0.CO;2-G](https://doi.org/10.1002/1096-9918(200008)30:1<273::AID-SIA715>3.0.CO;2-G).
- [79] K.K. Bando, K. Sayama, H. Kusama, K. Okabe, H. Arakawa, In-situ FT-IR study on CO2 hydrogenation over Cu catalysts supported on SiO2, Al2O3, and TiO2, *Appl. Catal. Gen.* 165 (1997) 391–409. [https://doi.org/10.1016/S0926-860X\(97\)00221-4](https://doi.org/10.1016/S0926-860X(97)00221-4).
- [80] G. Ramis, G. Busca, V. Lorenzelli, Low-temperature CO2 adsorption on metal oxides: spectroscopic characterization of some weakly adsorbed species, *Mater. Chem. Phys.* 29 (1991) 425–435. [https://doi.org/10.1016/0254-0584\(91\)90037-U](https://doi.org/10.1016/0254-0584(91)90037-U).
- [81] T. Blasco, J.M.L. Nieto, Oxidative dehydrogenation of short chain alkanes on supported vanadium oxide catalysts, *Appl. Catal. Gen.*

- 157 (1997) 117–142. [https://doi.org/10.1016/S0926-860X\(97\)00029-X](https://doi.org/10.1016/S0926-860X(97)00029-X).
- [82] Vicente. Sanchez Escribano, Guido. Busca, Vincenzo. Lorenzelli, Fourier transform infrared spectroscopic studies of the reactivity of vanadia-titania catalysts toward olefins. 1. Propylene, J. Phys. Chem. 94 (1990) 8939–8945. <https://doi.org/10.1021/j100389a017>.
- [83] M. El-Roz, P. Bazin, M. Daturi, F. Thibault-Starzyk, Operando Infrared (IR) Coupled to Steady-State Isotopic Transient Kinetic Analysis (SSITKA) for Photocatalysis: Reactivity and Mechanistic Studies, ACS Catal. 3 (2013) 2790–2798. <https://doi.org/10.1021/cs4006088>.
- [84] N.W. Alcock, V.M. Tracy, T.C. Waddington, Acetates and acetato-complexes. Part 2. Spectroscopic studies, J. Chem. Soc. Dalton Trans. 0 (1976) 2243–2246. <https://doi.org/10.1039/DT9760002243>.
- [85] S.E. Collins, M.A. Baltanás, A.L. Bonivardi, An infrared study of the intermediates of methanol synthesis from carbon dioxide over Pd/ $\beta$ -Ga<sub>2</sub>O<sub>3</sub>, J. Catal. 226 (2004) 410–421. <https://doi.org/10.1016/j.jcat.2004.06.012>.
- [86] Anatoli Davydov, Molecular Spectroscopy of Oxide Catalyst Surfaces, Wiley, 2003.
- [87] E.A. Mamedov, V. Cortés Corberán, Oxidative dehydrogenation of lower alkanes on vanadium oxide-based catalysts. The present state of the art and outlooks, Appl. Catal. Gen. 127 (1995) 1–40. [https://doi.org/10.1016/0926-860X\(95\)00056-9](https://doi.org/10.1016/0926-860X(95)00056-9).
- [88] A.E. Lewandowska, M. Calatayud, E. Lozano-Diz, C. Minot, M.A. Bññares, Combining theoretical description with experimental in situ studies on the effect of alkali additives on the structure and reactivity of vanadium oxide supported catalysts, Catal. Today. 139 (2008) 209–213. <https://doi.org/10.1016/j.cattod.2008.04.049>.



### **3.4. Kinetic study of propane ODH on electrospun vanadium oxide-based submicron diameter fiber catalyst.**

#### **Part I**

J. J. Ternero-Hidalgo, M.O. Guerrero-Pérez, J. Rodríguez-Mirasol, T. Cordero

Universidad de Málaga, Departamento de Ingeniería Química, Campus de Teatinos s/n, E29071 Málaga, Spain

**Keywords:** Propane ODH; Mixed-oxide catalysts; Fiber catalysts; Reaction mechanism; Kinetic study

#### **Abstract**

A rigorous kinetic study of the oxidative dehydrogenation (ODH) reaction of propane on a vanadium oxide-based submicron diameter fiber catalyst have been performed according to the reaction mechanism proposed from the FTIR-Raman *operando* results of a previous work. The proposed kinetic model simulates the conversion-selectivity profiles and the surface coverage of the different species present on the catalyst for the studied conditions of temperature, space-time and inlet partial pressures of propane and oxygen. The first hydrogen abstraction from propane is the rate determining step (RDS) and its calculated activation energy is 104.1 kJ·mol<sup>-1</sup>. The model predicts that although the reaction seems to be pseudo-zero order with respect to oxygen in a broad range of conditions, the catalyst may not be fully oxidized. The reduction degree of the catalyst will depend on its intrinsic chemical nature and reaction conditions, increasing with the space-time and in detriment of the overall reaction rate. Consequently, the propane turnover frequency (TOF) will also depend on the reaction conditions and space-time, even changing along the fixed-bed reactor.

## Nomenclature

ODH	Oxidative dehydrogenation
FTIR	Fourier-transform infrared spectroscopy
RDS	Rate determining step
TOF	Turnover frequency
TEM	Transmission electron microscopy
BET	Brunauer, Emmett and Teller
EDXA	Energy-dispersive X-ray analyzer
XPS	X-ray photoelectron spectroscopy
XRD	X-ray diffraction
STP	Standard temperature and pressure
GC	Gas chromatography
TCD	Thermal conductivity detector
FID	Flame ionization detector
V-O	Lattice oxygens (VO <sub>x</sub> ) in the form of V-O-V or V-O-Zr group
V=O	Terminal oxygen of the vanadyl group
V-OH	Protonated lattice oxygen
V-□	Vacancy in the lattice oxygen
$X$	Propane conversion
$S_i$	Selectivity to $i$ product
$Y_i$	Yield to $i$ product
$X_{exp}$	Experimental propane conversion
$S_{exp,i}$	Experimental selectivity to $i$ product
$Y_{exp,i}$	Experimental yield to $i$ product
$X_{sim}$	Simulated propane conversion
$S_{sim,i}$	Simulated selectivity to $i$ product
$Y_{sim,i}$	Simulated yield to $i$ product
$W_{cat}$	Mass of catalyst
$F_T$	Total volumetric gas flow
$F_{C3,o}$	Propane inlet volumetric flow
$\dot{F}_{C3,o}$	Propane inlet molar flow
$\dot{F}_i$	Inlet molar flow of $i$ compound
$n_i$	Number of carbon atoms per molecule of $i$ compound
$R_j$	Reaction step represented in Scheme 3.4.1
$Ads_j$	Adsorption step represented in Scheme 3.4.1
$r_j$	Reaction rate of $j$ step
$k_j$	Rate constant of $j$ reaction step
$k_{o,j}$	Preexponential factor of $j$ reaction step
$Ea_j$	Activation energy of $j$ reaction step
$k_{Appj}$	Apparent rate constant of $j$ reaction step
$k_{App,o,j}$	Apparent preexponential factor of $j$ reaction step
$Ea_{App,j}$	Apparent activation energy of $j$ reaction step
$K_j$	Equilibrium adsorption constant of $j$ step
$K_{o,j}$	Preexponential factor of $j$ adsorption step
$\Delta H_j$	Enthalpy of adsorption for $j$ step
$P_i$	Partial pressure of $i$ compound

$P_{i,o}$	Inlet partial pressure of $i$ compound
$\theta_i$	Surface coverage of $i$ species
$C_i$	Surface concentration of $i$ species
$C_T$	Active sites total surface concentration

### 3.4.1. Introduction

The global demand for propylene is growing up since the last decades due to their use as monomers/comonomers in the petrochemical industry for the production of many interest products (e.g. polypropylene, acrylonitrile, etc.) [1]. Nowadays, most of the propylene is obtained as byproduct from steam cracking of naphtha, fluid catalytic cracking in the oil refining and natural gas processing [1–3]. However, the current propylene demand is not satisfied by these technologies and it has been necessary to find alternatives [2,4]. The interest has mainly focused in producing propylene from propane, which is generally easily available and relatively low-cost [5–7]. One alternative for propylene production is the catalytic dehydrogenation of propane. However, this method is energetically very unfavorable because is a strong endothermic process that needs to be performed above 600°C and presents thermodynamic constraints that limit the propane conversion, as well as it has the problem of the rapid catalyst deactivation due to coke formation [3,8]. Oxidative dehydrogenation (ODH) of propane may be a promising alternative to obtain propylene from propane. This reaction is exothermic and can be performed at lower temperatures, it is thermodynamically unrestricted and the catalysts are not usually deactivated by coke deposition [3,8]. However, the propylene yields are still not sufficiently high to be profitable at industrial scale due to the undesirable combustion reactions to CO and CO<sub>2</sub> (CO<sub>x</sub>), which are difficult to control [3].

Dispersed vanadia species over different supports (ZrO<sub>2</sub>, TiO<sub>2</sub>, Al<sub>2</sub>O<sub>3</sub>, SiO<sub>2</sub>, etc.) seem to be the most selective catalysts to propylene in the propane ODH reaction [3,8–12], while the presence of crystalline vanadium has been reported to be detrimental for the catalytic activity [13,14]. Deep analysis of the reaction mechanism determining the kinetic parameters

would be a good strategy for improving the catalysts and to operate under the optimal reactor and reaction conditions in order to increase the yield and productivity to propylene. It seems that most of the authors agree that propane ODH reaction follows a Mars-van Krevelen type mechanism [8,15–22], where the lattice oxygens of the catalyst are the active sites. In this way, the catalyst is simultaneously reduced by the reaction with propane and reoxidized with gas phase oxygen or other oxidizing agents as  $N_2O$  [17,23]. Most of the reaction networks proposed in the literature usually have in common that the mechanism is a parallel-consecutive pathway, where propane and more probably the produced propylene can be totally oxidized forming  $CO_x$  [16]. The first hydrogen abstraction from propane is usually the rate determining step (RDS), and not so many deep studies have been found in the literature regarding the next steps involving the total oxidation [16].

Despite the vast propane ODH literature, not many articles describe a detailed reaction mechanism or kinetic study. Different kinetics models have been used (Power Law, Langmuir-Hinshelwood, Eley-Rideal, etc. [10,24–27]), but the Mars-van Krevelen expression [15] is the most frequently proposed for ODH reactions [8,16–22]. The kinetic parameter most frequently compared between the different catalysts is the activation energy of the first hydrogen abstraction from propane (i.e. RDS) [8,16]. However, a wide range of values can be found in the literature, probably due to the variety of different kinetic models used [8,10,14,16–22,24–32], which are sometimes oversimplified and/or frequently inconsistent and incorrect without physical relevance. Propane TOF is also widely used to compare the activity of the catalysts, however different tendencies can also be found. It has been reported that as the vanadium content of the catalyst increases, the propane turnover frequency (TOF) decreases [33,34], remains constant [8,35–37] or increases [28,38,39]. These discrepancies can be due to the use of different synthesis methods, supports and concentrations, which may result in different kind of vanadia surface species. Moreover, it cannot be discarded the possible existence of external

and/or internal mass and/or heat transport limitations, as well as contribution of homogenous phase reaction at high temperatures (above 500°C) and/or experiments with a total oxygen conversion.

The rate equation derived from the Mars-van Krevelen mechanism and used in the literature for more than 50 years to describe redox reactions is inconsistent for several reasons, and it should be only considered as a mathematical fitting function without physical relevance [40]. The major inconsistency (among others) is found in the rate of oxygen adsorption. Since if it is assumed that lattice oxygen are the active sites, the oxygen adsorption must have dissociative character. However, the equation used is the corresponding to molecular oxygen adsorption in a single site. Other inconsistencies come from the consideration of non-elementary steps in the rate equations and the non-inclusion of intermediate species or final products in the site balance, considering only oxygen ions (even though the equation represents molecular oxygen adsorption). Furthermore, many authors have simplified to zero-order dependence the rate equations assuming that the reoxidation reaction of the catalyst is much faster than the reduction reaction [14,25,26,28–32], and consequently, sometimes, even taking for granted that the catalyst is fully oxidized or nearly saturated with oxygen under reaction conditions [26,29]. These assumptions have become generalized and accepted in the literature for this kind of catalysts in ODH reactions, and probably it is right for a broad range of catalysts and operation conditions. However, it is possible that sometimes these assumptions are not true even at low conversions, since it will depend on the catalyst nature and reaction conditions.

In a previous work, FTIR and Raman *operando* spectroscopy were combined for the study of vanadium-based catalysts during propane ODH (*Section 3.3*). These experiments allowed the simultaneous characterization of the adsorbed species or reaction intermediates and of the catalyst structure, as well as the measurement of the activity results with both on line mass spectrometry and FTIR spectroscopy. The results obtained were used to establish a reaction mechanism and to identify the

role of different oxygen species bound to vanadium sites. The aim of the present work is to make a kinetic study of the propane ODH reaction on a vanadium oxide-based submicron diameter fiber catalyst already characterized in detail in a before paper ([41] or *Section 3.1*), establishing the kinetic equations in a rigorous way according to the reaction mechanism proposed in the previous work (*Section 3.3*). The use of electrospinning technique allowed the preparation of catalysts with very uniform composition and with submicrometric fibrous structure, what confers small internal diffusion resistance to the catalyst compared to traditional powdered catalysts, as well as less temperature gradients and lower pressure drop when they are packed in a fixed-bed [42]. These advantages made easier the performance of the experiments, without the addition of diluting inert material (e.g. silicon carbide [43,44]), while isolating the obtention of intrinsic kinetic data of the catalyst without the interference of other effects. In this way, a set of reaction experiments in a fixed-bed reactor has been performed to estimate the kinetic parameters, whose values have been analyzed. The proposed kinetic model can predict the surface coverage of the different adsorbed and vanadia species present on the catalyst at certain conditions of temperature, space-time and inlet partial pressures of propane and oxygen, which determines the conversion-selectivity profiles of the catalyst that adequately represents the experimental data for the studied conditions involving a broad range of conversion and selectivity values.

### **3.4.2. Materials and methods**

#### *3.4.2.1. Catalyst preparation and characterization*

The vanadium oxide based submicron-fiber catalyst, F-PZr-V5.0, was prepared using the electrospinning technique following the synthesis method previously described ([41] or *Section 3.1*). The electrospinning process was performed using a polymer solution prepared with zirconium (IV) propoxide, polyvinylpyrrolidone (PVP), acetylacetone, vanadyl acetylacetonate and 1-propanol. The polymer solution was vigorously

stirred for 24 h at room temperature before being electrospun in the electrospinning setup already described in previous articles ([41,45] or *Sections 3.1 and 3.2*). The distance between the needle and the collector was 20 cm, the electrical potential difference was 12 kV (the tip at +6 kV and the collector was at -6 kV), and the flow rate of the polymer solution through the spinneret was 0.5 mL/h. Then, the electrospun fibers were calcined in a conventional tubular furnace with a heating rate of 10 °C/min up to 500 °C, whose temperature was kept for 6 h in air flow (150 mL/min STP) to eliminate the organic part and the remaining solvent, as well as to stabilize the final inorganic zirconia fibers with a nominal vanadium mass concentration of 5.0% (F-PZr-V5.0).

A detailed characterization of the sample F-PZr-V5.0 has been already reported in a previous work ([41] or *Section 3.1*). The surface morphology was studied by transmission electron microscopy (TEM), where fibrous morphology of the catalyst with diameters ranging from 300 to 410 nm was observed. The porous texture was characterized by N<sub>2</sub> adsorption-desorption at -196°C, obtaining a type IVa isotherm corresponding to mesoporous solid and a BET surface area of 66 m<sup>2</sup>·g<sup>-1</sup>. The surface chemistry and crystal structure of the sample were analyzed by energy-dispersive X-ray (EDXA), X-ray photoelectron spectroscopy (XPS), in situ Raman and X-ray diffraction patterns (XRD). The results showed vanadium uniformly distributed along the fibers, being the vanadium mass concentration very close to the nominal value, 5.0%. It was confirmed the presence of VO<sub>x</sub> dispersed species, along the tetragonal zirconia, in form of monovanadate and polyvanadate species. Moreover, the presence of vanadium crystal structures as V<sub>2</sub>O<sub>5</sub> or ZrV<sub>2</sub>O<sub>7</sub> were not detected for this sample. Figure 3.4.1 and Table 3.4.1 summarize all the physicochemical characteristics above mentioned about F-PZr-V5.0.

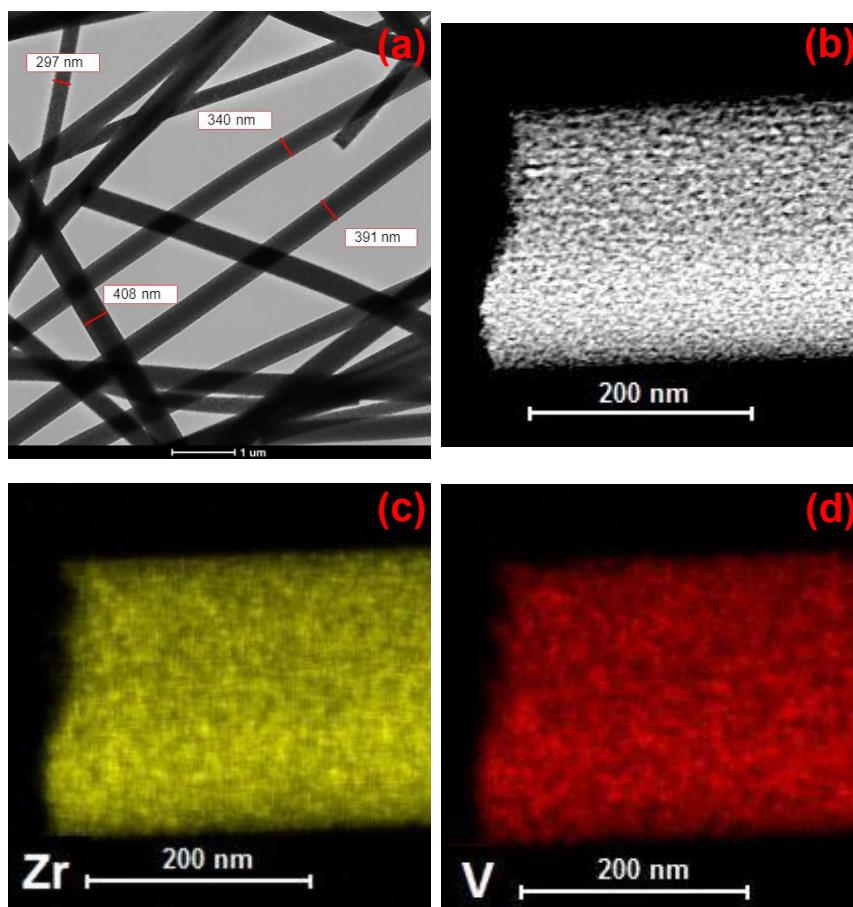


Figure 3.4.1. TEM (a) and HAADF-STEM (b) micrographs, and EDXA elemental mappings of Zr (c) and V (d) for the sample F-PZr-V5.0.

Table 3.4.1. Summary of the physicochemical characteristics of F-PZr-V5.0.

Property	Method	Result
Surface morphology	TEM	Submicron fibers with diameters of 300-410 nm
BET surface area	Adsorption-desorption of N <sub>2</sub> at -196°C	66 m <sup>2</sup> ·g <sup>-1</sup>
Surface chemistry and crystal structure	EDXA	4.7 wt.% V
	XPS	4.9 wt.% V <sub>2p</sub>
	Raman	VO <sub>x</sub> dispersed species (monovanadates and polyvanadates) and tetragonal ZrO <sub>2</sub>
	XRD	Tetragonal ZrO <sub>2</sub>



### 3.4.2.2. Propane ODH experiments

The catalyst F-PZr-V5.0 was used for the reaction of propane oxidative dehydrogenation (ODH) in a fixed bed microreactor (i.d. 4 mm) placed inside a vertical furnace with temperature control (the same than previous works ([41,45] or Sections 3.1 and 3.2)). The reaction temperature was varied from 300 to 400°C. The feed was prepared by a mixture of three gases: propane (99.95%), oxygen (99.999%) and helium (99.999%). The gases were mixed to obtain different feed compositions by using mass flow controllers, varying both the propane and oxygen inlet partial pressures ( $P_{C_3,o}$  and  $P_{O_2,o}$ , respectively) from 0.025 to 0.2 atm. The total volumetric gas flow ( $F_T$ ) and the mass of catalyst ( $W_{cat}$ ) were adjusted in order to vary the space-time ( $W_{cat}/F_{C_3,o}$ ) in the range of 0.1-1.0 g<sub>cat</sub>·s·mL<sup>-1</sup><sub>C<sub>3</sub>H<sub>8</sub></sub> (Volume was always expressed in STP conditions), which are typical units and range of values used in the literature [3]. The pipelines were heated at 120°C to pre-heat the reactant mixture upstream the reactor and to avoid condensation of products downstream the reactor.

Reactants and products were analyzed in steady state conditions by an on-line gas chromatograph (Perkin-Elmer, Clarus 500 GC), equipped with a Hayesep D 80/100 (length: 3 m; diameter: 1/8"; internal diameter: 2.1 mm) and an active carbon 80/100 (length: 2 m; diameter 1/8"; internal diameter: 2,1 mm) packed columns. Light gases (O<sub>2</sub>, CO and CO<sub>2</sub>) were detected by a thermal conductivity detector (TCD); and CH<sub>4</sub>, C<sub>2</sub>H<sub>4</sub>, C<sub>2</sub>H<sub>6</sub>, C<sub>3</sub>H<sub>6</sub> and C<sub>3</sub>H<sub>8</sub> were detected using a flame ionization detector (FID). In all the cases carbon and oxygen molar balances were closed with errors lower than 5%. The propane conversion and the selectivity or yield to  $i$  product are defined as  $X$  and  $S_i$  or  $Y_i$ , respectively:

$$X = \frac{\dot{F}_{C_3,o} - \dot{F}_{C_3}}{\dot{F}_{C_3,o}} \quad (1)$$

$$S_i = \frac{n_i \cdot \dot{F}_i}{n_{C_3} \cdot \dot{F}_{C_3,o} \cdot X} \quad (2)$$

$$Y_i = X \cdot S_i \quad (3)$$

where  $\dot{F}_{C_3,0}$  and  $\dot{F}_{C_3}$  are the molar flows of propane in the inlet and in the outlet streams, respectively.  $\dot{F}_i$  is the molar flow of  $i$  product in the outlet stream, and  $n_{C_3}$  or  $n_i$  are the number of carbon atoms per molecule of propane ( $n_{C_3}=3$ ) or  $i$  product, respectively.

In a previous work ([41] or *Section 3.1*), where the same sample and reactor were used, it was experimentally demonstrated that the possible catalyst deactivation during reaction, the contribution of homogenous phase reaction, the contribution of zirconia activity and the presence of external mass and heat transport limitations were negligible under the studied conditions. Moreover, internal mass and heat transport limitation can be discarded due to the quite small diameter of the submicron-fibers, and no pressure drop has been observed through the catalyst bed under the experimental conditions used due to the fibrous morphology of the catalyst [42].

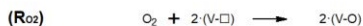
### 3.4.3. Results

#### 3.4.3.1. Propane ODH mechanism

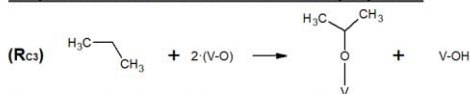
Scheme 3.4.1 represents the detailed mechanism proposed in the before work from the FTIR-Raman *operando* results (*Section 3.3*). It is assumed that only the lattice oxygen reacts with propane, adsorbed species, and reaction products present in the gas phase. Simultaneously, the gas phase oxygen reoxidizes the reduced vanadium sites in the  $VO_x$  lattice during the above reduction reactions, which is necessary to perpetuate the catalytic cycle. Note that lattice oxygens in the form of V-O-V or V-O-Zr groups have been represented in the same way, as (V-O), and it has been assumed that both have the same role in the mechanism, although is possible that they present different activity. It has been discarded the participation of V=O terminal groups in the reaction mechanism, since it seemed to be much less active than V-O sites. (V-OH) and (V-□) represent a protonated lattice

oxygen and a vacancy site, respectively. It is proposed that propane is firstly activated via dissociative chemisorption forming isopropoxide ( $R_{C_3}$ ), which can evolve as propylene or can be further oxidized to chemisorbed acetone ( $R_{Acetone}$ ). Propylene can adsorb again on a V-O site of the catalyst ( $Ads_{C_3=}$ ) and react with a neighbour V-OH as Bronsted acidic site forming isopropoxide ( $R_{C_3=}$ ) and continue with the subsequent oxidation steps. Then, oxidative cleavage of the C(1)-C(2) bond of chemisorbed acetone gives rise to the formation of bidentate formates and acetates ( $R_{Carboxylate}$ ). Afterwards, these carboxylates species evolve as CO in the gas phase ( $R_{Formate}$  and  $R_{Acetate}$ ). It should be noted that, unlike the formate species, acetate species require lattice oxygen to decompose. Finally, CO can be further oxidized to  $CO_2$  and desorb ( $R_{CO_2}$ ). Although it has not been represented in the scheme, it cannot be discarded the oxidation of formates, acetates and CO through the formation of carbonates species [20,46,47]. The necessary reoxidation reactions of the catalyst are represented by the equations  $R_{O_2}$  and  $R_{V-OH}$ , where the irreversible dissociative adsorption of  $O_2$  from the gas phase and the reversible recombination of V-OH forming  $H_2O$ , V-O and V-□ sites are required, respectively.

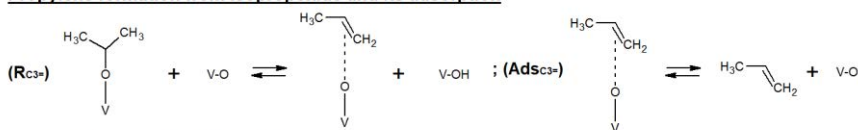
**Regeneration of the reduced catalyst**



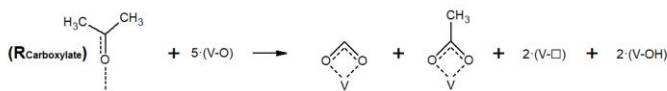
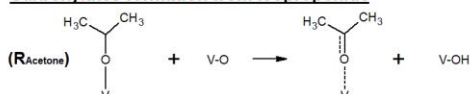
**Propane activation via formation of isopropoxide**



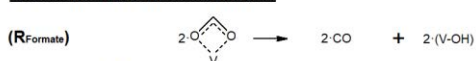
**Propylene formation from isopropoxide and its adsorption**



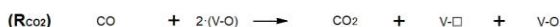
**Carboxylates formation from isopropoxide**



**CO formation from carboxylates**



**CO oxidation to CO<sub>2</sub>**



Scheme 3.4.1. Proposed detailed mechanism of the propane ODH (adapted from (Section 3.3)).

3.4.3.2. Rate equations

The kinetic equations will be derived from the proposed reaction mechanism shown in Scheme 3.4.1. Since surface oxidation reactions in redox mechanism usually consist of sequences of irreversible steps in nature, it will be assumed that all the steps are irreversible [40], except the ones related to the propylene formation and adsorption ( $R_{C_3=}$  and  $Ads_{C_3=}$ , respectively), in agreement with the experimental evidences from previous work (Section 3.3). With respect to the dehydration surface reaction ( $R_{V-OH}$ ), which is necessary for the catalyst reoxidation, it that has been assumed that kinetically acts as an irreversible reaction, although it has been reported to be reversible [48,49]. This means that the rate of the reverse reaction, where H<sub>2</sub>O is adsorbed and form two V-OH sites, has

been neglected, since the fully reoxidation of the catalyst was always achieved very fast (Section 3.3). The reactions  $R_{\text{Formate}}$  and  $R_{\text{CO}_2}$  will be considered second order with respect to the surface coverages of formate and active sites (V-O), respectively, assuming that carbonates species are formed as surface intermediates in such reactions. The reaction  $R_{\text{Carboxylate}}$  as expressed in Scheme 3.4.1 is a multi-body interaction that is very improbable that happens as an elementary step, probably should be expressed as a series of consecutive reactions to get its kinetic equation, but it will not be considered in this work because it is not kinetically significant or necessary in the development of the later equations. According to the above assumptions, the reaction rates are formulated as follows:

$$r_{V-OH} = k_{V-OH} \cdot \theta_{V-OH}^2 \quad (3)$$

$$r_{O_2} = k_{O_2} \cdot P_{O_2} \cdot \theta_{V-\square}^2 \quad (4)$$

$$r_{C_3} = k_{C_3} \cdot P_{C_3} \cdot \theta_{V-O}^2 \quad (5)$$

$$r_{C_3=} = k_{\xrightarrow{C_3=}} \cdot \theta_{\text{Isopropoxide}} \cdot \theta_{V-O} - k_{\xleftarrow{C_3=}} \cdot \theta_{V-O-C_3=} \cdot \theta_{V-OH} \quad (6)$$

$$r_{\text{Acetone}} = k_{\text{Acetone}} \cdot \theta_{\text{Isopropoxide}} \cdot \theta_{V-O} \quad (7)$$

$$r_{\text{Formate}} = k_{\text{Formate}} \cdot \theta_{\text{Formate}}^2 \quad (8)$$

$$r_{\text{Acetate}} = k_{\text{Acetate}} \cdot \theta_{\text{Acetate}} \cdot \theta_{V-O}^2 \quad (9)$$

$$r_{\text{CO}_2} = k_{\text{CO}_2} \cdot P_{\text{CO}} \cdot \theta_{V-O}^2 \quad (10)$$

where in Eqs. (3) and (4),  $r_{V-OH}$  and  $r_{O_2}$  are the consumption rates of V-OH sites and molecular oxygen to reoxidize the catalyst, respectively, being  $k_{V-OH}$  and  $k_{O_2}$  their respective rate constants;  $\theta_{V-OH}$  and  $\theta_{V-\square}$  are the surface coverages of V-OH and V- $\square$  sites, respectively; and  $P_{O_2}$  is the oxygen partial pressure. In Eq. (5),  $r_{C_3}$  is the rate of propane consumption, being  $k_{C_3}$  its rate constant,  $\theta_{V-O}$  is the surface coverage of V-O sites and  $P_{C_3}$  is the propane partial pressure. In Eq. (6),  $r_{C_3=}$  is the rate of the

reversible reaction of propylene formation on the V-O site, where  $k_{\xrightarrow{C_3=}}$  and  $k_{\xleftarrow{C_3=}}$  represent the forward and reverse rate constants, respectively; and  $\theta_{Isopropoxide}$  and  $\theta_{V-O-C_3=}$  are the surface coverages of isopropoxide and adsorbed propylene, respectively. In Eqs. (7), (8) and (9),  $r_{Acetone}$ ,  $r_{Formate}$  and  $r_{Acetate}$  are the formation rate of chemisorbed acetone, and the decomposition rates of formate and acetate species, respectively; being  $k_{Acetone}$ ,  $k_{Formate}$  and  $k_{Acetate}$  their respective rate constants; and  $\theta_{Formate}$  and  $\theta_{Acetate}$  are the fractions of sites covered by formate and acetate species, respectively. In Eq. (10),  $r_{CO_2}$  is the formation rate of CO<sub>2</sub> from oxidation of CO, being  $k_{CO_2}$  its rate constant and  $P_{CO}$  the CO partial pressure. Finally, the formation rate of CO can be derived from making a balance between the CO formed by the evolution of formate and acetate species, and the CO consumed in its oxidation to form CO<sub>2</sub>:

$$r_{CO} = r_{Formate} + 2 \cdot r_{Acetate} - r_{CO_2} \quad (11)$$

On the other hand, the site balance would be:

$$C_T = C_{V-O} + C_{V-OH} + C_{V-\square} + C_{Acetate} + C_{Formate} \quad (12)$$

where  $C_T$  is the total concentration of surface sites and  $C_i$  the surface concentration of  $i$  site. The surface concentrations of isopropoxide, adsorbed propylene and chemisorbed acetone have not been included, since they are negligible with respect to the other species, as it was already observed in the operando spectroscopic results obtained in the previous work (Section 3.3). Alternatively, Eq. (12) can be rewritten as a function of surface coverages if it is divided by  $C_T$ :

$$1 = \theta_{V-O} + \theta_{V-OH} + \theta_{V-\square} + \theta_{Acetate} + \theta_{Formate} \quad (12.1)$$

where each of the surface coverage values would be  $\leq 1$ . It should be noted that the rate equations (Eq. (3)-(11)) have been expressed as a function of surface coverages, then the rate constants include  $C_T$  combined with the preexponential factors, being  $k_i = C_T \cdot k'_i$ , resulting in a first-order

dependence on  $C_T$  for all the cases (not second-order) where  $k'_i$  contains the probability factor for nearest-neighbor [50].

It will be considered that the propane activation reaction (i.e. first hydrogen abstraction from propane), Eq. (5), is the rate-determining step (RDS) as reported elsewhere [16], which means that  $r_{C3}$  will determine the overall rate of the catalytic cycle and, then, also the propane conversion. In addition, it will be assumed that the propylene adsorption step ( $Ads_{C3=}$ ) is quasi-equilibrated. This assumption will only be valid if both the forward and reverse adsorption rates are several orders of magnitude greater than the RDS, which is reasonable. In this way, it could be possible to express the Eq. (6) as a function of propylene partial pressure,  $P_{C3=}$ , which can be measured during reaction, instead of surface coverage of adsorbed propylene,  $\theta_{V-O-C3=}$ , which is very difficult to quantify from experiment. Therefore, if the adsorption equilibrium constant of propylene is:

$$K_{Ads,C3=} = \frac{\theta_{V-O-C3=}}{P_{C3=} \cdot \theta_{V-O}} \quad (13)$$

and

$$k_{App,\leftarrow_{C3=}} = K_{Ads,C3=} \cdot k_{\leftarrow_{C3=}} \quad (14)$$

where  $k_{App,\leftarrow_{C3=}}$  is an apparent reaction rate constant that combines the equilibrium constant of propylene adsorption,  $K_{Ads,C3=}$ , and the reverse rate constant of the reversible reaction of adsorbed propylene formation,  $k_{\leftarrow_{C3=}}$ .

Then, Eq. (6) can now be rewritten as:

$$r_{C3=} = k_{\rightarrow_{C3=}} \cdot \theta_{Isopropoxide} \cdot \theta_{V-O} - k_{App,\leftarrow_{C3=}} \cdot P_{C3=} \cdot \theta_{V-O} \cdot \theta_{V-OH} \quad (6.1)$$

Moreover, as the catalyst is supposed to operate at steady-state conditions, then

$$r_{C3=} = r_{C3=} + r_{Acetone} \quad (15)$$

$$r_{Acetone} = r_{Carboxylate} = r_{Formate} = r_{Acetate} = \frac{r_{CO} + r_{CO2}}{3} \quad (16)$$

and

$$r_{C3} = r_{C3=} + \frac{r_{CO} + r_{CO2}}{3} \quad (15.1)$$

where  $r_{Carboxylate}$  is the formation rate of carboxylates from chemisorbed acetone in  $R_{Carboxylate}$  (Scheme 3.4.1), and  $r_{CO}$  and  $r_{CO2}$  are divided by 3 due to stoichiometry reasons. Eqs. (15) and (16) indicate that all the isopropoxide formed from the converted propane will be consumed by two parallel reactions; on one hand, forming adsorbed propylene that will evolve as propylene; and on the other hand, forming chemisorbed acetone that will evolve as CO, which also can be further oxidized to CO<sub>2</sub> (Eq. (15.1)). Therefore, the ratio among both parallel reactions for a given conditions will determine the selectivity to propylene and to CO<sub>x</sub>. It is interesting to note that the rate constants belonging to  $r_{C3=}$  and  $r_{Acetone}$  must be several orders greater than the ones belonging to the RDS, in this case  $r_{C3}$  as above mentioned.

Making balance and assuming pseudo-steady state for each adsorbed species, the rate of change in their respective surface coverages would be approximately zero:

$$\frac{d\theta_{Isopropoxide}}{dt} = r_{C3} - r_{C3=} - r_{Acetone} \approx 0 \quad (17)$$

$$\frac{d\theta_{Formate}}{dt} = r_{Carboxylate} - r_{Formate} \approx 0 \quad (18)$$

$$\frac{d\theta_{Acetate}}{dt} = r_{Carboxylate} - r_{Acetate} \approx 0 \quad (19)$$

$$\frac{d\theta_{V-OH}}{dt} = r_{C3} + r_{C3=} + r_{Acetone} + 2 \cdot r_{Carboxylate} + r_{Formate} + r_{Acetate} - r_{V-OH} \approx 0 \quad (20)$$

$$\frac{d\theta_{V-O}}{dt} = 2 \cdot r_{Carboxylate} + 2 \cdot r_{Acetate} + r_{CO2} + \frac{r_{V-OH}}{2} - 2 \cdot r_{O2} \approx 0 \quad (21)$$

$$\frac{d\theta_{V-O}}{dt} = 2 \cdot r_{O2} + \frac{r_{V-OH}}{2} - 2 \cdot r_{C3} - r_{Acetone} - 5 \cdot r_{Carboxylate} - 2 \cdot r_{Acetate} - r_{CO2} \approx 0 \quad (22)$$

Using these equations (Eqs. (17)-(22)) and taking into consideration the Eqs. (15) and (16) deduced from steady-state conditions together with Eqs.



(3)-(11) above proposed as rate expressions, it is possible to deduce the equations for the surface coverages of isopropoxide, formate and acetate adsorbed species, as well as those of V-OH and V-□ sites (Eqs. (23)-(27), respectively). It should be noted that the contribution of  $\theta_{V-OH}$  in Eq. (23) has been neglected when handling the balance of Eq. (20) to get the expression for the surface coverage of V-OH sites (Eq. (26)).



$$\theta_{\text{Isopropoxide}} = \frac{k_{C_3} \cdot P_{C_3} + k_{\text{App}, C_3} \cdot P_{C_3} \cdot \left(\frac{\theta_{V-OH}}{\theta_{V-O}}\right)}{k_{C_3} + k_{\text{Acetone}}} \cdot \theta_{V-O} \quad (23)$$

$$\theta_{\text{Formate}} = \sqrt{\frac{k_{\text{Acetone}}}{k_{\text{Formate}}} \cdot \theta_{\text{Isopropoxide}} \cdot \theta_{V-O}} \quad (24)$$

$$\theta_{\text{Acetate}} = \frac{k_{\text{Acetone}}}{k_{\text{Acetate}}} \cdot \theta_{\text{Isopropoxide}} \quad (25)$$

$$\theta_{V-OH} = \sqrt{\frac{2 \cdot k_{C_3} \cdot \left(k_{C_3} + 3 \cdot k_{\text{Acetone}}\right)}{k_{V-OH} \cdot \left(k_{C_3} + k_{\text{Acetone}}\right)} \cdot P_{C_3} \cdot \theta_{V-O}} \quad (26)$$

$$\theta_{V-\square} = \sqrt{\frac{k_{C_3} \cdot P_{C_3} \cdot \left(k_{C_3} + 7 \cdot k_{\text{Acetone}}\right) + 4 \cdot k_{\text{Acetone}} \cdot k_{\text{App}, C_3} \cdot P_{C_3} \cdot \left(\frac{\theta_{V-OH}}{\theta_{V-O}}\right) + \left(k_{C_3} + k_{\text{Acetone}}\right) k_{CO_2} \cdot P_{CO}}{2 \cdot k_{O_2} \cdot P_{O_2} \cdot \left(k_{C_3} + k_{\text{Acetone}}\right)}} \cdot \theta_{V-O} \quad (27)$$

and substituting the above equations (Eqs. (23)-(27)) in the site balance (Eq. (12.1)),  $\theta_{V-O}$  can be expressed as:

$$\theta_{V-O} = \frac{1 - \frac{k_{\text{Acetone}} \cdot \left(k_{C_3} \cdot P_{C_3} + k_{\text{App}, C_3} \cdot P_{C_3} \cdot \left(\frac{\theta_{V-OH}}{\theta_{V-O}}\right)\right)}{k_{\text{Acetate}} \cdot \left(k_{C_3} + k_{\text{Acetone}}\right)}}{1 + \left(\frac{\theta_{V-OH}}{\theta_{V-O}}\right) + \sqrt{\frac{k_{C_3} \cdot P_{C_3} \cdot \left(k_{C_3} + 7 \cdot k_{\text{Acetone}}\right) + 4 \cdot k_{\text{Acetone}} \cdot k_{\text{App}, C_3} \cdot P_{C_3} \cdot \left(\frac{\theta_{V-OH}}{\theta_{V-O}}\right) + \left(k_{C_3} + k_{\text{Acetone}}\right) k_{CO_2} \cdot P_{CO}}{2 \cdot k_{O_2} \cdot P_{O_2} \cdot \left(k_{C_3} + k_{\text{Acetone}}\right)}} + \sqrt{\frac{k_{\text{Acetone}} \cdot \left(k_{C_3} \cdot P_{C_3} + k_{\text{App}, C_3} \cdot P_{C_3} \cdot \left(\frac{\theta_{V-OH}}{\theta_{V-O}}\right)\right)}{k_{\text{Formate}} \cdot \left(k_{C_3} + k_{\text{Acetone}}\right)}}} \quad (28)$$

where, according to the Eq. (26):

$$\left(\frac{\theta_{V-OH}}{\theta_{V-O}}\right) = \sqrt{\frac{2 \cdot k_{C_3} \cdot \left(k_{C_3} + 3 \cdot k_{\text{Acetone}}\right)}{k_{V-OH} \cdot \left(k_{C_3} + k_{\text{Acetone}}\right)} \cdot P_{C_3}} \quad (26.1)$$

Then, Eq. (26.1) can be substituted in Eq. (28) to get the equation of  $\theta_{V-O}$  as a function of only rate constants and partial pressures ( $P_{C_3}$ ,  $P_{C_3=}$ ,  $P_{CO}$  and  $P_{O_2}$ ). In this way, it is possible to estimate the surface coverage of all the surface species for a given rate constants and partial pressures. It should be noted that each of the surface coverage values must be  $\leq 1$ .

It can be checked that the influence of the partial pressures and/or of the kinetic parameters in the Eqs. (23)-(28) for steady-state conditions is consistent with the experimental observations. For example, when the partial pressures of propane, propylene and CO are zero, at any oxygen concentration, the surface coverage for V-O is one (Eq. (28)), while for the other surface species are zero, which would mean that the catalyst is in its highest oxidation state as it can be observed when the catalyst is under airflow (Section 3.3). If the oxygen partial pressure is zero, at any propane, propylene and CO concentrations, the surface coverage for V-O (Eq. (28)) would be zero with V-□ sites as the majority species (Eq. (27)), being the catalyst in a deep reduced state as observed in the previous work (Section 3.3). In general, as the partial pressure of propane increases and/or of oxygen decreases at a constant temperature, the surface coverage of all the surface species increases (Eqs. (23)-(27)), except for the one of V-O sites (Eq. (28)), which decreases. The same effect occurs when propane conversion increases, as it can be deduced from how propylene and CO partial pressures contributes in the different expressions (Eqs (23)-(28)).

With respect to the influence of the kinetic parameters, Eq. (23) predicts that  $\theta_{Isopropoxide}$  should be very small, since  $k_{\xrightarrow{C_3=}}$  and  $k_{Acetone}$  are necessary to be several orders greater than  $k_{C_3}$  as above mentioned, according to the assumption of  $r_{C_3}$  as the RDS. This is consistent with the experimental spectroscopic evidences in a previous work where isopropoxide species were negligible or not detected in most of the reaction conditions (Section 3.3). Eqs. (24) and (25) predict that  $k_{Formate}$  and  $k_{Acetate}$  should be significantly smaller than  $k_{Acetone}$  if the surface coverage of formate and acetate are present in appreciable concentrations, as spectroscopically

observed in previous work (Section 3.3), otherwise these surface species would be in negligible concentrations as isopropoxide. Finally, since it was observed in the *operando* experiments (Section 3.3) that lattice oxygen ( $\theta_{V-O}$ ) was the most abundant species under reaction conditions, except in the absence of oxygen, it can be derived from Eqs. (26) and (27) that  $k_{V-OH}$  and  $k_{O_2}$  should be big enough to minimize  $\theta_{V-OH}$  and  $\theta_{V-\square}$  (reduced vanadia species), respectively, being both of them smaller than  $\theta_{V-O}$  (oxidized vanadia species) for most reaction conditions.

The necessary experimental data to validate the proposed model and determine the kinetic parameters of each rate equation have been obtained performing reaction experiments in a fixed-bed reactor. Molar balance equations of fixed-bed reactor have been used for the interpretation of the experimental data, assuming the following requirements: uniform distribution of active sites on the catalyst surface (as shown by the characterization data and in more detail in the previous work ([41] or Section 3.1)); axial dispersion and wall effects were discarded since the diameter of the fibers (submicron size) were several orders smaller than the length and diameter of the fixed-bed reactor, respectively; the reactor operated at steady-state conditions; diffusional constraints and transport limitations were discarded (as proven in a previous work using the same experimental procedure ([41] or Section 3.1)); and changes in temperature and pressure within the reactor were neglected. When these conditions are met, the molar balance equation for the fixed-bed reactor can be simplified obtaining the expression for the ideal plug-flow reactor (Eq. (29)):

$$-\frac{1}{P_{C_3,o}} \cdot \frac{dP_i}{d\left(\frac{W_{Cat}}{F_{C_3,o}}\right)} = r_i \quad (29)$$

where the space-time is expressed as  $W_{Cat}/F_{C_3,o}$  (ratio between catalyst weight and the inlet propane flow); and  $P_{C_3,o}$  and  $P_i$  are the partial pressures of initial propane and  $i$  reactant/product. Thus, combining molar balances (Eq. (29)) of oxygen, propane, propylene, carbon monoxide and carbon

dioxide, with their respective rate equations (Eqs. (4), (5), (6.1), (11) and (10)) and the corresponding surface coverage expressions (Eqs. (23)-(28)), the following system of differential equations is obtained:

$$-\frac{1}{P_{C3,o}} \cdot \frac{dP_{O2}}{d\left(\frac{W_{cat}}{F_{C3,o}}\right)} = k_{O2} \cdot P_{O2} \cdot \theta_{V-O}^2 \quad (30)$$

$$-\frac{1}{P_{C3,o}} \cdot \frac{dP_{C3}}{d\left(\frac{W_{cat}}{F_{C3,o}}\right)} = k_{C3} \cdot P_{C3} \cdot \theta_{V-O}^2 \quad (31)$$

$$\frac{1}{P_{C3,o}} \cdot \frac{dP_{C3}}{d\left(\frac{W_{cat}}{F_{C3,o}}\right)} = \frac{k_{C3\rightleftharpoons}}{k_{C3\leftarrow} + k_{Acetone}} \cdot \left( k_{C3} \cdot P_{C3} - \frac{k_{Acetone}}{k_{C3\leftarrow}} \cdot k_{App,C3\rightleftharpoons} \cdot P_{C3} \cdot \left( \frac{\theta_{V-OH}}{\theta_{V-O}} \right) \right) \cdot \theta_{V-O}^2 \quad (32)$$

$$\frac{1}{P_{C3,o}} \cdot \frac{dP_{CO}}{d\left(\frac{W_{cat}}{F_{C3,o}}\right)} = \frac{3 \cdot k_{Acetone}}{k_{C3\leftarrow} + k_{Acetone}} \cdot \left( k_{C3} \cdot P_{C3} + k_{App,C3\rightleftharpoons} \cdot P_{C3} \cdot \left( \frac{\theta_{V-OH}}{\theta_{V-O}} \right) \right) \cdot \theta_{V-O}^2 - k_{CO2} \cdot P_{CO} \cdot \theta_{V-O}^2 \quad (33)$$

$$\frac{1}{P_{C3,o}} \cdot \frac{dP_{CO2}}{d\left(\frac{W_{cat}}{F_{C3,o}}\right)} = k_{CO2} \cdot P_{CO} \cdot \theta_{V-O}^2 \quad (34)$$

It has been considered that the dependence of the kinetic and thermodynamic parameters with the temperature follow the Arrhenius law for the kinetic constants and Van't Hoff law for the equilibrium constants.

It can be checked that the balance equations obtained assuming steady-state conditions shown in Eq. (15.1) can be satisfied using the Eqs. (31)-(34), where

$$Eq.(31) = Eq.(32) + \frac{Eq.(33) + Eq.(34)}{3} \quad (15.2)$$

Moreover, it can be derived that the selectivity to propylene in a given conditions will be determined by the ratio  $k_{C3\rightleftharpoons}/k_{Acetone}$ , which only depends on the temperature, together with the propylene adsorption term  $k_{App,C3\rightleftharpoons} \cdot P_{C3} \cdot \left( \frac{\theta_{V-OH}}{\theta_{V-O}} \right)$ , which depends on the temperature as well as the propylene partial pressure (i.e. the conversion) and the ratio of the surface coverages of V-O and V-OH sites. Therefore, the maximum selectivity to propylene at a determined temperature will be obtained at low conversion values where  $P_{C3} \approx 0$ , and it will correspond, in this case, with the value of

$k_{\xrightarrow{C_3=}} / (k_{\xrightarrow{C_3=}} + k_{Acetone})$ , which would be the fraction of propane converted into propylene according to the Eq.(32). It should be noted that if the propylene adsorption step is neglected or not taken into consideration in the reaction mechanism (i.e.  $k_{App, \xrightarrow{C_3=}} \approx 0$  in Eq. (32) and (33)), the selectivity to propylene would reach the maximum value, which would remain constant with the space-time and without any dependence on the propane conversion. However, according to the results obtained in the previous works ([41,45] or Sections 3.1, 3.2 and 3.3) and those found in the literature about propane ODH [3,8,16], it seems very clear that propane conversion it has a great repercussion in the selectivity values, decreasing the one for propylene as the conversion is higher, which is the biggest drawback of this reaction, because it makes difficult to obtain high yields to propylene [3]. Then, it seems necessary to consider that propylene adsorption present an important contribution in the reaction mechanism of propane ODH. In fact, it has been reported elsewhere [8,16,32] that the majority of detected  $CO_x$  come from the combustion of the propylene previously formed, while direct propane combustion is usually neglected, which means that  $k_{\xrightarrow{C_3=}} / k_{Acetone}$  is very high in these cases denoting the higher stability of the molecule of propane than the one of propylene.

#### 3.4.3.3. Kinetic study

Integral packed fixed-bed reactor behaviour was considered using the molar balance Eqs. (30)-(34) for the interpretation of the experimental data. This system of differential equations was numerically solved, for the proposed kinetic parameters, to calculate the exit partial pressure of each reactant/product, as well as the surface coverage of each adsorbed species participating in the reaction mechanism. Then, the values of propane conversion, selectivity and yield to propylene, CO and CO<sub>2</sub> were calculated by using the partial pressures before obtained and Eqs. (1)-(3). The kinetic parameters were estimated by a modified Runge–Kutta method combined with an optimization routine based on the Levenberg–Marquardt algorithm implemented in Matlab R2016b software to minimize the *error* function:

$$error = \sum_j \left( \sqrt{(Y_{exp,C3=k} - Y_{sim,C3=k})^2} + \sqrt{(Y_{exp,CO,k} - Y_{sim,CO,k})^2} + \sqrt{(Y_{exp,CO2,k} - Y_{sim,CO2,k})^2} \right) \quad (35)$$

where  $Y_{exp,i,k}$  and  $Y_{sim,i,k}$  are the experimental and simulated yield, respectively, to the compound  $i$  for the experiment  $k$ . The optimization involved the Arrhenius and Van't Hoff parameters, and these kinetic parameters were used to simulate the conversion and selectivity values at different space-times, inlet partial pressures of propane and oxygen and temperatures. Table 3.4.2 summarizes the *error* function value, and the values obtained of preexponential factors and activation energies for all the reaction steps implied in the propane ODH reaction mechanism, whereas Figure 3.4.2 represents the simulated values of propane conversion or selectivity to compound  $i$  ( $X_{sim}$  or  $S_{sim,i}$ , respectively) versus the ones experimentally obtained ( $X_{exp}$  or  $S_{exp,i}$ , respectively) for these estimated kinetic parameters. The results show that the simulated values predict very well the experimental data, with an *error* function (Eq. (35)) value of 0.195, which validates the mathematical model equations presented in this study and consequently the reaction mechanism proposed previously (Section 3.3).

**Table 3.4.2.** Estimated kinetic parameters for the propane ODH reaction of the catalyst studied (F-PZr-V5.0).

	$k_{o,j}$ a,b,c,d ( $\text{mol}\cdot\text{s}^{-1}\cdot\text{g}^{-1}$ )	$Ea_j$ ( $\text{kJ}\cdot\text{mol}^{-1}$ )
$k_{V-OH}$	$2.05\cdot 10^8$	93.5
$k_{O_2}$	$^a 2.86\cdot 10^5$	97.9
$k_{C_3}$	$^b 3.35\cdot 10^4$	104.1
$k_{\xrightarrow{C_3=}}$	$2.31\cdot 10^{13}$	91.2
$k_{App,\xleftarrow{C_3=}}$	$^c 6.06\cdot 10^{12}$	112.0
$k_{Acetone}$	$1.83\cdot 10^9$	86.1
$k_{Formate}$	$1.63\cdot 10^{10}$	140.4
$k_{Acetate}$	$3.80\cdot 10^{11}$	180.5
$k_{CO_2}$	$^d 1.89\cdot 10^6$	115.7
<b>error</b>		<b>0.231</b>

<sup>a</sup> ( $\text{mol}\cdot\text{s}^{-1}\cdot\text{g}^{-1}\cdot\text{atm}^{-1}_{O_2}$ )

<sup>b</sup> ( $\text{mol}\cdot\text{s}^{-1}\cdot\text{g}^{-1}\cdot\text{atm}^{-1}_{C_3H_8}$ )

<sup>c</sup> ( $\text{mol}\cdot\text{s}^{-1}\cdot\text{g}^{-1}\cdot\text{atm}^{-1}_{C_3H_6}$ )

<sup>d</sup> ( $\text{mol}\cdot\text{s}^{-1}\cdot\text{g}^{-1}\cdot\text{atm}^{-1}_{CO}$ )

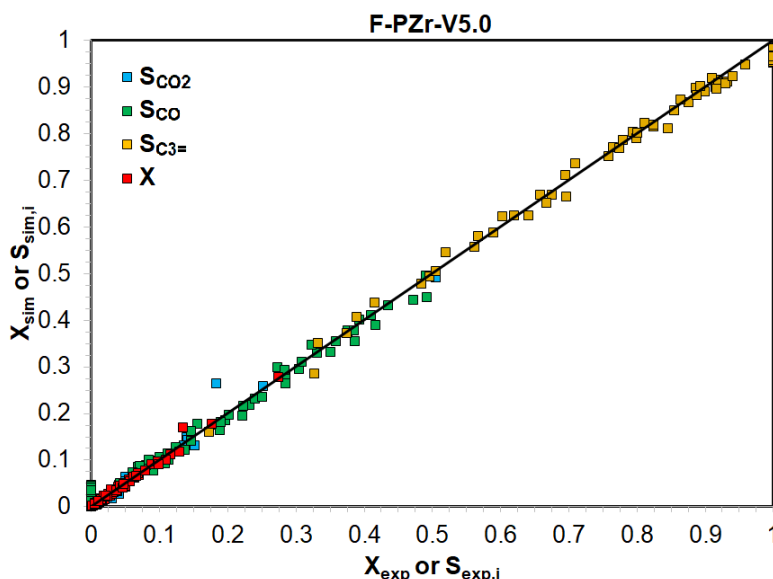


**Figure 3.4.2.** Simulated propane conversion and selectivity to propylene, CO or CO<sub>2</sub> ( $X_{sim}$  and  $S_{sim,i}$ , respectively) versus their respective conversion and selectivity experimentally obtained ( $X_{exp}$  and  $S_{exp,i}$ , respectively).

It should be reminded that  $k_{App,\xleftarrow{C_3=}}$  is the product between  $k_{\xleftarrow{C_3=}}$  and  $K_{Ads,C_3=}$ , constants of reaction and adsorption steps, respectively. Then:

$$k_{App,o,\xleftarrow{C_3=}} = k_{\xleftarrow{C_3=}} \cdot K_{Ads,o,C_3=} \quad (36)$$

$$Ea_{App,\xleftarrow{C_3=}} = Ea_{\xleftarrow{C_3=}} + \Delta H_{Ads,C_3=} \quad (37)$$



Among the kinetics parameters obtained in this work for propane ODH reaction (Table 3.4.2), the most comparable one with the literature is the activation energy of the propane activation step ( $Ea_{C_3}$ ), since this step is usually considered and most of the times as the RDS. The value obtained in this work ( $104.1 \text{ kJ}\cdot\text{mol}^{-1}$ ) is within the range of those reported for catalysts of vanadium oxide dispersed on  $\text{ZrO}_2$  [8,16], although there is a wide variety of values. Such variations among the different authors can reflect the use of different synthesis methods, supports and vanadium concentrations, which may result in different kind of vanadia surface species, as well as the wide range of different kinetic models used [8,10,14,16–22,24–32], which are sometimes oversimplified and/or frequently inconsistent and incorrect without physical relevance, as in the case of the Mars-van Krevelen expression [40]. On the other hand, in agreement with the previous work (Section 3.3), the activation energy obtained for the oxidation step of acetates ( $Ea_{Acetate}$ ) is higher than the one of formates ( $Ea_{Formate}$ ), and both of these values are higher than the one for the RDS ( $Ea_{C_3}$ ), as well as the latter value is higher than the activation energy for the oxidation of the catalyst via dissociative chemisorption of molecular oxygen ( $Ea_{O_2}$ ).

It can be also derived from Table 3.4.1 that  $k_{\xrightarrow{C_3=}}$  and  $k_{Acetone}$  are much greater than  $k_{C_3}$  (by  $10^{10}$  and  $10^6$  times, respectively) resulting in negligible values of  $\theta_{Isopropoxide}$  (Eq. (23)), which is consistent with assumptions made above and previous *operando* results (Section 3.3). Moreover, it can be calculated that the ratio  $k_{\xrightarrow{C_3=}}/k_{Acetone}$  is always very high, since  $k_{\xrightarrow{C_3=}}/(k_{\xrightarrow{C_3=}} + k_{Acetone})$  is always between 0.99 and 1.00 for the whole range of the studied temperatures (300–400°C), becoming even higher as temperature increases, since  $Ea_{\xrightarrow{C_3=}} > Ea_{Acetone}$ . This means that the fraction of converted propane that is directly oxidized to form  $\text{CO}_x$  is almost negligible, which is in very good accordance with results reported elsewhere [8,16,32]. Then, most of the  $\text{CO}_x$  formed come from the oxidation of the adsorbed propylene represented by the term of

$k_{App,C3=} \cdot P_{C3=} \cdot \left(\frac{\theta_{V-OH}}{\theta_{V-O}}\right)$ , where the  $E_{aApp,C3=}$  present a value of 112.0 kJ·mol<sup>-1</sup>. This latter value is higher than the activation energies of propane activation step ( $E_{aC3}=104.1$  kJ·mol<sup>-1</sup>), and adsorbed propylene formation ( $k_{C3=} = 91.2$  kJ·mol<sup>-1</sup>), which could mean that the selectivity to propylene would tend to be lower as temperature increases for same propane conversions, although it will also depend on the propylene partial pressure and the ratio of the surface coverages of V-O and V-OH sites. However. it should be noted that normally these kinds of catalysts are more selective as temperature increases [10,21,22,25].

Considering that it has been reported a propylene adsorption enthalpy on vanadia species ( $\Delta H_{Ads,C3=}$ ) of around -40.0 kJ·mol<sup>-1</sup> [32], the intrinsic activation energy of the oxidation of adsorbed propylene ( $E_{aC3=}$ ) could have an approximate value of around 150.0 kJ·mol<sup>-1</sup> (Eq. (37)). For a more accurate estimation of  $E_{aC3=}$ , it would be necessary to determine the real value of  $\Delta H_{Ads,C3=}$  for the catalyst used in this study, which could be different than the one found in the literature for another different catalyst.

The highest values of activation energies in Table 3.4.2 correspond to the CO and CO<sub>2</sub> formation steps ( $E_{aAcetate}=180.5$  kJ·mol<sup>-1</sup>,  $E_{aFormate}=140.4$  kJ·mol<sup>-1</sup> and  $E_{aCO2}=115.7$  kJ·mol<sup>-1</sup>) resulting in a certain accumulation of acetates and formates (CO precursor species) on the catalyst surface during reaction; as well as indicating that the subsequent formation of CO<sub>2</sub> will tend to occur mainly at high temperatures as observed in a before paper ([41] or Section 3.1). The high activation energies for the evolution of formate and acetate species result in low values of their respective rate constants,  $k_{Formate}$  and  $k_{Acetate}$ , being both significantly smaller than  $k_{Acetone}$  (by 10<sup>4</sup> and 10<sup>6</sup> times, respectively) and resulting in appreciable surface coverages of formate and acetate adsorbed species according to Eqs. (24) and (25), respectively, and previous spectroscopic results (Section 3.3). It can be also observed as  $E_{aAcetate}$  is  $> E_{aFormate}$ , which is in agreement with the higher thermal stability on the catalyst surface of

acetate species than formate species [47,51]. In addition, it can be checked that  $k_{V-OH}$  and  $k_{O_2}$  are several orders greater than the rate constant corresponding to the RDS,  $k_{C_3}$ , which allows  $\theta_{V-OH}$  and  $\theta_{V-O}$  to be smaller than  $\theta_{V-O}$  under most of the reaction conditions, in accordance with Eqs. (26)-(28) and previous results (Section 3.3).

#### 3.4.3.4. Influence of space-time

As shown in Figure 3.4.3, the model satisfactorily describes the conversion and selectivity profiles for F-PZr-V5.0 at different space-time and temperature, since experimental and simulated data match very well in most of the cases for a broad range of conversion and selectivity values. As expected for propane ODH, the conversion is higher as the temperature and space-time increase (Figure 3.4.3a), and the selectivity to propylene decreases as conversion increases (Figure 3.4.3b). When space-time tends to 0, propane conversion and selectivity to propylene tend to 0 and to 100%, respectively. However, if the space-time tended to infinite (not shown), the conversion would be 100% for the limitant reactant (propane or oxygen) and probably the selectivity to CO<sub>2</sub> could be 100% or very high (depending on the propane/oxygen ratio) in detriment of those to propylene and CO. The fact that selectivity to propylene can be close to 100% for some conditions (at low propane conversions), it can only occur when the fraction of  $k_{C_3=} / (k_{C_3=} + k_{Acetone})$  has a value of ~1. This means that almost all the converted propane is firstly forming propylene instead of being directly oxidized to CO<sub>x</sub>, whose mainly will come from the consecutive combustion of the propylene previously formed [8,16,32]. Consequently, the selectivity to CO and CO<sub>2</sub> (Figures 3.4.3c and 3.4.3d, respectively) is higher as the conversion increases (i.e. as the space-time and temperature increase). It is also possible to reach a point where the selectivity to CO start to decrease due to the further oxidation to form CO<sub>2</sub>, as can be observed at 400°C.

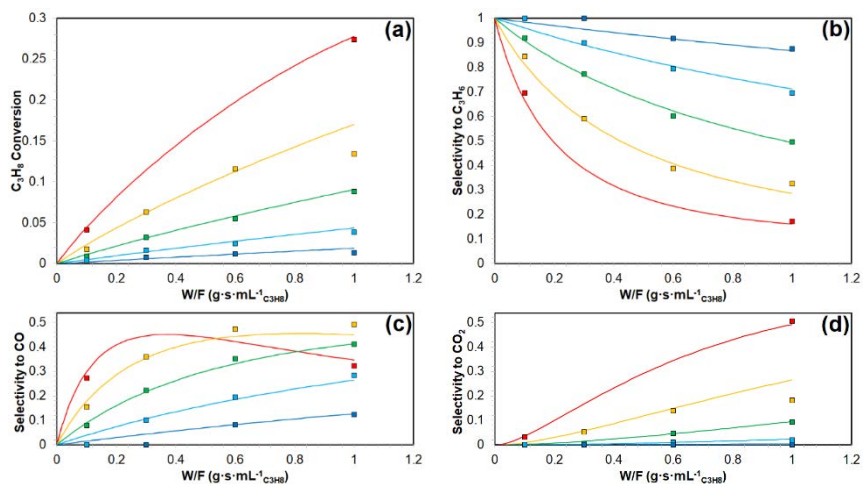


**Figure 3.4.3.** Steady-state propane conversion (a), selectivity to propylene (b), CO (c) and CO<sub>2</sub> (d) for F-PZr-V5.0 as a function of space-time and reaction temperature at inlet partial pressures of propane and oxygen of 0.1 atm (square symbols: experimental values; solid lines: simulated values; dark blue, light blue, green, yellow and red colors represent reaction temperatures of 300, 325, 350, 375 and 400°C, respectively).

Figure 3.4.4 represents the estimated evolution of the surface coverages for the different adsorbed and vanadia species as a function of the space-time, temperature and propane inlet partial pressure. Figure 3.4.4a and 3.4.4b show the simulation for a propane inlet partial pressure of 0.1 atm (same conditions than the experiments shown in Figure 3.4.3). It can be observed that in general the reduction degree of the catalyst along the fixed-bed reactor is higher as the space-time and temperature increase. This is evidenced by the successive loss of V-O sites and the growing appearance of surface vacancies in the VO<sub>x</sub> lattice (V-□) (Figure 3.4.4a), as well as the formation of more acetate and formate adsorbed species (Figure 3.4.4b). It can be seen that the concentration of acetate and formate adsorbed species increase with the temperature until 350°C, and above this temperature, these species decrease. Moreover, the proportion of acetate and formate species depend on the space-time and temperature, being the ratio  $\theta_{Acetate}/\theta_{Formate}$  lower than 1 at short space-time and higher than 1 at long space-time. It can also be observed that the surface coverage of V-OH sites is quite low with respect to the other vanadia species and it decreases as space-time or temperature increases (Figure 3.4.4b). As

expected, it can be confirmed that isopropoxide species appear in negligible concentrations (Section 3.3) (Figure 3.4.4b).

It is interesting to note that in these conditions  $\theta_{V-O}$  and  $\theta_{V-\square}$  represented most of the sites (Figure 3.4.4a), always covering more than the 97% of the surface sites, being  $\theta_{V-O}$  in the range of 0.60-0.90 and  $\theta_{V-\square}$  0.10-0.40. Then, the catalyst studied in this work is not always fully or almost fully oxidized during reaction as it can be found in the literature for similar catalysts [26,29]. Note that even when the space-time tends to 0,  $\theta_{V-O}$  already presents values around 0.88, which slightly decreases with temperature, indicating that this would be the equilibrium at steady-state conditions if there is no appreciable conversion (i.e. an atmosphere of propane and oxygen without propylene and  $CO_x$ ). However, as the reaction progresses (i.e. the conversion is higher) the propylene and CO formed compete with propane for the same active sites and they can be also adsorbed and further reduce the catalyst while producing  $CO_x$ . These reactions consume much more lattice oxygen than the propylene formation, which can explain the higher reduction state of the catalyst as the space-time is longer. Therefore, the oxidation state of the catalyst will depend on the feed composition, temperature and space-time, as well as will affect to the propane TOF, since the RDS is second-order with respect to  $\theta_{V-O}$ . This means that degree of reduction of the catalyst and TOF values could be different along the fixed-bed reactor. This appreciation was already considered by Deo *et al.* [36,37] to compare TOF values with more precision, although they used the Mars-van Krevelen expression, which is incorrect [40].

TOF values have been widely used for many authors to describe the catalytic activity of catalysts in the propane ODH reaction and to discern if monovanadate species are more, less or equally active than polyvanadates species. These studies have been typically based on analyzing the dependence of propane TOF values with respect to the vanadium content of the catalysts, which directly affect the proportion of polyvanadate species with respect to monovanadate ones, being higher as the vanadium surface

density is higher. However, different trends have been reported in the literature [17,28,33–39], which have been studied in an extensive review article by Carrero *et al.* [8] reaching to the conclusion that surface VO<sub>4</sub> monomer possess the same TOF as the surface VO<sub>4</sub> polymer. According to the results predicted by the kinetic model proposed in this work, this apparent non-universal behavior could be because as the vanadium content in a catalyst is higher (i.e. more active sites), the propane conversions will be higher for same reaction conditions, resulting in a deeper degree of reduction as above explained, and consequently the observed TOF could be lower in the catalyst with higher vanadium content, even though the intrinsic catalytic activity of the latter one is higher or same than the catalyst with lower vanadium content. Therefore, the comparison of propane TOF data of two catalysts should be done, at least, under the same conditions or it should be indicated if the conditions are different, otherwise it is possible to get wrong conclusions. Furthermore, it can be concluded that, unless the catalysts are always fully oxidized under reaction conditions, using only propane TOF values are not enough to reach solid conclusions about the activity of this kind of catalysts due to the non-linear variation of the catalyst oxidation state, which presents a complex dependence on many factors because of the reaction mechanism nature.

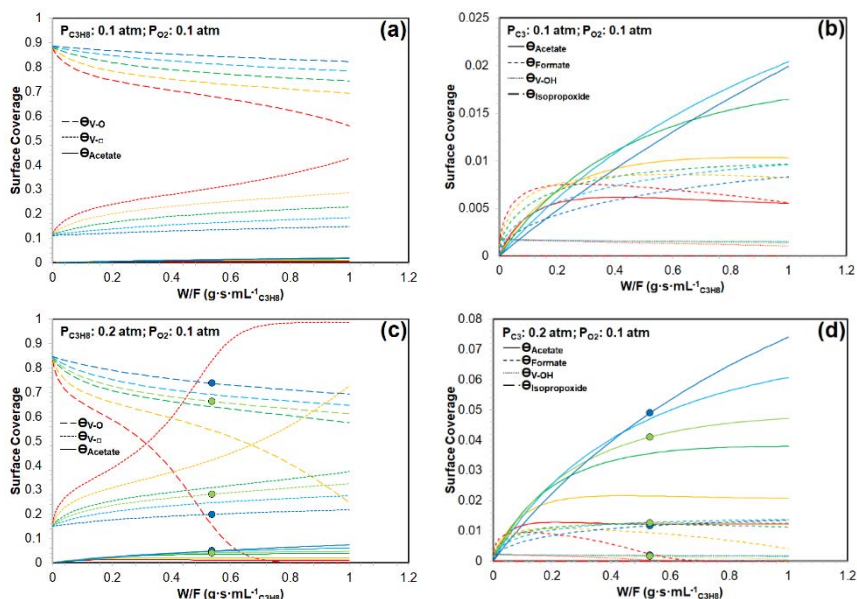


**Figure 3.4.4.** Steady-state surface coverages of V-O, V-□, acetate, formate, V-OH and isopropoxide for F-PZr-V5.0 as a function of space-time and reaction temperature at inlet partial pressures of oxygen of 0.1 atm and propane of 0.1 (a,b) and 0.2 (c,d) atm (dot symbols: predicted values of previous operando experiments; lines: simulated values; dark blue, light blue, light green, dark green, yellow and red colors represent reaction temperatures of 300, 325, 340, 350, 375 and 400°C, respectively).

Figures 3.4.4c and 3.4.4d are analogous to Figure 3.4.4a and 3.4.4b, respectively, but for a higher propane inlet partial pressure, 0.2 atm. In this case, it occurs the same effects explained above, but in a greater extent. In fact, the catalyst surface can be totally reduced at temperatures above 375°C for the conditions studied (Figure 3.4.4c). It can be observed as the lattice oxygen of the catalyst surface is almost exhausted at 400°C when the space-time is around 0.6-0.8  $\text{g}\cdot\text{s}\cdot\text{mL}^{-1}\text{C}_3\text{H}_8$ , becoming  $\theta_{\text{V-O}} \sim 0.99$ ,  $\theta_{\text{Acetate}} \sim 0.01$  and negligible surface coverages of the remaining species. At longer space-time, all the concentrations in the surface and in the gas phase remain constant denoting the deactivation of this part of the catalyst. The remaining acetate species can stay on the surface because they would require lattice oxygen to evolve as CO, while formate surface species are completely removed because they evolve without requiring lattice oxygen (Scheme 3.4.1). It should be noted that the molecular oxygen in the gas phase is also totally consumed around the space-time of 0.6-0.8  $\text{g}\cdot\text{s}\cdot\text{mL}^{-1}\text{C}_3\text{H}_8$ , which explains the subsequent total reduction and deactivation of the catalyst from this position, leaving without catalytic

activity more than half of the catalyst, as it can be seen in the picture of Figure 3.4.5. This picture was taken after performing the experiment at 400°C under the same conditions than in Figure 3.4.4c and 3.4.4d, and it can show as the catalyst become dark in color when is reduced, maybe due to coke deposition that occurs when the catalyst is in a high reduction degree (Section 3.3). Figure 3.4.5 also shows the simulated values of surface coverage for V-O and V-□ sites along the fixed-bed reactor. It is noteworthy that the change of color in the picture occurs halfway through the catalyst, coinciding with a point (space-time) where V-O sites start to be almost exhausted ( $\theta_{V-O} \approx 0.2$ ) according to the simulation, denoting the good agreement between the oxidation state of the catalyst predicted by the proposed kinetic model and the experimental observation. Moreover, it can be derived from the picture the flat radial velocity profile of the gas flow along the catalyst, confirming the plug-flow behavior of the reactor without significant deviation as assumed before.

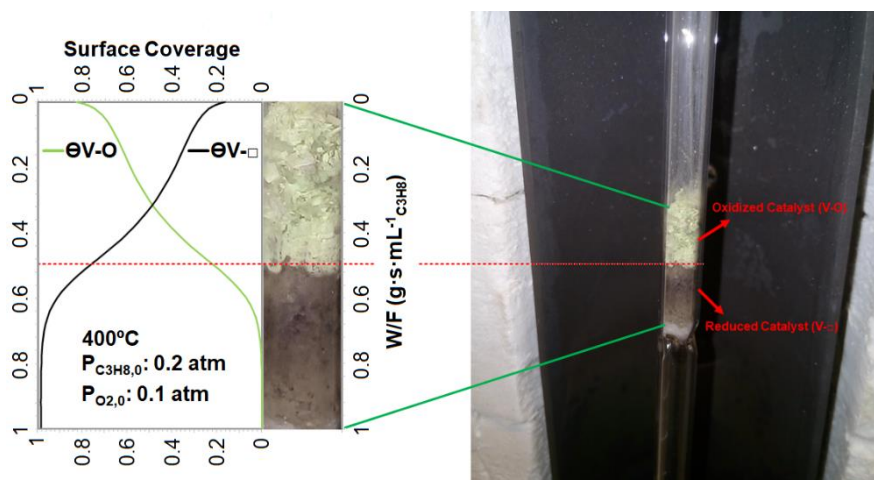


Figure 3.4.5. (Left) simulated values of surface coverage for V-O and V-□ sites along the fixed-bed reactor and (Right) picture of the fixed-bed reactor for F-PZr-V5.0 after reaction experiment at 400°C with a space-time of 1.0 g·s·mL<sup>-1</sup>C<sub>3</sub>H<sub>8</sub>, propane and oxygen inlet partial pressures of 0.2 and 0.1 atm, respectively.

Figures 3.4.4c and 3.4.4d also represent the predicted surface coverage for the operando experiments of the previous work (dot symbols), which was performed with an apparent space-time of  $\sim 0.53 \text{ g·s·mL}^{-1} \text{C}_3\text{H}_8$  (Section 3.3). Note that not quantitative data about the adsorbed species were obtained in the latter work, but the trend of these results can be compared



in a qualitative way with those predicted in this study, and it seems there is a good agreement between them. It can be observed that when the space-time is  $\sim 0.53 \text{ g}\cdot\text{s}\cdot\text{mL}^{-1}\text{C}_3\text{H}_8$  and the temperature is increased from 300 to 340°C,  $\theta_{V-O}$  decreases by 7%, the sum of  $\theta_{Acetate}$  and  $\theta_{Formate}$  decrease by a 11% and the ratio  $\theta_{Acetate}/\theta_{Formate}$  decrease from 4.2 to 3.2. Similar trends can be found observing the Raman and FTIR operando spectra obtained at the same reaction conditions, which validates once more the here proposed kinetic model.

#### *3.4.3.5. Influence of inlet partial pressure of propane and oxygen*

Figures 3.4.6 and 3.4.7 show conversion-selectivity profiles, while Figure 3.4.8 represents simulated surface coverages of vanadia and adsorbed species, as a function of temperature and inlet partial pressures of propane or oxygen for F-PZr-V5.0. It can be checked the good agreement between the experimental and simulated values of conversion and selectivity obtained in the whole range studied of propane and oxygen inlet partial pressures (Figure 3.4.6 and 3.4.7, respectively). As expected, the conversion and selectivity values markedly present a stronger influence with the inlet partial pressure of propane than with oxygen. Accordingly, the evolution of the surface coverages of the vanadia and adsorbed species as a function of propane or oxygen inlet partial pressure is also very different (Figure 3.4.8).

It can be derived from the comparison of Figures 3.4.3 and 3.4.6 that the influence of space-time and propane inlet partial pressure, respectively, on the conversion-selectivity profiles seems very similar. The conversion increases as the propane inlet partial pressure increases, and consequently the selectivity decreases. However, there are some differences when Figures 3.4.4a and 3.4.4b are compared with Figures 3.4.8a and 3.4.8b, respectively. It can be observed that the increase of propane inlet partial pressure tends to promote the reduction of the catalyst in more extent than the increase of space-time, denoted by the faster decrease of lattice oxygen concentration and the faster increase of adsorbed species, mainly as

acetate. Moreover, it can be seen in Figure 3.4.8a that when the propane inlet pressure tends to 0,  $\theta_{V-O}$  become 1.00, which is consistent because the catalyst would be under an oxidant atmosphere without propane. This is different from what observed in Figure 3.4.4a, where at space-time of 0 the catalyst presented already certain reduction degree.

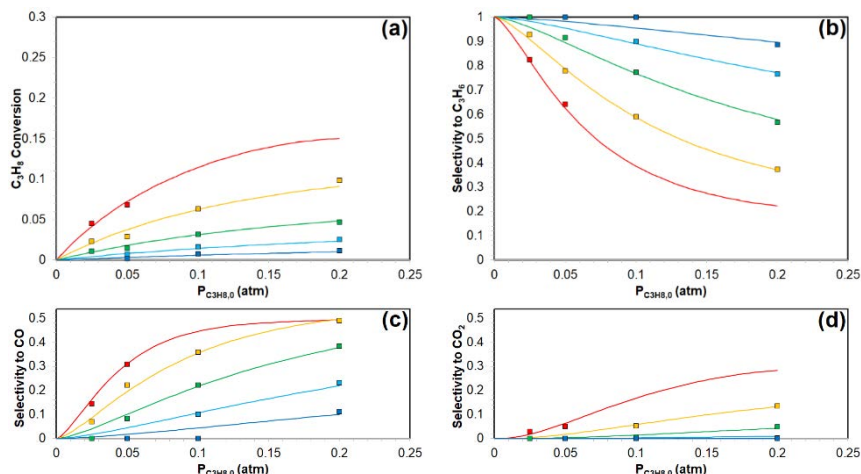


**Figure 3.4.6.** Steady-state propane conversion (a), selectivity to propylene (b), CO (c) and CO<sub>2</sub> (d) for F-PZr-V5.0 versus propane inlet partial pressure and reaction temperature at space-time of  $0.3 \text{ g} \cdot \text{s} \cdot \text{mL}^{-1} \text{C}_3\text{H}_8$  and oxygen inlet partial pressure of 0.1 (square symbols: experimental values; solid lines: simulated values; dark blue, light blue, green, yellow and red colors represent reaction temperatures of 300, 325, 350, 375 and 400°C, respectively).

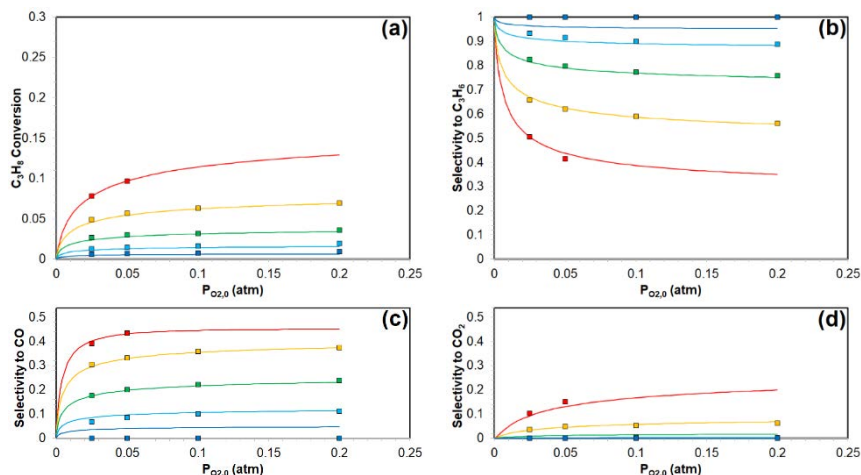


**Figure 3.4.7.** Steady-state propane conversion (a), selectivity to propylene (b), CO (c) and CO<sub>2</sub> (d) for F-PZr-V5.0 versus oxygen inlet partial pressure and reaction temperature at space-time of  $0.3 \text{ g} \cdot \text{s} \cdot \text{mL}^{-1} \text{C}_3\text{H}_8$  and propane inlet partial pressure of 0.1 atm (square symbols: experimental values; solid lines: simulated values; dark blue, light blue, green, yellow and red colors represent reaction temperatures of 300, 325, 350, 375 and 400°C, respectively).

It can be observed in Figures 3.4.7, 3.4.8c and 3.4.8d that exists a strong influence of the oxygen at low partial pressures on the conversion-selectivity profiles and on the surface coverages of vanadia and adsorbed species, respectively. This strong influence disappears once exceeded a certain value of oxygen concentration in the gas phase, becoming the kinetic of the reaction pseudo-zero order with respect to oxygen in these conditions. However, the presence of oxygen in the gas phase is still necessary for the reoxidation of the catalyst to perpetuate the catalytic cycle, otherwise the activity would be null as predicted in Figure 3.4.7a, since the active sites would be exhausted (i.e.  $\theta_{V-O} \approx 0$ ) as shown in Figure 3.4.8c.

The fact that the RDS is second-order with respect to  $\theta_{V-O}$  (Eq. (5)) means that the propane conversion profile will be determined in part by the surface coverage of the lattice oxygen, which in turn will be as a function of the reaction conditions according to Eq. (28). Then, the evolution of  $\theta_{V-O}$  as a function of oxygen inlet partial pressure predicted in Figure 3.4.8c can justify why the propane conversion sharply change at low oxygen concentrations, while is almost constant at higher oxygen inlet partial pressures (Figure 3.4.7). Moreover, it should be noted that it is predicted that the catalyst is not fully oxidized even for the highest oxygen inlet partial pressures used in this work (Figure 3.4.8c), which means that although the reaction is pseudo-zero order with respect to the oxygen partial pressure, it does not mean that the catalyst has to be nearly saturated with oxygen under the assumption that probably the reoxidation reaction of the catalyst is much faster than the reduction. In this way, many authors have reported zero-order dependence in the ODH reaction [14,25,26,28–32] assuming that the reoxidation reaction of the catalyst is several orders faster than the reduction reaction, and then, sometimes it has also considered that the catalyst is fully oxidized under reaction conditions [26,29]. However, these assumptions are not always right, since it will depend on each catalyst nature and reaction conditions as above observed.

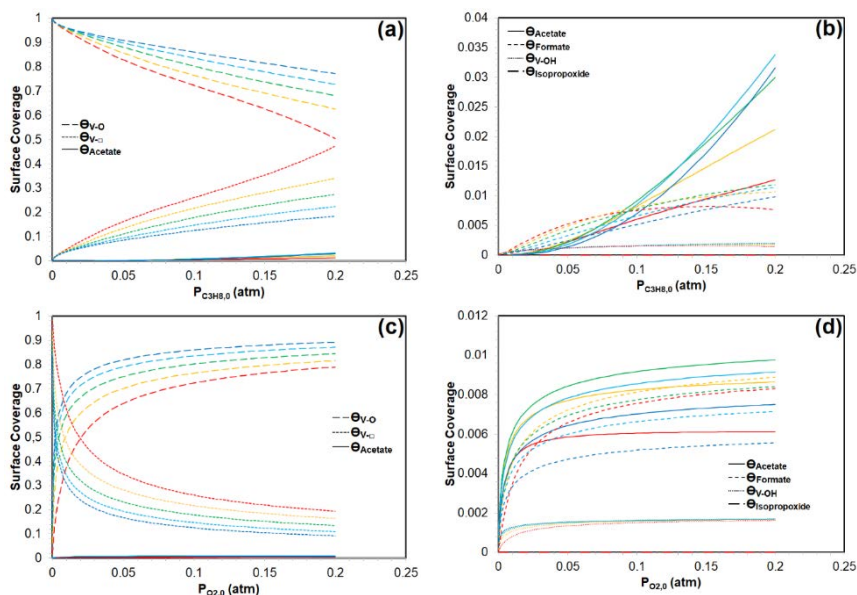


**Figure 3.4.8.** Simulation of steady-state surface coverages of V-O, V-O, acetate, formate, V-OH and isopropoxide for F-PZr-V5.0 versus reaction temperature and inlet partial pressures of propane (a,b) or oxygen (c,d) at space-time of  $0.3 \text{ g} \cdot \text{s} \cdot \text{mL}^{-1} \text{C}_3\text{H}_8$ . The inlet partial pressure of oxygen or propane was 0.1 atm in (a,b) and (c,d), respectively. (dark blue, light blue, green, yellow and red colors represent reaction temperatures of 300, 325, 350, 375 and 400°C, respectively).

### 3.4.4. Conclusions

A rigorous kinetic study of the propane ODH reaction on a vanadium oxide-based submicron (diameter) fiber catalyst have been carried out establishing the kinetic equations according to the reaction mechanism proposed from the FTIR-Raman *operando* results of a previous work. The shape and the size of the catalyst allowed the relatively easier obtention of intrinsic kinetic data of the catalyst, without the interference of other effects, compared to the traditional powdered catalysts. The proposed kinetic model with the estimated kinetic parameters satisfactorily predicts the conversion and selectivity profiles and the surface coverage of the different species present on the catalyst for all the studied conditions of temperature, space-time and inlet partial pressures of propane and oxygen, covering a broad range of conversion and selectivity values. The first hydrogen abstraction from propane is the rate determining step (RDS) and the calculated activation energy ( $104.1 \text{ kJ} \cdot \text{mol}^{-1}$ ) is within the range of those ones reported for similar catalysts. Although, there is a wide variety of

values in the literature, probably due to the use of the inconsistent Mars-van Krevelen expression or oversimplified models.

The conversion and selectivity values, as well as the surface coverages of the different species, present a strong dependence on temperature, space-time and propane inlet partial pressure. However, the influence of oxygen concentration is only strong at low oxygen partial pressures, becoming pseudo-zero order dependence (i.e. independent) with respect to oxygen concentration once exceeded a certain value. Moreover, the model predicts that the catalyst used in this work is not fully oxidized under reaction conditions even for the highest oxygen inlet partial pressures used and neither when the space-time tends to zero (i.e. negligible conversions). Which means that although the reaction is pseudo-zero order with respect to oxygen in a broad range of conditions, the catalyst may not be fully oxidized, even though the reoxidation reaction of the catalyst may be much faster than the reduction. Then the tempting assumption of considering that the catalyst is always fully oxidized to simplify the equations could be wrong sometimes. In fact, the model predicts that the catalyst oxidation state under reaction conditions will depend on its intrinsic chemical nature, the feed composition, temperature and space-time. Furthermore, as the RDS is considered second-order with respect to the surface coverage of lattice oxygen, it can be derived that propane TOF will also depend on the reaction conditions and space-time, and so, it will change along the fixed-bed reactor. Therefore, the comparison of propane TOF data of two catalysts only should be done under the same conditions, although using only this parameter is not enough to reach solid conclusions about the activity of this kind of catalysts, unless the catalysts are always fully oxidized under reaction conditions. This is due to the non-linear variation of the catalyst oxidation state, which presents a complex dependence on many factors because of the reaction mechanism nature.

## Acknowledgements

This work was supported by the Spanish Ministry of Economy and Competitiveness and FEDER [CTQ-2012-36408 and CTQ-2015-68654-R]. J.J.T.H. acknowledges the assistance of the Ministry of Economy and Competitiveness of Spain for the award of a FPI Grant [BES-2013-064425].

## 3.4.5. References

- [1] J. Lazonby, Propene (Propylene), (n.d.). <http://www.essentialchemicalindustry.org/chemicals/propene.html>. (accessed April 15, 2019).
- [2] A. Agarwal, D. Sengupta, M. El-Halwagi, Sustainable Process Design Approach for On-Purpose Propylene Production and Intensification, *ACS Sustain. Chem. Eng.* 6 (2018) 2407–2421. <https://doi.org/10.1021/acssuschemeng.7b03854>.
- [3] F. Cavani, N. Ballarini, A. Cericola, Oxidative dehydrogenation of ethane and propane: How far from commercial implementation?, *Catal. Today.* 127 (2007) 113–131. <https://doi.org/10.1016/j.cattod.2007.05.009>.
- [4] The Propylene Gap: How Can It Be Filled?, *Am. Chem. Soc.* (n.d.). <https://www.acs.org/content/acs/en/pressroom/cutting-edge-chemistry/the-propylene-gap-how-can-it-be-filled.html> (accessed April 15, 2019).
- [5] J.F. Brazdil, Strategies for the selective catalytic oxidation of alkanes, *Top. Catal.* 38 (2006) 289–294. <https://doi.org/10.1007/s11244-006-0027-4>.
- [6] R.K. Grasselli, Advances and future trends in selective oxidation and ammoxidation catalysis, *Catal. Today.* 49 (1999) 141–153. [https://doi.org/10.1016/S0920-5861\(98\)00418-0](https://doi.org/10.1016/S0920-5861(98)00418-0).
- [7] I. Amghizar, L.A. Vandewalle, K.M. Van Geem, G.B. Marin, New Trends in Olefin Production, *Engineering.* 3 (2017) 171–178. <https://doi.org/10.1016/J.ENG.2017.02.006>.

- [8] C.A. Carrero, R. Schloegl, I.E. Wachs, R. Schomaecker, Critical Literature Review of the Kinetics for the Oxidative Dehydrogenation of Propane over Well-Defined Supported Vanadium Oxide Catalysts, *ACS Catal.* 4 (2014) 3357–3380. <https://doi.org/10.1021/cs5003417>.
- [9] A. Corma, J.M. López-Nieto, N. Paredes, M. Pérez, Y. Shen, H. Cao, S.L. Suib, Oxidative Dehydrogenation Of Propane Over Supported-Vanadium Oxide Catalysts, in: P. Ruiz, B. Delmon (Eds.), *Stud. Surf. Sci. Catal.*, Elsevier, 1992: pp. 213–220. [https://doi.org/10.1016/S0167-2991\(08\)61673-0](https://doi.org/10.1016/S0167-2991(08)61673-0).
- [10] B. Frank, A. Dinse, O. Ovsitser, E.V. Kondratenko, R. Schomäcker, Mass and heat transfer effects on the oxidative dehydrogenation of propane (ODP) over a low loaded VOx/Al<sub>2</sub>O<sub>3</sub> catalyst, *Appl. Catal. Gen.* 323 (2007) 66–76. <https://doi.org/10.1016/j.apcata.2007.02.006>.
- [11] Y.-M. Liu, Y. Cao, K.-K. Zhu, S.-R. Yan, W.-L. Dai, H.-Y. He, K.-N. Fan, Highly efficient VOx/SBA-15 mesoporous catalysts for oxidative dehydrogenation of propane, *Chem. Commun.* 0 (2002) 2832–2833. <https://doi.org/10.1039/B208177F>.
- [12] Y.-M. Liu, Y. Cao, N. Yi, W.-L. Feng, W.-L. Dai, S.-R. Yan, H.-Y. He, K.-N. Fan, Vanadium oxide supported on mesoporous SBA-15 as highly selective catalysts in the oxidative dehydrogenation of propane, *J. Catal.* 224 (2004) 417–428. <https://doi.org/10.1016/j.jcat.2004.03.010>.
- [13] M.O. Guerrero-Pérez, Supported, bulk and bulk-supported vanadium oxide catalysts: A short review with an historical perspective, *Catal. Today.* 285 (2017) 226–233. <https://doi.org/10.1016/j.cattod.2017.01.037>.
- [14] A. Khodakov, J. Yang, S. Su, E. Iglesia, A.T. Bell, Structure and properties of vanadium oxide-zirconia catalysts for propane oxidative dehydrogenation, *J. Catal.* 177 (1998) 343–351. <https://doi.org/10.1006/jcat.1998.2143>.

- [15] P. Mars, D.W. van Krevelen, Oxidations carried out by means of vanadium oxide catalysts, *Chem. Eng. Sci.* 3 (1954) 41–59. [https://doi.org/10.1016/S0009-2509\(54\)80005-4](https://doi.org/10.1016/S0009-2509(54)80005-4).
- [16] R. Grabowski, Kinetics of Oxidative Dehydrogenation of C2-C3 Alkanes on Oxide Catalysts, *Catal. Rev.* 48 (2006) 199–268. <https://doi.org/10.1080/01614940600631413>.
- [17] E.V. Kondratenko, M. Cherian, M. Baerns, D. Su, R. Schlögl, X. Wang, I.E. Wachs, Oxidative dehydrogenation of propane over V/MCM-41 catalysts: comparison of O<sub>2</sub> and N<sub>2</sub>O as oxidants, *J. Catal.* 234 (2005) 131–142. <https://doi.org/10.1016/j.jcat.2005.05.025>.
- [18] A. Dinse, B. Frank, C. Hess, D. Habel, R. Schomäcker, Oxidative dehydrogenation of propane over low-loaded vanadia catalysts: Impact of the support material on kinetics and selectivity, *J. Mol. Catal. Chem.* 289 (2008) 28–37. <https://doi.org/10.1016/j.molcata.2008.04.007>.
- [19] B.Y. Jibril, S.M. Al-Zahrani, A.E. Abasaheed, R. Hughes, Propane oxidative dehydrogenation on Cs-doped Cr-Mo-Al-O catalyst: kinetics and mechanism, *Chem. Eng. J.* 103 (2004) 59–67. <https://doi.org/10.1016/j.cej.2004.03.006>.
- [20] M. Baldi, E. Finocchio, C. Pistarino, G. Busca, Evaluation of the mechanism of the oxy-dehydrogenation of propane over manganese oxide, *Appl. Catal. Gen.* 173 (1998) 61–74. [https://doi.org/10.1016/S0926-860X\(98\)00129-X](https://doi.org/10.1016/S0926-860X(98)00129-X).
- [21] K. Routray, K.R.S.K. Reddy, G. Deo, Oxidative dehydrogenation of propane on V<sub>2</sub>O<sub>5</sub>/Al<sub>2</sub>O<sub>3</sub> and V<sub>2</sub>O<sub>5</sub>/TiO<sub>2</sub> catalysts: understanding the effect of support by parameter estimation, *Appl. Catal. Gen.* 265 (2004) 103–113. <https://doi.org/10.1016/j.apcata.2004.01.006>.
- [22] S. Chakraborty, S.C. Nayak, G. Deo, TiO<sub>2</sub>/SiO<sub>2</sub> supported vanadia catalysts for the ODH of propane, *Catal. Today.* 254 (2015) 62–71. <https://doi.org/10.1016/j.cattod.2015.01.047>.
- [23] E.V. Kondratenko, M. Baerns, Catalytic oxidative dehydrogenation of propane in the presence of O<sub>2</sub> and N<sub>2</sub>O—the role of vanadia



- distribution and oxidant activation, *Appl. Catal. Gen.* 222 (2001) 133–143. [https://doi.org/10.1016/S0926-860X\(01\)00836-5](https://doi.org/10.1016/S0926-860X(01)00836-5).
- [24] A. Bottino, G. Capannelli, A. Comite, S. Storace, R. Di Felice, Kinetic investigations on the oxidehydrogenation of propane over vanadium supported on  $\gamma$ -Al<sub>2</sub>O<sub>3</sub>, *Chem. Eng. J.* 94 (2003) 11–18. [https://doi.org/10.1016/S1385-8947\(03\)00003-2](https://doi.org/10.1016/S1385-8947(03)00003-2).
- [25] M.D. Argyle, K. Chen, A.T. Bell, E. Iglesia, Effect of Catalyst Structure on Oxidative Dehydrogenation of Ethane and Propane on Alumina-Supported Vanadia, *J. Catal.* 208 (2002) 139–149. <https://doi.org/10.1006/jcat.2002.3570>.
- [26] D. Creaser, B. Andersson, Oxidative dehydrogenation of propane over V-Mg-O: kinetic investigation by nonlinear regression analysis, *Appl. Catal. Gen.* 141 (1996) 131–152. [https://doi.org/10.1016/0926-860X\(96\)00029-4](https://doi.org/10.1016/0926-860X(96)00029-4).
- [27] S.L.T. Andersson, Kinetic study of the oxidative dehydrogenation of propane over vanadia supported on amorphous AlPO<sub>4</sub>, *Appl. Catal. Gen.* 112 (1994) 209–218. [https://doi.org/10.1016/0926-860X\(94\)80220-3](https://doi.org/10.1016/0926-860X(94)80220-3).
- [28] A. Khodakov, B. Olthof, A.T. Bell, E. Iglesia, Structure and Catalytic Properties of Supported Vanadium Oxides: Support Effects on Oxidative Dehydrogenation Reactions, *J. Catal.* 181 (1999) 205–216. <https://doi.org/10.1006/jcat.1998.2295>.
- [29] C. Carrero, M. Kauer, A. Dinse, T. Wolfram, N. Hamilton, A. Trunschke, R. Schlögl, R. Schomäcker, High performance (VO<sub>x</sub>)<sub>n</sub>–(TiO<sub>x</sub>)<sub>m</sub>/SBA-15 catalysts for the oxidative dehydrogenation of propane, *Catal. Sci. Technol.* 4 (2014) 786–794. <https://doi.org/10.1039/C3CY00625E>.
- [30] S. Zhang, H. Liu, Oxidative dehydrogenation of propane over Mg-V-O oxides supported on MgO-coated silica: Structural evolution and catalytic consequence, *Appl. Catal. Gen.* 573 (2019) 41–48. <https://doi.org/10.1016/j.apcata.2019.01.012>.
- [31] J.N. Michaels, D.L. Stern, R.K. Grasselli, Oxydehydrogenation of propane over Mg-V-Sb-oxide catalysts. II. Reaction kinetics and

- mechanism, *Catal. Lett.* 42 (1996) 139–148. <https://doi.org/10.1007/BF00810679>.
- [32] A. Dinse, S. Khennache, B. Frank, C. Hess, R. Herbert, S. Wrabetz, R. Schlögl, R. Schomäcker, Oxidative dehydrogenation of propane on silica (SBA-15) supported vanadia catalysts: A kinetic investigation, *J. Mol. Catal. Chem.* 307 (2009) 43–50. <https://doi.org/10.1016/j.molcata.2009.03.008>.
- [33] B. Solsona, T. Blasco, J.M. López Nieto, M.L. Peña, F. Rey, A. Vidal-Moya, Vanadium Oxide Supported on Mesoporous MCM-41 as Selective Catalysts in the Oxidative Dehydrogenation of Alkanes, *J. Catal.* 203 (2001) 443–452. <https://doi.org/10.1006/jcat.2001.3326>.
- [34] A. Christodoulakis, M. Machli, A.A. Lemonidou, S. Boghosian, Molecular structure and reactivity of vanadia-based catalysts for propane oxidative dehydrogenation studied by in situ Raman spectroscopy and catalytic activity measurements, *J. Catal.* 222 (2004) 293–306. <https://doi.org/10.1016/j.jcat.2003.10.007>.
- [35] X. Gao, J.-M. Jehng, I.E. Wachs, In Situ UV–vis–NIR Diffuse Reflectance and Raman Spectroscopic Studies of Propane Oxidation over ZrO<sub>2</sub>-Supported Vanadium Oxide Catalysts, *J. Catal.* 209 (2002) 43–50. <https://doi.org/10.1006/jcat.2002.3635>.
- [36] D. Shee, T.V.M. Rao, G. Deo, Kinetic parameter estimation for supported vanadium oxide catalysts for propane ODH reaction: Effect of loading and support, *Catal. Today.* 118 (2006) 288–297. <https://doi.org/10.1016/j.cattod.2006.07.017>.
- [37] T.V.M. Rao, G. Deo, Kinetic parameter analysis for propane ODH: V<sub>2</sub>O<sub>5</sub>/Al<sub>2</sub>O<sub>3</sub> and MoO<sub>3</sub>/Al<sub>2</sub>O<sub>3</sub> catalysts, *AIChE J.* 53 (2007) 1538–1549. <https://doi.org/10.1002/aic.11176>.
- [38] K. Chen, A.T. Bell, E. Iglesia, The Relationship between the Electronic and Redox Properties of Dispersed Metal Oxides and Their Turnover Rates in Oxidative Dehydrogenation Reactions, *J. Catal.* 209 (2002) 35–42. <https://doi.org/10.1006/jcat.2002.3620>.
- [39] P. Viparelli, P. Ciambelli, L. Lisi, G. Ruoppolo, G. Russo, J.C. Volta, Oxidative dehydrogenation of propane over vanadium and niobium

- oxides supported catalysts, *Appl. Catal. Gen.* 184 (1999) 291–301. [https://doi.org/10.1016/S0926-860X\(99\)00104-0](https://doi.org/10.1016/S0926-860X(99)00104-0).
- [40] M.A. Vannice, An analysis of the Mars–van Krevelen rate expression, *Catal. Today.* 123 (2007) 18–22. <https://doi.org/10.1016/j.cattod.2007.02.002>.
- [41] J.J. Ternero-Hidalgo, J. Torres-Liñán, M.O. Guerrero-Pérez, J. Rodríguez-Mirasol, T. Cordero, Electrospun vanadium oxide based submicron diameter fiber catalysts. Part I: Preparation procedure and propane ODH application, *Catal. Today.* (2018). <https://doi.org/10.1016/j.cattod.2018.10.073>.
- [42] E. Reichelt, M.P. Heddrich, M. Jahn, A. Michaelis, Fiber based structured materials for catalytic applications, *Appl. Catal. Gen.* 476 (2014) 78–90. <https://doi.org/10.1016/j.apcata.2014.02.021>.
- [43] J. Pérez-Ramírez, R.J. Berger, G. Mul, F. Kapteijn, J.A. Moulijn, Six-flow reactor technology a review on fast catalyst screening and kinetic studies, *Catal. Today.* 60 (2000) 93–109. [https://doi.org/10.1016/S0920-5861\(00\)00321-7](https://doi.org/10.1016/S0920-5861(00)00321-7).
- [44] R.J. Berger, J. Pérez-Ramírez, F. Kapteijn, J.A. Moulijn, Catalyst performance testing: The influence of catalyst bed dilution on the conversion observed, *Chem. Eng. J.* 90 (2002) 173–183. [https://doi.org/10.1016/S1385-8947\(02\)00078-5](https://doi.org/10.1016/S1385-8947(02)00078-5).
- [45] J.J. Ternero-Hidalgo, M.O. Guerrero-Pérez, J. Rodríguez-Mirasol, T. Cordero, Electrospun vanadium oxide based submicron diameter fiber catalysts. Part II: Effect of chemical formulation and dopants, *Catal. Today.* (2018). <https://doi.org/10.1016/j.cattod.2018.10.072>.
- [46] G. Busca, E. Finocchio, V. Lorenzelli, G. Ramis, M. Baldi, IR studies on the activation of C–H hydrocarbon bonds on oxidation catalysts, *Catal. Today.* 49 (1999) 453–465. [https://doi.org/10.1016/S0920-5861\(98\)00441-6](https://doi.org/10.1016/S0920-5861(98)00441-6).
- [47] E. Finocchio, G. Busca, V. Lorenzelli, R.J. Willey, FTIR studies on the selective oxidation and combustion of light hydrocarbons at metal oxide surfaces. Propane and propene oxidation on MgCr<sub>2</sub>O<sub>4</sub>, J.

- Chem. Soc. Faraday Trans. 90 (1994) 3347–3356.  
<https://doi.org/10.1039/FT9949003347>.
- [48] K. Chen, A.T. Bell, E. Iglesia, Kinetics and Mechanism of Oxidative Dehydrogenation of Propane on Vanadium, Molybdenum, and Tungsten Oxides, *J. Phys. Chem. B.* 104 (2000) 1292–1299.  
<https://doi.org/10.1021/jp9933875>.
- [49] K. Chen, A. Khodakov, J. Yang, A.T. Bell, E. Iglesia, Isotopic Tracer and Kinetic Studies of Oxidative Dehydrogenation Pathways on Vanadium Oxide Catalysts, *J. Catal.* 186 (1999) 325–333.  
<https://doi.org/10.1006/jcat.1999.2510>.
- [50] M.A. Vannice, *Kinetics of catalytic reactions*, Springer, New York, 2005.
- [51] E. Finocchio, G. Busca, V. Lorenzelli, V.S. Escribano, FTIR studies on the selective oxidation and combustion of light hydrocarbons at metal oxide surfaces. Part 2.—Propane and propene oxidation on  $\text{Co}_3\text{O}_4$ , *J. Chem. Soc. Faraday Trans.* 92 (1996) 1587–1593.  
<https://doi.org/10.1039/FT9969201587>.

### **3.5. Kinetic study of propane ODH on electrospun vanadium oxide-based submicron diameter fiber catalysts. Part II**

J. J. Ternero-Hidalgo<sup>1</sup>, C. Tsao<sup>2</sup>, M.O. Guerrero-Pérez<sup>1</sup>, J. Rodríguez-Mirasol<sup>1</sup>, T. Cordero<sup>1</sup>

<sup>1</sup>Universidad de Málaga, Departamento de Ingeniería Química, Campus de Teatinos s/n, E29071 Málaga, Spain

<sup>2</sup>National Ilan University, Department of Environmental Engineering, 1, Sec. 1, Shen-Lung Road, I-Lan, 260, Taiwan

**Keywords:** Propane ODH; Mixed-oxide catalysts; Fiber catalysts; Structure-activity relationships; Kinetic study

#### **Abstract**

The kinetic parameters for the oxidative dehydrogenation (ODH) of four different submicron diameter fiber catalysts based on V-Zr and V-Mo-Zr mixed oxides have been determined by using the kinetic model proposed in the previous paper. The simulated data have matched very well with the experimental results. The kinetic model has been used to simulate the optimum conditions to get the maximum values of yield and productivity that can be obtained for a given space-time and temperature. It has been predicted that yields close to 100% or higher productivities than the best ones reported in the literature can be possible for all the catalysts studied in this work, as long as the reaction is performed under the proper conditions. Therefore, low yield or productivity should not be the main obstacle that avoids the industrial implementation of propane ODH as alternative to produce propylene. The main issue could be if such high yield or productivity values can be obtained in affordable conditions for a given catalyst, or to find catalysts that simultaneously present high yield and productivity. In this way, the best catalyst studied in this work was the one containing the highest proportion of polyvanadate species without forming vanadium crystalline phases.

## Nomenclature

SC	Steam cracking
FCC	Fluid catalytic cracking
ODH	Oxidative dehydrogenation
FTIR	Fourier-transform infrared spectroscopy
RDS	Rate determining step
TOF	Turnover frequency
TEM	Transmission electron microscopy
BET	Brunauer, Emmett and Teller
EDXA	Energy-dispersive X-ray analyzer
XPS	X-ray photoelectron spectroscopy
XRD	X-ray diffraction
STP	Standard temperature and pressure
GC	Gas chromatography
TCD	Thermal conductivity detector
FID	Flame ionization detector
V-O	Lattice oxygens (VO <sub>x</sub> ) in the form of V-O-V or V-O-Zr group
V=O	Terminal oxygen of the vanadyl group
V-OH	Protonated lattice oxygen
V-□	Vacancy in the lattice oxygen
<i>X</i>	Propane conversion
<i>S<sub>i</sub></i>	Selectivity to <i>i</i> product
<i>Y<sub>i</sub></i>	Yield to <i>i</i> product
<i>X<sub>exp</sub></i>	Experimental propane conversion
<i>S<sub>exp,i</sub></i>	Experimental selectivity to <i>i</i> product
<i>Y<sub>exp,i</sub></i>	Experimental yield to <i>i</i> product
<i>X<sub>sim</sub></i>	Simulated propane conversion
<i>S<sub>sim,i</sub></i>	Simulated selectivity to <i>i</i> product
<i>Y<sub>sim,i</sub></i>	Simulated yield to <i>i</i> product
<i>W<sub>Cat</sub></i>	Mass of catalyst
<i>F<sub>T</sub></i>	Total volumetric gas flow
<i>F<sub>C3,o</sub></i>	Propane inlet volumetric flow
<i>Ḟ<sub>C3,o</sub></i>	Propane inlet molar flow
<i>Ḟ<sub>i</sub></i>	Inlet molar flow of <i>i</i> compound
<i>n<sub>i</sub></i>	Number of carbon atoms per molecule of <i>i</i> compound
<i>M<sub>C3=</sub></i>	Molar mass of propylene
<i>R<sub>j</sub></i>	Reaction step represented in Scheme 3.5.1
<i>Ads<sub>j</sub></i>	Adsorption step represented in Scheme 3.5.1
<i>r<sub>j</sub></i>	Reaction rate of <i>j</i> step
<i>k<sub>j</sub></i>	Rate constant of <i>j</i> reaction step
<i>k<sub>o,j</sub></i>	Preexponential factor of <i>j</i> reaction step
<i>E<sub>a,j</sub></i>	Activation energy of <i>j</i> reaction rate
<i>k<sub>App,j</sub></i>	Apparent rate constant of <i>j</i> reaction step
<i>k<sub>App,o,j</sub></i>	Apparent preexponential factor of <i>j</i> reaction step
<i>E<sub>a,App,j</sub></i>	Apparent activation energy of <i>j</i> reaction step
<i>K<sub>j</sub></i>	Adsorption constant of <i>j</i> step

$K_{o,j}$	Preexponential factor of $j$ adsorption step
$\Delta H_j$	Enthalpy of adsorption for $j$ step
$P_i$	Partial pressure of $i$ compound
$P_{i,o}$	Inlet partial pressure of $i$ compound
$\theta_i$	Surface coverage of $i$ species

### 3.5.1. Introduction

Over the past decades, propylene demand has been steadily growing and has become the second most-produced building block (after ethylene) in the petrochemical industry. Propylene is the starting material for many demanded materials in the world market (polypropylene, acrylonitrile, oxo-alcohols, propylene oxide, cumene, acrylic acid, etc) [1,2]. The global demand in 2014 was about 89-109 million tons and is expected to be about 165 million tons by 2030 [2,3]. Traditionally, the propylene demand has been indirectly satisfied by its production as byproduct of ethylene from steam cracking (SC), and as a byproduct of gasoline from fluid catalytic cracking (FCC) in refineries [2–4]. However, these technologies only can supply around the 85-90% of the propylene market since last decade. This is due to the increase of the propylene demand together with the improvement of ethylene and gasoline yields obtained by SC and by FCC, respectively, in detriment of propylene [3–5]. Therefore, it is necessary to fill this gap created between the demand and the supply by SC and FCC with so-called “on-purpose propylene technologies”.

In this way, propane dehydrogenation with catalysts of Pt-Sn or Cr<sub>2</sub>O<sub>3</sub> supported on alumina (for Oleflex or Catofin technologies, respectively) is becoming commercially viable to obtain propylene, especially due to the abundance of cheap propane derived from shale gas and stranded gas [5]. However, this is a strong endothermic process that works above 600°C, and then presents a very high energy consumption. In addition, the propane conversion is thermodynamically restricted and the catalyst is progressively deactivated by coke deposition [6,7]. Thereby, oxidative dehydrogenation (ODH) of propane to obtain propylene could also be a promising alternative.

This reaction consumes much less energy, since is very exothermic and is performed at lower temperatures. Moreover, it is not thermodynamically limited and the catalysts are not usually deactivated during the process [6,7]. Nevertheless, propane ODH has never been so interesting for the industry due to the low yield and productivity to propylene obtained until now, even though it has been investigated for last decades [6–8]. This is due to the undesirable combustion reactions forming CO and CO<sub>2</sub> (CO<sub>x</sub>), which are difficult to avoid [6]. Most of the yields obtained by propane ODH are lower than 30% with propylene selectivity not higher than 70% [6], while for propane dehydrogenation the yield is usually around 40% with propylene selectivity higher than 90% [3,9]. Therefore, yield and selectivity should increase in propane ODH in order to be competitive with propane dehydrogenation. Then, it would be necessary to improve the existing catalysts or to find new ones and/or to optimize the reaction conditions in order to obtain higher yield and/or productivity.

Most of the authors have focused on the preparation and characterization of the catalysts followed by testing them under a given reaction conditions to compare conversion-selectivity profiles, propane consumption TOF, yields and/or productivity values. However, not so much effort has been put into the optimization of the reaction conditions to get the maximum yield or productivity for a given catalyst. Dispersed vanadium and molybdenum based catalysts over different supports (ZrO<sub>2</sub>, TiO<sub>2</sub>, Al<sub>2</sub>O<sub>3</sub>, SiO<sub>2</sub>, etc.) are the most reported catalysts for propane ODH [6,7,10–16], where the formation of crystalline vanadium phases is detrimental [17,18]. Mars Van Krevelen type mechanism is the most frequently proposed mechanism for the reaction [19]. However, the role of the active sites during the reaction and their relationship with the conversion and selectivity are still unclear, and some discrepancies can be found about which species are the most active. It is well-known that the VO<sub>x</sub> lattice oxygen are active species [6,7], but it seems that there is not a complete unanimity about the different activity between the bridging oxygen sites (V-O-V and V-O-Support) and terminal oxygen sites (V=O) [20–22]. Moreover, it is not so clear about



which species are more active, monovanadate or polyvanadate species, or if they just present the same activity [7,20,21]. *Operando* spectroscopy together with a kinetic study of the propane ODH can be a good combination to get new insights about the reaction mechanism, what could be useful to improve the catalysts and to optimize the reaction conditions getting the maximum values of yield and productivity for a given catalyst.

The FTIR and Raman *operando* results obtained in a previous work showed that the activity of V=O terminal oxygen sites were negligible with respect to V-O bridging oxygen sites (*Section 3.3*). Moreover, a detailed reaction mechanism was proposed according to the spectroscopic and activity results. In the following paper (*Section 3.4*), a rigorous kinetic model was proposed establishing the kinetic equations based on the above reaction mechanism. In the present work, a kinetic study using the above proposed model has been performed using four different submicron diameter fiber catalysts based on V-Zr and V-Mo-Zr mixed oxides, which were already thoroughly characterized in previous papers ([23,24] or *Sections 3.1 and 3.2*). In this way, it has been studied the influence of the vanadium concentration and of the presence of molybdenum in the catalysts, in order to find out some insights about the structure-activity relationship of polyvanadate, monovanadate, crystalline  $ZrV_2O_7$  and V-Mo-O species. Reaction experiments varying the temperature, the propane and oxygen inlet partial pressure and the space-time have been performed in a fixed-bed reactor to estimate the kinetic parameters of each catalyst studied. These parameters have been analyzed and compared among the different catalysts. In all the cases, the simulation data matched very well with the experimental results. Finally, it has been simulated values of yield and productivity in a broad range of conditions to study their dependence and to try to find the theoretical optimum conditions to get their maximum values. This catalytic information could be very useful to determine if a catalyst can be suitable to be used on an industrial scale.

### **3.5.2. Materials and methods**

#### *3.5.2.1. Catalysts preparation and characterization*

Four vanadium oxide based submicron-fiber catalysts were prepared using the electrospinning technique following the synthesis method previously described in previous works ([23,24] or *Sections 3.1 and 3.2*). Three of the catalysts consist of V-Zr-O systems with different vanadium mass concentrations, while the other sample also presents Mo in its formula giving rise to a V-Mo-Zr-O catalyst. The synthesis of the samples involved the use of the following chemicals: Zirconium (IV) propoxide solution (70 wt. % in 1-propanol), zirconium acetate solution (Zr ~16 wt % in acetic acid), polyvinylpyrrolidone (PVP), acetylacetone, 1-propanol, acetic acid, vanadyl acetylacetonate and ammonium heptamolybdate tetrahydrate. For the V-containing fibers, the electrospinning process was performed using polymer solutions prepared with different amounts of the corresponding reagents in order to obtain final fibers with elemental vanadium mass concentrations of 2.5, 5.0 and 6.4%, named as F-PZr-V2.5, F-PZr-V5.0 and F-PZr-V6.4, respectively ([23] or *Section 3.1*). For the V-Mo-containing fibers, they have been prepared with a final mass concentration of 0.8 and 4.3 of vanadium and molybdenum, respectively, named as F-AZr-V0.8-Mo4.3 ([24] or *Section 3.2*). Finally, the electrospun fibers were calcined in a conventional tubular furnace at 500 °C under air flow (150 mL/min STP) for 6 h to eliminate the organic part and the remaining solvent, as well as to stabilize the final inorganic zirconia fibers. A heating rate of 10°C·min<sup>-1</sup> was always used to reach the calcination temperature.

Table 3.5.1 summarizes the main physicochemical characteristics of the catalysts studied in the present work. A more detailed characterization has been reported in previous papers ([23,24] or *Sections 3.1 and 3.2*). The fibrous morphology of all the samples was confirmed by using transmission electron microscopy (TEM), where it was observed diameters ranging from 150 to 620 nm. The porous texture was characterized by N<sub>2</sub> adsorption-desorption isotherms at -196°C, obtaining a type IVa isotherm

corresponding to mesoporous solid in the samples F-PZr-V2.5, F-PZr-V5.0 and F-PZr-V6.4, while type II isotherm characteristic of solids with a quite low developed porous structure was found in F-AZr-V0.8-Mo4.3. The BET surface areas were calculated from the N<sub>2</sub> isotherms obtaining very similar values (59-66 m<sup>2</sup>/g) for the V-Zr-O catalysts (F-PZr-V2.5, F-PZr-V5.0 and F-PZr-V6.4) and very low value (6 m<sup>2</sup>/g) for the Mo-containing sample (F-AZr-V0.8-Mo4.3). The above differences observed in the porous texture are associated to the different zirconium precursor used in F-AZr-V0.8-Mo4.3 (zirconium acetate) with respect to F-PZr-V2.5, F-PZr-V5.0 and F-PZr-V6.4 (zirconium propoxide) ([24] or Section 3.2). The surface chemistry and crystal structure of the samples were analyzed by energy-dispersive X-ray analyzer (EDXA), X-ray photoelectron spectroscopy (XPS), in situ Raman and X-ray diffraction patterns (XRD). The results showed vanadium and molybdenum homogeneously distributed along the fibers, being their elemental mass concentrations relatively close to the nominal values in all the cases. Moreover, it was confirmed the presence of dispersed species of mono and poly VO<sub>x</sub> and MoO<sub>x</sub> structures and V-Mo-O phases along the tetragonal zirconia, as well as it was not found crystalline phases of V<sub>2</sub>O<sub>5</sub> and MoO<sub>3</sub>. It should be noted that the proportion of polyvanadates with respect to monovanadates is higher as the vanadium concentration of the samples increases, and incipient ZrV<sub>2</sub>O<sub>7</sub> phases was observed in the Raman spectra of F-PZr-V6.4.

**Table 3.5.1.** Physicochemical characteristics of the catalysts F-PZr-V6.4, F-PZr-V5.0, F-PZr-V2.5 and F-AZr-V0.8-Mo4.3.

Catalyst	Diameter (nm)	<sup>a</sup> A <sub>BET</sub> (m <sup>2</sup> /g)	EDXA (wt.%)		XPS (wt.%)		Active species
			V	Mo	V2p	Mo3d	
<b>F-PZr-V6.4</b>	260-410	59	6.2	-	6.0	-	↓ Mono/↑ poly VO <sub>x</sub> and incipient ZrV <sub>2</sub> O <sub>7</sub>
<b>F-PZr-V5.0</b>	300-410	66	4.7	-	4.9	-	Mono/↑ poly VO <sub>x</sub>
<b>F-PZr-V2.5</b>	270-620	59	2.4	-	2.7	-	Mono/poly VO <sub>x</sub>
<b>F-AZr-V0.8-Mo4.3</b>	150-290	6	1.0	5.5	1.3	3.5	Mono/poly VO <sub>x</sub> /MoO <sub>x</sub> and V-Mo-O phases

<sup>a</sup>from N<sub>2</sub> adsorption-desorption isotherms.

### 3.5.2.2. Propane ODH experiments

The catalytic experiments about the propane oxidative dehydrogenation (ODH) reaction were performed in a fixed bed microreactor (i.d. 4 mm) placed inside a vertical furnace with temperature control ([23,24] or Sections 3.1, 3.2 and 3.4). Mass flow controllers were used to feed the reactor with the desired mixtures of propane (99.95%), oxygen (99.999%) and helium (99.999%) gases. The reaction temperature was varied from 300 to 480°C, the propane and oxygen inlet partial pressures ( $P_{C_3,o}$  and  $P_{O_2,o}$ , respectively) was varied from 0.025 to 0.2 atm, and the total volumetric gas flow ( $F_T$ ) together with the mass of catalyst ( $W_{cat}$ ) were adjusted in order to vary the space-time ( $W_{cat}/F_{C_3,o}$ ) in the range of 0.1-1.0  $g_{cat} \cdot s \cdot mL^{-1} C_3H_8$  (Volume was always expressed in STP conditions). In order to pre-heat the reactant mixture upstream the reactor and to avoid condensation of products downstream the reactor the lines were heated at 120°C.

Reactants and products were analyzed in steady state conditions by an on-line gas chromatograph (Perkin-Elmer, Clarus 500 GC), equipped with a Hayesep D 80/100 (length: 3 m; diameter: 1/8"; internal diameter: 2.1 mm) and an active carbon 80/100 (length: 2 m; diameter 1/8"; internal diameter: 2,1 mm) packed columns. Light gases ( $O_2$ , CO and  $CO_2$ ) were detected by a thermal conductivity detector (TCD); and  $CH_4$ ,  $C_2H_4$ ,  $C_2H_6$ ,  $C_3H_6$  and  $C_3H_8$  were detected using a flame ionization detector (FID). In all the cases carbon and oxygen molar balances were closed with errors lower than 5%. The propane conversion and the selectivity or yield to  $i$  product are defined as  $X$  and  $S_i$  or  $Y_i$ , respectively:

$$X = \frac{\dot{F}_{C_3,o} - \dot{F}_{C_3}}{\dot{F}_{C_3,o}} \quad (1)$$

$$S_i = \frac{n_i \cdot \dot{F}_i}{n_{C_3} \cdot \dot{F}_{C_3,o} \cdot X} \quad (2)$$

$$Y_i = X \cdot S_i \quad (3)$$

where  $\dot{F}_{C3,o}$  and  $\dot{F}_{C3}$  are the molar flows of propane in the inlet and in the outlet streams, respectively.  $\dot{F}_i$  is the molar flow of  $i$  product in the outlet stream, and  $n_{C3}$  or  $n_i$  are the number of carbon atoms per molecule of propane ( $n_{C3}=3$ ) or  $i$  product, respectively. Propylene productivity values were calculated using Eq. (4). It indicates the propylene mass obtained per mass of catalyst and time:

$$\text{Propylene productivity} = \frac{\dot{F}_{C3,o} \cdot Y_{C3=} \cdot M_{C3=}}{W_{cat}} \quad (4)$$

where  $M_{C3=}$  is the molar mass of propylene.

The possible catalyst deactivation during reaction, the contribution of homogenous phase reaction, the contribution of zirconia activity and the presence of external mass and heat transport limitations were experimentally discarded within the studied conditions in a previous work ([23] or *Section 3.1*). On the other hand, internal mass and heat transport limitations have been assumed negligible due to the quite small diameter of the submicron-fibers. Moreover, no pressure drop has been observed through the catalyst bed under the experimental conditions used probably due to the fibrous morphology of the catalyst [25].

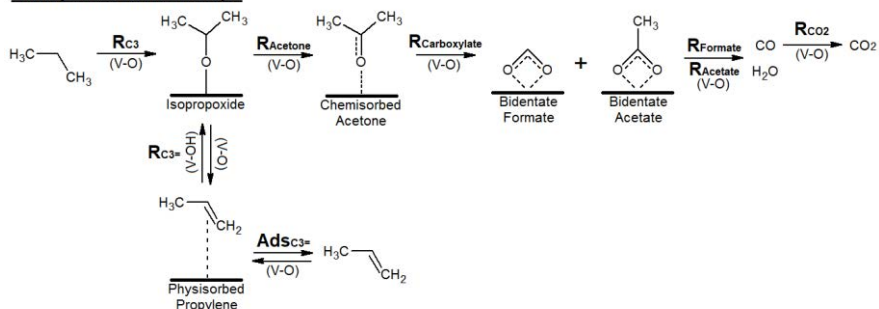
### 3.5.3. Results and discussion

#### 3.5.3.1. Kinetic model

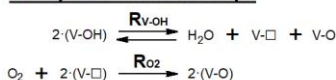
A detailed description of the kinetic model used in this work and its mathematical deduction was already reported in the previous article (*Section 3.4*). This kinetic model was based on the propane ODH mechanism proposed (Scheme 3.5.1) in a before work according to the FTIR-Raman *operando* results obtained (*Section 3.3*). The proposed mechanism assumes that lattice oxygen (V-O) are the only active sites responsible of the propane oxidation to form propylene or combustion

products, CO and CO<sub>2</sub> (CO<sub>x</sub>). However, the gas phase oxygen also plays an important role in the mechanism, since it is necessary to reoxidizes the catalyst and perpetuate the catalytic cycle. The lattice oxygen in the form of V-O-V or V-O-Zr groups have been represented as (V-O), and it has been assumed that both of them have the same role in the mechanism, although they may be different in terms of activity. However, it has been discarded the activity or participation of the V=O terminal groups. Protonated lattice oxygens and reduced vanadium sites have been represented as (V-OH) and (V-□). Irreversible dissociative chemisorption of propane forming isopropoxide is proposed as the first step and RDS (R<sub>C3</sub>). Isopropoxide can evolve as propylene (R<sub>C3=</sub> followed by Ad<sub>C3=</sub>) or can be further oxidized forming chemisorbed acetone (R<sub>Acetone</sub>). Propylene can be adsorbed on a V-O site (Ad<sub>C3=</sub>) and react with a neighbour V-OH as Bronsted acidic site to form isopropoxide (R<sub>C3=</sub>). The oxidative cleavage of the C(1)-C(2) bond of chemisorbed acetone produces bidentate formates and bidentate acetates (R<sub>Carboxylate</sub>), which are removed as CO in the gas phase (R<sub>Formate</sub> and R<sub>Acetate</sub>, respectively). Finally, part of the CO can be further oxidized to CO<sub>2</sub> in the gas phase (R<sub>CO2</sub>). The reoxidation reactions of the catalyst are represented by equations R<sub>V-OH</sub> and R<sub>O2</sub>, where the reversible recombination of V-OH forming H<sub>2</sub>O, V-O and V-□ sites and the irreversible dissociative chemisorption of O<sub>2</sub> from the gas phase are involved, respectively.

### Catalyst Reduction Steps



### Catalyst Reoxidation Steps



**Scheme 3.5.1.** Propane ODH reaction mechanism proposed in previous works (*Sections 3.3 and 3.4*). (V-O), (V-OH) and (V- $\square$ ) represent lattice oxygens (V-O-V or V-O-Zr bonds), protonated lattice oxygens, and vacancies in the  $\text{VO}_x$  lattice, respectively.

Molar balance equations of plug-flow reactor (Eq. (5)) have been used for the interpretation of the experimental catalytic data determining the intrinsic kinetic parameters for the catalysts studied in this work.

$$-\frac{1}{P_{\text{C}_{3,0}}} \cdot \frac{dP_i}{d\left(\frac{W_{\text{Cat}}}{F_{\text{C}_{3,0}}}\right)} = r_j \quad (5)$$

where the space-time is expressed as  $W_{\text{Cat}}/F_{\text{C}_{3,0}}$  (ratio between catalyst weight and the inlet propane flow); and  $P_{\text{C}_{3,0}}$  and  $P_i$  are the partial pressures of initial propane and  $i$  reactant/product. It was possible to simplify the molar balance equation of the fixed-bed reactor into the one for the ideal plug-flow reactor (Eq. (5)) because the following conditions were accomplished for all the catalysts: homogeneous distribution of active sites on the catalyst surface (as indicated in the characterization section and explained in more detail in the previous works ([23,24] or *Sections 3.1 and 3.2*)); axial dispersion and wall effects were discarded since the diameter of the fibers (submicron size) were several orders smaller than the length and diameter of the fixed-bed reactor; the reactor operated at steady-state conditions; diffusional constraints and transport limitations were discarded (as proven in a previous work using the same experimental procedure ([23] or *Section*

3.1)); and changes in temperature and pressure within the reactor were neglected.

The combination of the molar balances (Eq. (5)) of oxygen, propane, propylene, carbon monoxide and carbon dioxide with the rate equations (Eqs. (3)-(11) in (Section 3.4)) deduced from the proposed elementary steps gives rises to the following system of differential equations (Section 3.4):

$$-\frac{1}{P_{C3,o}} \cdot \frac{dP_{O2}}{d\left(\frac{W_{cat}}{F_{C3,o}}\right)} = k_{O2} \cdot P_{O2} \cdot \theta_{V-\square}^2 \quad (6)$$

$$-\frac{1}{P_{C3,o}} \cdot \frac{dP_{C3}}{d\left(\frac{W_{cat}}{F_{C3,o}}\right)} = k_{C3} \cdot P_{C3} \cdot \theta_{V-O}^2 \quad (7)$$

$$\frac{1}{P_{C3,o}} \cdot \frac{dP_{C3=}}{d\left(\frac{W_{cat}}{F_{C3,o}}\right)} = \frac{k_{C3=}^{\rightarrow}}{k_{C3=}^{\rightarrow} + k_{Acetone}} \cdot \left( k_{C3} \cdot P_{C3} - \frac{k_{Acetone}}{k_{C3=}^{\rightarrow}} \cdot k_{App,C3=} \cdot P_{C3=} \cdot \left( \frac{\theta_{V-OH}}{\theta_{V-O}} \right) \right) \cdot \theta_{V-O}^2 \quad (8)$$

$$\frac{1}{P_{C3,o}} \cdot \frac{dP_{CO}}{d\left(\frac{W_{cat}}{F_{C3,o}}\right)} = \frac{3 \cdot k_{Acetone}}{k_{C3=}^{\rightarrow} + k_{Acetone}} \cdot \left( k_{C3} \cdot P_{C3} + k_{App,C3=} \cdot P_{C3=} \cdot \left( \frac{\theta_{V-OH}}{\theta_{V-O}} \right) \right) \cdot \theta_{V-O}^2 - k_{CO2} \cdot P_{CO} \cdot \theta_{V-O}^2 \quad (9)$$

$$\frac{1}{P_{C3,o}} \cdot \frac{dP_{CO2}}{d\left(\frac{W_{cat}}{F_{C3,o}}\right)} = k_{CO2} \cdot P_{CO} \cdot \theta_{V-O}^2 \quad (10)$$

where  $P_{O2}$ ,  $P_{C3}$ ,  $P_{C3=}$ ,  $P_{CO}$  and  $P_{CO2}$  are the partial pressures of oxygen, propane, propylene, carbon monoxide and carbon dioxide, respectively. Arrhenius and Van't Hoff laws have been considered to determine the dependence on temperature of the kinetic and equilibrium constants, respectively.  $k_{O2}$  is the rate constant of the dissociative chemisorption of gas phase oxygen on the vacancies in the  $VO_x$  lattice ( $V-\square$ ) to reoxidize the catalyst ( $RO_2$ ).  $k_{C3}$  is the rate constant of the propane activation via dissociative chemisorption on the  $VO_x$  lattice ( $V-O$ ) forming isopropoxide and  $V-OH$  bonds ( $RC_3$ ).  $k_{C3=}^{\rightarrow}$  and  $k_{App,C3=}^{\leftarrow}$  are the forward and apparent reverse rate constants, respectively, of the reversible reaction of adsorbed propylene formation ( $RC_3=$ ).  $k_{App,C3=}^{\leftarrow}$  combines the equilibrium constant of propylene adsorption ( $Ads_{C3=}$ ),  $K_{C3=}$ , and the reverse rate constant of the reversible reaction of adsorbed propylene formation,  $k_{C3=}^{\leftarrow}$ .  $k_{Acetone}$  is the



rate constant of the formation rate of chemisorbed acetone from isopropoxide ( $R_{\text{Acetone}}$ ), which will produce CO in next steps.  $k_{\text{CO}_2}$  is the rate constant of the oxidation rate of CO to form  $\text{CO}_2$ .  $\theta_{\text{V-O}}$ ,  $\theta_{\text{V-}\square}$  and  $\theta_{\text{V-OH}}$  are the surface coverages of V-O, V- $\square$  and V-OH sites, and the mathematical expressions to calculate their values as a function of rate constants and partial pressures ( $P_{\text{C}_3}$ ,  $P_{\text{C}_3=}$ ,  $P_{\text{CO}}$  and  $P_{\text{O}_2}$ ) have been deduced in a previous work (Section 3.4). The same for the expressions of  $\theta_{\text{Isopropoxide}}$ ,  $\theta_{\text{Formate}}$  and  $\theta_{\text{Acetate}}$ , which represent the surface coverages of isopropoxide, formate and acetate species.

### 3.5.3.2. Kinetic study

The system of differential equations corresponding to the molar balance of oxygen, propane, propylene, carbon monoxide and carbon dioxide (Eqs. (6)-(10), respectively) has been numerically solved with each set of proposed kinetic parameters, considering integral packed fixed-bed reactor behaviour and Arrhenius and Van't Hoff laws, in order to calculate the exit partial pressure of each reactant/product, as well as the surface coverage of each adsorbed species participating in the reaction mechanism by using the Eqs. (23-28) in Section 3.4. Subsequently, the simulated values of propane conversion, selectivity and yield to propylene, CO and  $\text{CO}_2$  were calculated with Eqs. (1)-(3). The kinetic parameters were estimated by a modified Runge–Kutta method combined with an optimization routine based on the Levenberg–Marquardt algorithm implemented in Matlab R2016b software to minimize the *error* function:

$$\text{error} = \sum_k \left( \sqrt{(Y_{\text{exp,C}_3=k} - Y_{\text{sim,C}_3=k})^2} + \sqrt{(Y_{\text{exp,CO},k} - Y_{\text{sim,CO},k})^2} + \sqrt{(Y_{\text{exp,CO}_2,k} - Y_{\text{sim,CO}_2,k})^2} \right) \quad (11)$$

where  $Y_{\text{exp},i,k}$  and  $Y_{\text{sim},i,k}$  are the experimental and simulated yield to the compound  $i$  for the experiment  $k$ . Table 3.5.2 shows the preexponential factors and activation energies for all the reaction steps involved in the proposed propane ODH reaction mechanism and for all the catalysts studied in this work. Note that  $k_{\text{Formate}}$  and  $k_{\text{Acetate}}$  are the rate constants of the evolution rates of formate and acetate species in form of CO in the

gas phase ( $R_{\text{Formate}}$  and  $R_{\text{Acetate}}$ , respectively), while  $k_{V-OH}$  is the rate constant of the dehydration reaction between two V-OH sites ( $R_{V-OH}$ ). Figure 3.5.1 depicts the simulated values of propane conversion or selectivity to compound  $i$  ( $X_{sim}$  or  $S_{sim,i}$ , respectively) versus the ones experimentally obtained ( $X_{exp}$  or  $S_{exp,i}$ , respectively) for each catalyst. It can be observed that the simulated values are quite similar to the experimental data, with *error* function values of 0.216, 0.231, 0.020 and 0.037 for the catalysts F-PZr-V6.4, F-PZr-V5.0, F-PZr-V2.5 and F-AZr-V0.8-Mo4.3, respectively, which validates both the reaction mechanism and the kinetic model proposed in the previous works (Sections 3.3 and 3.4). The error function values of F-PZr-V6.4 and F-PZr-V5.0 present around one magnitude order higher than those of F-PZr-V2.5 and F-AZr-V0.8-Mo4.3, probably due to the fact that the former catalysts have propane conversions approximately one magnitude order higher than the latter catalysts for the studied conditions. It can be observed in Figure 3.5.1 that the propylene selectivity values obtained for the catalysts F-PZr-V2.5 and F-AZr-V0.8-Mo4.3 are generally higher than for F-PZr-V6.4 and F-PZr-V5.0, which also leads to lower CO and almost negligible CO<sub>2</sub> selectivity values, probably due to the lower propane conversions obtained for the former catalysts.

**Table 3.5.2.** Estimated kinetic parameters for the propane ODH reaction of the different catalysts studied: F-PZr-V6.4, F-PZr-V5.0, F-PZr-V2.5 and F-AZr-V0.8-Mo4.3.

	F-PZr-V6.4		F-PZr-V5.0		F-PZr-V2.5		F-AZr-V0.8-Mo4.3	
	$k_{o,j}$	${}^fE_{a,j}$	$k_{o,j}$	${}^fE_{a,j}$	$k_{o,j}$	${}^fE_{a,j}$	$k_{o,j}$	${}^fE_{a,j}$
$k_{V-OH}$	<sup>e</sup> 2.83·10 <sup>9</sup>	55.7	<sup>e</sup> 2.05·10 <sup>8</sup>	93.5	<sup>e</sup> 1.91·10 <sup>9</sup>	143.7	<sup>e</sup> 1.36·10 <sup>9</sup>	147.0
$k_{O_2}$	<sup>a</sup> 3.74·10 <sup>2</sup>	60.1	<sup>a</sup> 2.86·10 <sup>5</sup>	97.9	<sup>a</sup> 1.90·10 <sup>5</sup>	104.4	<sup>a</sup> 3.61·10 <sup>9</sup>	158.6
$k_{C_3}$	<sup>b</sup> 8.14·10 <sup>3</sup>	96.0	<sup>b</sup> 3.35·10 <sup>4</sup>	104.1	<sup>b</sup> 1.42·10 <sup>4</sup>	112.3	<sup>b</sup> 3.33·10 <sup>3</sup>	117.7
$k_{\frac{C_3}{C_3=}}$	<sup>e</sup> 9.41·10 <sup>12</sup>	71.3	<sup>e</sup> 2.31·10 <sup>13</sup>	91.2	<sup>e</sup> 1.17·10 <sup>12</sup>	105.9	<sup>e</sup> 1.85·10 <sup>14</sup>	132.9
$k_{App,\frac{C_3}{C_3=}}$	<sup>c</sup> 8.18·10 <sup>11</sup>	67.3	<sup>c</sup> 6.06·10 <sup>12</sup>	112.0	<sup>c</sup> 8.27·10 <sup>10</sup>	113.9	<sup>c</sup> 2.83·10 <sup>13</sup>	160.6
$k_{Acetone}$	<sup>e</sup> 5.29·10 <sup>8</sup>	68.3	<sup>e</sup> 1.83·10 <sup>9</sup>	86.1	<sup>e</sup> 8.28·10 <sup>7</sup>	100.2	<sup>e</sup> 1.03·10 <sup>9</sup>	116.0
$k_{Formate}$	<sup>e</sup> 1.04·10 <sup>9</sup>	121.7	<sup>e</sup> 1.63·10 <sup>10</sup>	140.4	<sup>e</sup> 9.31·10 <sup>7</sup>	146.6	<sup>e</sup> 5.24·10 <sup>7</sup>	147.2
$k_{Acetate}$	<sup>e</sup> 1.85·10 <sup>7</sup>	130.4	<sup>e</sup> 3.80·10 <sup>11</sup>	180.5	<sup>e</sup> 9.03·10 <sup>10</sup>	192.5	<sup>e</sup> 2.63·10 <sup>9</sup>	193.8
$k_{CO_2}$	<sup>d</sup> 6.27·10 <sup>1</sup>	60.0	<sup>d</sup> 1.89·10 <sup>6</sup>	115.7	<sup>d</sup> 1.24·10 <sup>6</sup>	119.8	<sup>d</sup> 1.58·10 <sup>7</sup>	158.7
<i>error</i>		0.216	<i>error</i>	0.231	<i>error</i>	0.020	<i>error</i>	0.037

<sup>a</sup> (mol·s<sup>-1</sup>·g<sup>-1</sup>·atm<sup>-1</sup>O<sub>2</sub>)  
<sup>b</sup> (mol·s<sup>-1</sup>·g<sup>-1</sup>·atm<sup>-1</sup>C<sub>3</sub>H<sub>6</sub>)  
<sup>c</sup> (mol·s<sup>-1</sup>·g<sup>-1</sup>·atm<sup>-1</sup>C<sub>3</sub>H<sub>6</sub>)  
<sup>d</sup> (mol·s<sup>-1</sup>·g<sup>-1</sup>·atm<sup>-1</sup>CO)  
<sup>e</sup> (mol·s<sup>-1</sup>·g<sup>-1</sup>)  
<sup>f</sup> (kJ·mol<sup>-1</sup>)

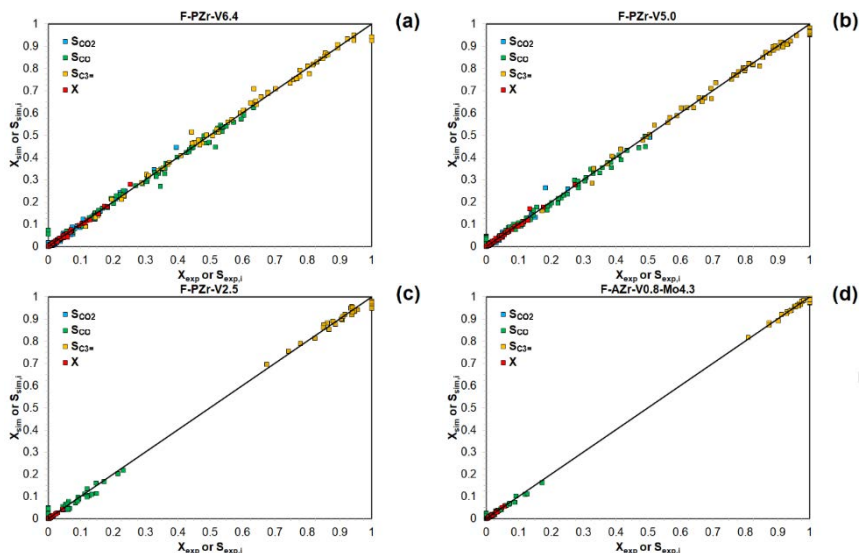


**Figure 3.5.1.** Simulated propane conversion and selectivity to propylene, CO or CO<sub>2</sub> ( $X_{sim}$  and  $S_{sim,i}$ , respectively) versus their respective conversion and selectivity experimentally obtained ( $X_{exp}$  and  $S_{exp,i}$ , respectively) for the different catalysts studied: (a) F-PZr-V6.4, (b) F-PZr-V5.0, (c) F-PZr-V2.5 and (d) F-AZr-V0.8-Mo4.3.

It can be observed that the vanadium concentration in the catalyst and/or the addition of molybdenum to the sample have a great influence in all the kinetic parameters, suggesting that both determine the intrinsic catalytic activity of the catalyst. It is noteworthy that the activation energy should not be affected by the variation of the vanadium concentration unless it involved a change in the active sites or in the environment that surrounds them. However, the preexponential factor will be determined by the nature of the catalyst and will also be proportional to the surface area and total concentration of active sites ([26] and Section 3.4). This means that if the increase of the concentration of the active sites did not involve a change in the nature of the catalyst, the activation energy would be constant and the preexponential factor would proportionally change to that concentration increase and to the variation of the surface area. However, Table 3.5.1 shows an increase of the activation energy values of all reaction steps as the vanadium concentration decreases and/or molybdenum is added to the catalyst. With respect to the preexponential factors, they seem to present a more complex dependence, and except for  $k_{O,V-OH}$ , there is an increase from F-PZr-V2.5 to F-PZr-V5.0 that could be related to the higher vanadium

concentration; and a decrease from F-PZr-V5.0 to F-PZr-V6.4 that could be related to the agglomeration of dispersed vanadia to form more condensed structures [27], which results in the exposure of less active sites as well as different active sites with different intrinsic catalytic activity. This is coherent with the Raman results obtained for these samples in a previous paper ([23] or *Section 3.1*), where incipient  $ZrV_2O_7$  was observed in detriment of dispersed  $VO_x$  species in F-PZr-V6.4. It should be noted that the differences among the preexponential factors in F-PZr-V6.4, F-PZr-V5.0 and F-PZr-V2.5 are not related to the BET surface areas, since these latter values are similar for these catalysts, unlike for F-AZr-V0.8-Mo4.3 that is much lower (Table 3.5.1). On the other hand, the variation observed when molybdenum is added in the preexponential factors with respect to the catalysts free of Mo does not follow a clear trend, being  $k_{o,i}$  increased or decreased depending on the reaction steps. This suggests that the nature of F-AZr-V0.8-Mo4.3 is very different compared to F-PZr-V2.5, F-PZr-V5.0 and F-PZr-V6.4, as it can be supported by the Raman spectra of F-AZr-V0.8-Mo4.3 obtained in a previous work ([24] or *Section 3.2*), where the presence of dispersed  $MoO_x$  and V-Mo-O phases were also detected.

It should be noted that all the kinetic parameters (activation energies and preexponential factors) have an influence in the overall catalytic activity, selectivity and surface coverage of adsorbed species and vanadium sites. However, some of them will have more repercussion in some characteristics of the catalyst than in others. The kinetic parameters associated to the RDS will be the ones that have more influence in the overall catalytic activity of the catalyst. Since the propane activation step is usually considered as the RDS for propane ODH reaction,  $Ea_{C_3}$  is the kinetic parameter more used to compare the catalysts in the literature [7,8], although it can be found a wide range of values among similar catalysts. This broad range of values could be due to the different vanadium concentrations, supports and/or added dopants, as well as the different kinetics models used [7,8,11,18,21,27–40], which are sometimes oversimplified and/or frequently inconsistent and incorrect without physical

relevance, as in the case of the Mars-van Krevelen expression [41]. In this work, the  $Ea_{C_3}$  presents values of 96.0, 104.1, 112.3 and 117.7 kJ·mol<sup>-1</sup> for the catalysts F-PZr-V6.4, F-PZr-V5.0, F-PZr-V2.5 and F-AZr-V0.8-Mo4.3, respectively, which are within the range of those reported for catalysts of vanadium oxide dispersed on ZrO<sub>2</sub> [7,8]. The increase of  $Ea_{C_3}$  suggests a decrease of the intrinsic catalytic activity, and therefore a change in the active sites and/or in the environment that surrounds them, as the vanadium concentration is lower and/or molybdenum is added to the sample. According to the characterization of these samples in a before article ([23] or *Section 3.1*), there is a decrease in the proportion of polyvanadates with respect to monovanadates as the vanadium concentration in the sample decreases. These results suggest that polyvanadates present lower  $Ea_{C_3}$  than monovanadates, and then, a higher catalytic activity. Nevertheless, some discrepancies can be found in the literature about the activity of these species, it has been reported that polyvanadates are more, less or equally actives than monovanadates [7,20,21]. With respect to F-AZr-V0.8-Mo4.3, the lower vanadium concentration and the presence of dispersed MoO<sub>x</sub> and V-Mo-O phases detected in the Raman spectra ([24] or *Section 3.2*) could be related to its higher  $Ea_{C_3}$ , and in turn, to the possible lower catalytic activity with respect to the other catalysts. It should be also noted that  $Ea_{C_3}$  is always higher than  $Ea_{O_2}$  for the V-Zr-O catalysts, which is in agreement with the deductions made according to the *operando* results obtained in the previous work (*Section 3.3*). However,  $Ea_{C_3}$  is lower than  $Ea_{O_2}$  in the V-Mo-Zr-O catalyst, suggesting the different catalytic nature of the active surface species present on the Mo-containing catalyst with respect to those free of Mo.

The selectivity of each catalyst could be mainly determined by the kinetic parameters associated to the rate constants  $k_{\xrightarrow{C_3=}}$ ,  $k_{App,\xleftarrow{C_3=}}$ ,  $k_{V-OH}$  and  $k_{Acetone}$ . The observed increase of their respective activation energy values ( $Ea_{\xrightarrow{C_3=}}$ ,  $Ea_{App,\xleftarrow{C_3=}}$ ,  $Ea_{V-OH}$  and  $Ea_{Acetone}$ , respectively) as the vanadium concentration is lower and/or molybdenum is added to the sample will directly affect decreasing the reaction rates of the propylene formation, the

propylene adsorption and reaction with a V-OH site to form isopropoxide species, the dehydration reaction to remove the V-OH sites, and the chemisorbed acetone formation (precursor of CO production), respectively. The relative changes of these kinetic parameters among the studied catalysts will mainly determine the relative differences of their selectivity results. From the data shown in Table 3.5.1, it can be derived that  $k_{\xrightarrow{C_3=}}$  is always several magnitude orders higher than  $k_{Acetone}$  in the range of studied temperatures (300-480°C), being the ratio  $k_{\xrightarrow{C_3=}} / (k_{\xrightarrow{C_3=}} + k_{Acetone})$  always between 0.99 and 1.00 and higher as the temperature increases, since  $Ea_{\xrightarrow{C_3=}} > Ea_{Acetone}$  for all the catalysts. These results indicate that the direct combustion of propane presents a negligible contribution with respect to the consecutive combustion of the formed propylene, which is in agreement with results reported elsewhere [7,8,40]. Therefore, the selectivity of the catalysts will be mainly determined by the term  $k_{App, \overleftarrow{C_3=}} \cdot P_{C_3=} \cdot \left( \frac{\theta_{V-OH}}{\theta_{V-O}} \right)$  associated to the propylene adsorption that appears in the molar balances of propylene and CO (Eqs. (8) and (9), respectively).  $P_{C_3=}$  will depend on the conversion and in turn also on  $k_{C_3=}$ , while  $\left( \frac{\theta_{V-OH}}{\theta_{V-O}} \right)$  will mainly depend on  $k_{V-OH}$ ,  $k_{C_3=}$  and  $P_{C_3=}$  (Eq. (26.1) in Section 3.4). This means that, according to the above equations, higher conversions and/or propane partial pressures will promote the propylene adsorption, with the subsequent decrease of the selectivity. It should be reminded that  $k_{App, \overleftarrow{C_3=}}$  is a combination between the equilibrium constant of propylene adsorption ( $K_{C_3=}$ ) and the reverse rate constant of the reversible reaction of adsorbed propylene formation ( $k_{\xrightarrow{C_3=}}$ ). It is interesting to note that  $Ea_{App, \overleftarrow{C_3=}}$  for F-PZr-V6.4 and F-AZr-V0.8-Mo4.3 are markedly lower and higher, respectively, than the very similar values showed by F-PZr-V5.0 and F-PZr-V2.5. It seems that the presence of incipient  $ZrV_2O_7$  promotes the adsorption of propylene with respect to polyvanadate and monovanadate species, while V-Mo-O phases avoid such adsorption improving the propylene selectivity as was already reported in a previous work ([24] or Section 3.2). On the

other hand, the lower values of  $Ea_{V-OH}$  in F-PZr-V6.4 and F-PZr-V5.0 with respect to F-PZr-V2.5 and F-AZr-V0.8-Mo4.3 will result in faster removal rates of V-OH sites in the former catalysts, and then decreasing the surface concentration of sites where adsorbed propylene can react to form isopropoxide, what could increase the selectivity. It seems that higher surface density of vanadia species promote the dehydration reaction between two V-OH sites. Then, although F-PZr-V5.0 and F-PZr-V2.5 present very similar values of  $Ea_{App, C_3=}$ , F-PZr-V5.0 could be more selective at isoconversion values than F-PZr-V2.5, due to its lower value of  $Ea_{V-OH}$ , suggesting that polyvanadates could be more selective than monovanadates.

The rate constants associated to the CO and CO<sub>2</sub> formation steps are  $k_{Formate}$ ,  $k_{Acetate}$  and  $k_{CO_2}$ . Their main contribution is related to the surface coverages of formate and acetate species for  $k_{Formate}$  and  $k_{Acetate}$ , respectively, and to the CO/CO<sub>2</sub> product ratio for  $k_{CO_2}$ . The corresponding activation energies of these rate constants ( $Ea_{Formate}$ ,  $Ea_{Acetate}$  and  $Ea_{CO_2}$ ) are the highest values of each catalyst, and are higher as the vanadium concentration decreases and/or when molybdenum is added to the sample. This means that, the CO<sub>2</sub> formation will tend to occur mainly at high temperatures and in more extent in Mo-free-catalysts with high vanadium concentrations. It seems evident the different nature of the active sites in F-PZr-V6.4 and F-AZr-V0.8-Mo4.3 compared to F-PZr-V5.0 and F-PZr-V2.5, since  $Ea_{CO_2}$  is much lower for F-PZr-V6.4 and much higher for F-AZr-V0.8-Mo4.3, indicating that incipient ZrV<sub>2</sub>O<sub>7</sub> would promote the CO oxidation to CO<sub>2</sub> in comparison with dispersed mono/poly VO<sub>x</sub> species, while V-Mo-O phases would be much less active for such oxidation step. With respect to the surface coverages of formate and acetate species, the high activation energies for their evolution will result in low values of their respective rate constants ( $k_{Formate}$  and  $k_{Acetate}$ , respectively), being both significantly smaller than  $k_{Acetone}$  (by more than 10<sup>4</sup> times) and probably resulting in appreciable surface coverages of formate and acetate adsorbed species according to Eqs. (24) and (25) in Section 3.4 and previous spectroscopic

results (Section 3.3). It can be also observed as  $Ea_{Acetate}$  is always higher than  $Ea_{Formate}$  in all the samples, as also deduced in a previous work (Section 3.3), which denotes the higher thermal stability of acetate species than formate species on the catalyst surface [42,43]. This difference between  $Ea_{Formate}$  and  $Ea_{Acetate}$  is significantly smaller in F-PZr-V6.4 than for the other catalysts. This could be due to the more condensed vanadia species found in F-PZr-V6.4, which results in a high surface density of vanadia species that can easily supply the necessary lattice oxygen to oxidize the acetate species, unlike the evolution of formate species that do not require lattice oxygen. However, the other catalysts that present a lower surface density of vanadia species could relatively present more difficulties to oxidize acetate species than formate species, resulting in higher difference between  $Ea_{Formate}$  and  $Ea_{Acetate}$ .

The reoxidation of the catalyst will be determined by the rate constants  $k_{V-OH}$  and  $k_{O_2}$ . It can be derived that  $k_{V-OH}$  and  $k_{O_2}$  are always several orders greater than the rate constant corresponding to the RDS ( $k_{C_3}$ ) for all the studied catalysts, which means that  $\theta_{V-OH}$  and  $\theta_{V-\square}$  could be smaller than  $\theta_{V-O}$  under most of the reaction conditions according to Eqs. (26)-(28) in Section 3.4 and in agreement with previous results (Section 3.3). Moreover, it can be predicted negligible values of  $\theta_{Isopropoxide}$  for all the catalysts according to the Eq. (23) in Section 3.4, since  $k_{\frac{\rightarrow}{C_3=}}$  and  $k_{Acetone}$  are always more than  $10^5$  times greater than  $k_{C_3}$ , as expected taking into account previous *operando* results (Section 3.3). In addition, it can be observed as the activation energy value for F-PZr-V6.4 is much lower than for the other catalysts, suggesting that as the surface density of vanadia species is higher, the reoxidation reactions could be faster. This seems coherent since each of these two reactions steps involve two vanadium sites (two V-OH or two V- $\square$  sites in  $R_{V-OH}$  or  $R_{O_2}$ , respectively), and therefore, the reaction could be promoted if such sites are closer. This could explain the greater difficulty in reoxidizing the catalyst containing 2.5 wt. % of vanadium with respect to the other with higher vanadium content observed in previous *operando* results (Section 3.3). It should be also noted



that, there is a significant increase of the  $Ea_{O_2}$  from F-PZr-V2.5 (104.4 kJ·mol<sup>-1</sup>) to F-AZr-V0.8-Mo4.3 (158.6 kJ·mol<sup>-1</sup>), which is in agreement with the slower mobility of molybdena species than vanadia species reported in the literature [44], due to the higher Tamman temperature of molybdenum oxide with respect to vanadium oxide. It can be derived that the mobility of these species presents a great influence on the required migration of such species during the dissociative chemisorption of O<sub>2</sub>, which could be similarly extrapolated for the dissociative chemisorption of propane step as well. This could also have a certain influence on the different activity observed with different metal oxides.

### *3.5.3.3. Influence of space-time and oxygen inlet partial pressure*

Figure 3.5.2 shows that the conversion-selectivity profiles simulated by the kinetic model as a function of space-time and temperature match very well with the experimental results obtained in this work, despite the different broad ranges of conversion and selectivity values given for each catalyst studied. Note that the results showed for the catalysts F-PZr-V6.4, F-PZr-V5.0 and F-PZr-V2.5 (Figure 3.5.2a, 3.5.2b and 3.5.2c, respectively) are obtained in a temperature range of 300-400°C, while those for F-AZr-V0.8-Mo4.3 are obtained at 400-480°C (Figure 3.5.2d) to get conversions in the same magnitude order than for the other catalysts, since the latter one is much less active. For the sake of brevity, the simulated and experimental data of selectivity to CO and CO<sub>2</sub> is not shown (Figure 3.5.1.S in supplementary info). As typical in the propane ODH reaction, the propane conversion is higher as the temperature and/or the space-time increases, and the selectivity to propylene decreases as conversion increases. It can be observed that the highest conversion values are obtained for the catalysts F-PZr-V6.4 and F-PZr-V5.0, which are quite similar (Figure 3.5.2a and 3.5.2b) despite the lower value of  $Ea_{C_3}$  in F-PZr-V6.4. This could be explained by the also lower value of  $k_{o,C_3}$  in F-PZr-V6.4 (Table 3.5.2) due to the agglomeration of vanadia species resulting in a less exposure of active sites. F-PZr-V6.4 always presents significantly lower propylene

selectivity values than F-PZr-V5.0 at isoconversion values and same experimental conditions. It was already mentioned in the before section that F-PZr-V6.4 was expected to be the least selective to propylene, since it presents the lowest value of  $Ea_{App, \xi_{C_3=}}$  (Table 3.5.2), which is related to the propylene adsorption followed by its oxidation. The lowest propane conversion results are obtained with the catalysts F-PZr-V2.5 and F-AZr-V0.8-Mo4.3, being also these conversions very similar among them, although each catalyst have worked at different temperatures (Figure 3.5.2c and 3.5.2d). It can be seen that the propylene selectivity values obtained with F-AZr-V0.8-Mo4.3 are markedly higher than those obtained with F-PZr-V2.5. This could be due to the temperature difference, since it has been reported elsewhere [11,27,32,34] that for isoconversion values, higher temperature leads to higher propylene selectivity values. However, it could be also due to the highest value of  $Ea_{App, \xi_{C_3=}}$  in F-AZr-V0.8-Mo4.3 (Table 3.5.2) that denotes a low contribution of propylene adsorption, which is the main source of  $CO_x$ , as it was explained in the previous section.

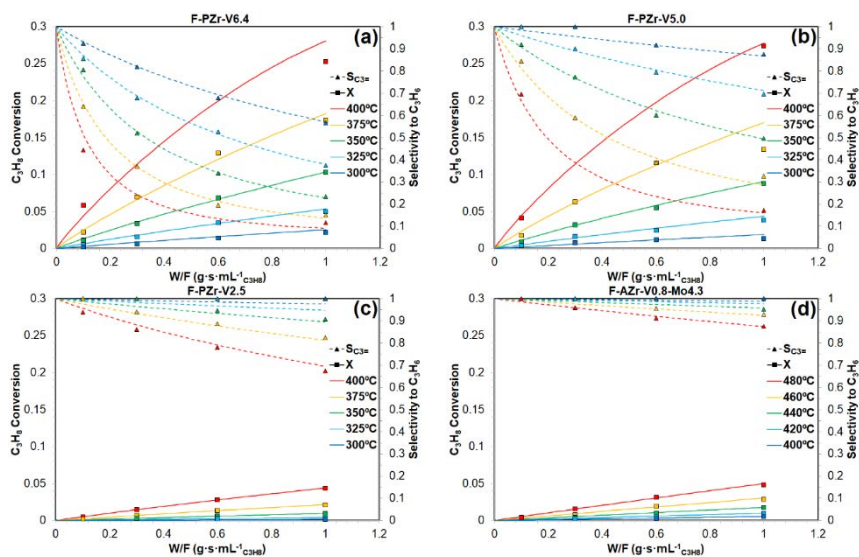


**Figure 3.5.2.** Steady-state (•) propane conversion and (▲) selectivity to propylene for (a) F-PZr-V6.4, (b) F-PZr-V5.0, (c) F-PZr-V2.5 and (d) F-AZr-V0.8-Mo4.3 as a function of space-time and reaction temperature at inlet partial pressures of propane and oxygen of 0.1 atm (symbols: experimental values; lines: simulated values).

The predicted surface coverage values for the different adsorbed species and vanadium sites are depicted as a function of space-time and temperature for each catalyst in Figure 3.5.3. In general, it can be observed that most of the surface is clean of adsorbed species, as expected, since the first proton abstraction from propane is the rate-determining step and the subsequent oxidation steps are kinetically favored. In this way, more than the 90% of the catalyst surface is represented by free sites of V-O and V-□ in all the catalysts and reaction conditions studied in this work. The evolution of the surface species presents a quite complex dependence on the experimental conditions and on the catalyst (i.e. the kinetic parameters that define the catalyst). It can be observed that formate and acetate species are present in different concentrations and proportions on each catalyst, and that their surface coverage values increase as the space-time is longer. However, they have different dependences on the temperature in each sample for the conditions studied. As the temperature increases, in the catalysts F-PZr-V6.4 and F-PZr-V5.0 there is a decrease of acetate and formate species (Figure 3.5.3b and 3.5.3d, respectively), while these species increase in F-PZr-V2.5 and F-AZr-V0.8-Mo4.3 (Figure 3.5.3f and 3.5.3f, respectively). Moreover, it can be observed that the highest surface coverage values of adsorbed species are found in F-PZr-V6.4 and F-PZr-V2.5.  $\theta_{Acetate}$  is higher than  $\theta_{Formate}$  in F-PZr-V6.4 and F-PZr-V5.0 in most of the conditions, and  $\theta_{Acetate}$  is lower than  $\theta_{Formate}$  in F-PZr-V2.5 and F-AZr-V0.8-Mo4.3. These differences observed among the catalysts F-PZr-V6.4, F-PZr-V5.0 and F-PZr-V2.5 are in good accordance with the FTIR and Raman *operando* obtained in a previous work (Section 3.3). According to the surface coverage of V-OH sites, it can be observed that they decrease as space-time and/or temperature is higher, as well as they appear in higher proportion with respect to the other adsorbed species as the vanadium concentration is lower and/or molybdenum is added to the catalyst. This can be due to the dehydration reaction ( $R_{V-OH}$ ) and to the reaction of adsorbed propylene with V-OH sites forming isopropoxide ( $R_{C3=}$ ). Such steps involve the consumption of V-OH sites and are favored in Mo-free-catalysts with high vanadium surface density (as explained in

the before section). Finally, it can be confirmed that isopropoxide species appear in negligible concentrations as expected for all the catalysts studied in this work (Section 3.3) (Figure 3.5.3b, 3.5.3d, 3.5.3f and 3.5.3h).

On the other hand, it can be observed for all the catalysts that there is an increase of the reduction degree along the fixed-bed reactor, evidenced by the loss of V-O bonds in favor of the apparition of V-□ sites as the space-time and/or the temperature is higher. This effect is more obvious in F-PZr-V6.4 and F-PZr-V5.0 (Figure 3.5.3a and 3.5.3c, respectively) than in F-PZr-V2.5 (Figure 3.5.3e) and negligible in F-AZr-V0.8-Mo4.3 (Figure 3.5.3g). Moreover, all the catalysts present a certain reduction degree even when the space-time and propane conversions tends to zero, which means that the catalyst is not always fully oxidized during reaction, in contrast with some works that can be found in the literature for similar catalysts [35,37]. The reduction degree of the catalyst will depend on the reaction conditions and the catalyst, which can be defined by its kinetic parameters. In the case of F-AZr-V0.8-Mo4.3, the reduction degree is always very low ( $\theta_{V-O}$  is always around 0.95) and practically keeps constant with space-time and temperature. The main reason could be the high propylene selectivity that this catalyst presents under these reaction conditions, always around 90% or higher (Figure 3.5.2d), which reduces the oxygen consumption from the catalyst, since the formation of the combustion products ( $CO_x$ ) consume much more lattice oxygen than the solely propylene formation. The propylene formation consumes only one oxygen atom from the  $VO_x$  lattice, while CO and  $CO_2$  formation consumes 7/3 and 10/3, respectively. Then, unlike the catalysts F-PZr-V6.4, F-PZr-V5.0 and F-PZr-V2.5, it can be considered that F-AZr-V0.8-Mo4.3 is almost fully oxidized under a broad range of reaction conditions. The fact that the RDS is second-order with respect to  $\theta_{V-O}$  means that TOF values will be different along the fixed-bed reactor decreasing as the space-time is longer for the catalysts F-PZr-V6.4, F-PZr-V5.0 and F-PZr-V2.5, while it could be relatively constant for F-AZr-V0.8-Mo4.3. Then, it can be concluded that the comparison of TOF values for this reaction could not be rigorous enough to reach solid conclusions

about which catalysts or active species are more active, unless the catalysts are always fully oxidized under reaction conditions, since even for the same experimental conditions the degree of reduction of the catalysts can be very different, and so affecting the TOF value misleading the real differences among the catalysts.

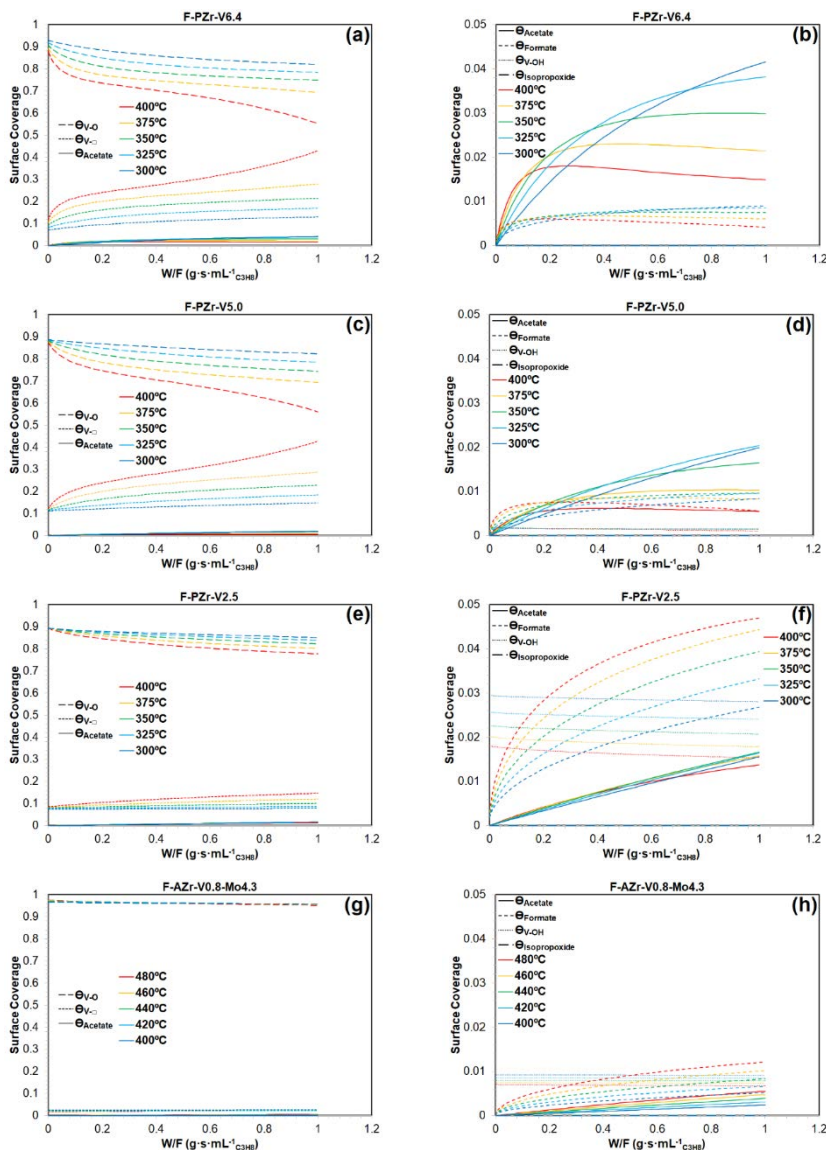


**Figure 3.5.3.** Steady-state surface coverages of V-O, V-O, acetate, formate, V-OH and isopropoxide for (a,b) F-PZr-V6.4, (c,d) F-PZr-V5.0, (e,f) F-PZr-V2.5 and (g,h) F-AZr-V0.8-Mo4.3 as a function of space-time and reaction temperature at inlet partial pressures of propane and oxygen of 0.1 atm.

Figure 3.5.4 represents the simulated and experimental conversion-selectivity profiles, as well as the predicted surface coverages of V-O, V-□ and acetate species, for each catalyst studied in this work as a function of inlet partial pressure of oxygen and temperature. Formate, V-OH and isopropoxide species are shown in Figure 3.5.2 of the supplementary info. There is a good agreement between the experimental and simulated values of conversion and selectivity obtained in the whole range studied of oxygen inlet partial pressures and temperatures. It can be seen that the influence of oxygen on the conversion-selectivity profiles is very strong at low inlet partial pressures. When this partial pressure tends to 0, the conversion and the selectivity tends to 0 and 100%, respectively. This means, as expected, that oxygen in the gas phase is always necessary to perpetuate the catalytic cycle. However, from a relatively low value of inlet partial pressure of oxygen, the conversion and selectivity keep constant having a pseudo-zero order dependence with respect to oxygen. It seems that this turning point has a lower value of oxygen partial pressure as the catalyst presents lower consumption of oxygen for a given conditions (i.e. lower propane conversion and/or higher propylene selectivity values) as can be derived when comparing the catalysts F-PZr-V6.4, F-PZr-V5.0, F-PZr-V2.5 and F-AZr-V0.8-Mo4.3.

The same trends are found for the surface coverages of surface species (Figures 3.5.4b, 3.5.4d, 3.5.4f and 3.5.4h and Figure 3.5.2.S in supplementary info), where a sharply change of the values are observed at low inlet partial pressures of oxygen and then almost constant values are found at higher oxygen inlet partial pressures. As expected, since the catalytic activity and the surface species are interrelated. In fact, the RDS presents a second-order dependence with respect to  $\theta_{V-O}$ . When the catalytic activity shows a pseudo-zero order dependence, it means that  $\theta_{V-O}$  is constant with the oxygen inlet partial pressure, although not necessarily the catalyst must be fully oxidized. Among the samples studied in this work, only F-AZr-V0.8-Mo4.3 could be considered that is fully oxidized in most of the conditions showed.

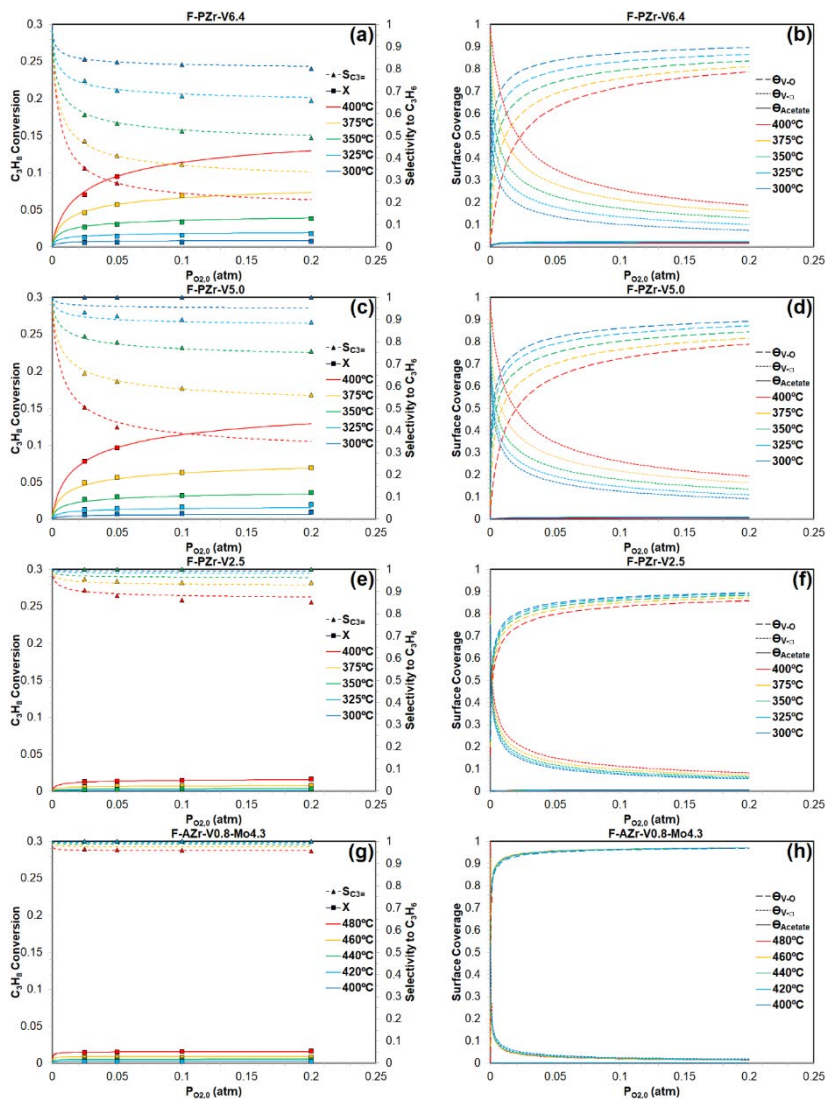


**Figure 3.5.4.** Steady-state propane conversion and selectivity to propylene (a,c,e,g), and surface coverages of V-O, V-O and acetate species (b,d,f,h), for F-PZr-V6.4 (a,b), F-PZr-V5.0 (c,d), F-PZr-V2.5 (e,f) and F-AZr-V0.8-Mo4.3 (g,h) as a function of oxygen inlet partial pressure and reaction temperature at space-time of 0.3 g·s·mL<sup>-1</sup>C<sub>3</sub>H<sub>8</sub> and propane inlet partial pressure of 0.1 atm (symbols: experimental values; lines: simulated values).

### 3.5.3.4. Simulation of yield and productivity to propylene

Simulated and experimental values of selectivity versus conversion at different temperatures have been plotted in Figure 3.5.5 for the catalysts studied. In this way, it can be possible to observe how the selectivity varies with temperature at isoconversion values for each catalyst and to compare

them. It can be checked that the simulation predicts very well the data experimentally obtained. In Figure 3.5.5a the space-time is varied in the range of 0.02-1 g·s·mL<sup>-1</sup>C<sub>3</sub>H<sub>8</sub> and at constant propane inlet partial pressure of 0.1 atm. For these conditions, the catalyst that presents the highest propylene selectivity at isoconversion values is F-AZr-V0.8-Mo4.3, followed by F-PZr-V2.5 and F-PZr-V5.0 with very similar selectivity, and the catalyst with the lowest selectivity is F-PZr-V6.4. The differences in the  $Ea_{App, \overleftarrow{C_{3=}}}$  among these catalysts follow the same trend of these results (Table 3.5.2), being the highest value for F-AZr-V0.8-Mo4.3, intermediate and very similar values for F-PZr-V2.5 and F-PZr-V5.0, and the lowest value for F-PZr-V6.4. Note that the decrease of  $Ea_{App, \overleftarrow{C_{3=}}}$  contributes increasing the propylene adsorption followed by its reaction with V-OH sites to form isopropoxide species. This suggests that the variation of space-time in these experiments specially highlights the  $Ea_{App, \overleftarrow{C_{3=}}}$  value from the adsorption term  $(k_{App, \overleftarrow{C_{3=}}} \cdot P_{C_{3=}} \cdot \left(\frac{\theta_{V-OH}}{\theta_{V-O}}\right))$  in each catalyst, which determines the selectivity. Moreover, it can be derived from Figure 3.5.5a that the selectivity dependence on temperature for these experiments can be different for each catalyst. The selectivity increases at isoconversion values when the temperature is higher in F-PZr-V6.4, conversely to the results observed in F-PZr-V5.0. The selectivity also increases in F-PZr-V2.5 and decreases in F-AZr-V0.8-Mo4.3 at higher temperatures, but the influence of temperature on these two latter catalysts is much lower or almost negligible.



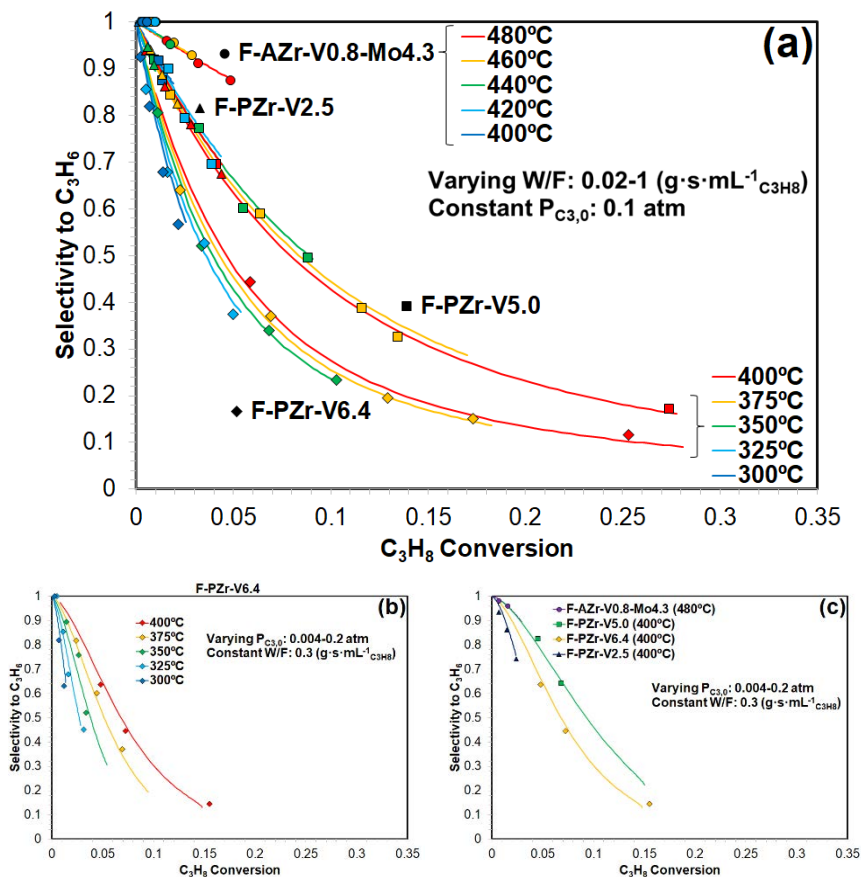


**Figure 3.5.5.** Simulated (lines) and experimental (symbols) values of selectivity to propylene versus propane conversion at different temperatures: (a) varying the space-time from 0.02 to 1.00  $g \cdot s \cdot mL^{-1} C_3H_8$  at inlet partial pressure of propane of 0.1 atm for all the catalysts studied, (b) varying the propane inlet partial pressure from 0.004 to 0.2 atm at space time of 0.3  $g \cdot s \cdot mL^{-1} C_3H_8$  for F-PZr-V6.4, and (c) at 400°C for F-PZr-V6.4, F-PZr-V5.0 and F-PZr-V2.5 and at 480°C for F-AZr-V0.8-Mo4.3. The oxygen inlet partial pressure was always 0.1 atm.

Figure 3.5.5b and 3.5.5c are analogous to Figure 3.5.5a but in this case the propane inlet partial pressure is varied in the range of 0.004-0.2 atm and at constant space-time of 0.3  $g \cdot s \cdot mL^{-1} C_3H_8$ . It can be observed that the selectivity increases for isoconversion values at higher temperatures in F-PZr-V6.4 (Figure 3.5.5b), being this increase of selectivity significantly higher than in Figure 3.5.5a, where the space-time was varied while keeping constant the propane inlet partial pressure. The same has been observed for the other samples studied in this work (Figure 3.5.3.S in supplementary info), even for F-PZr-V5.0 and F-AZr-V0.8-Mo4.3 that presented opposite trends with temperature in Figure 3.5.5a. The

comparison of the selectivity trajectories among the different catalysts, at 400°C for the Mo-free-catalysts and at 480°C for the Mo-containing catalyst, is represented in Figure 3.5.5c. Note that the influence of temperature in F-AZr-V0.8-Mo4.3 is almost negligible and it has been represented the data at 480 instead of 400°C to be able to show higher conversions. In this case, it can be observed that F-AZr-V0.8-Mo4.3 and F-PZr-V5.0 (with similar results) present the highest selectivity at isoconversion values, followed by F-PZr-V6.4 and then by F-PZr-V2.5, which shows the lowest selectivity. It seems that different selectivity trends at isoconversion values can be observed comparing Figure 3.5.5a and Figure 3.5.5c. It is possible that the variation of the propane inlet partial pressure introduces higher influence on the  $P_{C3=}$ ,  $\theta_{V-O}$  and  $\theta_{V-OH}$  values of the adsorption term ( $k_{App, \leftarrow C3=} \cdot P_{C3=} \cdot \left(\frac{\theta_{V-OH}}{\theta_{V-O}}\right)$ ) than the variation of the space-time, as expected according to the Eqs. (26) and (28) in Section 3.4 and to the results showed in such section. Therefore, other rate constants different than  $k_{App, \leftarrow C3=}$ , such as  $k_{\rightarrow C3=}$ ,  $k_{V-OH}$  and  $k_{Acetone}$ , will also be important in the selectivity dependence of each catalyst.

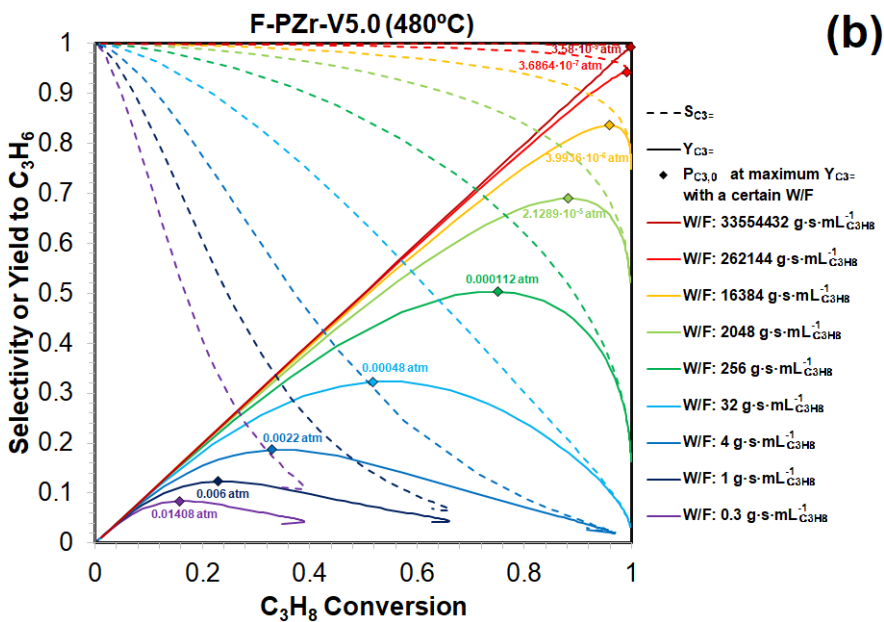
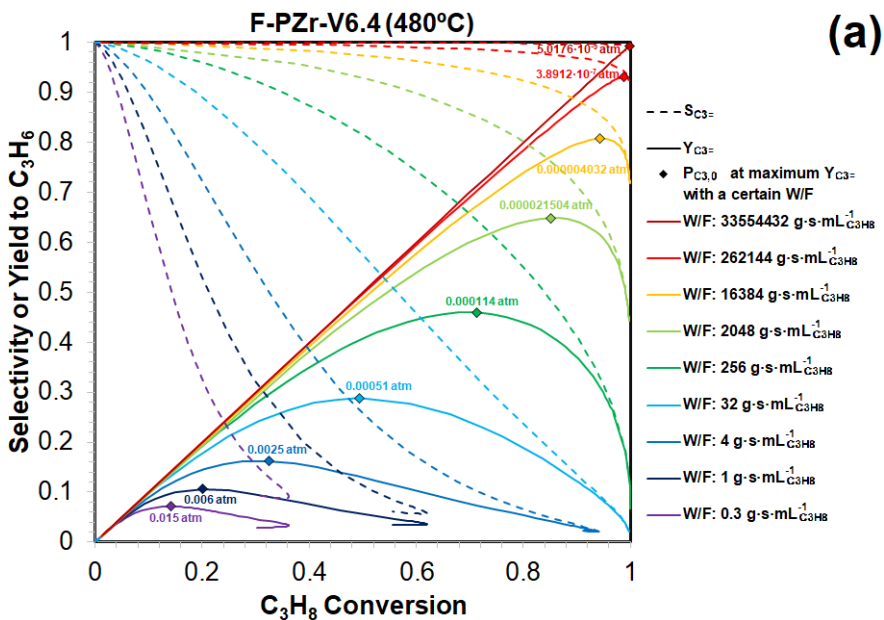
In general, it can be concluded that F-AZr-V0.8-Mo4.3 is always the most selective and the less active catalyst among the samples studied in this work, while F-PZr-V5.0 seems to be the sample with the best ratio of conversion and selectivity. On the other hand, F-PZr-V2.5 can be as selective as F-PZr-V5.0 at isoconversion values when the space-time is varied (Figure 3.5.5a) because of their similar value of  $Ea_{App, \leftarrow C3=}$ , while it can be the catalyst with the least selectivity at isoconversion values when the propane inlet partial pressure is varied, mainly due to the high value of  $Ea_{V-OH}$ , that decreases the dehydration reaction rate of V-OH sites, increasing the value of  $\theta_{V-OH}$  that can react with adsorbed propylene forming isopropoxide. It should be noted that if only Figure 3.5.5a had been showed and not Figure 3.5.5c, a wrong conclusion could have been achieved, since those preliminary results could induce to conclude that F-PZr-V5.0 and F-PZr-V2.5 are equally selective, and then that

polyvanadates present the same selectivity than monovanadates. Generally, it has been reported in the literature that the propylene selectivity of the propane ODH reaction increases with the temperature at isoconversion values due to the higher activation energy to produce propylene than the one for the combustion forming  $\text{CO}_x$  [11,27,32,34]. However, it has been observed that the selectivity dependence on temperature is not so simple as reported in the literature. The propylene selectivity at isoconversion values will usually tend to increase at higher temperatures, but it will also depend on the reaction conditions and on the catalytic properties of the catalyst.

Figure 3.5.6 represents the simulation curves of selectivity and yield to propylene as a function of propane conversion at different space-times and 480°C for all the catalysts studied in this work. For each space-time value, the propane inlet partial pressure has been varied to obtain the curves, from very low propane conversions to total propane or oxygen conversions, and the partial pressure value has been indicated in the point of maximum yield to propylene. When the total conversion of oxygen occurs for a given space-time, the conversion of propane decreases with the increase of the propane inlet partial pressure, as can be observed in the endings of some curves. Note that the oxygen inlet partial pressure has been always 0.1 atm. Surprisingly, the model predicts that all the catalysts can reach yields to propylene quite close to 100%. Such yield values have never been reported before and it seems contradictory to the traditional inverse dependence of the selectivity on conversion that never allows to get so high yields to propylene [6–8]. Very high yields to propylene could be possible due to the different influence of the space-time and the propane inlet partial pressure on the propane conversion and propylene selectivity. This is because an increase of the conversion via increasing the space-time results in a lower selectivity decrease than when the same conversion increase has been obtained increasing the propane inlet partial pressure. Therefore, for a given conversion point, if the space-time is increased to get a higher conversion, a decrease of the propane inlet partial pressure to come back

to the initial conversion will involve a selectivity increase higher than the decrease produced by the previous space-time increase. Then, it can be obtained the same conversion than initially but with higher selectivity, which results in higher yield to propylene. It can be concluded that the successive increase of space-time together with the decrease of the propane inlet partial pressure can result in a higher conversion and selectivity, and so, in higher yield to propylene reaching values close to 100% as can be observed for all the catalysts in Figure 3.5.6.

From the comparison of the simulated results showed in Figure 3.5.6, it seems that all the catalysts can reproduce any desired value of yield to propylene, and that the difference among them is in the required reactions conditions to reach such yield value. Then, the best catalyst would be the one that requires the most affordable conditions to get the desired catalytic result. It can be observed that, for a given space-time value, the highest yields to propylene are always obtained by F-PZr-V5.0, followed by F-PZr-V6.4, then by F-PZr-V2.5 and finally by F-AZr-V0.8-Mo4.3. It can be also seen that the necessary propane inlet partial pressure to get the same maximum propylene yields for a given space-time is always the highest for F-AZr-V0.8-Mo4.3, followed by F-PZr-V2.5, then by F-PZr-V5.0 and finally by F-PZr-V6.4. The same graphics than Figure 3.5.6 but at 400°C show the same differences among the catalysts (Figure 3.5.4.S in supplementary info). It can be checked that lower yield values are obtained at lower temperatures for a given conditions. In general, in all the cases the high yields to propylene could be only obtained at very high space-times and very low propane inlet partial pressures, which would probably result in very low productivity to propylene despite the high yield.



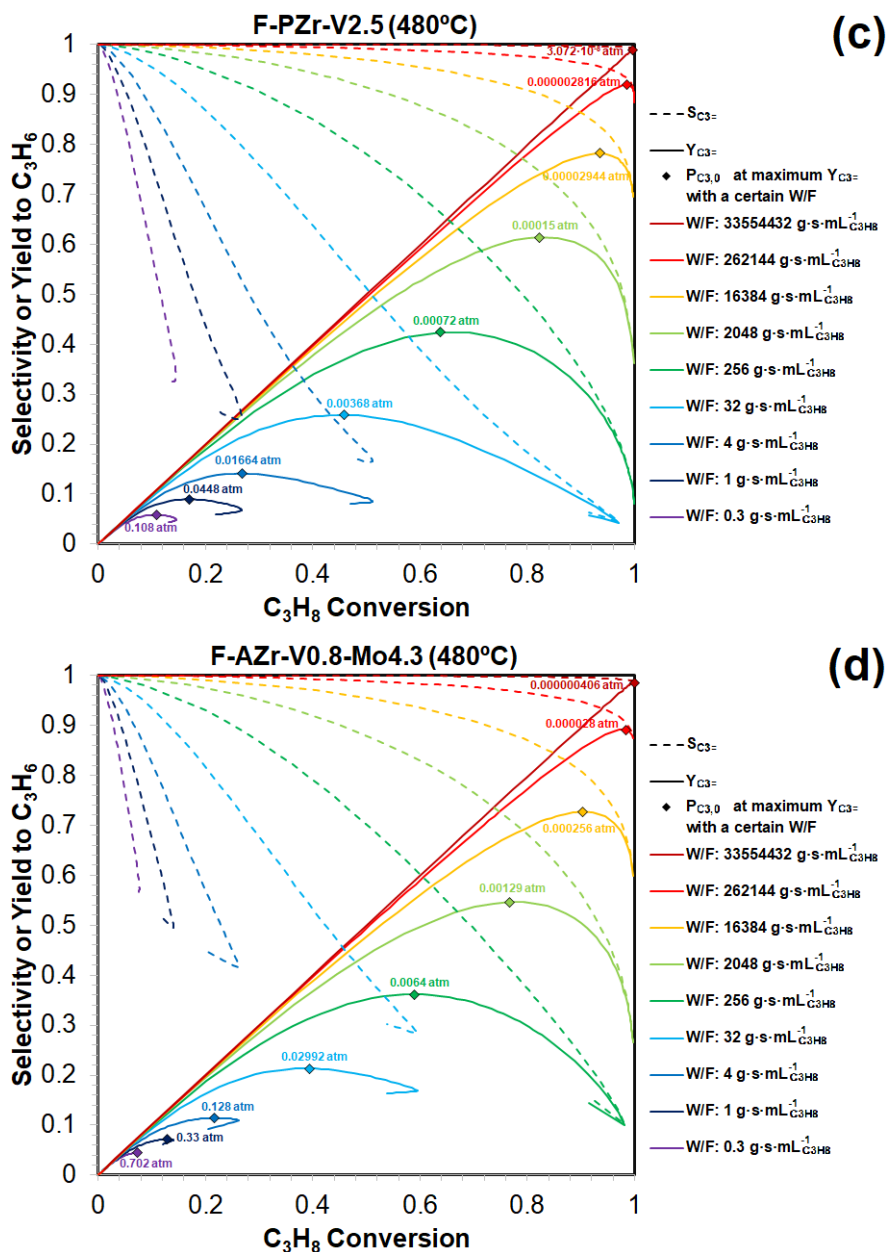
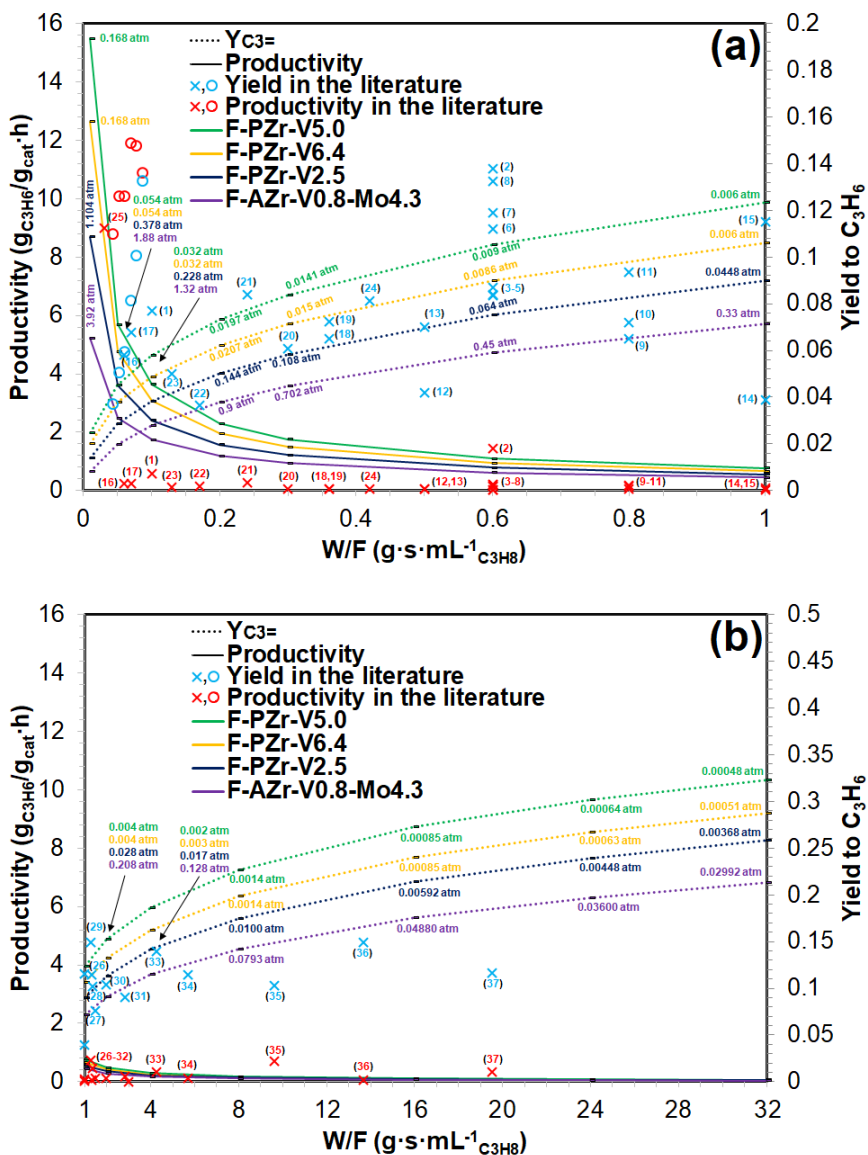


Figure 3.5.6. Simulated selectivity and yield to propylene as a function of propane conversion at different space-times, 0.1 atm of oxygen inlet partial pressure and 480°C for (a) F-PZr-V6.4, (b) F-PZr-V5.0, (c) F-PZr-V2.5 and (d) F-AZr-V0.8-Mo4.3. For each space-time value, the propane inlet partial pressure has been varied and its value has been indicated in the point of maximum yield to propylene.

According to Eq. (4), the productivity to propylene will depend on the inverse of the space-time and on the yield to propylene. Then, the maximum productivity that can be obtained at a given space-time and temperature will correspond to the point of maximum yield, which will be reached at a certain propane inlet partial pressure as represented in Figure 3.5.6. Note that the oxygen inlet partial pressure will also have some influence on the yield/productivity to propylene, but if it is high enough, the dependence would be pseudo-zero order with respect to the oxygen. Figure 3.5.7 simulates the maximum yield and productivity to propylene that can be obtained at different space-times and at 480°C for all the catalysts studied in this work. It has also been indicated the corresponding propane inlet partial pressure used for each point. Moreover, yield and productivity data from the literature (mainly from [6,45,46]) using different catalysts are also represented, and Table 3.5.3 indicates the temperature, catalyst and reference of such experiments. In this way, a proper comparison of the catalytic activity of the different catalysts can be done, instead of using the typical conversion-selectivity plots, which sometimes does not give information enough to state solid conclusions. It should be noted that the results obtained in the literature at 450-500°C (with many different catalysts) follow the same dependency predicted by the kinetic model on yield and productivity values as a function of the reaction conditions for the catalysts studied in this work. This validates the proposed kinetic model to explain the catalytic behavior of most of the catalysts in the propane ODH, and probably in other partial oxidation reactions that follow similar reaction mechanism. Only the catalysts based on elemental boron (represented by “o” dots) presents some significant different trends with respect to the catalysts studied in this work and to those used in the literature, probably because these boron-containing catalysts follow a different mechanism.



**Figure 3.5.7.** Simulation of maximum values of yield and productivity to propylene at different space-times with an oxygen inlet partial pressure of 0.1 atm and at 480°C for F-PZr-V6.4, F-PZr-V5.0, F-PZr-V2.5 and F-AZr-V0.8-Mo4.3. Propane inlet partial pressure corresponding to each point is indicated. Yield and productivity results obtained in the literature between ~450-500°C are also represented (Table 3.5.3). (o) Symbols without numbers represents values for elemental boron catalysts and (x) symbols with numbers for the rest of catalysts.



**Table 3.5.3.** Temperature, catalyst and reference of the data from the literature (mainly from [6,45,46]) represented in Figure 3.5.7.

Number	Temperature (°C)	Catalyst	Reference
1	455	V <sub>2</sub> O <sub>5</sub> -ZrO <sub>2</sub>	[47]
2	500	V/Mg/O	[48]
3	480	V/Mg/Al/O	[49]
4	500	V <sub>2</sub> O <sub>5</sub> -SmVO <sub>4</sub>	[50]
5	450	V/Sm/O	[51,52]
6	500	V-HMS	[53]
7	500	V-HMS	[54]
8	500	V/Sb/O	[55]
9	500	Co/Mo/O-MCM-41	[56]
10	500	MoO <sub>3</sub> /K-ZrO <sub>2</sub>	[57]
11	450	Cr <sub>2</sub> O <sub>3</sub> -Al <sub>2</sub> O <sub>3</sub>	[58]
12	450	Ni/Mo/O+Sb/O+prom N <sub>2</sub> O	[59]
13	500	V/silic. Beta	[60]
14	445	V/Zr/O-PILC	[61]
15	450	Co/Sr/O-hydr. apatite	[62,63]
16	450	V <sub>2</sub> O <sub>5</sub> -Ga <sub>2</sub> O <sub>3</sub>	[64]
17	500	V/Mg/Al/O	[65]
18	500	V <sub>2</sub> O <sub>5</sub> -TiO <sub>2</sub>	[14]
19	500	MoO <sub>3</sub> -Al <sub>2</sub> O <sub>3</sub>	[14]
20	500	V <sub>2</sub> O <sub>5</sub> -ZrO <sub>2</sub>	[20]
21	500	V-MCM-41	[66]
22	500	Ga-USY	[67]
23	470	MoO <sub>3</sub> -Al <sub>2</sub> O <sub>3</sub>	[68]
24	500	MoO <sub>3</sub> -Al <sub>2</sub> O <sub>3</sub>	[69]
25	500	V/Ti/SBA-15	[37]
26	475	V <sub>2</sub> O <sub>5</sub> /K-Al <sub>2</sub> O <sub>3</sub>	[70]
27	500	Ag/Mo/P/O	[71]
28	500	Na-V <sub>2</sub> O <sub>5</sub> /Al <sub>2</sub> O <sub>3</sub>	[72]
29	500	SrVMoO <sub>x</sub> /Al <sub>2</sub> O <sub>3</sub>	[73]
30	500	P <sub>2</sub> O <sub>5</sub> -Nanodiamond	[74]
31	450	Cr <sub>2</sub> O <sub>3</sub> /Al <sub>2</sub> O <sub>3</sub>	[75]
32	450	Ni/Al/O	[76]
33	450	MoO <sub>3</sub> /K-Si-TiO <sub>2</sub>	[77]
34	450	CMK-3	[78]
35	500	Mesoporous NiO	[79]
36	450	NiO-POM	[80]
37	475	Meso-NiMoO <sub>4</sub>	[81]
No number	500	Elemental Boron	[46]

Regarding the simulated values of the catalysts prepared in this work, the results show that the maximum propylene productivity predicted, at a given space-time, exponentially increases as the space-time tends to zero and tends to zero as the space-time tends to infinity. However, in the case of

the propylene yield, the prediction shows that tends to zero as the space-time tend to zero, and tends to 100% as the space-time tends to infinity as shown in Figure 3.5.6. The required propane inlet partial pressure increases as the maximum productivity is higher. The reaction conditions that promote the increase of the productivity (short space-times and high propane inlet partial pressures) would lead to experiments with very low propane conversions and very high propylene selectivity. It should be noted that it can be obtained better yield and productivity values at higher temperature for a given conditions, but it has not been simulated since around 500°C the homogeneous reaction in the gas phase starts to have some contribution ([23,24] or *Sections 3.1 and 3.2*), and this phenomenon has not been considered in the kinetic model used in this work.

The prediction of the here reported yield and productivity dependence has never found or addressed in the literature before. In fact, it has been repeatedly reported over the past 30 years that the main reason of the low industrial interest in the propane ODH is the low yields obtained [6–8], being most of them lower than 30% [6]. On the other hand, maybe the only reason is not due to the low yields, since productivity to propylene is also very important to make the process economically profitable on an industrial scale. The highest productivity found in the literature for transition metal based catalysts is  $9 \text{ g}_{\text{C}_3\text{H}_6} \cdot \text{g}_{\text{cat}}^{-1} \cdot \text{h}^{-1}$  [37]. However, it has been demonstrated that all the catalysts used in this work can reach yields values of 100% or much higher productivity values than  $9 \text{ g}_{\text{C}_3\text{H}_6} \cdot \text{g}_{\text{cat}}^{-1} \cdot \text{h}^{-1}$ , if proper reaction conditions are used. Therefore, it can be concluded that, instead of low yield or productivity values, the main problems of the industrial implementation of the propane ODH reaction could be to optimize the reaction conditions and to find catalysts that can reach the desired values of yield or productivity in affordable conditions, or to find catalysts that simultaneously present high yield and productivity. Unfortunately, the values of productivity and yield to propylene follow different directions for this reaction. The ideal situation would be that both results follow the same direction.

Comparing the simulated yield and productivity values obtained for each catalyst, the catalyst F-PZr-V5.0 always presents the highest yield and productivity values in the whole range of space-times, followed by F-PZr-V6.4, then by F-PZr-V2.5 and finally by F-AZr-V0.8-Mo4.3. Moreover, the necessary propane inlet partial pressures to get the maximum yield in each point becomes higher in the same above order of catalysts. Even higher propane inlet partial pressures than 1 atm could be required for F-AZr-V0.8-Mo4.3 and F-PZr-V2.5. However, despite the higher amounts of propane used in these latter catalysts for each space-time, the amount of propylene obtained is always higher using the catalysts F-PZr-V5.0 and F-PZr-V6.4. It should be noted that most of the results showed in Figure 3.5.6 and Figure 3.5.7 have not been experimentally reproduced, because the best results of yield or productivity require conditions difficult to properly reproduce in the set up used in this study. Since the used mass flow controllers only can work in a limited range of gas flow and do not allow to get very low inlet partial pressures of propane. With respect to the space-time, the dimensions of the reactor are not adequate to hold so large or so small amounts of catalyst keeping the plug-flow reactor behavior. For example, to get yield values close to 100%, it would be necessary a space-time of  $33554432 \text{ g}_{\text{cat}} \cdot \text{s} \cdot \text{mL}^{-1} \text{C}_3\text{H}_8$  and propane inlet partial pressures of  $5.02 \cdot 10^{-9}$ ,  $3.58 \cdot 10^{-9}$ ,  $3.07 \cdot 10^{-8}$  and  $4.06 \cdot 10^{-7}$  atm for F-PZr-V6.4, F-PZr-V5.0, F-PZr-V2.5 and F-AZr-V0.8-Mo4.3, respectively (Figure 3.5.6). If a total flow of 100 mL/min was fixed (very common flow at laboratory scale), the corresponding mass of each catalyst would be 0.281, 0.200, 1.718 and 22.705 g, respectively. It can be observed as the propane inlet partial pressures are too low in all the cases and the mass of catalyst are too high for F-PZr-V2.5 and F-AZr-V0.8-Mo4.3. A redesign of the set up would be necessary to perform this kind of experiments.

It can be concluded that the best catalyst prepared in this work is F-PZr-V5.0, which presents the highest proportion of polyvanadate species without forming crystalline phases of vanadium, because it has the best combination of activity and selectivity. However, F-AZr-V0.8-Mo4.3, which

presents V-Mo-O phases, is the most selective catalyst, but its lower activity results in lower values of yield and productivity to propylene. Perhaps, it could be possible to prepare better catalysts than F-PZr-V5.0 finding the optimum composition of vanadium and molybdenum to combine the high activity of polyvanadate species with the high selectivity of V-Mo-O phases. The presence of other dopant elements to improve the catalyst would not be discarded. Moreover, it can be possible that catalysts close to the optimum composition already exist in the vast propane ODH literature, but maybe the conditions to get the best values of productivity and/or yield have not been found. The kinetic model proposed in the previous work and used in this article could help to find that hypothetical composition and those desired optimum conditions.

#### **3.5.4. Conclusions**

In a previous work, a rigorous kinetic model was proposed for the propane ODH reaction on vanadium oxide-based catalysts according to the FTIR-Raman *operando* results obtained in a before paper. This proposed model has been used to estimate the kinetic parameters and to obtain insights about the structure-activity relationship of the catalysts, as well as to simulate values of conversion, selectivity, yield, productivity and surface coverages of adsorbed species and vanadium sites for the different catalysts prepared in this work. The simulation has satisfactorily predicted the experimental results for a broad range of reaction conditions and results of conversion and selectivity, even though the catalytic behavior of each sample was very different.

It has been observed that the vanadium concentration in the catalyst and/or the addition of molybdenum to the sample have a great influence in all the kinetic parameters, suggesting the presence of different active species and/or environments that surround them. Somehow all the kinetic parameters have influence in the conversion and selectivity of the catalyst. However, the conversion of the catalysts will be mainly determined by the kinetic parameters associated to the dissociative chemisorption of propane

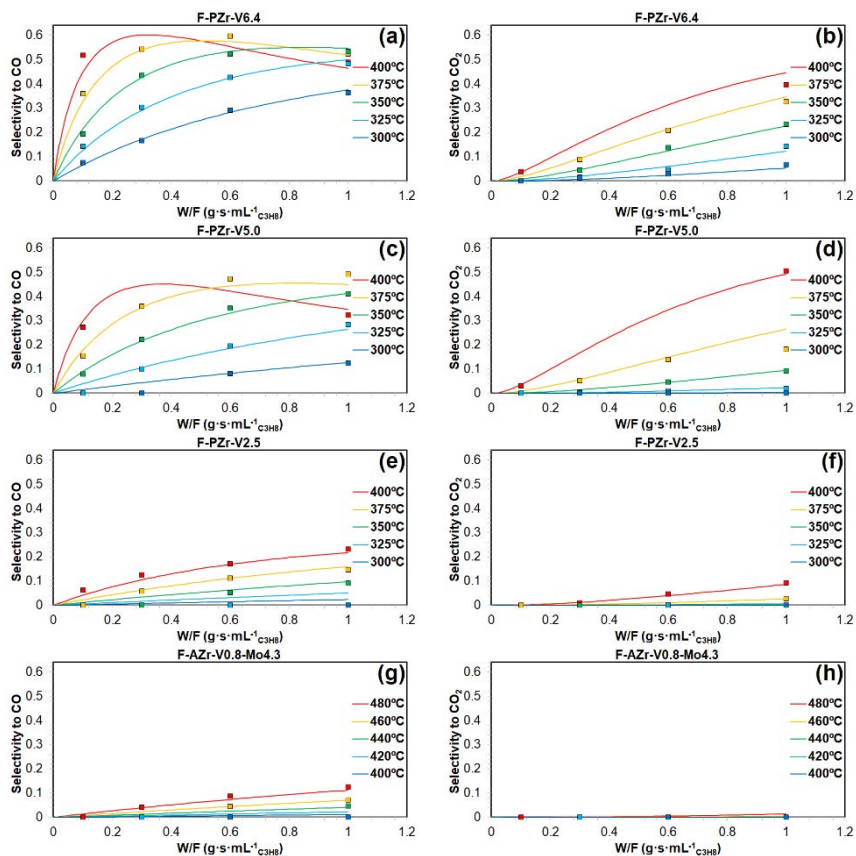
(RDS), while the propylene selectivity will be mainly determined by the kinetic parameters belonging to both the propylene adsorption followed by reaction with V-OH sites forming isopropoxide and the dehydration reaction for the removal of such V-OH sites. According to the results obtained with the catalysts used in this work, polyvanadate species present the best combination of catalytic activity and propylene selectivity. Monovanadate species are slightly less active and selective to propylene than polyvanadate species. The tendency to adsorb propylene of both species are similar, but the slower removal rate of V-OH sites in mono VO<sub>x</sub> structures than in poly VO<sub>x</sub> structures is the responsible for the lower selectivity of monovanadate species. Incipient ZrV<sub>2</sub>O<sub>7</sub> are slightly more active than polyvanadate species, but the fraction of exposed active sites decreases in the former species due to the vanadium agglomeration into more condensed structures. Moreover, incipient ZrV<sub>2</sub>O<sub>7</sub> are less selective than polyvanadate species for propane ODH mainly due to their faster rate of propylene adsorption followed by reaction with V-OH sites forming isopropoxide species. V-Mo-O phases are the least active and the most selective sites among the different active species studied in this work. The slow rate of propylene adsorption followed by reaction with V-OH sites forming isopropoxide species is the responsible for the high selectivity of the latter species.

Using the simulation data obtained from the kinetic model, the propane inlet partial pressure has been optimized for each catalyst to get the highest yield and productivity at 400 and 480°C for a broad range of given space-times and an oxygen inlet partial pressure of 0.1 atm. The catalyst containing the highest proportion of polyvanadate species without forming crystalline phases of ZrV<sub>2</sub>O<sub>7</sub> or V<sub>2</sub>O<sub>5</sub> is the one that presented the best yield and productivity values in the whole range of conditions. However, the sample that also contained V-Mo-O phases was the most selective, but the least active, which resulted in the catalyst with the lowest yield and productivity values in the whole range of conditions. It is possible that V-Mo-O phases in an optimum composition could be the best catalyst, although the

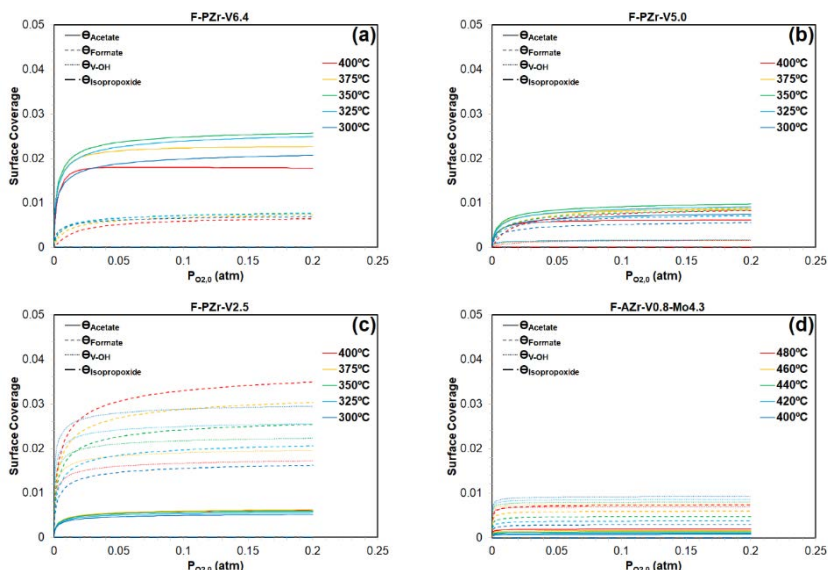
presence of another dopant elements would not be discarded. The idea would be, at least, trying to be as active as the polyvanadate species and as selective as the V-Mo-O phases.

It should be noted that the study of the yield and productivity results found in the literature, for a wide variety of catalysts, followed the same trends predicted by the kinetic model, what validates the proposed kinetic model explaining the catalytic behavior of most of the catalysts in the propane ODH, and probably in other partial oxidation reactions that follow similar reaction mechanism. The predicted yield and productivity values for the catalysts used in this work can be much higher than the values usually found in the literature as long as the reaction is performed under the proper conditions. Therefore, the main problem of the industrial implementation of the propane ODH reaction should not be related to the low yield or productivity values, but to find catalysts that can reach the desired yields and productivities under affordable conditions or to find catalysts that simultaneously present high yield and productivity.

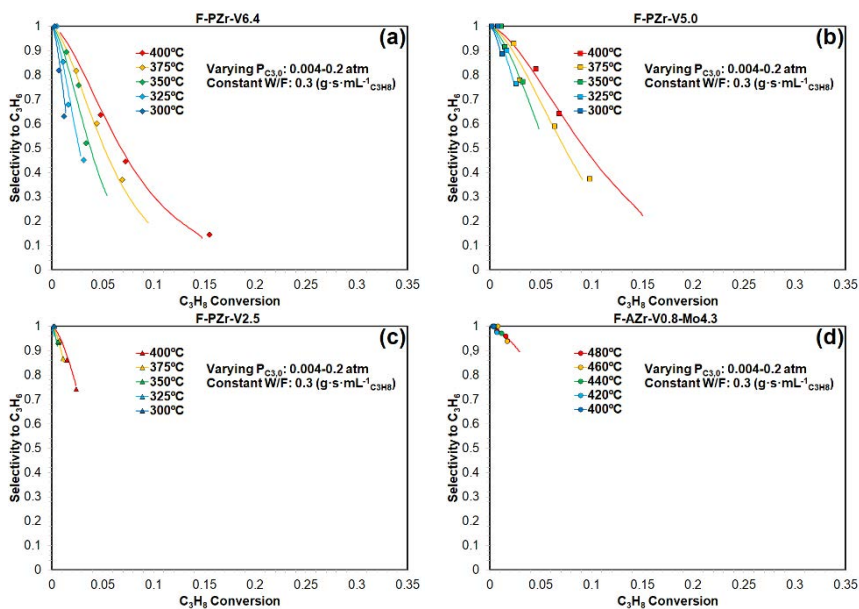
### 3.5.5. Supplementary information



**Figure 3.5.1.S.** Steady-state values of selectivity to (a,c,e,g) CO and (b,d,f,h) CO<sub>2</sub> for (a,b) F-PZr-V6.4, (c,d) F-PZr-V5.0, (e,f) F-PZr-V2.5 and (g,h) F-AZr-V0.8-Mo4.3 as a function of space-time and reaction temperature at inlet partial pressures of propane and oxygen of 0.1 atm (symbols: experimental values; lines: simulated values).

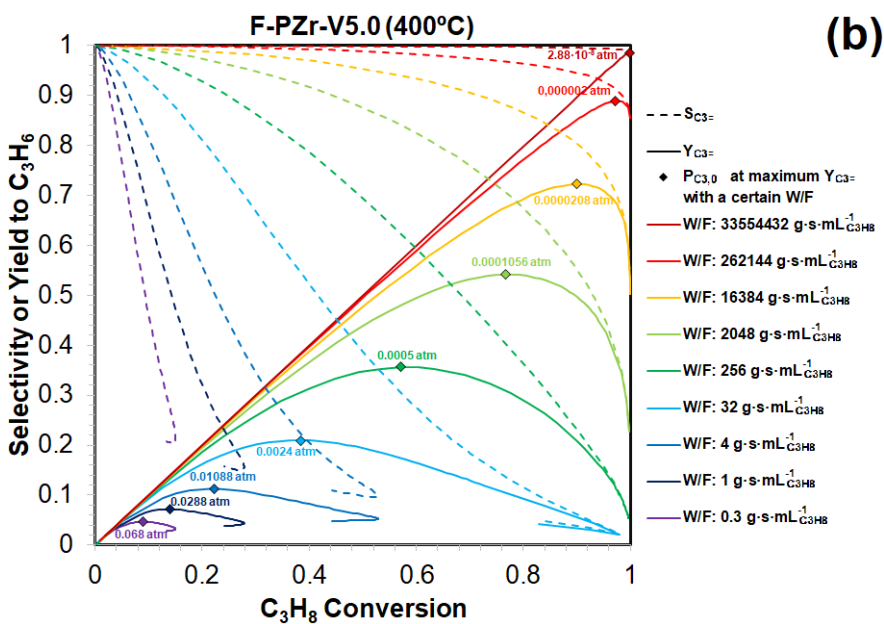
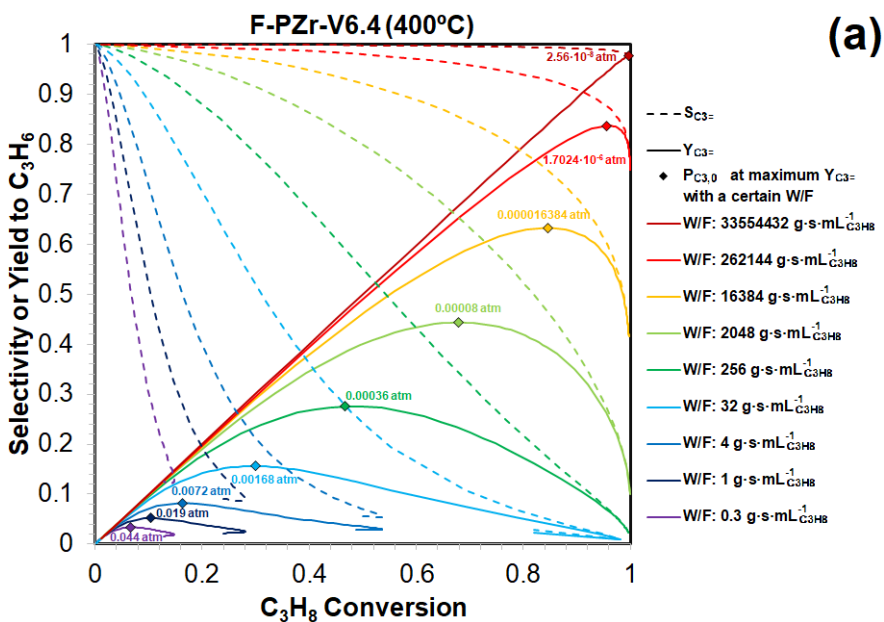


**Figure 3.5.2.S.** Steady-state surface coverages of acetate, formate, V-OH and isopropoxide species for (a) F-PZr-V6.4, (b) F-PZr-V5.0, (c) F-PZr-V2.5 and (d) F-AZr-V0.8-Mo4.3 as a function of oxygen inlet partial pressure and reaction temperature at space-time of  $0.3 \text{ g} \cdot \text{s} \cdot \text{mL}^{-1} \text{C}_3\text{H}_8$  and propane inlet partial pressure of 0.1 atm.



**Figure 3.5.3.S.** Simulated (lines) and experimental (symbols) values of selectivity to propylene versus propane conversion at different temperatures varying the propane inlet partial pressure from 0.004 to 0.2 atm at a space time of  $0.3 \text{ g} \cdot \text{s} \cdot \text{mL}^{-1} \text{C}_3\text{H}_8$  for (a) F-PZr-V6.4, (b) F-PZr-V5.0 and (c) F-PZr-V2.5 and (d) F-AZr-V0.8-Mo4.3. The oxygen inlet partial pressure was always 0.1 atm.





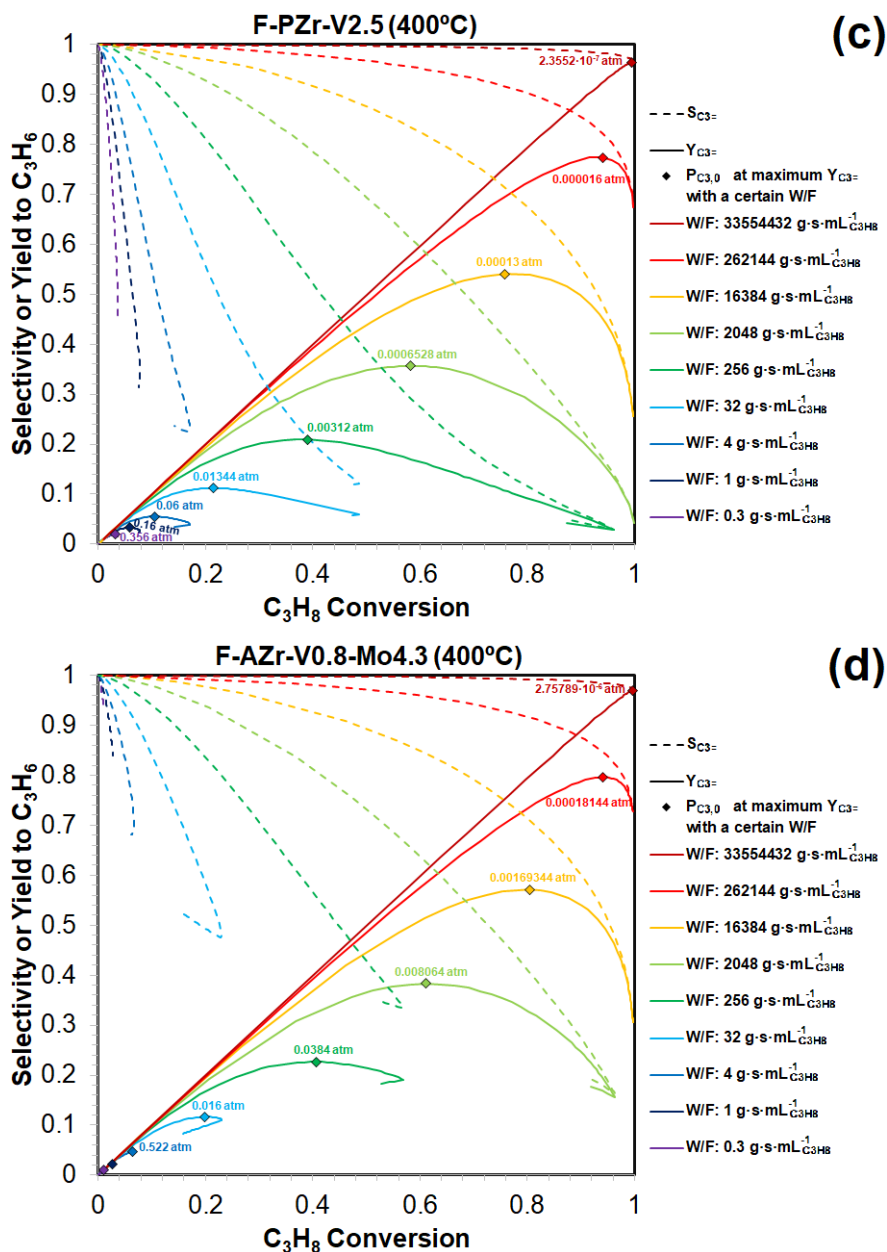


**Figure 3.5.4.S.** Simulated selectivity and yield to propylene as a function of propane conversion at different space-times, 0.1 atm of oxygen inlet partial pressure and 400°C for (a) F-PZr-V6.4, (b) F-PZr-V5.0, (c) F-PZr-V2.5 and (d) F-AZr-V0.8-Mo4.3. For each space-time value, the propane inlet partial pressure has been varied and its value has been indicated in the point of maximum yield to propylene.

## Acknowledgements

This work was supported by the Spanish Ministry of Economy and Competitiveness and FEDER [CTQ-2012-36408 and CTQ-2015-68654-R]. C.Tsao acknowledges the support of the Erasmus Mundus Action-2 Strand-2 (EMA2/S2) EURASIACAT project. J.J.T.H. acknowledges the assistance of the Ministry of Economy and Competitiveness of Spain for the award of a FPI Grant [BES-2013-064425].

## 3.5.6. References

- [1] J. Lazonby, Propene (Propylene), (n.d.).  
<http://www.essentialchemicalindustry.org/chemicals/propene.html>  
(accessed June 3, 2019).
- [2] The Propylene Gap: How Can It Be Filled?, Am. Chem. Soc. (n.d.).  
<https://www.acs.org/content/acs/en/pressroom/cutting-edge-chemistry/the-propylene-gap-how-can-it-be-filled.html> (accessed June 3, 2019).
- [3] A. Agarwal, D. Sengupta, M. El-Halwagi, Sustainable Process Design Approach for On-Purpose Propylene Production and Intensification, ACS Sustain. Chem. Eng. 6 (2018) 2407–2421.  
<https://doi.org/10.1021/acssuschemeng.7b03854>.
- [4] A. Akah, M. Al-Ghrami, Maximizing propylene production via FCC technology, Appl. Petrochem. Res. 5 (2015) 377–392.  
<https://doi.org/10.1007/s13203-015-0104-3>.
- [5] I. Amghizar, L.A. Vandewalle, G. Van, G.B. Marin, New Trends in Olefin Production, 3 (2017) 171–178.  
<https://doi.org/10.1016/J.ENG.2017.02.006>.
- [6] F. Cavani, N. Ballarini, A. Cericola, Oxidative dehydrogenation of ethane and propane: How far from commercial implementation?, Catal. Today. 127 (2007) 113–131.  
<https://doi.org/10.1016/j.cattod.2007.05.009>.
- [7] C.A. Carrero, R. Schloegl, I.E. Wachs, R. Schomaecker, Critical Literature Review of the Kinetics for the Oxidative Dehydrogenation

- of Propane over Well-Defined Supported Vanadium Oxide Catalysts, *ACS Catal.* 4 (2014) 3357–3380. <https://doi.org/10.1021/cs5003417>.
- [8] R. Grabowski, Kinetics of Oxidative Dehydrogenation of C2-C3 Alkanes on Oxide Catalysts, *Catal. Rev.* 48 (2006) 199–268. <https://doi.org/10.1080/01614940600631413>.
- [9] Y. Shan, Z. Sui, Y. Zhu, D. Chen, X. Zhou, Effect of steam addition on the structure and activity of Pt–Sn catalysts in propane dehydrogenation, *Chem. Eng. J.* 278 (2015) 240–248. <https://doi.org/10.1016/j.cej.2014.09.107>.
- [10] A. Corma, J.M. López-Nieto, N. Paredes, M. Pérez, Y. Shen, H. Cao, S.L. Suib, Oxidative Dehydrogenation Of Propane Over Supported-Vanadium Oxide Catalysts, in: P. Ruiz, B. Delmon (Eds.), *Stud. Surf. Sci. Catal.*, Elsevier, 1992: pp. 213–220. [https://doi.org/10.1016/S0167-2991\(08\)61673-0](https://doi.org/10.1016/S0167-2991(08)61673-0).
- [11] B. Frank, A. Dinse, O. Ovsitser, E.V. Kondratenko, R. Schomäcker, Mass and heat transfer effects on the oxidative dehydrogenation of propane (ODP) over a low loaded VOx/Al2O3 catalyst, *Appl. Catal. Gen.* 323 (2007) 66–76. <https://doi.org/10.1016/j.apcata.2007.02.006>.
- [12] Y.-M. Liu, Y. Cao, K.-K. Zhu, S.-R. Yan, W.-L. Dai, H.-Y. He, K.-N. Fan, Highly efficient VOx/SBA-15 mesoporous catalysts for oxidative dehydrogenation of propane, *Chem. Commun.* 0 (2002) 2832–2833. <https://doi.org/10.1039/B208177F>.
- [13] Y.-M. Liu, Y. Cao, N. Yi, W.-L. Feng, W.-L. Dai, S.-R. Yan, H.-Y. He, K.-N. Fan, Vanadium oxide supported on mesoporous SBA-15 as highly selective catalysts in the oxidative dehydrogenation of propane, *J. Catal.* 224 (2004) 417–428. <https://doi.org/10.1016/j.jcat.2004.03.010>.
- [14] E. Heracleous, M. Machli, A.A. Lemonidou, I.A. Vasalos, Oxidative dehydrogenation of ethane and propane over vanadia and molybdena supported catalysts, *J. Mol. Catal. Chem.* 232 (2005) 29–39. <https://doi.org/10.1016/j.molcata.2005.01.027>.

- [15] M. Høj, T. Kessler, P. Beato, A.D. Jensen, J.-D. Grunwaldt, Structure, activity and kinetics of supported molybdenum oxide and mixed molybdenum–vanadium oxide catalysts prepared by flame spray pyrolysis for propane OHD, *Appl. Catal. Gen.* 472 (2014) 29–38. <https://doi.org/10.1016/j.apcata.2013.11.027>.
- [16] E.M. Thorsteinson, T.P. Wilson, F.G. Young, P.H. Kasai, The oxidative dehydrogenation of ethane over catalysts containing mixed oxides of molybdenum and vanadium, *J. Catal.* 52 (1978) 116–132. [https://doi.org/10.1016/0021-9517\(78\)90128-8](https://doi.org/10.1016/0021-9517(78)90128-8).
- [17] M.O. Guerrero-Pérez, Supported, bulk and bulk-supported vanadium oxide catalysts: A short review with an historical perspective, *Catal. Today.* 285 (2017) 226–233. <https://doi.org/10.1016/j.cattod.2017.01.037>.
- [18] A. Khodakov, J. Yang, S. Su, E. Iglesia, A.T. Bell, Structure and properties of vanadium oxide-zirconia catalysts for propane oxidative dehydrogenation, *J. Catal.* 177 (1998) 343–351. <https://doi.org/10.1006/jcat.1998.2143>.
- [19] P. Mars, D.W. van Krevelen, Oxidations carried out by means of vanadium oxide catalysts, *Chem. Eng. Sci.* 3 (1954) 41–59. [https://doi.org/10.1016/S0009-2509\(54\)80005-4](https://doi.org/10.1016/S0009-2509(54)80005-4).
- [20] A. Christodoulakis, M. Machli, A.A. Lemonidou, S. Boghosian, Molecular structure and reactivity of vanadia-based catalysts for propane oxidative dehydrogenation studied by in situ Raman spectroscopy and catalytic activity measurements, *J. Catal.* 222 (2004) 293–306. <https://doi.org/10.1016/j.jcat.2003.10.007>.
- [21] A. Khodakov, B. Olthof, A.T. Bell, E. Iglesia, Structure and Catalytic Properties of Supported Vanadium Oxides: Support Effects on Oxidative Dehydrogenation Reactions, *J. Catal.* 181 (1999) 205–216. <https://doi.org/10.1006/jcat.1998.2295>.
- [22] A.S. Sandupatla, S.C. Nayak, C. Sivananda, G. Deo, DFT investigation into the experimentally observed influence of oxide support in the ODH of propane over supported vanadia catalysts, *Catal. Today.* (2019). <https://doi.org/10.1016/j.cattod.2018.05.058>.

- [23] J.J. Ternero-Hidalgo, J. Torres-Liñán, M.O. Guerrero-Pérez, J. Rodríguez-Mirasol, T. Cordero, Electrospun vanadium oxide based submicron diameter fiber catalysts. Part I: Preparation procedure and propane ODH application, *Catal. Today*. (2018). <https://doi.org/10.1016/j.cattod.2018.10.073>.
- [24] J.J. Ternero-Hidalgo, M.O. Guerrero-Pérez, J. Rodríguez-Mirasol, T. Cordero, Electrospun vanadium oxide based submicron diameter fiber catalysts. Part II: Effect of chemical formulation and dopants, *Catal. Today*. (2018). <https://doi.org/10.1016/j.cattod.2018.10.072>.
- [25] E. Reichelt, M.P. Heddrich, M. Jahn, A. Michaelis, Fiber based structured materials for catalytic applications, *Appl. Catal. Gen.* 476 (2014) 78–90. <https://doi.org/10.1016/j.apcata.2014.02.021>.
- [26] M.A. Vannice, *Kinetics of catalytic reactions*, Springer, New York, 2005.
- [27] S. Chakraborty, S.C. Nayak, G. Deo, TiO<sub>2</sub>/SiO<sub>2</sub> supported vanadia catalysts for the ODH of propane, *Catal. Today*. 254 (2015) 62–71. <https://doi.org/10.1016/j.cattod.2015.01.047>.
- [28] E.V. Kondratenko, M. Cherian, M. Baerns, D. Su, R. Schlögl, X. Wang, I.E. Wachs, Oxidative dehydrogenation of propane over V/MCM-41 catalysts: comparison of O<sub>2</sub> and N<sub>2</sub>O as oxidants, *J. Catal.* 234 (2005) 131–142. <https://doi.org/10.1016/j.jcat.2005.05.025>.
- [29] A. Dinse, B. Frank, C. Hess, D. Habel, R. Schomäcker, Oxidative dehydrogenation of propane over low-loaded vanadia catalysts: Impact of the support material on kinetics and selectivity, *J. Mol. Catal. Chem.* 289 (2008) 28–37. <https://doi.org/10.1016/j.molcata.2008.04.007>.
- [30] B.Y. Jibril, S.M. Al-Zahrani, A.E. Abasaheed, R. Hughes, Propane oxidative dehydrogenation on Cs-doped Cr-Mo-Al-O catalyst: kinetics and mechanism, *Chem. Eng. J.* 103 (2004) 59–67. <https://doi.org/10.1016/j.cej.2004.03.006>.
- [31] M. Baldi, E. Finocchio, C. Pistarino, G. Busca, Evaluation of the mechanism of the oxy-dehydrogenation of propane over

- manganese oxide, *Appl. Catal. Gen.* 173 (1998) 61–74. [https://doi.org/10.1016/S0926-860X\(98\)00129-X](https://doi.org/10.1016/S0926-860X(98)00129-X).
- [32] K. Routray, K.R.S.K. Reddy, G. Deo, Oxidative dehydrogenation of propane on V<sub>2</sub>O<sub>5</sub>/Al<sub>2</sub>O<sub>3</sub> and V<sub>2</sub>O<sub>5</sub>/TiO<sub>2</sub> catalysts: understanding the effect of support by parameter estimation, *Appl. Catal. Gen.* 265 (2004) 103–113. <https://doi.org/10.1016/j.apcata.2004.01.006>.
- [33] A. Bottino, G. Capannelli, A. Comite, S. Storace, R. Di Felice, Kinetic investigations on the oxidized hydrogenation of propane over vanadium supported on  $\gamma$ -Al<sub>2</sub>O<sub>3</sub>, *Chem. Eng. J.* 94 (2003) 11–18. [https://doi.org/10.1016/S1385-8947\(03\)00003-2](https://doi.org/10.1016/S1385-8947(03)00003-2).
- [34] M.D. Argyle, K. Chen, A.T. Bell, E. Iglesia, Effect of Catalyst Structure on Oxidative Dehydrogenation of Ethane and Propane on Alumina-Supported Vanadia, *J. Catal.* 208 (2002) 139–149. <https://doi.org/10.1006/jcat.2002.3570>.
- [35] D. Creaser, B. Andersson, Oxidative dehydrogenation of propane over V-Mg-O: kinetic investigation by nonlinear regression analysis, *Appl. Catal. Gen.* 141 (1996) 131–152. [https://doi.org/10.1016/0926-860X\(96\)00029-4](https://doi.org/10.1016/0926-860X(96)00029-4).
- [36] S.L.T. Andersson, Kinetic study of the oxidative dehydrogenation of propane over vanadia supported on amorphous AlPO<sub>4</sub>, *Appl. Catal. Gen.* 112 (1994) 209–218. [https://doi.org/10.1016/0926-860X\(94\)80220-3](https://doi.org/10.1016/0926-860X(94)80220-3).
- [37] C. Carrero, M. Kauer, A. Dinse, T. Wolfram, N. Hamilton, A. Trunschke, R. Schlögl, R. Schomäcker, High performance (VO<sub>x</sub>)<sub>n</sub>–(TiO<sub>x</sub>)<sub>m</sub>/SBA-15 catalysts for the oxidative dehydrogenation of propane, *Catal. Sci. Technol.* 4 (2014) 786–794. <https://doi.org/10.1039/C3CY00625E>.
- [38] S. Zhang, H. Liu, Oxidative dehydrogenation of propane over Mg-V-O oxides supported on MgO-coated silica: Structural evolution and catalytic consequence, *Appl. Catal. Gen.* 573 (2019) 41–48. <https://doi.org/10.1016/j.apcata.2019.01.012>.
- [39] J.N. Michaels, D.L. Stern, R.K. Grasselli, Oxidative dehydrogenation of propane over Mg-V-Sb-oxide catalysts. II. Reaction kinetics and

- mechanism, *Catal. Lett.* 42 (1996) 139–148.  
<https://doi.org/10.1007/BF00810679>.
- [40] A. Dinse, S. Khennache, B. Frank, C. Hess, R. Herbert, S. Wrabetz, R. Schlögl, R. Schomäcker, Oxidative dehydrogenation of propane on silica (SBA-15) supported vanadia catalysts: A kinetic investigation, *J. Mol. Catal. Chem.* 307 (2009) 43–50.  
<https://doi.org/10.1016/j.molcata.2009.03.008>.
- [41] M.A. Vannice, An analysis of the Mars–van Krevelen rate expression, *Catal. Today.* 123 (2007) 18–22.  
<https://doi.org/10.1016/j.cattod.2007.02.002>.
- [42] E. Finocchio, G. Busca, V. Lorenzelli, R.J. Willey, FTIR studies on the selective oxidation and combustion of light hydrocarbons at metal oxide surfaces. Propane and propene oxidation on MgCr<sub>2</sub>O<sub>4</sub>, *J. Chem. Soc. Faraday Trans.* 90 (1994) 3347–3356.  
<https://doi.org/10.1039/FT9949003347>.
- [43] E. Finocchio, G. Busca, V. Lorenzelli, V.S. Escribano, FTIR studies on the selective oxidation and combustion of light hydrocarbons at metal oxide surfaces. Part 2.—Propane and propene oxidation on Co<sub>3</sub>O<sub>4</sub>, *J. Chem. Soc. Faraday Trans.* 92 (1996) 1587–1593.  
<https://doi.org/10.1039/FT9969201587>.
- [44] K. Chen, A.T. Bell, E. Iglesia, Kinetics and Mechanism of Oxidative Dehydrogenation of Propane on Vanadium, Molybdenum, and Tungsten Oxides, *J. Phys. Chem. B.* 104 (2000) 1292–1299.  
<https://doi.org/10.1021/jp9933875>.
- [45] L. Shi, Y. Wang, B. Yan, W. Song, D. Shao, A.-H. Lu, Progress in selective oxidative dehydrogenation of light alkanes to olefins promoted by boron nitride catalysts, *Chem. Commun.* 54 (2018) 10936–10946. <https://doi.org/10.1039/C8CC04604B>.
- [46] J.T. Grant, W.P. McDermott, J.M. Venegas, S.P. Burt, J. Micka, S.P. Phivilay, C.A. Carrero, I. Hermans, Boron and Boron-Containing Catalysts for the Oxidative Dehydrogenation of Propane, *ChemCatChem.* 9 (2017) 3622–3622.  
<https://doi.org/10.1002/cctc.201701473>.



- [47] C.L. Pieck, M.A. Bañares, J.L.G. Fierro, Propane oxidative dehydrogenation on VOx/ZrO<sub>2</sub> catalysts, *J. Catal.* 224 (2004) 1–7. <https://doi.org/10.1016/j.jcat.2004.02.024>.
- [48] E.V. Kondratenko, O.V. Buyevskaya, M. Baerns, Characterisation of vanadium-oxide-based catalysts for the oxidative dehydrogenation of propane to propene, *Top. Catal.* 15 (2001) 175–180. <https://doi.org/10.1023/A:1016649731881>.
- [49] R. Dula, K. Wcisło, J. Stoch, B. Grzybowska, E.M. Serwicka, F. Kooli, K. Bahranowski, A. Gawęł, Layered double hydroxide-derived vanadium catalysts for oxidative dehydrogenation of propane: Influence of interlayer-doping versus layer-doping, *Appl. Catal. Gen.* 230 (2002) 281–291. [https://doi.org/10.1016/S0926-860X\(02\)00041-8](https://doi.org/10.1016/S0926-860X(02)00041-8).
- [50] B.P. Barbero, L.E. Cadus, Vanadium species: Sm-V-O catalytic system for oxidative dehydrogenation of propane, *Appl. Catal. Gen.* 244 (2003) 235–249. [https://doi.org/10.1016/S0926-860X\(02\)00568-9](https://doi.org/10.1016/S0926-860X(02)00568-9).
- [51] B.P. Barbero, L.E. Cadus, Evaluation and characterization of Sm-V-O catalytic system for propane oxydehydrogenation: Sm<sub>2</sub>O<sub>3</sub>-impregnated V<sub>2</sub>O<sub>5</sub> catalysts, *Appl. Catal. Gen.* 234 (2002) 245–258. [https://doi.org/10.1016/S0926-860X\(02\)00228-4](https://doi.org/10.1016/S0926-860X(02)00228-4).
- [52] B.P. Barbero, L.E. Cadus, V<sub>2</sub>O<sub>5</sub>–SmVO<sub>4</sub> mechanical mixture: oxidative dehydrogenation of propane, *Appl. Catal. Gen.* 237 (2002) 263–273. [https://doi.org/10.1016/S0926-860X\(02\)00336-8](https://doi.org/10.1016/S0926-860X(02)00336-8).
- [53] R. Zhou, Y. Cao, S. Yan, K. Fan, Rare earth (Y, La, Ce)-promoted V-HMS mesoporous catalysts for oxidative dehydrogenation of propane, *Appl. Catal. Gen.* 236 (2002) 103–111. [https://doi.org/10.1016/S0926-860X\(02\)00281-8](https://doi.org/10.1016/S0926-860X(02)00281-8).
- [54] R. Zhou, Y. Cao, S. Yan, J. Deng, Y. Liao, B. Hong, Oxidative Dehydrogenation of Propane over Mesoporous HMS Silica Supported Vanadia, *Catal. Lett.* 75 (2001) 107–112. <https://doi.org/10.1023/A:1016684218041>.

- [55] P. Moggi, M. Devillers, P. Ruiz, G. Predieri, D. Cauzzi, S. Morselli, O. Ligabue, Oxidative dehydrogenation of propane on pure and silica-dispersed multimetallic oxides based on vanadium and niobium prepared via hydrolytic and non-hydrolytic sol-gel methods, *Catal. Today*. 81 (2003) 77–85. [https://doi.org/10.1016/S0920-5861\(03\)00114-7](https://doi.org/10.1016/S0920-5861(03)00114-7).
- [56] B.Y. Jibril, S. Ahmed, Oxidative dehydrogenation of propane over Co, Ni and Mo mixed oxides/MCM-41 catalysts: Effects of intra- and extra-framework locations of metals on product distributions, *Catal. Commun.* 7 (2006) 990–996. <https://doi.org/10.1016/j.catcom.2006.04.017>.
- [57] S.N. Koc, G. Gurdag, S. Geissler, M. Guraya, M. Orbay, M. Muhler, The oxidative dehydrogenation of propane over potassium-promoted molybdenum oxide/sol-gel zirconia catalysts, *J. Mol. Catal. Chem.* 225 (2005) 197–202. <https://doi.org/10.1016/j.molcata.2004.09.009>.
- [58] S.M. Al-Zahrani, B.Y. Jibril, A.E. Abasaeed, Activities of  $\gamma$ -Al<sub>2</sub>O<sub>3</sub>-Supported Metal Oxide Catalysts in Propane Oxidative Dehydrogenation, *Catal. Lett.* 85 (2003) 57–67. <https://doi.org/10.1023/A:1022116723773>.
- [59] O. Demoulin, F. Dury, M. Navez, E.M. Gaigneaux, P. Ruiz, Modification of active catalytic sites with N<sub>2</sub>O and CO<sub>2</sub> as gas promoters during oxidation reactions, *Catal. Today*. 91–92 (2004) 27–31. <https://doi.org/10.1016/j.cattod.2004.03.005>.
- [60] S. Dźwigaj, I. Gressel, B. Grzybowska, K. Samson, Oxidative dehydrogenation of propane on VSi $\beta$  catalysts, *Catal. Today*. 114 (2006) 237–241. <https://doi.org/10.1016/j.cattod.2006.02.022>.
- [61] K. Bahranowski, R. Grabowski, B. Grzybowska, A. Kielski, E.M. Serwicka, K. Wcisło, E. Wisła-Walsh, K. Wodnicka, Synthesis and physicochemical properties of vanadium-doped zirconia-pillared montmorillonites in relation to oxidative dehydrogenation of propane, *Top. Catal.* 11 (2000) 255. <https://doi.org/10.1023/A:1027247914281>.

- [62] S. Sugiyama, H. Hayashi, Role of Hydroxide Groups in Hydroxyapatite Catalysts for the Oxidative Dehydrogenation of Alkanes, *Int. J. Mod. Phys. B.* 17 (2003) 1476–1481. <https://doi.org/10.1142/S0217979203019186>.
- [63] S. Sugiyama, T. Shono, D. Makino, T. Moriga, H. Hayashi, Enhancement of the catalytic activities in propane oxidation and H–D exchangeability of hydroxyl groups by the incorporation with cobalt into strontium hydroxyapatite, *J. Catal.* 214 (2003) 8–14. [https://doi.org/10.1016/S0021-9517\(02\)00101-X](https://doi.org/10.1016/S0021-9517(02)00101-X).
- [64] A. Pérez Pujol, R.X. Valenzuela, A. Fuerte, E. Wloch, A. Kubacka, Z. Olejniczak, B. Sulikowski, V. Cortés Corberán, High performance of V–Ga–O catalysts for oxidehydrogenation of propane, *Catal. Today.* 78 (2003) 247–256. [https://doi.org/10.1016/S0920-5861\(02\)00348-6](https://doi.org/10.1016/S0920-5861(02)00348-6).
- [65] K. Bahranowski, G. Bueno, V. Cortés Corberán, F. Kooli, E.M. Serwicka, R.X. Valenzuela, K. Wcislo, Oxidative dehydrogenation of propane over calcined vanadate-exchanged Mg,Al-layered double hydroxides, *Appl. Catal. Gen.* 185 (1999) 65–73. [https://doi.org/10.1016/S0926-860X\(99\)00113-1](https://doi.org/10.1016/S0926-860X(99)00113-1).
- [66] Y. Wang, Q. Zhang, Y. Ohishi, T. Shishido, K. Takehira, Synthesis of V-MCM-41 by template-ion exchange method and its catalytic properties in propane oxidative dehydrogenation, *Catal. Lett.* 72 (2001) 215–219. <https://doi.org/10.1023/A:1009001707280>.
- [67] A. Kubacka, E. Wloch, B. Sulikowski, R.X. Valenzuela, V. Cortés Corberán, Oxidative dehydrogenation of propane on zeolite catalysts, *Catal. Today.* 61 (2000) 343–352. [https://doi.org/10.1016/S0920-5861\(00\)00394-1](https://doi.org/10.1016/S0920-5861(00)00394-1).
- [68] M.A. Bañares, S.J. Khatib, Structure–activity relationships in alumina-supported molybdena–vanadia catalysts for propane oxidative dehydrogenation, *Catal. Today.* 96 (2004) 251–257. <https://doi.org/10.1016/j.cattod.2004.06.152>.
- [69] M.C. Abello, M.F. Gomez, O. Ferretti, Oxidative Conversion of Propane over Al<sub>2</sub>O<sub>3</sub>-Supported Molybdenum and Chromium

- Oxides, Catal. Lett. 87 (2003) 43–49.  
<https://doi.org/10.1023/A:1022801126269>.
- [70] G. Garcia Cortez, J.L.G. Fierro, M.A. Bañares, Role of potassium on the structure and activity of alumina-supported vanadium oxide catalysts for propane oxidative dehydrogenation, Catal. Today. 78 (2003) 219–228. [https://doi.org/10.1016/S0920-5861\(02\)00341-3](https://doi.org/10.1016/S0920-5861(02)00341-3).
- [71] X. Zhang, H. Wan, W. Weng, X. Yi, Effect of Ag promoter on redox properties and catalytic performance of Ag-Mo-P-O catalysts for oxidative dehydrogenation of propane, Appl. Surf. Sci. 220 (2003) 117–124. [https://doi.org/10.1016/S0169-4332\(03\)00837-7](https://doi.org/10.1016/S0169-4332(03)00837-7).
- [72] A.A. Lemonidou, L. Nalbandian, I.A. Vasalos, Oxidative dehydrogenation of propane over vanadium oxide based catalysts: Effect of support and alkali promoter, Catal. Today. 61 (2000) 333–341. [https://doi.org/10.1016/S0920-5861\(00\)00393-X](https://doi.org/10.1016/S0920-5861(00)00393-X).
- [73] M.D. Putra, S.M. Al-Zahrani, A.E. Abasaeed, Oxidative dehydrogenation of propane to propylene over Al<sub>2</sub>O<sub>3</sub>-supported Sr–V–Mo catalysts, Catal. Commun. 14 (2011) 107–110. <https://doi.org/10.1016/j.catcom.2011.07.025>.
- [74] X. Sun, Y. Ding, B. Zhang, R. Huang, D. Chen, D.S. Su, Insight into the Enhanced Selectivity of Phosphate-Modified Annealed Nanodiamond for Oxidative Dehydrogenation Reactions, ACS Catal. 5 (2015) 2436–2444. <https://doi.org/10.1021/acscatal.5b00042>.
- [75] B.Y. Jibril, Propane oxidative dehydrogenation over chromium oxide-based catalysts, Appl. Catal. Gen. 264 (2004) 193–202. <https://doi.org/10.1016/j.apcata.2003.12.054>.
- [76] J. Słoczyński, J. Ziółkowski, B. Grzybowska, R. Grabowski, D. Jachewicz, K. Wcisło, L. Gengembre, Oxidative Dehydrogenation of Propane on Ni<sub>x</sub>Mg<sub>1-x</sub>Al<sub>2</sub>O<sub>4</sub> and NiCr<sub>2</sub>O<sub>4</sub> Spinels, J. Catal. 187 (1999) 410–418. <https://doi.org/10.1006/jcat.1999.2626>.
- [77] R.B. Watson, U.S. Ozkan, K/Mo Catalysts Supported over Sol–Gel Silica–Titania Mixed Oxides in the Oxidative Dehydrogenation of

- Propane, J. Catal. 191 (2000) 12–29.  
<https://doi.org/10.1006/jcat.1999.2781>.
- [78] P. Michorczyk, P. Kuśtrowski, P. Niebrzydowska, A. Wach, Catalytic performance of sucrose-derived CMK-3 in oxidative dehydrogenation of propane to propene, Appl. Catal. Gen. 445–446 (2012) 321–328. <https://doi.org/10.1016/j.apcata.2012.08.044>.
- [79] J.-H. Li, C.-C. Wang, C.-J. Huang, Y.-F. Sun, W.-Z. Weng, H.-L. Wan, Mesoporous nickel oxides as effective catalysts for oxidative dehydrogenation of propane to propene, Appl. Catal. Gen. 382 (2010) 99–105. <https://doi.org/10.1016/j.apcata.2010.04.034>.
- [80] Q. Zhang, C. Cao, T. Xu, M. Sun, J. Zhang, Y. Wang, H. Wan, NiO–polyoxometalate nanocomposites as efficient catalysts for the oxidative dehydrogenation of propane and isobutane, Chem. Commun. (2009) 2376–2378. <https://doi.org/10.1039/B823369A>.
- [81] B. Farin, P. Eloy, C. Poleunis, M. Devillers, E.M. Gaigneaux, Self-assembled hybrid precursors towards more efficient propane ODH NiMoO<sub>4</sub> catalysts, Catal. Sci. Technol. 6 (2016) 6046–6056. <https://doi.org/10.1039/C6CY00167J>.

## **GENERAL CONCLUSIONS**



## 4. GENERAL CONCLUSIONS

It has been described a new procedure for the preparation of porous ZrO<sub>2</sub> submicrometric fibers with catalytically active species such as VO<sub>x</sub>, NbO<sub>x</sub>, MoO<sub>x</sub> and/or their mixed oxides. This method only involves one calcination step and is a versatile, simple and straightforward procedure based on the electrospinning technique. The dispersion of VO<sub>x</sub>, NbO<sub>x</sub> and/or MoO<sub>x</sub> during the ZrO<sub>2</sub> fiber formation delay the crystallization of amorphous zirconia and inhibit the conversion of metastable tetragonal to monoclinic phase in zirconia, while favoring the development of the porous texture and avoiding the formation of V<sub>2</sub>O<sub>5</sub>, Nb<sub>2</sub>O<sub>5</sub> and MoO<sub>3</sub> crystals.

TOF and propylene productivity obtained during the propane ODH with the catalysts prepared in this work present similar values than those reported in the literature. Moreover, the fibrous catalysts do not present deactivation processes and are stable under time of stream. These results validate the new procedure method for the preparation of submicrometric fiber catalysts by the electrospinning technique, which allow to obtain materials with homogenous compositions of different metal oxides.

The results obtained in the *operando* experiments performed in the new IRRaman reactor have shown some insights about the structure-activity relationships of V-Zr-O based catalysts in the propane ODH. The results indicate that the reaction occurs via a Mars-van Krevelen type mechanism, where the catalyst lattice oxygen sites in the form of bridging V-O-V/V-O-Zr bonds are significantly more active than those of terminal V=O bonds. In addition, a general mechanism has been proposed, according to the results obtained. It has been proposed that propane oxidation occurs via the irreversible isopropoxide formation, which can give rise to propylene in the gas phase or can be parallelly further oxidized to chemisorbed acetone by some secondary reactions. Furthermore, the propylene formed can be adsorbed on the surface and be oxidized to isopropoxide species through a neighbour V-OH as Bronsted acidic site and continue with the subsequent



oxidation steps. Then, from chemisorbed acetone, bidentate formates and bidentate acetates are formed by oxidative cleavage of the C(1)-C(2) bond. These oxygenate species evolve leading CO in the gas phase, which can be further oxidized to CO<sub>2</sub>. The required reoxidation reactions of the catalyst consists of the irreversible dissociative adsorption of oxygen from the gas phase, as well as the reversible OH recombination forming water, an oxygen active site and a vacancy center.

By this manner, a rigorous kinetic study has been performed to estimate the kinetic parameters of the propane ODH reaction over vanadium oxide-based submicrometric fiber catalysts. The fibrous shape and the submicrometric diameter size of the catalysts allowed the relatively easier obtention of intrinsic kinetic data compared to the traditional powdered catalysts, without the interference of other effects, even though it has not been used any diluting inert materials or pelletization of the catalysts. The proposed kinetic model with the estimated kinetic parameters satisfactorily predicts the conversion and selectivity profiles and the surface coverage of the different species present on the catalyst for all the studied conditions of temperature, space-time and inlet partial pressures of propane and oxygen, covering a broad range of conversion and selectivity values for all the catalysts.

The kinetic study reveals that the activation energy of the rate determining step (first hydrogen abstraction from propane) presented values between 96.0-117.7 kJ·mol<sup>-1</sup> for the catalysts studied, which are within the range of those ones reported for equivalent catalytic systems (same support and composition). Moreover, it also shows that polyvanadates present the best combination of catalytic activity and propylene selectivity, whereas monovanadates are slightly less active and selective to propylene. Crystalline ZrV<sub>2</sub>O<sub>7</sub> species are significantly less selective to propylene and slightly more active than polyvanadate species, but the fraction of exposed active sites decreases in the former species due to the vanadium agglomeration into more condensed structures. V-Mo-O phases are the

least active and the most selective sites among the different active species studied in this work.

The kinetic model predicts that the catalysts used in this work are not fully oxidized under reaction conditions even for the highest oxygen inlet partial pressures used and neither when the space-time tends to zero with negligible conversions. Then, the tempting assumption of considering that the catalyst is always fully oxidized to simplify the equations could be wrong sometimes. Moreover, the model also predicts that the catalyst oxidation state decreases as the space-time is longer. Then, as the rate determining step is second-order with respect to the surface coverage of lattice oxygen, it can be derived that propane TOF will also depend on the catalyst oxidation state, and then, on the reaction conditions and space-time, and so, it will change along the fixed-bed reactor. Therefore, the comparison of propane TOF data of two catalysts only should be done under the same conditions, although using only this parameter is not enough to reach definitive conclusions about the activity of this kind of catalysts, unless the catalysts are always fully oxidized under reaction conditions.

The values of yield and productivity towards propylene predicted by the kinetic model for all the catalysts used in this work are much higher than the values usually found in the literature, if the reaction is performed under the optimal conditions. Short space-times and high propane inlet partial pressures lead to high productivity and low yield, with very low propane conversion and very high propylene selectivity. However, very low propane inlet partial pressure and long space-time give rise to the high yield and low productivity, with very high conversion and selectivity. It should be noted that the study of the yield and productivity results found in the literature, for a wide variety of catalysts, followed these same trends, what validates the proposed kinetic model explaining the catalytic behavior of most of the catalysts in the propane ODH, and probably in other partial oxidation reactions that follow similar reaction mechanism. It is possible that instead of low yield or productivity values, the main problems of the industrial implementation of the propane ODH reaction could be to optimize the

reaction conditions and to find catalysts that can reach the desired values of yield or productivity in affordable conditions, or to find catalysts that simultaneously present high yield and productivity. Unfortunately, the conditions to obtain high productivity lead to low yield and vice versa, the ideal situation would be that both parameters follow the same dependency.



## **SUMMARY IN ENGLISH**



## SUMMARY IN ENGLISH

### Introduction

Propylene has become the second most-demanded building block (after ethylene) in the petrochemical industry due to its use as monomers/comonomers to produce many interest products (e.g. polypropylene, acrylonitrile, oxo-alcohols, propylene oxide, cumene, acrylic acid, etc). The traditional technologies to obtain propylene as by product in the steam cracking and in the fluid catalytic cracking have experienced some changes in the operating conditions during last decade to improve the yields toward ethylene and gasoline, respectively, in detriment of the propylene yield. In fact, it has been necessary to find new alternatives to fully satisfy the growing propylene demand. This situation has encouraged the production of propylene from propane, which is an abundant and low-cost feedstock due to the current proliferation of the shale gas.

Nowadays, non-oxidative dehydrogenation of propane is commercially implemented in the industry to produce propylene by using catalysts of Pt-Sn or Cr<sub>2</sub>O<sub>3</sub> supported on alumina (Oleflex or Catofin technologies, respectively). However, this process suffers from several limitations, since it is an endothermic reaction that works above 600°C (energy-intensive process) and that is thermodynamically restricted (limiting the conversion and selectivity). Furthermore, side reactions and coke deposition resulting in catalyst deactivation are apparent at working temperatures. Thereby, oxidative dehydrogenation (ODH) of propane appears as a promising alternative to overcome these limitations. This process requires the introduction of an oxidizing agent (generally oxygen) into the reaction mixture and involves an exothermic reaction that can be performed at lower temperatures (300-600°C), what significantly reduces the energy consumption. Moreover, the reaction is not thermodynamically restricted and the catalyst deactivation by coke deposition is practically negligible. However, propane ODH has not been industrially implemented, since the propylene yields are still low due to the undesirable combustion reactions

to CO and CO<sub>2</sub> (CO<sub>x</sub>), which are difficult to control. Moreover, it presents other drawbacks such as the removal of heat, flammability of the reaction mixture, and the possibility of reaction runaway, what can give rise to explosions and/or damage the catalyst. Then, it would be necessary to improve the existing catalysts or to find new ones, to optimize the reaction conditions and/or to find the optimal reactor in order to work under safe operative conditions while obtaining higher yield and/or productivity.

Catalysts based on dispersed vanadia species over different supports (ZrO<sub>2</sub>, TiO<sub>2</sub>, Al<sub>2</sub>O<sub>3</sub>, SiO<sub>2</sub>, etc.) are the most reported in the literature for the propane ODH, where the formation of crystalline vanadium phases is generally detrimental for the catalytic activity. The addition of additives such as alkalis or alkaline earth, transition metals and phosphorus as promoters in the vanadia based catalysts have been reported to affect their redox and acid-basic properties, and hence their catalytic activity and selectivity. Generally, the addition of redox elements or P leads to an increase of the activity and a decrease of the selectivity, while the doping with alkalis elements leads to a decrease of the activity and an increase of the selectivity.

The use of catalytic materials with fibrous structure of submicrometric size may present several advantages with respect to the traditional powdered ones, but their use in the propane ODH has not been published before in the literature. They show very small resistance to internal diffusion and high surface area to volume ratio because of their submicrometric diameter; as well as less significant temperature gradients and lower pressure drop in a fixed bed than those in powder form due to the high void fractions or bed porosity offered by these fibrous structures. Furthermore, they are easy to handle and can be packed or constructed in the best form to fit the particular use or application due to their geometric flexibility. All these differences would still be more appreciable in the use of these catalysts on an industrial scale. Since the powder catalysts can easily overcome all these intrinsic disadvantages at laboratory scale adding a diluting inert material (glass, quartz,  $\alpha$ -alumina or silicon carbide) and/or making pellets (not necessary

for submicrometric fibers), which may not be so operative at industrial level. Moreover, pellet size should be small enough to avoid high resistance to internal diffusion and big enough to avoid high pressure drop in a fixed bed, which is not possible sometimes. Consequently, fibers have potentially higher fluidodynamics and transfer properties which may reduce the probability of hot spot formation allowing to work under safer conditions, what may make them more feasible to scale up to industrial level.

Some authors have investigated the use of membrane reactors for the propane ODH, which allow dosing the oxidant continuously along the reactor decreasing the overall oxygen concentration that interact with the catalyst, hindering the appearance of hot spots, as well as increasing the selectivity at isoconversion values. In this way, these reactors can be fed with high hydrocarbon concentration without risk of explosion. However, the use of membranes can also be dangerous in the case of membrane damage or other reactor leakages. Among these types of reactors, fluidized bed membrane reactors (FLBMR) with distributed oxidant supply seem to be the most promising reactors for strongly exothermic reactions as alkanes ODH. This is due to the combination of the excellent heat transfer of fluidized bed with the advantageous principle of distributed oxidant dosing, which allow the operation in a broad conditions range with respect to the hydrocarbon to oxygen ratio. Moreover, these reactors are especially robust against oscillations and disturbances in the reactant feed, what confers a higher operation safety. It has been shown that the use of FLBMR can improve the selectivity and yield value towards olefin with respect to fixed bed membrane reactors (FBMR) and fixed bed reactors (FBR). However, it seems that the use of membrane reactors in the propane ODH has not generally brought remarkable improvements with respect to the conventional reactor configurations as the FBR.

It has been established that propane ODH reaction proceeds via Mars-van Krevelen type mechanism, which means that the lattice oxygens of the catalyst ( $\text{VO}_x$ ) are the active sites. In this way, the mechanism involves the consecutive reduction and oxidation of the catalyst surface by the reaction



with propane and oxygen (or other oxidizing agents as  $N_2O$ ), respectively. The general reaction network most accepted in the literature is a parallel-consecutive pathway, where propane is oxidized to propylene, and both of them can be totally oxidized to  $CO_x$ . Moreover, it appears to be a consensus that the activation of the secondary C-H bond of propane is the rate determining step (RDS) via the formation of propyl or (iso)propoxy species as first reaction intermediates, which leads to propylene in the gas phase or oxygenate species adsorbed on the catalyst, that are usually further oxidized giving rise to  $CO_x$  in the gas phase. However, although it is generally accepted that bridging oxygen sites (V-O-V/V-O-Support) are the most active sites, there are still authors reporting that terminal oxygen sites (V=O) are the active sites. It is not so clear about which species are more active, monovanadate or polyvanadate species, or if they just present the same activity. Furthermore, despite the vast propane ODH literature, not many details are usually given about the nature and number of the next steps of the mechanism involving the formation of carbon oxides.

Not many articles describe a detailed reaction mechanism or kinetic study. Different kinetics models have been used (Power Law, Langmuir-Hinshelwood, Eley-Rideal, etc.), but the Mars-van Krevelen expression is the most frequently proposed for ODH reactions. The kinetic parameter most frequently compared between the different catalysts is the activation energy of the first hydrogen abstraction from propane (i.e. RDS). However, a wide range of values can be found in the literature even for equivalent catalysts (e.g. same support and composition), probably due to the variety of different kinetic models used, which are sometimes oversimplified and/or frequently inconsistent and incorrect without physical relevance. Propane TOF is also widely used to compare the activity of the catalysts, especially to study the influence of the vanadia content to try discerning if monovanadates are more, less or equally active than polyvanadates. However different tendencies can also be found. It has been reported that as the vanadium content of the catalyst increases, the propane turnover frequency (TOF) decreases, remains constant or increases. These

discrepancies can be due to the use of different synthesis methods, supports and concentrations, which may result in different kind of vanadia surface species. Moreover, it cannot be discarded the possible existence of external and/or internal mass and/or heat transport limitations, as well as contribution of homogenous phase reaction at high temperatures (above 500°C) and/or experiments with a total oxygen conversion.

Thus, the objectives of this PhD thesis are, on the one hand, the preparation of zirconia submicron sized fibrous catalytic materials with dispersed  $\text{VO}_x$  active species by electrospinning technique for the propane ODH reaction, as well as the incorporation of Mo and Nb additives to these fibrillar materials in order to try to modulate their activity and selectivity. The submicron fiber shape should confer to the catalyst small internal diffusion resistance compared to traditional powdered catalysts, as well as less temperature gradients and lower pressure drop when they are packed in a fixed bed, allowing the operation in a safer conditions. Moreover, these advantages should make easier the performance of the experiments, without the addition of diluting inert material (e.g. silicon carbide), while isolating the obtention of intrinsic kinetic data of the catalyst without the interference of other effects. On the other hand, simultaneous FTIR and Raman *operando* experiments in a new IRRaman reactor will be performed to study the structure-activity relationships of the catalysts during the propane ODH reaction and to propose a reaction mechanism, while providing the required bases to perform a future rigorous kinetic study. Subsequently, reaction experiments in a conventional fixed bed reactor varying the temperature, the propane and oxygen inlet partial pressure and the space-time will be performed for the kinetic study to estimate the kinetic parameters of the catalysts. In this way, it will be studied the influence of the vanadium concentration and of the presence of molybdenum or niobium on the estimated kinetic parameters values, in order to find out kinetic information from polyvanadate, monovanadate, crystalline  $\text{ZrV}_2\text{O}_7$ , V-Mo-O and V-Nb-O species. Finally, it will be simulated values of yield and productivity towards propylene by using the kinetic model proposed in this

work, in an attempt to find the theoretical optimum conditions to get their maximum values. This catalytic information could be very useful to design better catalysts, to find the optimal reactor and reaction conditions, and subsequently, to determine if a catalyst can be suitable to be used on an industrial scale.

### **Sections 3.1 and 3.2**

In these sections, fiber catalysts based on Zr, Zr-V, Zr-Mo, Zr-Nb, Zr-V-Mo and Zr-V-Nb mixed oxides have been prepared by using the electrospinning technique, in order to be studied in the propane ODH reaction. A new versatile, simple and straightforward procedure is proposed for the preparation of such catalysts, which involves the electrospun of the polymer solution containing all the required metallic precursors of zirconium, vanadium, niobium and/or molybdenum, followed by only one calcination step to obtain the final submicron-fiber catalysts. However, traditional methods for the preparation of supported catalysts (e.g. incipient wetness impregnation method) usually require at least two calcination steps: one for the preparation of the catalytic support and another one after the support impregnation with the active phase precursor.

Both zirconium propoxide or zirconium acetate solutions have been used as zirconia precursor during the preparation of the electrospinning polymer solutions in order to evaluate the effect of the precursor. Vanadyl acetylacetonate, ammonium heptamolybdate and ammonium niobate oxalate have been used as vanadium, molybdenum and niobium precursors, respectively. Then, the electrospun fibers were recovered in form of non-woven cloth and calcined at 500°C in order to eliminate the remaining solvent and the organic part of the polymer solution. In this way, it has been prepared catalysts with different vanadium, molybdenum and/or niobium content in the final catalyst using both zirconium precursors (propoxide or acetate).

All the catalysts presented a very homogenous metallic composition along the fibers. Most of these materials showed a quite high length to diameter

ratio and without presenting fused zones or beads, which confirmed that the fibrous morphology of the samples was successfully achieved with a diameter size of the order of 100 nanometers (submicrometric). In all the cases, the diameters were thicker for the samples prepared with propoxide, probably due to the lower applied voltage required during the electrospinning process in these samples compared to the ones prepared with acetate, although the influence of other solution parameters as viscosity or electrical conductivity cannot be discarded. Moreover, it has been generally observed that the incorporation of vanadium decreases the diameter in the case of the propoxide materials, probably due to the increase of the electrical conductivity of the polymer solution because of the presence of vanadium precursor. The same occurred, but to a much lesser extent, when the niobium or molybdenum precursor was added to the polymer solution. However, different trends occurred when the vanadium, molybdenum or niobium precursors were incorporated into the polymer solutions prepared using zirconium acetate. It is also noteworthy that the fibers containing molybdenum prepared with propoxide were apparently more fragile than the ones prepared with acetate.

The materials prepared using propoxide presented a more developed porous texture and therefore higher BET surface area values in all the cases. Moreover, when vanadium was added to the polymer solution, the BET surface area values increased for the preparation with both precursors, obtaining maximum values of  $66 \text{ m}^2 \cdot \text{g}^{-1}$  or  $42 \text{ m}^2 \cdot \text{g}^{-1}$  at around 5.0 wt % of vanadium content when using propoxide or acetate as zirconium precursor, respectively. Higher vanadium contents than 5.0 wt % resulted in a decrease of the BET surface area, probably due to the formation of vanadium crystalline phases that can partially block the porous texture. Similar effects were also observed, but in a lower extent, when Nb or Mo were added to the fiber.

The pattern of zirconia tetragonal phase was detected in all the samples, whereas crystalline phases such as  $\text{V}_2\text{O}_5$ ,  $\text{Nb}_2\text{O}_5$  or  $\text{MoO}_3$ , were not observed. Amorphous and dispersed vanadium in the form of monovanate

and polyvanadate species has been observed in all the catalysts containing vanadium, being higher the polyvanadate to monovanadates ratio as the vanadium concentration was higher. Crystalline  $ZrV_2O_7$  was formed when the vanadium content exceeded a certain value, which was higher in the catalysts prepared using propoxide with respect to those prepared with acetate. This suggested that the formation of more condensed or crystalline vanadium structures are favored when zirconium acetate was used, probably due to the lower porosity development when this zirconium precursor was incorporated to the polymer solution. Regarding the catalysts containing molybdenum or niobium, it was observed their amorphous or dispersed phases in all the samples, whereas their corresponding crystalline phases or their crystalline mixed oxides phases with zirconium were not detected, probably because the concentrations of molybdenum or niobium in the catalysts were never so high.

All the catalysts were tested in the propane ODH reaction in a fixed bed microreactor. The propane and oxygen partial pressures were always 0.2 and 0.1 atm, respectively, the reaction temperature was varied between 300 and 480°C, the total volumetric gas flow and the mass of catalyst were adjusted in order to vary the space-time in the range of 0.1-1.0  $g_{cat} \cdot s \cdot mL^{-1} C_3H_8$  (Volume was always expressed in STP conditions).

For all the catalysts, an increase of the temperature or of the space-time resulted in an increase of the propane conversion and a decrease of the propylene selectivity due to the overoxidation reactions leading to the formation of  $CO_x$ . In the case of the V-Zr-O catalysts, it was observed that the most active catalysts were the ones with the highest amount of dispersed vanadia ( $VO_x$ ) without the presence of crystalline  $ZrV_2O_7$ . Moreover, the results suggested that among the dispersed vanadia species, polyvanadates were more active than monovanadates. The presence of crystalline  $ZrV_2O_7$  in the catalysts resulted in a significantly decrease of the propylene selectivity. In the case of the Mo-Zr-O and Nb-Zr-O catalysts, they were the least active catalysts, in fact their activity values were negligible at lower temperature than 480°C, being both the

activity and selectivity always higher in the Mo-containing catalyst with respect to the Nb-containing catalyst. Regarding the V-Mo-Zr-O and V-Nb-Zr-O catalysts, the incorporation of Nb in the V-Zr-O system did not result in any improvement of the catalytic performance, at least in the proportion used in this work, while the incorporation of Mo somehow gave rise to a synergic interaction that significantly improved the propylene selectivity at isoconversion values. It seems that the interaction between V and Mo species avoid the overoxidation reactions to CO<sub>x</sub>.

All the catalysts presented propylene selectivity values of 100% at very low propane conversion values. Then, as the conversion was higher, the selectivity to CO also started to be appreciable, as well as that to propylene, but not to CO<sub>2</sub>. Finally, the presence of CO<sub>2</sub> was also observed at relative high conversion values. These results suggested that the reaction mechanism could occur in a consecutive pathway, where propylene is firstly formed, followed by CO and finally CO<sub>2</sub>, although the direct combustion of propane cannot be discarded, especially at high temperatures.

It should be noted that the catalysts prepared in this chapter presented similar results in terms of TOF and propylene productivity with respect to those reported in the literature. Moreover, the fibrous catalysts were stable under time of stream up to 24 h without noticeable deactivation at the operation conditions studied. These results are quite promising and validate the new procedure method for the preparation of submicron fiber catalysts by the electrospinning technique.

### Section 3.3

The aim of this section was to gain deeper insight about the propane ODH mechanism over V-Zr-O catalysts. In this way, it has been used a new homemade *operando* IRRaman reactor that allowed to obtain in a single experiment, with space and time consistency, information about the structure of the catalyst (mainly from Raman), the adsorbed species (mainly from FTIR) and the reactivity (online gases measurements) during reaction.

Which offered a higher possibility to directly observe more relevant details about the structure-activity relationships of the catalysts during reaction.

Three V-Zr-O catalysts with different vanadium content, and consequently with different monovanadate to polyvanadate ratio, were used to study the different catalytic behavior of these two surface active species. It should be noted that the structured fiber catalysts were grinded and pressed into self-supported wafers to perform the *operando* experiments in the IRRaman reactor. The temperature during experiments varied from room temperature to 340°C, the weight of catalyst wafer ( $W_{\text{cat}}$ ) and the total volumetric gas flow ( $F_T$ ) were always around 31.5 mg and 18.1 mL·min<sup>-1</sup>, respectively, and the propane and oxygen inlet partial pressures were always 0.2 and 0.1 atm, respectively.

The *operando* results obtained in this work during propane ODH showed that the catalysts were partly reduced during reaction, while part of the propane was oxidized giving rise to propylene (desired product), as well as oxygenated adsorbed species, behaving as active intermediates in the mechanism for the total oxidation to CO<sub>x</sub> (undesired products). With respect to the surface species, acetates and formates were generally the most abundant reaction intermediates (MARI) with minor amounts of acrylates, for most of the reaction conditions studied. Other previous intermediate species than carboxylates was also expected during reaction, but they were not detected in the studied conditions, probably due to their low or negligible surface concentrations, as a result of the relative low stability of such species with respect to those related to the rate determining step (propane activation). Moreover, the fact that the oxygenated species were stable and accumulated on the surface below the reaction temperature suggested that the activation energy values for the oxidation steps of such species should be higher than the one for the rate determining step. This was also consistent with the decrease of the amount of adsorbed species as the temperature increased, with the subsequent increase of the conversion values. Furthermore, this decrease of the adsorbed species with the temperature was relatively higher for formate than for acetate species,

which suggested that the activation energy of the oxidation step for acetates is higher than for formates. This is consistent with the higher stability of acetates with respect to formates reported in the literature.

With respect to the lattice oxygen, V=O and V-O-V/V-O-Zr bonds showed changes during reaction, which were quickly reversible under subsequent oxidation, but the biggest changes were observed in the bridging V-O-V and V-O-Zr bonds, as well as these bonds seemed to start interacting with propane at lower temperature than the terminal oxygens, suggesting that bridging oxygens are most probably the active sites during propane ODH. The slight decrease of bridging V-O-V/V-O-Zr bonds with the increase of the reaction temperature indicated a lower activation energy value for the catalyst reoxidation reaction of these bonds with respect to the activation energy value for the rate determining step, which determine the rate of the different catalyst reduction reactions. In the case of the slight perturbations observed in the V=O band could somehow be associated with the interaction of these bonds with the adsorbed species, since these shifts were only observed when these species were present, and they disappeared just when the oxygenates were removed, regardless of whether the catalyst had been reoxidized or not.

Transient *operando* experiments using propane flow without oxygen in the feed (20% propane in argon) were also performed. The fact that propylene, CO and CO<sub>2</sub> were detected during some minutes, even though oxygen was not present in the gas phase, confirmed the participation of the lattice oxygen of the catalyst during reaction, as in a Mars-Van Krevelen type mechanism. These results showed that the V-O-V/V-O-Zr sites (lattice bridging oxygens) are able to complete the whole catalytic cycle of the propane ODH reaction without the participation of oxygen from the gas phase or V=O sites (terminal vanadyl oxygens), since all the gas phase products and adsorbed species of such reaction were fully formed during the first minute of reaction with the only consumption of the bridging oxygens. Therefore, the results revealed that terminal oxygen bonds (V=O) present some activity, but much lower than the bridging oxygens (V-O-V/V-



O-Zr). These results confirmed the predictions made by other authors in the past, about the higher activity of bridging oxygens with respect to terminal oxygens. It should be also noted that the simultaneous analysis by FTIR and Raman of the gas phase, of the catalyst structure and of the adsorbed species was crucial to fully and directly observe these findings in an unambiguous way. Furthermore, space and time consistency offered by the IRRaman reactor, due to its very small dead volume, was also crucial to successfully perform such transient experiments.

An experiment feeding propylene and oxygen was also performed, since propylene is more reactive than propane and, consequently, allows running the reaction at lower temperatures than propane, which may enable the detection of less stable intermediates. Moreover, as it is well known that the main source of CO<sub>x</sub> during propane ODH is the consecutive oxidation of the propylene formed, this experiment could give more information about the oxidations steps that take place during the total oxidation pathway. The results showed that propylene activation mainly proceeded via isopropoxide species formation giving rise to chemisorbed acetone and then carboxylates as observed in some previous works, in contrast to other studies that have reported the activation through allyl-alkoxides giving rise to chemisorbed acrolein and then acrylates surface species. It was derived that probably both propylene oxidation routes can simultaneously happen, and that the catalyst nature determine the most favorable pathway or the contribution of each one for the total oxidation steps. On the other hand, it was assumed that propane is also activated via isopropoxide species formation as reported elsewhere, which would mean that a common surface intermediate is responsible of both parallel reactions, the propylene formation step and the total oxidation steps of propane or propylene.

A general mechanism has been proposed according to the results obtained. The lattice oxygens in the form of V-O-V or V-O-Zr bonds have been considered as the main active sites. It has been proposed that propane oxidation occurs via the irreversible isopropoxide formation, which can give rise to propylene in the gas phase or can be further oxidized to chemisorbed

acetone. The propylene formed can be adsorbed on the surface and be oxidized to isopropoxide species through a neighbour V-OH as Bronsted acidic site and continue with the subsequent oxidation steps. Then, from chemisorbed acetone, bidentate formates and bidentate acetates are formed by oxidative cleavage of the C(1)-C(2) bond. These oxygenate species evolve leading CO in the gas phase, which can be further oxidized to CO<sub>2</sub>. The required reoxidation reactions of the catalyst consisted of the irreversible dissociative adsorption of oxygen from the gas phase, as well as the reversible OH recombination forming water, an oxygen active site and a vacancy center.

As described, it was possible to experimentally observe that the reaction occurs via a Mars-van Krevelen type mechanism showing clear evidences that the V-O-V/V-O-Zr sites are much more active than terminal V=O bonds. In addition, also the required steps for the total oxidation to CO<sub>x</sub> have been identified, at least for V-Zr-O catalysts, which could be useful to know how to proceed to avoid in some extent the total oxidation of propane, so increasing the selectivity towards propylene.

### **Sections 3.4 and 3.5**

The objective of these sections was to make a kinetic study of the propane ODH reaction over the submicron diameter fiber catalysts already prepared by electrospinning and thoroughly characterized in the *Sections 3.1* and *3.2*, establishing the kinetic equations in a rigorous way using the reaction mechanism proposed in the *Section 3.3* according to the FTIR-Raman *operando* results obtained in the IRRaman reactor. The kinetic study has been performed over four different catalysts in order to study the influence of the vanadium concentration and of the presence of molybdenum on the catalysts, and consequently, to find out kinetic information from polyvanadate, monovanadate, crystalline ZrV<sub>2</sub>O<sub>7</sub> and V-Mo-O species. In this way, the kinetic parameters of each catalysts have been analyzed and compared. Finally, it has been simulated values of yield and productivity in a broad range of conditions to study their dependence and to try to find the

theoretical optimum conditions to get their maximum values. This catalytic information could be very useful to determine if a catalyst can be suitable to be used on an industrial scale.

The use of electrospinning technique allowed the preparation of catalysts with very uniform composition and with submicrometric fibrous structure, what confers small internal diffusion resistance to the catalyst compared to traditional powdered catalysts, as well as less temperature gradients and lower pressure drop when they are packed in a fixed bed reactor. These advantages made easier the performance of the reaction experiments, without the addition of any diluting inert material (e.g. silicon carbide), while isolating the obtention of intrinsic kinetic data of the catalyst without the interference of other effects. In this way, a set of reaction experiments in a fixed bed microreactor for each catalyst was performed varying the temperature from 300 to 480°C, the propane and oxygen inlet partial pressure from 0.025 to 0.2 atm and the space-time from 0.1 to 1.0 g·s·mL<sup>-1</sup><sub>C<sub>3</sub>H<sub>8</sub></sub>.

Firstly, the kinetic equations were derived from the proposed mechanism and *operando* spectroscopic results in the *Section 3.3*. It has been assumed steady state and that most of the surface oxidation reactions are irreversible steps, as typical in surface oxidation reactions in redox mechanism, and that the different oxidation steps of the hydrocarbon species occur through the lattice oxygen of the catalyst. It has been also assumed that the bridging oxygen sites, V-O-V and V-O-Zr bonds, are kinetically equivalent and present the same role in the mechanism, although may be different. Moreover, the contribution of the terminal oxygen sites, V=O bonds, have been discarded. In the adsorbed species and site balance, it has been neglected the contribution of the surface coverages of isopropoxide, adsorbed propylene and chemisorbed acetone. The expressions to determine the surface coverages were obtained assuming pseudo-steady state and making balance of each site or adsorbed species.

Molar balance equation of fixed-bed reactor and integral reactor behaviour have been used for the interpretation of the experimental data, assuming the following requirements: uniform distribution of active sites on the catalyst surface (as shown by the characterization data and in more detail in *Sections 3.1* and *3.2*); axial dispersion and wall effects were discarded since the diameter of the fibers (submicron size) were several orders smaller than the length and diameter of the fixed-bed reactor, respectively; the reactor operated at steady-state conditions; diffusional constraints and transport limitations were discarded (as proven in *Section 3.1* using the same experimental procedure); and changes in temperature and pressure within the reactor were neglected. Since all the above conditions were met, the molar balance equation for the fixed-bed reactor was simplified into the simple molar balance equation of the ideal plug flow reactor. Thus, combining the molar balances of oxygen, propane, propylene, carbon monoxide and carbon dioxide, with their respective rate equations and the corresponding surface coverage expressions, the differential equations of the molar balance for each of the reactants and products were obtained.

This system of differential equations was numerically solved, for the proposed kinetic parameters in each iteration, to calculate the values of conversion, selectivity and yield, as well as the surface coverage of each site and adsorbed species participating in the reaction mechanism. The kinetic parameters were estimated by a modified Runge-Kutta method combined with an optimization routine based on the Levenberg-Marquardt algorithm implemented in Matlab R2016b software to minimize the error function between the experimental and simulated data. The optimization involved the Arrhenius and Van't Hoff parameters, and the final estimated kinetic parameters were used to simulate the conversion, selectivity, yield and productivity values at different space-times, inlet partial pressures of propane and oxygen and temperatures. The proposed kinetic model was able to successfully predict the surface coverages of the different adsorbed and vanadia species present on the catalyst at certain conditions of temperature, space-time and inlet partial pressures of propane and oxygen,

which also determined the conversion-selectivity profiles of the catalyst that adequately represented the experimental data for the studied conditions involving a broad range of conversion and selectivity values.

It has been observed that the vanadium concentration in the catalyst and/or the addition of molybdenum to the sample had a great influence in all the kinetic parameters, suggesting the formation of different active species and/or environments that surround them. Somehow conversion and selectivity of the catalysts will be influenced by all the kinetic parameters. However, the conversion of the catalysts will be mainly determined by the kinetic parameters associated to the dissociative chemisorption of propane (i.e. RDS), while the propylene selectivity will be mainly determined by the kinetic parameters belonging to both the propylene adsorption followed by reaction with V-OH sites forming isopropoxide and the dehydration reaction for the removal of such V-OH sites. According to the results obtained with the catalysts used in this work, polyvanadate species present the best combination of catalytic activity and propylene selectivity. Monovanadate species are slightly less active and selective to propylene than polyvanadate species. The tendency to adsorb propylene of both species is similar, but the slower removal rate of V-OH sites in mono  $\text{VO}_x$  structures than in poly  $\text{VO}_x$  structures is the responsible for the lower selectivity of monovanadate species. Incipient  $\text{ZrV}_2\text{O}_7$  are slightly more active than polyvanadate species, but the fraction of exposed active sites decreases in the former species due to the vanadium agglomeration into more condensed structures. Moreover, incipient  $\text{ZrV}_2\text{O}_7$  are less selective than polyvanadate species for propane ODH mainly due to their faster rate of propylene adsorption followed by reaction with V-OH sites forming isopropoxide species. V-Mo-O phases are the least active and the most selective sites among the different active species studied in this work. The slow rate of propylene adsorption followed by reaction with V-OH sites forming isopropoxide species is the responsible for the high selectivity of the latter species.

Moreover, the model predicts that the catalysts used in this work are not fully oxidized under reaction conditions even for the highest oxygen inlet partial pressures used and neither when the space-time tends to zero (i.e. negligible conversions). Which means that although the reaction is pseudo-zero order with respect to oxygen in a broad range of conditions, the catalyst may not be fully oxidized, even though the reoxidation reaction of the catalyst may be much faster than the reduction. Then, the tempting assumption of considering that the catalyst is always fully oxidized to simplify the equations could be wrong sometimes. In fact, the model predicts that the catalyst oxidation state under reaction conditions will depend on its intrinsic chemical nature, the composition of the gas phase, temperature and space-time. Furthermore, as the reaction rate of the RDS is considered second-order with respect to the surface coverage of lattice oxygen, it can be derived that propane TOF will also depend on the catalyst oxidation state, and then, on the reaction conditions and space-time, and so, it will change along the fixed-bed reactor. Therefore, the comparison of propane TOF data of two catalysts only should be done under the same conditions, although using only this parameter is not enough to reach solid conclusions about the activity of this kind of catalysts, unless the catalysts are always fully oxidized under reaction conditions. This is due to the non-linear variation of the catalyst oxidation state, which presents a complex dependence on many factors because of the reaction mechanism nature.

Finally, using the proposed kinetic model with the estimated kinetics constant, the propane inlet partial pressure has been optimized for each catalyst to get the highest yield and productivity at 400 and 480°C for a broad range of space-times and an oxygen inlet partial pressure of 0.1 atm. For a given reaction conditions, the catalyst that presented the best yield and productivity values in the whole range of conditions was the one of V-Zr-O with 5 wt % of vanadium, which contained the highest proportion of polyvanadate species without forming crystalline  $ZrV_2O_7$  phase. The catalyst containing V-Mo-O phases was the most selective. However, it was also the least active, which resulted in the catalyst with the lowest yield and

productivity values in the whole range of conditions. It is possible that V-Mo-O phases in an optimum composition could be the best catalyst for propane ODH, although the presence of another additive elements could also be beneficial. The idea would be, at least, trying to be as active as the polyvanadate species and as selective as the V-Mo-O phases present on the previously mentioned catalyst. The predicted yield and productivity values by the kinetic model for all the catalysts used in this work are much higher than the values usually found in the literature, if the reaction is performed under the proper conditions. The maximum propylene productivity predicted, at a given space-time, exponentially increased as the space-time tended to zero, and tended to zero as the space-time tended to infinity. As the maximum productivity was higher, the required propane inlet partial pressure increased. The reaction conditions that promote the increase of the productivity (short space-times and high propane inlet partial pressures) would lead to experiments with very low propane conversions and very high propylene selectivity. However, regarding the propylene yield, it was observed an opposite trend, the prediction showed that tended to zero as the space-time tended to zero, and tended to 100% as the space-time tended to infinity, although very low propane inlet partial pressure would be required in this case to achieve such value. In addition, the values of yield and productivity were better as the temperature increased in all the cases. It should be noted that the study of the yield and productivity results found in the literature, for a wide variety of catalysts, followed the same trends, what validates the proposed kinetic model explaining the catalytic behavior of most of the catalysts in the propane ODH, and probably in other partial oxidation reactions that follow similar reaction mechanism.

The prediction of the here reported yield and productivity dependence has never found or addressed in the literature before. In fact, it has been repeatedly reported over the past 30 years that the main reason of the low industrial interest in the propane ODH is the low yields obtained, being most of them lower than 30%. Perhaps, the low yield usually obtained in this process is not the only reason, since productivity to propylene is also very

important to make the process economically profitable on an industrial scale. The highest productivity found in the literature among transition metal based catalysts is  $9 \text{ g}_{\text{C}_3\text{H}_6} \cdot \text{g}_{\text{cat}}^{-1} \cdot \text{h}^{-1}$ . However, it has been demonstrated that all the catalysts used in this work can reach yields values of 100% or much higher productivity values than  $9 \text{ g}_{\text{C}_3\text{H}_6} \cdot \text{g}_{\text{cat}}^{-1} \cdot \text{h}^{-1}$ , if proper reaction conditions are used. Therefore, it can be concluded that, instead of low yield or productivity values, the main problems of the industrial implementation of the propane ODH reaction could be to optimize the reaction conditions and to find catalysts that can reach the desired values of yield or productivity in affordable conditions, or to find catalysts that simultaneously present high yield and productivity. Unfortunately, the values of productivity and yield to propylene follow different directions for this reaction. The ideal situation would be that both results follow the same direction.







## **RESUMEN EN ESPAÑOL**



## RESUMEN EN ESPAÑOL

### Introducción

El propileno se ha convertido en el segundo reactivo más importante, tras el etileno, en la industria petroquímica debido a que a partir de él se producen una gran variedad de productos de interés como por ejemplo polipropileno, acrilonitrilo, oxo-alcoholes, óxido de propileno, cumeno, ácido acrílico, etc. El propileno se ha obtenido tradicionalmente como subproducto en los procesos de craqueo al vapor y craqueo catalítico, los cuales han mejorado los rendimientos a sus respectivos productos deseados durante la última década, etileno y gasolina, disminuyendo así el rendimiento a propileno. Esta situación, junto con el incremento de la demanda de propileno, ha incentivado la aparición de tecnologías alternativas para producir propileno, generalmente a partir de propano, el cual es muy abundante y barato actualmente, debido a la proliferación del gas de lutita (“shale gas”).

Hoy en día, la deshidrogenación de propano no oxidativa para producir propileno está ya implementada en la industria utilizando catalizadores de Pt-Sn o Cr<sub>2</sub>O<sub>3</sub> soportados sobre alúmina para las tecnologías Oleflex o Catofin, respectivamente. Sin embargo, este proceso sufre de muchas desventajas, puesto que es una reacción muy endotérmica que trabaja por encima de los 600°C (es un proceso que consume mucha energía) y que está termodinámicamente restringida (limitando la conversión y selectividad). Además, la ocurrencia de reacciones secundarias y de desactivación del catalizador por deposición de coque son aparentes en las condiciones de temperatura de trabajo. Por tanto, de este modo, la deshidrogenación oxidativa (ODH) de propano para obtener propileno aparece como una alternativa prometedora para superar todas las limitaciones anteriores. Este proceso requiere de la introducción de un agente oxidante (generalmente oxígeno) en la mezcla de reacción, siendo una reacción exotérmica que puede ser llevada a cabo a bajas temperaturas (300-600°C), lo que reduce significativamente el consumo de

energía. Además, la reacción no está termodinámicamente restringida y la desactivación del catalizador por deposición de coque es prácticamente inexistente. Sin embargo, la ODH de propano no ha sido industrialmente implementada debido a que los rendimientos hacia propileno obtenidos con este proceso, a día de hoy, son bajos todavía, debido a la ocurrencia indeseada de reacciones de combustión dando lugar a CO y CO<sub>2</sub>, las cuales son difíciles de evitar o controlar. Además, la ODH presenta otros inconvenientes tales como la eliminación del calor formado, inflamabilidad de la mezcla de reacción, y la posibilidad de que la reacción se des controle, lo que puede dar lugar a explosiones y/o dañar el catalizador. Por consiguiente, sería necesario mejorar los catalizadores ya existentes o encontrar nuevos, optimizar las condiciones de reacción y/o diseñar el reactor óptimo con objeto de trabajar bajo condiciones seguras mientras que se puedan obtener altos rendimientos y/o productividades.

Los catalizadores basados en especies de óxidos de vanadio dispersos sobre diferentes soportes (ZrO<sub>2</sub>, TiO<sub>2</sub>, Al<sub>2</sub>O<sub>3</sub>, SiO<sub>2</sub>, etc.) son los más utilizados en la literatura para la ODH de propano, donde es bien conocido que la formación de fases cristalinas de vanadio es generalmente perjudicial para la actividad catalítica. La adición de aditivos tales como alcalinos o alcalinotérreos, metales de transición y fósforo como promotores en los catalizadores basados en óxido de vanadio ha sido reportada en la bibliografía indicando que afecta a las propiedades redox y ácido-base de los catalizadores, y por tanto influye en su actividad catalítica y selectividad. En general, la adición de elementos redox o fósforo provoca un incremento de la actividad y un descenso de la selectividad, mientras que el dopaje con elementos alcalinos promueve un descenso de la actividad y un incremento de la selectividad.

El uso de catalizadores con estructura fibrilar de tamaño submicrométrico podría presentar varias ventajas con respecto a los catalizadores tradicionales en polvo, pero su uso en la ODH de propano todavía no ha sido publicado en la bibliografía. Este tipo de catalizadores muestran muy baja resistencia a la difusión interna y tienen una relación alta de área con

respecto a volumen debido a su diámetro submicrométrico; así como que, cuando se encuentran en un lecho fijo, presentan gradientes de temperatura mucho más bajos y menores pérdidas de carga que los catalizadores en polvo, debido a la alta fracción de huecos o porosidad del lecho que ofrece los materiales fibrilares. Además, son fáciles de manejar y se pueden embalar o construir de la mejor forma para adaptarse al uso o aplicación particular debido a su flexibilidad geométrica. Todas estas diferencias aún serían más apreciables en el uso de estos catalizadores a escala industrial, dado que los catalizadores en polvo pueden superar fácilmente todas estas desventajas intrínsecas a escala de laboratorio agregando un material inerte diluyente (vidrio, cuarzo,  $\alpha$ -alúmina o carburo de silicio) y/o haciendo pellets (lo cual no es necesario para las fibras submicrométricas) que puede que no sea tan beneficioso u operativo a nivel industrial. Además, el tamaño de los pellets debe ser lo suficientemente pequeño como para evitar una alta resistencia a la difusión interna y lo suficientemente grande como para evitar una alta pérdida de carga en el lecho fijo, lo que a veces no es posible. En definitiva, las fibras tienen propiedades de transferencia y fluidodinámicas potencialmente mejores que pueden reducir la probabilidad de formación de puntos calientes permitiendo trabajar en condiciones más seguras, lo que puede hacer que sean más factibles para escalar a nivel industrial.

Algunos autores han investigado el uso de reactores de membrana para la ODH de propano, el cual permite dosificar el oxígeno continuamente a lo largo del reactor disminuyendo la concentración media de oxígeno que interactúa con el catalizador, lo que en cierta medida evita la aparición de puntos calientes en el catalizador, así como incrementa la selectividad en condiciones de isoconversión. De este modo, estos reactores pueden ser alimentados con altas concentraciones de hidrocarburo sin riesgo de explosión. Sin embargo, el uso de membranas puede ser también peligroso en el caso de que la membrana presente alguna rotura o fuga. Entre este tipo de reactores, los reactores de membrana de lecho fluidizado (FLBMR) con alimento de oxígeno distribuido parecen ser los más prometedores

para reacciones muy exotérmicas como es el caso de la ODH de alcanos. Esto es debido a la combinación de la excelente transferencia de calor en el lecho fluidizado con la ventaja de la dosificación de oxígeno a lo largo del reactor, lo que permite la operación en un amplio rango de condiciones con respecto al ratio hidrocarburo/oxígeno en la alimentación del reactor. Además, estos reactores son especialmente robustos contra oscilaciones y perturbaciones en la alimentación, lo que confiere alta seguridad durante la operación. Se ha mostrado que el uso de FLBMR puede mejorar los valores de selectividad y rendimiento hacia olefinas con respecto al uso de reactores de membrana de lecho fijo (FBMR) y reactores de lecho fijo (FBR). Sin embargo, parece ser que el uso de reactores de membrana en la ODH de propano no ha llevado a una mejora significativa de los resultados con respecto a los reactores convencionales, como es el caso de los FBR.

Parece estar claro en la literatura que la ODH de propano procede a través de un mecanismo del tipo de Mars-van Krevelen, lo que significa que el oxígeno estructural del catalizador ( $\text{VO}_x$ ) son los sitios activos. De este modo, el mecanismo involucra las reacciones consecutivas de reducción y oxidación de la superficie del catalizador con propano y oxígeno (u otros agentes oxidantes como  $\text{N}_2\text{O}$ ), respectivamente. El mecanismo general más aceptado en la literatura es a través de reacciones paralelas y consecutivas, donde el propano es oxidado a propileno, y ambos pueden ser totalmente oxidados a  $\text{CO}_x$ . Además, parece haber un consenso en que la activación de propano, la cual ocurre a través del enlace C-H secundario, es la etapa controlante del mecanismo de reacción mediante la formación de especies de radicales propilo o isopropoxido como primeros intermedios de reacción, a partir de los cuales dan lugar a la formación de propileno en la fase gas o especies oxigenadas adsorbidas sobre el catalizador, que normalmente son oxidadas dando lugar a  $\text{CO}_x$  en la fase gas. Aunque parezca haber un acuerdo en que los oxígenos puentes (V-O-V/V-O-Soporte) son los más activos, todavía hay autores que reportan actualmente que los oxígenos terminales (V=O) son más activos. Tampoco

está claro qué especies son más activas, monovanadatos o polivanadatos, o si presentan la misma actividad. Además, a pesar de la gran cantidad de artículos publicados sobre la ODH de propano, no se han dado muchos detalles sobre la naturaleza y número de reacciones elementales del mecanismo de reacción que da lugar a la formación de CO y CO<sub>2</sub>.

No hay muchos artículos en la bibliografía que describan a fondo el mecanismo de reacción o lleven a cabo un estudio cinético de forma detallada. Se han utilizado diferentes modelos cinéticos (Power Law, Langmuir-Hinshelwood, Eley-Rideal, etc.), pero la expresión de Mars-van Krevelen es la propuesta más frecuentemente para reacciones de ODH. El parámetro cinético comparado habitualmente entre los diferentes catalizadores es la energía de activación de la primera abstracción de hidrógeno del propano, o dicho de otra forma, la etapa controlante. En la literatura se puede encontrar un amplio rango de valores de energías de activación incluso entre catalizadores equivalentes (utilizando el mismo soporte y con la misma composición), probablemente debido a la variedad de diferentes modelos cinéticos utilizados, los cuales son a veces simplificados en exceso y/o frecuentemente inconsistentes e incorrectos sin relevancia física. El estudio de la variación de los valores de TOF de propano con respecto a la concentración de vanadio se ha utilizado ampliamente en la literatura para tratar de discernir si los monovanadatos son más, menos o igualmente activos que los polivanadatos. Puesto que la proporción de estas especies superficiales dependen de la carga de vanadio, siendo la proporción de polivanadatos con respecto monovanadatos más alta conforme la concentración de vanadio es más alta. Sin embargo, se pueden encontrar tendencias diferentes entre distintos autores. Se ha reportado que conforme el contenido de vanadio del catalizador aumenta, el TOF disminuye, aumenta o permanece constante. Estas discrepancias pueden ser debidas al uso de diferentes métodos de preparación, soportes y concentraciones, los cuales pueden resultar en diferentes tipos de especies superficiales de óxidos de vanadio. Además, no se puede descartar la posible existencia de problemas





difusionales de transferencia interna y/o externa de materia y/o energía, así como contribución de la reacción en fase homogénea a altas temperaturas (por encima de 500°C) y/o experimentos con conversión total de oxígeno.

Por tanto, los objetivos de esta tesis son, por un lado, la preparación de catalizadores fibrilares de tamaño submicrométrico de óxido de vanadio disperso sobre zirconia mediante la técnica de electrospinning para la reacción de ODH de propano, así como la incorporación de aditivos como Mo y Nb a dichos materiales fibrilares para tratar de modular su actividad y selectividad. La forma de fibra submicrométrica debería de conferir a los catalizadores una muy baja resistencia a la difusión interna comparado con los catalizadores tradicionales en forma de polvo, así como menos problemas de gradientes de temperatura y pérdida de carga cuando estos materiales se encuentran empacados en un lecho fijo, permitiendo que las condiciones de operación sean más seguras. Además, estas ventajas deberían facilitar la realización de los experimentos, sin la necesidad de tener que añadir ningún tipo de material inerte para diluir el lecho (por ejemplo, carburo de silicio), al mismo tiempo que se facilita la obtención aislada de datos cinéticos intrínsecos de los catalizadores sin la interferencia de otros efectos. Por otro lado, serán realizados experimentos *operando*, en un nuevo reactor (“IRRaman reactor”), con la obtención simultánea de espectros FTIR y Raman, con objeto de estudiar la relación que hay entre la actividad y la estructura de la superficie del catalizador durante la reacción de la ODH de propano, y así proponer un mecanismo de reacción, mientras que se proveen las bases requeridas para llevar a cabo un futuro estudio cinético riguroso. Posteriormente, serán llevado a cabo experimentos de ODH de propano en un reactor de lecho fijo convencional variando la temperatura, las presiones parciales iniciales de propano y oxígeno y el tiempo espacial con objeto de realizar un estudio cinético y estimar los valores de las constantes cinéticas de los catalizadores. De este modo, será estudiada la influencia de la concentración de vanadio y de la presencia de molibdeno o niobio sobre

los valores estimados de las constantes cinéticas, para intentar averiguar información cinética de las especies de polivanadatos, monovanadatos,  $ZrV_2O_7$  cristalino, V-Mo-O y V-Nb-O. Finalmente serán simulados los valores de rendimiento y productividad hacia propileno usando el modelo cinético propuesto en este trabajo, en un intento de encontrar las condiciones teóricamente óptimas para conseguir sus valores máximos. Esta información catalítica podría ser muy útil para diseñar catalizadores mejores, utilizar el reactor adecuado y trabajar en las condiciones de reacción óptimas, y por tanto, determinar si un catalizador podría ser adecuado para su uso a escala industrial.

### **Secciones 3.1 y 3.2**

En estas secciones se han preparado catalizadores fibrilares basados en óxidos metálicos de Zr, Zr-V, Zr-Mo, Zr-Nb, Zr-V-Mo o Zr-V-Nb mediante la técnica de electrospinning para estudiar la reacción de la ODH de propano. Se ha propuesto un nuevo procedimiento que es simple, versátil y directo para la preparación de dichos catalizadores. En dicho procedimiento, se realiza el electrohilado de la disolución polimérica que contiene todos los precursores metálicos requeridos de zirconia, vanadio, niobio y/o molibdeno, seguido de un solo paso de calcinación para obtener los catalizadores finales con forma de fibras submicrométricas. Sin embargo, los métodos tradicionales para preparar catalizadores soportados, tales como el de impregnación por humedad incipiente, normalmente requieren al menos dos etapas de calcinación: uno para la preparación del soporte catalítico y otro después de la impregnación de dicho soporte con el precursor de la fase activa.

Las disoluciones poliméricas para llevar a cabo el electrohilado se han preparado utilizando dos precursores de zirconio distintos, acetato de zirconio o propóxido de zirconio, para evaluar la influencia del tipo de precursor. Mientras que los precursores de vanadio, molibdeno y niobio siempre fueron los mismos, acetilacetonato de vanadilo, heptamolibdato de amonio tetrahidratado y oxalato de niobato de amonio hidratado,

respectivamente. Tras el electrohilado, las fibras fueron calcinadas a 500°C en atmósfera de aire para eliminar la materia orgánica y el disolvente remanente de la disolución polimérica. De esta manera se han preparado una serie de catalizadores cambiando la concentración de vanadio, molibdeno o niobio final en la muestra para ambos precursores de zirconia.

Todos los catalizadores presentaron una composición metálica muy homogénea a lo largo de las fibras. La mayoría de estos materiales mostraron una ratio muy alto de longitud/diámetro y sin la presencia de zonas fundidas o gotas, lo que confirmó que la morfología fibrilar de las muestras fue conseguida satisfactoriamente con un diámetro del orden de los 100 nanómetros (submicrométrico). En todos los casos, las muestras preparadas usando propóxido presentaron fibras con diámetros más gruesos comparado con las muestras preparadas con acetato, probablemente debido al menor voltaje aplicado que requirió las muestras preparadas con propóxido durante el proceso de electrohilado, aunque la influencia de otros parámetros de la disolución como la viscosidad o conductividad eléctrica no deberían de ser descartados. Además, se ha observado de forma generalizada que la incorporación de vanadio disminuye el diámetro en el caso de los materiales preparados con propóxido, probablemente debido al incremento de la conductividad eléctrica de la disolución polimérica como consecuencia de la presencia del precursor de vanadio. Lo mismo ocurrió, pero en menor medida, cuando los precursores de niobio o molibdeno fueron añadidos a la disolución polimérica. Sin embargo, otras tendencias fueron observadas cuando los precursores de vanadio, molibdeno o niobio fueron añadidos a las disoluciones poliméricas preparadas con acetato de zirconio. Cabe destacar que las fibras de molibdeno preparadas con el precursor de propóxido fueron aparentemente más frágiles que aquellas preparadas con el precursor de acetato.

Se ha observado que los catalizadores obtenidos utilizando el precursor de propóxido de zirconio tienden a presentar una textura porosa más desarrollada en todo el rango de microporos y mesoporos, dando lugar a

valores de superficie específica más altos, que aquellos obtenidos usando el acetato de zirconio como precursor. Además, para ambos precursores de zirconio, se ha observado que la presencia del precursor de vanadio durante la etapa de calcinación favorece el desarrollo de la textura porosa del catalizador. Sin embargo, llegado a un determinado contenido de V (5% en masa), el área específica del catalizador empieza a disminuir como resultado de la formación cristales de V que posiblemente puedan bloquear parcialmente los poros. Este mismo fenómeno también se observó, pero en menor medida, cuando se utilizaron los precursores de Mo ó Nb.

Independientemente del precursor de zirconia utilizado, los resultados obtenidos mediante difracción de rayos X, espectroscopía Raman y XPS revelaron que todos los catalizadores presentaban zirconia cristalina en fase tetragonal, mientras que no fueron detectadas ninguna de las fases cristalinas de  $V_2O_5$ ,  $Nb_2O_5$  ó  $MoO_3$ . En aquellos catalizadores que contenían vanadio, éste se encontraba en forma de óxido de vanadio amorfo y disperso sobre la zirconia. Estas especies de vanadio se encontraban formando estructuras de monovanadatos y polivanadatos, aumentando la proporción de estos últimos a medida que la densidad superficial de vanadio final era mayor. Además, se ha observado que llegado a una cierta densidad superficial de vanadio, se empezó a favorecer la formación de cristales de  $ZrV_2O_7$ , lo cual coincidió con el momento en el que la superficie específica final del catalizador empezó a descender. En el caso de los catalizadores preparados a partir del precursor de acetato de zirconio, la formación de cristales de  $ZrV_2O_7$  comenzó a favorecerse a concentraciones de vanadio más bajas, lo que sugiere que el uso de acetato como precursor tiende a favorecer más la formación estructuras de vanadio condensadas que cuando se usa propóxido como precursor. En cuanto a los catalizadores que contenían Mo ó Nb, también se ha observado la fase amorfa o dispersa de sus respectivos óxidos. Sin embargo, no se han observado las fases cristalinas correspondientes, quizás porque las concentraciones de estos metales en el catalizador nunca fueron demasiado altas.

Todos estos catalizadores también fueron probados en la reacción de ODH de propano en un reactor de lecho fijo. Con respecto a las condiciones de reacción, la temperatura de reacción se varió de 300 a 480°C, la presión parcial inicial de propano y de oxígeno fue de 0,2 y 0,1 atm, respectivamente, y el flujo total de gas y la masa de catalizador se ajustó para obtener tiempos espaciales en el rango de 0,1 a 1,0 g·s·mL<sup>-1</sup>C<sub>3</sub>H<sub>8</sub> (el volumen siempre es expresado en condiciones STP).

Para todos los catalizadores, un aumento de la temperatura o del tiempo espacial conllevó a un aumento en la conversión de propano y a una disminución de la selectividad hacia propileno, o lo que es lo mismo, a un aumento de la selectividad hacia CO<sub>x</sub>. En el caso de los catalizadores de V-Zr-O, se observó que los más activos eran aquellos que, sin llegar a contener especies de ZrV<sub>2</sub>O<sub>7</sub> cristalinas, contenían más cantidad de óxido de vanadio disperso (VO<sub>x</sub>), siendo más activos en la forma de polivanadatos que de monovanadatos. Se observó una notable disminución de la selectividad a propileno cuando la muestra presentaba cristales de ZrV<sub>2</sub>O<sub>7</sub>, mostrando que estas especies son menos convenientes para la reacción que el óxido de vanadio amorfo y disperso (VO<sub>x</sub>). Por otro lado, los catalizadores de Mo-Zr-O y de Nb-Zr-O también fueron probados en las mismas condiciones de reacción que los anteriores. Los resultados obtenidos mostraron que la actividad catalítica de ambos materiales es despreciable a temperaturas más bajas de 480°C, siendo el de Mo-Zr-O algo más activo que el de Nb-Zr-O. Sin embargo, aunque los catalizadores de V-Mo-Zr-O presentaron conversiones más bajas que aquellos de V-Zr-O para unas mismas condiciones dadas, se ha observado que los de V-Mo-Zr-O presentaron una selectividad notablemente más alta comparando resultados de misma conversión para ambos catalizadores. Estos resultados sugieren que las especies de vanadio y molibdeno, de algún modo, deben interaccionar entre sí dando lugar a sitios activos que tienden a formar propileno evitando la oxidación total dando CO<sub>x</sub>. Por otro lado, los catalizadores de Zr-V-Nb no mostraron una mejora significativa

en el comportamiento catalítico con respecto a los catalizadores de Zr-V, al menos en las proporciones estudiadas en este trabajo.

Todos los catalizadores presentaron valores de selectividades a propileno del 100% a conversiones de propano muy bajas. Luego, conforme la conversión fue incrementando, la selectividad a CO empezó a ser apreciable junto a la de propileno, pero no a CO<sub>2</sub>. Finalmente, la presencia de CO<sub>2</sub> también empezó a ser observada a conversiones relativamente altas. Estos resultados sugirieron que el mecanismo de la reacción podría ocurrir de forma consecutiva, donde primeramente se forma propileno, luego CO y finalmente CO<sub>2</sub>, aunque la combustión directa de propano no debería ser descartada, especialmente a altas temperaturas.

Hay que destacar que los catalizadores en las condiciones estudiadas fueron muy estables y no dieron síntomas de sufrir desactivación con el paso del tiempo. Además, los resultados obtenidos de TOF y productividades a propileno con estos catalizadores fueron comparables con los mejores encontrados en bibliografía, mostrando la validez de este nuevo método de preparación con la técnica de electrospinning para este tipo de catalizadores en forma de fibras.

### Sección 3.3

El objetivo de esta sección era obtener información acerca del mecanismo de la reacción de la ODH de propano sobre catalizadores de V-Zr-O. De este modo, se ha utilizado una nueva celda *operando* (“IRRaman reactor”) que permite la caracterización de la superficie del catalizador mediante la obtención de espectros FTIR y Raman, con medida simultánea de la actividad catalítica a través de un espectrómetro de masas y un espectrofotómetro de FTIR que se sitúan a la salida de la celda para analizar la fase gaseosa. Por tanto, dicho reactor puede ser muy útil para correlacionar la actividad catalítica del catalizador con los cambios producidos en su estructura y las especies adsorbidas en su superficie, pudiendo establecerse mecanismos de reacción y siendo posible la identificación de especies activas e intermedios de reacción.

Se realizaron experimentos con tres catalizadores de V-Zr-O con distintas concentraciones de vanadio, puesto que dicha concentración afecta a la proporción de especies superficiales de polivanadatos y monovanadatos, el estudio comparativo de ellas podía ser importante para entender el mecanismo de reacción y la influencia de cada una de las especies. Cabe destacar que los catalizadores fibrilares fueron machacados y prensados en forma de pastilla para realizar los experimentos *operando* en la celda. Con respecto a las condiciones de operación, la temperatura se varió desde temperatura ambiente hasta 340°C, la masa de catalizador y el flujo total volumétrico de gas fueron de 31,5 mg y 18,1 mL·min<sup>-1</sup>, respectivamente, y las presiones parciales iniciales de propano y oxígeno fueron siempre de 0,2 y 0,1 atm, respectivamente.

Los resultados operando obtenidos en este trabajo durante la reacción de la ODH de propano mostraron que los catalizadores eran parcialmente reducidos durante reacción, mientras que parte del propano era oxidado dando lugar a propileno (producto deseado), así como especies oxigenadas adsorbidas sobre la superficie del catalizador actuando como intermedios de reacción en el mecanismo para la oxidación total a CO<sub>x</sub> (productos indeseados). Con respecto a las especies superficiales, acetatos y formiatos fueron generalmente los intermedios de reacción más abundantes (MARI), junto con pequeñas cantidades de acrilatos, para la mayoría de las condiciones de reacción estudiadas. Se esperaba también la formación de otras especies intermedias de reacción previas a los carboxilatos, pero no fueron detectadas en las condiciones estudiadas, probablemente debido a sus bajas o despreciables concentraciones superficiales, como resultado de la relativa baja estabilidad de tales especies con respecto a aquellas involucradas en la etapa controlante (activación de propano).

Además, el hecho de que las especies oxigenadas fueran estables y acumuladas sobre la superficie por debajo de la temperatura de reacción sugirió que los valores de las energías de activación para las reacciones de oxidación de dichas especies deberían ser más altas que la de la etapa

controlante. Esto fue consistente con el descenso de la cantidad de especies adsorbidas con el incremento de la temperatura y el correspondiente aumento de la conversión. Por otro lado, los formiatos empezaron a descomponerse en forma de CO a temperaturas más bajas que los acetatos, lo que sugirió que la energía de activación de la oxidación de acetatos es más alta que la de formiatos. Esto es consistente con la mayor estabilidad de las especies de acetatos con respecto a formiatos, lo cual ya se ha reportado en la bibliografía.

Con respecto al oxígeno estructural, los enlaces V=O y V-O-V/V-O-Zr mostraron cambios durante la reacción, los cuales fueron rápidamente reversibles hacia el estado inicial en presencia de aire. Los cambios más notorios fueron observados en los enlaces puentes de oxígenos V-O-V y V-O-Zr. Además, estos enlaces empezaron a interactuar con propano a temperaturas más bajas que los oxígenos terminales (V=O), sugiriendo que probablemente los enlaces V-O-V y V-O-Zr son los sitios más activos de estos catalizadores en la reacción de la ODH de propano. El ligero descenso de la cantidad de estos enlaces con el incremento de la temperatura de reacción indicó que la energía de activación de la reoxidación de dichos enlaces es más baja que la de la etapa controlante, la cual determina la velocidad de las distintas reacciones de reducción que ocurren en la superficie del catalizador. Para el caso de los enlaces terminales de oxígeno (V=O), las pequeñas perturbaciones observadas podrían ser asociadas a la interacción de estos sitios de oxígenos con las especies adsorbidas, puesto que estos cambios sólo se observaron cuando dichas especies adsorbidas estaban presentes y desaparecían cuando estos oxigenados eran eliminados, independientemente de si el catalizador había sido reoxidado o no.

También fueron realizados experimentos *operando* en régimen transitorio utilizando flujos de propano sin oxígeno en la alimentación (20% de propano en argón). El hecho de que propileno, CO y CO<sub>2</sub> fueron detectados durante algunos minutos, incluso aunque no había oxígeno en la fase gas, confirmó la participación del oxígeno estructural del catalizador durante la



reacción, al igual que en los mecanismos de reacción del tipo Mars-van Krevelen. Estos resultados mostraron que los sitios V-O-V/V-O-Zr (enlaces de oxígenos puentes contenidos en la estructura del catalizador) son capaces de completar el ciclo catalítico completo de la reacción de la ODH de propano sin la participación del oxígeno de la fase gaseosa o de los enlaces de oxígenos terminales (V=O), puesto que todos los productos de la fase gas y todas las especies adsorbidas que se forman durante tal reacción fueron formados durante el primer minuto de reacción con el consumo único y exclusivo de los oxígenos puentes de la estructura del catalizador. Por consiguiente, los resultados revelaron que los enlaces de oxígenos terminales (V=O) presentan algo de actividad, pero mucho más baja que los enlaces de oxígenos puente (V-O-V/V-O-Zr). Ésto va en la línea de predicciones anteriores reportadas por otros autores sobre la más alta actividad de los oxígenos puente con respecto a los oxígenos terminales. Cabe destacar que el análisis simultáneo de los espectros FTIR y Raman de la fase gas, de la estructura del catalizador y de las especies adsorbidas fue crucial para observar directamente la diferencia de actividades entre los distintos sitios de oxígeno. Además, la consistencia en el espacio y tiempo ofrecida por el "IRRaman reactor", debido a su muy pequeño volumen muerto, fue también crucial para llevar a cabo satisfactoriamente estos experimentos en régimen transitorio.

Por último, también se realizó un experimento alimentando propileno y oxígeno, puesto que el propileno es más reactivo que el propano, y entonces permite empezar la reacción a temperaturas más bajas, a las cuales puede que las especies intermedias de reacción menos estables aparezcan ahora con una mayor concentración superficial y puedan ser detectables. Además, como es bien conocido que la principal fuente de CO<sub>x</sub> durante la ODH de propano es la oxidación consecutiva del propileno formado, este experimento podría dar información acerca de las reacciones de oxidación que tienen lugar durante la vía de oxidación total. Los resultados mostraron que la activación del propileno ocurre principalmente a través de la formación de especies de isopropóxido que

posteriormente se oxida a acetona quimisorbida y después a carboxilatos, como ya también fue observado en trabajos anteriores, a diferencia de otros estudios donde se ha descrito la activación de propileno a través de la formación de alil-alcóxidos dando lugar posteriormente a acroleína quimisorbida y después acrilatos. Se concluyó que probablemente ambas rutas de oxidación del propileno pueden ocurrir simultáneamente, y que la naturaleza del catalizador determina el camino de oxidación más favorable o la contribución de cada uno en la oxidación total del propileno. Por otro lado, fue asumido que la activación del propano ocurre también a través de isopropóxido, como ha sido reportado en otros trabajos, lo que significaría que hay un intermedio de reacción común responsable de las dos reacciones paralelas, la formación de propileno y la oxidación total de propano o propileno.

Acorde a todos los resultados obtenidos, se ha propuesto un mecanismo general de reacción. Se han considerado que los enlaces V-O-V y V-O-Zr son los sitios más activos. Se ha propuesto que la oxidación de propano en estos catalizadores ocurre a través de la formación irreversible de isopropóxido, el cual puede dar lugar a propileno en la fase gas o continuar oxidándose a acetona quimisorbida. El propileno formado puede adsorberse de nuevo y reaccionar con un sitio V-OH (que actuaría como sitio ácido de Bronsted) dando lugar a isopropóxido, que luego se puede oxidar a acetona quimisorbida, que por escisión oxidativa da lugar a la formación de una mezcla de especies adsorbidas de formiatos y acetatos bidentados, los cuales se descomponen dando  $\text{CO}_x$  en la fase gaseosa (productos indeseados).

Tal y como se ha descrito, ha sido posible observar experimentalmente que la reacción ocurre a través de un mecanismo del tipo Mars-van Krevelen, mostrando claras evidencias de que los sitios de oxígeno puentes (V-O-V/V-O-Zr) son mucho más activos que los sitios de oxígeno terminales (V=O). Además, se han identificado los pasos requeridos para la oxidación total hacia  $\text{CO}_x$ , al menos para los catalizadores de V-Zr-O, lo cual podría ser útil para saber cómo proceder para evitar de alguna manera la

oxidación total de propano, y por tanto, aumentando la selectividad hacia propileno.

### Secciones 3.4 y 3.5

El objetivo de estas secciones fue hacer un estudio cinético de la reacción ODH de propano sobre los catalizadores fibrilares de diámetro submicrométrico ya preparados por electrospinning y caracterizados a fondo en las *Secciones 3.1 y 3.2*, estableciendo las ecuaciones cinéticas de manera rigurosa y utilizando el mecanismo de reacción propuesto en la *Sección 3.3*, de acuerdo con los resultados *operando* FTIR-Raman obtenidos en el “IRRaman reactor”. El estudio cinético se ha realizado sobre cuatro catalizadores diferentes para estudiar la influencia de la concentración de vanadio y la presencia de molibdeno en los catalizadores y, en consecuencia, para encontrar información cinética de las especies de polivanadato, monovanadato,  $ZrV_2O_7$  cristalino y V-Mo-O. De esta manera, los parámetros cinéticos de cada catalizador han sido analizados y comparados. Finalmente, se han simulado valores de rendimiento y productividad hacia propileno en un amplio rango de condiciones para estudiar su dependencia y tratar de encontrar las condiciones teóricas óptimas para obtener sus valores máximos. Esta información catalítica podría ser muy útil para determinar si un catalizador puede ser adecuado para su uso a escala industrial.

El uso de la técnica de electrospinning permitió la preparación de catalizadores con una composición muy uniforme y con una estructura fibrilar de diámetro submicrométrico, lo que le confiere al catalizador bajas resistencias a la difusión interna durante la reacción, así como menores gradientes de temperatura y de pérdidas de carga a lo largo del lecho en comparación con los catalizadores en polvo tradicionales, cuando éstos se empacan en un reactor convencional de lecho fijo. Estas ventajas hicieron más fácil la realización de los experimentos de reacción, sin la necesidad de la adición de materiales inertes (por ejemplo, carburo de silicio) como diluyente en el lecho fijo, obteniendo de forma aislada información cinética

intrínseca del catalizador, minimizando así la interferencia de otros efectos. En este sentido, se llevaron a cabo los experimentos en un reactor de lecho fijo, y para cada catalizador se varió la temperatura de 300 a 480°C, las presiones parciales iniciales de propano y oxígeno se varió entre 0,025 y 0,2 atm, y el tiempo espacial entre 0,1 y 1,0 g·s·mL<sup>-1</sup>C<sub>3</sub>H<sub>8</sub>.

Para la realización del estudio cinético, primeramente, se propusieron las ecuaciones cinéticas acorde al mecanismo propuesto y los resultados espectroscópicos en *operando* obtenidos en la *Sección 3.3*. Se ha asumido estado estacionario y que la mayoría de las reacciones superficiales de oxidación de cada una de las especies intermedias involucradas en el mecanismo son irreversibles, lo cual suele ser una buena aproximación en este tipo de reacciones superficiales de oxidación. Además, se ha asumido que las reacciones de oxidación de las distintas especies de hidrocarburos ocurren a través del oxígeno estructural del catalizador. Por simplificación, en las ecuaciones cinéticas no se ha hecho distinción entre los dos tipos de oxígeno de la estructura del catalizador que son activos, V-O-V y V-O-Zr, aunque puede que sean distintos. Se ha considerado despreciable la posible contribución durante la reacción del oxígeno contenido en forma de enlaces terminales V=O. En el balance de sitios y de especies adsorbidas, el grado de cobertura de propileno adsorbido, isopropóxido y acetona quimisorbida se ha despreciado frente al resto de especies presentes. Las expresiones para determinar las coberturas superficiales fueron obtenidas asumiendo estado pseudo estacionario y haciendo balance para cada sitio o especie adsorbida.

Para la interpretación de los datos experimentales, se ha utilizado la ecuación de balance de materia para reactor de lecho fijo, así como se ha considerado comportamiento de reactor integral. También se asume el cumplimiento de los siguientes requerimientos: distribución uniforme de sitios activos en la superficie del catalizador (como se muestra en los datos de caracterización y con más detalle en las *Secciones 3.1* y *3.2*); la dispersión axial y los efectos de pared se descartaron ya que el diámetro de las fibras (submicrométrico) eran varios órdenes de magnitud menor

que la longitud y el diámetro del reactor de lecho fijo, respectivamente; el reactor operó en condiciones estacionarias; se descartó la posible presencia de problemas difusionales (como se demostró en la *Sección 3.1* usando el mismo procedimiento experimental); y se consideraron despreciables los gradientes de temperatura y pérdidas de carga dentro del reactor. Puesto que se cumplieron todas las condiciones anteriores, la ecuación de balance de materia para el reactor de lecho fijo se simplificó dando lugar a la del reactor ideal de flujo pistón. De modo que, combinando los balances de materia de oxígeno, propano, propileno, monóxido de carbono y dióxido de carbono, con sus respectivas ecuaciones de velocidad y las correspondientes expresiones de cobertura superficial, se obtuvieron las ecuaciones diferenciales del balance de materia para cada uno de los reactivos y productos.

Este sistema de ecuaciones diferenciales fue numéricamente resuelto, para los parámetros cinéticos propuestos en cada iteración, con objeto de calcular los valores de conversión, selectividad y rendimiento, así como las coberturas superficiales de cada uno de los sitios y especies adsorbidas que participan en el mecanismo de reacción. Todas estas ecuaciones se han resuelto numéricamente, para la optimización de las constantes cinéticas estimadas, utilizando la herramienta de Matlab. Para la optimización se tuvo en cuenta que los parámetros cinéticos cumplieran las leyes de Arrhenius y Van't Hoff. Los parámetros cinéticos estimados fueron utilizados para simular los valores de conversión, selectividad, rendimiento y productividad a diferentes temperaturas, tiempos espaciales y presiones parciales iniciales de propano y oxígeno. La comparación de los resultados obtenidos experimentalmente con aquellos simulados mostró que el ajuste cinético ha sido satisfactorio para cada catalizador estudiado. El modelo cinético fue también capaz de predecir el grado de cobertura de cada una de las especies intermedios de reacción, así como de las especies de vanadio involucradas en el mecanismo, a lo largo del lecho catalítico para unas condiciones dadas de temperatura, tiempo espacial, presión parcial inicial de propano y de oxígeno.

Se ha observado que la concentración de vanadio en el catalizador y/o la adición de molibdeno al catalizador tuvo una gran influencia en todos los parámetros cinéticos, sugiriendo la formación de diferentes especies activas y/o entornos que los rodea. De alguna manera la conversión y la selectividad de los catalizadores serán influenciados por todos los parámetros cinéticos. Sin embargo, la conversión de los catalizadores será principalmente determinada por los parámetros cinéticos asociados a la etapa controlante (quimisorción disociativa de propano), mientras que la selectividad a propileno será determinada por los parámetros cinéticos pertenecientes a la adsorción de propileno con posterior reacción con sitios V-OH formando isopropóxido y a la reacción de deshidratación para la eliminación de tales sitios de V-OH. Acorde a los resultados obtenidos en este trabajo, las especies de polivanadatos presentaron la mejor combinación de actividad catalítica y selectividad a propileno. Las especies de monovanadatos son ligeramente menos activas y selectivas a propileno que las especies de polivanadatos. La tendencia del propileno a adsorberse sobre ambas especies es similar, pero la velocidad de deshidratación de los sitios V-OH en los monovanadatos es más lenta, lo que explica que estas especies sean menos selectivas que los polivanadatos. Las fases cristalinas de  $ZrV_2O_7$  son más activas que los polivanadatos, pero la fracción de sitios activos expuestos en estas especies disminuye como consecuencia de la aglomeración y formación de estructuras más condensadas. Además, estas especies cristalinas favorecen la adsorción de propileno para ser oxidado a isopropóxido, lo que resulta en un descenso de la selectividad a propileno incentivando la oxidación total a  $CO_x$ . Por otro lado, las fases de V-Mo-O son las menos activas y las más selectivas entre las distintas especies activas consideradas en este trabajo. La baja velocidad de adsorción de propileno para su posterior oxidación hacia isopropóxido es la razón de la alta selectividad a propileno que presentan estas últimas especies.

Además, el modelo predice que los catalizadores utilizados en este trabajo no se encuentran totalmente oxidados cuando están en condiciones de

reacción, incluso para los experimentos con las presiones parciales iniciales de oxígeno más altas o para cuando el tiempo espacial tiende a cero (conversión despreciable). Esto significa que, aunque la reacción es de pseudo-cero orden con respecto al oxígeno en un amplio rango de condiciones, el catalizador puede que no esté totalmente oxidado, incluso aunque la velocidad de reoxidación del catalizador es mucho más rápida que la de reducción. Entonces, la asunción de considerar que el catalizador está siempre totalmente oxidado para simplificar las ecuaciones podría a veces ser errónea o no del todo cierta. De hecho, el modelo predice que el estado de oxidación del catalizador en condiciones de reacción dependerá de su naturaleza química intrínseca, la composición de la fase gas, temperatura y tiempo espacial. Además, puesto que la velocidad de reacción de la etapa controlante es considerada ser de segundo orden con respecto a la cobertura superficial de los sitios activos, se puede deducir que el TOF de propano depende del estado de oxidación del catalizador, y entonces también dependerá de las condiciones de reacción y tiempo espacial, y por tanto variará a lo largo del lecho catalítico. Por consiguiente, la comparación de valores de TOF de propano de dos catalizadores distintos debería de ser realizada siempre en las mismas condiciones, aunque usando sólo este parámetro no es suficiente para lograr conclusiones definitivas sobre la actividad de este tipo de catalizadores, a menos que los catalizadores estén totalmente oxidados durante la reacción. Esto es debido a la dependencia no lineal y compleja que presenta el estado de oxidación del catalizador, el cual depende de muchos factores distintos, debido a la naturaleza del mecanismo de reacción.

Finalmente, utilizando el modelo cinético propuesto con las constantes cinéticas estimadas, ha sido optimizada para cada catalizador la presión parcial inicial de propano para conseguir los rendimientos y productividades más altos posibles a 400 y 480°C para un amplio rango de tiempos espaciales y una presión parcial inicial de oxígeno de 0,1 atm. Para unas mismas condiciones de reacción, el catalizador que siempre presentó mejores rendimientos y productividades fue el de V-Zr-O con un 5% de

vanadio, el cual contenía la proporción más alta de polivanadatos en su superficie sin la formación de especies cristalinas de  $ZrV_2O_7$ . El catalizador que contenía fases de V-Mo-O fue el más selectivo. Sin embargo, también fue el menos activo, lo que resultó en los valores de rendimientos y productividades más bajos para todo el rango de condiciones estudiadas. Es posible que el mejor catalizador podría ser la fase V-Mo-O (sin descartar la adición de otro aditivo) en una composición de vanadio y molibdeno óptima, tal que, fuera tan activo como las especies de polivanadatos y tan selectivo como las fases de V-Mo-O observadas en el catalizador estudiado en este trabajo.

Los valores de rendimientos y productividades predichos por el modelo cinético para todos los catalizadores utilizados en este trabajo pueden llegar ser mucho más altos que los valores normalmente encontrados en la literatura, siempre y cuando la reacción sea llevada a cabo en las condiciones apropiadas. La productividad máxima de propileno estimada, a un tiempo espacial dado, aumentó exponencialmente a medida que el tiempo espacial tendía a cero, y tendía a cero a medida que el tiempo espacial tendía a infinito. Conforme la productividad máxima fue mayor, la presión parcial de entrada de propano requerida para ello aumentó. Las condiciones de reacción que promueven el aumento de la productividad (tiempos espaciales bajos y presiones parciales iniciales de propano altas) condujeron a experimentos con conversiones de propano muy bajas y una selectividad de propileno muy alta. Sin embargo, con respecto al rendimiento de propileno se observó una tendencia opuesta a la productividad, la predicción mostró que tendía a cero conforme el tiempo espacial tendía a cero, y tendía al 100% conforme el tiempo espacial tendía al infinito, aunque en este caso se requeriría una presión parcial inicial de propano muy baja para lograr tal valor. Además, los valores de rendimiento y productividad aumentaron con el aumento de la temperatura en todos los casos. Cabe destacar que el análisis de los resultados de rendimiento y productividad encontrados en la bibliografía, para una amplia variedad de catalizadores, siguieron estas mismas tendencias, lo que valida el modelo



cinético propuesto pudiendo explicar el comportamiento catalítico de la mayoría de los catalizadores en la ODH de propano, y probablemente de forma similar en otras reacciones de oxidación parcial que puedan presentar mecanismos de reacción parecidos.

La predicción de la dependencia de los valores de rendimiento y productividad en función de las condiciones de operación mostrada en este trabajo nunca ha sido descrita en la literatura. De hecho, se ha mencionado en muchas ocasiones que la razón principal del bajo interés industrial de la ODH de propano ha sido siempre los bajos rendimientos, los cuales raramente llegan a superar el 30%. Por otro lado, no sólo los bajos rendimientos han frenado la implementación industrial de este proceso, puesto que la productividad es también importante. La productividad más alta publicada hasta el momento es de  $9 \text{ g}_{\text{C}_3\text{H}_6} \cdot \text{g}_{\text{cat}}^{-1} \cdot \text{h}^{-1}$ . Sin embargo, ha sido demostrado que todos los catalizadores usados en este trabajo podrían alcanzar rendimientos del 100% o productividades mucho más altas que  $9 \text{ g}_{\text{C}_3\text{H}_6} \cdot \text{g}_{\text{cat}}^{-1} \cdot \text{h}^{-1}$ , siempre y cuando se utilicen las condiciones de operación adecuadas. Por consiguiente, puede ser concluido que, en vez de los bajos rendimientos o productividades, el principal problema para la industrialización de la ODH de propano podría ser la optimización de las condiciones de reacción, y encontrar catalizadores que puedan alcanzar los valores deseados de rendimiento y productividad en unas condiciones viables de operación, o encontrar catalizadores que puedan dar simultáneamente altos valores de rendimientos y productividad. Desafortunadamente, los valores de productividad y rendimiento siguen distintas direcciones. La situación ideal sería que ambos siguieran la misma dirección.



## ACKNOWLEDGEMENTS

Llegados a este momento, me siento muy feliz por acabar mi tesis doctoral y ver que todo el esfuerzo ha tenido su recompensa. Pero, sobre todo, estoy muy agradecido y me siento muy afortunado por toda la gente que ha estado a mi alrededor durante estos años.

En primer lugar, quiero dejar constancia de mi agradecimiento a mis directores de tesis doctoral, Dr. D. José Rodríguez Mirasol y Dra. Dña. María Olga Guerrero Pérez, por la paciencia que han tenido conmigo y por la sabiduría que me han transmitido, la cual tiene un valor incalculable. Me siento muy orgulloso de haberlos tenido como directores. Y por supuesto, quiero agradecer a Dr. D. Tomás Cordero Alcántara, por haber sido también, aunque no de manera oficial, director de mi tesis. También me ha enseñado mucho, y sus consejos y dedicación han sido imprescindibles para que todo haya sido posible. Además, me ha apoyado y ayudado en todo momento.

En el apartado de los agradecimientos institucionales, he de agradecer al Ministerio de Economía y Competitividad (MINECO) por la financiación de los proyectos en los que he participado (CTQ-2012-36408 y CTQ2015-68654-R), la concesión de una beca FPI (BES-2013-064425) y de una ayuda (EEBB-I-16-10749) para realizar una estancia de 4 meses en Caen, Francia. También agradecer al programa Erasmus Mundus (EM) “Advanced Education European-Asiatic Exchange Programme in Materials Science and Catalysis” por la financiación del proyecto EURASIACAT y concesión de una beca predoctoral para realizar una estancia en Hong Kong durante 1 año.

Además, agradezco al grupo Terma y al Departamento de Ingeniería Química de la Universidad de Málaga por haberme acogido y haberme dejado utilizar sus instalaciones para realizar los experimentos de mi tesis doctoral. También quiero señalar la importancia de la magnífica labor de todos los técnicos del Servicio Central de Apoyo a la Investigación (SCAI)



de la Universidad de Málaga, donde se ha llevado a cabo gran parte de la caracterización de los materiales preparados en esta tesis. En especial, quisiera resaltar el trabajo de la Dra. Dña. María Dolores Marqués Gutiérrez del laboratorio de Sólidos Porosos, siempre muy amable y eficiente.

Tengo que decir que estoy tremendamente agradecido con todos los miembros del grupo Terma. Hemos compartido muchas horas de laboratorio, al mismo tiempo que se forjaban muy buenas amistades, en especial con José Palomo. Especial mención también para Javier Torres, quien colaboró conmigo muy activamente durante el trabajo realizado para el primer capítulo de la presente tesis doctoral. Aquí también tengo que nombrar a Nani, Ramiro, María José, Aurora, Fran, Raúl, Mari Carmen, Elisa, Imane, Tomás Jr., los migueles (Miguel y Miguel Ángel), Alicia, June, Lourdes, Eli, Olaya, Hugo, Paul, Mpho, Lilia, Rafael...Y creo que no se me olvida nadie. Algunos han estado presentes durante toda mi tesis doctoral, otros sólo al principio o al final de ésta, pero todos han hecho que fuera un placer ir a trabajar cada día.

I would also like to thank the good support that I received from my supervisors in the LCS group, Dr. D. Marco Daturi, Dr. D. Guillaume Clet and Dr. D. Philippe Bazin. They taught me a lot about FTIR and Raman *operando* spectroscopies during my 4 months stay in Caen, France. I cannot forget to name the good friends I met in this research group: Eli, Sandra, Clement, Julien, Stijn, Kamila, Eddy...They made me feel very comfortable in the lab and they integrated me into the group since the very first day.

I also found the love of my life during these years, Claudia. I met her in my stay in Hong Kong. I am also very grateful to her, she has been very patient and understanding with me and has given me the support I needed in the worst moments, even though sometimes I was not able to give her so much attention when I was very busy at work. I also can say that I made very good friends in Hong Kong, specially people from SKCC residence. For the sake of brevity, I will not show their names, but they have also been a very



important support during my PhD thesis. I did not feel alone, despite of being on the other side of the Earth.

También quiero agradecer de corazón todo lo que mi familia hace y ha hecho por mí durante todo este tiempo. Ellos han sido totalmente imprescindibles, me han aportado el cariño, la confianza, los recursos y la estabilidad necesaria para que yo haya llegado hasta aquí y pueda tener un futuro mejor. En este sentido, nombrar a mi familia más cercana: mis padres, María Luisa y Juan; mi hermano y cuñada, Daniel y Rocío; y mis sobrinos, Guillermo y Daniel. Por supuesto, también tengo que agradecer el apoyo que he tenido siempre de mis amigos que tengo desde la infancia o de las distintas etapas académicas de las que he vivido en el colegio, instituto y universidad.

Gracias a todos,

Juan José Ternero Hidalgo

Málaga, diciembre de 2019





## CURRICULUM

### Articles

This PhD is a compendium of the following publications:

- [1] J.J. Ternero-Hidalgo, J. Torres-Liñán, M.O. Guerrero-Pérez, J. Rodríguez-Mirasol, T. Cordero, Electrospun vanadium oxide based submicron diameter fiber catalysts. Part I: Preparation procedure and propane ODH application, *Catal. Today*. (2018). <https://doi.org/10.1016/j.cattod.2018.10.073>.
- [2] J.J. Ternero-Hidalgo, M.O. Guerrero-Pérez, J. Rodríguez-Mirasol, T. Cordero, Electrospun vanadium oxide based submicron diameter fiber catalysts. Part II: Effect of chemical formulation and dopants, *Catal. Today*. 325 (2019) 144–150. <https://doi.org/10.1016/j.cattod.2018.10.072>.
- [3] J.J. Ternero-Hidalgo, M.O. Guerrero-Pérez, J. Rodríguez-Mirasol, T. Cordero<sup>1</sup>, M. A. Bañares, R. Portela<sup>2</sup>, P. Bazin<sup>3</sup>, G. Clet<sup>3</sup>, M. Daturi, Simultaneous operando FTIR & Raman characterization (IRRaman) for the extended study of gas-phase reactions with solid catalysts. *Submitted*.
- [4] J.J. Ternero-Hidalgo, M. Daturi, G. Clet, P. Bazin, M. A. Bañares, R. Portela, M.O. Guerrero-Pérez, J. Rodríguez-Mirasol, T. Cordero, A simultaneous operando FTIR & Raman study of propane ODH mechanism over V-Zr-O catalysts. *Submitted*.
- [5] J.J. Ternero-Hidalgo, M.O. Guerrero-Pérez, J. Rodríguez-Mirasol, T. Cordero, Kinetic study of propane ODH on electrospun vanadium oxide-based submicron diameter fiber catalyst. Part I. *Submitted*.
- [6] J.J. Ternero-Hidalgo, C. Tsao, M.O. Guerrero-Pérez, J. Rodríguez-Mirasol, T. Cordero, Kinetic study of propane ODH on electrospun vanadium oxide-based submicron diameter fiber catalysts. Part II. *Submitted*.

## Other articles by the author:

- [1] J.J. Ternero-Hidalgo, F.F. Budihardjo, K.L. Yeung, Rapid synthesis of zeolite film coating on stainless steel, *Catal. Today*. (2019). <https://doi.org/10.1016/j.cattod.2019.08.057>.
- [2] L. Sabantina, M.Á. Rodríguez-Cano, M. Klöcker, F.J. García-Mateos, J.J. Ternero-Hidalgo, A. Mamun, F. Beermann, M. Schwakenberg, A.-L. Voigt, J. Rodríguez-Mirasol, T. Cordero, A. Ehrmann, Fixing PAN Nanofiber Mats during Stabilization for Carbonization and Creating Novel Metal/Carbon Composites, *Polymers*. 10 (2018) 735. <https://doi.org/10.3390/polym10070735>.
- [3] T. Cordero-Lanzac, J.M. Rosas, F.J. García-Mateos, J.J. Ternero-Hidalgo, J. Palomo, J. Rodríguez-Mirasol, T. Cordero, Role of different nitrogen functionalities on the electrochemical performance of activated carbons, *Carbon*. 126 (2018) 65–76. <https://doi.org/10.1016/j.carbon.2017.09.092>.
- [4] J. Palomo, J.J. Ternero-Hidalgo, J.M. Rosas, J. Rodríguez-Mirasol, T. Cordero, Selective nitrogen functionalization of phosphorus-containing activated carbons, *Fuel Process. Technol.* 156 (2017) 438–445. <https://doi.org/10.1016/j.fuproc.2016.10.006>.
- [5] J.J. Ternero-Hidalgo, J.M. Rosas, J. Palomo, M.J. Valero-Romero, J. Rodríguez-Mirasol, T. Cordero, Functionalization of activated carbons by HNO<sub>3</sub> treatment: Influence of phosphorus surface groups, *Carbon*. 101 (2016) 409–419. <https://doi.org/10.1016/j.carbon.2016.02.015>.



## Congress contributions

This PhD thesis has also generated the following congress contributions:

- [1] J.J. Ternero-Hidalgo, C. Tsao, M.O. Guerrero-Pérez, J. Rodríguez-Mirasol, T. Cordero, Alkane activation over V-Mo-O fibrous catalysts: a kinetic study, EURASIACAT Final Meeting (2018) (Hong Kong).
- [2] J.J. Ternero-Hidalgo, J. Torres-Liñán, M.O. Guerrero-Pérez, J. Rodríguez-Mirasol, T. Cordero, Group V elements based nanofiber catalysts prepared in one step by electrospinning for partial oxidation reaction, 9th International Symposium on Group Five Elements (2017) (Nueva Delhi, India).
- [3] J.J. Ternero-Hidalgo, J. Torres-Liñán, M.O. Guerrero-Pérez, J. Rodríguez-Mirasol, T. Cordero, Multilayered VOx/ZrO<sub>2</sub> nanofibers prepared in one step by electrospinning and their use as catalysts for propane ODH, 10th World Congress of Chemical Engineering (2017) (Barcelona, España).
- [4] J.J. Ternero-Hidalgo, M.O. Guerrero-Pérez, J. Rodríguez-Mirasol, T. Cordero, P. Bazin, G. Clet, M. Daturi, Unraveling the propane ODH mechanism by simultaneous FTIR-Raman operando studies over VOx/ZrO<sub>2</sub> catalysts, XXXVI Reunión Bienal de la Sociedad Española de Química (2017) (Sitges, Barcelona, España).
- [5] J.J. Ternero-Hidalgo, J. Torres-Liñán, F.J. García-Mateos, M.O. Guerrero-Pérez, J. Rodríguez-Mirasol, T. Cordero, VPO catalysts using activated carbons as a template. ODH of propane, 6th EuCheMS Chemistry Congress (2016) (Sevilla, España).



And the other works have also derived in the following congress contributions:

- [1] J. Palomo, J.J. Ternero-Hidalgo, J. María Rosas, J. Rodríguez-Mirasol, T. Cordero, Preparación de carbones activos de alto desarrollo poroso por activación química con  $H_2SO_4$  Y  $H_3PO_4$ , XIV Reunión del GEC (2017) (Málaga, España).
- [2] J.J. Ternero-Hidalgo, J. Palomo, J.M. Rosas, J. Rodríguez-Mirasol, Tomás Cordero, Selective nitrogen functionalization of P-containing carbons, The World Conference on Carbon (2016) (Pennsylvania, USA).
- [3] J.J. Ternero-Hidalgo, J. Palomo, J.M. Rosas, J. Rodríguez-Mirasol, T. Cordero, Influencia de la presencia de compuestos superficiales de P sobre la funcionalización de carbones activos con  $HNO_3$ , XIII Reunión del GEC en Alicante (2015) (España).
- [4] J. Palomo, J.J. Ternero-Hidalgo, J.M. Rosas, J. Rodríguez-Mirasol, T. Cordero, Funcionalización superficial de carbones activos con grupos nitrogenados mediante reacciones de oxidación/reducción, XIII Reunión del GEC en Alicante (2015) (España).
- [5] J.J. Ternero-Hidalgo, E. Polido, J. Rodríguez-Mirasol, T. Cordero, Funcionalización superficial de carbón activo: introducción de grupos aminos, XII Reunión del GEC en Madrid (2013) (España).



## Participation in projects

- [1] Referencia del proyecto: CTQ-2012-36408
- Título: Catalizadores ácidos/básicos de carbón a partir de residuos lignocelulósicos para la obtención de productos químicos de interés industrial
- Investigador principal: José Rodríguez Mirasol
- Entidad financiadora: MINECO
- Convocatoria: 2012
- Duración: Desde enero de 2013 a diciembre de 2015
- Financiación recibida: 143910,00 €
- Tipo de participación: Becario FPI
- [2] Referencia del proyecto: CTQ-2015-68654-R
- Título: Catalizadores avanzados de base biomásica para la síntesis de dimetil éter en una etapa.
- Investigador principal: José Rodríguez Mirasol
- Entidad financiadora: MINECO
- Convocatoria: 2015
- Duración: Desde enero de 2016 a diciembre de 2018
- Financiación recibida: 157300,00 €
- Tipo de participación: Equipo de trabajo



- [3] Title: EURASIACAT: Advanced Education European-Asiatic Exchange Programme in Materials Science and Catalysis.

ID: 552067-EM-1-2014-1-ES-ERA MUNDUS-EMA22

Programme: EM

Call: EACEA/18/13

Action / Strand / Lot: EMA2 / S2 / LOT.03

Geographical Area: EU + Hong Kong / Taiwan / Singapore / Macau

Levels: MAS+PHD+POS+STA

Date (start): 15/07/2014

Date (end): 15/07/2018

Duration: 48 months

Coord: University of Malaga (UMA), ES



## Grants

- [1] Beca FPI concedida (BES-2013-064425) por el Ministerio de Economía y Competitividad (MINECO) para la realización de la tesis doctoral en el Departamento de Ingeniería Química de la Universidad de Málaga con el grupo de investigación Terma.

Título del proyecto: “Catalizadores ácidos/básicos de carbón a partir de residuos lignocelulósicos para la obtención de productos químicos de interés industrial”

Centro de I+D de la ayuda: Universidad de Málaga

Investigador principal del proyecto: José Rodríguez Mirasol

Línea de investigación: Ingeniería Química y Tecnología Ambiental

### Predoctoral research stays:

- [2] Ayuda a la movilidad predoctoral concedida (EEBB-I-16-10749) por el Ministerio de Economía y Competitividad (MINECO) para la realización de una estancia breve de 4 meses durante el año 2016 en Caen (Francia) en el grupo del catedrático Dr. Marco Daturi

Organismo de I+D receptor: Universidad de Caen

Centro: Escuela Nacional Superior de Ingenieros (ENSICAEN)

Departamento: Laboratoire Catalyse et Spectrochimie (LCS)



- [3] Concedida una beca por el programa Erasmus Mundus (EM), con el título de “Advanced Education European-Asiatic Exchange Programme in Materials Science and Catalysis” para la realización de una estancia breve de 6-7 meses en Hong Kong durante el año 2018 como doctorando en el grupo del catedrático Dr. King Lun YEUNG. Dicha estancia fue extendida haciendo un total de 12 meses

Organismo de I+D receptor: Hong Kong University of Science and Technology

Departamento: Department of Chemical and Biomolecular Engineering (CBE)

